# Characteristics and origin of polymetallic mineralisation in the Kopaonik region of Serbia and Kosovo, with particular reference to the Belo Brdo Pb-Zn (Ag) deposit

## Milica Veselinović-Williams

**A thesis submitted in partial fulfilment of the requirements of Kingston University for the degree of Doctor of Philosophy**

**October 2011**

Veselinovic-Williams, M.
EThOS ID 542473.

Please do NOT digitise the following figures:

| | |
|---|---|
| Figure 1.1 | p.2 |
| Figure 2.1 | p.7 |
| Figure 2.2 | p.8 |
| Figure 2.3 | p.10 |
| Figure 2.4 | p.11 |
| Figure 2.5 | p.15 |
| Figure 2.6 | p.17 |
| Figure 2.7 | p.17 |
| Figure 2.8 | p.19 |
| Figure 2.9 | p.21 |
| Figure 2.10 | p.23 |
| Figure 2.11 | p.25 |
| Figure 2.12 | p.26 |
| Figure 2.13 | p.27 |
| Figure 2.14 | p.28 |
| Figure 2.15 | p.30 |
| Figure 3.1 | p.33 |
| Figure 3.2 | p.34 |
| Figure 3.3 | p.34 |
| Figure 3.4 | p.35 |
| Figure 4.1 | p.67 |
| Figure 4.20 | p.97 |
| Figure 5.1 | p.105 |
| Figure 5.2 | p.105 |
| Figure 6.6 | p.125 |
| Figure 6.15 | p.137 |
| Figure 9.1 | p.182 |
| Figure 9.2 | p.189 |
| Figure 9.3 | p.202 |

THESIS CONTAINS
CD/DVD

# ABSTRACT

This project was initiated with the aim of determining the origin and evolution of the Belo Brdo Pb-Zn (Ag) carbonate-replacement and vein-type deposit in the Kopaonik metallogenic district of Serbia and Kosovo and to test its potential genetic association to nearby porphyry Cu-Au and skarn deposits. Hydrothermal-replacement, stockwork, skarn and vein-type base metal deposits in the region are related to a Tertiary (65.5 to 1.8 Ma) volcano-magmatic complex that intruded a tectonic nappe pile that includes a Triassic (251 to 199.6 Ma) Metamorphic Complex, a Jurassic (199.6 to 145.5 Ma) Ophiolite Unit and an Upper Cretaceous (99.6 to 65.5 Ma) Flysch Unit. Petrographic and geochemical investigations of the Tertiary igneous rocks confirm a calc-alkaline chemistry for regionally distributed andesitic-dacitic and quartz-latite rocks. These volcanic rocks show a clear subduction-related character.

The Pb-Zn (Ag) mineralisation at Belo Brdo evolved as a result of several successive stages of mineralisation including: (1) pre-ore stage, including early hydrothermal alteration and listwanisation followed by the deposition of Ni-Co-As sulphides; (2) main-ore stage, represented by massive sulphides including sphalerite, galena, pyrite, arsenopyrite, chalcopyrite, Ag-tetrahedrite-tennantite, bournonite; and (3) post-ore stage represented by quartz, carbonates ±pyrite.

A combination of fluid inclusion microthermometry, sphalerite and arsenopyrite geothermometry, and oxygen-isotope geothermometry suggests that the hydrothermal mineralisation at Belo Brdo was deposited from epithermal- to moderately high temperature (160–350°C), low salinity (6.5 eq. wt. % NaCl) fluids. Calculated $\delta^{18}O$ (6.5 to 10 ‰) and $\delta D$ (- 38 to – 62 ‰) values of water in equilibrium with sericite, tourmaline and quartz of the pre-ore stage are consistent with the ore fluids being derived from a magmatic source. Additionally, calculated oxygen isotopic composition of the main-ore stage fluid also shows magmatic signatures (5.9 to 7.7‰). However, the water from fluid inclusions hosted by quartz from the late- ore stage breccia exhibits lower $\delta D$ (-93 to -96‰) and $\delta^{18}O$ (4.8 to 2.3 ‰) values, indicating an involvement of a more dilute, low-temperature meteoric hydrothermal fluids. Meteoric water played an increasing role toward the later stages of ore deposit evolution. The $\delta^{34}S$ values of the sulphides at Belo Brdo are homogeneous (average 4.4‰) and similar to those from nearby Cu-Au porphyry and skarn deposits in the study area, indicating a common source of sulphur for all deposits.

The hydrothermal deposits in the study area show homogeneous lead isotopic compositions ($^{206}Pb/^{204}Pb$= 18.68 to 18.76, $^{207}Pb/^{204}Pb$= 15.67 to 15.68, and $^{208}Pb/^{204}Pb$ = 38.87 to 38.91), similar to those of local calc-alkaline volcanic rocks ($^{206}Pb/^{204}Pb$ = 18.76-18.82, $^{207}Pb/^{204}Pb$ 15.66-15.68 and $^{208}Pb/^{204}Pb$ 38.87-38.97) indicating a genetic link between mineralisation and magmatism.

The data suggests that the Belo Brdo and the nearby Pb-Zn deposits are not Mississippi Valley type, but similar to a high temperature carbonate-replacement massive sulphide deposits associated with calc-alkaline magmatism in a supra-subduction zone setting.

# ACKNOWLEDGEMENTS

Firstly, I would like to thank my director of studies, Professor Peter Treloar for his invaluable advice, contributions and constant support during the duration of my research. This dissertation would not be possible without his insights, an expert guidance and understanding. Secondly, but no less importantly, I am thankful to Professor Andy Rankin for his support, advice and numerous contributions to this project, especially in the fields of fluid inclusions and mineralising systems.

I am grateful to the Crustal Processes and Geodynamics Research group of the Centre for Earth and Environmental Science Research at Kingston University for the full funding of this project. I am also thankful to the Natural Environment Research Council (NERC) Isotope Geosciences Laboratory for providing financial support for stable and radiogenic isotope analyses.

Further, I am appreciative of the advice and assistance from Dr. Stella Bignold, Professor Ian Jarvis, Dr. Kym Jarvis, Richard Giddens, Ian Gill, Rob Ravenhill, Simon Crust, Tracey Davis, Claire Ivison, Kevin Attree and Simon De Mars. I am also very grateful for discussion with, and advice from, persons away from Kingston, namely Professor Ladislav Palinkaš and Dr. Sabina Strmić-Palinkaš (Zagreb University), Dr. Adrian Boyce, Alison McDonald, Julie Dougans and Chris Taylor (stable isotope facility, the Scottish Universities Environmental Research Centre-“SUERC”) as well as Drs. Ian Millar and Jonathan Naden (radiogenic isotope facility, NERC, British Geological Survey, UK).

Many thanks for organising the access to the Belo Brdo mine and supervision go to Professor Ladislav Palinkaš (Geology Department, University of Zagreb, Croatia), Mr. Ivan Forjan (Development Officer of Trepca Mines Complex, under UNMIK), Mr. Stevica Vidosavljević (Director, RMHK Trepča RIF Kopaonik) and Mr. Branislav Kokerić (Technical Supervisor, Belo Brdo Mine). Special thanks for organising access to the Karavansalija and Rudnitza prospects go to Dr. Vertrees "Mac" Canby (Freeport McMoRan) and Dr. Dejan Koželj (South Danube Metals). First class logistical field support in Raška from the staff of Freeport McMoRan Copper & Gold, Inc. and EuroMax Resources Ltd. is sincerely appreciated.

Mališa Mladenović, Stanoje Milutinović, Krstibor Vukojević, Živko Dimitrijević, Veroljub Ilić and Milanko Kovačević are thanked for their hospitably and lively discussions on geology of the Kopaonik region.

I would like to thank all of my friends in the School of Geography, Geology and the Environment for the friendship and support during my post- graduate study.

Finally, I would like to thank my husband David, our daughters Michaela and Nicola, and my mum Ljuba for their love, patience, and encouragement during this study.

# TABLE OF CONTENTS

## CHAPTER 1: INTRODUCTION AND BACKGROUND

## CHAPTER 2: REGIONAL GEOLOGICAL SETTING

## CHAPTER 3: LOCAL GEOLOGY, PETROGRAPHYAND GEOCHEMISTRY OF IGNEOUS ROCKS IN THE KOPAONIK AREA

## CHAPTER 4: MINERALOGY OF THE BELO BRDO DEPOSIT

## CHAPTER 5: MINERALOGY OF THE KARAVANSALIJA SKARN DEPOSIT

## CHAPTER 6: FLUID INCLUSION STUDIES OF THE BELO BRDO DEPOSIT

APPENDICES are saved on a CD-ROM enclosed at the back of this report

# CHAPTER 1:
# INTRODUCTION AND BACKGROUND

## 1.1 Introduction

The magmatic-hydrothermal class of ore deposits encompass a wide variety of economically important deposits types, namely the porphyry Cu (±Au)-Mo deposits, epithermal precious-metal, intrusion-related gold, greisen-related Sn-W, polymetallic skarn and pegmatite-related deposits (Robb, 2005; Pirajno, 2009). Major geological processes responsible for the formation of these deposits include the generation of hydrous silicate magmas, the exsolution of aqueous fluids from magmas as they cool and crystallise, vapour-brine immiscibility, fluid-mineral interactions and the precipitation of ore minerals (e.g., Burnham and Ohmoto, 1980; Whitney and Naldrett, 1989; Hedenquist and Lowenstern, 1994; Burnham, 1997; Audétat et al., 1998).

*Porphyry Cu (±Au)-Mo systems* are the main source of Cu and Mo and a significant source of Au, Ag, Sn, W, Pb and Zn (Cox, 1986; Guilbert and Parks, 1986; Kesler, 1994). They are generally characterised by distinct hydrothermal alteration and sulphide mineralisation halos that are concentrically zoned around porphyritic intrusions emplaced at a shallow crustal level (< 5 km) (e.g., Sillitoe 1973; 2000). The mineralisation typically occurs in dense, multidirectional veinlets (stockworks) and sporadic disseminations (Lowell and Guilbert, 1970; Sillitoe, 1973; Titley and Beane, 1981; Titley, 1982). Porphyry deposits are formed in association with the emplacement and crystallisation of intermediate to felsic granitic intrusions derived from hydrous, mainly magnetite-series (oxidised), magmas generated at convergent plate margin settings (Mitchell and Garson, 1972; Sillitoe, 1972, 1987, 1991; Ishihara, 1981; Corbett and Leach, 1998). These intrusives may, according to Burnham (1967; 1979; 1997), reach water saturation due to decompression during upward emplacement ("first boiling") resulting in the exsolution of the ore-bearing aqueous fluid and subsequent fracturing of the carapace and surrounding rocks. Such fractured country rocks provide good ground preparation for the circulation of ore-bearing fluids which interact with the wall-rocks resulting in hydrothermal alteration and mineral precipitation. The porphyry intrusions act as the source for volatiles and metals as well as the heat responsible for the development of large, circulating cells of magmatic-meteoric hydrothermal fluids (for example, Burnham, 1979; Sillitoe and Hedenquist, 2003). The porphyry ore fluids are initially dominated by hot (400-700°) magmatic, hypersaline brines, which usually coexist with a low density vapour (for example, Heinrich, 2005). The aqueous fluids (100-400°C) of low salinity and meteoric origin are common in the later stage of deposits evolution and play an important role by cooling and diluting the magmatic fluid (Bodnar, 1995). If the exsolved magmatic fluids interact with surrounding calcareous sediments, *polymetallic skarn* deposits may form, which in turn give way to *carbonate-replacement Pb-Zn-Ag (±Au)* type of mineralisation (Sillitoe, 1989; 2010). The fluids may extend some distance from the source intrusion into the shallow environment where *base-metal veins* and *epithermal Au-Ag (± Cu) deposits* may form. The epithermal Au-Ag (± Cu) deposits, including high-sulphidation (HS), low-sulphidation (LS) and intermediate-sulphidation (IS) types, terms introduced by Hedenquist (1987) and Hedenquist et al., (2000), are often regarded as end-members in a continuum of hydrothermal-magmatic processes that progressively incorporate more non-magmatic waters as the magmatic system wanes, or as one moves away from the igneous centre (Sillitoe, 1973, 1989; Hedenquist et al., 2000; Einaudi et al., 2003; Sillitoe and Hedenquist, 2003). A conceptual model for porphyry -epithermal transition system is presented in Figure 1.1.

**Figure 1.1:** Conceptual model for types of mineral deposits in porphyry system (taken from Corbett and Leach, 1998).

Porphyry systems are among the most studied types of deposits within the magmatic-hydrothermal class. Since the interest for precious metals increased during recent years, the geological studies intensified and concentrated mainly on gold-rich porphyry and epithermal Au-Ag deposits (Einaudi et al., 2003; Heinrich, 2005; Camprubi and Albinson, 2006). However, less consideration has been given to peripheral base-metal carbonate-replacement and polymetallic vein deposits which can form in-between the two end-members of the porphyry system. This transitional environment is the focus of this study.

## 1.2 Aims and objectives of this study

The Kopaonik metallogenic district in southern Serbia and Kosovo is a region with a proud mining history (Ellis 2005). The district is well known for its economically significant deposits of lead-zinc, antimony, silver, chromium and nickel, as well as smaller copper, iron and gold mineralisation. Deposit types include stockworks, skarn, carbonate-replacement bodies and veins (Janković, 1990). Such a variety and diversity of mineral deposits in a geographically restricted area is indicative of a suite of ore-forming processes, which, until now, have not been studied in detail, particularly in the context of modern ore genetic theories. Pre-1990 knowledge of the metallogenic evolution of the region was insufficient to reliably constrain the important processes of ore formation (Karamata and Janković, 2000). There is little post-1990 western literature that deals with the genesis of ore deposits in this region. This is partly because research since then was curtailed by the wars that affected the former Yugoslavia. The region is thus ripe for a study that embraces modern techniques and concepts. This study was carried out to test *the hypothesis that the Pb-Zn ±(Ag) deposits of the Kopaonik metallogenic district represent epigenetic peripheral mineralised bodies linked to a larger, perhaps porphyry system at depth, with significant input of trace elements from related ophiolites.*

The porphyry-type systems, outlined above, are evident elsewhere in the world in subduction and supra-subduction environments, such as the Circum-Pacific, the central Asian collages of island arcs and the Carpathian arc of Eastern Europe (Sinclair, 2007). However, the model has not previously been tested within the Vardar ophiolitic suture zone of the Dinaride-Hellenide belt in Serbia and Kosovo and would have important metallogenic implications for the region. Testing of the system-scale magmatic-hydrothermal model including the Belo Brdo Pb-Zn (Ag) deposit, the Karavansalija Cu-Au skarn and the Rudnitza Cu-Au porphyry mineralisation is the main focus of this research.

The prime aims of this study are to:

- Determine the nature and origin of the hydrothermal ore-forming environment at the Belo Brdo Pb-Zn (Ag) carbonate-replacement and vein-type deposit and to carry out a comparable study with other Pb-Zn (±Ag) occurrences in the district;
- Investigate the role of calc-alkaline magmas, associated ophiolites and sedimentary rocks in providing fluids and ore components for the various types of Pb-Zn-Ag-Cu-(Au)-(Sb) deposits in the Kopaonik mining district;
- Develop a genetic model for the evolution of Pb-Zn-Ag deposits within the study area in order to refine exploration models for similar deposits including Au occurrences in the region;
- Demonstrate that carbonate-replacement Pb-Zn deposits in the Kopaonik district are not Mississippi Valley- type (MVT).

No previous scientific research including mineral chemistry, fluid inclusion, stable and radiogenic isotope studies has been carried out in the Belo Brdo ore field. The results of the first-hand, robust data, collected by the author, will enhance our understanding of Pb-Zn (Ag) deposits in the region and contribute to the geologic history of the Vardar Zone magmatism in the Dinarides.

### 1.3 Geographic setting

The study area (43°14' N, 20°50'E) is located partly in southern Serbia, about 280 km south from the capital Belgrade and partly in northern Kosovo (Figure 1.2). The topography is mountainous with altitudes up to about 2,000 m. The average elevation is around 1,200 m. Two major mountain ranges, namely Kopaonik and Rogozna, are situated in the centre of the study area. The main drainage is the 270 km long river Ibar and its tributary Raška. The Ibar flows from Montenegro through Kosovo into the West Morava, which in turn flows into the river Danube in Serbia. They are part of the Black Sea drainage basin. The climate is continental, with hot summers and cold and snowy winters and relatively moderate precipitation, occurring mostly in summer. The access to the study area is available by the main transport routes through Serbia, Kosovo and Macedonia. Also, it has a well-developed rail network which connects the area with central Europe and the Near East.

Figure 1.2: Geographic location of the study area.

International air links are provided from across Europe to Priština in Kosovo and Niš in Southern Serbia. The largest town in the study area is Novi Pazar with a population of 100,000. Smaller towns are Raška in Serbia and Leposavić in Kosovo.

The area was an important mining centre during medieval times with many Saxons operating in the area as miners.

## 1.4 Methods applied

The methods employed to reach the objectives of this thesis include (i) field work, (ii) petrographic studies (Scanning Electron Microscopy [SEM], Cathodoluminescence [CL], reflected and transmitted light microscopy), (iii) fluid inclusion studies (microthermometry), and (iv) geochemical studies including whole-rock geochemistry, stable ($\delta^{13}C$, $\delta^{18}O$, $\delta D$, $\delta^{34}S$) and radiogenic (strontium: $^{87}Sr/^{86}Sr$; and lead: $^{207}Pb/^{204}Pb$, $^{206}Pb/^{204}Pb$ and $^{208}Pb/^{204}Pb$) isotope geochemistry and Rare Earth Elements (REE) analyses on carbonate gangue minerals. The resultant data will be presented and briefly discussed in the following chapters. These data will then be combined to develop a robust metallogenic model for the origin of the carbonate-replacement deposits in the Kopaonik Metallogenic district. This model incorporates all aspects of metallogeny including regional setting, mineralisation style, nature and origin of the fluids, their metal-, sulphur- and carbonate components and implications for further exploration.

Most data presented in this study concern the Pb-Zn (Ag) Belo Brdo deposit. However, in order to establish a sound metallogenetic model for the study area, data from other deposits, such as the Cu-Au skarn in Karavansalija, Cu-Au porphyry in Rudnitza and small Pb-Zn vein deposit in Karadak near Rudnitza will also be taken into consideration when discussing the general model for metallogeny of the Kopaonik district.

# CHAPTER 2:
# REGIONAL GEOLOGICAL SETTING

## 2.1 Introduction

The Tethyan orogenic system (or Alpine-Himalayan) (Figure 2.1A) developed during the Late Mesozoic-Tertiary convergence of the Indian, Arabian and African plates and their on-going collision with Eurasia (e.g., Şengör, 1989). Progressive closure of the Tethys oceanic basins occurred through multistage subduction, followed by obduction, accretion, and syn- to post-orogenic extension processes along the active margin of southern Eurasia. The Eastern Mediterranean realm of the Tethyan orogenic system includes the Alpine-Balkan-Carpathian-Dinaride orogenic chain (ABCD province) (Figure 2.1B). The Kopaonik metallogenic district is located within the Vardar ophiolite zone (Figure 2.1C), which is the easternmost tectonic unit of the Dinaride-Hellenide branch of the ABCD province. The Vardar ophiolite zone separates the Africa-Arabia plate from the Eurasian plate. Details on the tectonic evolution of the Tethyan orogen are beyond the scope of the current study, but there is ample literature on the topic (e.g., Smith, 1971, 2006; McKenzie, 1972, 1978; Dewey, et al., 1973; Dercourt, et al., 1986, 1993, 2000; Dixon and Robertson, 1984; Şengör, 1989; Stampfli and Borel, 2002; Robertson and Mountrakis, 2006). Whilst the Alps and Carpathians have been extensively studied by generations of Earth scientists from all over the world, the Dinaride branch of the ABCD province remained the least documented within the region. However, the opening of borders between western and eastern parts of Europe played an important role in releasing new information related to the recent geological research carried out in the region.

This chapter introduces the general features of the Dinarides including a summary of the main tectono-stratigraphic units. An overview of the geodynamic evolution of the orogen, mainly based on recently published literature (Robertson et al., 2009; 2009a; Schmidt et.al., 2008) is presented in Section 2.4. A brief review of the Dinaride's major mineral deposits within the region of former Yugoslavia is presented in Section 2.5, whilst more details on mineral deposits of the Kopaonik metallogenic district is presented in Section 2.6.

## 2.2 General features of the Dinarides

The Dinaride orogenic chain represents the south-western margin of the ABCD province (Figure 2.1). Together with the Hellenides, they compose a 2000 km-long NW–SE trending fold and thrust orogenic belt of Alpine age, covering parts of Slovenia, Croatia, Bosnia and Herzegovina, Serbia, Montenegro, Albania and part of Greece (Figure 2.1). The belt is connected with the Southern Alps in the north. To the north-east, the Dinarides have been overprinted by

**Figure 2.1:** Regional geological setting. A- Tethyan orogenic system; red square is inset showing the ABCD province in B; red lines indicate cross section shown in Figure 2.2; C- Dinaride-Hellenide belt (Modified after Dimitrijević, 2001; Karamata, 2006 and Schmid et al., 2008).

tectonic processes controlling the evolution of the Neogene Pannonian Basin. Towards the east, the Dinarides are separated from the Carpathian/Balkanides by the Vardar Ophiolite Zone, which in turn is bounded by the European- derived Serbo-Macedonian unit, generally considered to be the stable margin of the Eurasian Plate (Dimitrijević, 2001). The Dinarides are bounded to the west by the undeformed Apulia Zone (Figure 2.1). The Dinaride-Hellenide belt became a part of the Alpine orogenic system during the Late Mesozoic and Cenozoic, when the Mediterranean region experienced complex subduction events and associated collisions, resulting in mountain building, magmatism, foreland and hinterland deformation, sedimentary basin evolution, escape tectonics, orogenic collapse, and the opening of small ocean basins (Dilek, 2006). The diachronous collision of Adria microplate (McKenzie, 1972) with Europe along its irregular margins created the Alps, the Apennines and the Dinaride-Hellenide mountain belt at different times and affected the Carpathians in the east, resulting in the formation of the arcuate-shaped orogenic system (Figure 2.1B) (Ilić and Neubauer, 2005; Dilek, 2006).

The Dinaride-Hellenide belt displays a double- vergent structural architecture with east-vergent thrust fault systems in the internal zone to the east, and west-vergent thrust faults in its external zone to the west (Figure 2.2). The east-directed thrusts are believed to be related to ophiolite emplacement in the Late Jurassic-Early Cretaceous (Schmid et al., 2008). The west-southwest-directed thrust faults developed as a result of oblique collision between Adria and Eurasia, starting around 55 Ma, and subsequently migrating westward into the Peri-Adriatic depression (Figure 2.2) (Dilek, 2006).

**Figure 2.2:** Simplified tectonic cross section across Dinaride-Hellenide segment of the Alpine orogenic belt (Modified after Dilek, 2006; Schmid et al., 2008).

Early attempts to define a regional structural framework of the Dinarides in former Yugoslavia took place during the first half of the 20th century, when the importance of the "Alpine-type" overthrusts and nappes were already recognised and applied to the Dinarides, which were subdivided into three geotectonic units composed of seven large-scale nappes (Kosmat, 1924; Kober, 1924). This early concept of fold-and-thrust belts, comprising external structural units overthrusted by internal ones, was accepted by most of the local authors and used as a base for further research (Besić, 1954; Petković, 1961; Aubouin, 1973; Grubić, 1980; Dimitrijević 1982, 1997, 2001; Andjelković, 1982; Herak, 1986; Pamić et al., 1998; Tari and Pamić, 1998). Many of these papers were published in local journals and thus not easily accessible to the international geological community. In most of these papers the authors stressed their own geotectonic approach, in line with, the then, current understanding and with a major emphasis on terminology, not seriously departing from Kosmat's and Kober's (1924) views. However, a review of ophiolitic belts in central and south-western parts of the Balkan Peninsular by Robertson and Karamata (1994), as well as papers by Karamata et al. (2000) and Pamić et al. (2002) initiated a new approach to the interpretation of the Mesozoic evolution of the region. Those authors recognised the presence of two ophiolite belts namely the *Dinaride Ophiolite Zone*, which extends from Croatia through Albania (the Mirdita zone), and into northern Greece, as the Mesohellenic ophiolites (e.g. Pindos and Vourinos ophiolites) and the *Vardar Ophiolite Zone*, which extends from Serbia through Thessaloniki in Greece (Axios zone) (Figure 2.1). The two ophiolite zones are in tectonic contact with the continental Drina-Ivanjica, Jadar and Pelagonian "blocks" (Karamata et al., 2000). Most of the authors view these two ophiolite belts as representing two distinct oceanic realms, while the intervening continental blocks were regarded as microcontinents or "terranes" that separated them (e.g. Karamata, 2006). There is, however, an ongoing debate on the existence of the microcontinents and the number of oceans that existed during the Mesozoic (see Section 2.4).

## 2.3 Overview of the major tectono-stratigraphic units within the Dinarides

The Dinarides have been divided into a series of northwest-southeast trending tectono-stratigraphic zones, as shown in Figures 2.1C and 2.3. From southwest to northeast, the following tectono-stratigraphic units can be distinguished: 1- External Dinaride Zone (carbonate platform formations), including the Bosnian Flysch Unit, 2- Dinaride Ophiolite Zone (including ophiolites associated with related sedimentary formations), 3- Drina-Ivanjica-Jadar Zone (Palaeozoic–Triassic nappes) and, 4- Vardar Ophiolite Zone (including Upper Cretaceous-Paleogene flysch, tectonised olistostrome mélange, metamorphic and granitoid rocks) (Pamić et al., 1998; Karamata and Vujnović, 2000; Hrvatović and Pamić, 2005; Karamata, 2006) (Figure 2.3). The Dinaride tectono-stratigraphic units constitute a stack of thrust sheets with the External Dinaride Zone at the base and the Vardar Ophiolite Zone at the top.

***2.3.1 The External Dinaride Zone***, or the Adriatic-Dinaridic carbonate platform, represents the proximal parts of the Adriatic continental margin. The following allochtonous tectonic units have been distinguished from SW to NE: the Adriatic-Dalmatian Zone, the Budva-Cukali Zone, the Dalmatian-Herzegovian Zone (or High Karst Unit), the Una-Kuci Zone, the Central Bosnian Mountains Unit and the East Bosnian-Durmitor Zone (Hrvatović and Pamić, 2005). All tectonic units were tectonically emplaced during the Alpine deformation, forming a complex fold and thrust belt (Figure 2.3). The Adriatic-Dinaridic carbonate platform is made up of Triassic-Cenozoic continental sedimentary successions deposited on the Adriatic continental crust basement. The successions represent a typical continental margin evolution closed by the sedimentation of the flysch deposits. The basement of the sedimentary succession is composed of Middle Devonian-Middle Permian metamorphic rocks, affected by the Variscan deformations.

The Late Permian to Late Triassic sequence of clastics and platform carbonates and associated synsedimentary igneous rocks were deposited during the initial rifting stage of the Alpine cycle (Pamić et al., 1998). In some areas the carbonates are interlayered with chert, shale, pyroclastic and volcanic rocks, which accumulated in platform depressions (Figure 2.4 A). The deposition of thick carbonate platform sequences continued during the Norian (216.5 to 203.6 Ma). The stable shallow-marine environments prevailed during the Jurassic-Cretaceous and lasted till the Middle Eocene, temporarily interrupted by several pelagic incursions (Figure 2.4A). The carbonate platforms are interspersed by intervening narrow deep-water basins (intra-platform rift basins), whose successions generally begin with Triassic deep-water facies and end with Cenozoic flysch (Schmid et al. 2008), such as those in the Pindos-Olonos Zone (Greece), Krasta-Čukali Zone (Albania) and Budva Zone (Montenegro) (Dimitrijević, 1997).

**Figure 2.3:** Outline tectonic map of the Dinarides, showing the tectonic zonation. (Modified after Hrvatović and Pamić, 2005; Karamata, 2006).

*The Bosnian Flysch Unit* (Figures. 2.3 and 2.4 B), which was deposited on the slope of the Adriatic-Dinaridic carbonate shelf (Pamić et al. 1998), is characterised by an intensely folded stack of Middle Jurassic to Cretaceous mixed carbonate and siliciclastic sediments. Within this unit, which is about 3000 m thick, two subunits can be distinguished (Olujić, 1978); 1- "Vranduk

Subgroup" is characterised by thick-bedded radiolarian chert, which pass upwards into pelagic carbonates, interbedded with sandstone turbidites and shales. 2- The "Ugar Subgroup" is a typical carbonate flysch series from the carbonate shelf margin with the youngest exposed succession ending with marls and sandstone turbidites of Palaeocene age.

**Figure 2.4:** Correlation charts for major tectono-stratigraphic units of the Dinarides (taken from Hrvatović and Pamić, 2005).

***2.3.2 The Internal Dinaride Zone*** (Middle Triassic – Late Jurassic oceanic domain) or the Dinaride Ophiolite Belt, (e.g. Dimitrijević, 1982), lies to the northeast of the Adriatic-Dinaridic carbonate platform and related units, and is bounded by the Drina–Ivanjica unit to the northeast (Figures 2.1; 2.3).

This belt, referred to by most authors as the Dinaridic ophiolites (Pamić et al., 2002; Karamata, 2006), is also known as the Central Dinaridic ophiolite belt (Lugović et al., 1991) and represents the remnants of the former Dinaric (Pamić et al., 2002) or Intradinaric ocean (Dimitrijević, 2001). The Dinaride ophiolite belt consists of two fundamental allochthonous components. The first is a mélange, traditionally known as the Dinaride olistostrome, and the second is variably dismembered, mainly ultramafic bodies, known as the Dinaride ophiolites (Karamata, 2006). The mélange consists of detached blocks and dismembered thrust sheets of various lithologies and ages set in a sheared clastic sedimentary matrix (Figure 2.4C). Radiolarian cherts, indicative of deep-water or oceanic conditions, are locally intercalated with basalts, with either primary depositional or tectonic contacts, and are also present as individual chert- blocks in the mélange. The sedimentary blocks occur as olistoliths and dismembered limestone thrust sheets. These commonly include Upper Triassic shallow- water limestone and Upper Triassic pelagic limestones (Robertson et al., 2009a). Within the Dinaride ophiolite belt mid-ocean ridge- type basalt (MORB) occurs as pillow lava, massive lava and lava breccia, mainly as blocks and dismembered thrust sheets (Robertson and Karamata, 1994). Ophiolites are mainly peridotites with subordinate basalt-diabase and gabbro. Ultramafic units occur at high structural levels of the tectono–stratigraphy, commonly tectonically overlying mélange. Mantle tectonite ultramafics make up the largest of the ultramafic bodies, of which the best studied, is Zlatibor (western Serbia). These ophiolitic bodies are relatively thin sheets, 2–3 km thick (Roksandić, 1971). Their basal contacts are tectonic, with a discontinuous metamorphic sole in some places. Recent mineral chemistry studies within the Dinaride Ophiolite Belt show that the ultramafic bodies fall into two main classes (Bazylev et al., 2003, 2006, 2009). The first is mainly fertile spinel and plagioclase lherzolites interpreted as tectonically emplaced (exhumed) sub-continental mantle lithosphere. The second class is composed of depleted spinel harzburgite and may also include ultramafic rocks internally ranging from lherzolite to depleted harzburgite (Bazylev et al., 2009). This assemblage is attributed to formation in a supra-subduction zone-type oceanic setting (Bazylev et al., 2003, 2009). The Dinaride ophiolite belt is locally covered by transgressive shallow-water limestones and clastic sediments of Late Jurassic–Early Cretaceous age (Pogari Series).

***2.3.3 The Pelagonian-Drina-Ivanjica Zone*** (continental domain) is represented by an Upper Triassic to Upper Cretaceous sedimentary succession, unconformably overlying a Paleozoic continental crust basement composed of terrigenous sedimentary and mafic volcanic rocks, metamorphosed to greenschist facies (Figure 2.4E) (Milovanović, 1984). This unit was initially described as a regional-scale anticlinorium (Ćirić and von Gaertner, 1962) and was later interpreted as a folded or upthrust window of a regional Adria–Dinaride platform (Golija unit of Aubouin et al., 1970; Rampnoux, 1970). More recently, the Drina–Ivanjica unit has been interpreted as a microcontinent that rifted from Adria (Dimitrijević, 1982; Robertson and Karamata, 1994; Dimitrijević, 1997, 2001). However, the Drina–Ivanjica unit has also been correlated with Eurasia, since it also shows some facies similarities with the Palaeozoic of Western Europe (Pamić et al., 1998; Hrvatović and Pamić, 2005). Recently, Schmid et al. (2008) infer that the Drina–Ivanjica unit is part of Adria, which extends right under the Dinaride ophiolite belt.

***2.3.4 The Vardar zone*** (Late Triassic-Maastrichtian) (Figures 2.1 and 2.3) is a composite terrane, characterised by both oceanic- and continental- derived tectonic units (Figure 2.4D), such as: the ophiolite mélange; dismembered ophiolitic rocks; Cretaceous-Early Paleogene flysch (Dimitrijević and Dimitrijević, 1985); Late Paleogene regionally metamorphic sequences originated from surrounding Late Cretaceous flysch; syn-kinematic granitoids and post-orogenic volcanics (Robertson and Karamata, 1994; Trubelja et al., 1995; Dimitrijević, 2001). Karamata (1994) distinguished two branches of the Vardar Zone namely the Vardar Zone Western Belt, and the Eastern Vardar Zone (also known as Main Vardar Zone). The Vardar Zone Western Belt is a large region of ophiolites and mélange (Karamata et al. 1980) and is largely equivalent to the Sava Zone of Pamić et al., (1998; 2002), who interpreted it as the most internal unit of the Dinarides. This belt is also referred to as the Inner Dinaridic ophiolite belt (Lugović et al., 1991), the External Vardar Subzone (Dimitrijević 1997, 2001) or simply the Vardar Zone (Pamić et al., 2002). The Vardar Zone Western Belt is dominated by depleted mantle rocks (harzburgites) with a suprasubduction geochemical signature (i.e. Spray et al. 1984; Lugović et al. 1991). The East Vardar Zone comprises the ophiolites east from Kopaonik in Serbia, the Guevgueli complex in F.Y.R. of Macedonia, and the Peonias zone in Greece. Ophiolite rocks found in the Romanian South Apuseni Mountains are interpreted as members of this ophiolite zone (Bortolotti et al., 2002). The common features of the East Vardar Zone are as follows: the present structural position of these ophiolites is characterised by eastward vergence, opposite to other ophiolites of the Balkan Peninsula; they consist predominantly of gabbro-diabase assemblages, whereas basaltic pillow lavas and obducted peridotite sheets are relatively rare; they are overlain by Tithonian (150.8 to 145.5 Ma) limestones, and they are closely associated with intermediate and acid calc-alkaline rocks (Karamata, 2006; Šarić et al., 2009).

## 2.4 Geodynamic evolution of the Dinarides

The evolution of the Dinaride-Hellenide belt was governed by the interaction of the Afro-Arabian plate with the Eurasian plate and intervening continental terranes. Jurassic and Early Cretaceous opening of the Central Atlantic initiated convergence and collision between the Adria microplate and the intra-Carpathian terranes. This early tectonism represents the onset of orogenic activity in the ABCD area. Several contrasting tectonic models have been proposed to reconstruct the regional evolution of the Mediterranean region, including the Dinaride-Hellenide belt (Robertson and Mountrakis, 2006). The main points of debate have been concentrated around a number of issues such as: the nature of the Paleozoic Palaeotethyan ocean ("Palaeotethys") and its relationship to younger Mesozoic Tethyan ("Neo-Tethyan") oceanic basins; the number of oceans and micro-continents that existed during the Mesozoic; the number of subduction zones in the area of the present Balkan Peninsula; the direction and character of subduction; the direction and character of obduction and emplacement of the ophiolites; the nature and paleogeographical location of the Drina-Ivanjica zone; and dating and determination of the main regional tectonic phases. Some of these points and the summary of the recently proposed geodynamic models regarding the evolution of the Dinaride-Hellenide belt are presented below.

In general, the geodynamic evolution of the Dinarides was controlled by a sequence of tectonic processes, including continental rifting, development of passive margins, opening of the Neo-Tethyan oceanic basins, subduction processes, emplacement of ophiolites and collision (Robertson et al., 2009).

### *2.4.1 Triassic rifting and continental break-up*

The earliest Alpine phases of the evolution of the Dinarides commenced with Late Permian-Middle Triassic continental rifting related to opening of an early Mesozoic oceanic basin (Dimitrijević and Dimitrijević, 1973; Dimitrijević, 1982, 2001; Robertson and Karamata, 1994; Pamić et al., 1998; Bortolotti et al., 2004). Rifting took place within the Variscan basement of Adria and started with deposition of siliciclastic sediments, restricted marine environment evaporites, and local organic lagoonal mudstones (Hrvatović, 2006). The igneous rocks and related sedimentary rocks indicate that rifting was followed by Early–Mid Triassic rift-related subsidence, accompanied by bimodal magmatism, which ended in the Late Triassic by establishment of the Adriatic-Dinaric carbonate platform and its passive margin. The evidence for rifting within the Dinarides is preserved within Adria, the Budva zone, the Dinaride carbonate platform and the Drina–Ivanjica unit (Hrvatović, 2006). Within the Budva rift zone, volcanics include basaltic pillow lavas, pyroclastic debris and epiclastic sediments (e.g. volcaniclastic sandstones), interbedded with deep-water sedimentary rocks of mainly Mid-Triassic age. Rift features are also preserved in the Bosnian Flysch Unit and in the Dinaride ophiolite belt. Additional rift-related units are preserved within the Dinaride ophiolite belt. These relate to the transition from continental to oceanic crust and are equivalent to the continent–ocean transition zone of the modern oceans (e.g. central North Atlantic; Red Sea/Gulf of Aden). Such settings include marginal rift fault blocks, exhumed continental crust and exhumed mantle lithosphere (Robertson et. al., 2009a).

Three main alternative models have been proposed for Triassic rifting in the Mediterranean region as shown in Figure 2.5. According to Şengör (1984), a Late Palaeozoic Palaeotethyan ocean (Figure 2.5a) subducted southward beneath the North Gondwana margin during Late Palaeozoic-Triassic time, opening several Neo-Tethyan back-arc basins during the Triassic. Karamata (2006) supports this model and implies that rifting took place along the northern margin of Adria during Late Permian–Middle Triassic, including the Budva zone, eventually opening the Dinaride ocean to the north during Late Triassic–Early Jurassic time. This model is supported by the presence of voluminous Triassic calc- alkaline igneous rocks within the Adria, Budva and Dinaride units (Knežević and Cvetković, 2000). However, there is little evidence of a subduction-related magmatic arc along the northern periphery of Adria.

**Figure 2.5:** Alternative tectonic models for Triassic rifting in the Northern Balkan Peninsula (taken from Robertson et al., 2009a).

In an alternative model (Figure 2.5b), Palaeotethys subducted northward during the Triassic, opening a back-arc basin within the northern continental margin of Eurasia (Stampfli and Borel, 2002; Garfunkel, 2004). In this interpretation the Dinaride ocean rifted during the Early–Middle Triassic within the southern margin of Eurasia to form a back-arc marginal basin. Palaeotethys closed regionally by the end of the Triassic, amalgamating Gondwanan and Eurasian continental units while the Dinaride ocean continued to widen. In this model however, the Triassic rift-related igneous rocks do not show evidence of contemporaneous subduction (Robertson et al., 2009a).

In a third model (Figure 2.5c), the northern margin of Gondwana experienced pulsed rifting that culminated in break-up to create several Neo-Tethyan oceanic basins during Early Mesozoic time (Smith et al., 1975; Dercourt et al., 1986, 1993, 2000; Robertson and Dixon, 1984; Robertson et al., 2004). Continental fragments such as Adria, Drina–Ivanjica, Kopaonik and Pelagonia have been interpreted by Karamata (2006) as microcontinents or "terranes" rifted from Gondwana. A possible cause of rifting was slab–pull related to northward subduction of Palaeotethyan ocean beneath Eurasia. The subduction is indicated by evidence from the Pontides of northern Turkey

(Robertson, 2006). However, there is so far, little reported evidence of Permo–Triassic northward subduction beneath the Eurasian margin in former Yugoslavia, although this may be concealed by Cenozoic collision and metamorphism within the Serbo–Macedonian composite unit.

### *2.4.2 Ophiolite genesis and emplacement*

The rifting of Adria was followed by oceanic spreading during the Middle/Late Triassic-Early Jurassic and the opening of the Neo-Tethyan ocean basins. There are two main models for the genesis of ophiolites and their emplacement namely the "multi-ocean" model (Robertson and Karamata, 1994; Dimitrijević, 1997, 2001; Karamata, 2006; Dilek et al., 2008) and the "single-ocean" model (Bernoulli and Laubscher, 1972; Smith and Spray, 1984; Pamić et al. 2002; Gawlick et al., 2008). There is also an on-going debate as to whether (Dimitrijević and Dimitrijević, 1973; Robertson and Karamata, 1994; Karamata et al., 2000; Karamata, 2006) or not (Pamić et al., 1998; 2002; Bortolotti et al., 2005) the Mesozoic Tethyan basin enclosed a discrete microcontinent.

**The "single-ocean" model** in early interpretations implied an existence of a wide ocean opened in the Triassic (Aubouin et al., 1970; Aubouin, 1973) (Figure 2.6A). This single ocean basin closed northwards and sutured by Late Jurassic–Early Cretaceous time, creating the mélange and emplacing ophiolites south-westwards, onto the Adria continental margin. The suture experienced post-collisional shortening during Late Cretaceous–Early Cenozoic time. A comparable model was adopted by several other authors (e.g. Pamić et al., 1998; Pamić et al., 2002). Dimitrijević (2001) proposed an alternative single-ocean model which implies complete closure of the ocean during Late Jurassic time followed by re-opening (Figure 2.6B) to create a new Cretaceous ocean. A new rifting event in the Drina-Ivanjica zone took place during the Late Cretaceous, which led to the opening of the Upper Cretaceous Vardar zone oceanic domain. The Upper Cretaceous Vardar ocean domain is interpreted as a back-arc basin, located at the west of the present Western Vardar zone, at the contact with the Drina-Ivanjica zone.

The third single-oceanic model (Figure 2.6C) favours an intra-oceanic subduction process, which was initiated during the Mid-Jurassic (Stampfli et al., 1998). The mélange of the Dinaride Ophiolite Belt and the Vardar Zone Western Belt were all created within a single subduction zone. New oceanic crust formed within an intra-oceanic marginal basin in a back-arc environment. The trench then collided with the Adria– Dinaride passive margin and the Dinaride and Vardar ophiolites were thrust south-westward over the Drina–Ivanjica, Kopaonik and Jadar unit, interpreted here as parts of the Adria passive continental margin. Oceanic lithosphere of the Main Vardar ocean subducted north-eastward causing Late Cretaceous– Palaeogene arc magmatism.

**The "multi-ocean" model** assumes the existence of more than one oceanic basin, separated by one, or several, microcontinents (Dimitrijević and Dimitrijević, 1973; Robertson and Karamata, 1994; Karamata, 2006). Robertson and Karamata (1994) interpret the Drina-Ivanjica unit as a microcontinent within the Jurassic Tethyan ocean, which they compared with the Korabi zone of

Albania and the Pelagonian zone of Greece. The multiple ocean models are favoured by many authors for Greece and Albania (e.g. Robertson et al., 1991; 1996; Smith, 1993; Dilek et al., 2005; 2008; Smith, 2006). Three main alternative models have been postulated as shown in Figure 2.7.

**Figure 2.6:** Alternative tectonic models for ophiolite genesis and emplacement that involve the opening and closure of a single Mesozoic oceanic basin (taken from Robertson et al., 2009a).

**Figure 2.7:** Alternative tectonic models for ophiolite genesis and emplacement that involve the opening and closure of a several Mesozoic oceanic basins separated by microcontinents (taken from Robertson et al., 2009a).

*The multi-oceans with a Cretaceous marginal basin model* (Figure 2.7A) is supported by Pamić et al., (2002) and assumes that the Drina-Ivanjica microcontinent rifted from Adria.

According to this model, a wide Dinaridic Tethyan basin, characterised by mid-ocean ridge oceanic lithosphere (Pamić et al., 2000; Bortolotti et al., 2004; Saccani et al., 2004) existed between the two continents. Subduction (Figure 2.7 A) started in the Late Jurassic as indicated by ophiolite emplacement accompanied by the generation of an "amphibolite facies metamorphic sole" composed of amphibolites. During emplacement, rocks of the oceanic crust were dismembered and ophiolite fragments included in olistostrome mélange. Late Jurassic subduction initiated gradual closure of the Dinaridic domain of Tethys and the initiation of a magmatic arc characterised by granite plutonism and basalt-rhyolite volcanism. This magmatic arc later split to form a Cretaceous back-arc basin within the Sava–Vardar zone. This back-arc basin probably formed the westernmost part of the huge north Tethyan subduction zone stretching eastwards to Greece, Turkey, Iran and Afghanistan (Pamić et al., 1998; Pamić, 2002). In a later interpretation, Pamić (2002) suggested that the Dinaride ocean closed by the Early Cretaceous, but re-opened above a subduction zone located within the Budva zone, during which time Upper Cretaceous ophiolites formed. Closure of the back-arc was accompanied by calc- alkaline arc magmatism.

Tectonic movements, which took place by the end of the Late Eocene and Early Oligocene, mark the closure of the Dinaridic Tethys. This phase was characterised by: 1) tectonisation of the Dinaride Ophiolite mélange, generation of the Vardar Zone ophiolite mélange and emplacement of a second ophiolite on top of the Dinaride zone ophiolites, obducted during the first Late Jurassic obduction, 2) medium-grade metamorphism of Late Cretaceous-Early Paleogene flysch sequences with emplacement of accompanying igneous rocks, and 3) synkinematic calc-alkaline granitoid plutonism. This final Eocene-aged orogenic phase marks the completion of the Dinaride structural framework.

*The Multi-ocean terrane model* (Figures. 2.7B and 2.8) was proposed by Karamata et al., (2000a; 2003) and Karamata (2006). In this model the Vardar ocean evolved from a pre-existing Main Vardar ocean, which was considered to be an equivalent to Palaeotethys and was subducted beneath the Eurasian continent. A Palaeotethyan Vardar ocean also subducted southward, initiating opening of a Triassic marginal basin along the northern margin of Adria. Drina–Ivanjica and Kopaonik microcontinents rifted from the Adria during Middle and Late Triassic initiating an opening of the Dinaride ocean. This ocean subducted north-eastwards beneath the Drina–Ivanjica microcontinent in the beginning of the Late Triassic, resulting in formation of the Dinaride mélange and south-westward emplacement of the Dinaride ophiolites. The Dinaride ocean was finally closed by Middle–Late Jurassic time. The western branch of the Vardar ocean (the Vardar Zone Western Belt) opened in the Late Triassic. After the closure of the Main Vardar ocean during Middle–Late Jurassic, the Vardar Zone Western Belt remained as a wide ocean between Adria and Eurasia until the Maastrichtian. North-eastward subduction during the Cretaceous triggered formation of the supra-subduction zone oceanic crust (Kozara ophiolite) and initiated Upper Cretaceous–Palaeogene arc volcanism along the southern margin of Eurasia.

In the *third alternative multi-ocean model* (Figure 2.7C), which was proposed by Robertson and Karamata (1994), the Jurassic Dinaride ophiolites formed by supra-subduction spreading above a south-west dipping intra-oceanic subduction zone. The Drina–Ivanjica unit drifted away from Adria, opening the Dinaride ocean basin during Late Triassic–Early Jurassic, which, during the late Early to Mid-Jurassic, subducted to the southwest. The subduction events were associated with accretion and mélange development, as well as with obduction of the Jurassic oceanic crust. The obducted hot oceanic crust metamorphosed the underlying continental margin of the Adria plate, developing the metamorphic soles. The subduction trench collided with the intra-oceanic Drina–Ivanjica microcontinent and the Dinaride ophiolites and sub-continental mantle bodies were thrust north-eastwards onto the Drina–Ivanjica microcontinent. In this interpretation, the ophiolites and mélanges of the Vardar Zone Western Belt are a continuation of the Dinaride Ophiolite Belt (e.g. ultramafic rocks of the southern Kozara Mountains).

**Figure 2.8:** Tectonic sketch map and location of terranes in the former Yugoslavia (after Karamata, 2000). SMTC–Serbomacedonian Composite Terrane; VZWB – Western belt of Vardar Zone; MVZ – Main Vardar zone; KB – Kopaonik block/ridge; JBT – Jadar Block Terrane; DIT – Drina-Ivanjica Terrane; DOBT – Dinaride Ophiolite Belt Terrane; EBDT – East Bosnian-Durmitor Terrane; CBMT – Central Bosnia Mountains Block/Terrane.

In their recent analysis of the Alpine-Carpathian-Dinaridic system, based on a newly compiled tectonic map that includes the entire system, Schmid et al. (2008) proposed a new interpretation which strongly deviates from the view expressed by practically all previous authors who regarded the Drina-Ivanjica Unit as a continental terrane that was originally located between two separate oceanic basins (e.g., Dimitrijević and Dimitrijević 1973; Robertson and Karamata 1994; Dimitrijević 2001; Karamata 2006) or who postulated that this terrane was derived by out-of-sequence thrusting from the European margin (Pamić et al., 1998; Hrvatović and Pamić 2005). Schmid et al. (2008) support the 'single ocean' model and consider the two belts of ophiolites (Dinaride and Vardar Zone Western belt) as relics of the same, formerly coherent ophiolitic sheet that was obducted onto the Adriatic passive margin in the Late Jurassic and was disrupted by Cretaceous to Tertiary thrusting. Thrusting has exposed units derived from the Adriatic margin below the ophiolitic units, in the form of windows, which were interpreted as Drina-Ivanjica, Jadar and Kopaonik microcontinents by earlier authors. According to Schmid et al. (2008), the narrow belt of the East Vardar Zone represents a different geotectonic entity from that of the Dinaride and West Vardar ophiolites located farther west. Schmid et al. (2008) suggest that the East Vardar Zone represents a part of the Carpatho-Balkan Orogen and is structurally separated from the Western Vardar Ophiolitic Unit by the Sava Zone. Therefore, the collective term "Vardar Zone" should not be used any longer.

In summary, insufficient data exist at present to confirm one specific model. Hence the geodynamic setting of the Vardar ophiolites is still a matter of debate, owing to a lack of reliable data on their geochemical affinity.

Convergence between Adria and Eurasia led to a mature continental collision stage during Late Cretaceous - Early Paleogene. During the Tertiary the whole area of the Balkan Peninsula has been affected by extensional tectonics and regional uplift, associated with related extrusive and intrusive magmatic activity (Dilek, 2006). In the Vardar Zone, continental collision was also accompanied by emplacement of calc-alkaline granitoids, mainly of Late Eocene - Early Oligocene age (e.g., Pamić and Balen, 2001). The neotectonic activity during the Quaternary affected the area of the Dinarides and the Vardar zone due to continuous underplating of the Adria plate beneath the Dinarides, which is also still active. This deformation phase formed the NE-SW, NW-SE and NNW-SSE striking faults.

## 2.5 Major mineral deposits in the Dinaride belt

### *2.5.1 Introduction*

The metallogenic evolution of the Dinarides is largely influenced by geotectonic processes operating during the evolution of the Tethyan orogenic belt. The Tethyan orogenic system, which occupies an area of more than 5 million km$^2$, is of similar size to, and broadly coeval with, the Cordilleran orogenic belt of the Americas (Porter, 1998). Tethyan metallogeny is characterised by a spectrum of metal deposits associated with major calc-alkaline magmatism, as well as extensional and metamorphic stages during the evolution of the orogen (Dixon and Pereira, 1974; Janković, 1977; Porter, 1998; Lescuyer, et al., 2003; Canby, 2007; Lips, 2007). The Western Mediterranean branch or the Alpine–Balkan–Carpathian–Dinaride (ABCD) belt is one of Europe's major metallogenic provinces. Broadly, three spatially and temporally distinct tectonic and metallogenic zones can be distinguished within the region. They are associated with Late Cretaceous to Neogene magmatism (Figure 2.9), namely:

1) *The Eastern Zone*, which comprises Late Cretaceous, subduction-related calc-alkaline intrusive and volcanic rocks, also known as the Banat-Timok-Srednoegorie or "Banatitic" metallogenic belt, extends from Romania through Serbia into Bulgaria. This zone hosts significant economically world-class Cu-Au deposits, such as the Moldova Noua Cu porphyry in Romania, Majdenpek, Veliki Krivelj Cu-Au and Bor Cu-Au porphyry (± epithermal) in Serbia, and the Elatsite, Medet and Assarel Cu porphyry and Chelopech Au epithermal deposits in Bulgaria (Janković, 1997; Heinrich and Neubauer, 2002).

**Figure 2.9:** Simplified tectonic map displaying the distribution of major tectonic units and ore deposits in the Alpine-Balkan- Carpathian-Dinaride (ABCD) region (Modified after Forward, 2008).

2) *The Western Zone*, which is characterised by Eocene-Oligocene and Oligocene-Miocene calc-alkaline activity within the Serbo-Macedonian-Rhodopian region and ophiolite belts. It hosts several significant epi- to mesothermal Pb-Zn (Ag, Au) vein and carbonate- replacement deposits in Serbia, Macedonia, Bulgaria and Greece. The Buchim (Macedonia) and Skouries (Greece) porphyry Au-Cu deposits belong to this metallogenic region. Calc-alkaline activity here is mainly related to post-subduction and continent-continent collision (e.g. Harkovska et al. 1998).

3) *The Northern zone* comprises Neogene/Quaternary subduction- related, calc-alkaline to alkaline volcanic chain of the Carpathians. It is one of Europe's major metallogenic provinces, which hosts some important epithermal gold- polymetallic ore deposits such as the Rosia Montana epithermal gold and Rosia Poieni Cu-Au porphyry in Romania.

Unfortunately, a comprehensive review of mineral deposits and their geotectonic setting within the ABCD province is beyond the scope of this study. Most recent information about the tectonic setting of the mineral deposits within this province can be found in the following publications: Blundell et al. (2002; 2005), Heinrich and Neubauer (2002), Eliopoulos et al. (2003), Von Quadt, et al. (2004; 2005; 2007), Jelenković et al. (2008).

### *2.5.2 Mineral deposits within the Dinarides*

The Dinaride belt is characterised by a diversity of mineral deposits, which can be divided, according to their tectonic setting, into four major groups as follows (Janković, 1990; 1997; Karamata and Janković, 2000; Palinkaš et al., 2008):

*1) Late Permian-Triassic intracontinental rifting.* Thermal doming and Pangea break up induced intensive, deep hydrothermal circulation cells. Engagement of brine-derived, heated fluids and leaching of iron from the thick shale sedimentary sequences led to the formation of epigenetic, metasomatic siderite deposits. These demarcate the opening of the Tethys from Eastern, Central and NW Bosnia (Ljubija), in Central Croatia (Trgovska and Petrova Gora Mts.) (Figure 2.10), Rude-Samobor and may be traced to Hungary (Rudabanya), and as siderite and magnesite deposits in Slovakia (Gemerides) and Eastern Alps (Erzberg), (Palinkaš, 2000). They are located within the Internal Dinarides.

The Ljubija Fe carbonate-sulphide-barite ore field is located at the margin of the Mesozoic carbonate platform, within Palaeozoic rocks of the Sana-Una River terrain. Mineralisation is hosted by Middle Carboniferous sediments, represented by clastic (subgreywackes, greywackes, sandstones and shales) and carbonate blocks contained within a shale sequence (Protić, 2003). Fe carbonates occur as stratabound siderite and ankerite replacement in limestones and as siderite-sulphide veins within shales (Strmić et al., 2003). Barite veins with fluorite occur within upper parts of the ore deposit (Palinkaš, 1988; Borojević- Šoštarić, 2004; Strmić-Palinkaš, 2004).

Middle/Late Triassic advanced rifting phase, prior to the opening of the Tethys ocean, is the time of formation of extensive Fe-Mn sedimentary exhalative (SEDEX) deposits within the Internal Dinaride region. The biggest are the hematite-siderite deposits of Vareš and Veovača, Čevljanovići (Mn), situated in Central Bosnia, and Buzim (Mn) in NW Bosnia. At Idrija (Slovenia) (Figure 2.10), and Draževići (Central Bosnia) epigenetic-syngenetic Hg-deposits are also a product of Triassic rifting. Idrija is a typical Hg-SEDEX deposit with a well-developed feeder zone that bears large reserves of epigenetic mineralisation within Carboniferous, Permian and Lower Triassic strata. Acid, explosive, submarine volcanism produced the Kuroko type Pb-Zn deposit Šuplja Stijena in the Internal Dinarides of NW Montenegro (Janković, 1990). Deep seated, low temperature, connate brines within the carbonate platform, driven by pressure of the overlying sediment burden, and expelled into favourable sites, precipitated carbonate-hosted Pb-Zn mineralisation. Good examples are at Olovo (Central Bosnia), St.Jacob (Central Croatia), equivalents of Mežica, Bleiberg, Reibl and other carbonate hosted Pb-Zn deposits within the Southern and Northern Calcareous Alps.

*2) Jurassic intraoceanic rifting - ophiolite complex.* Deposits related to Jurassic ocean formation and formation of ophiolites are scarce in the Dinarides. In the ophiolite zone low-quality podiform chromite deposits are present in lherzolites associated with pyroxenites (Dubostica ore deposit, Central Bosnia). In contrast, chromite deposits are widespread in the Vardar Zone where they are related to harzburgite-dunite ophiolites (Janković, 1990).

**Figure 2.10:** Major mineral deposits in the former Yugoslavia (Modified after Janković, 1990; Hrvatović and Pamić, 2005; Karamata, 2006; Palinkaš et al., 2008).

*3) Subduction-related setting.* Cretaceous-Paleogene subduction related magmatism in the NW Dinarides, characterised by remnants of magmatic arc formation (basalts, rhyolites and minor granite bodies) is devoid of mineralisation. However, subduction-related mineral deposits are well known in the Carpatho-Balkan metallogenic province which hosts major porphyry copper deposits, lesser skarn deposits (iron, locally Pb-Zn), massive Cu sulphide (e.g. Bor) accompanied locally by replacement type Pb-Zn, epithermal gold deposits, associated with calc-alkaline igneous complexes of the Early Tertiary-Late Cretaceous, and Neogene gold/silver and base metals deposits. These types of deposits have not yet been discovered in the Central Dinaride belt.

*4) Tertiary, post-subduction plutonism.* Intrusion of igneous bodies (granodiorites, monzogranites, tonalites) and migmatization formed beryl-containing pegmatite-aplites and W-Mo-Sn-sulphide pneumatolitic greisen in N Bosnia and W Serbia. The post-collisional continent-continent setting includes numerous Pb-Zn, Sb, As, Au-Cu deposits located within the Vardar Zone. These deposits are believed to be associated with volcano-plutonic complexes of calc-alkaline affinity (Janković, 1990). The Oligocene-Neogene volcanism is the major source of hydrothermal lead and zinc (±Sb, or ± Ag, or ±Au) deposits in the Vardar Zone. The Pb-Zn deposits extend from Kosovo (Trepča, Crnac, Belo Brdo and Koporić) through western Serbia (Kiževak, Sastavci, Rudnik and Veliki Majdan), to easternmost Bosnia (Srebrenica) (Figure 2.10). Pb-Zn mineralisation in this study is related to this mineralisation epoch.

The Oligocene-Miocene Serbo-Macedonian-Rhodope magmatic and metallogenic zone of Serbia, Macedonia, Bulgaria and Greece includes numerous volcanic–hosted (Lece) and vein-type (Kratovo) Pb-Zn deposits (Figure 2.10), skarn-type polymetallic deposits (Toranitza, Sasa, and Golema Reka), porphyry Cu-Au-Mo (Bučim and Skouries) mineralisation and epithermal Au deposits (Janković, 1997; Neubauer et al., 2003). Some of these deposits will be investigated during the course of this study.

## 2.6 Brief review of mineral deposits in the Vardar zone and the Kopaonik district

Numerous economically significant deposits of lead-zinc, antimony, bismuth and molybdenum, as well as smaller copper, iron, tin, tungsten and gold deposits are distributed within the NNW-SSE trending Vardar tectonic zone (Janković, 1990; Janković et al., 2003).

Lead and zinc mineral deposits of Serbia and Kosovo (Figure 2.11) are concentrated within several larger metallogenic districts namely Kopaonik, Golija, Šumadija and Srebrenica, with Kopaonik being the most significant. These deposits are believed to be related to Tertiary calc-alkaline magmatic complexes that intruded not only pre-Tertiary rocks of the Vardar Zone, but also those of the Serbo-Macedonian zone (Neubauer et al., 2003). Silver also represents a characteristic commodity of the Vardar Zone. In the Kopaonik region silver production is assessed at more than 4,500 t (Monthel et al., 2002), most of which comes from the Trepča mine. Copper, although occurring extensively in the Vardar Zone does not form economically significant concentrations

(Janković, 1990). However, within individual deposits it reaches economically significant levels such as 0.7% Cu at the Suvo Rudište deposits. According to Janković, et al. (2003) the origin of the copper might be traced to ultramafic rocks, from where it was mobilized by hydrothermal solutions. They observe that all deposits where increased copper concentrations occur in the Vardar zone are located close to serpentinised peridotites (Rudnik, Kremići, Bučim porphyry).

Little is known about the geochemistry of gold and its association with mineralisation in the Vardar Zone and Kopaonik mineral belt, as no exploration or research has been carried out (Janković et al., 2003). Gold is known only locally from exploration for other deposits. According to present knowledge, the deposits within the Kopaonik district are poor in gold (Janković et al., 2003). However, a recently compiled simplified mineral deposit database of Serbia (Monthel et al., 2002) reported that most of the Pb-Zn deposits of the Kopaonik district contain gold (Figure 2.12), but data are sparse. Between 1950 and 1985, Trepča produced 8.7 t of gold, or an average of 250 kg per year. The main deposits reputed to be gold bearing are Belo Brdo, Novo Brdo and Ajvalija (Monthel et al., 2002).

**Figure 2.11:** Important Pb-Zn deposits in Serbia and Kosovo (taken from Monthel et al., 2002).

The Kopaonik metallogenic district (Figure 2.13), hosts several skarn, hydrothermal replacement and vein type Pb-Zn (Ag) deposits (Janković, 1995). The hydrothermal replacement lead-zinc deposits are mainly irregular, but compact, bodies hosted in limestone and siliceous rocks that range from several thousand to several million tons of ore. It is one of the largest Pb-Zn ore districts of Europe, with a metal tonnage produced of nearly 3 Mt lead and 2 Mt zinc. The Trepča deposit, which is a skarn and hydrothermal replacement type deposit, has to date been the largest individual source of lead-zinc ore in Serbia.

The structure of the Kopaonik metallogenic district is dominated by NNW-SSE trending structures (Figures 2.13 and 2.14). Many of the Vardar structures may be reactivated Variscan structures marginal to the Serbo-Macedonian Massif. This tectonic zone, within which the Balkan

**Figure 2.12:** Important Au deposits in Serbia (taken from Monthel et al., 2002).

**Figure 2.13:** Simplified geological map showing more important mineral deposits within the Kopaonik metallogenic belt (Modified after Dimitrijević, 1997; 2001; Karamata, 1995; Sudar and Kovács, 2006).

Pb-Zn-Ag deposits are located (Janković, 1990), is marked by lineaments and fracture zones striking NW-SE. It can be followed approximately 700 km along a strike from Bosnia, through Kosovo and Macedonia into Greece and varies in width from 40 to 60 kilometres.

In the southern part of the Kopaonik metallogenic belt, also known as the Trepča Mineral Belt, three regional zones of mineralisation that extend over 80 km in northern Kosovo can be recognised (Figure 2.14):

- Zone I – includes Artana (Novo Brdo) – Batllave. Zone I follows the boundary between the Kosovo sector of the Serbo-Macedonian Massif, which is marked here by extensive Neogene calc-alkaline volcanics and intrusives, with the Vardar Zone.
- Zone II – extends from the Hajvalija- Kishnica district in the south to Belo Brdo in the north, and includes the Trepča (Stari Trg) mine and numerous other occurrences. Zone II

follows the major fault that marks the eastern margin of the Miocene Priština basin, and its extension to the NNW and the intrusive and volcanic complexes in northern Kosovo.

- Zone III – includes the Crnac mine, and extends along a number of lead-zinc occurrences on the western border of the Vardar Zone, where it is in contact with the Dinaride Drina-Ivanjica structural block.

**Figure 2.14**: The southern Kopaonik metallogenic belt ("Trepča Mineral Belt") consisting of three regional NNW-SSE trending mineralising zones (Modified after UNMIK, 2005).

### *2.6.1 History of mining in the Kopaonik district*

The silver-bearing lead and zinc resources of the Kopaonik metallogenic district have been known from ancient times, judging by numerous medieval workings, old dug pits, mining equipment and tools found in the area. Despite such a long history of mining activity, it is only since 1930 that modern mining was established at Trepča by the British company Seltrust. Since then, Trepča experienced a period of massive growth through the 60's and 70's, employing 20,000 people in nine operating mines. This was followed by an almost catastrophic decline in the 80s and 90s. Today, approximately 2,000 workers are employed as the modernisation of the core mining facilities is completed and production is gradually increasing. Whilst the 80's and 90's were characterised, at least partly, by a lack of exploration, the known deposits are not exhausted. Mineable reserves and measured resources at the five key mines totalled 7.068 million tonnes at 5.46% lead, 5.64% zinc and 116 g/tonne silver. An exploration programme is currently being initiated by UNMIK in terms of underground definition drilling, as well as regional exploration to define new deposits around Trepča. Recent geological work strongly indicates the likelihood of additional ore reserves within the Trepča Mineral Belt, as the mineralisation is structurally and/or fault controlled (UNMIK, 2005). Consequently, the Trepča mineral belt holds a high potential, not only for lead, zinc and silver but also for copper and gold. This will be investigated during the course of this study.

On a wider scale, no modern aerial or ground geophysical exploration has been undertaken anywhere in the Trepča Belt. In addition, no modern geochemical research has been carried out thus far in the area.

### *2.6.2 Belo Brdo mine: exploration and mining history*

The Belo Brdo Mine works an underground lead, zinc and silver deposit located in northern Kosovo. The mine was explored by Trepča Mines Ltd in 1927 and high-grade Pb-Zn-ore was exploited on five levels until 1941. During this period, a total of 183,000 t of ore was produced. By 1990 a main shaft, drifts and production stopes had been established with 13 levels, from the lowest haulage level elevation at 1000 m to the highest at 1425 m above sea level.

From 1972 to 1984 the average production rate approached 100,000 tonnes/year. The highest yearly production was in 1977 when more than 110,000 tonnes were mined. Average mill feed grades for this period were: Pb 4.2% and Zn 3.3%. From 1985-1990, Belo Brdo declined in ore production from approximately 90,000 to 60,000 tonnes per year. The break up of Yugoslavia around 1991 caused a sudden production fall to less than 10,000 tonnes per annum in 1994. A slight increase occurred after this with around 30,000 tonnes annually being mined in 1995/6 but falling again to less than 20,000 tonnes up to closure in 1998. The grade of ore during this time also dropped to an average of Pb 4.0% and Zn 3.5%. The mine was reopened in 2003. Its main access level is an adit some 3 km long from the Kosovo side of the mountain into the ore-zone. A shaft accesses the six mining levels, 50 m vertically apart. Access to the hoist is along an adit from Serbia. Mining is carried out by underhand cut-and-fill methods with open pit quarried aggregate from the Serbian side being used as fill material.

Three main ore bodies namely GI, GII and GIII are of a hydrothermal carbonate-hosted type, with an elongated columnar form that plunges at 25-40° (Miletić and Mladenović, 1995). Additional hydrothermal vein deposits are located within overlying andesite volcanics. The vein extends approximately 400 m along strike, and over 250 m in depth (Figure 2.15).

The mine currently exploits the GII hydrothermal replacement body and the GII/12 vein-type mineralisation. Larger zones are mined by underhand cut-and-fill and the vein is mined by overhand cut-and-fill method. Backfill, sourced from a quarry in Serbia, is emplaced pneumatically.

Over the past 2 years, previous Yugoslav estimates and all available mine and geological data have been extensively revised. Original data conformed to the reserve standards common within former Eastern bloc countries. More recent calculations allow Western standards and currently stand at 1.4 Mt at 5.99% Pb, 5.26% Zn and 86 g/t Ag.

**Figure 2.15:** 3D oblique view of the Belo Brdo ore bodies (UNMIK, 2005).

# CHAPTER 3:

# LOCAL GEOLOGY, PETROGRAPHYAND GEOCHEMISTRY OF IGNEOUS ROCKS IN THE KOPAONIK AREA

## 3.1 Introduction

In this chapter the local geology of the Kopaonik area, including its structural and stratigraphic characteristics, is outlined. The petrologic characteristics of the principal lithologies in the study area are described and the mineral chemical data from primary and secondary mineral phases of the host rocks presented. In addition, major and trace element whole-rock geochemical data for the igneous rocks are discussed. These results can be combined to constrain the geotectonic environment of the parent magma.

Current knowledge of Serbian geology is mainly based on 1:100 000 scale geological maps published by the Geological Survey of Yugoslavia between 1970 and 1973. The geological relationships between the main lithological units described in this chapter draw on the following sources: the 1: 100 000 scale geological map of Novi Pazar (Urosević et al., 1973); the overviews published by Dimitrijević (1997) and the Symposium Committee (1995); and the primary observations made during fieldwork. Petrographic descriptions, mineral chemistry and geochemical interpretation are based on the results of primary investigations carried out in this study.

## 3.2 Sampling and Methods

The Kopaonik district contains a wide range of rock types of variable composition. A total of 81 rock samples were collected during fieldwork carried out in September 2006, May 2007 and August 2008. They were prepared as thin sections, polished thin sections, polished blocks and doubly polished wafers at Kingston University. A list of samples and their localities are provided in Appendix 1, which is saved on a CD-ROM enclosed at the back of this report. For the purpose of *petrographic analysis*, a group of representative rock samples were taken randomly from different lithological units outcropping in the Kopaonik area, including the Belo Brdo and Raška (Karavansalija) ore fields. Additionally, several groups of representative host rock lithologies were collected from the Belo Brdo Pb-Zn (Ag) underground mine and drill cores of the Karavansalija Cu-Au skarn and the Rudnitza Cu-Au porphyry exploration prospects. A total of 45 polished thin sections were studied using Optical Transmitted Light Microscope and Cathodoluminescence (CL) with the aim of (i) characterising the petrology of the host rocks in the study area, (ii) better understanding of the textures of the mineral phases and (iii) defining the secondary alteration mineralogy. Modal proportions of individual mineral phases were visually estimated and wherever possible, identification of preserved primary minerals was determined by means of their optical properties. Representative key samples and those with more complex textures were further analysed using the SEM with an electron microprobe facility at Kingston University to characterise *mineral chemistry and microtextures*. The polished, carbon-coated samples were examined by Zeiss EVO50 Scanning Electron Microscope (SEM) fitted with both energy dispersive X-ray (EDX, Oxford Instruments INCA ENERGY 450) and wavelength dispersive (WDS, Oxford Instruments INCA WAVE 500) detection systems. Natural mineral standards were used for calibration and the following operating conditions were applied: accelerating voltage 20 kV, working distance 8.5mm, beam current 1.5 nA detector process time 4. The information about instrumentation and the mineral chemistry data are presented in Appendix 2.

As the study area is located in the centre of a major mineralised district, most of the collected samples show various degrees of hydrothermal alteration; hence it was difficult to collect suitable fresh host rocks for geochemical investigations. A total of 22 least altered volcanic rocks were *geochemically analysed* for major, trace, and rare earth elements using Inductively Coupled Plasma Mass Spectrometry (ICP-MS) and Inductively Coupled Plasma Atomic Emission Spectroscopy (ICP-AES) techniques. The whole-rock geochemical data as well as the procedures for the preparation of the samples are presented in Appendix 3. All Appendices are provided on a CD-ROM enclosed at the back of the report.

## 3.3 Geological and structural setting

The NNW-SSE trending Kopaonik unit ("Kopaonik block and ridge" unit of Karamata, 1995, 2006) is characterised by both, oceanic and continental rocks. Along its eastern margin, an east dipping Cretaceous/Paleogene suture zone (southern prolongation of the "Sava Zone"), as defined by Schmid et al. (2008), separates the Dinarides in the west from the Carpatho-Balkan orogen that consists of the Serbomacedonian "Massif" tectonically overlain by the Eastern Vardar Ophiolitic Unit (Figure 3.1). The latter unit is covered by Lower Cretaceous unmetamorphic flysch ("Paraflysch", of Dimitrijević and Dimitrijević, 1987; Dimitrijević, 1997). Along the western margin, the present-day tectonic contact with the Drina-Ivanjica unit is steeply dipping with a dextral strike-slip component (Gerzina and Csontos, 2003). This contact marks the ophiolitic "Zvornik suture" (Dimitrijević, 1997) that separates the continental Drina-Ivanjica and Jadar-Kopaonik "block terranes" (Karamata, 2006). According to Schmid et al. (2008), the Drina-Ivanjica and the Jadar-Kopaonik units represent thrust sheets derived from the most distal Adriatic passive margin, now exposed as windows, and the Zvornik "suture" simply represents the north-western continuation of the long belt of Late Cretaceous ("Senonian") flysch, which marks the tectonic boundary between the Drina-Ivanjica and Jadar-Kopaonik thrust sheets (Fig. 3.1). Besides the Kopaonik window, a smaller Paleozoic-Mesozoic complex, referred to as the Studenica slice (Dimitrijević, 1997), crops out in the region (Figure 3.2). The Kopaonik-Studenica Metamorphic

**Figure 3.1:** Regional tectonic map of the Alps, Carpathians, and Dinarides (modified after Schefer et al., 2010; Schmid et al., 2008).

Series are overlain by a Mid- to Late Jurassic ophiolitic mélange that lies beneath the obducted Western Vardar Ophiolitic Unit. These three units are unconformably overlain by Late Cretaceous ("Senonian") flysch that contains large olistoliths, including ophiolitic blocks and reworked metamorphic rocks (Schmid et al., 2008). Tertiary geodynamics of the region is dominated by collision/post-collision tectonics that followed the final closure of the Tethyan domain. Subduction of part of the Tethyan Vardar Ocean occurred during the Late Mesozoic to Early Palaeogene, followed by Eocene collision and Oligocene to Pliocene post-collisional collapse of the Dinarides (Karamata and Krstić, 1996; Karamata et al., 1999). Grubić et al. (1995) and Schmid et al. (2008), suggest that the Kopaonik window represents a late stage antiformal structure (Figure 3.3) that folded the previously obducted Western Vardar Ophiolitic Unit, which is preserved on both sides of this structure (see also Sudar and Kovács, 2006). On the eastern flank of this antiform, which was intruded by an Oligocene granodiorite, Senonian flysch rests unconformably on either the Western Vardar ophiolites or the underlying Triassic continental units of the Kopaonik window. The Senonian flysch is over-thrust by the Eastern Vardar Ophiolitic Unit that was earlier obducted onto the Serbo-Macedonian Massif. This east-dipping thrust fault is regarded by Schmid et al. (2008) as a first order tectonic contact that marks the suture between the Dinarides in a lower-plate position and the Carpatho-Balkan orogen in an upper-plate position. Towards the hanging-wall this Senonian flysch contains olistoliths, as well as abundant detrital material that was eroded from the overriding Eastern Vardar Ophiolitic Unit, thus dating the closure of this flysch basin as Late Senonian (89 to 70.6 Ma) (Schmid et al., 2008).

**Figure 3.2:** Simplified regional geological map of the Kopaonik district (Modified after Dimitrijević, 1997; Karamata, 1995; Schmid et. al, 2008).

**Figure 3.3:** Schematic tectonic cross-section of the Vardar Zone in the northern area of the Kopaonik Mt. (modified after Sudar and Kovacs, 2006). 1 – Oligocene granodiorites; 2 – ultramafic rocks; 3 – Upper Cretaceous deposits of the Kopaonik Block; 4 – Cretaceous paraflysch/flysch: a – Lower Cretaceous paraflysch of the Eastern Kopaonik; b – Upper Cretaceous flysch of the Eastern Kopaonik; 5 – Ophiolitic melange of the Vardar Zone Western Belt; 6 – Ophiolitic melange of the Eastern Kopaonik, slightly metamorphosed; 7 – Triassic and Paleozoic metamorphic rocks; 8 – deposits of the Drina-Ivanjica Terrane (DIE); 9 – metamorphic rocks of the Serbo- Macedonian Composite Terrane (SMCT).

## 3.4 Main lithological units

The study area is characterised by various lithostratigraphical units that range in age from Triassic to Recent (Dimitrijević, 1997). The tectonic nappe pile includes, from bottom to top: aTriassic metamorphic complex; a Jurassic-Cretaceous Ophiolite mélange Unit; a Jurassic Ophiolite Unit; and an Upper Cretaceous Flysch Unit (Figs. 3.3 and 3.4).

**Figure 3.4:** A) Geological map of the Kopaonik district (modified after Urosević, 1970); B) Cross section of the Belo Brdo ore field (note: horizontal scale exaggerated; the cross section based on 1:25 000 geological map).

During the Early Oligocene, the tectonic stack was intruded by the I-type Kopaonik intrusive complex (Dimitrijević, 2001; Zelić et al., 2010a). Very few data on the continental units of the Kopaonik area are available (Schefer et al., 2010a; Zelić, et al., 2010), whilst the oceanic units of the Dinarides in general have attracted more interest since the beginning of the 21st Century. Several papers presenting new data and interpretations of the ophiolites and related units of the Balkan Peninsula, with particular emphasis on former Yugoslavia, have been published in a special issue of LITHOS (Robertson et al., 2009), following an international field workshop: "Mesozoic Ophiolite Belts of the Northern Part of the Balkan Peninsula, Serbia and Montenegro – Bosnia and Herzegovina" held out in 2006. Despite the recent increased interest in the geology of Serbia and Kosovo, the Kopaonik area still remains underexplored.

### *3.4.1 Triassic Kopaonik Metamorphic Complex*

The oldest rocks outcropping in the study area belong to the "Kopaonik Metamorphic Complex", which stratigraphically rests on the Paleozoic schists (Schmid et al., 2008). Early studies dealt principally with rock description and petrography and resulted in the recognition of several "series" known under different names, such as: the "Suvo Rudište Formation" (Wilson, 1933) or "Central Kopaonik Series" (Urosević et al., 1970, 1973) in the north; the "Metamorphic Trepča Series" or "Stari Trg Series" (Brammall, 1930) in the south; the "Rogozna and Golija" (Urosević, 1970; 1973) and "Studenica"(Simić, 1956) in the west, the "Footwall Series" at Belo Brdo mine (Kandić, 1987). More recent studies aimed at interpreting the geotectonic environment include the works of Grubić (1995) and Grubić et al. (1995) who considered these series as the equivalents of the Alpine "schistes lustres" formed in deep-water environment. On the contrary, Karamata et al. (2000) consider these series as deposits of the continental slope at the margin of the Vardar Ocean.

The Kopaonik Metamorphic Complex, previously considered as Paleozoic is, according to Mićić et al. (1972) and Sudar (1986), of Middle and Late Triassic age. The recognised conodont fauna from meta-limestones (Sudar, 1986) more precisely confirmed Carnian (228-216.5 Ma) and Norian (216.5-203.6 Ma) ages. The metamorphic sequence has a maximum thickness of ~ 400 m and is composed of sericite-chlorite, chlorite-epidote-actinolite schists; metasandstones; greenschist-facies metabasalts; and thin-bedded crystalline limestones (Figure 3.5). The Triassic metasediments are present in almost all the underground Pb-Zn mines within the Kopaonik metallogenic district (Belo Brdo, Stari Trg, Ajvalija - Kišnica, Novo Brdo, Radanj, Suvo Rudište and Rogozna). The lower part of the stratigraphic column is represented by sericite-chlorite schists and chlorite-epidote-actinolite schists, which are overlain by the organic-rich limestones (Figure 3.5) of Middle Triassic age (Robertson et al., 2009a). The upper part of the column is characterised by the Upper Triassic metasedimentary and metabasic rocks, which are folded together with the metasediments into a 200 m thick succession (Zelić et al., 2005; 2010). Although the relationships between the metabasic rocks and the metasedimentary rocks are still unclear, this succession has been interpreted as a single rifting-related Triassic volcano-sedimentary formation by Dimitrijević (2001).

The interpretation is based on the recognition of the same deformation and metamorphic features in both metabasic and metasedimentary rocks. According to recent studies carried out by Zelić et al., (2005), these rocks show a complex deformation history that includes two phases developed under upper greenschist- upper amphibolite P-T conditions followed by subsequent two phases characterised by very-low grade metamorphism. The geochemical affinity of the igneous protoliths indicates that basaltic magmas were generated at continental arc settings (Zelić, et al., 2005). At the contact with the Oligocene granodiorite, the metabasic rocks of the Kopaonik Metamorphic Complex are metamorphosed to hornfels and the limestones to spectacular skarns and marbles (Figure 3.5).

**Figure 3.5:** Field occurrence of the Triassic metamorphic rocks. A) Very dark, almost black, thin to medium-bedded limestones with sporadic bedding-parallel calcite veins; B) Folding developed in interbedded metapelites and dark grey cherty meta-limestones; C) light- to medium grey thin bedded crystalline limestones with interlayers of creamy-yellow pelitic-psammitic rocks; D) Formation of Iron skarns and marbles at the contact of Oligocene granodiorite and Upper Triassic limestones.

Metasedimentary rocks consist of grey, thin-bedded crystalline limestones, metapelites and meta-sandstones (Figure 3.5). The meta-carbonates are composed of alternating 30– 180 cm thick, white to grey, fine-grained marble layers and 10–140 cm thick, white to yellowish meta-dolostone layers. Fine-grained impure marbles with minor quartz are also present (Figure 3.6).

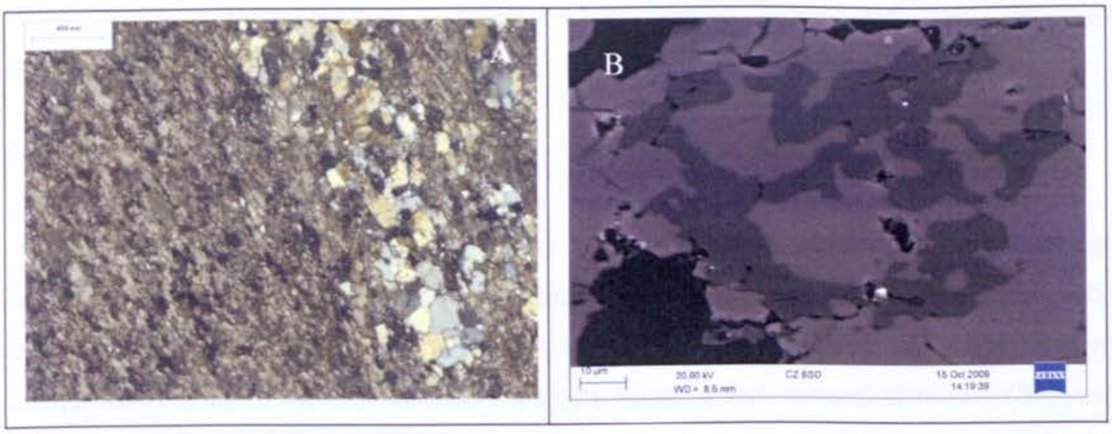

**Figure 3.6**: Photomicrograph (A) and BSE image (B) of the Upper Triassic meta-limestones. A) Meta-limestones with well developed foliation and parallel meta-arenite lamination (sample Z-3); B) Silicified fine-grained meta-limestones from Belo Brdo mine (sample Zap-1). (scale = 100 microns).

The Triassic meta-limestones represent one of the host rocks to the Pb-Zn mineralisation in the Belo Brdo deposit. Triassic lithologies are overlain by the Jurassic Ophiolite mélange on both flanks of the Kopaonik unit.

### *3.4.2 Jurassic-Cretaceous Ophiolite Mélange Unit*

Ophiolite mélanges, often referred in the literature as the "diabase-chert formation", occur throughout the western Vardar Ophiolite Belt. In the Kopaonik area, the Ophiolite Mélange Unit consists of large olistoliths including Triassic limestones, greenschists and metabasalts as well as sedimentary rocks represented by sandstones, mudstones, breccia and conglomerates (Figure 3.7).

**Figure 3.7** Field occurrence of ophiolite mélange: A) An olistostrome containing a large block of interbedded mudstones and sandstones in sharp contact with metre-thick beds of green and red cherts; B) a block of breccia containing fragments of carbonates, chert and basalts.

Chert is sporadic through the formation. This unit also contains dismembered ophiolitic rocks such as basalts, gabbros, radiolarites and ultramafic rocks (Dimitrijević and Dimitrijević, 1973; Dimitrijević, 1995; Karamata and Krstić, 1996; Zelić et al., 2010). The ophiolitic mélange commonly has a quartz- and mica-rich shaly matrix. Palynomorphs from the shaly matrix and radiolarians from siliceous clasts have yielded Late Triassic, Jurassic and Early Cretaceous ages (Vishnevskaya et al., 2006).

### 3.4.3 Jurassic Ophiolite Unit

The Kopaonik district contains a wide variety of dismembered ophiolitic rocks such as serpentinised ultrabasic rocks, known as the Ibar Massif, gabbros and basalts. Peridotites within the main mapped area of the Kopaonik district are characterised by depleted harzburgites and are interpreted as being of supra-subduction zone type based on their mineral chemistry (Bazylev et al., 2009). Most of the ultramafic rocks in the study area have experienced severe serpentinisation. The serpentinite in the vicinity of Belo Brdo is strongly brecciated and tectonised. The relationship between the serpentinites and the younger mélange unit is of tectonic origin with the ultramafic bodies thrust onto an ophiolite olistostrome mélange (Dimitrijević, M. 1995). The contact between dismembered gabbros and mélange is also sharp, probably due to the sliding of gabbro blocks into the olistostrome. Basalts are developed as pillow lavas with small pillows up to 0.5 m in size. The obduction of ophiolites was followed by the metamorphism of underlying olistostrome mélange under amphibolite facies due to still hot ultramafic body emplacement.

The age of the ophiolitic ultramafic and mafic rocks within the Western Vardar Ophiolitic Unit is Middle to early Late Jurassic (163–148 Ma), based on radiometric age determinations (Spray et al., 1984; Bazylev et al., 2006).

In Belo Brdo deposit, serpentinites are hydrothermally altered to listwanites and represent an important host rock to the "GII" carbonate-replacement ore body (see Chapter 4).

#### 3.4.3.1 Petrography of the peridotites

Petrographic observations of several peridotite samples identified harzburgite as the main rock type (Figure 3.8). Generally, all samples display similar textures and mineral assemblages containing olivine (70-90%), orthopyroxene (10-30%), Cr-spinel (up to 2%) and in one sample clinopyroxene (up to 5%). According to the classification of Streckeisen (1973) of plutonic ultramafic rocks, most samples from our study classify as harzburgites and one as clinopyroxene-bearing harzburgite.

All the samples show various degrees of serpentinisation ranging from partial, in which 50% of primary minerals have been replaced by serpentine minerals (Figure 3.8A and B) to severe, in which hardly any primary minerals are preserved (Figure 3.8C- F). In the case of severe serpentinisation, the primary phases were reconstructed by means of identifying the following microtextures: mesh-textured serpentine (Figure 3.8A and C-F), pseudomorphing primary olivine; bastite pseudomorphs of primary orthopyroxene (Figure 3.8B); tremolite-actinolite clusters, replacing primary clinopyroxene (Figure 3.8E); and magnetite developed at the rims of primary

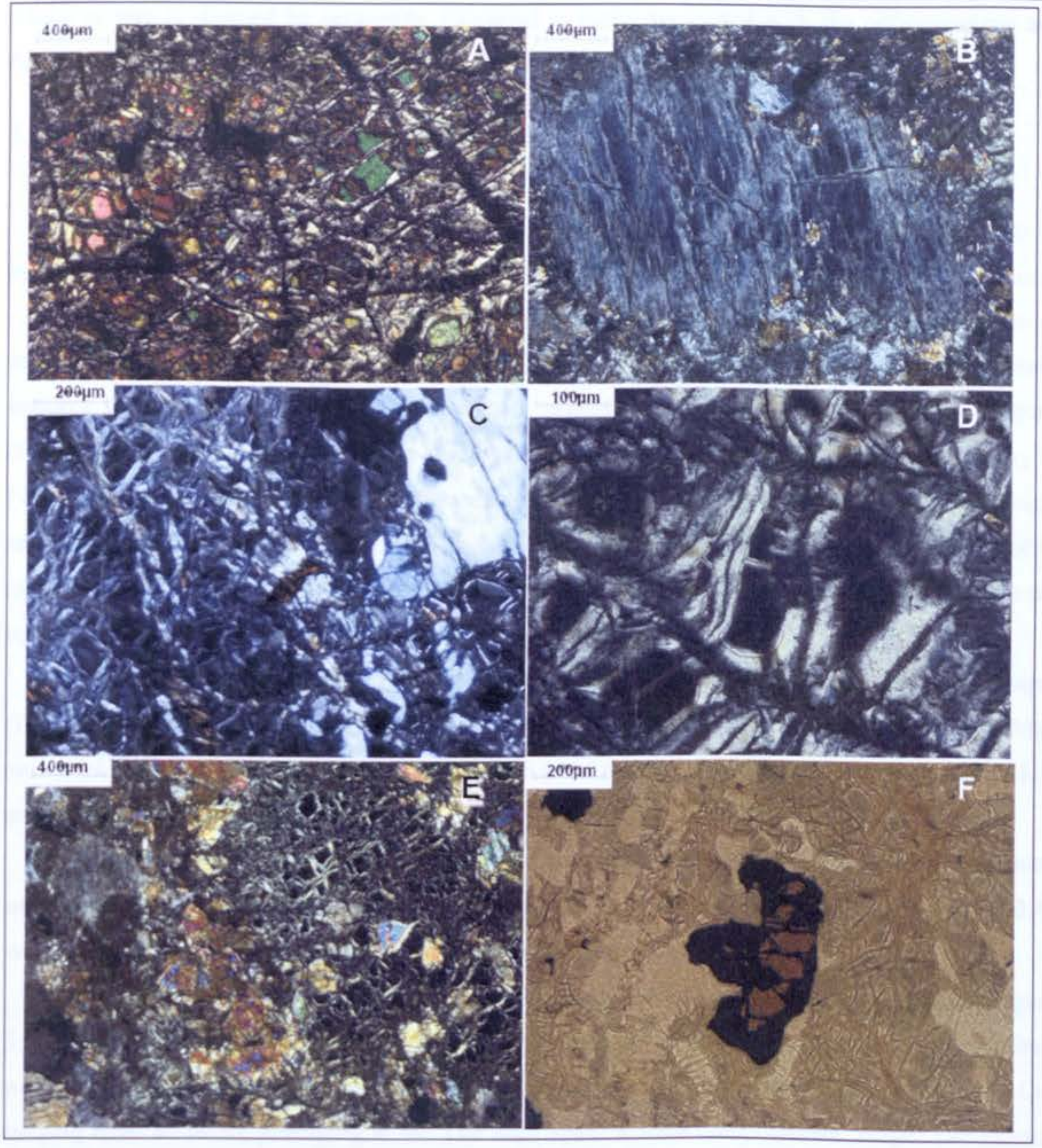

**Figure 3.8**: Photomicrographs of serpentinised peridotites in cross-polarized light (A-E) and plain-polarised light (F) showing main mineral phases and textures of harzburgites. A) Mesh texture of serpentine with relict olivine crystals (sample P-4); B) Kinked orthopyroxene porphyroclast pseudomorphed by bastite (sample 1000/1); C) Mesh texture of serpentine completely replacing olivine (sample SRP-1); D) Hourglass texture (sample P-4); E) Tremolite-actinolite replacement of clinopyroxene in olivine matrix (sample 1000/1); F) Holly-leaf crystal of spinel associated with anhedral to interstitial orthopyroxene crystals in serpentinised olivine matrix (sample SRP-1).

Cr-spinels (Figure 3.8F). The microtextures of serpentinised harzburgite are represented mainly by pseudomorphic mesh and hourglass textures, whilst the coarse-grained textured rocks (Nicolas and Poirier, 1976; Mercier, 1985) can contain orthopyroxene porphyroclasts that exceed 1 cm in size. Orthopyroxene crystals are also found recrystallised in polygonal grains (< 0.5 mm). They are commonly altered to bastite (Figure 3.8B) and locally to tremolite-actinolite. In these rocks, spinel is generally reddish-brown and forms holly-leaf crystals, whose rims grade to magnetite. Some Cr-spinel grains exhibit a zonation in which euhedral Cr-spinel core is rimmed by ferritchromite, which in turn is rimmed by magnetite. Cr-spinel is rarely associated with the orthopyroxene and forms isolated crystals within the olivine matrix (Figure 3.8F).

### *3.4.3.2 Mineral chemistry of the peridotites*

Mineral chemistry studies were conducted on four peridotite samples. The compositions of primary olivine, pyroxenes, as well as spinels and amphiboles are listed in Table 3.1 in Appendix 2.

Primary *olivine* compositions were obtained from only two samples, in which the degree of serpentinisation was less than that of the rest of the samples. The abundant serpentine mesh textures suggest that olivine was the dominant primary igneous phase in all the thin sections (Figure 3.8). Their compositions are quite uniform and forsterite content ranges from $Fo_{89.5}$ to $Fo_{90.4}$, except for one crystal which shows $Fo_{93.4}$ (Figure 3.9A). Variation in Fo within a single sample is typically less than ±0.5%. Olivine has rather uniform Mg# (Mg x 100/[Mg + $Fe^{2+}$] mol%) of 89.5–90.3. and one value of 94 which relates to the highest Fo content. Their NiO contents are up to 0.57 wt% (Figure 3.9A).

The *orthopyroxene* (enstatite) compositions ($En_{89}$) were obtained from only one fresh sample (Figure 3.9B) representing clinopyroxene-bearing harzburgite. They are characterised by high Mg# values (92 to 93) and relatively low CaO content (<0.81 wt%). The $Al_2O_3$ contents are rather low and range from 2.7–4.6 wt.%.

The *clinopyroxene* (diopside) (Figure 3.9B) compositions were determined from the same sample as orthopyroxenes and they are characterised by low $Na_2O$ (< 1 wt %) and $TiO_2$ (<0.46 wt.% ) as well as low $Cr_2O_3$ contents. Their Mg# values are between 92 and 96.

*Cr-Spinel* is present in all the samples and is characterised by variable compositions (Figure 3.9C). Cr# of spinels (Cr x100/[Cr + Al] mol%) are high in weakly mineralised host serpentinites, where spinels are commonly transferred to magnetite. Non-mineralised serpentinites have Cr# ranging from 47 to 80, averaging at 60. The Mg# spans a wide compositional range. The Fe-rich spinels in mineralised samples have low Mg# (<20), whilst non-mineralised samples are characterised by more Mg-rich spinels, having Mg# of 55-78. Compared with the spinel cores, the spinel rims were enriched in Fe but were deficient in Al, Mg and Cr. Concentrations of $TiO_2$ do not exceed 1wt%. $Al_2O_3$ contents of all analysed Cr-spinels are low and do not exceed 17%. Magmatic amphiboles have not been observed in analysed harzburgites. Amphiboles have been determined from one sample from Belo Brdo mine where they replace clinopyroxene. They are calcic (Leake et al., 1997), with compositions corresponding to tremolite (Figure 3.9C).

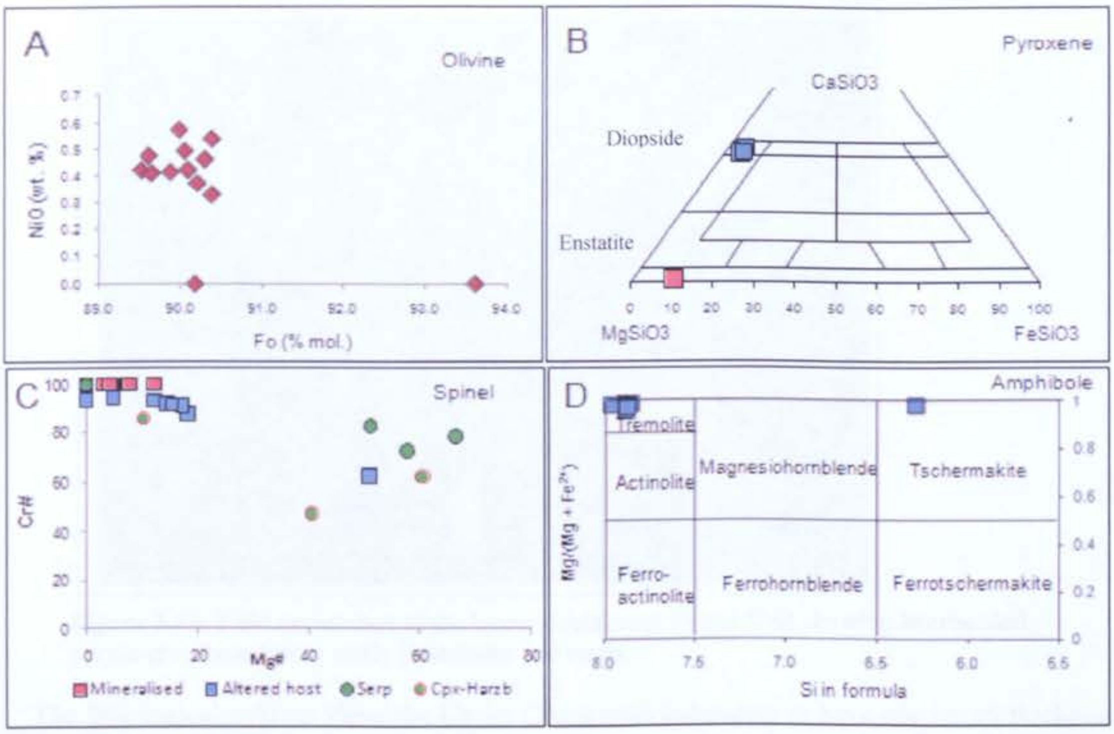

**Figure 3.9:** Mineral chemistry of olivine, pyroxene, spinel and amphibole in harzburgites. A) Chemical analysis of forsterite in olivine (n=13); B) Chemical composition of pyroxenes (n= 14); red=orthopyroxene, blue=clinopyroxene; C) Variation diagram Mg# (Mg/(Mg + $Fe^{2+}$) - Cr# (Cr/(Cr + Al) of Cr-spinels (n= 26); (D) Chemistry of amphiboles (n=12; classification after Leake et al., 1997).

### *3.4.4 Upper Cretaceous Flysch Unit*

The Upper Cretaceous sedimentary cover is post-tectonic and post-metamorphic with respect to the Late Jurassic to earliest Cretaceous obduction of the Western Vardar Ophiolitic Unit and to Early to mid-Cretaceous deformations. Above a major unconformity, Cenomanian to Maastrichtian sediments commence with shallow water clastic rocks, including conglomerates and rudist limestones, which grade upward into marly limestones and a thick pile of sandstone turbidites ("Kosovska Mitrovica Flysch"; Dimitrijević and Dimitrijević, 1987) (Figure 3.10).

These series unconformably cover, from west to east, Paleozoic to Mesozoic strata of the Drina-Ivanjica thrust sheet, ultramafic rocks and mélange of the Western Vardar Ophiolitic Unit, as well as the Triassic Kopaonik Metamorphic Complex.

Massive reef limestones occur in the vicinity of the Belo Brdo mine and on Vojetin Hill, where they are transgressive over Triassic metamorphic rocks. Brecciated at the base, the limestones grade upward into white limestones and, locally, marbles. The fossil content indicated a Senonian age for all Cretaceous sedimentary rocks (Kandić, 1987).The clastic rocks consist of conglomerates and conglomerate breccia at the base of the Upper Cretaceous.

**Figure 3.10:** Field occurrence of the Upper Cretaceous Flysch Unit showing interbedded purple-grey limestones, marly limestones and marls.

The lithological column show the Upper Cretaceous sediments to have maximum thickness of 350 m . The Upper Cretaceous in the Kopaonik district is clearly stratigraphically and lithologically defined. The Upper Cretaceous age (*Hippurites felixi, Cunolites profundus and of. discoidens, Pachygiraorbigvi, Rhynchonella diformis and Alectryonis anguleta*) in the basal part is related to the Coniacian (89.3-85.8 Ma). The Senonian age is confirmed by rudistic fauna of the hippurites species (*Hippurites-Orbignya-nabresiensis, gosavinesis, giganteus, oppeli, sulcatus* etc.) in reef limestones of central Kopaonik. In the higher levels, the Senonian age is substantiated by numerous *Globotruncana* species (*Stuarti, Arca, Fornicata, Contusa*) in marly limestones, and in flysch sediments by *Lapparenti* forms (*Lapparenti, Ttricarinata, Stuarti, Arca* etc.) (Sladić-Trifunović, 1995).

### 3.4.5 Tertiary Igneous Rocks

Tertiary igneous activity in Europe is recognised in a continuous belt that extends from the eastern Alps in the north of the study area, extending across the southern Pannonian Basin (Slovenia and Croatia) and the Dinarides (Serbia, Macedonia) into the Rhodope-Thrace region (Bulgaria and Greece) to the south of the Kopaonik district ( Pamić et al., 1995; 2002a; Christofides et al., 1998; 2001; Harkovska et al., 1998; Marchev et al., 1998; Yilmaz and Polat 1998; Jovanović et al., 2001; Prelević et al., 2001; Cvetković, 2002; Cvetković et al., 2004; 2007). This igneous belt comprises Eocene to Oligocene granitoid bodies, Oligocene to Miocene shoshonites, high-K calc-alkaline volcanic rocks and ultrapotassic rocks (lamproites and leucitites) (Harangi et al., 2006 and therein). Within the Kopaonik district, which forms an integral part of this Tertiary belt, igneous activity produced voluminous volcanic and plutonic rocks (Figure 3.11).

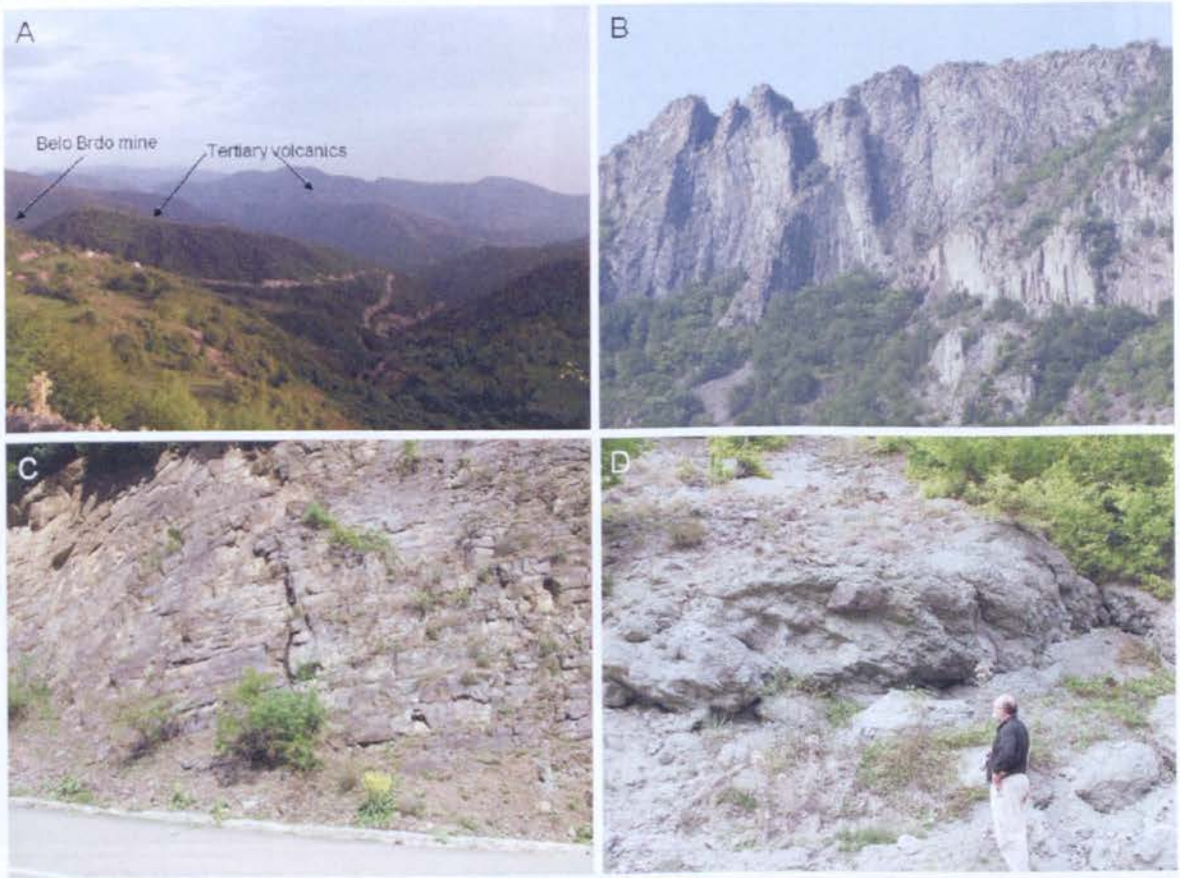

**Figure 3.11:** Field occurrences of the first phase volcanics. A) panoramic view looking SW to the Belo Brdo mine; B) Columnar jointed andesitic lavas; C) stratified andesitic lavas; D) andesitic pyroclastic deposits.

Earlier investigations of Tertiary igneous rocks in this area dealt mainly with petrography (Dimitrijević and Dragić, 1957; Stefanović and Pavlović, 1960; Mićić, 1980) and age determination of the Kopaonik granodiorite (Karamata et al., 1992). Very little geochemical work has been carried out until now (Zelić, et al., 2010).

At least three phases of volcano-intrusive activity have been recognized by Mićić (1980). The first two phases are volcanic in character, whilst the youngest, third phase is represented by granodioritic plutonism.

The first volcanic phase is characterised by andesites and occasional occurrence of dacites. They occupy the lower level of the volcano-intrusive complex. The volcanics of this phase occur mainly as lava flows and thick volcaniclastic deposits, whilst dykes are rare (Figure 3.11). Thick flows often consist of massive interiors with columnar jointing. Andesites vary from a dark grey colour to medium grey and grey-green colour, whilst dacites appear light to medium gray on fresh surfaces (Figure 3.12). The magmatic rocks of the Kopaonik district are deeply eroded, so their true extent and thickness is difficult to reconstruct. Thus far, the maximum thickness of the rocks belonging to the first volcanic phase has been reported to be up to 300 m (Urosević et al., 1973).

**Figure 3.12:** Hand specimens (A and C), field occurrence (B) and drill core close-up (D) of the rocks from the first volcanic phase. A) Fine grained- almost aphanitic andesite; B) In situ dacitic dyke with centimetre-sized feldspars - xenocrysts; C) Plagioclase- and hornblende-phyric trachytic-textured andesite; D) Dacite porphyry.

The second volcanic phase, which makes up the upper part of the volcanic complex, is dominated by latites and quartz latites and most of the mineralisation in the study area is related to the rocks of this volcanic phase. It includes large bodies of lava and volcaniclastic deposits along the Ibar Valley, on Rogozna Mountain (Karavansalija area) and around Trepca to the south east (Figure 3.13). The quartz latites also occur as steeply-deeping dykes discordant to stratigraphy (Figure 3.13A) and commonly intrude fault zones (Figure 3.13B). Within the Karavansalija prospect, ENE-WSW trending latite and quartz latite dyke swarms occur perpendicularly to the regional NNW structural fabric of the Western Vardar Ophiolite Zone. The samples from drill cores are medium grained plagioclase- hornblende-phyric rocks, light grey to medium grey in colour and lack trachytic textures found in lavas (Figure 3.13D and E). They can be best described as latite and quartz latite porphyries.

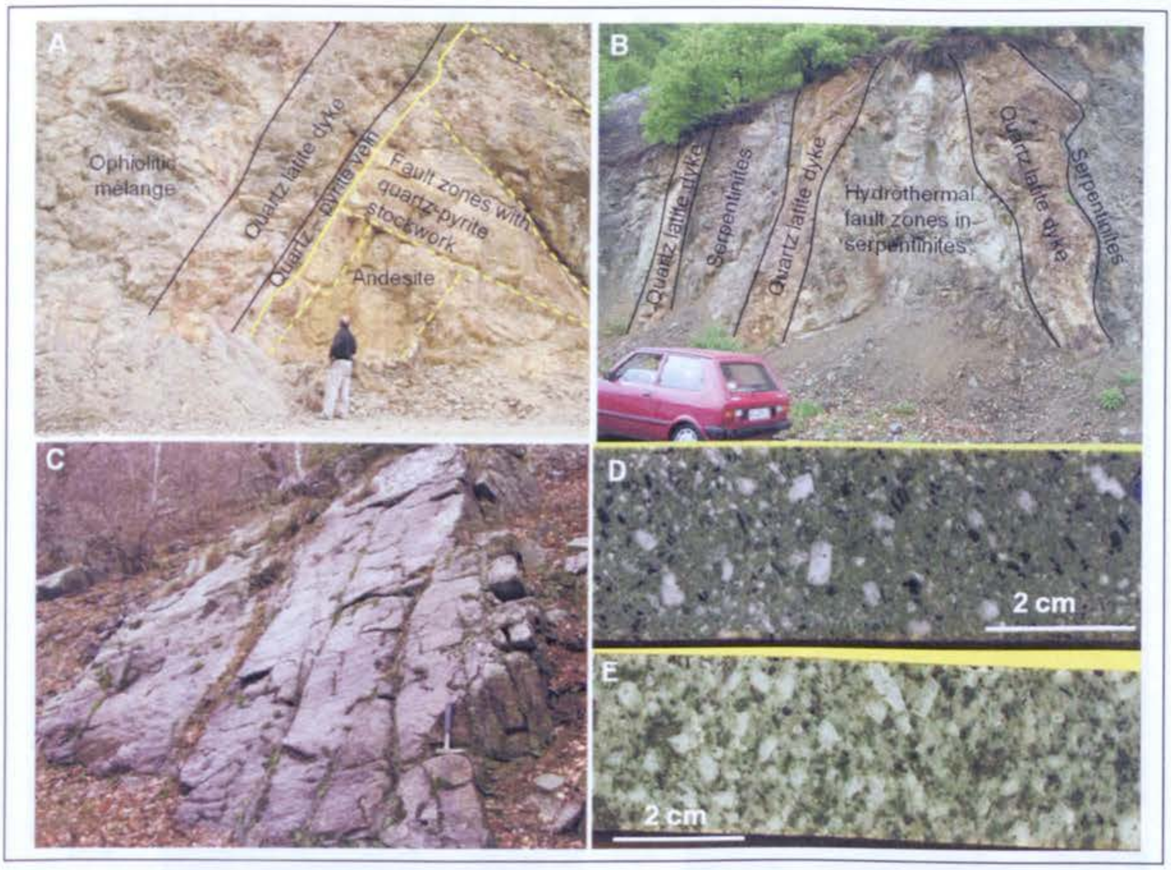

**Figure 3.13:** Field occurrences (A-C) and drill core close-ups (D and E) of the rocks of the second volcanic phase. A) Quartz latite dyke and pyrite stockwork; B) quartz latite dykes intruding serpentinites; C) q-latite dyke Karavansalija K8; D) Close-up of a drill core (sample KU27) showing coarse-grained plagioclase and hornblende- phyric latite porphyry; E) Coarse- grained phenocryst-rich quartz latite porphyry (sample KU17).

## 3.5 Petrography of the Tertiary Igneous Rocks

### *3.5.1 The first volcanic phase*

Petrographic observations of the rocks of the first volcanic phase identified the following rock types: amphibole-, amphibole-biotite-, amphibole-pyroxene andesites and amphibole-biotite dacites. *Andesites* (Figures. 3.14A-F and 3.15A-D) are holocrystalline and display porphyritic textures, which range from moderately porphyritic (15–20% phenocrysts) (Figure 3.14A) to phenocryst-rich (30-40% phenocrysts) (Figure 3.14B). The phenocrysts consist of plagioclase, amphibole, biotite and rare clinopyroxene. Fine- to medium-coarse grained euhedral plagioclase (0.05-2 mm) is the most abundant phenocryst phase in all samples (40-50 % modal abundance) and occurs as both seriate textured (Figure 3.14B) to more evenly sized phenocryst populations (Figure 3.15 C). Additionally, plagioclase phenocrysts exhibit concentric oscillatory zoning (Figures.3.14C and D) and several disequilibrium textures including sieve textured bands (Figure3.14E), resorption (Figure 3.14F) and corroded cores (Figures. 3.14B, G and H) that are partially replaced by clay

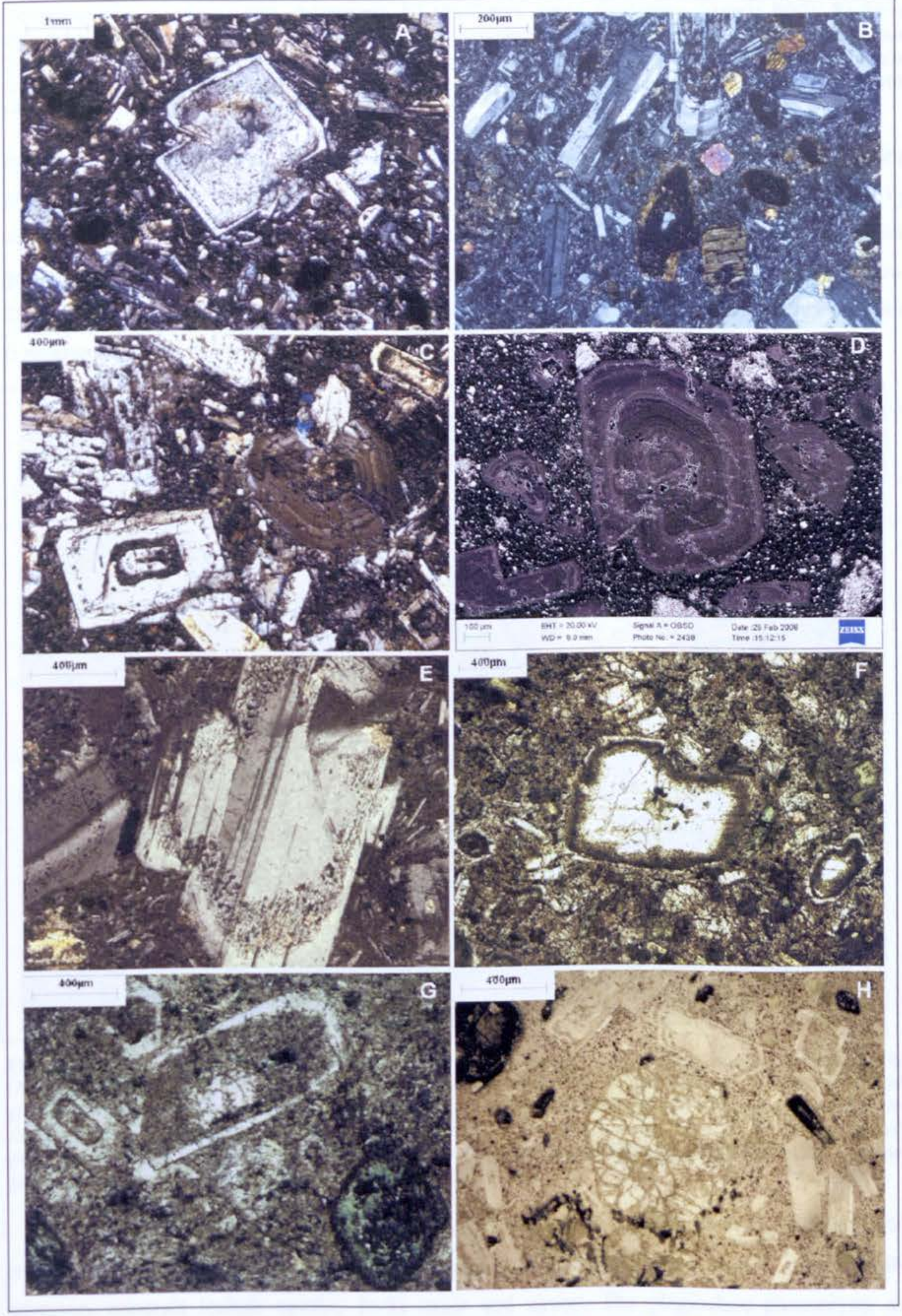

**Figure 3.14:** Photomicrographs of andesites taken under crossed polarised transmitted light (A-C and E); plane polarised transmitted light (F-H) and BSE image showing normal and disequilibrium textures of andesites. A) Moderately rich porphyritic andesite showing sieve textured core plagioclase phenocryst with unaltered rim (sample BB3); B) Amphibole-biotite andesite showing typical phenocryst-rich porphyritic texture; note some plagioclase phenocrysts are corroded (sample BB2); C) Phenocryst-rich andesite with complex oscillatory zoned plagioclase (sample BB3-1); note boxy-cellular and corroded plagioclase

(*continued from previous page*) phenocrysts; D) Oscillatory zoned plagioclase (sample BB2); E) Sieve textured plagioclase in a microcrystalline groundmass (sample BB2); F) Resorbed phenocrysts of plagioclase (sample T3); G) Sieve-textured and corroded phenocryst of plagioclase in altered amphibole-biotite andesite (sample 1235/1); H) Clinopyroxene- bearing andesite consisting of two populations of plagioclase, one with sieved cores and the other fairly fresh (sample BB2).

minerals. Hornblende and plagioclase phenocrysts often cluster in aggregates forming glomeroporphyritic textures (Figure 3.15A, B). Medium- grained rounded amygdales filled by secondary minerals (quartz or calcite) are present in small modal proportions. The microcrystalline groundmass consists mainly of plagioclase, sporadic anhedral alkali feldspar, rare augite and iron-titanium oxides. Plagioclase occurs as groundmass microlites or laths, which sometimes exhibit flow-aligned (trachytic) textures. The accessory minerals are apatite, zircon, and Ti-magnetite.

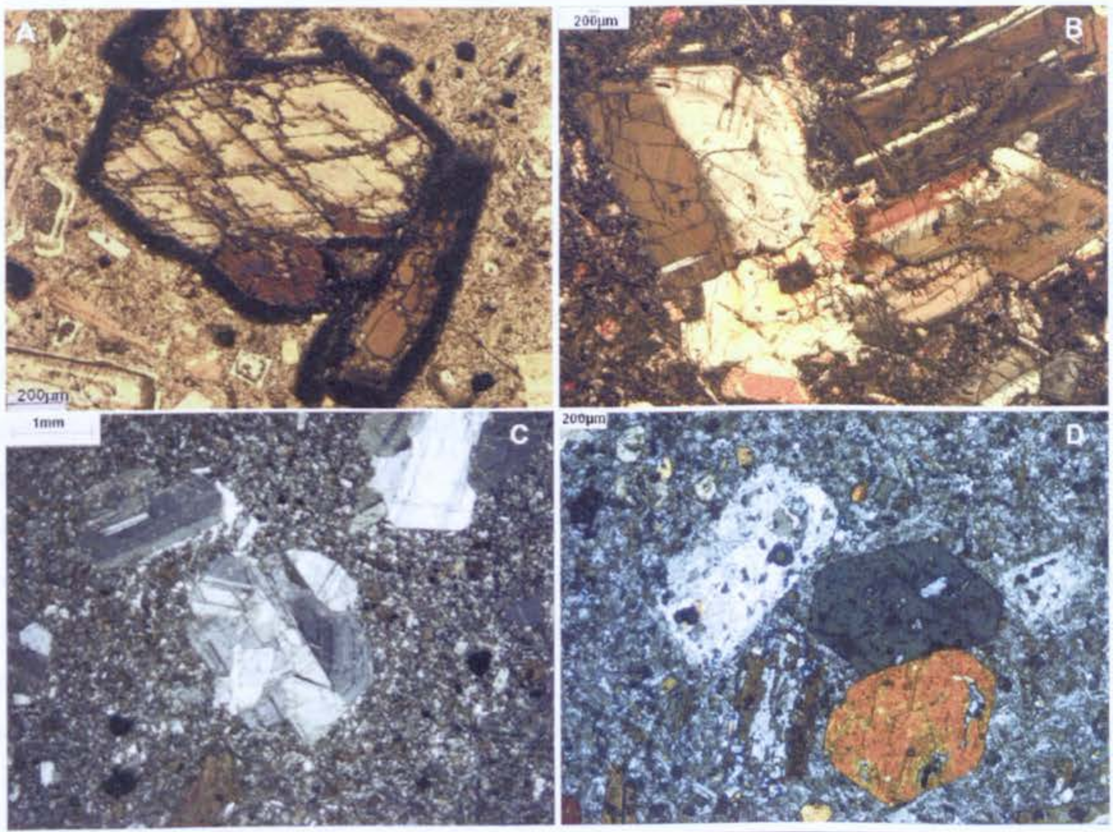

**Figure 3.15:** Photomicrographs of andesites (A and B) and dacites (C and D) showing glomeroporphyritic (A-C) and poikilitic (D) textures taken under crossed polarised transmitted light. A) Brown hornblende glomerocrysts showing dehydration reaction rims (Fe-Ti oxide) (sample BB2); B) Large glomeroporphyritic cluster of plagioclase crystals within the fine grained groundmass (sample T3); C) Biotite-dacite with glomeroporphyritic texture (sample Kop-1); D) Porphyritic amphibole-biotite dacites in fine-grained groundmass; note poikilitic texture of plagioclase (sample KU45).

*Dacites* are holocrystalline with glomeroporphyritic and porphyritic textures (Figure 3.15C and D). The phenocrysts are composed of plagioclase, hornblende, biotite and quartz, whilst accessory minerals include apatite, Fe-Ti oxide and zircon. The plagioclase phenocrysts are typically zoned and show euhedral to subhedral shapes (up to 1 cm in diameter), sometimes poikilitic (Figure 3.15D). Microcrystalline to cryptocrystalline groundmass is composed of plagioclase, some alkali feldspar, rare clinopyroxene, quartz, opaque minerals and apatite.

### 3.5.2 The second volcanic phase

Latites and quartz latites (Figure 3.16) are the predominant rock types of this volcanic phase. They are generally coarser grained relative to the rocks of the first volcanic phase. They may contain plagioclase and alkali feldspar megacrysts of up to three centimetres in diameter.

*Latites* are porphyritic (Figure 3.16A), rarely trachytic (Figure 3.16B) with hypocrystalline groundmass. They are composed of phenocrysts of medium- to coarse- grained euhedral plagioclase, amphibole, biotite, rare clinopyroxene and alkali feldspar, set in a groundmass of subhedral alkali feldspar, quartz, biotite, clinopyroxene and amphibole. Accessory minerals include apatite, zircon, sphene and opaque minerals.

*Quartz latites* (Figure 3.16C-F) are represented by biotite and biotite-amphibole varieties. They are characterised by holo- to hypocrystalline, rarely glassy groundmass and porphyritic (Figure 3.16C and D) to trachytic textures (Figure 3.16E and F). The phenocrysts are made up of plagioclase, sanidine and quartz with variable proportions of amphibole, biotite and clinopyroxene. Plagioclase is the main phenocryst in most samples and occurs as euhedral to subhedral grains, often zoned and as rare glomerocrysts. In some instances plagioclase appears as xenocrysts, indicating disequilibrium with the host rock (Figure 3.17A). Sanidine occurs as coarse euhedral elongate grains with simple Carlsbad twinning (Figure 3.16E and F). Quartz phenocrysts are sparsely scattered through the rock. Some are euhedral to subhedral in form, but most have suffered severe magmatic resorption (Figure 3.17B). In contrast with the rocks of the first volcanic phase, phenocrysts of hornblende are generally euhedral and do not exhibit the dehydration reaction rim textures found in andesitic lavas of the first volcanic phase. In some samples hornblende occurs as megacrysts enclosing numerous plagioclase crystals (Figure 3.17C). The groundmass is composed of microlites of plagioclase, alkali feldspar, quartz, opaque minerals, apatite and amphibole. Accessory minerals are represented by apatite, often characterised by oscillatory zoning (Figure 3.17D), zircon and opaque minerals.

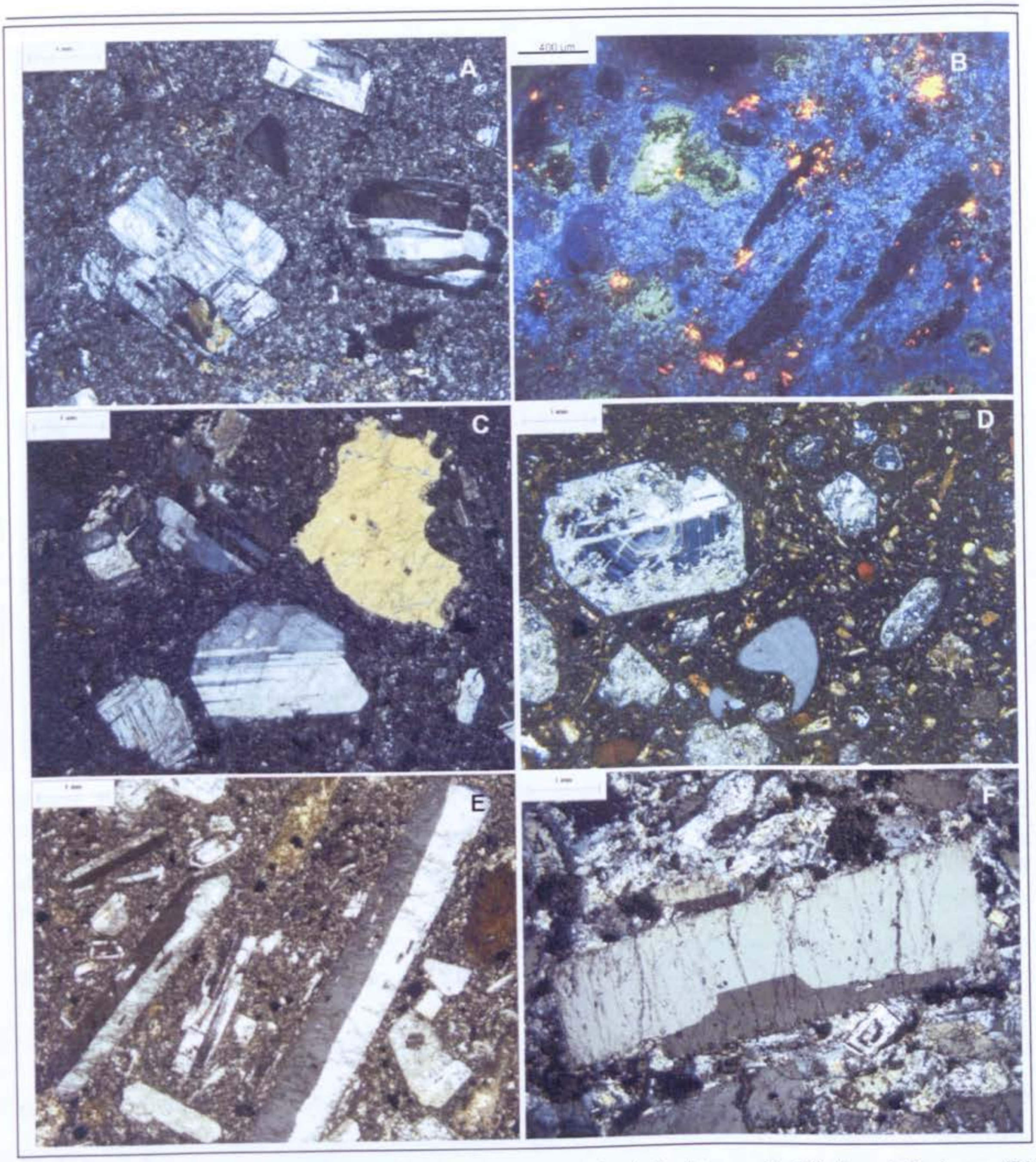

**Figure 3.16:** Photomicrographs (A; C-F) taken under crossed polarised transmitted light and CL image (B) showing volcanic textures of the rocks of the second volcanic phase. A) Moderately rich porphyritic latite with glomerocrysts of plagioclase (sample KU1A); B) Amphibole-latite showing trachytic texture defined by amphibole laths (black) in the fine-grained groundmass composed of alkali feldspar (bright blue) and quartz (dark blue); green crystals are plagioclase glomerocrysts and yellow-red is carbonate alteration (sample 1235); C) Moderately rich porphyritic quartz latite with resorbed quartz phenocryst (sample KU18); D) Phenocryst-rich amphibole-biotite quartz latite with oscillatory zoned plagioclase showing some degree of alteration and with an embayed quartz crystal (sample KU26); E) Seriate, trachytoid- textured (defined by alkali feldspar and plagioclase phenocrysts) amphibole-biotite quartz latite showing tabular flow-aligned sanidine megacrysts (sample KG1); F) Sanidine-phyric quartz latite composed mainly of alkali feldspar with only minor mafic minerals (sample CVrh). Scale=1mm except in B=400μm.

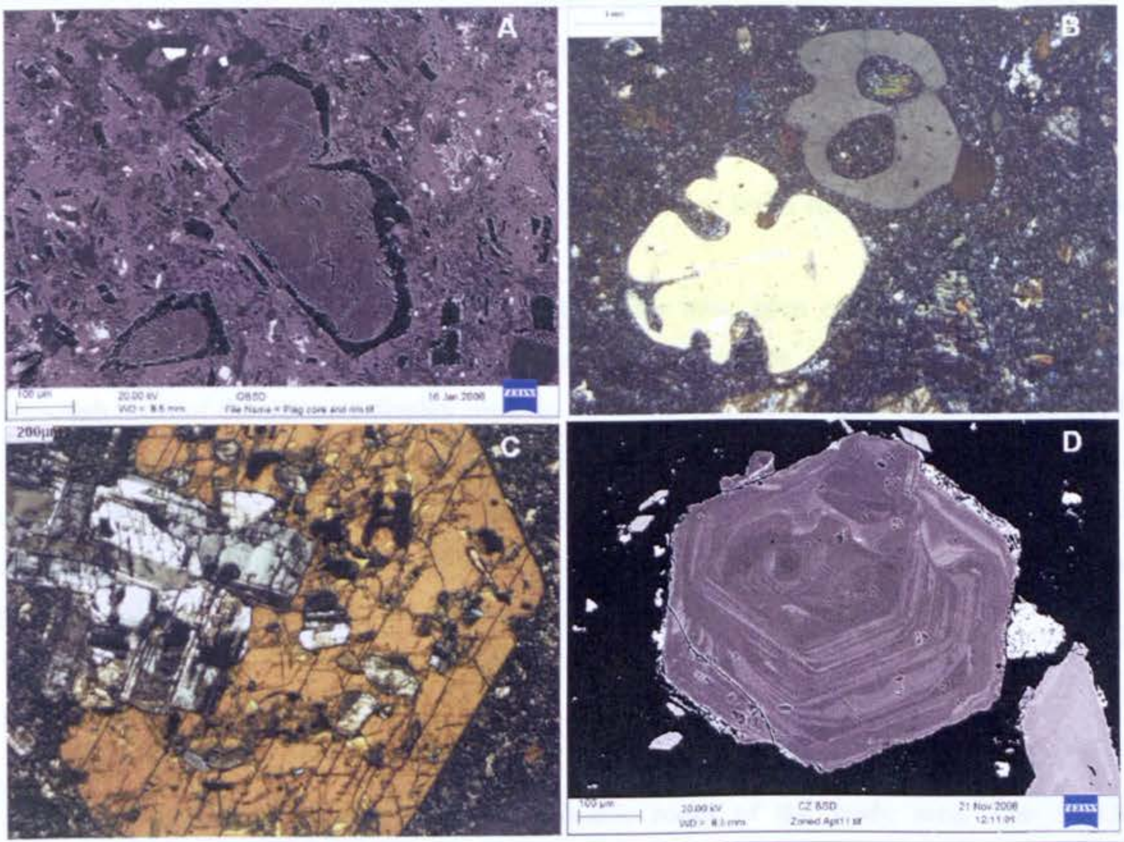

**Figure 3.17:** BSE Image (A and D) and photomicrographs (B and C) taken under crossed polarised transmitted light showing disequilibrium (A, B and D) and poikilitic textures of quartz latites. A) Xenocryst of plagioclase (sample KU18); B) Embayed quartz crystals (sample KU32); C) Large hornblende phenocryst enclosing and partially enclosing crystals of plagioclase in poikilitic texture (sample KG1); D) Complex zoning of apatite (sample CVrh).

### *3.5.3 The Kopaonik intrusive*

The Kopaonik intrusive displays a zonal distribution of granitoid varieties that show gradual transitions between each other (Cvetković et al., 2002). The southern part is represented by porphyritic granodiorite to quartzmonzonite characterised by the presence of cm-sized K- feldspars. Towards the north, the intrusive rocks are more equigranular in texture and granodioritic to quartzdioritic in composition. In general, these granitoids are composed of quartz, plagioclase ($An_{35-55}$), K- feldspar (Or $_{>86}$), biotite, and magnesiohornblende, with titanite, epidote, allanite, apatite, zircon, and magnetite as accessory minerals. The Kopaonik rocks have silica contents ranging from 57 to 67 wt% $SiO_2$. They are medium-K calc-alkaline, metaluminous ($Al_2O_3$-[$K_2O$+ Na2O]\1), I-type granitoid rocks, with LILE- and LREE enriched trace element patterns. Because of slightly elevated $K_2O$ concentrations (≥ 2.5–3 wt%), the Kopaonik quartzmonzonites occurring in the south exhibit a high-K calc-alkaline character and are richer in incompatible elements compared to the Kopaonik granodiorites (Schefer et al., 2010).

According to Schefer et al. (2010), U–Pb (ID-TIMS) dating on single zircons from the Kopaonik igneous rocks revealed an Oligocene (31.77–30.70 Ma) age group. It consists of I-type granitoids with positive Hf values of the zircons, indicating a moderate crustal influence in their origin, and it is proposed that this group formed via partial melting of mantle-derived lower crustal protoliths (Schefer et al., 2010).

## 3.6 Mineral chemistry of the main phenocryst phases from the Tertiary igneous rocks

The compositions of the main phenocryst phases have been obtained from representative samples of rocks of the first and second volcanic phase and are described here in more detail. Although most of the samples display weak to moderate propylitic alteration, great care has been taken in making sure that unaltered phenocryst phases (plagioclase, hornblende and pyroxene) analysed by SEM are considered in the final interpretation. The chemical analyses of plagioclase, atomic formulas calculated on the basis of 8 oxygens and An-Ab-Or content are given in Table 3.2 (the first volcanic phase) and Table 3 (the second volcanic phase) in Appendix 2.

### *3.6.1 Feldspars*

The feldspars are ubiquitous in the volcanic rocks of the study area. The Ab-Or-An classification diagrams (Figure 3.18) show the range of feldspar compositions of the analysed samples. Plagioclase is the main phenocryst phase in most of the analysed rocks (Figure 3.18A and B) and the predominant constituent of the groundmass. Alkali feldspar (sanidine) is the predominant phenocryst phase in quartz latite trachytic-textured lavas (Figure 3.18B), and a common groundmass constituent in latites, whilst its presence is less common in groundmass of andesites and dacites (Fig 3.18A). It can also occur as a product of reaction rims around xenocrysts in quartz latite lavas (Figs. 3.17A). There is a compositional continuity of plagioclase phenocrysts from andesites (labradorite to andesine) to dacites (andesine) and quartz latites (andesine-oligoclase). In andesites, the anorthite content of plagioclase phenocrysts shows a range from $An_{42}$ to $An_{65}$ and in dacites from $An_{31}$ to $An_{45}$. The plagioclase phenocrysts in the rocks of the second volcanic phase have anorthite compositions that range between $An_{23}$ and $An_{46}$. In most of the lithologies plagioclase crystals are zoned showing normal zoning, but in some andesite lavas they show reversed and oscillatory pattern with $An_{54-60}$ cores and $An_{60-71}$ rims (Figure 3.18A, samples BB2 and T3). In reversed zoning, the observed maximum compositional range from core to rim is 14.4 mole % An. Plagioclase microlites are generally more sodic ($An_{18-43}$, rarely up to $An_{53}$). The K-feldspar with the lowest $K_2O$ content ($Or_{55-68}$) appears sporadically in the groundmass of the rocks belonging to the first volcanic phase (Figure 3.18A), whereas the phenocrysts and microlites of sanidine are widespread in the rocks of the second volcanic phase. Alkali feldspars also occur around plagioclase xenocrysts in the rocks of second volcanic phase and are usually more potassic (Or>60).

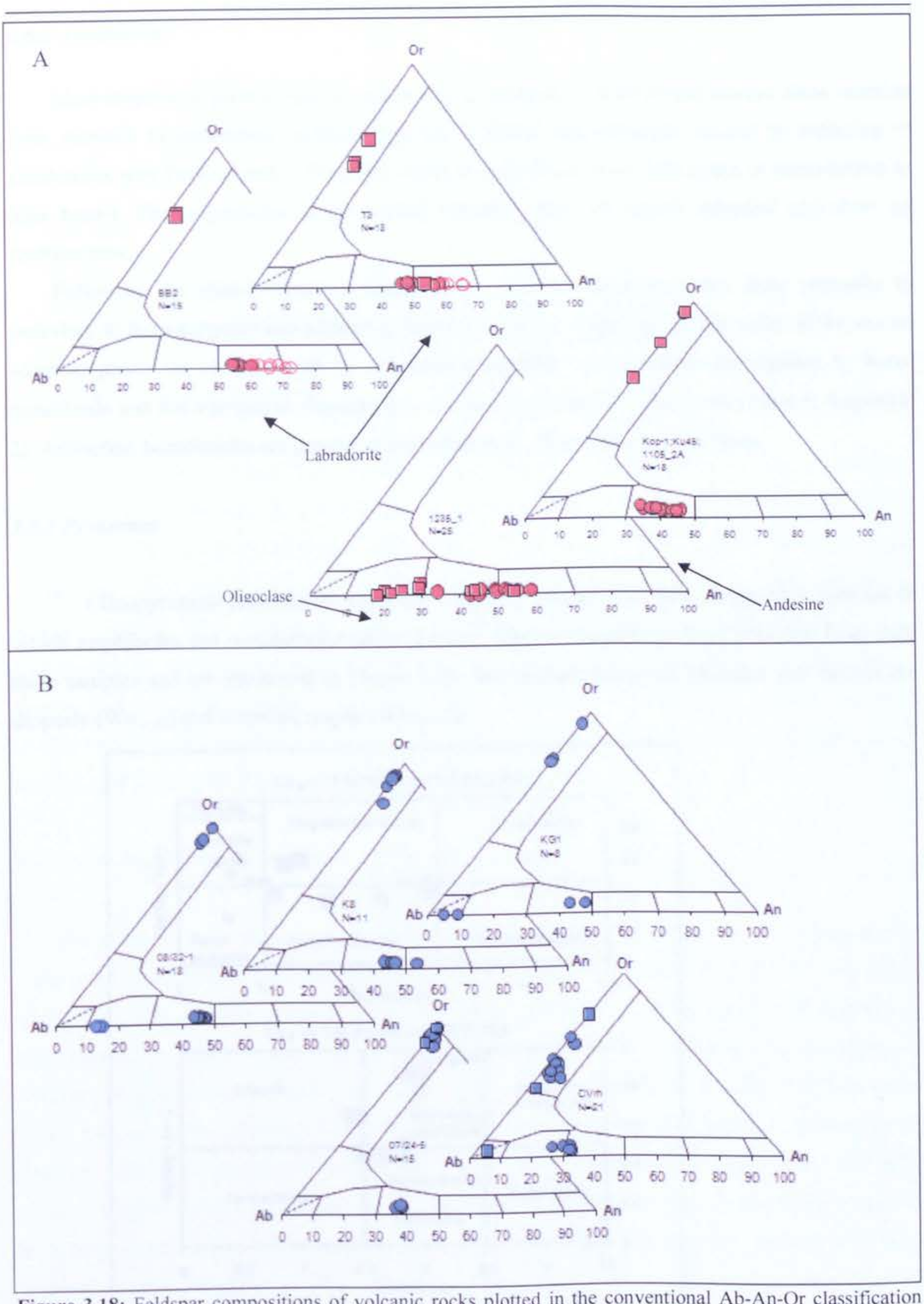

**Figure 3.18:** Feldspar compositions of volcanic rocks plotted in the conventional Ab-An-Or classification scheme. A) First volcanic phase; B) Second volcanic phase. Abbreviations: Ab, Albite; An, Anorthite; Or, Orthoclase. N is number of analyses. Solid circles = phenocryst cores; open circles = phenocryst rims; solid squares = groundmass phases. Some phenocrysts are altered and replaced by albite (samples 08/32-1 and KG8).

### 3.6.2 Amphiboles

Most amphibole phenocrysts in andesites are anhedral crystals which always show reaction rims, partially to completely oxidised forming "opacite" pseudomorphs caused by replacing of amphiboles with Fe-Ti oxides. The phenocrysts are pleochroic from dark green or green-brown to light brown. The amphiboles of the second volcanic phase are mainly euhedral and show no reaction rims.

Following the classification of Leake et al. (1997) amphiboles vary from pargasite in andesites, to ferro-pargasite and edenite in dacites (Table 3.2, Appendix 2). The rocks of the second volcanic phase are characterised by magnesio-hornblende and magnesio-hastingsites to ferro-hornblende and ferro-pargasite, depending on Na and K contents (Figure 3.19) (Table 3, Appendix 2). Actinolitic hornblendes are present in hydrothermally altered quartz latite lavas.

### 3.6.3 Pyroxenes

Clinopyroxene phenocrysts, relatively minor in volume have been observed in samples in which amphiboles are pseudomorphed by opacite. Their compositions were obtained from only three samples and are illustrated in Figure 3.20. The clinopyroxenes in andesites and dacites are diopside (Wo $_{>45}$) and diopsidic augite (Wo $_{41-45}$).

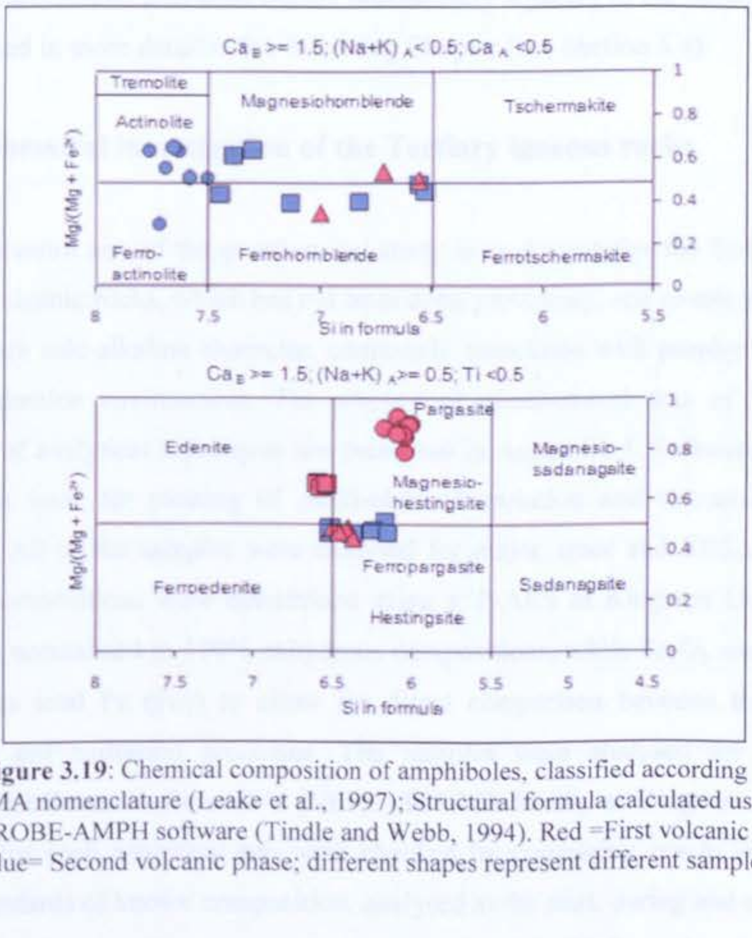

**Figure 3.19**: Chemical composition of amphiboles, classified according to the IMA nomenclature (Leake et al., 1997); Structural formula calculated using PROBE-AMPH software (Tindle and Webb, 1994). Red =First volcanic phase; Blue= Second volcanic phase; different shapes represent different sample numbers.

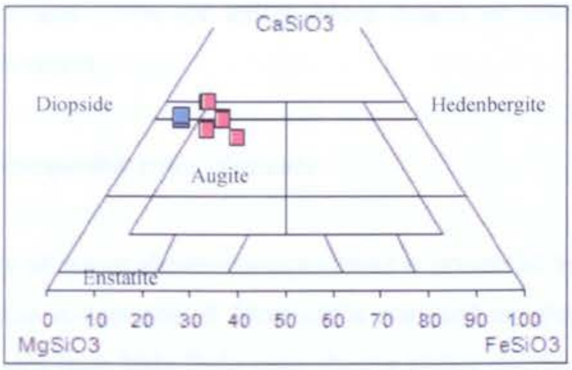

**Figure 3.20:** Composition of clinopyroxenes (after Morimoto et al., 1988).
Red squares=First volcanic phase; Blue squares= Second volcanic phase.

## 3.7 Hydrothermal alteration

Most of the samples show varying degrees of hydrothermal alteration with a secondary mineralogy consistent with propylitic (epidote+calcite+chlorite), phyllic (quartz+sericite+ pyrite) and argillic (quartz+clay) alteration assemblages. The rocks of the second volcanic phase additionally carry abundant pyrite as disseminations and fracture fillings. Many samples are partially masked by a retrograde weathering assemblage of goethite, kaolin and pyrolusite. Ferromagnesian minerals are most affected and they have been variably altered to chlorite, calcite, epidote and magnetite. Feldspars have been partially altered to sericite and calcite. The most intense hydrothermal alteration occurs immediately adjacent to the mineralised ore bodies and will be discussed in more detail in the following Chapter (see Section 4.4).

## 3.8 Geochemical investigation of the Tertiary igneous rocks

The overall aim of the geochemical study is to characterise the Belo Brdo and Karavansalija Tertiary volcanic rocks, which has not been done previously, and to test if the volcanic rocks are of intermediate calc-alkaline character, commonly associated with porphyry-type Cu-Au deposits in supra-subduction environment. The whole-rock geochemical data of twenty two samples and summary of analytical techniques are presented in Appendix 3. Software GCDkit (Vojtěch, et al., 2006) was used for plotting of multi-element variation and tectono-magmatic discrimination diagrams. All of the samples were analysed for major, trace and REE contents. Major and trace element compositions were determined using ICP-AES at Kingston University. Major elements have been normalised to 100% anhydrous compositions, while $Fe_2O_3$ and FeO contents have been reported as total Fe ($Fe_T$) to allow for direct comparison between the samples, regardless of oxidation and hydration processes. The samples were analysed for REE using the Natural Environment Research Council 's (NERC) ICP-MS facility at Kingston University. Precision and accuracy for each analytical run were checked by comparing results of a suite of international USGS standards of known composition, analysed at the start, during and end of each analytical run. The analyses are considered accurate within limits of 2–5% for major elements, 10–15% or better for trace elements and 1–5% for REEs. More details on precision and accuracy are given in Appendix 3 of this report.

### *3.8.1 Major and compatible trace elements*

The summary of major element compositions is presented in Table 3.1 below and the full data results are presented in Appendix 3. Most of the analysed samples show some secondary alteration. Of these samples, six from Belo Brdo mine show a higher degree of alteration comparing to the rest of the analysed samples. Hence they have been separately grouped as the altered first volcanic phase in order to be treated with caution and to avoid their misinterpretation. The secondary mineral phases of altered samples have been determined entirely by optical mineralogy, since it is not possible to estimate the degree of alteration using the ICP techniques. All the analysed samples of the study area show a restricted compositional range (Table 3.1).

All the samples show a narrow range of $SiO_2$ contents, from 57 to 63 wt %, which are typical for rocks of andesitic compositions. However, there is a difference in silica and alkali content between rocks of the first (Belo Brdo ore field) and second (Karavansalija prospect) volcanic phase, indicating a bimodal character for the rocks of the Kopaonik district. The rocks of the Belo Brdo ore field show lower silica (average 59.9 wt %) and K contents (average 2.2 wt % $K_2O$) than those of the Karavansalija prospect (average 62.4 wt % $SiO_2$ and 4.6 wt % $K_2O$ respectively) (Table 3.1). All of the rocks are rich in $Al_2O_3$ (>15wt %) and their Mg number (Mg # = molecular Mg/[Mg + $Fe_T$] x 100), range from 35 to 56 in each volcanic phase.

**Table 3.1**. Summary of major elemental data normalised to 100% anhydrous (wt.%). Full data presented in Appendix 3.

| Volc | Stats | $SiO_2$ | $TiO_2$ | $Al_2O_3$ | $FeO_T$ | MnO | MgO | CaO | $Na_2O$ | $K_2O$ | $P_2O_5$ |
|---|---|---|---|---|---|---|---|---|---|---|---|
| First Volc Phase | BB max | 62.40 | 0.85 | 18.48 | 7.62 | 0.16 | 4.26 | 8.43 | 3.94 | 4.57 | 0.29 |
| | BB min | 57.36 | 0.63 | 16.17 | 5.38 | 0.08 | 1.65 | 5.48 | 0.17 | 1.42 | 0.15 |
| | Mean BB | 59.93 | 0.73 | 17.65 | 6.40 | 0.11 | 3.33 | 6.47 | 2.98 | 2.21 | 0.19 |
| | STD | 1.65 | 0.09 | 0.78 | 0.75 | 0.02 | 0.83 | 1.04 | 1.19 | 1.03 | 0.04 |
| Second Volc Phase | Ka max | 63.48 | 0.70 | 19.12 | 6.30 | 0.18 | 3.30 | 6.26 | 5.07 | 5.93 | 0.59 |
| | Ka min | 61.45 | 0.54 | 15.47 | 3.49 | 0.03 | 0.16 | 1.94 | 1.98 | 2.41 | 0.17 |
| | Mean Ka | 62.41 | 0.65 | 16.82 | 5.07 | 0.11 | 2.24 | 4.74 | 2.97 | 4.65 | 0.35 |
| | STD | 0.91 | 0.05 | 1.18 | 0.90 | 0.04 | 1.02 | 1.33 | 0.95 | 1.22 | 0.13 |
| Altered First Volc Phase | Alt max | 66.90 | 0.90 | 18.45 | 5.80 | 0.29 | 7.73 | 6.87 | 3.71 | 5.03 | 0.31 |
| | Alt min | 62.58 | 0.57 | 15.79 | 2.63 | 0.02 | 3.27 | 0.14 | 0.09 | 1.34 | 0.15 |
| | Mean alt | 64.72 | 0.70 | 17.34 | 4.61 | 0.11 | 4.40 | 3.48 | 1.49 | 2.96 | 0.21 |
| | STD | 1.80 | 0.12 | 1.00 | 1.24 | 0.10 | 1.71 | 2.21 | 1.47 | 1.37 | 0.05 |

$TiO_2$ contents are always <1 wt % with slightly lower values in the rocks of the second volcanic phase. Cr and Ni contents gradually decrease from the rocks of the first volcanic phase (from 112 ppm Cr and 48 ppm Ni) to the rocks of the second volcanic phase (to 46 ppm Cr and 38 ppm Ni). Average contents of Co, V and Cu also decrease from rocks of the first volcanic phase

(18.3 ppm; 115.3 ppm and 20.1 ppm) towards rocks of the second volcanic phase (10.7 ppm; 84.3 ppm and 13.4 ppm respectively).

Classification of the volcanic rocks has been made on the basis of the total alkali-silica (TAS) diagram (Le Bas et al., 1986; Figure 3.21A) and also following the criteria of Irvine and Baragar (1971; Figure 3.21B). All, except one sample (C-Vrh, showing higher degree of hydrothermal alteration) from the study area plot in the field of subalkaline rock type. The two principal volcanic compositions are evident from the TAS diagram. They range from andesites and dacites (first volcanic phase), to trachyandesites (second volcanic phase) (Figure 3.21A), although the clustering of points supports the predominantly andesitic composition. All the compositions plot along a calc-alkaline trend on an AFM (A= $Na_2O + K_2O$; F= FeO; M= MgO) diagram of Irvine and Baragar (1971) (Figure 3.21B). However, one sample exhibits post crystallisation iron enrichment attributable to weathering, which pushes values towards the tholeiitic field.

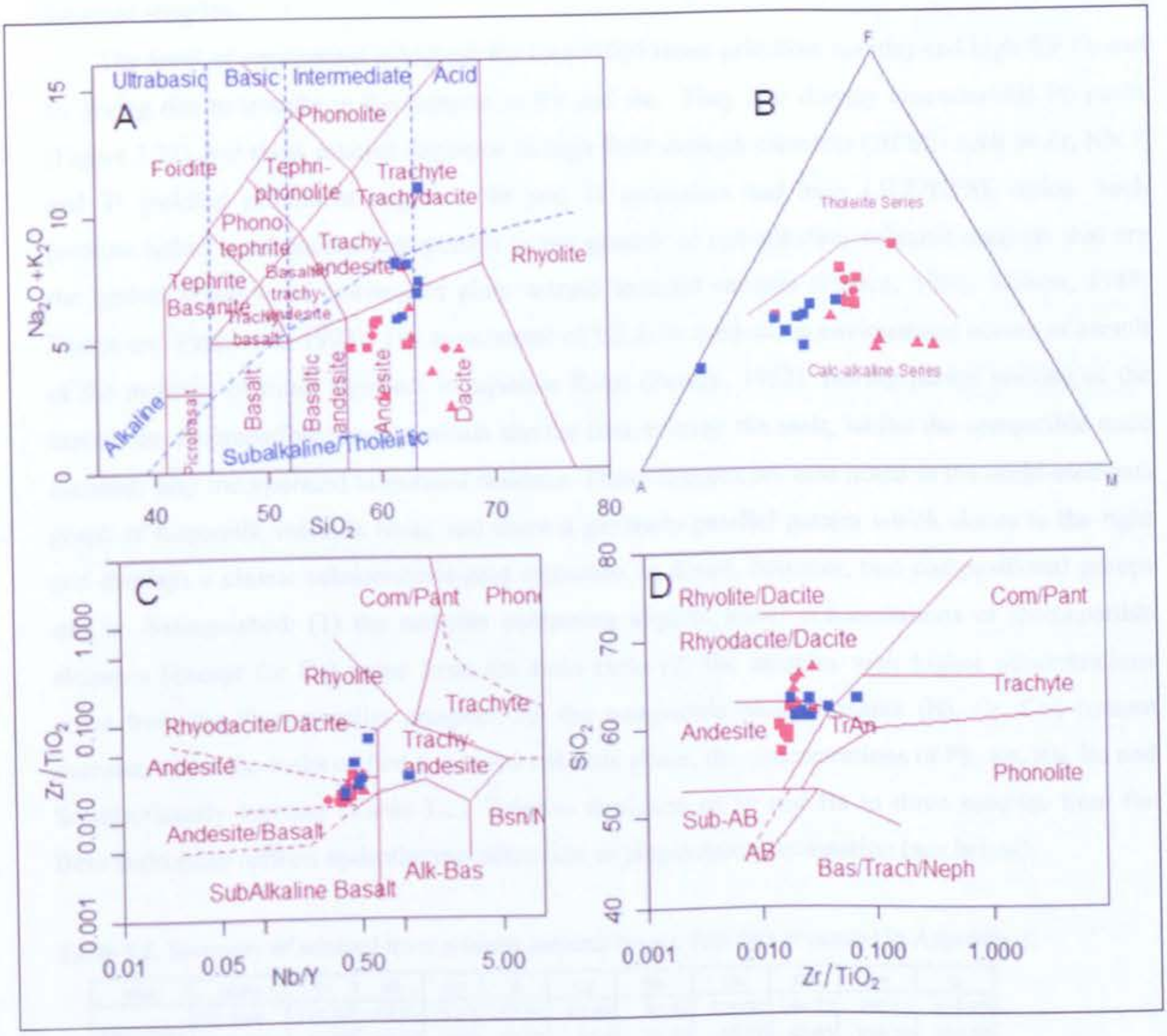

**Figure 3.21:** Rock classification diagrams. A) Total alkalis-silica (TAS) plot (anhydrous basis) of analysed rocks. Field boundaries after Le Bas et al. (1986); B) After Irvine and Baragar, 1971. C) Classification diagrams of Winchester & Floyd (1977) based on immobile element ratios. Red squares = First volcanic phase, Belo Brdo; Red circles = First volcanic phase, Rudnitza; Red triangles = Altered first volcanic phase. Blue squares = Karavansalija, mainly second volcanic phase.

Considering that most of the samples in this study are altered to various degrees, the use of more immobile elements would be more suitable for their classification. On the rock classification diagrams of Winchester and Floyd (1977) using less mobile elements (Nb/Y- Log Zr/TiO$_2$; Log Zr/TiO$_2$-SiO$_2$, Figure 3.21C and D respectively), the two principal volcanic compositions (andesite and rhyodacite/dacite) are also evident.

### *3.8.2 Incompatible trace elements*

Incompatible trace element variations are summarised in primitive mantle normalised multi-element diagrams and presented in Figure 3.22. The trace element patterns display generally similar features for all lithologies. They are characterised by extreme enrichment of large ion lithophile elements (LILE) such as Cs, Rb, Th, U, in the range of 100–800 times primitive mantle for most samples.

The level of enrichment is highest for Cs (>5000 times primitive mantle) and high for Th and U, giving rise to troughs in the patterns at Rb and Ba. They also display characteristic Pb peaks (Figure 3.22), but show relative depletion in high field strength elements (HFSE) such as Zr, Nb, P and Ti yielding prominent negative Nb and Ti anomalies and high LILE/HFSE ratios. Such patterns reflect a subduction component in the genesis of calc-alkaline volcanic magmas that are the typical products of convergent plate margin tectonic settings (Pearce, 1982; Wilson, 1989; Pearce and Parkinson, 1993). The enrichment of LILE in subduction environment occurs as aresult of the mobility of those elements in aqueous fluids (Pearce, 1982). During partial melting of the mantle the incompatible trace elements are the first to enter the melt, whilst the compatible trace elements stay incorporated in mineral residues. Those features are also noted in the multi-elements graph of Kopaonik volcanic rocks and show a generally parallel pattern which slopes to the right and displays a classic subduction-related signature. In detail, however, two compositional groups can be distinguished: (1) the samples containing slightly lower concentrations of incompatible elements (except for Cs) come from the Belo Brdo (2) the samples with higher concentrations come from the Karavansalija prospect. As the compatible trace elements (Ni, Cr, Co) content decreases from the rocks of first to second volcanic phase, the concentrations of Pb, Zn, Rb, Ba and Sr significantly increase (Table 3.2). Relative depletion of Sr and Ba in three samples from the Belo Brdo mine reflects hydrothermal alteration or plagioclase fractionation (see below).

**Table 3.2.** Summary of selected trace element contents (ppm). Full data presented in Appendix 3.

| Volc | Stats | Cr | Ni | Co | V | Cu | Pb | Zn | Rb | Ba | Sr |
|---|---|---|---|---|---|---|---|---|---|---|---|
| First Volc Phase | BB max | 111.64 | 47.75 | 25.99 | 161.19 | 45.44 | 32.51 | 105.92 | 184.22 | 750.33 | 629.05 |
| | BB min | 32.89 | 26.36 | 12.06 | 93.95 | 9.74 | 15.12 | 57.20 | 42.61 | 159.50 | 210.28 |
| | Mean BB | 63.82 | 39.06 | 18.34 | 115.26 | 20.13 | 20.92 | 71.83 | 97.48 | 416.83 | 433.20 |
| Second Volc Phase | Ka max | 46.25 | 37.64 | 28.94 | 117.66 | 36.62 | 187.78 | 705.61 | 216.73 | 1836.88 | 1903.08 |
| | Ka min | 28.51 | 29.12 | 3.80 | 61.92 | 1.06 | 21.16 | 46.27 | 91.97 | 541.11 | 409.45 |
| | Mean Ka | 36.85 | 33.00 | 10.71 | 84.25 | 13.41 | 72.96 | 184.40 | 151.13 | 1208.00 | 953.14 |
| Altered First Volc Phase | Alt max | 289.50 | 179.53 | 13.62 | 159.38 | 859.91 | 1783.20 | 4003.57 | 332.65 | 588.97 | 358.56 |
| | Alt min | 40.13 | 32.72 | 1.49 | 91.02 | 2.00 | 14.68 | 22.28 | 43.95 | 87.18 | 97.84 |
| | Mean alt | 83.12 | 61.60 | 8.69 | 105.28 | 268.41 | 387.80 | 712.91 | 179.09 | 325.14 | 198.59 |

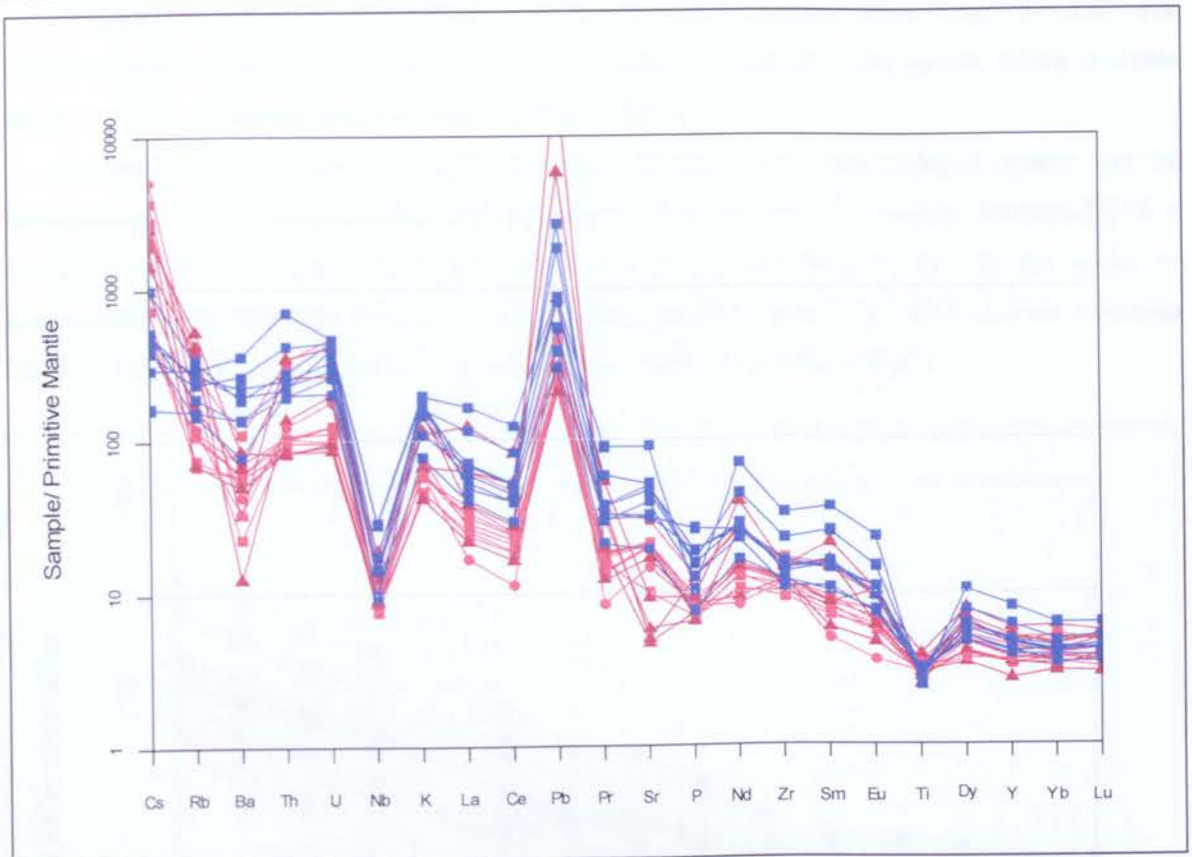

**Figure 3.22:** Multi-element variation diagram for the Kopaonik volcanic rocks normalised to primitive mantle values (Sun and McDonough, 1989). Normalisation removes "spiky" nature of trace element pattern due to variation in abundances, allowing the direct comparison of different rock suites on a single diagram. Negative anomalies for all rocks in Nb and Ti (Ta not plotted) and positive anomaly in Pb, as well as a general enrichment in incompatible elements, are characteristic features of arc magmas (Sun and McDonough, 1989; Pearce and Peate, 1995). Red squares = First volcanic phase, Belo Brdo; Red circles = First volcanic phase, Rudnitza; Brown triangles = Altered first volcanic phase. Blue squares = Second volcanic phase, Karavansalija.

### *3.8.3 Rare earth elements (REE)*

Volcanic rocks from both volcanic phases in the study area have similar chondrite-normalised REE convex-upward patterns relative to chondritic values (Figure 3.23), showing enrichment in the light rare earth (LREE) over the heavy rare earth elements (HREE). Most samples are characterised by weak to negligible negative europium anomalies (Eu/Eu* = 0.8 to 0.9; Eu/Eu* = Eu $_N$/sqrt $(Sm)_N*(Gd)_N$] (Taylor and McLennan, 1985). One sample of dacite has a lower negative Eu anomaly (Eu/Eu* = 0.7) compared to the rest of the samples. Only one sample displays a positive Eu anomaly, which could be attributed to hydrothermal alteration and calcite-filled fractures. Europium depletion or enrichment is generally attributed to europiums tendency to be readily incorporated into plagioclase, where it substitutes for calcium ($Ca^{2+}$), preferentially over other minerals. Rocks that have accumulated plagioclase show positive anomalies, whilst a removal of plagioclase from the melt by fractional crystallisation or partial melting of a rock containing plagioclase displays negative Eu anomalies.

The studied rocks are also characterised by flat HREE patterns ($Tb_N/Yb_N = 1 - 1.5$). The HREE concentrations are in a region of 10 x chondritic, suggesting that garnet, which is stable below ~ 60 km, is absent from the source (Wilson, 1989).

In detail, however, as seen with the trace elements, two compositional groups can be distinguished: (1) the samples from the Belo Brdo show lower total REE content (average ΣREE = 111.5) and display lower fractionation from La to Lu ($La_N/Yb_N$ 6-12); (2) the rocks of Karavansalija prospect (the second volcanic phase) exhibit higher total REE content (average ΣREE = 240) and higher light rare earth element enrichment ($La_N/Yb_N = 9-25$).

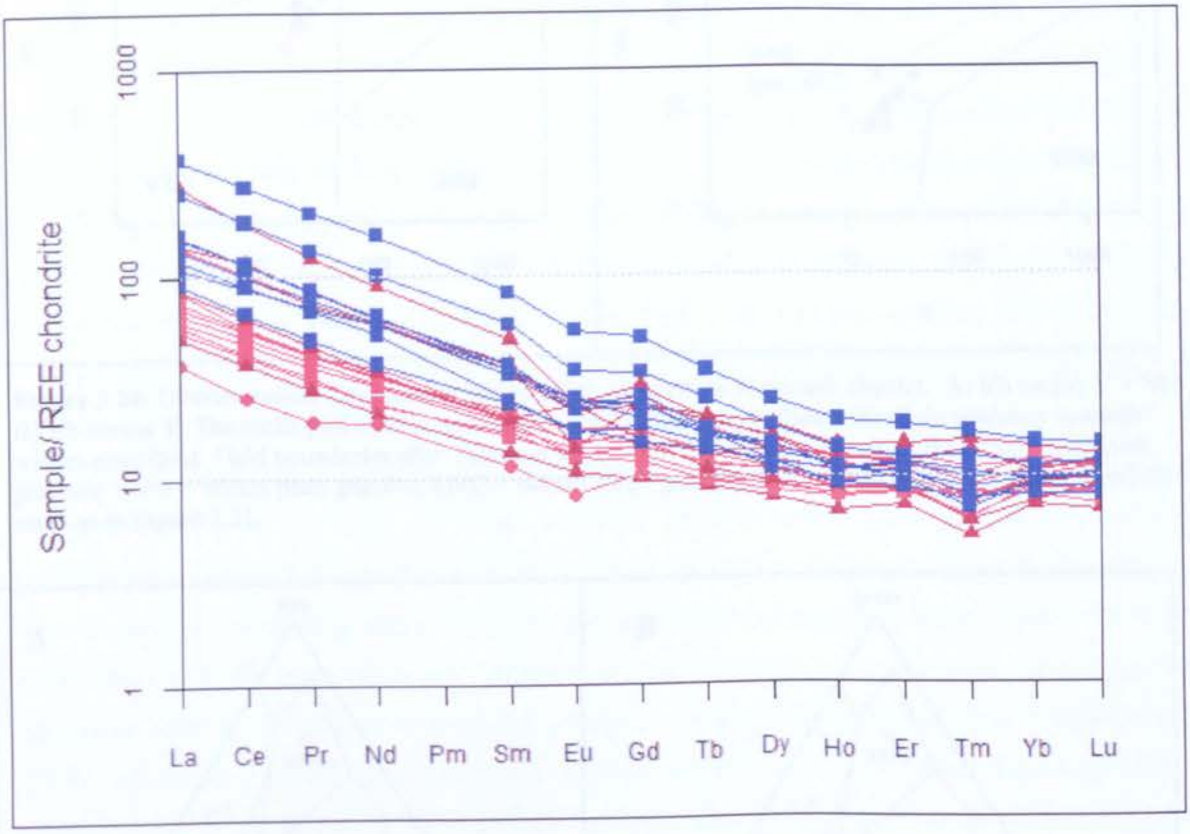

**Figure 3.23**: Chondrite-normalised rare earth element (REE) patterns (normalisation factors from Boynton, 1984). Normalisation "smooths-out" the odd-even atomic abundance differences between elements. Symbols same as in previous figure.

### 3.9 Tectono-magmatic affinities

The trace element data can be used in "tectonomagmatic discrimination diagrams" to elucidate tectonic setting associated with particular magma types (Pearce and Cann, 1973; Wood, 1980; Pearce 1982; Pearce et al., 1984). Many of the diagrams use HFSE such as Ti, Zr, Y and Nb which are relatively immobile in aqueous fluids and stable under conditions of hydrothermal, sea-floor weathering and up to medium metamorphic grades (Rollinson, 1993). Two of the most widely used plots utilise Rb versus Y + Nb (Figure 3.24 A) and Nb versus Y (Figure 3.24 B). Because Y substitutes mainly for Ca in pyroxene, amphibole and apatite, it is concentrated in mafic cumulates and primitive (MORB) basaltic rocks (Wilson, 1989). Niobium behaviour is complex and is only partly controlled by differentiation, whereas Rb is an excellent indicator of differentiation and continental crustal components.

The trace element characteristics of the volcanic rocks in the study area show features of magmas erupted in volcanic arc settings. On the discrimination plots, the rocks plot mostly within calc-alkaline basalt fields (Figs 3.24 A and B).

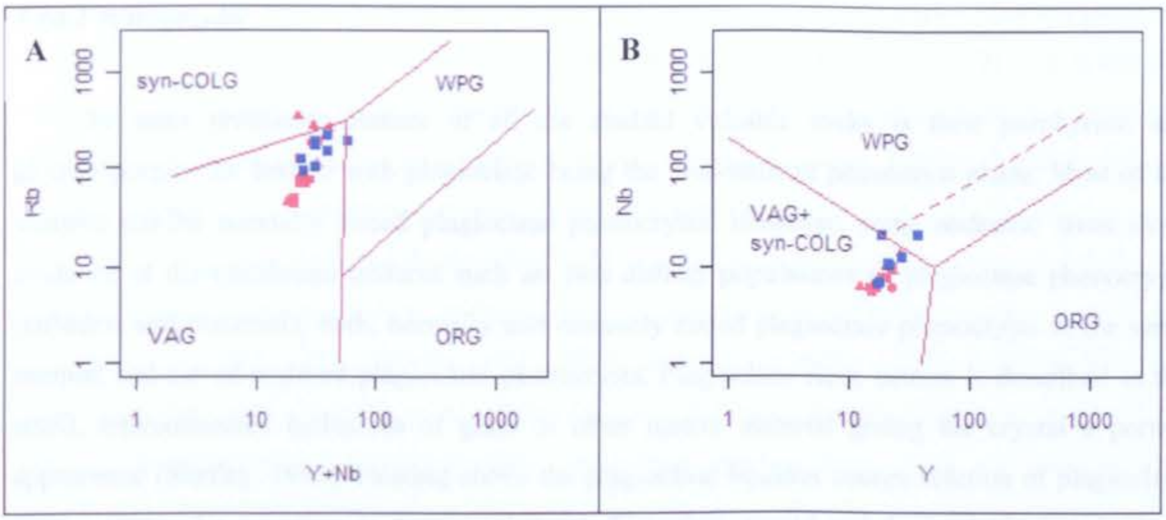

**Figure 3.24:** Discrimination diagrams for the volcanic rocks of the Kopaonik district. A) Rb versus Y + Nb; B) Nb versus Y. The rocks plot mainly within destructive plate margin filed with slight tendency towards within-plate field. Field boundaries after Pearce et al., (1984). Abbreviations: syn-COLG = syn-collisional granites; WPG = within plate granites; ORG = ocean- ridge granites; VAG = volcanic arc granites. Symbols same as in Figure 3.21.

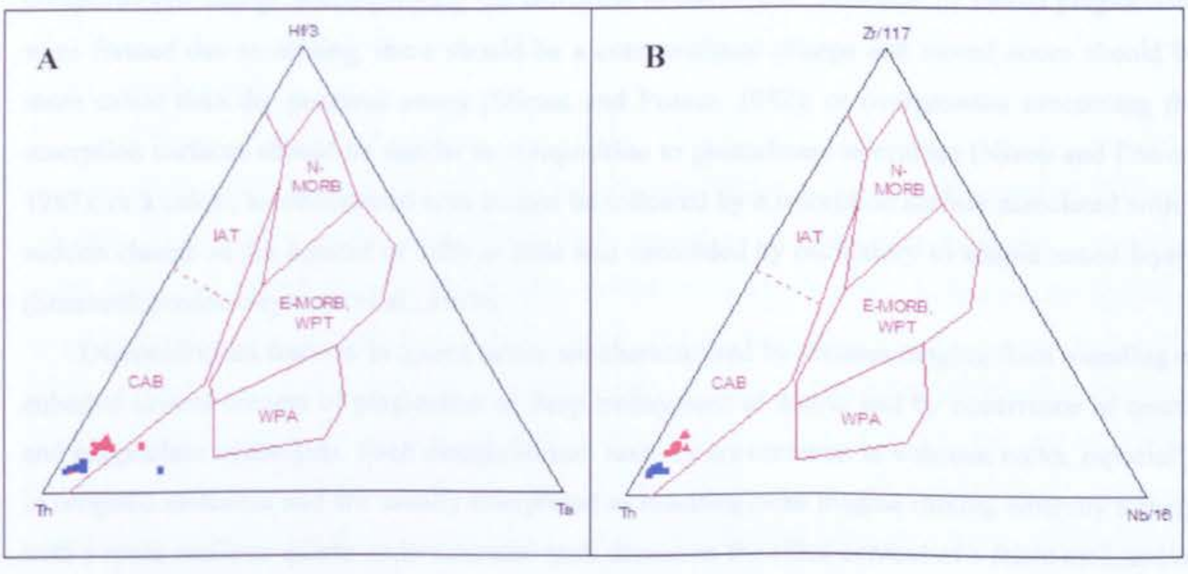

**Figure 3.25:** Hf/3-Th-Ta (A) and Zr/117-Th-Ta (B) tectonomagmatic discrimination diagrams for the volcanic rocks of the Kopaonik district (after Wood, 1980). Abbreviations: N-MORB= Normal - Mid Oceanic Ridge Basalts (MORB); E-MORB, WPT= Enriched - MORB and Tholeiitic Within- Plate Basalts; WPA= Alkaline Within-Plate Basalts; IAT= Island Arc Tholeiitic Basalts; CAB= Continental Arc Basalts (Destructive plate margin basalts). Symbols same as in Figure 3.21.

In terms of the ternary Hf-Th-Ta and Zr-Th-Nb plots of Wood (1980), they plot also within the destructive plate margin field (Figure 3.25 A and B). Affinities to destructive plate margin volcanics on these discrimination plots are possibly due to the relative low Ti and high Th characteristics of the volcanic suite.

## 3.10 Interpretation of Petrographic and Geochemical data for the Tertiary volcanic rocks

### 3.10.1 Petrography

The most prominent feature of all the studied volcanic rocks is their porphyritic and glomeroporphyritic texture with plagioclase being the predominant phenocryst phase. Most of the samples exhibit normally zoned plagioclase phenocrysts. However, some andesitic lavas show evidence of disequilibrium textures such as: two distinct populations of plagioclase phenocrysts (euhedral and resorbed); both, normally and reversely zoned plagioclase phenocrysts in the same sample; and sieved-textured plagioclase phenocrysts. Plagioclase sieve texture is described as the small, interconnected inclusions of glass or other matrix material giving the crystal a porous appearance (Shelley, 1993). Heating above the plagioclase liquidus causes solution of plagioclase phenocrysts and a rounding of the crystal shape. Therefore, sieved and dusty plagioclase textures are commonly reported in igneous rocks of proposed magma mixing origin (Tsuchiyama, 1985). Sieve texture also forms due to decompression when magma rises towards the surface (Nelson and Montana, 1992). In the case of rapid adiabatic decompression there should not be any compositional change accompanying the corrosion of the crystal. However, if sieved plagioclases were formed due to mixing, there should be a compositional change and sieved zones should be more calcic than the previous zones (Stimac and Pearce, 1992); or overgrowths succeeding the resorption surfaces should be similar in composition to groundmass microlites (Nixon and Pearce, 1987); or a calcic, sieve-textured core should be followed by a resorption surface associated with a sudden change in An content of 10% at least and succeeded by oscillatory to simple zoned layers (Stamatelopoulou-Seymour et al., 1990).

Disequilibrium features in quartz latites are characterised by textures ranging from rounding of euhedral crystal corners of plagioclase to deep embayment of quartz and by occurrence of quartz and plagioclase xenocrysts. Such disequilibrium textures are common in volcanic rocks, especially in orogenic andesites and are usually interpreted as resulting from magma mixing whereby mixing with a more mafic or quartz-undersaturated melt decreases the silica content of a felsic melt and/or increases the melt temperature, resulting in the resorption of early formed plagioclase and quartz (e.g. Dungan and Rhodes, 1978; Sakuyama, 1981; Tsuchiyama, 1985; Kuscu and Floyd, 2001). Chang and Meinert (2004) found extensive embayments of quartz phenocrysts in the Empire Mine Cu–Zn skarn deposit located in south-central Idaho. Based on detailed geochemical and textural analysis, they concluded that the embayments formed due to resorption during the magmatic–hydrothermal transition. Deep embayments of quartz phenocrysts and resorption of K-feldspar and plagioclase can also occur due to quartz under-saturation in the magma caused by rapid decompression as the magma ascended to a shallow magma reservoir (Nelson and Montana, 1992). Thus, shallow crustal processes might have had an important role in the petrogenesis of the studied rocks.

The major ferromagnesian phase in the studied rocks from both volcanic phases is the calcic amphibole, whilst biotite represents the second most common mafic mineral. Most primary amphiboles are rich in alkali elements (Na + K > 0.5), while secondary amphiboles are relatively depleted in alkali elements (Na + K < 0.5) and belong to groups of actinolite and actinolitic hornblende. The andesites are characterised by high-Al amphiboles ($Al_2O_3$ > 12 wt %; pargasites), which could have crystallised at high temperature and elevated pressure. Amphibole phenocrysts in these rocks exhibit breakdown textures of reaction rims. Formation of this texture has been attributed to solid-state hornblende dehydration in response to water loss from the coexisting melt during relatively slow or adiabatic magma ascent or introduction and mixing of water-poor melt (Rutherford and Hill, 1993; Buckley et al., 2002). Amphiboles of the second volcanic phase are more silicic and have much lower Al content ($Al_2O_3$ < 8.5 wt%; mainly edenitic hornblende, Fe- and Mg- hornblende) and could have been crystallised at lower temperature and pressure than amphiboles of the first volcanic phase. Mineral chemistry data indicate that there is no transition in amphibole end-members between the two volcanic phases. The general absence of dehydration reaction rims is a characteristic of the rocks of second volcanic phase. This feature suggests that emplacement of the hydrous magmas was not associated with sufficient or slow degassing to cause dehydration reactions during ascent (Bryan, 2002).

### *3.10.2 Geochemistry*

The Kopaonik metallogenic district comprises calc-alkaline volcanic rocks generated through two phases of volcanic activity. The first phase is represented mainly by andesitic-dacitic volcanic rocks, while the second volcanic phase includes latites and quartz latites. In general, all the rocks are characterised by relatively narrow $SiO_2$ contents (57-63 wt%), low $TiO_2$ (< 1wt %), high $Al_2O_3$ (>15 wt%) and low to moderate MgO contents ( 1.6 – 4.2 wt %). On primitive mantle-normalised multi-element diagrams all the rocks display relative enrichment in LILE (Cs, Rb, Ba, K, Sr) and Pb and depletion in HFSE (Nb,Ta,Ti, Zr and Hf) (Saunders et al., 1991). Their chondrite-normalised REE patterns show enrichment in LREE, flat HREE ($La/Sm_N$ = 3.2-4.9; $Gd/Yb_N$ = 1.2-3.3; $La/Yb_N$ = 6.3-23) and the presence of a minor negative Eu anomaly. All these geochemical characteristics indicate clear subduction-related magmatic signatures for all volcanic rocks (McDonough, 1990; McCulloch and Gamble, 1991; Pearce and Peate, 1995). The differences between the rocks of first and second volcanic phase are not significant in terms of most major element values, except alkali and Si contents, which are higher in the quartz latite phase. The rocks of the second volcanic phase are slightly more potassic with $K_2O/Na_2O$ ratios mostly between 0.5 and 2, which is consistent with the post-collisional nature of magmatism in the Vardar Zone

(Cvetković et al, 2004). The difference between the rocks of the two phases exists in their trace element abundances in that the rocks of the second volcanic phase are more enriched in incompatible elements with respect to primitive mantle, than the rocks of the first volcanic phase. Additionally, bivariate plots (Figure 3.26A and B) indicate that the rocks first and second volcanic phases might not be co-genetic. However, the fractionations of LILE/LREE, LILE/HFSE and REE/HFSE (e.g. La/Nb, La/Yb, Zr/Nb) from both groups indicate subduction-related metasomatism for (Gill, 1981; Pearce, 1982) and the melt source involved in the genesis of these lavas was possibly a subduction- modified mantle. The slightly more potassic and more trace-element enriched volcanic rocks of the second volcanic phase, as well as their high Pb contents indicate crustal contamination. The $^{87}Sr/^{86}Sr$ and $^{206}Pb/^{204}Pb$ radiogenic isotope data provide further evidence for the importance of continental crustal material in the genesis of these magmas (see Chapter 8).

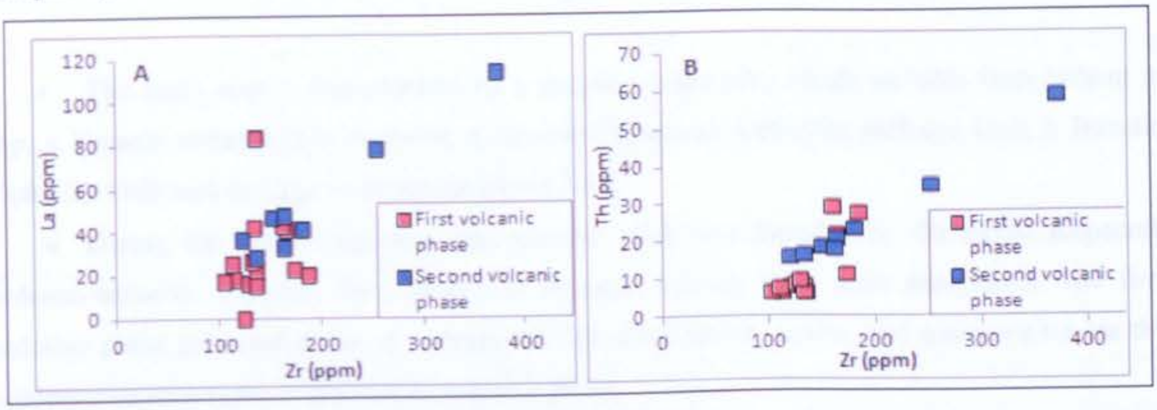

**Figure 3.26**: Bivariate plots Zr vs. La (A) and Zr vs. Th (B).

Magmas with subduction-related geochemical signatures are well known for their occurrence in active subduction zones, where they originate by dehydration of the subducted oceanic slab and interaction of these fluids with the overlying mantle wedge. Such magmas have trace element and isotopic fingerprints that reflect fluid involvement in their genesis. The LILE and LREE are soluble in aqueous fluids (Tatsumi et al., 1986) and during these processes they go preferentially into the fluid phase, whereas HFSEs are retained in the stable titanium phases (titanite, rutile) (Saunders et al., 1991 and references therein). Therefore the LILE are enriched relative to the immobile HFSE, MREE and HREE (Gill, 1981; Pearce, 1982; Ellam and Hawkesworth, 1988; Pearce and Peate, 1995). This is reflected by negative anomalies in HFSE and the relative enrichment of LILE in trace element patterns in primitive mantle-normalized multi-element diagrams.

In the Vardar zone of Serbia and Kosovo, the Tertiary was a period of collisional and post-collisional magmatism characterised by voluminous intermediate to acidic magmatism (Prelević et al., 2001; 2007; Cvetković et al., 2004; 2004a; 2007;). The calc-alkaline volcanism developed in the early Oligocene, well after the end of subduction of the Vardar Ocean beneath the southern European margin at the Upper Cretaceous/Tertiary boundary (Karamata et al., 2000) and following the collision, which occurred during the Eocene (Cvetković et al., 2004). High-K calc-alkaline to shoshonitic and ultrapotassic volcanic rocks and related intrusions were formed.

Widespread magmatism developed in the other areas of the Alpine-Mediterranean region (Wilson and Downes, 1991, Wilson and Bianchini, 1999; Lustrino, 2000; Harangi et al., 2006), where the processes of subduction, back-arc extension and lithospheric delamination were accompanied by eruption of a wide range of magma types during Tertiary. The dominant magma type is calc-alkaline, but in some places, a transition from calc-alkaline to alkaline volcanism is observed. This transition is commonly interpreted as a change in the magma source region as a result of changing geodynamic conditions from compression to extension (Harangi et al., 2006 and references therein).

## 3.11 Summary and conclusions

- The study area is characterised by a tectonic nappe pile, which includes from bottom to top: a Triassic metamorphic complex; a Jurassic-Cretaceous Ophiolite mélange Unit; a Jurassic Ophiolite Unit; and an Upper Cretaceous Flysch Unit.
- During the Early Oligocene, the tectonic stack was intruded by the I-type Kopaonik volcano-intrusive complex. Two phases of volcanic activity have been recognised. The first volcanic phase produced rocks of andesitic-dacitic composition. Latites and quartz latites are the predominant rock types of the second volcanic phase.
- Petrographic and geochemical data indicate subduction-related signatures for the magmatic rocks. All volcanic rocks are characterised by porphyritic and glomeroporphyritic textures, typical of those found in orogenic belts.
- Some volcanic rocks display disequilibrium textures such as: resorbed plagioclase phenocrysts; sieved-textured plagioclase; rounding of euhedral crystal corners of plagioclase; deep embayment of quartz; and occurrence of quartz and plagioclase xenocrysts. Such disequilibrium textures are common in volcanic rocks, especially in orogenic andesites and are usually interpreted as a result of magma mixing.
- The geochemical data indicate that the volcanic rocks from the first and second volcanic phase exhibit typical "subduction-related" composition as reflected by the enrichment of the LILE (Cs, Rb, Th, U, K) and Pb over LREE and MREE, and depletion of the HFSE (Zr, Nb, Ti, and P). The volcanic rocks classify as subalkaline and exhibit a calc-alkaline to mildly alkaline character.
- On "tectonomagmatic discrimination diagrams" (Rb vs. Y + Nb and Nb vs. Y) and the ternary Hf-Th-Ta and Zr-Th-Nb diagrams, they all plot in the field of magmas erupted in volcanic arc settings.

# CHAPTER 4:

# MINERALOGY OF THE BELO BRDO DEPOSIT

## 4.1 Introduction

The mineralisation at Belo Brdo mine has not previously been described in any detail in the literature, other than a brief report by Radosavljević (1989).

In this chapter, a detailed description of the ore petrography and mineralogy of the Belo Brdo Pb-Zn (Ag) deposit, including the wall- rock alteration is presented. Particular emphasis is placed on the paragenetic sequence of ore deposition as evidenced by mineralogical textures, zonation, and crosscutting relationships in the mineralised system. These mineralogical data, together with the REE geochemical data of different carbonate generations and sphalerite geothermometry and arsenopyrite geothermometry data, provide an insight into the origin and evolution of the Belo Brdo mineralisation. Further evidence for the genesis of the mineralising fluids based on fluid inclusion and stable isotope data will be presented and discussed in the following chapters.

## 4.2 Sampling and Methods

Samples from Belo Brdo were collected from three levels and two sub-levels, covering approximately 235 m of GII replacement-type ore body up and down dip and along strike. Samples were also taken from one level of the GII/12 vein-type ore body. A list of samples with their locations and schematic plan showing sampling positions from all mine levels is presented in Appendix 1. Additionally, a group of representative mineralised rock samples were taken from 9 drill- cores from the Karavansalija Cu-Au skarn and Rudnitza Cu-Au porphyry prospects. All samples were washed, dried and photographed to ensure capture of hand specimen sized textural data. The hand specimens were sorted according to ore structures and textures. A suite of representative samples was cut and lapped for a preliminary macro-scale study of ore textures and for photographing.

A total of 49 polished thick sections and 10 polished blocks were examined using optical reflective light microscope in order to define ore textures and the paragenetic sequence of ore deposition, as well as post-deposition effects, such as recrystallisation and alteration of primary mineralogy. Representative samples were further analysed using SEM techniques to characterise mineral chemistry and complex textures. Quantitative analysis of sulphides using the WDS was carried out on the main ore-stage mineralisation to characterise trace element contents of sphalerite and galena from 4 representative samples. WDS analyses of trace elements in sphalerite were used to calculate the formation temperatures (geothermometry). Additionally, 14 samples of different carbonate generations were analysed for REE contents using ICP-MS techniques to characterise the chemical environment of carbonate deposition. The data are presented in Appendix 3.

## 4.3. Nature of ore bodies

Several styles of mineralisation have been recognised at Belo Brdo deposit, namely: hydrothermal replacement (GII ore body); vein (GII/12 ore body); and skarn (GI ore body) (Kandić, 1987; Miletić and Mladenović, 1995; Mladenović, 2005) (Figure 4.1).

**Figure 4.1:** Simplified geological map of the underground level 1105 m, Belo Brdo deposit. 1 = Quartz-latite; 2 = Andesite; 3 = Reef limestones; 4 = Serpentinite; 5 = Ore body; 6 = Faults. (Modified after Miletic and Mladenovic, 1995).

The skarn mineralisation is reported to be spatially separated from the replacement and vein-type mineralisation. It was developed in the Cretaceous carbonates of the GI ore body, which has now been completely mined out. It consisted of magnetite, pyrrhotite, galena, sphalerite and chalcopyrite (Kandić, 1987; Janković, 1990). There are reports of skarn mineralisation of limited appearance at level 1000 (Mladenović, 2005), but access to this level was not possible during this study. In this work, therefore, the focus of research is on replacement- and vein- type ore bodies, as they are currently the most economic and are being mined at the present day.

### 4.3.1 Hydrothermal replacement mineralisation

This is the predominant and economically most important style of mineralisation in the Belo Brdo deposit. The GII ore body is irregularly shaped and plunges to the SE at 20° - 30°. It occurs, at, or close to, the tectonic contacts between the Cretaceous carbonates (rarely Triassic marbles) and Tertiary volcanic rocks and/or Jurassic serpentinites (Figure 4.1). The degree of replacement of the carbonate rocks varies from local replacement in marginal parts of the ore body, to complete in the ore body when only minor relicts of carbonate hosts are preserved (Figure 4.2A and B). The limestone is dolomitised and brecciated. A pervasive orange-brown iron-rich hydrothermal alteration locally colours the otherwise medium gray dolomitic limestone (Figure 4.2A). Some parts of the mineralised ore body are also strongly brecciated. Much of the ore in the breccias appears as angular mineralised fragments (Figure 4.2C). Early sulphides and carbonate veins are broken, rotated and transported as mineralised clasts that may be cemented by younger sulphides. Massive sulphide ore is found in replacement zones of the carbonate host rocks and is dominated by pyrite, sphalerite and galena, together with variable amounts of arsenopyrite and chalcopyrite. Quartz, dolomites and ankerites are the main hydrothermal gangue minerals.

A wide variety of ore textures have been recognised in the GII ore body, including: early breccia formation (Figure 4.3A), open-space filling of small fractures and vugs (Figure 4.3B), typical massive replacement ore (Figure 4.3C-E) and fractured and cataclastic ore (Figure 4.3F). Small cavity-fillings are characterised by concentric deposition of sulphides, quartz and carbonates. However, these cavities are only up to tens of centimetres in size and confined to the breccias (Figure 4.3B). No infilling of karst cavities, typical for Mississippi-type carbonate replacement deposits have been observed. A banded style of mineralisation (Figure 4.3D) occurs only sporadically, and it does not represent a typical ore texture in the Belo Brdo deposit. It is believed that banded style of mineralisation is confined to the Triassic metasedimentary sequence. Although massive monomineralic aggregates of sphalerite and galena ore are known and occur as large, probably recrystallised ore with the grain size locally increased to the multi-centimetre level, most of the ores are predominantly polymineralic granular aggregates (Figure 4.3C-E). The ore bodies are associated with zones of intense hydrothermal alteration controlled by syn-tectonic faults (Figure 4.4B-D). Such zones are also characterised by minor stockwork and veinlet types of mineralisation. These sub-economic styles of mineralisation occur peripheral to the main ore bodies. Stockwork structures consisting of quartz-carbonate and quartz-tourmaline veins have been recognised at the contact of serpentinites with limestones and/or andesitic volcaniclastic rocks, at the margins of GII ore body, whilst small pyrite and galena veinlets cross-cut hydrothermally altered andesitic volcaniclastic rocks at level 1235.

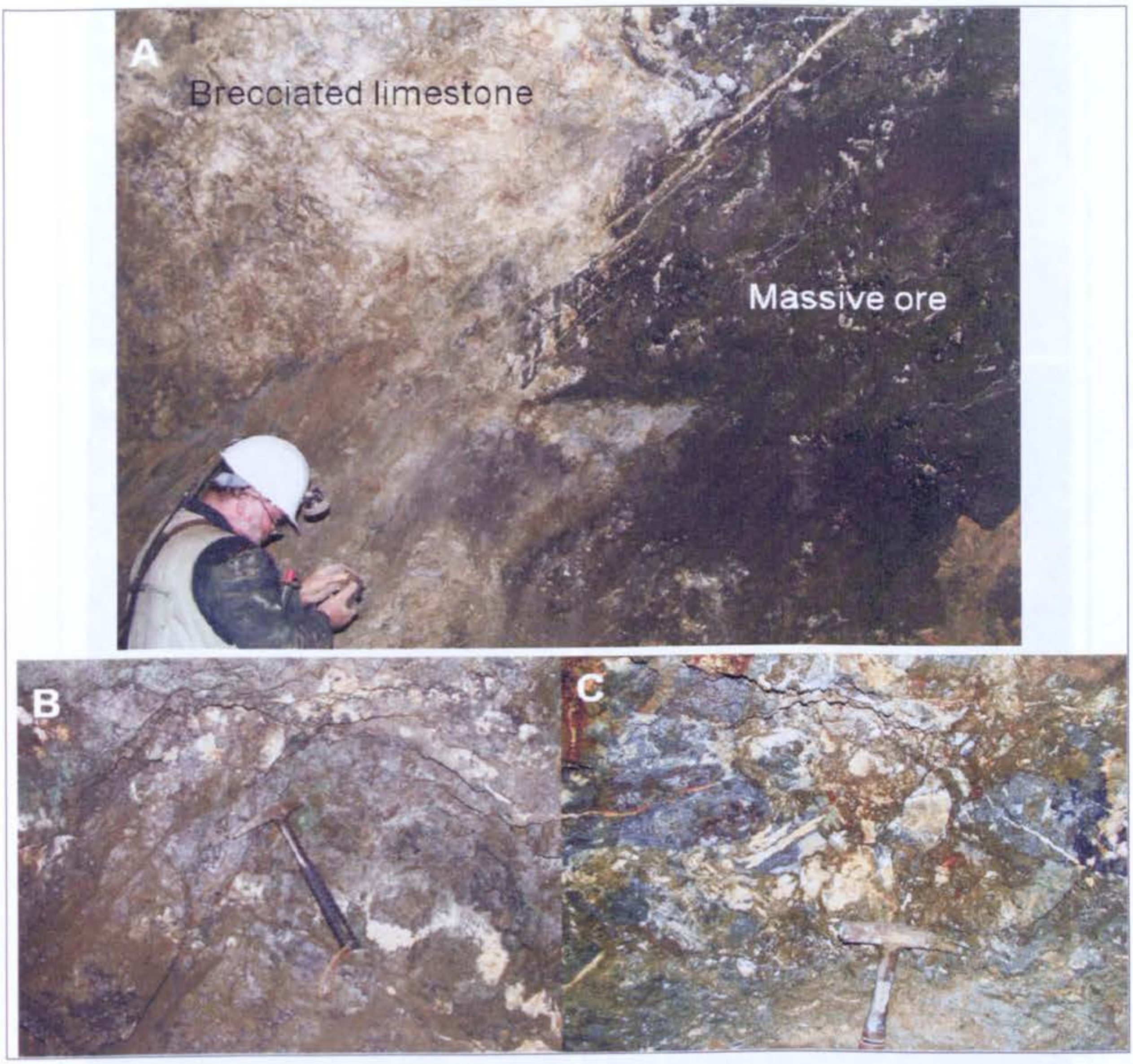

**Figure 4.2:** Underground exposure of the GII ore body. A) Massive sulphides (galena and sphalerite) replacing brecciated limestones; late stage carbonate veins cutting mineralisation; level 1055. B) Massive sulphide ore with only relicts of brecciated carbonates and discontinuous veins; level 1105. C) Breccia ore-"pebble type" containing angular carbonate rock fragments and mineralised fragments cemented by sulphide mineralisation; level 1055.

Two main types of *breccia* have been recognised in Belo Brdo namely "pebble type" and hydrothermal fluidised breccia. The late mineral "pebble type"(Figure 4.2C), often found in Cu porphyry deposits (Sillitoe, 1985) represents irregular mineralised bodies of up to 2m in size. They are composed of angular and semi-angular rock fragments, as well as mineralised fragments cemented by later sulphide mineralisation indicating late mineralisation stage.

Hydrothermal fluidised breccia is of pre-mineralisation age. Polygenetic breccias filling fractures have been observed on 1055 level (Figure 4.4 E) and 1130 sub-level. The thorough mixing of fragments of different origins cemented by hydrothermal phases indicates transport by fluidisation (McCallum, 1985).

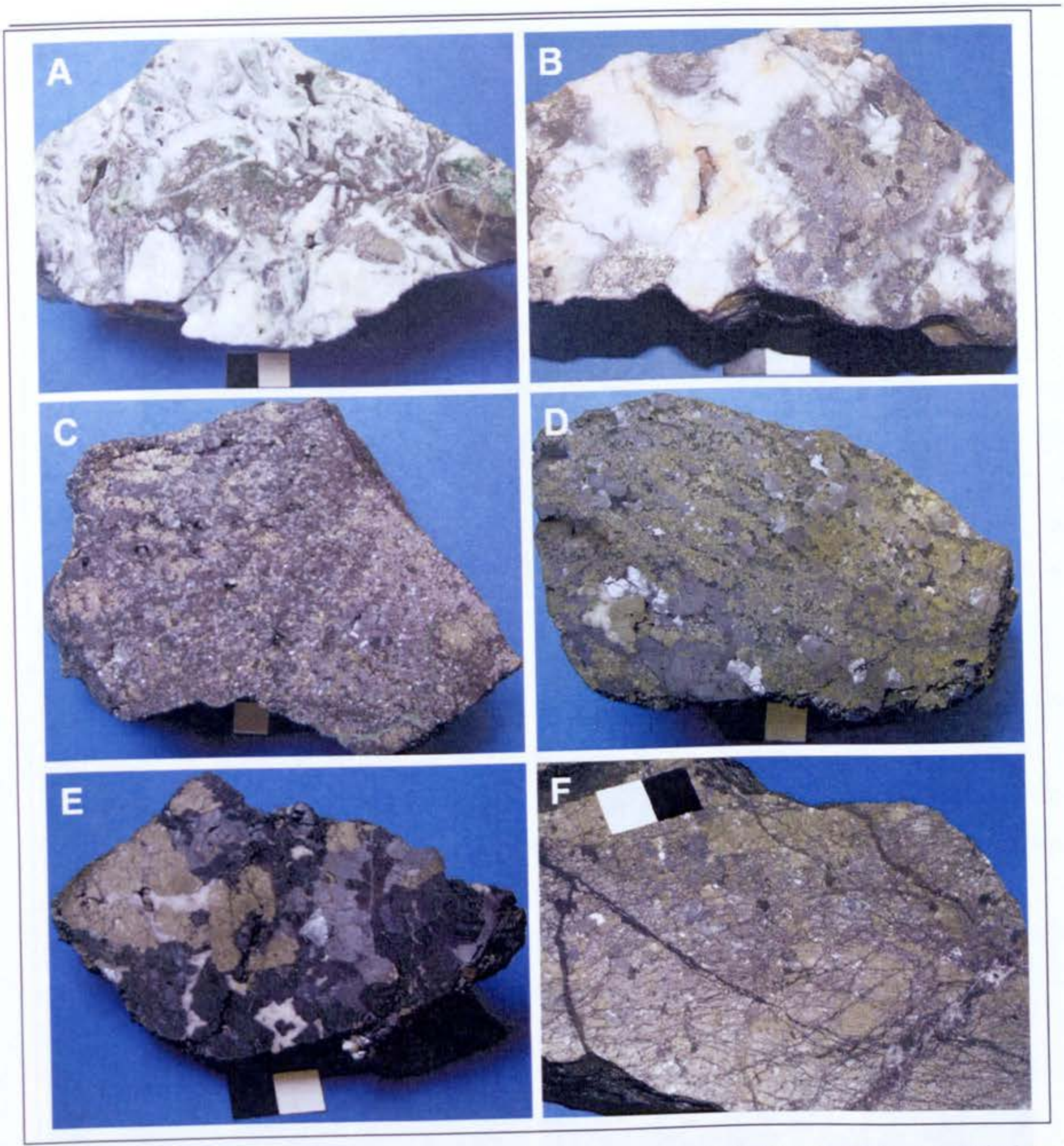

**Figure 4.3:** Macro-scale ore textures characteristic for the replacement-type ore body. A) Early breccia formation with rounded clasts of mineralised (listwanite) and non-mineralised fragments of host rocks, cemented by hydrothermal-stage ankeritic dolomite, sample 1055/1B; B) Small cavity filling and colloform texture consisting mainly of pyrite and galena with minor sphalerite, followed by deposition of post-mineralised dolomite; note cross-cutting quartz-carbonate veins, sample 1055/4D; C) Massive sulphide texture of evenly distributed, granular ore comprised of sphalerite (dark grey), galena (medium grey) and aggregates of fine-grained pyrite (brass yellow); the grain size of the ore minerals is on the order of 2-5 mm, sample 1080/1; D) Banded coarse-grained granulated pyrite (brass yellow) and galena (grey) followed by quartz and dolomite gangue minerals, the grain size of the ore minerals vary from of 2-3 mm in finer bands, to 2 cm in coarser bands, sample 1080/3. E) Coarse- grained massive sphalerite-dominant mineralisation; pyrite has been replaced by galena and sphalerite, sample 1105/4; F) Fractured, cataclastic pyrite-arsenopyrite ore cemented by quartz, sample 1055/6.

### *4.3.2 Vein-type mineralisation*

The GII/12 ore body (Figure 4.4 A) is hosted by Tertiary andesitic rocks. It consists of a NE-SW trending quartz-carbonate-sulphide vein 1-2 m thick, with a strike length of 400 m. There is no evidence thus far to suggest that the vein ore body crosscuts the GII ore body at any underground

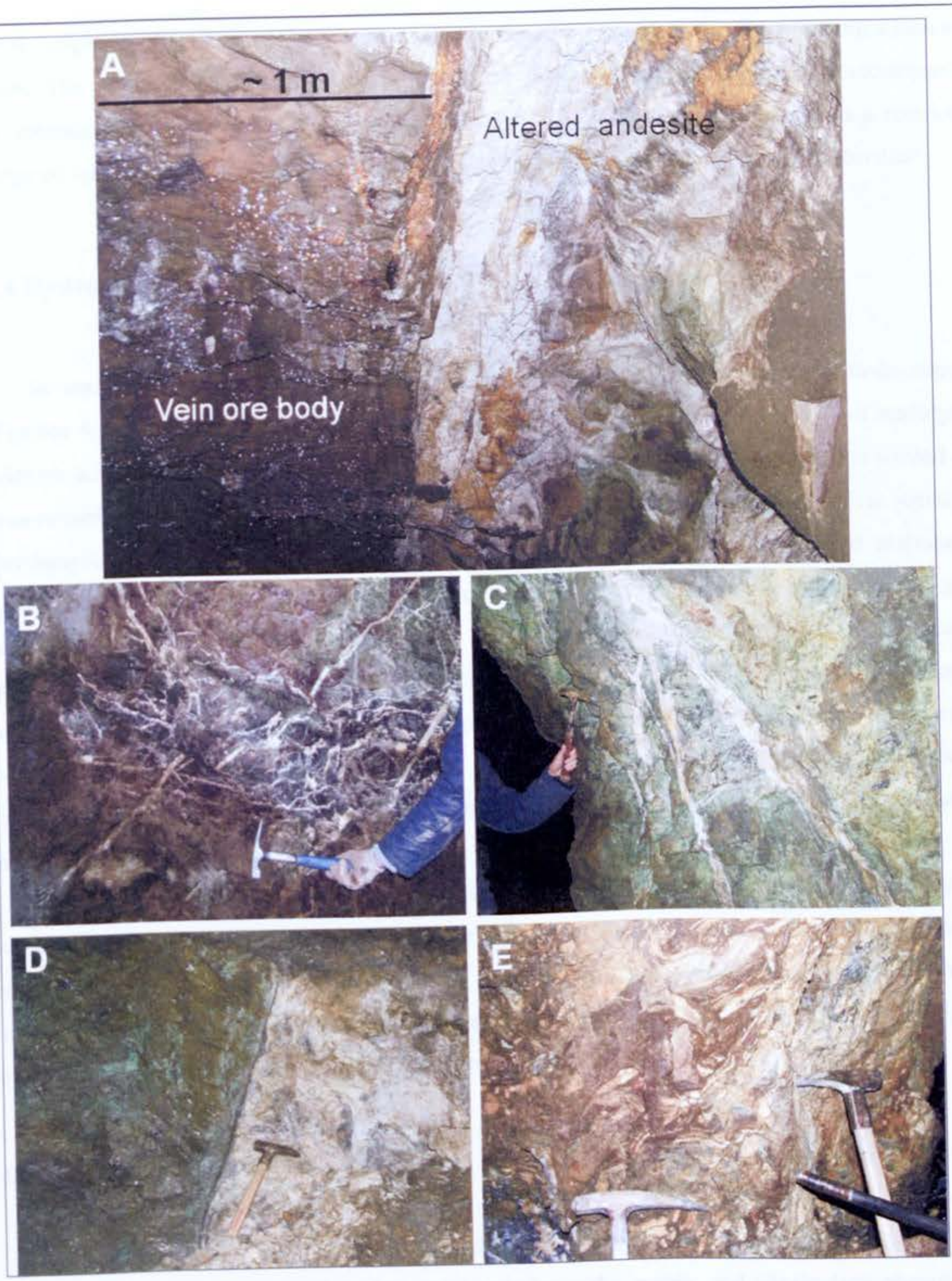

**Figure 4.4:** Underground exposure of vein-type GII/12 ore body (A); and structurally controlled (B-D) and brecciated GII ore body. A) Vein-type ore body hosted by pervasively altered andesites; level 1235; B) Stockwork zone comprised of at least three generations of quartz-carbonate veins developed at contact of serpentinites and carbonates; thicknesses of veins vary from a mm to 3 cm in size; folded, thinner veinlets represent an earlier generation than the thicker, steeper dipping quartz-carbonate veins; note several faults post-dating quartz-carbonate vein network; level 1055; C) Stockwork of quartz-carbonate veins; the thickness of veins varies from few mm to 12 cm; the quartz-tourmaline breccia zone developed in the central part of a stockwork; level 1055; D) Listwanite mineralisation (green) associated with a fault zone, which developed at the contact of andesitic dyke (right) with a bedded sedimentary sequence (far right and top right) and serpentinites (left); level 1080; E) Hydrothermal breccia consisting of three types of clasts: elongated fragments of silicified grey limestone; sub-rounded clasts of less altered laminar limestones; and yellow-brown broken ankeritic veins, cemented by sulphides; the variable orientation of the laminar texture in limestone fragments indicate that the fragments have been moved relative to each other; level 1055.

level. Sulphide minerals occur within the quartz-carbonate vein material as fine disseminations and blebs. The essential ore mineral assemblage consists of galena, sphalerite and pyrite, accompanied by arsenopyrite, minor chalcopyrite, stibnite and barite. The mineralisation exhibits a restricted range of open space filling textures including rhythmic banding, crustification and brecciation.

## 4.4 Hydrothermal alteration of host rocks

Several styles of hydrothermal alteration have been recognised in the Belo Brdo deposit (Figures 4.5 - 4.9). The Tertiary volcanic rocks in and around Belo Brdo mine have undergone widespread propylitic alteration (Figure 4.5A and B) that extends hundreds of metres around the mineralised ore bodies. It is characterised by chlorite, epidote, carbonate and magnetite replacing ferromagnesian minerals, whilst feldspars have been partially altered to sericite and carbonates. Such an alteration type is usually found in the outer zones of copper porphyry and epithermal gold deposits (Corbett and Leach, 1998). The preliminary formation temperature of chlorite (Cathelineau, 1988) from one propylitised sample was estimated at ~260°C. The data is presented in Appendix 2. Intermediate argillic alteration (also known in older literature as argillic) of volcanic rocks occurs in the marginal parts of the mineralised area. It consists of a clay- sericite-carbonate assemblage which replaces plagioclase to various degrees (Figure 4.5C). Mafic minerals are replaced by chlorite and clay minerals.

Before the deposition of the main mineralisation stage at Belo Brdo, the rocks in the deposit were subjected to intensive hydrothermal alteration which developed at the contact of the andesitic rocks and serpentinites and at the contact of the igneous rocks with carbonates adjacent to the mineralised ore bodies. Several styles of intense hydrothermal alteration have been distinguished including: sericitisation, quartz-tourmaline alteration and listwanisation.

### *4.4.1 Sericitic (phyllic) alteration*

This is the most common form of hydrothermal alteration of the andesitic rocks at Belo Brdo deposit. In andesitic wall rocks, sericite replaces the matrix and plagioclase phenocrysts (Figure 4.5E). Quartz occurs as a secondary phase in the matrix. Additionally, quartz-tourmaline-pyrite veins crosscut the wall-rock (Figure 4.5F). Carbonates completely replace feldspars (Figure 4.5D). Minor amounts of clay minerals also occur, while pyrite is disseminated throughout the sericitised rocks, as well as associated with quartz-tourmaline veins. SEM analyses of tourmalines reveal their dravite composition (Appendix 2). Rutile is a minor alteration phase, occurring mainly in pseudomorphs after mafic minerals (Figure 4.5A). Slight enrichment in La, Ce and Nd is evident in secondary epidote that occurs as replacement of mafic minerals (Figure 4.5B).

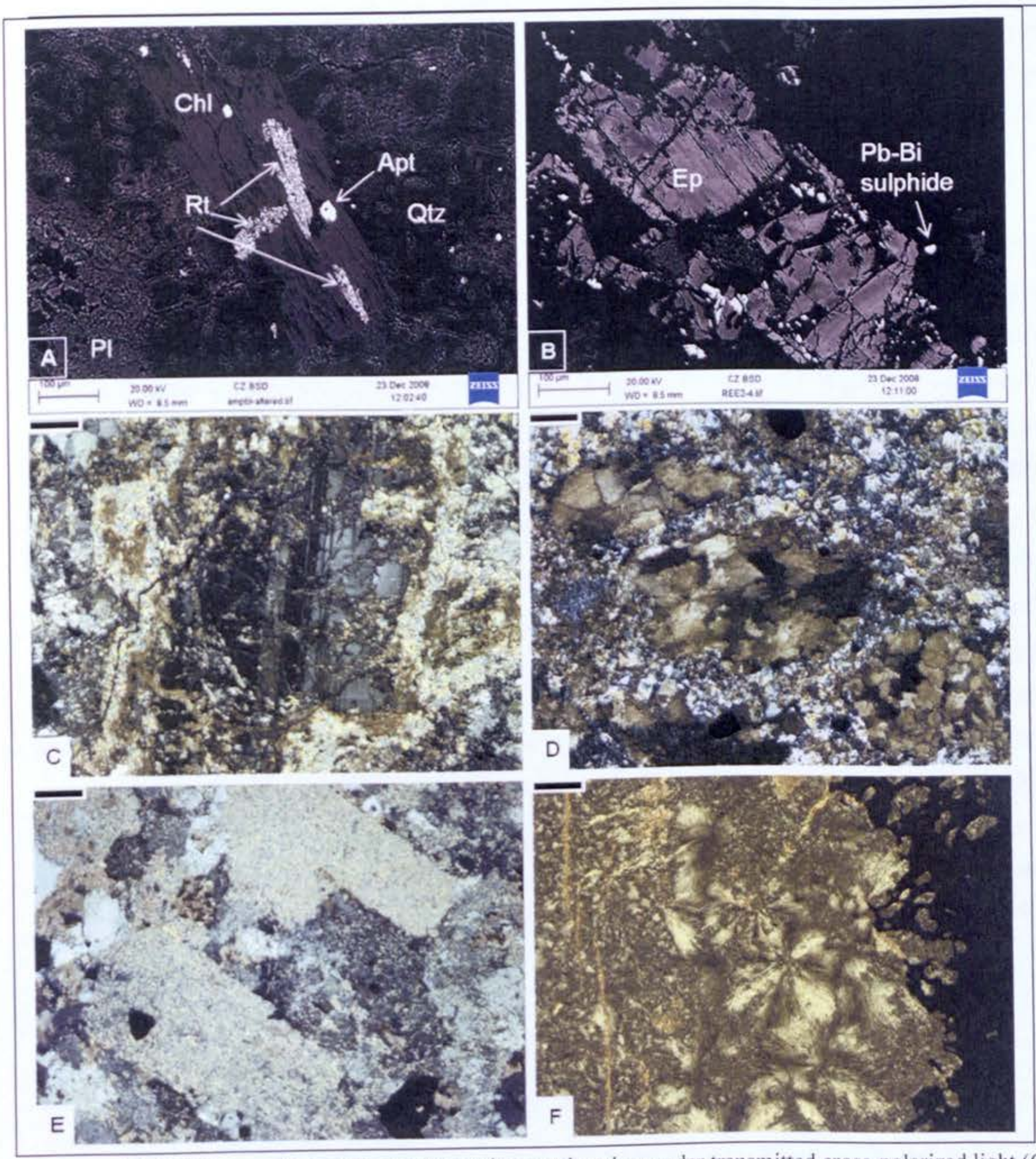

**Figure 4.5:** BSE images (A and B) and photomicrographs taken under transmitted cross-polarized light (C-F) showing hydrothermal alteration of andesitic rocks of the Belo Brdo deposit. A) Propylitic alteration; rutile pseudomorphs after mafic minerals and minor accessory apatite; plagioclase replaced by sericite and carbonates; mafic mineral completely replaced by chlorite (sample 1105/5); B) Epidotisation of mafic minerals and dissemination of Pb-Bi sulphides (sample 1105/5); C) Intermediate argillic alteration; sericite and clay minerals partially replace plagioclase; the matrix is composed of chlorite and quartz (sample 1235/7D); D) Carbonatisation of plagioclase phenocrysts in silicified and sericitised matrix (sample 180/3A); E) Complete sericitisation of plagioclase and silicification of the matrix (sample 1105/2A); F) Quartz-tourmaline veins with associated pyritisation (black right), cross-cutting the wall-rock; acicular tourmaline; note late carbonate veinlets cross-cuting the altered rocks (sample 180/3C); bar=100 microns (A and B) and 200microns (C-F).

Chemical analyses of altered andesites (Appendix 3) show enrichment of Si and K and general depletions of Na, Ca, Mn and Fe relative to fresh andesites due to the presence of secondary mineral phases. The addition of Si is consistent with the widespread silicification, which is a major feature of phyllic alteration. Evident enrichments in K, Rb, and volatiles (lower totals due to added water) and depletions in Na, Mg, and Sr, point to the replacement of plagioclase and amphibole by

K- feldspar and K- mica respectively. Variable additions of Cu, Pb and Fe indicate the presence of sulphides (chalcopyrite, galena, and pyrite), whereas the inconsistent enrichment of Ca and to a lesser extent Mg and Mn are related to the presence of secondary carbonates (Figure 4.5D).

### *4.4.2 Quartz-tourmaline alteration*

Apart from quartz-tourmaline veins cross-cutting the andesitic volcanic rocks (level 1080), a pervasive quartz-tourmaline alteration of the wall-rocks and the formation of quartz-tourmaline breccia (Figure 4.6A-E) has been observed at the fault zone marked by steeply dipping quartz-carbonate veins and stockwork on level 1055 (Figure 4.4 C).The wall-rock was previously described in the local literature as a skarn (Mladenović, Pers. Com.). However, in our investigation, no skarn mineralogy was observed at this level. The alteration assemblage is represented by Cr-bearing tourmaline ($Cr_2O_3$ contents up to 9%), quartz, carbonates (ferroan and manganoan dolomite), Cr-mica (fuchsite, with $Cr_2O_3$ contents up to 9%), and minor rutile and apatite. Tourmaline commonly occurs as rosettes and clusters as fillings in vesicles or drusy cavities and as small prisms disseminated in the matrix. SEM analyses were carried out on tourmaline, carbonates and mica (Appendix 2). Tourmaline often exhibits oscillatory zoning (Figure 4.6B) that range in composition from schorl to dravite and rarely from dravite to uvite The composition of Cr-bearing tourmalines is most likely influenced by the composition of the host rocks (source of Mg, Fe, Ca and Cr) and the nature of the hydrothermal fluid (Si, Al, and B). The type of carbonate alteration reflects the ferromagnesian content of the primary host lithology. Additionally, the presence of Cr-spinel, Cr-bearing tourmaline and Cr-mica indicate the ultramafic nature of the host rock. The altered rock is cut by younger dolomitic veinlets.

### *4.4.3 Listwanisation (carbonatisation of ultramafic rocks)*

Listwanite (listvenite, listwaenite) is a term introduced by Soviet geologists to describe the type locality at Beresovsk in the Ural Mountains of central Russia (Goncharenko, 1970; Kuleshevich, 1984). It describes a mineralogical assemblage that results from the carbonatisation of serpentinised ultramafic rocks and represents a distinctive alteration suite that is commonly associated with quartz-carbonate lode gold deposits (Hall and Zhao, 1995; Ash, 2001).

At Belo Brdo, high degrees of alteration occur along high-angle fracture zones (Figure 4.4 B-D), which served as high permeability pathways for percolation of hydrothermal fluids. A halo of carbonate alteration extends for tens of metres into wall-rock adjacent to the controlling fracture. The intensity of alteration locally ranges from minor quartz-carbonate (±Fe, ±Mn dolomite) veining and stockwork (Figure 4.7A) to pervasive alteration resulting in completely replaced ultramafic rock (Figure 4.7C) composed primarily of carbonates, quartz, Cr-mica and pyrite. The predominant carbonate phase is dolomite with variable contents of iron (up to 14% Fe) and

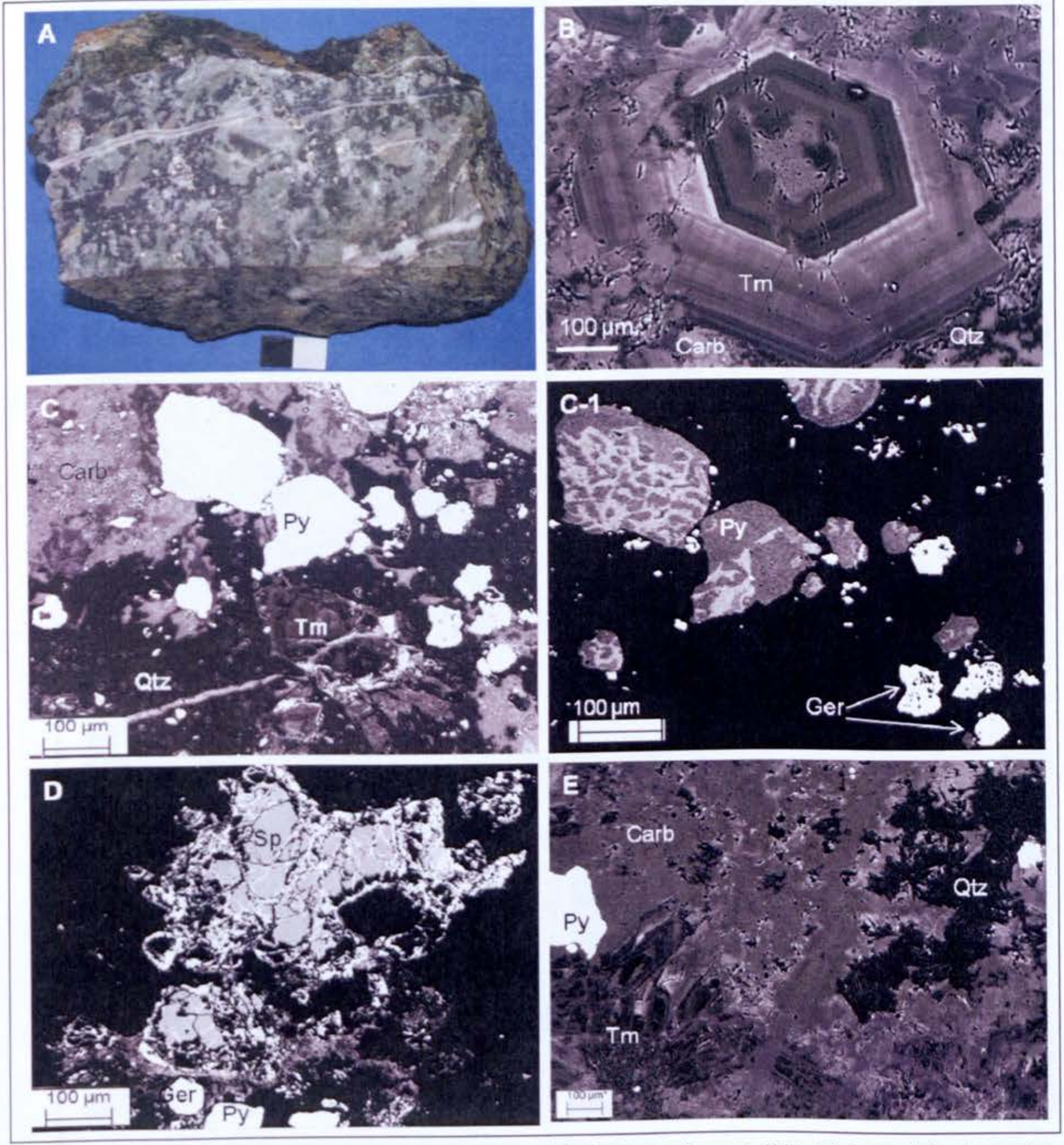

**Figure 4.6:** Quartz-tourmaline alteration of carbonitised ultramafic protolith. A) Lapped hand specimen showing quartz-tourmaline breccia, consisting of fragments of carbonate-silica rock, cemented by later quartz and tourmaline; note sulphide mineralisation (pyrite, arsenopyrite and Bi-bearing galena associated with quartz-tourmaline cement (also shown in C); also late stage quartz-carbonate veinlets crosscutting the quartz-tourmaline breccia; scale=2 cm; B) BSE image of coarser, concentrically zoned early tourmaline affected and corroded by younger quartz-tourmaline phase; the concentric dark core is of dravite-uvite composition and the lighter concentric rims are dravite-schorl. C and C-1) BSE images showing sulphide mineralisation (pyrite and gersdorffite) associated with quartz-tourmaline alteration of carbonitised ultramafic rock; note irregular zoning of Ni-bearing pyrite shown in C-1. D) BSE image of Cr spinel transferring into Zn-bearing spinel along fractures in carbonitised ultramafic rock affected by quartz-tourmaline alteration; E) Carbonatised ultramafic breccia cemented by tourmaline and quartz, followed by sulphides; prismatic growth of tourmaline filling the void; late ferroan dolomite vein cross-cutting the rock.

manganese (up to 4% Mn). Cr- chlorite, Cr-spinel, magnetite, serpentine and talc occur as accessory minerals. Variability in Fe, Mn, Ca and Mg contents of carbonates possibly reflects the composition of primary silicate phases, as well as multiple hydrothermal pulsations. The listwanites are often intensely brecciated (Figure 4.8A). If the carbonatisation is complete, the primary silicate

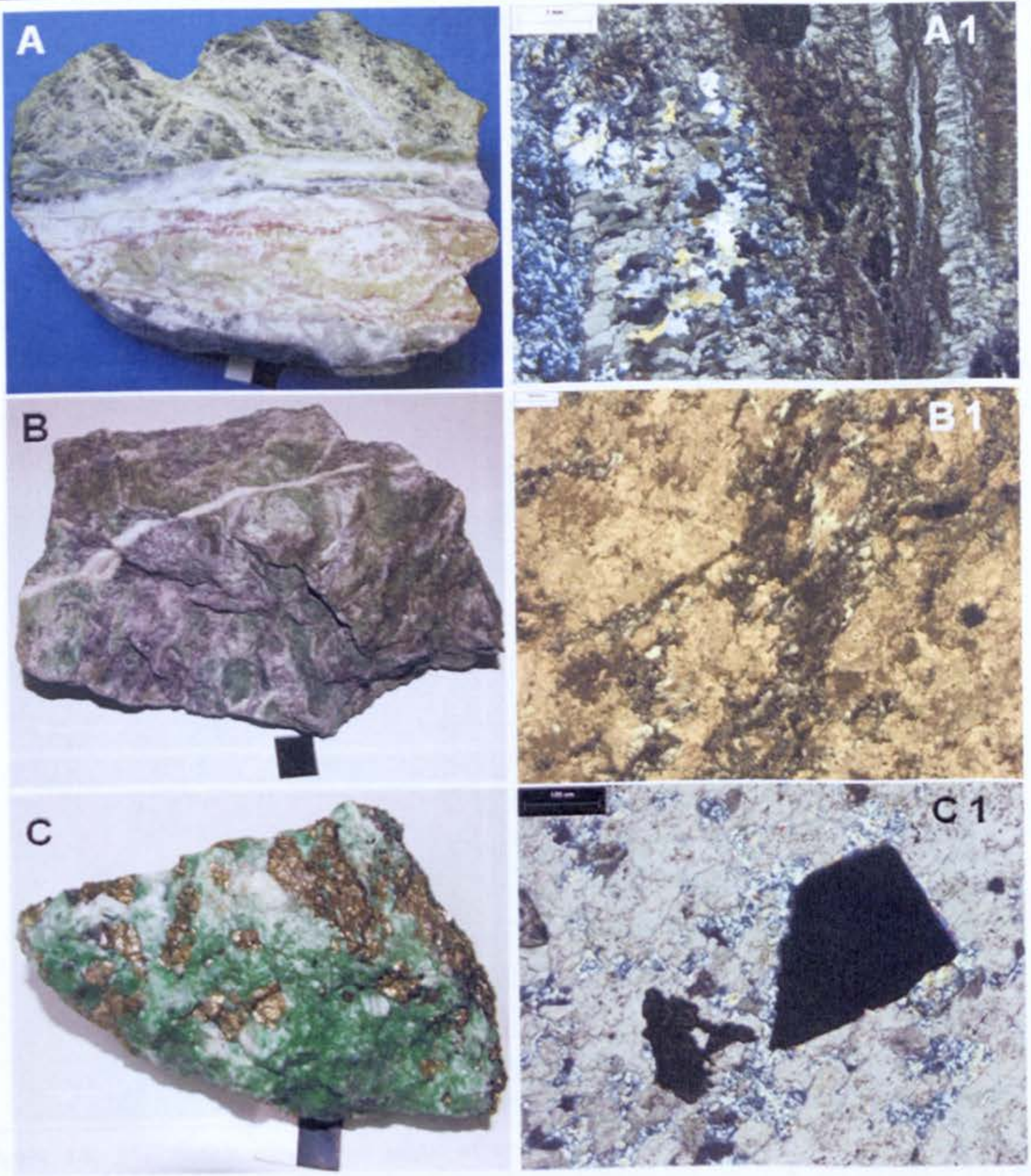

**Figure 4.7:** Hand specimens (A-C) and photomicrographs (A1-C1) taken under transmitted cross-polarized light, showing various degrees of alteration of ultramafic rocks and the formation of listwanite rocks. A) early quartz- (Mg, Fe) carbonate stockwork developed in a highly altered ultramafic rock cross-cut by later quartz-carbonate vein (sample 1005/6); A1) Same rock in thin section; the early generation of carbonates have psuedomorphed the original fabric of the schistose serpentinite; disseminated pyrite grains associated with later quartz-carbonate veins; scale 1mm; B) Poorly- mineralised listwanite breccia cross-cut by late dolomitic veins; this rock-type was mapped as limestone by local workers (sample 1055/1C); B1) Relicts of serpentine minerals in carbonate rock, indicating their ultramafic origin; scale 200μm; C) Massive mineralised listwanite with a distinctive green colour derived from abundant Cr-micas; it is composed of carbonates (dolomite-ankerite, roughly 60 vol.% of the rock), quartz (15 vol.% ), Cr-micas (10 vol.% ) and sulphides (pyrite >> arsenopyrite > gersdorffite, 15 vol.% ) (sample 1055/T2). C1) Euhedral - to subhedral arsenopyrite grain associated with quartz- fuchsite- Cr-chlorite alteration assemblage; scale 100 μm.

minerals of the ultramafic rocks are not recognisable and only Cr-spinel relicts are seen to be resistant to chemical changes during alteration processes (Figure 4.8B). Hydrothermal dolomite is

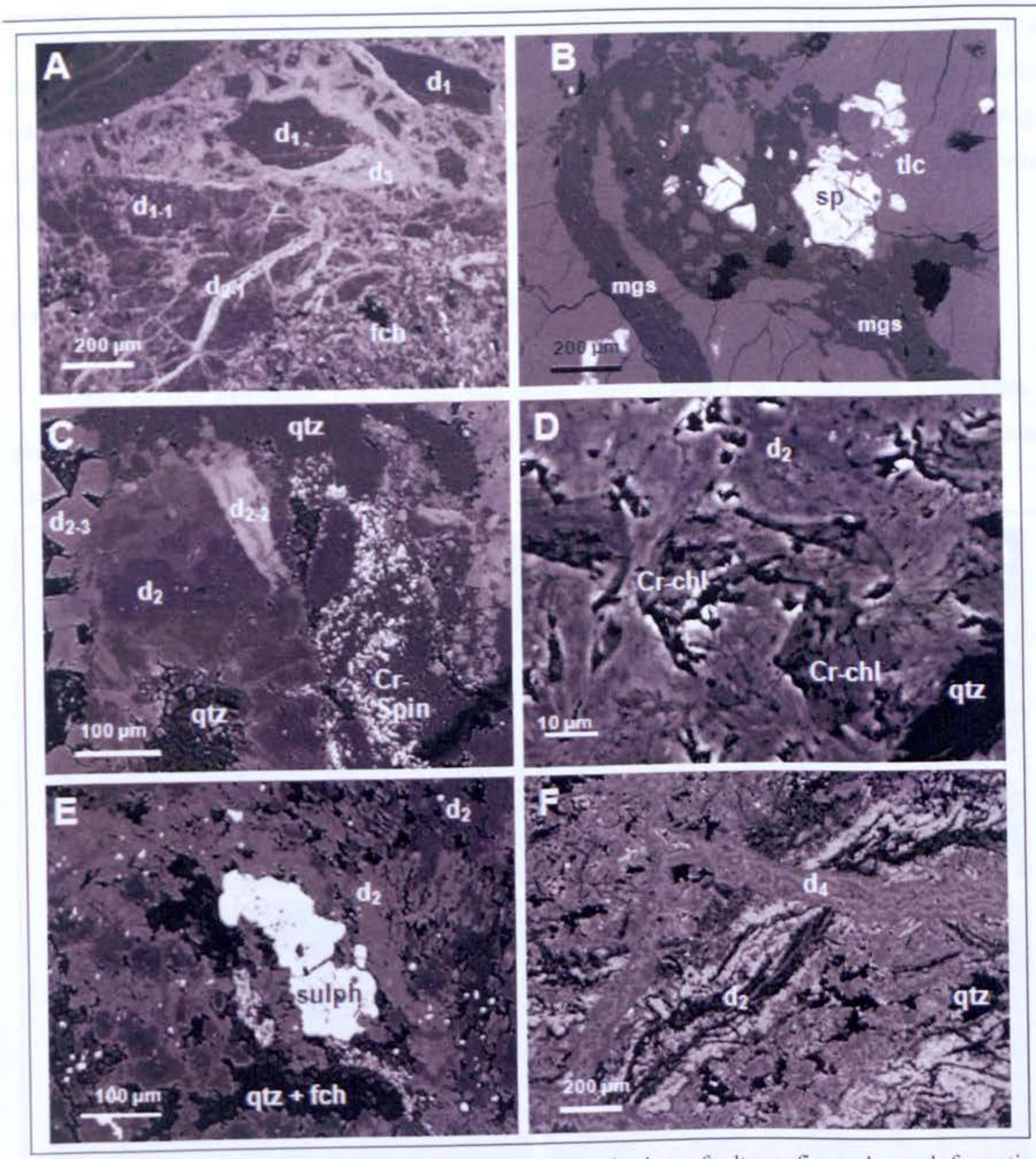

**Figure 4.8:** BSE images of different stages of carbonatisation of ultramafic rocks and formation of listwanites. A) Listwanite breccia consisting of angular fragments of unmineralised host carbonates ($d_1$) and fragments of carbonate breccias ($d_2$) intensively crosscut by different generations of iron-rich carbonate veins ($_{d1-2}$), cemented by hydrothermal ankerites ($_{d3-1}$); disseminated sulphides are associated with fuchsite (fch) and quartz (sample 1055/1C); B) Altered ultramafic rock consisting of relicts of primary Cr-spinel (sp), magnesite veins (mgs), replacing most likely serpentine veins and talc (tlc) after orthopyroxenes (sample 1105/2B); C) Pervasive carbonatisation ($d_2$) replacing original ultramafic rock, evident by relicts of Cr-micas and Cr-chlorites; note different tones of grey colour in carbonates, reflecting different contents of Fe and Mg; also, euhedral dolomitic rhombs (lighter grey) growing in an open space; late quartz-Cr-mica alteration filling cavities (sample 1055/1C/new); D) "flaky" Cr-chlorite and pervasive carbonate alteration ($d_2$) (sample 1055/2B); E). The first appearance of Fe- and Ni-As sulphides replacing early hydrothermal dolomites ($d_2$); the sulphides are associated with microcrystalline quartz and Cr-mica (sample 1055/1C); F) Massive listwanite formed as a result of pervasive alteration of ultramafic rock, evident by carbonate ($d_2$) textures, clearly replacing fibrous-textured serpentinites; also shown are the late-stage carbonate veins ($d_4$) crosscutting massive listwanite (sample 1105/3B).

often crystallised as euhedral vugs precipitates within the veins (Figure 4.8C). Trace amounts of subhedral apatite is also present in listwanites. Besides carbonates and quartz, fuchsite is the next most common secondary mineral and occurs with quartz (Figure 4.8E), mainly as vein-filling minerals. Sulphides are often found associated with those veins (Figure 4.8E), or to a lesser extent disseminated throughout the rock. Green Cr-bearing chlorite has been observed in veins, fractures, vugs, and breccia matrix and shows usually an anhedral platy form and fibrous clusters (Figure 4.8D). SEM analyses were carried out on carbonates, mica and chlorite (Appendix 2). Chlorite is classified as pycnochlorite and diabantite.

### *4.4.4 Silicification and dolomitisation of limestones*

Most of the carbonate host rocks that have been mapped as Cretaceous limestones by geologists in the Belo Brdo mine and sampled for this study proved to be carbonatised ultramafic rocks, known as listwanites. Only fragments of dolomitised limestones (Figure 4.9) that form the parts of tectonic breccias found in fault zones within the underground mine have been observed in this study. The fragments show that pervasive dolomitisation and silicification of the limestone host rock resulted in silicified dolomites that generally destroyed fossils and original textures. Locally, some unrecognizable fossil relicts, which have been replaced by dolomite, still

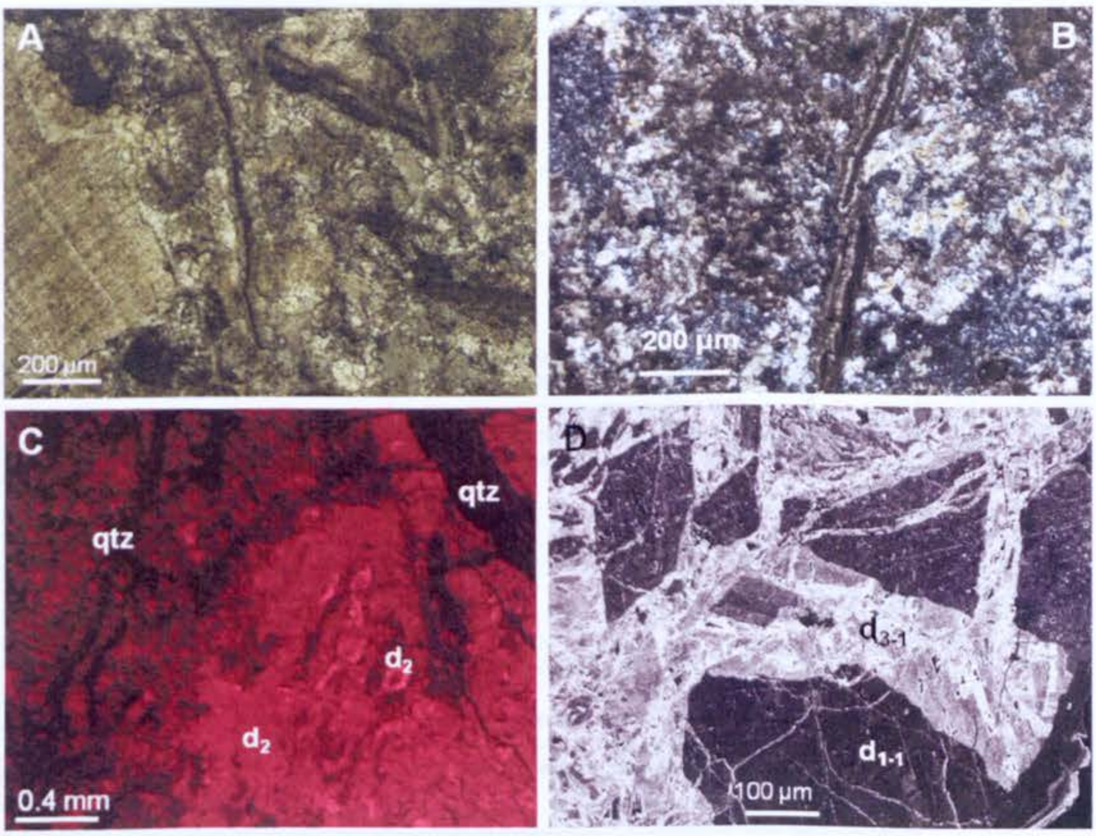

**Figure 4.9:** Photomicrographs taken under transmitted cross-polarized light (A and B); CT image (C) and BSE image (D) of Cretaceous limestones. A) Non-mineralised fossiliferous reef-limestones (sample LIM-1); B) Pervasive silicification of carbonates and relict of unknown fossils preserved (sample 180/3A); C) Fragments of brecciated dolomitised ($d_2$) limestones, resulting in a complete destruction of original textures; note quartz veins crosscutting the altered wall rock (sample 1055/1C); D) Angular fragments of dolomite breccia ($d_{1-1}$) cemented by later hydrothermal ankerites ($d_{3-1}$) (sample 1055/1A).

retain some indications of their original shape (Figure 4.9B). Dolomite developed after the porosity of limestones was enhanced by fluid circulation through fractures (Figure 4.9C and D).

## 4.5 Ore Petrography and Paragenesis

Detailed studies of the textural and mineralogical relations within the deposit have revealed a complex multistage paragenesis, which can be broadly classified into three major stages: (1) pre-ore stage, (2) main-ore stage, which has been subdivided into early and late sub-stages and (3) post-ore stage (Figure 4.10).

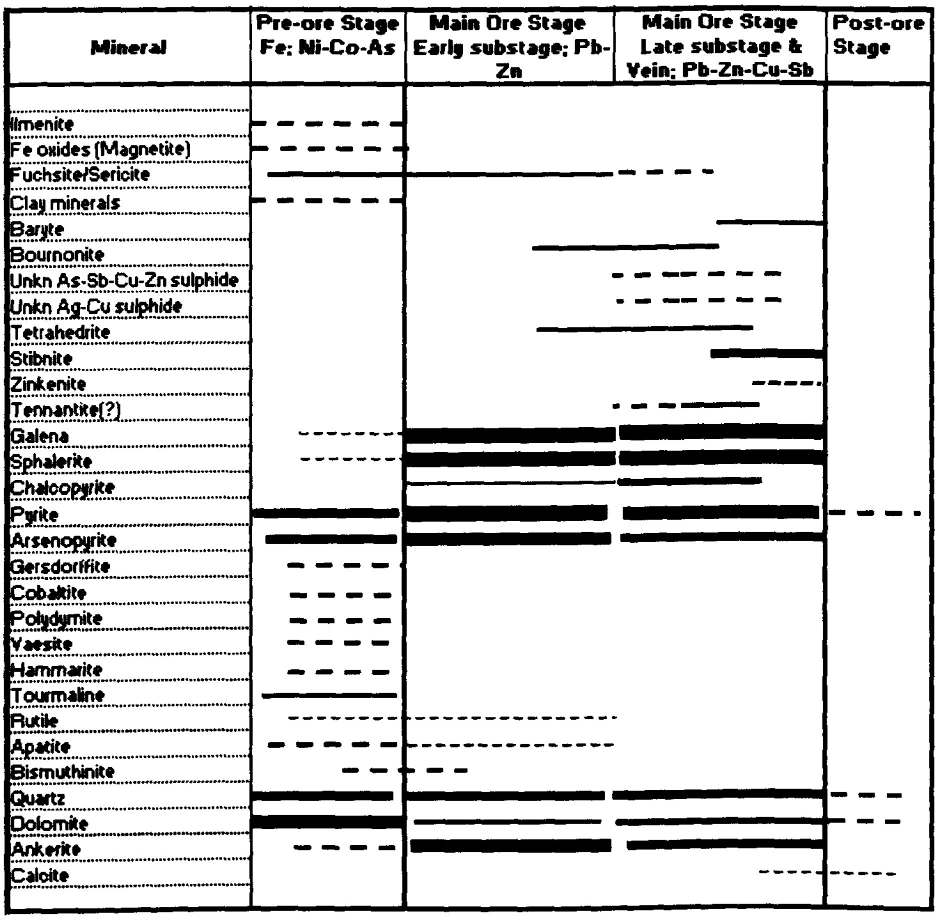

**Figure 4.10:** Simplified paragenetic sequences for the assemblages of principal ore and alteration minerals at the Belo Brdo deposit. Line thickness represents schematically the relative abundances of the mineral deposited.

Several criteria were used in determining mineral relationships and relative ages of minerals in polished sections, namely pseudomorphs, relict structures, non-matching walls of fractures, overgrowth, irregular borders, cross-cutting relationships and crystal forms (Stanton, 1972; Ramdohr, 1980; Guilbert and Park, 1986; Craig and Vaughan 1994; Ixer and Duller, 1998; Marshall, et all. 2004;). Ore textures in the Belo Brdo deposit indicate that replacement is the dominant process in the formation of sulphide mineralisation. Besides the minerals of the host rocks and the early hydrothermal dolomites, replacement has also affected the earlier formed ore minerals. The resulting textures are varied and described below.

### 4.5.1 Pre-ore stage

The early hydrothermal stage corresponds to a locally dense network of irregular carbonate veining. Several generations of crosscutting carbonate veins indicate repeated fracturing of the host rocks. The carbonate veining, as well as pervasive carbonatisation of ultramafic rocks resulted in formation of listwanites, as described in section 4.4.3 The veining was followed by brecciation of listwanites and brecciation and dolomitisation of the hanging wall limestones. Both, the listwanisation and dolomitisation could be interpreted to have formed contemporaneously during the same hydrothermal alteration (see section 4.7) prior to mineralisation. During the pre-ore stage, quartz-tourmaline veins and breccias also formed, as described in section 4.4.2. The pre-ore stage does not carry economic concentrations of sulphide mineralisation. However, it is an important stage in terms of preparing the ground for later deposition of massive sulphide ore and hosting a sulphide mineralogy that indicates magmatic signatures of the mineralising fluids.

Dissemination (Figure 4.11) is the predominant ore texture of early sulphide mineralisation. Pyrite is the most abundant ore mineral of the pre-stage. Fine grained disseminated pyrite ($py_1$) formed synchronously with the formation of massive listwanites, as well as veining and silicification of limestones. This early generation of pyrite displays mainly euhedral shapes and no zonation (Figure 4.11 A). Subhedral pyrite is found in quartz-pyrite veinlets cross-cutting the serpentinised ultramafic rocks and quartz-tourmaline veins cutting the andesitic wall rock (see Figure 4.5 F). Further brecciation and silicification of listwanites, as well as formation of quartz-tourmaline breccias was followed by the precipitation of compositionally zoned Ni-Co bearing pyrite ($py_2$) (Figure 4.11B) and arsenopyrite ($apy_1$) (Figure 4.11C), as well as Ni-Co-As-bearing sulphides (Figure 4.11D-F and also 4.6C and C-1), such as gersdorffite $(Ni_{0.71}Fe_{0.23}Co_{0.07})_{\Sigma 1.01}(As_{0.95}Sb_{0.01}Zn_{0.02})_{\Sigma 0.96}S_{1.03}$, cobaltite $[Co_{0.55}Fe_{0.08}Ni_{0.39}]_{\Sigma=1.02}As_{0.94}S_{1.04}$), and minor polydimite ($[Ni_{2.67}Co_{0.08}Fe_{0.19}]_{\Sigma=2.94}As_{0.067}S_4$), vaesite ($[Ni_{0.66}Fe_{0.27}]_{\Sigma 0.93}[As_{0.14}S_{1.93}]_{\Sigma 2.07}$), and krutovite ($[Ni_{0.94}Fe_{0.07}]_{\Sigma 1.01}[As_{1.43}S_{0.56}]_{\Sigma 1.99}$). Pyrite occurs as aggregates of euhedral to subhedral crystals, commonly associated with individual or clustered rhombic grains of early arsenopyrite, which is commonly zoned and sometimes contains inclusions of pyrite (Figure 4.11 B). Pyrite ($py_2$) commonly overgrows gersdorffite and cobaltite (Figure 4.11 D-F).

The Ni-Co-As-bearing sulphides are finely disseminated within the altered host rocks as well as within thin quartz veins, accompanied by fuchsite (Cr-mica) and sericite. Gersdorffite is the predominant Ni sulphide and occurs in several textural forms, namely fine grained euhedral to subhedral grains; anhedral; corroded and embayed. Embayed gersdorffite is occasionally rimmed by small bismuth- and tellurium- bearing lead sulphosalts and galena (Figure 4.11E). Occurrence of

Bi- and Te- bearing minerals, as well as an increased amount of galena indicates the transition to the early main-ore stage (Figure 4.11F). Bismuth- and tellurium-bearing minerals are a common feature in many high- and intermediate-sulphidation epithermal deposits with dominantly magmatic signatures of the mineralising fluids (Kouzmanov et al., 2005).

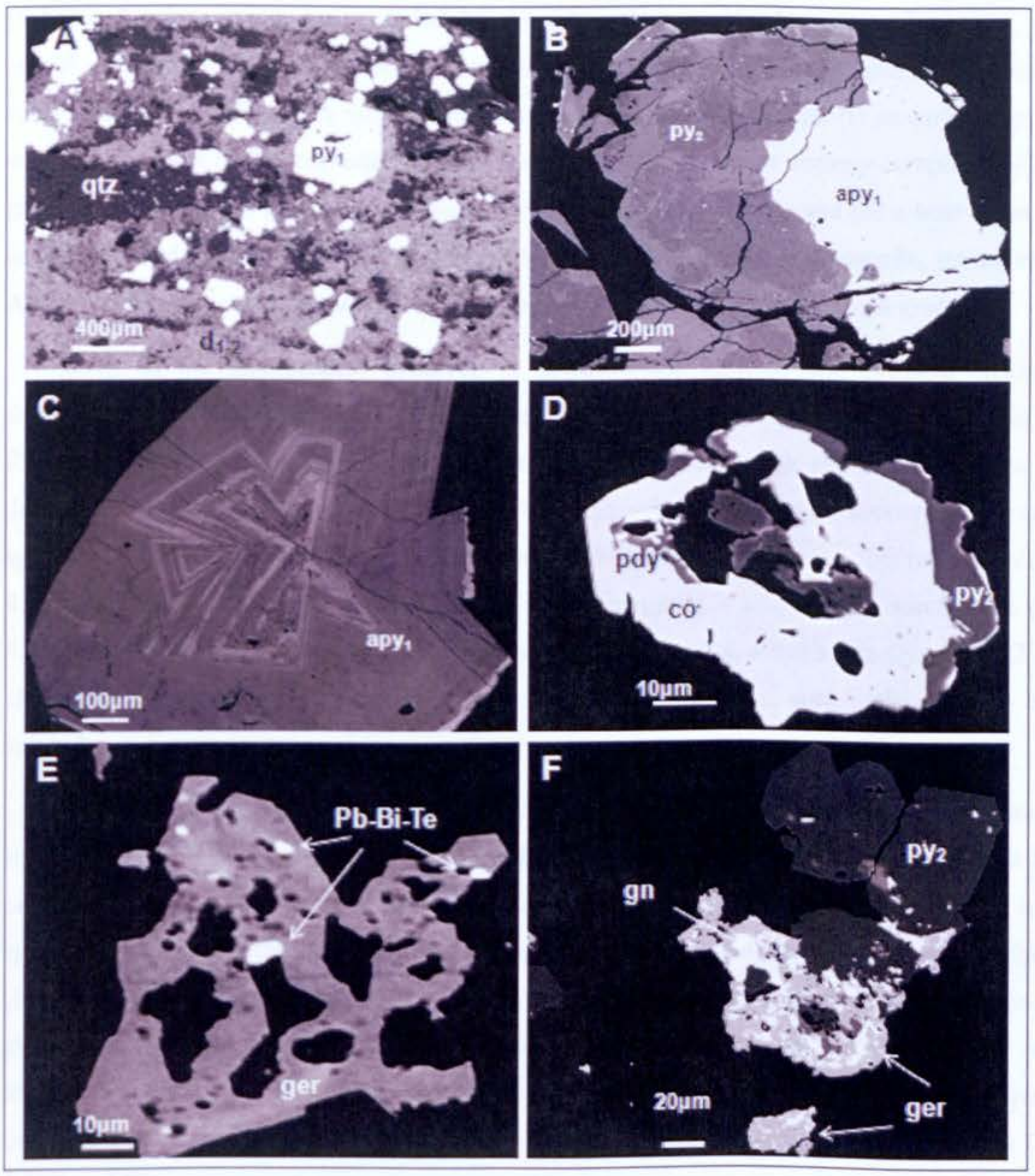

**Figure 4.11:** BSE images of the pre-ore stage sulphide assemblages. A) Early formation of fine-grained (< 1 mm in size) euhedral to subhedral pyrite with no compositional zoning; pyrite is disseminated within the silicified and veined carbonate wall rock (sample 1155/2B); B) Texture indicating coeval crystallisation of second generation of pyrite (py$_2$) and arsenopyrite associated with hydrothermal ankerites and cut by later carbonate veins; pyrite shows irregular compositional zoning with respect to Ni (sample 1055/1A); C) Second generation of euhedral arsenopyrite showing twinning and compositional zoning, (bright zones contain up to 5 wt. % Ni) (sample 1055/1A); D) Subhedral cobaltite with inclusions of early pyrite and gangue minerals; cobaltite is overgrown by younger pyrite (sample 1055/1C); E) Small blebs of Pb-Bi-Te sulphides rimming embayed gersdorffite (1055/2B); F) Euhedral, slightly zoned pyrite replaced by gersdorffite, which in turn has been replaced by galena, sample BB-T2.

### 4.5.2 Main-ore Stage

The poorly mineralised pre-ore stage is succeeded by sulphide and gangue minerals of the main mineralisation event. The dominant ore minerals in this stage are coarse-grained sphalerite ($sph_1$) and galena ($gn_1$), accompanied by As-rich pyrite ($py_3$) and arsenopyrite ($apy_2$), and by significant amounts of chalcopyrite. Cogenetic gangue minerals are quartz, ankerite, dolomite, Cr-mica and chlorite. The main mineralisation stage can be subdivided into (i) an early stage, which accounts for most of the sulphide mineralisation and which is almost entirely composed of coarse-grained sphalerite and galena accompanied by pyrite and arsenopyrite and (ii) a later stage, which is characterised by mixed sulphides (sphalerite, galena, chalcopyrite, arsenopyrite, pyrite, and Cu-, As-, Sb-, Pb- sulphosalts; Appendix 2). The transition between the two stages is gradual.

Many of the relationships observed in polished thin sections and polished blocks were developed by replacement and relatively little evidence of deposition in open spaces was found. Replacement textures are the predominant ore textures in both early and late sub-stages of ore deposition, as depicted in figures 4.12 and 4.13 respectively. The main economic minerals are sphalerite and galena, both occurring intergrown with pyrite ($py_3$) and arsenopyrite ($apy_2$) (Figure 4.12A) or, as co-existing minerals replacing an earlier pyrite – arsenopyrite assemblage (Figure 4.12 B-D). In the early sub-stage of massive sulphide deposition, tetrahedrite (Figure 4.12 E) and chalcopyrite (Figure 4.12 F) are locally present and other sulphides, such as Bi- and Te- bearing sulphides and sulphosalts are observed only in trace amounts.

The later sub-stage of main-ore deposition is marked by the introduction of the epithermal-style mineralisation (Figure 4.13). In the GII ore body this sub-stage is characterised by the presence of the second generation of galena ($gn_2$) (Figure 4.13A), euhedral pyrite, massive sphalerite and introduction of significant amounts of chalcopyrite and Cu-Sb-Pb-As sulphosalts (Figure 4.13B-D), such as Ag-tetrahedrite, Ag- bearing tennantite and bournonite. Chalcopyrite extensively replaces iron-rich sphalerite, which becomes poorer in iron content and is here identified as the second generation of sphalerite ($sph_2$). The iron-poor, third generation of sphalerite ($sph_3$) and second generation of galena ($gn_2$) are often associated with Cu-rich minerals (Figure 4.13B and D).

The economic mineralisation of the GII/12 vein ore body is characterised by the pyrite-galena-sphalerite paragenesis with considerable amount of arsenopyrite (Figure 4.13 E), followed by the deposition of Sb-rich sulphides (Figure 4.13 F), namely stibnite and zinkenite accompanied by quartz, barite and carbonates (dolomites).

Pyrite is present in every sample studied and appears to have been deposited throughout most of the sequence including both the early and late stage of main ore deposition. It forms sub-mm to several mm- sized euhedral crystals, commonly compositionally zoned (Figure 4.14A), or massive granular aggregates weakly anisotropic. Pyrite is often the earliest sulphide precipitate of the early

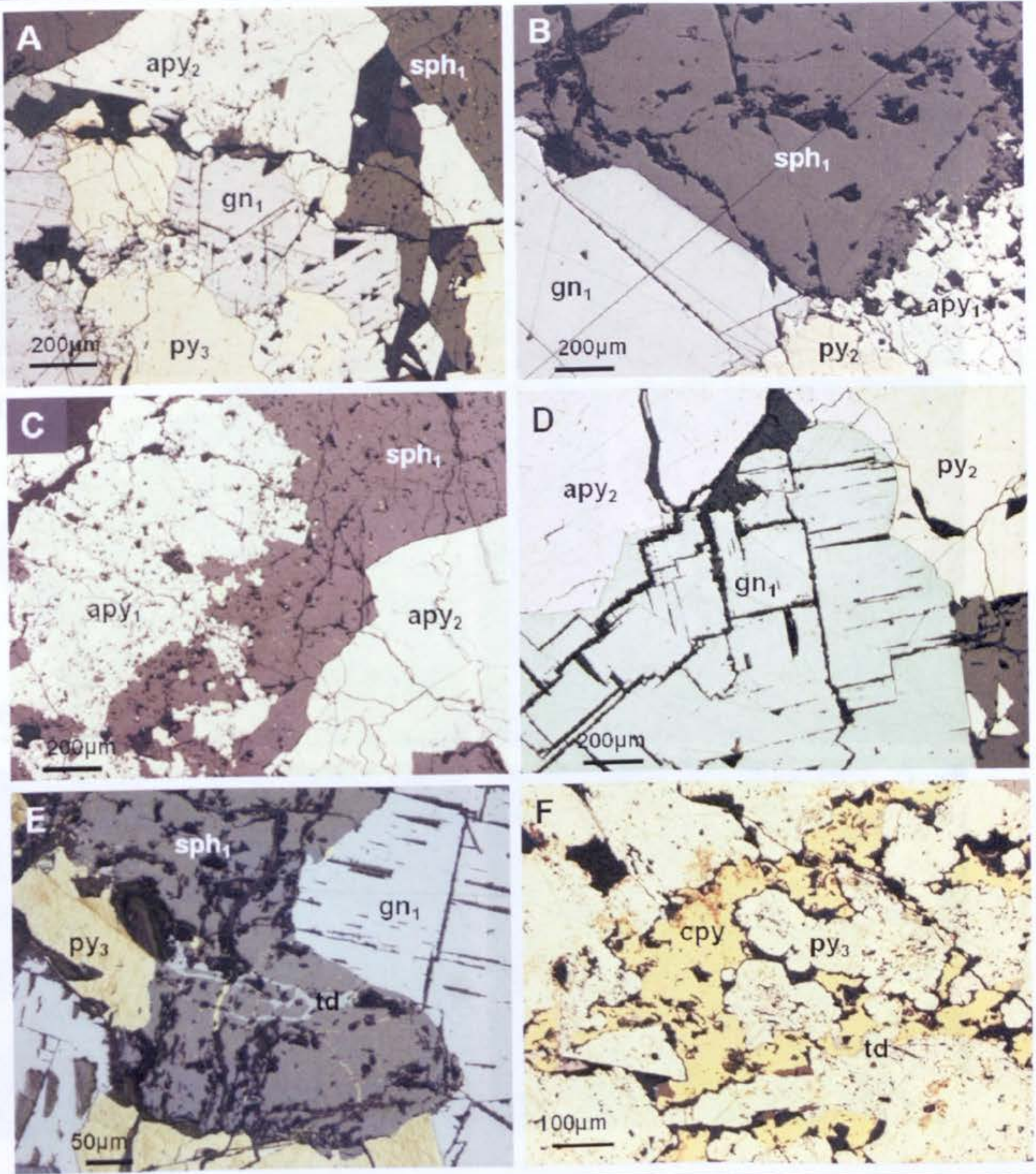

**Figure 4.12:** Reflected light photomicrographs taken under plane-polarized light (PPL) of the main-ore mineralisation stage, showing representative ore textures of an early deposition stage (A-D) and transition towards later, epithermal-style mineralisation (E and F). A) Typical massive sulphide intergrowth textures of pyrite, arsenopyrite, sphalerite and galena; the gangue mineral is quartz (black) (sample 1105/4); B) Euhedral, coarse-grained sphalerite co-existing with galena and replacing earlier pyrite-arsenopyrite aggregates (sample 1155/1B); C) Sphalerite with "chalcopyrite disease", co-existing with the coarse-grained arsenopyrite and replacing earlier finer-grained aggregates of arsenopyrite and pyrite (sample 1055/4D); D) Concave surface of well-cleaved galena, replacing an early pyrite; the different orientations of the triangular polishing pits within galena show that it comprises a number of separate crystals (sample 1055/4D); E) Selective association: fractured second generation of sphalerite rather than galena or pyrite is invaded by tetrahedrite after an increase of Cu-Sb activity in fluids; veins filled by tetrahedrite terminate at sphalerite-galena ($gn_2$) boundary, indicating that galena was deposited as a later phase (sample 180/1F); F) Granular aggregates of pyrite, with intergranular and along fracture replacement by chalcopyrite, which in turn is partially rimmed by tetrahedrite (light grey) (sample 1055/8).

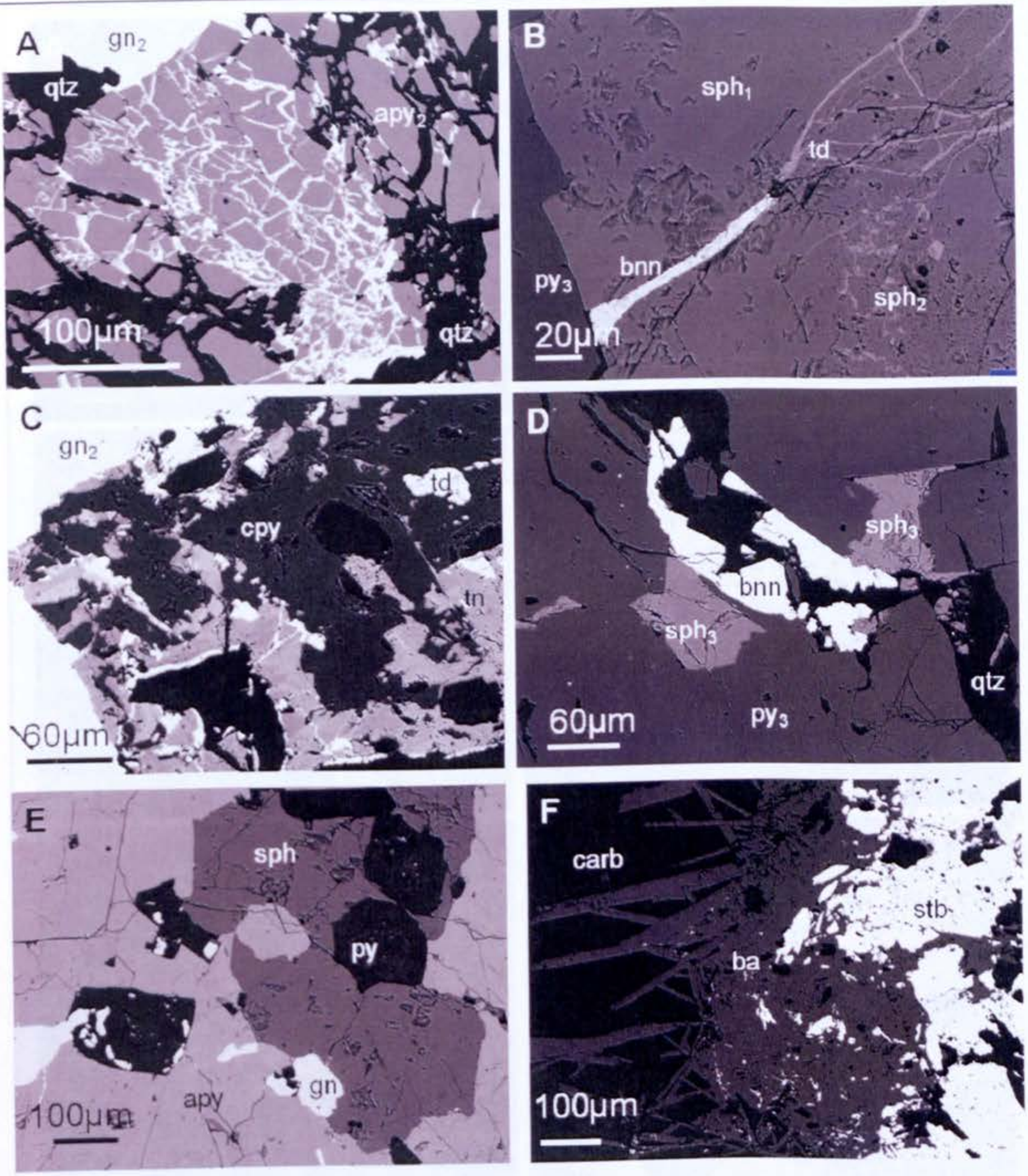

**4.13:** BSE images showing representative ore textures of the later main-ore mineralisation stage from the GII ore body (A-D) and the mineralisation textures of the GII/12 vein ore body (E and F). A) Fractured arsenopyrite (apy$_2$) replaced by galena (gn$_2$) and cemented by quartz (qtz) (sample 1105/3A); B) Thin veins of bournonite (bnn) and tetrahedrite (td) cross-cutting iron-rich sphalerite (sph1) coexisting with pyrite (py$_3$); note also irregular patches of tetrahedrite replacing sphalerite, leaving behind a Fe-depleted and Cu-enriched variety of sphalerite (sph$_2$) (sample 1130/1A); C) Chalcopyrite (cpy) replaced by Ag-rich tetrahedrite and tennantite (tn), all surrounded by galena (sample 180/1F); D) Fe-poor sphalerite (sph$_3$) associated with bournonite and replaces pyrite; note late stage quartz veinlets cross-cutting the ore minerals (sample 1130/1B); E) Sulphide-rich ore composed of arsenopyrite, Fe-rich sphalerite, compositionally zoned As-rich pyrite and galena in the vein-ore body (sample 1235/7B); F) Later stage of vein infilling, represented by early stibnite (stb) overgrown by massive and needle-like barite enclosed in carbonates (sample 1235/5B1).

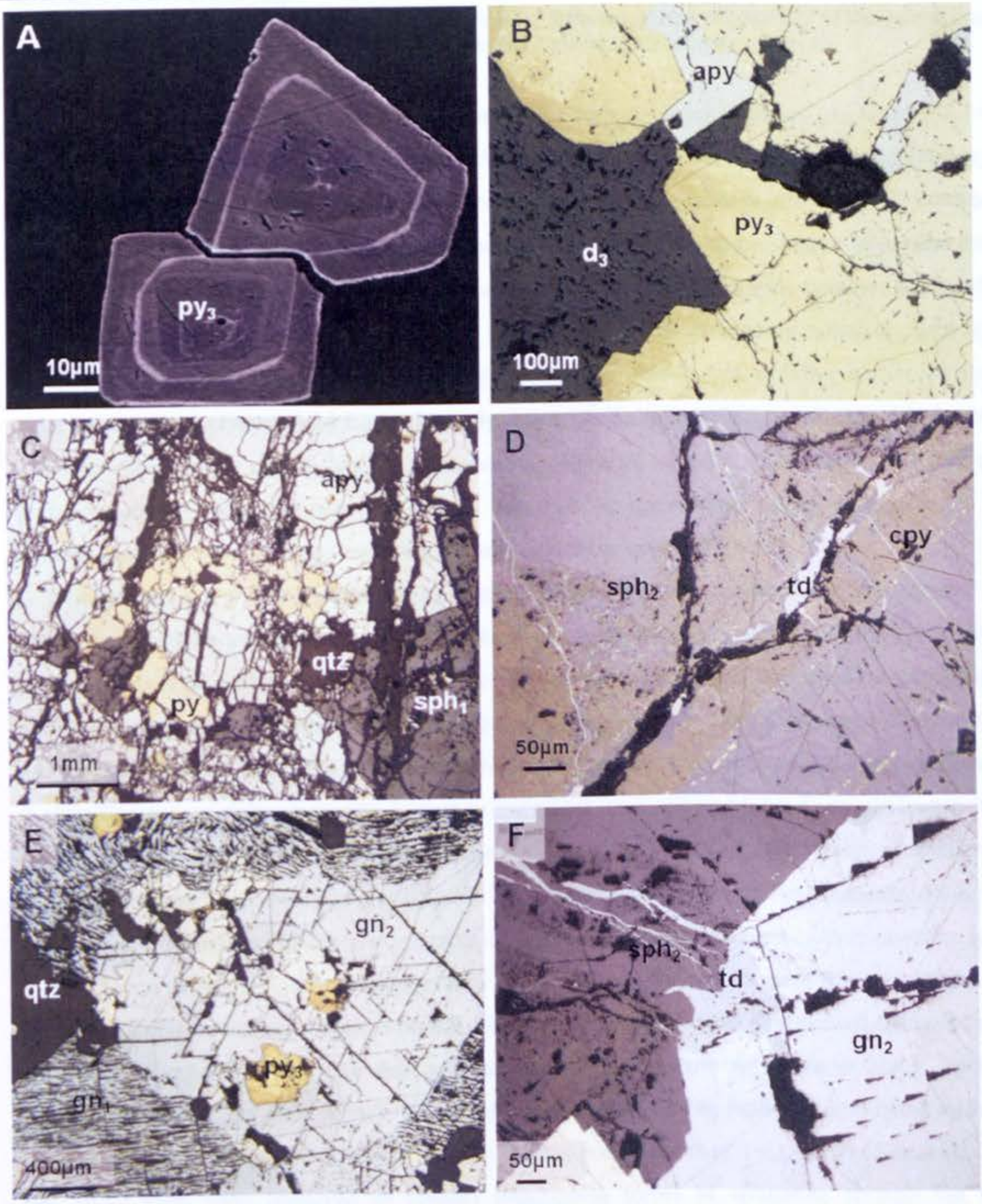

**Figure 4.14:** BSE image (A) and reflected light photomicrographs taken under PPL (B-F) showing mineral textures of the GII replacement-type ore body. A) Concentrically growth-zoned euhedral fine-grained pyrite (bright zones contain up to 8 wt. % As) (sample 1055/1A); (2). B) Coarser, euhedral pyrite crystals associated with arsenopyrite and hydrothermal ankerite ($d_3$) at an early stage of the main ore deposition; (although pyrite shows some compositional zoning, the variety in colouring is also consequence of removal of carbon-coating) (sample 1055/8); C) Cataclastic arsenopyrite associated with pyrite and sphalerite, which is also fractured by quartz filled veins (sample 1105/3A); D) Sphalerite ($sph_2$) with extensive chalcopyrite disease along crystal boundaries and fractures; note the variation in surface colour of the diseased sphalerite (yellow-brown to purple-brown), which is controlled by the density of the fine chalcopyrite inclusions; sphalerite is also cut by tetrahedrite-filled veinlets (sample 1130/1A); E) Two generations of galena; the earlier ($gn_1$) shows curved cleavage planes, whilst the second, coarse grained galena ($gn_2$) does not display deformation textures and contains island shaped relics of earlier pyrite and arsenopyrite, indicating replacement of those minerals; note also the differences in polishing between pitted (top, bottom left and

(*continued from previous page*)
bottom right) and well polished galena grains reflecting different crystal orientations of the galena (sample 180/1F). Tetrahedrite (td), replacing sphalerite ($sph_2$) and galena ($gn_2$) (sample 1130/1A).

main-ore stage and associated with arsenopyrite in the carbonate-rich domains ($d_3$) (Figure 4.14 B). However, two samples from small vugs (1055/4A and 1105/4) show successive euhedral pyrite deposition after sphalerite and galena. Arsenopyrite is an abundant ore mineral, commonly occurring as euhedral to subhedral crystals that vary in size from sub-millimetre to several mm in length. When euhedral, it occurs as individual or clustered rhombic grains commonly associated with As-bearing pyrite ($py_3$) (Figure 4.14 B and C) and is not commonly zoned as seen in the arsenopyrite of the pre-ore stage. Arsenopyrite is also found overgrowing earlier pyrite. A cataclastic texture (Figure 4.14 C) of the early arsenopyrite aggregates, associated with the pyrite and later cemented by quartz, has been observed in couple of samples. The cataclastic deformation textures occur towards the end of the early stage of the main mineralising event. This is also evident from textures showing fracturing of early sphalerite grains (Figure 4.14C).

Sphalerite is a widely distributed ore mineral within the main ore stage. It is associated with pyrite, arsenopyrite and galena in the early main ore stage and with galena and the Cu-sulphides and sulphosalts at a later mineralisation stage. It occurs mainly as anhedral massive replacements and large aggregates with chalcopyrite inclusions (chalcopyrite disease). Two major textural types are readily identified under the microscope: dark brown to black (opaque) sphalerite ($sph_1$), which is classified as iron-rich variety also known as marmatite, and yellow-brown to purple-brown ($sph_2$) sphalerite extensively replaced by chalcopyrite ($sph_2$) (Fig 4.14 D). The dark variety of sphalerite is the most common textural type and displays no colour zoning. It contains moderate amounts of chalcopyrite inclusions, which are irregular in shape. The early sphalerite often contains island shaped forms of pyrite and arsenopyrite providing evidence for replacement of those minerals. It can also exhibit fracturing, which is mainly filled by gangue minerals. The second textural variety of sphalerite represents the one that suffered severe chalcopyrite replacement along fractures, crystal boundaries and twin planes. The third variety of sphalerite ($sph_3$) is associated with Cu-sulphosalts and was identified using the SEM as iron-poor (less than 1 wt.% Fe) (Appendix 2). A few small vugs were observed to contain tetrahedron forms of sphalerite crystals but these instances are not so common.

Galena is the second most important major ore mineral at Belo Brdo. It occurs as anhedral to subhedral masses showing perfect cleavage visible as triangular pits. The grain size of galena varies from sub-mm to several millimetres in size. As seen in sphalerite, the island shaped relics of pyrite and arsenopyrite are frequently seen in galena. Additionally, galena penetrates arsenopyrite along fractures and also replaces pyrite and arsenopyrite along grain boundaries. Two textural varieties of galena have been identified based on the effects of post-depositional processes. The first generation of galena ($gn_1$) shows deformational textures, such as curved and kinked cleavage planes, whilst the second generation ($gn_2$) shows no obvious deformation textures (Figure 4.14E).

The early galena is found associated with sphalerite, pyrite and arsenopyrite, whilst the second generation of galena is associated with sphalerite, chalcopyrite and Cu-sulphosalts at a later stage of main ore deposition (Figure 4.14F).

Chalcopyrite occurs both as small inclusions in sphalerite and as a primary ore, which often replaces earlier sulphides along fractures. It also occurs as aggregates of fine to medium coarse grained anhedral crystals.

Tetrahedrite, tennantite and bournonite are the most common of the sulphosalts group in this deposit and occur specifically during the late mineralisation stage, associated with chalcopyrite sphalerite and galena. Ag-rich tetrahedrite replaces sphalerite and galena as veinlets and along crystal boundaries (Figure 4.14F), whilst tetrahedrite itself is often rimmed by bournonite. Tetrahedrite also occurs as rims around chalcopyrite, and with tennantite it forms irregular shaped solid-solution (see Figure 4.13C) series replacing chalcopyrite.

Barite is a minor mineral constituent in Belo Brdo deposit and is restricted to the late stage vein ore body development.

The gangue mineralisation consists mainly of iron and magnesium carbonates (ankerite, ferroan dolomite) as well as quartz, Cr-mica and chlorite. The carbonates are compositionally zoned and their chemistry will be presented in Section 4.6. Quartz, Cr-mica and chlorite are locally present as fillings of small vugs and as late fracture fillings.

### *4.5.3 Post-ore Stage*

The mineralogy in this stage is very simple and consists mainly of late carbonate (dolomite) vugs filling (see Figure 4.3B) and post-depositional veinlets (Figure 4.8F) occasionally accompanied by quartz and late pyrite which does not display any zoning.

## 4.6 Ore Mineral Chemistry

The electron probe microanalysis of all mineral phases was performed at Kingston University using a Zeiss EVO50 SEM instrument. The details about instrumentation and the mineral chemistry data are provided in Appendix2 on a CD-ROM enclosed at the back of the report.

### *4.6.1 Ni-Co sulphide composition*

The Ni-Co sulphide mineralisation has been observed only in the pre-ore stage of the GII replacement-type ore body. The predominant Ni-Co ore mineral is gersdorffite, which occurs in massive listwanite as well as in quartz-tourmaline breccias, whilst the minor ore mineral phases, such as cobaltite (average measured composition $[Co_{0.55}Fe_{0.08}Ni_{0.39}]_{\Sigma=1.02}As_{0.94}S_{1.04}$), polydimite ($[Ni_{2.67}Co_{0.08}Fe_{0.19}]_{\Sigma=2.94}As_{0.067}S_4$), vaesite ($[Ni_{0.66}Fe_{0.27}]_{\Sigma 0.93}[As_{0.14}S_{1.93}]_{\Sigma 2.07}$), and krutovite

($[Ni_{0.94}Fe_{0.07}]_{\Sigma 1.01}[As_{1.43}S_{0.56}]_{\Sigma 1.99}$) are found only in listwanite breccias. Gersdorffite has the ideal composition of NiAsS, but in Belo Brdo, significant amounts of iron and cobalt substitute for nickel and minor amounts of antimony and zinc substitute for arsenic, resulting in a variety of compositions with an average formula of $(Ni_{0.71}Fe_{0.23}Co_{0.07})_{\Sigma 1.01}(As_{0.95}Sb_{0.01}Zn_{0.02})_{\Sigma 0.98}S_{1.03}$. Based on compositions in Ni–Co–Fe space, gersdorffite displays a wide range of compositions which can be grouped into three different populations (Figure 4.15). A preliminary attempt to estimate formation temperatures comparing compositional populations of gersdorffite from Belo Brdo with experimentally determined gersdorffite solid solution fields of Klemm (1965) has been made (Figure 4.15).

Gersdorffite in massive listwanite occurs as euhedral grains, often disseminated in quartz –Cr-mica-chlorite veinlets and associated with As-bearing pyrite. It comprises the highest Ni content, whilst Fe and Co contents are generally low. Low concentrations of Sb are present in this population, which has the average formula of $(Ni_{0.95}Fe_{0.04}Co_{0.01})_{\Sigma 1.01}$ $(As_{0.95}Sb_{0.03})_{\Sigma 0.98}$ $S_{1.01}$. In the ternary Ni–Co–Fe diagram this population of gersdorffite displays a tight cluster, indicating a homogeneous composition and formation temperatures of < 300° C. Less silicified listwanite breccia hosts slightly zoned gersdorffite, which comprises the highest Co contents (up to 11.4 wt.%) and displays smooth transition from gersdorffite to cobaltite, thus indicating crystallisation in the triclinic space group at temperature of 300–550° C (Figure 4.15).

Gersdorffite from the quartz-tourmaline breccia, with an average composition of $(Ni_{0.59}Fe_{0.31}Co_{0.10})_{\Sigma 1.02}$ $(As_{0.95}Sb_{0.02})_{\Sigma 0.97}$ $S_{1.01}$ contains significantly more Fe (up to 12.7 wt.%) and variable amounts of Co (1-8 wt.%). It is also characterised by an abundance of Zn (up to 3 wt. %), which is not found in other gersdorffite populations. Gersdorffite of this population occurs mainly as anhedral and corroded grains, often associated with irregularly zoned Ni-Co-As bearing pyrite ($py_2$). Trace amounts of Bi-Te-Pb unidentified minerals occasionally rim corroded gersdorffite.

Listwanite breccias cemented by iron-rich carbonates (ankerite and ankeritic dolomite) host euhedral to subhedral gersdorffite associated with pyrite ($py_2$) and arsenopyrite ($apy_1$). It has variable iron contents (6-13wt.%) and low Co (up to 1wt.%). Gersdorffite in this host rock is also found as inclusions in the third generation of pyrite ($py_3$). Here, gersdorffite population has an average composition $(Ni_{0.71}Fe_{0.28}Co_{0.01})_{\Sigma 1.00}$ $As_{0.93}$ $S_{1.07}$. In the ternary Ni–Co–Fe diagram (Figure 4.15) gersdorffite from both, quartz-tourmaline breccias and brecciated listwanite display wider ranges in compositions, indicating more heterogeneous fluid composition. The formation temperatures in these cases could not be reliably determined, as gersdorffite compositions do not reflect equilibrium values. However, the data indicate that those two populations of gersdorffite, which is associated with arsenopyrite, could have been crystallised at temperatures greater than 300°C. More precise analytical work needs to be done to further confirm formation temperatures. There is strong evidence that the Ni-Co mineralisation described above is hydrothermal. The unquestionable evidence is the occurrence of the gersdorffite and Ni-Co bearing pyrite in veins and veinlets associated with hydrothermal phases, such as Cr- mica, chlorite, carbonate and quartz, that

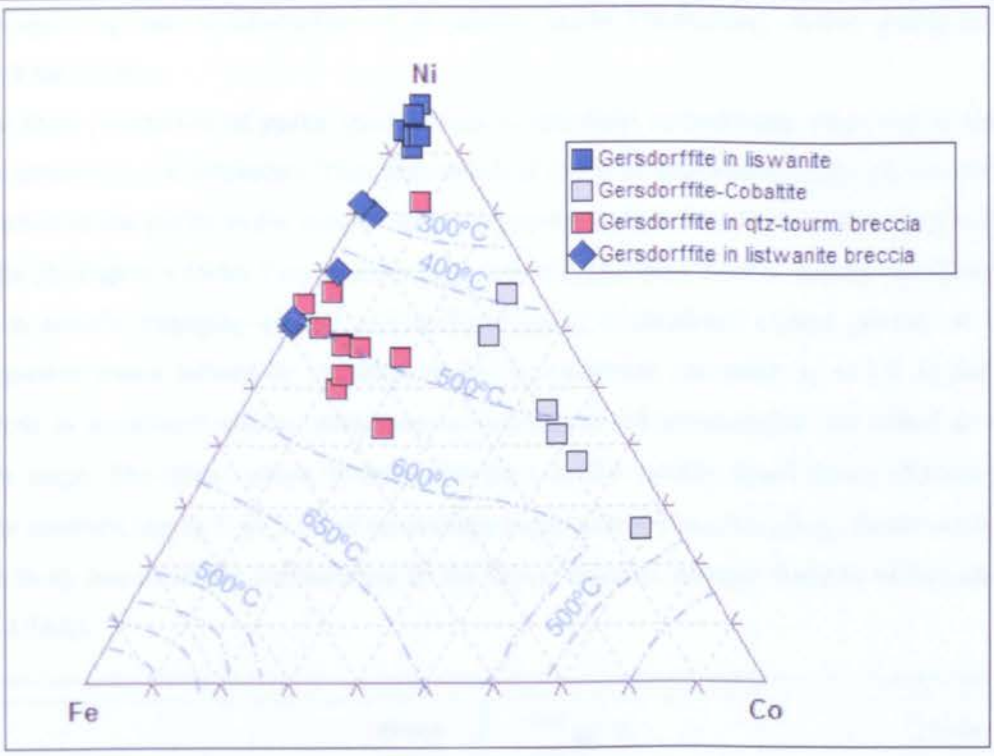

**Figure 4.15:** Plot of compositional variations of gersdorffite in terms of atomic% Ni-Fe-Co in the system NiAsS-FeAsS-CoAsS; dashed blue lines represent isotherms from Klemm (1965).

replace the carbonitised ultramafic rocks and listwanite breccias, indicating that the mineralisation post-dated the formation of the early listwanite breccia. This assemblage of hydrothermal minerals formed at temperatures lower than 550° C.

### *4.6.2 Pyrite*

Pyrite is the most abundant sulphide at Belo Brdo. Three main generations of pyrite have been identified on the basis of textural and compositional differences. The first type is characterised by euhedral to subhedral crystals, which are disseminated within the silicified wall rocks and quartz veins. These pyrite grains are commonly homogeneous and have no or very low As contents of between 0.6 to 1.2 wt.% As (0.02-0.04 atomic %) (Figure 4.16A) (Appendix 2).

The second generation of pyrite is associated with the Ni-Co-As-bearing sulphides of the pre-ore stage. It contains variable concentrations of Ni, Co and As with up to 8.9 wt% Ni, 3.6 wt% Co and 7.6 wt% As respectively (Figure 4.16A). Two compositional varieties of pyrite with respect to Co contents could be distinguished. The Co-poor Ni-rich pyrite is found in listwanite breccias, often overgrowing gersdorffite and has an average composition of $(Fe_{0.95}Ni_{0.04})_{\Sigma 0.99}As_{0.02}S_{1.99}$. The Co-rich pyrite is hosted by quartz-tourmaline breccia and has a higher As content (up to 7.6 wt.%) comparing to the former. Its average composition is $(Fe_{0.89}Ni_{0.04}Co_{0.04})_{\Sigma 0.97}As_{0.15}S_{1.88}$. This type of pyrite shows complex grains and compositional zoning with respect to As and Co contents, characterised by irregular boundaries between the As-Co rich outer zones and As-Co poor inner zones, suggesting partial dissolution of an earlier pyrite (Ni-bearing, As-Co poor) before the growth of the latter.

The third generation of pyrite (py$_3$) occurs in the main mineralising stage and is associated with the economic ore sulphides. This generation of pyrite is characteristically nickel- and cobalt poor relative to the pyrite in the pre-ore stage but contains high As concentrations (up to 8 wt. %, Appendix 2) (Figure 4.16A). Two textural types are distinguished. One is usually oscillatory zoned and often reveals changing crystal morphology (cube, octahedron) during growth. It contains several growth zones defined by variation in As content which can reach up to 7.8 wt percent As. This pyrite is associated mainly with compositionally zoned arsenopyrite and found at an early main-ore stage. The other, which is more abundant, is the weakly zoned pyrite characterised by lower As contents (up to 3 wt.%) and an average composition $Fe_{0.99}As_{0.05}S_{1.96}$. Pyrite in the GII/12 vein ore body has a similar composition to the latter, with an average formula of $Fe_{0.99}As_{0.06}S_{1.95}$ (Figure 4.16A).

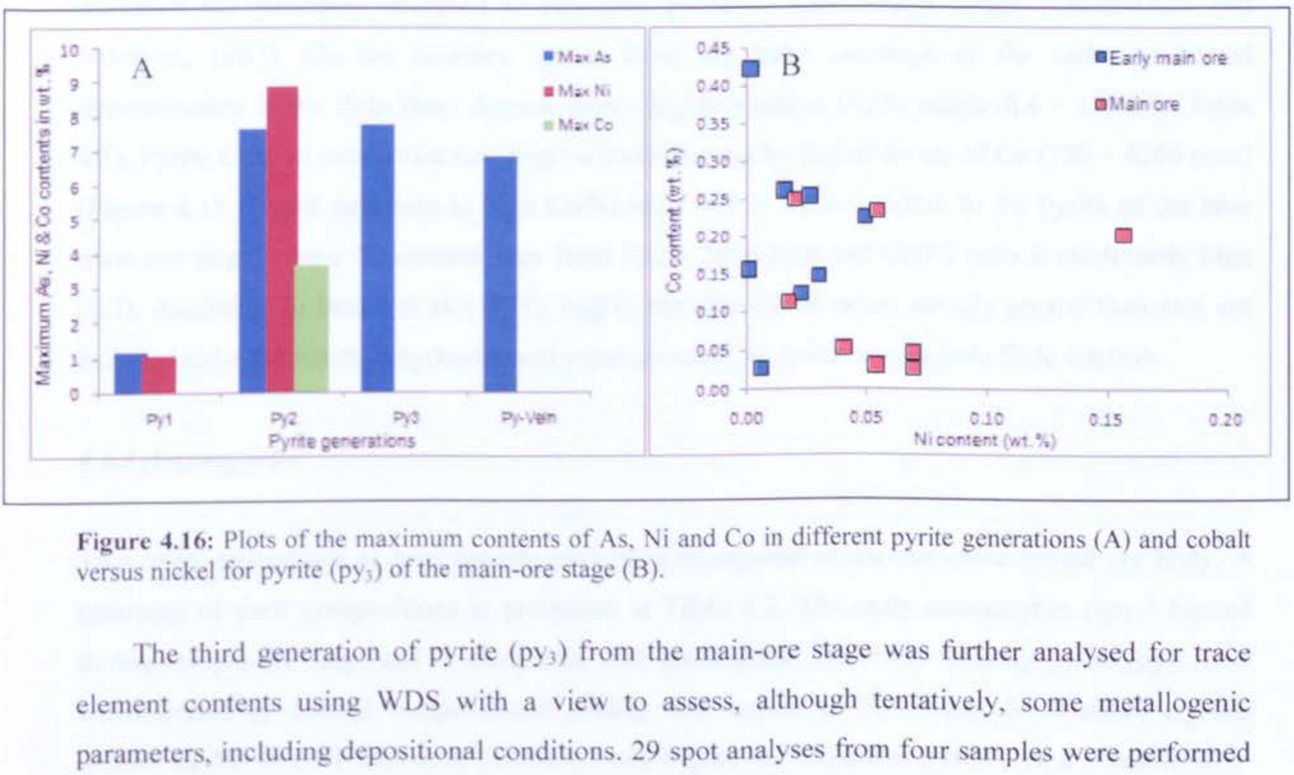

**Figure 4.16:** Plots of the maximum contents of As, Ni and Co in different pyrite generations (A) and cobalt versus nickel for pyrite (py$_3$) of the main-ore stage (B).

The third generation of pyrite (py$_3$) from the main-ore stage was further analysed for trace element contents using WDS with a view to assess, although tentatively, some metallogenic parameters, including depositional conditions. 29 spot analyses from four samples were performed and the summary of the elemental concentrations are presented in Table 4.1.

**Table 4.1**: Summary of trace element composition of main-ore stage pyrite in wt.%.

| Element | Co | Ni | Mn | Cu | Zn | As | Ag | Cd | Au | Co/Ni |
|---|---|---|---|---|---|---|---|---|---|---|
| Min | 0.023 | 0.001 | 0.013 | 0.013 | 0.006 | 0.012 | 0.005 | 0.008 | 0.022 | 0.40 |
| Max | 0.421 | 0.157 | 0.070 | 0.218 | 0.164 | 2.540 | 0.051 | 0.091 | 0.076 | 129.86 |
| Mean | **0.153** | **0.044** | **0.032** | **0.071** | **0.051** | **1.220** | **0.027** | **0.045** | **0.047** | **13.55** |

Arsenic, cobalt, nickel and cadmium were found to be the most common trace elements in this generation of pyrite and occur in almost all analysed samples. The other trace elements, such as Cu, Zn, Mn, Ag and Au are sporadically distributed within the analysed samples and are present in variable concentrations. Pyrite is locally auriferous; however the results have to be taken cautiously, as only four analyses out of 29 contain significant concentrations of gold (220 -760 ppm). The Co/Ni ratio in pyrite (Figure 4.16B) has been used here in an attempt to get a preliminary understanding of the ore deposition. Many authors have used the Co/Ni ratio as an empirical indicator of different styles of mineralisation and the environment of deposition (Loftus-Hills and Solomon, 1967; Bralia et al., 1979; Roberts, 1982; Campbell and Ethier, 1984; Raymond, 1996; Craig et al., 1998). The Co/Ni ratio may reflect the temperature of initial formation independent of metamorphic grade (Walshe and Solomon, 1981; Cook, 1996). Up to 9 wt.% cobalt can be included in pyrite at temperatures of 400°C, and at elevated temperatures (>700°C) complete $FeS_2$–$CoS_2$ solid solution can occur (Moh, 1980). Cobalt content in pyrite is suggested to be higher in copper-rich ores formed at higher temperatures within feeder zones to massive deposits (Cook, 1996). Low Co and Ni concentrations and Co/Ni ratios of less than one with a low standard deviation are generally accepted to represent pyrite of sedimentary origin (Loftus-Hills and Solomon, 1967). On the contrary, pyrite from the main ore-stage of the carbonate-hosted mineralisation in the Belo Brdo deposit shows highly variable Co/Ni ratios (0.4 – 129.86) (Table 4.1). Pyrite from an early main-ore stage is characterised by higher levels of Co (280 – 4200 ppm) (Figure 4.15 B) and moderate to high Co/Ni ratio (4.5 – 129.9) relative to the pyrite of the later main-ore stage, where Co content vary from 230 – 2900 ppm and Co/Ni ratio is moderately high (4.2). According to Bralia et al. (1979), highly variable Co/Ni ratios, usually greater than one, are believed to be the result of hydrothermal mineralisation, as is the case in Belo Brdo deposit.

### *4.6.3 Arsenopyrite*

Two main generations of arsenopyrite have been recognised in the carbonate-hosted ore body. A summary of their compositions is presented in Table 4.2. The early arsenopyrite ($apy_1$) formed during the pre-ore stage and is associated with gersdorffite and Ni-Co bearing pyrite ($py_2$). It is characterised by distinct compositional zoning with respect to Ni content. Most zoned crystals exhibit an As- and Ni- rich core (Table 4.2 and Figure 4.17A) and a S-rich rim, a characteristic

**Table 4.2**: Summary of the average compositions of different arsenopyrite generations (tr= traces; n.d= not detected) in atomic proportions

| Apy generation | Fe | As | S | Ni |
|---|---|---|---|---|
| $Apy_1$-core (n=7) | 30.19 | 32.45 | 34.83 | 2.53 |
| $Apy_1$-rim (n=8) | 32.82 | 30.36 | 36.82 | tr |
| $Apy_2$ (n=21) | 33.31 | 30.05 | 36.65 | tr |
| Apy-vein (n=6) | 33.68 | 29.71 | 36.61 | n.d |

found mainly in arsenopyrites of primary origin (Lentz, 2002). Ni-rich zones may contain up to 6.0 wt. % Ni (5.5 atomic proportions). The main-ore stage arsenopyrite (apy$_2$), which is associated with pyrite (py$_3$), sphalerite (sph$_1$) and galena (gn$_1$), appears optically homogeneous and contains no significant Ni content (Figure 4.17A). Arsenopyrite of the late ore stage found in the vein-ore body is of similar composition as the arsenopyrite of the main- ore stage (Table 4.2 and Figure 4.17A). In general, the samples show substantial As–S variability from 27.9 to 33.9 atom % As, but most fall between 29.5 and 31.5 mole % As (Figure 4.17B).

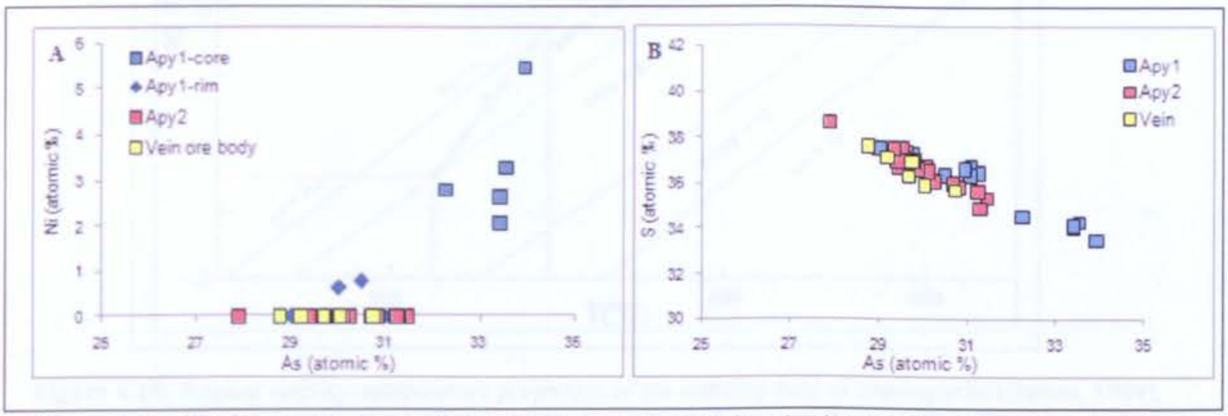

**Figure 4.17:** Concentrations of arsenic versus nickel (A) and sulphur (B) in arsenopyrites from pre-ore stage (apy$_1$), main-ore stage (apy$_2$) and late ore stage (vein ore body) from the Belo Brdo deposit.

*4.6.3.1 Arsenopyrite geothermometry*

Assuming equilibrium conditions between the sulphides (pyrite, sphalerite) and sulpharsenides (arsenopyrite), the composition of arsenopyrite is a function of $fS_2$ (sulphur fugacity) and temperature. It is possible to estimate the formation conditions of arsenopyrite based on the Fe-As-S mineral assemblage and the As at.% content of arsenopyrite (Barton, 1969; Kretschmar and Scott, 1976; Scott, 1983; Sharp et al.,1985). Using the equilibria established by Kretschmar and Scott (1976), the high As contents (32.5 to 33.9 atom % As) in some of the cores of pre-ore stage arsenopyrite can be interpreted as a sign of high-temperature deposition of sulphide (430° to 500°C). However, this type of arsenopyrite contains more than 0.5 atom % Ni and Co and was not used for geothermometry, because higher amounts of these elements may affect the As/S value of arsenopyrite (Scott, 1983; Sharp et al. 1985). In order to detect any zonation within arsenopyrite, points from grain cores and rims were routinely analysed. The chemistry of the optically more homogeneous, discretely zoned arsenopyrite (apy$_2$) of the main-ore stage was used for geothermometry. This type of arsenopyrite, which coexists with main-ore stage pyrite and sphalerite, has a narrow As/S ratio (0.78-0.89) and was chosen as the most suitable for the thermometry calculations. Most As contents fall between 29.4 and 31.5 with a mean value of 30.05 atom % As (Table 4.2). In the vein ore body the values are between 28.8 and 30.7 atom % As with a mean value of 29.7 atom % As. This assemblage implies a temperature range of 311 to 348 °C (Figure 4.18) using the calibration of Kretschmar and Scott (1976). $f$ S$_2$ was between $10^{-8.3}$ and ~$10^{-10.5}$ bar. The arsenic content of arsenopyrites coexisting with pyrite from the same samples studied for fluid inclusions indicates temperatures broadly similar to those obtained from fluid inclusions (see Chapter 6).

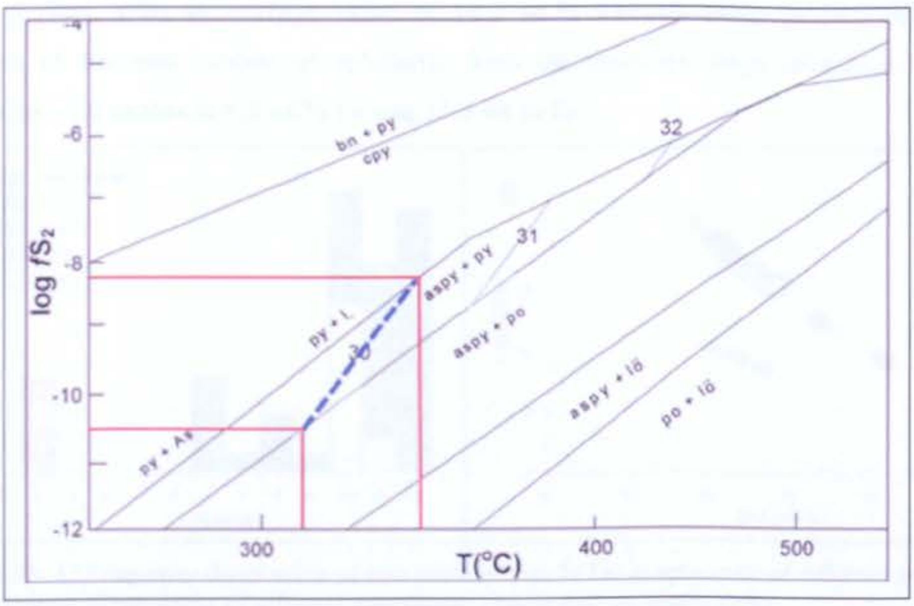

**Figure 4.18:** Sulphur activity–temperature projection of the stability field of arsenopyrite (Barton, 1969), with atom. wt.% As arsenopyrite-buffered curves from Kretschmar and Scott (1976). The blue dashed line depicts the average As content of 30.05 atomic %; the red lines show temperature range and $fS_2$ conditions of precipitation for the arsenopyrite-pyrite-sphalerite assemblage of the main mineralising ore stage, as well as for the vein-type ore body in the Belo Brdo deposit. Symbols: As = arsenic, aspy =arsenopyrite, l = liquid, lö = löllingite, bn = bornite, po = pyrrhotite, py = pyrite.

### *4.6.4 Sphalerite*

Sphalerite, together with galena, is a major constituent of the ore sulphide mineral paragenesis of the Belo Brdo deposit. Within the pre-ore stage, sphalerite occurs rarely and has been detected only in the quartz-tourmaline breccias. Here, sphalerite occurs as anhedral crystals with gersdorffite and galena inclusions. Several spot analyses have been performed to detect any zoning; however, the grains are fairly homogeneous and contain on average 5.3 wt% Fe (Figure 4.19A), which correspond to ~ 9 mol.% FeS (Figure 4.19B) and average formula of $Zn_{0.90}Fe_{0.1}S$.

Three main compositional populations of sphalerite have been distinguished corresponding to the principal textural generations of sphalerite identified within the main-ore stage paragenesis. These populations represent (i) iron-rich coarse-grained sphalerite ($sph_1$), (ii) sphalerite which has been affected by corrosion and replaced by copper minerals ($sph_2$) and (iii) euhedral, fine-grained iron-poor sphalerite ($sph_3$). The most commonly occurring type is the iron- rich ($sph_1$) variety, which accounts for almost 80% of all analysed crystals occurring throughout the main stage of mineralisation, including an earlier paragenesis with pyrite, arsenopyrite and galena of the carbonate-hosted ore body, as well as the later paragenesis of the vein ore body (Fig 4.19A). The iron-rich sphalerite does not show significant variations in average Fe content between the carbonate-hosted and vein ore bodies. The average composition of this type of sphalerite is $Zn_{0.82}Fe_{0.18}S$ in the carbonate-hosted ore body and $Zn_{0.84}$ $Fe_{0.16}S$ in the vein ore body. In detail, however, the compositional variability is much more apparent in the carbonate-hosted ore body, where the Fe content varies between 7.4 and 11.5 wt.% (12.5 -19.7 mol.% FeS respectively) (Figure 4.19A), with an average value of 10.2 wt.% corresponding to 17.5 mol. % FeS. A histogram of the iron content of sphalerite from the main-ore stage reveals a weak bimodal distribution with modes at 9.5 wt.% Fe and 11.5 wt.% Fe.

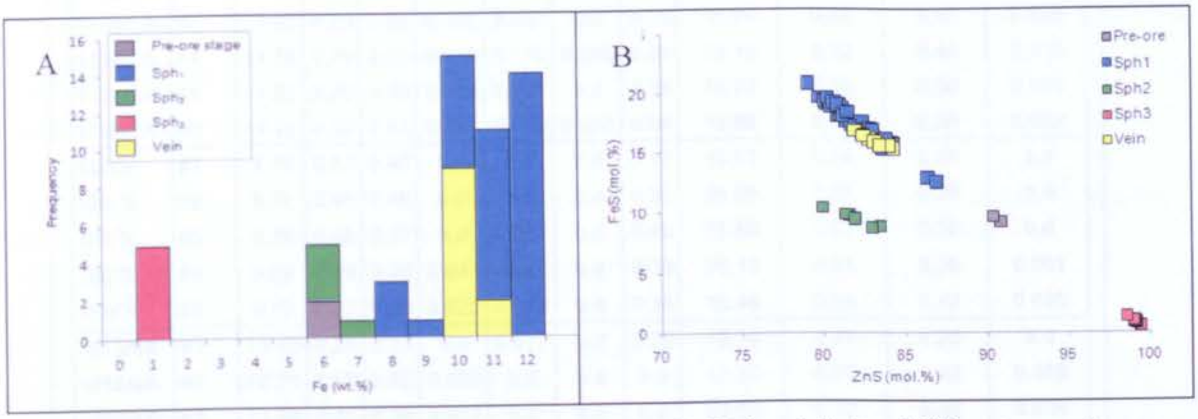

**Figure 4.19:** A) Frequency distribution of iron contents (wt. % Fe) in sphalerite of different generations; B) Composition of sphalerite of different generations (mol% FeS vs. mol% ZnS).

The iron-rich sphalerite in the vein ore body exhibits a narrow compositional range with iron content between 9.1 and 10.5 wt.% (15.3 and 17 mol.% FeS respectively) and an average value of 9.7 wt.% corresponding to 16 mol.% FeS.

The second generation of sphalerite (sph$_2$) has Fe contents with a narrow range of 5.2 -6.2 wt.% Fe, which are markedly lower than that of the iron-rich sphalerite. The average composition of this type of sphalerite, which contains significant amount of copper is $Zn_{0.82}$ $Fe_{0.10}Cu_{0.09}S$.

The third generation of sphalerite (sph$_3$) has iron content which is characteristically lower than that of the first and second generations with values that range from 0.36-0.79 wt.% Fe (Figure 4.19 A), corresponding to an average of 0.97 mol% FeS (Figure4.19 B) and an average formula $Zn_{0.99}$ $Fe_{0.01}S$.

### 4.6.5 Trace elements in Sphalerite and Galena

Sphalerite can incorporate various elements in its structure and is therefore especially suited for trace element studies. Fe, Cd and Cu commonly substitute for Zn in sphalerite, whereas Pb, In, Ga, Ge, Hg, Sn and Mn occur more sporadically (Barton et al. 1977; Burke and Kieft, 1980; McLimans et al. 1980, Oen et al., 1980; Möller, 1985; Johan 1988; Viets et al., 1992; Pattrick et al., 1993; Dini et al. 1995, Kuhlemann and Zeeh, 1995). WDS analyses were used to characterise trace element contents in sphalerite (Table 4.3) and galena (Table 4.4) from different underground levels of the carbonate-hosted ore body, with a view to constrain some genetic information about deposition of Belo Brdo mineralisation, as the chemical composition of sphalerite, in particular, is a good indicator of physicochemical conditions of ore formation.

**Table 4.3**: Major and trace element compositions of sphalerite from four representative samples of the main-ore stage; n.d= not determined; b.d below detection) in wt.% unless specified. Note: Mn was not determined in sample 1155/1B.

| Sample | Sph | Fe | Mn | Cd | Cu | Co | Ni | As | FeS (mole %) | MnS (mole %) | CdS (mole %) | CuS (mole %) |
|---|---|---|---|---|---|---|---|---|---|---|---|---|
| 1130/1A | #1 | 11.02 | 0.30 | 0.36 | b.d | 0.173 | 0.019 | 0.15 | 18.82 | 0.52 | 0.31 | b.d |
| 1130/1A | #2 | 11.40 | 0.29 | 0.38 | b.d | b.d | b.d | 0.34 | 19.34 | 0.50 | 0.32 | b.d |
| 1130/1A | #3 | 11.43 | 0.29 | 0.50 | 0.006 | 0.053 | b.d | 0.36 | 19.04 | 0.48 | 0.42 | 0.009 |
| 1130/1A | #4 | 11.38 | 0.19 | 0.53 | 0.080 | 0.117 | 0.005 | 0.31 | 19.16 | 0.32 | 0.44 | 0.119 |
| 1130/1A | #5 | 11.22 | 0.20 | 0.45 | 0.054 | 0.037 | b.d | 0.35 | 19.02 | 0.34 | 0.38 | 0.080 |
| 1130/1A | #6 | 11.25 | 0.33 | 0.44 | 0.035 | 0.098 | 0.037 | 0.04 | 18.85 | 0.56 | 0.36 | 0.052 |
| 180/3I | #1 | 9.79 | 0.31 | 0.46 | b.d | b.d | b.d | 0.47 | 16.53 | 0.54 | 0.38 | b.d |
| 180/3I | #2 | 9.84 | 0.45 | 0.46 | b.d | b.d | b.d | 0.35 | 16.59 | 0.77 | 0.39 | b.d |
| 180/3I | #3 | 9.39 | 0.45 | 0.47 | b.d | 0.064 | b.d | 0.40 | 15.90 | 0.78 | 0.39 | b.d |
| 180/3I | #4 | 9.59 | 0.40 | 0.46 | 0.041 | b.d | b.d | 0.33 | 16.18 | 0.68 | 0.39 | 0.061 |
| 180/3I | #5 | 9.73 | 0.37 | 0.50 | 0.023 | 0.042 | b.d | 0.36 | 16.48 | 0.64 | 0.42 | 0.035 |
| 1055/4A | #1 | 11.43 | 0.24 | 0.33 | b.d | 0.077 | b.d | 0.28 | 19.34 | 0.41 | 0.28 | b.d |
| 1055/4A | #2 | 10.31 | 0.53 | 0.52 | 0.060 | b.d | b.d | b.d | 17.30 | 0.90 | 0.43 | 0.089 |
| 1055/4A | #3 | 11.04 | 0.46 | 0.38 | 0.024 | b.d | b.d | b.d | 18.59 | 0.79 | 0.32 | 0.036 |
| 1055/4A | #4 | 10.46 | 0.46 | 0.50 | 0.015 | b.d | b.d | b.d | 17.68 | 0.79 | 0.42 | 0.022 |
| 1055/4A | #5 | 10.61 | 0.52 | 0.53 | 0.009 | b.d | b.d | 0.30 | 17.95 | 0.90 | 0.45 | 0.013 |
| 1155/1B | #1 | 10.82 | n.d | 0.55 | b.d | 0.014 | 0.025 | 0.48 | 18.28 | 0.00 | 0.46 | 0.000 |
| 1155/1B | #2 | 10.76 | n.d | 0.55 | 0.064 | 0.068 | b.d | 0.10 | 18.39 | 0.00 | 0.46 | 0.096 |
| 1155/1B | #3 | 10.78 | n.d | 0.42 | b.d | 0.078 | b.d | 0.07 | 18.68 | 0.00 | 0.36 | 0.000 |
| 1155/1B | #4 | 10.66 | n.d | 0.51 | 0.003 | 0.077 | b.d | 0.31 | 18.37 | 0.00 | 0.44 | 0.005 |
| 1155/1B | #5 | 9.93 | n.d | 0.48 | 0.038 | b.d | 0.005 | 0.28 | 17.02 | 0.00 | 0.41 | 0.058 |
| 1155/1B | #6 | 10.52 | n.d | 0.42 | b.d | b.d | b.d | 0.14 | 18.16 | 0.00 | 0.36 | 0.000 |
| Min | | 9.39 | 0.19 | 0.33 | 0.003 | 0.014 | 0.005 | 0.04 | 15.90 | 0.321 | 0.280 | 0.009 |
| Max | | 11.43 | 0.53 | 0.55 | 0.080 | 0.173 | 0.037 | 0.48 | 19.34 | 0.903 | 0.449 | 0.119 |
| Mean | | 10.61 | 0.36 | 0.45 | 0.035 | 0.083 | 0.020 | 0.31 | 17.92 | 0.620 | 0.381 | 0.051 |
| std | | 0.65 | 0.11 | 0.06 | 0.024 | 0.041 | 0.014 | 0.13 | 1.25 | 0.189 | 0.051 | 0.036 |

The sphalerite grains analysed in this study display a restricted composition. Iron, Mn and Cd are predominant trace elements in all samples (Table 4.3). All three elements show quite uniform concentrations in sphalerites from different underground levels of the mine and range between 9.39-11.43 wt.% Fe, 1900-5300 ppm Mn and 3300-5500 ppm Cd. Ni is commonly below detection limit, with a maximum concentration of 370 ppm. Co is more common than Ni and shows significant variations in concentrations between 140-1730 ppm. The Cu content of sphalerite is consistently low, usually below 800 ppm. Concentrations of Se, Te, Sn, Hg, Ge, Ga are all below the detection limit of the WDS probe.

The FeS contents show a limited range from 15.9 to 19.34 mol% with an average composition of 17.9 mol%. The MnS and CdS contents are less than 1 and 0.5 mol% respectively. Such an iron-rich and moderately high Mn and Cd chemistry is a common feature of sphalerites in the skarn and hydrothermal Pb-Zn Trepca deposit in Kosovo (Strmić-Palinkaš, 2009), as well as in many Cordilleran-type base metal deposits (Bendezú and Fontboté, 2009). In contrast, in carbonate-hosted Mississippi Valley type deposits, for instance, Fe content in sphalerite is generally low (e.g. Hagni, 1976). For example, Craig et al. (1983) gave average Fe and Cd contents of 0.27 and 0.38

wt.% respectively for sphalerites from 16 deposits in Tennessee. South African Mississippi Valley type deposits do not exceed 4 wt% Fe (Schaefer, 2009). Our data clearly indicate much higher temperatures of formation, which will be confirmed by the fluid inclusion study and presented in Chapter 6.

The only trace elements present in significant concentrations in galena are Ag, Mn and Cd (Tab. 4.4). Cu, Zn and Fe are usually elevated if small inclusions of pyrite, sphalerite and chalcopyrite are present. The Ag content in galena is highest for the second generation of galena, which is mainly associated with chalcopyrite, tennantite and tetrahedrite of the later main-ore stage mineralisation. Here, the Ag values commonly reach up to 0.13wt.% . Galena of an earlier main ore-mineralisation stage have much lower Ag contents between 140 and 810 ppm. Cadmium concentrations in galena are rather high and consistent in all samples, with an average of 0.12 wt.% (Table 4.4).

**Table 4.4**: Summary of major and trace element compositions of galena from three representative samples of the main-ore stage; n.d= not determined; b.d below detection) in wt.% unless specified. Note: As commonly below detection limit; Ni and Co were not determined.

| Sample | Stat | Fe | Mn | Cd | Cu | Ag | Zn | Fe (mole%) | Mn (mole%) | Cd (mole%) | Cu (mole%) |
|---|---|---|---|---|---|---|---|---|---|---|---|
| 1130/1A | Min | 0.007 | 0.030 | 0.030 | 0.020 | 0.008 | 0.008 | 0.03 | 0.13 | 0.06 | 0.07 |
| | Max | 0.047 | 0.090 | 0.216 | 0.145 | 0.177 | 0.021 | 0.20 | 0.39 | 0.46 | 0.53 |
| | MEAN | 0.023 | 0.059 | 0.115 | 0.061 | 0.061 | 0.015 | 0.10 | 0.26 | 0.24 | 0.23 |
| | STD | 0.014 | 0.025 | 0.050 | 0.041 | 0.066 | 0.009 | 0.06 | 0.10 | 0.11 | 0.15 |
| 180/3I | Min | 0.005 | 0.011 | 0.055 | 0.007 | 0.007 | 0.035 | 0.02 | 0.05 | 0.12 | 0.03 |
| | Max | 0.047 | 0.151 | 0.234 | 0.116 | 0.134 | 0.155 | 0.20 | 0.66 | 0.50 | 0.44 |
| | MEAN | 0.023 | 0.062 | 0.114 | 0.063 | 0.060 | 0.098 | 0.09 | 0.21 | 0.28 | 0.17 |
| | STD | 0.015 | 0.047 | 0.061 | 0.051 | 0.054 | 0.052 | 0.03 | 0.19 | 0.18 | 0.23 |
| 1055/4A | Min | 0.014 | 0.011 | 0.014 | 0.052 | 0.008 | b.d | 0.06 | 0.05 | 0.03 | 0.20 |
| | Max | 0.081 | 0.068 | 0.232 | 0.089 | 0.106 | 0.079 | 0.34 | 0.30 | 0.50 | 0.34 |
| | MEAN | 0.043 | 0.030 | 0.125 | 0.070 | 0.055 | 0.079 | 0.19 | 0.13 | 0.27 | 0.27 |
| | STD | 0.026 | 0.026 | 0.069 | 0.018 | 0.042 | n.d | 0.11 | 0.11 | 0.15 | 0.07 |
| Min | | 0.005 | 0.011 | 0.014 | 0.007 | 0.007 | 0.008 | 0.02 | 0.05 | 0.06 | 0.03 |
| Max | | 0.081 | 0.151 | 0.234 | 0.145 | 0.177 | 0.155 | 0.20 | 0.66 | 0.50 | 0.53 |
| Mean | | 0.030 | 0.052 | 0.118 | 0.064 | 0.059 | 0.071 | 0.10 | 0.26 | 0.24 | 0.23 |
| std | | 0.021 | 0.037 | 0.059 | 0.039 | 0.051 | 0.054 | 0.06 | 0.16 | 0.12 | 0.16 |

Such a narrow range of trace element distributions in both, sphalerite and galena from different underground levels in Belo Brdo mine reflect a similar mode of mineral growth.

Trace element concentrations in sulphide minerals and mineral pairs have also been used to establish a series of geothermometers. The temperature and pressure dependence of the fractionation of Cd and Mn between cogenetic sphalerite and galena that form under equilibrium conditions was studied by Bethke and Barton (1971) and Geletii et al. (1979). Application of these two geothermometers to the data derived from three samples in this study results in very low Cd and Mn fractionation factors ($Cd_{sph}/Cd_{gn} \sim 4$ and $Mn_{sph}/Mn_{gn} \sim 6$) that result in unreasonably high temperature estimates (above 650°C) that far exceed temperature estimates derived from arsenopyrite geothermometry and fluid inclusion studies (Chapter 5) and suggest that incorporation of Mn and Cd into sphalerite and galena took place under disequilibrium conditions (Bethke and Barton, 1971; Geletii et al., 1979).

The FeS content in sphalerite has been proposed as a sensitive indicator for $f\mathrm{S}$ during ore precipitation (Barton and Toulmin, 1966). A log $f\mathrm{S}_2$–temperature (1000/K) composition map has been constructed by Lusk and Calder (2004) for sphalerite using Lusk and Bray's (2002) data for a sequence of buffer reactions in the Cu–Fe–S and Fe–S systems. The equation: $\log_{10}f\mathrm{S}_2=11.01-9.49\ (1000/\mathrm{K})+[0.187-0.252\ (1000/\mathrm{K})]\ (\mathrm{mol.\%\ FeS})+[0.35-0.2\ (1000/\mathrm{K})]\ (\mathrm{mol.\%\ CuS\ in\ sphalerite})$ can be applied to sphalerites that have equilibrated with buffer assemblages containing pyrite, or pyrite and pyrrhotite, in both the Fe–Zn-S and Cu-Fe-Zn-S systems at temperatures between 250 and 550°C at 1 bar (Lusk and Calder, 2004). This equation incorporates data from Lusk and Calder (2004) experiment and from a selection of published experimental data that are fitted to within 10%. In our study, sphalerite with mean mol.% FeS composition of 18; minimum mol.% CuS composition of 0.009 and maximum 0.12; and values for sulphur fugacity of $10^{-8.3}$ and $\sim 10^{-10.5}$ obtained from arsenopyrite geothermometry were used to estimate formation temperatures. The 1000/K values range from 1.60 to 1.77 and correspond to 290 to 350°C (Figure 4.20).

**Figure 4.20:** Log $f\mathrm{S}_2$ vs. T diagram illustrating the approximate cooling path (black arrow) of fluids from pre-ore stage (blue square) to main-ore stage (red dotted line) based on gersdorffite, arsenopyrite and FeS-CuS geothermometry, as well as on the mineral assemblages (modified from Einaudi et al., 2003; Lusk and Calder, 2004; Bendezú and Fontboté, 2009).

The FeS content of the main-mineralising stage in Belo Brdo is typical of sphalerite occurring along the pyrite-pyrrhotite solvus, where the composition is approximately constrained to 20 mol

% FeS (Scott and Barnes, 1971; Scott, 1973). According to Lusk and Calder (2004), sphalerite compositions indicate large increases in the mol% FeS content and the Fe/Cu ratio with decreasing sulphur fugacity at given temperatures (Figure 4.20). In this study, a decrease in sulphur fugacity as well as cooling of the hydrothermal fluid is suggested to be an important mechanism of the ore deposition. This is shown by an increase in FeS content from sphalerites of the pre-ore stage to main-ore stage, as well as reduction in formation temperatures between the two stages. The data also confirm an intermediate sulphidation state of the hydrothermal ore fluids.

## 4.7 Carbonate Mineral Chemistry

Study of different generations of carbonates by conventional petrographic methods (transmitted and reflected light microscopy), cathodoluminescence, back-scattered electron imaging (BSE), and energy dispersive X–ray spectroscopy (EDS) revealed textural and compositional changes that can be related to different stages of carbonate and sulphide precipitation. Quantitative EDS analyses of carbonate minerals were obtained using the following operating conditions: 15kV acceleration voltage, 1nA beam current, and count time 50s.

At least four carbonate generations have been recognised in the Belo Brdo deposit and four carbonate minerals have been determined, namely dolomite, ankerite, calcite and magnesite (Figure 4.21). Calcite is a major constituent of the non-mineralised limestones, but is absent from the

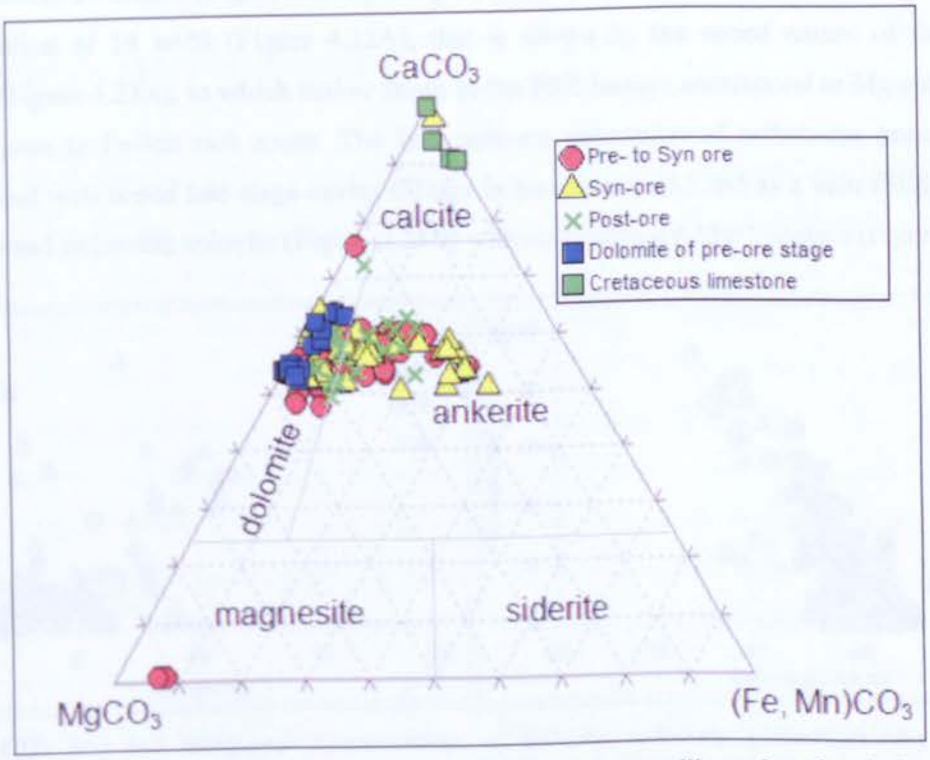

**Figure 4.21:** Ternary $CaCO_3$-$MgCO_3$-(Fe+Mn)$CO_3$ diagram illustrating chemical composition of carbonate minerals from different carbonate generations in Belo Brdo deposit; (compositional divisions after Nakamura and Kato, 2004).

hydrothermal stages of ore deposition except for one sample, where it occurs as a late stage phase. Similarly, magnesite has been detected as a vein filling with dolomite in only one sample (see Figure 4.8B).

The first generation of carbonates (d$_1$) represents unmineralised Cretaceous limestones (see also Figures 4.8A and 4.9A), which are composed of calcite (Figure 4.21). The host limestones underwent dolomitisation, brecciation and silicification during the pre-ore stage. This stage was followed by formation of the second generation of carbonates and is characterised by pervasive carbonation (d$_2$), and veining (d$_{2-1}$ and d$_{2-2}$) of ultramafic rocks, resulting in formation of listwanites (see also Figure 4.8C-F). Carbonate minerals in listwanites are dolomite, ferroan dolomite (5-10mol.% FeCO$_3$) and ankerite (> 10mol.% FeCO$_3$) (Figure 4.21), which contain substantial amounts of MnO (up to 9 wt.%) (Figure 4.22A). Variability in MgO, FeO and MnO contents probably reflects the nature of the primary mafic host minerals and redistribution of those components into dolomites and ankerites during hydrothermal alteration. It is noted that the listwanite breccias are cemented mainly by ankerites (±Mn), which suggests that hydrothermal carbonates were precipitated from magnesium-and iron-rich (±Mn) fluids (Figure 4.22B). The carbonate mineral replacing plagioclase in Tertiary volcanics is dolomite. Ferroan dolomite, which contains up to 2 mol.% MnCO$_3$, is the main carbonate mineral in quartz-tourmaline breccias, as well as in andesitic host rocks where it replaces mafic minerals. The third generation of carbonates (d$_3$) is associated with massive sulphide ore and is characterised mainly by ankerites and to a lesser extent ferroan dolomites (Figure 4.23A). They contain variable amounts of MnO, with a maximum concentration of 16 wt.% (Figure 4.22A), that is shown by the zoned nature of the carbonate crystals (Figure 4.23A), in which darker zones in the BSE images correspond to Mg-rich bands and lighter zones to Fe-Mn rich zones. The last, post-ore generation of carbonates occur as coarse-grained and well zoned late-stage cavity fillings in breccia ore (d$_3$) and as a vein filling by ferroan dolomite and dolomitic ankerite (Figure 4.23B) with no significant MnO content (Figure 4.22A).

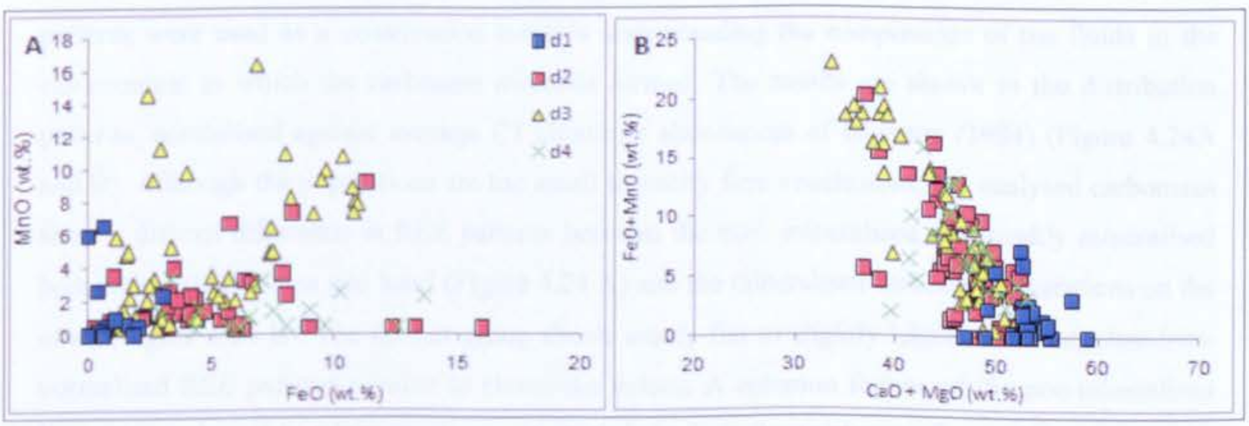

**Figure 4.22:** Iron and manganese concentrations of different carbonate generations (A); calcium and magnesium vs. iron and manganese concentrations of different carbonate generations indicating their strong negative correlation (B). Abbreviations: d$_1$= unmineralised carbonates including Cretaceous limestones; d$_2$=pre-ore stage carbonates including carbonatisation of ultramafic rocks; d$_3$=syn-ore stage hydrothermal carbonates; d$_4$=post-ore stage.

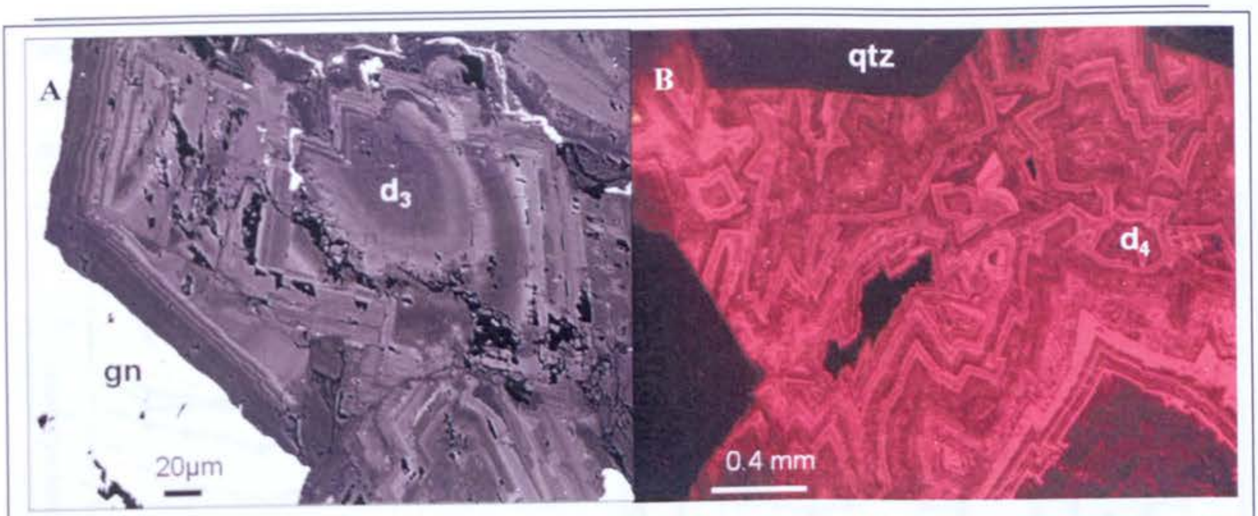

**Figure 4.23:** BSE image (A) and CL microphotograph (B) of zoned carbonates. A) Compositionally zoned ankerite with high contents of Mn (bright zones) and Mg (dark bands) associated with galena (gn) of the the main-ore stage. B) Late stage coarsely crystalline dolomite associated with euhedral late stage quartz; dolomite is strongly zoned, with alternating luminescent (iron-rich) and cloudy zones; this type of dolomite fills voids and small fractures and cross-cuts earlier ankerites, indicating that they postdate the main Pb–Zn mineralization phase.

In general, the compositional trend characterised by an increase in FeO and MnO and decrease in CaO and MgO (Figure 4.22B) reflects the evolution of hydrothermal fluids from an early, pre-ore stage in which non-ferroan dolomite formed, through to the main-ore stage, characterised by ferroan dolomite, ankerite and manganoan ankerite.

## 4.8 REE geochemistry of carbonates

Rare earth element analyses were conducted on 14 samples representing different carbonate generations including non-mineralised host limestone, weakly mineralised listwanite and hydrothermal breccia of the pre-ore stage, syn-ore carbonates and post-ore dolomite. The REE patterns were used as a contribution towards understanding the composition of the fluids in the environment in which the carbonate minerals formed. The results are shown in the distribution patterns, normalised against average C1 chondrite abundances of Boynton (1984) (Figure 4.24A and B). Although the populations are too small to justify firm conclusions, the analysed carbonates show a distinct difference in REE patterns between the non- mineralised and weakly mineralised host rock carbonates on one hand (Figure 4.24 A) and the mineralised carbonate generations on the other (Figure 4.24 B). The former group shows nearly flat to slightly LREE enriched, chondrite-normalised REE patterns relative to chondritic values. A common feature of the non-mineralised limestone and weakly mineralised pre-ore stage breccia is the existence of negative anomalies in $Ce_N$, being higher in non-mineralised host rocks ($Ce/Ce^* = 0.36$ in Triassic metalimestones and 0.69 in Cretaceous limestone) than in dolomite fragments of hydrothermal pre-ore breccia ($Ce/Ce^* = 0.84$-$0.95$), whilst listwanite breccia and silicified carbonate host rock does not exhibit any $Ce_N$ anomaly. A negative $Eu_N$ anomaly is also evident in the non-mineralised carbonate host rocks ranging from 0.75 (Triassic metalimestones) to 0.96 (Cretaceous limestones), whilst the pre-ore breccias exhibit negligible positive $Eu_N$ anomalies (Eu/Eu*= 1.12-1.30) (Figure 4.24 A).

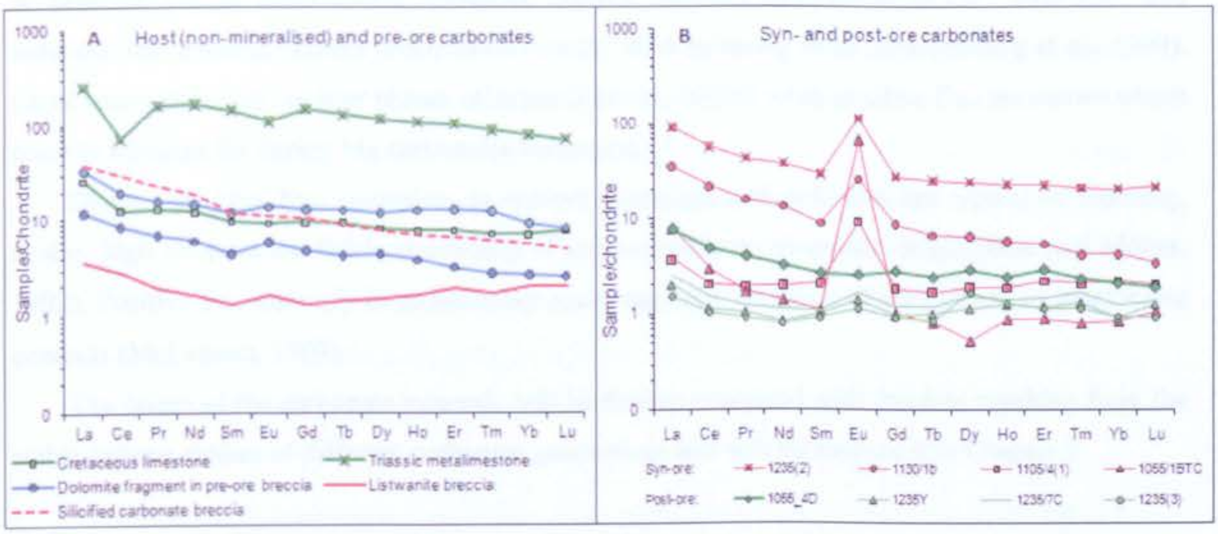

**Figure 4.24:** Chondrite-normalised rare-earth element distributions of non-mineralised limestone host rocks and weakly mineralised breccias from pre-ore stage (A) and syn-ore and post-ore carbonates (B).

In contrast, the syn-ore stage carbonates show high positive $Eu_N$ anomalies with a Eu/Eu* range of 3-5, and with one sample showing an extremely high Eu/Eu*value of 66. The negative $Ce_N$ anomalies vary between 0.76 and 0.91 (Figure 4.24 B).

The post-ore stage carbonates have weak positive $Eu_N$ anomalies (1.2-1.5) and show a narrow range of negative $Ce_N$ anomalies between 0.8 and 0.87 (Figure 4.24 A).

The rare earth element distribution in minerals and hydrothermal fluids has been used for a better understanding of the behaviour of these elements during interactions of hydrothermal solutions with host rocks (Bau and Möller, 1991). Eu, in particular, has been used for temperature determination. The $Eu^{3+}/Eu^{2+}$ redox potential in aqueous solutions depends on pressure, pH and REE speciation. But theoretical considerations (Bau and Möller, 1992) as well as experimental results (Sverjensky, 1984) reveal that the most important parameter controlling the valency of Eu is temperature. $Eu^{3+}$ dominates at low temperatures, and at temperature exceeding 200°C (P=0.5 kbar) divalent Eu should predominate (Sverjensky, 1984). Therefore, $Eu_N$ anomalies will readily develop at temperatures >200°C and under at least mildly reducing conditions (Bau and Möller, 1992), while oxidising fluids will exhibit a negative Ce-anomaly. Negative Ce anomaly is typical features of marine water (Hu et. al, 1988). Due to oxidising conditions in seawater $Ce^{3+}$ is oxidised to $Ce^{4+}$ which is less mobile resulting in Ce depletion of the seawater itself. Therefore marine water commonly possesses a negative Ce anomaly (Elderfield and Greaves, 1982; de Baar et al., 1985), which is then inherited by carbonates formed in a marine environment.

Our data clearly indicate that the REE distribution pattern for non-mineralised limestones reflects the marine environment for their origin, as they are characterised by negative $Eu_N$ and $Ce_N$ anomalies. Most of the other analysed carbonates display weak negative $Ce_N$ anomalies, which could possibly be inherited from the primary carbonate sediments, and positive $Eu_N$ anomaly. Negative $Ce_N$ anomalies and positive $Eu_N$ anomalies cannot build up in the same physico-chemical environment, but are indicative of changing redox conditions during fluid migration. The absence of negative $Ce_N$ in ankerite-rich listwanite breccia suggests domination of $Ce^{3+}$ over $Ce^{4+}$ and indicates that ankerite cement precipitated directly from reducing fluid (Spangenberg et al., 1999). Light sparry dolomite, as later phases of mineralisation, exhibit weak positive $Eu_N$ anomalies which point to trivalent Eu during Mg carbonates formation.

Distinct positive $Eu_N$ anomalies in syn-ore dolomites and ankerites are typical of reducing, acidic, high temperature fluids commonly of metamorphic or magmatic origin (Bau and Möller, 1992). Positive $Eu_N$ anomaly in sedimentary rocks may also be result of enrichment of plagioclase contents (McLennan, 1989).

The origin of the carbonate minerals will be further examined with the data resulting from the stable isotope studies of different carbonate generations and will be discussed in Chapter 7.

## 4.9 Summary and conclusions

- Formation of irregular and tabular carbonate-replacement Pb-Zn (Ag) ore bodies at the Belo Brdo deposit is controlled by steeply dipping fault zones developed at contacts between different lithologies (serpentinites/Tertiary volcanics; Cretaceous limestones/ volcanics).
- Petrographic data presented here show that listwanites, in addition to Cretaceous limestones, represent an important host rock to the carbonate-replacement type of mineralisation. An additional hydrothermal vein deposit is located within Tertiary andesites.
- The listwanites are composed primarily of carbonates, quartz, Cr-mica and pyrite. The predominant carbonate phase is dolomite with variable contents of iron (up to 14% Fe) and manganese (up to 4% Mn). Cr- chlorite, Cr-spinel, magnetite, serpentine and talc occur as accessory minerals.
- The paragenesis of the Belo Brdo deposit is very complex. At least three major stages of the mineral deposition have been recognised in Belo Brdo based on petrographic and mineral chemistry data, namely: (1) pre-ore stage, characterised by hydrothermal alteration of host rocks (listwanisation, quartz-sericite-pyrite, quartz-tourmaline, propylitic and intermediate argillic) followed by the deposition of Ni-Co-As sulphides; (2) main-ore stage, represented by massive sulphides consisting mainly of pyrite, galena and iron-rich sphalerite with a significant amount of arsenopyrite and chalcopyrite mixed with varying amounts of quartz, fuchsite and ankeritic-dolomitic gangue; and (3) post-ore stage (quartz, carbonates ±pyrite). Additionally, stibnite and barite associated with the pyrite-galena-sphalerite paragenesis have been recognised in the vein-ore body.

- Field evidence, microtextures and mineral chemistry data indicate that sulphide formation in massive listwanites was associated with quartz veining, carbonatisation and fuchsite (Cr-mica) metasomatism.

- The pre-ore stage sulphides are characterised by two distinct groups of gersdorffite, a high temperature gersdorffite (>400°C) found in listwanite breccias, and a lower temperature gersdorffite ($\leq$ 300 °C) which formed in massive listwanites.

- The most commonly occurring type of sphalerite is the Fe-rich variety with an average ~18 mol.% FeS. Estimated formation temperatures for the main-ore stage using sphalerite with mean composition of 18 mol.% FeS and CuS compositions between 0.009 and 0.12 mol.% CuS, range between 290 and 350°C. Arsenopyrite geothermometry yielded formation temperatures between 311 and 348°C and sulphur fugacity ($fS_2$) of between $10^{-8.3}$ and $\sim 10^{-10.5}$ bar.

- Co/Ni ratio and Fe, Mn and Cd contents in pyrite and sphalerite respectively do not support MVT deposits.

- At least four carbonate generations have been recognised in the Belo Brdo deposit. The predominant carbonate phases are dolomites and ankerites.

- The compositional trend of carbonate phases is characterised by an increase in FeO and MnO and decrease in CaO and MgO from an early, pre-ore stage through to the main-ore stage.

- The REE patterns for the main-ore stage carbonates show distinct positive $Eu_N$ anomalies, indicating precipitation from reducing, acidic and high temperature fluids, whereas those for the non-mineralised limestones reflect the marine environment for their origin.

# CHAPTER 5:

# MINERALOGY OF THE KARAVANSALIJA SKARN DEPOSIT

## 5.1 Introduction

The Karavansalija Cu-Au (Pb-Zn) skarn prospect is situated on Rogozna Mountain, about 20 km southwest of Belo Brdo (see Chapter 1) and covers an area of roughly 12 km$^2$ (Carter, 2008). The area has long been known for its Pb-Zn prospectors, but became the target for Cu-Au exploration, after 2003 by Freeport-McMoRan Exploration Corporation and subsequently by EurOmax Resources since 2008. Recent exploration, which included outcrop mapping, rock chips and soil geochemistry, geophysical surveys, metallurgical tests and 32 diamond drill holes indicated a 600 metre long mineralised zone to a depth of 200 m.

During this study, several intersections of the sulphide ore were observed and a set of samples (Appendix 1), which encompassed the different stages of skarn formation and mineralisation that could be identified during field mapping, were collected from six drill cores. These samples were studied with a view to characterise the paragenetic sequence of ore deposition and to carry out fluid inclusion and stable isotope studies to compare with the Belo Brdo deposit. Twenty one polished thin sections were prepared for petrologic studies.

This chapter aims to provide a brief description of the mineralogy, textures, paragenetic sequence of deposition and mineral chemistry of the Karavansalija skarn deposit, based mainly on a new observation of dataset. It focuses predominantly on those minerals that are important for fluid inclusions and stable isotope studies, which will be discussed in later chapters.

## 5.2 Geological setting

The Karavansalija prospect belongs to the Kopaonik metallogenic district and is located within the Western Vardar Ophiolite Zone, near its contact with the Drina-Ivanjica geotectonic unit (see Chapter 2). The geology is characterised by Jurassic serpentinites, overlain by Upper Cretaceous flysch and Tertiary andesites. The whole sequence was later intruded by an Oligocene (Borojević-Šoštarić, 2009) quartz latite dyke swarm (Figure 5.1). Regional and local geology of the study area has been described in more detail in Chapters 2 and 3 of this study and will not be discussed again. Instead, additional geochemical characteristics of the igneous rocks pertinent to the skarn formation are briefly described below. A simplified geology and the SW-NE long section are depicted in Figures 5.1 and 5.2 respectively.

The emplacement of the quartz-latite dykes appears to have been structurally controlled, since they are emplaced along ENE-WSW faults perpendicular to the regional NNW-SSE structural trend of the Vardar Zone (Figure 5.1). These calc-alkaline rocks are andesitic to rhyodacitic/dacitic

**Figure 5.1:** Simplified geological map of the Karavansalija skarn prospect, also indicating locations of sampled boreholes; long section (red line) shown in Figure 5. 2 (Modified after Milutinović, 2008).

**Figure 5.2:** The Karavansalija long section (after Milutinović, 2008).

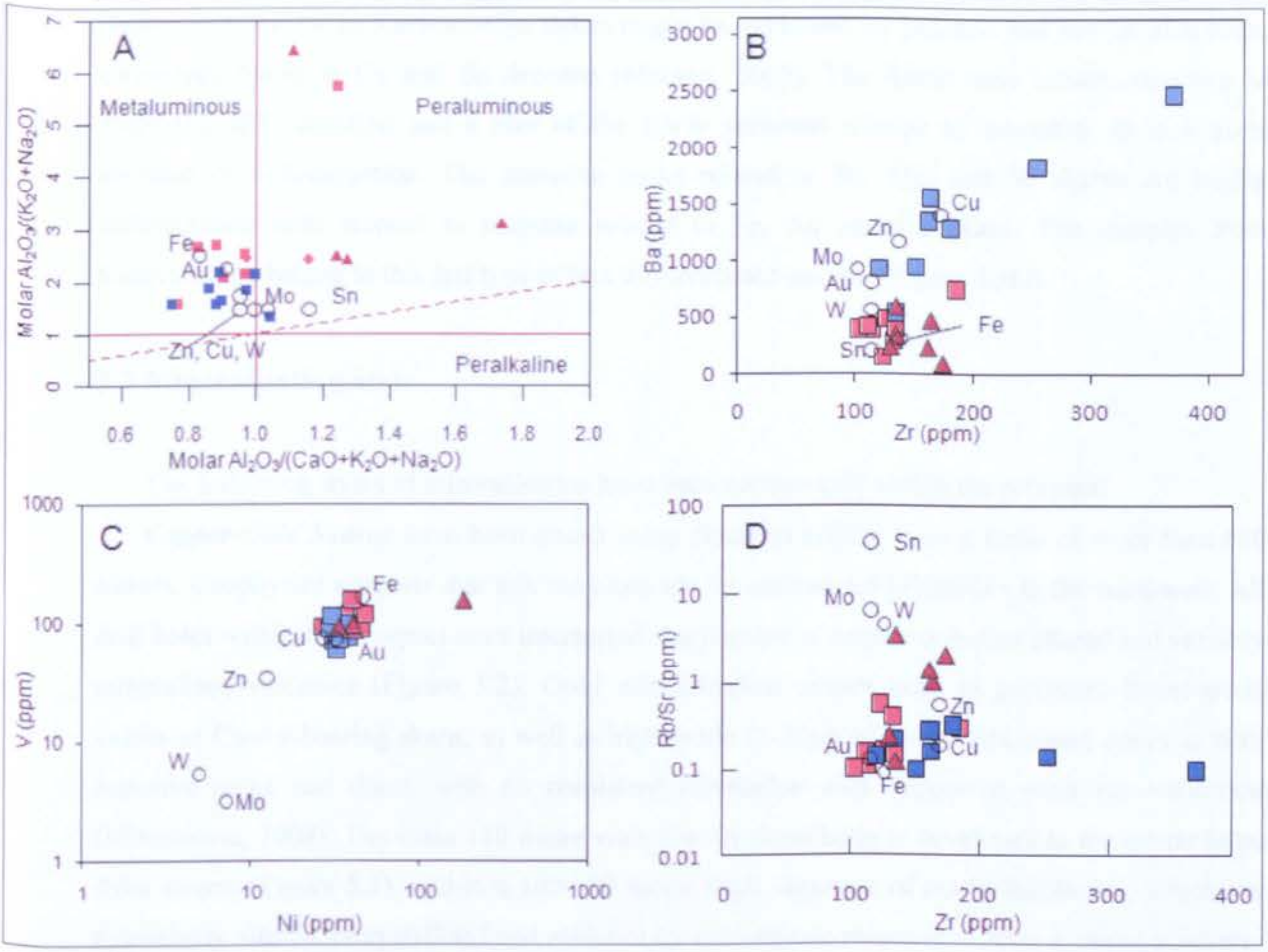

**Figure 5.3:** Major (A) and trace-element (B-D) chemistry of the Kopaonik igneous rocks (solid markers) compared to the plutons (open circles) associated with various types of skarn deposits (data from Meinert, 1995). A) Illustration of Al-saturation (A/CKN vs. A/KN diagram, according to Shand, 1943). B) Zr vs. Ba; C) Ni vs. V; and D) Zr vs. Rb/Sr plots of the Kopaonik igneous rocks. Red squares = Andesites of the First volcanic phase, Belo Brdo; Blue squares = Quartz-latites of the Second volcanic phase, Karavansalija skarn prospect; Brown triangles = Altered volcanics of the First volcanic phase. Open circles = Mean composition of plutons associated with skarn deposits world-wide.

in composition (see Chapter 3) and in terms of aluminium saturation, most compositions plot within metaluminous field or close to the division between metaluminous and peraluminous, a composition typical of intrusions associated with Fe, Cu, Au and Zn skarn deposits (Figure 5.3A) (Kwak and White, 1982; Meinert, 1993, 1995; Titley, 1993). None would be classified as peralkaline, whilst most hydrothermally altered rocks skater within the peraluminous field (Figure 5.3A). The quartz-latite dykes are also characterised by the absence of ilmenite and relative abundance of titanite and magnetite, indicating oxidised rather than reduced state of their parental magma (Frost, 1991, Frost et al., 2001; Frost and Lindsley, 1991). As with plutons associated with other Cu, Au and Fe skarns, igneous rocks of Karavansalija prospect exhibit slight enrichment in compatible elements such as Ni and V comparing to the calc-alkaline plutons associated with Mo, W and Sn skarn mineralisation (Figure 5.3C). Barium contents of Karavansalija dykes are comparable with those found in plutons associated with Cu and Zn skarns (Figure 5.3B). Ba can substitute for K in both K-feldspar and in mica and for Ca in plagioclase, amphibole and pyroxene.

Barium enrichment in Karavansalija dykes might be explained by potassic and phyllic alteration, commonly found in Cu and Zn deposits (Meinert, 2007). The Rb/Sr ratio is very sensitive to magmatic differentiation and a plot of the Rb/Sr variation relative to immobile Zr is a good measure of differentiation. The intrusive rocks related to Sn, Mo, and W skarns are highly differentiated with respect to magmas related to Fe, Au and Cu skarn. The samples from Karavansalija belong to this last type of less differentiated magma (Figure 5.3D).

## 5.3 Mineralisation style

The following styles of mineralisation have been encountered within the prospect:

***Copper-Gold Skarns*** have been traced using diamond drilling over a strike of more than 600 meters. Geophysics suggests that this zone extends for another 1.5 kilometers to the southwest. All drill holes within the prospect have intersected skarn either at surface or below altered and variably mineralised volcanics (Figure 5.2). Gold mineralisation occurs both as persistent lower-grade values in Cu-Au-bearing skarn, as well as high-grade (5-20g/t of gold) mineralised zones in both intrusive rocks and skarn, with no consistent correlation with copper or other mineralisation (Milutinović, 2008). The main 150 metre wide Cu-Au skarn body is developed in the quartz latite dyke swarm (Figure 5.1), within a 500-600 meter thick sequence of marly limestones, which are extensively altered, recrystallised and replaced by calc-silicate minerals to form a calcic exoskarn. The skarn shows evidence of prograde (Figure 5.4A and B) and superimposed retrograde stages (e.g. Einaudi et al., 1981) (Figure 5.4C-H). The prograde stage exoskarn has a massive texture (Figure 5.4A) and is composed predominantly of brown-red to honey-yellow garnet and subordinate green pyroxene (Figure 5.4A and B). Other textures, such as irregular pods, lenses and breccias are common, particularly in skarn that exhibits retrograde mineralogy (5.4 E-H), characterised by epidote, amphibole chlorite, calcite and quartz. Pyrite and chalcopyrite are disseminated throughout the host rock, but mineralisation also occurs in massive sulphide pods (Figure 5.4C) and in cross-cutting pyrrhotite-arsenopyrite and pyrite-sphalerite-galena veins (Figure 5.4 B and D).

***Lead-Zinc-Copper-Gold Skarns*** were historically exploited from the uppermost levels of the currently explored skarn system. More recent exploration indicated locally high grade mineralisation. Within the prospect, the lead-zinc skarns have not been systematically explored and their extent is unclear. However, a few kilometers southeast from the prospect the extensive lead-zinc vein stockwork has been mined by underground workings at the Crnac deposit.

***Volcanic Hosted Gold*** is found in silicified zones with massive and disseminated sulphides. Based on the results of only two drill holes the volcanic hosted gold mineralisation has a strike of at least 200 meters with a similar width. Diamond drill hole PDMC-0503 intersected 42 meters from

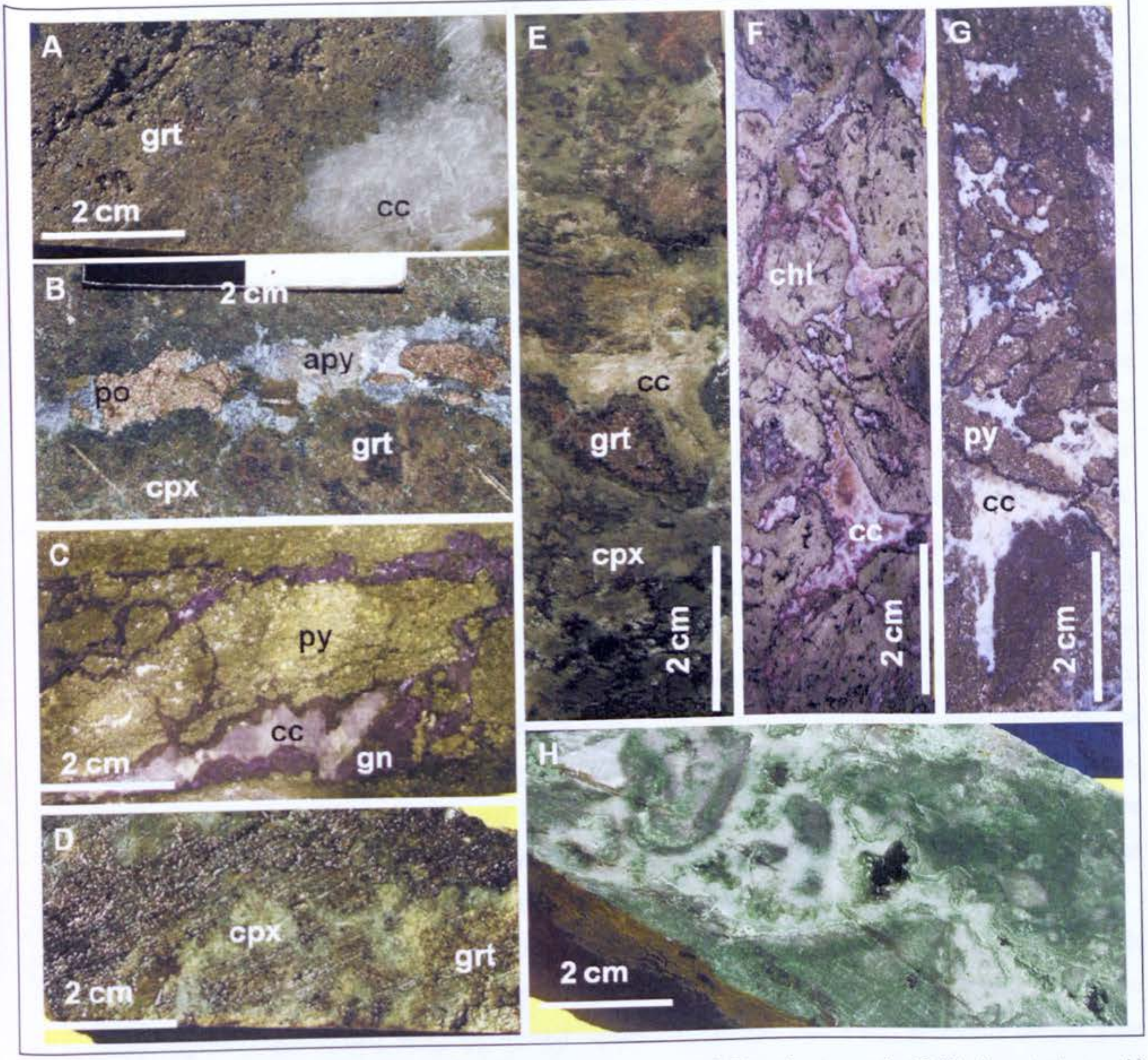

**Figure 5.4:** Photographs of drill core showing prograde (A and B) and retrograde (C-H) skarn textures. A) Massive skarn composed of garnet with pods of late stage coarse-grained calcite (sample KU 29). B) Garnet and pyroxene skarn cross-cut by pyrrhotite, arsenopyrite, quartz-carbonate vein (sample KU08-31-3). C) Massive sulphide pods of pyrite, galena and sphalerite cemented by late stage calcite (sample KU07-24-3). D) Pyrrhotite and chalcopyrite vein cutting garnet-pyroxene skarn (sample KU36). E) Pods of coarse-grained garnet and pyroxene replaced by chlorite and cemented by calcite (sample KU08-31-1). F) Breccia composed mainly of chlorite, cemented by calcite (sample KU07-24-1). G) Ore breccia composed of pyrite aggregates, succeeded by galena and cemented by calcite (sample KU07-24-2). H) Epithermal-type silica breccia composed mainly of quartz and epidote with rare disseminations of Ni-Co minerals; prismatic late-stage quartz crystals fill the vug cavities (sample KU71). Abbreviations: apy-arsenopyrite, cc-calcite, chl-chlorite, cpx-clinopyroxene, cpy- chalcopyrite, gn-galena, grt-garnet, py-pyrite.

surface at 3.1 g/t gold including 28 meters at 4.37 g/t gold.

***Silica Breccias.*** Five diamond drill holes at the eastern end of the exposed copper-gold skarn mineralisation intersected epithermal textured (Figure 5.4 H) silica breccia beneath altered volcanics (Figure 5.2). No hole has penetrated the silica breccia unit and it does not outcrop, consequently its areal extent is unclear. A high order gravity anomaly at depth beneath the silica-breccia remains unidentified.

## 5.4 Skarn petrography and mineralogy

The principal skarn minerals in the Karavansalija deposit are garnet, clinopyroxene, epidote, and amphibole, together with quartz, chlorite, titanite, calcite, and apatite as subordinate or accessory minerals. Paragenetic studies based on macro- and microtextures show that the formation of skarn occurred in several stages, similar to other skarns globally (Meinert, 1992; 2007). The early mineral phases are anhydrous, whereas later, retrograde stages are predominantly hydrous. The alteration of the host rock marble in the Karavansalija prospect is marked by the formation of coarsely crystalline skarn lenses due to the introduction of Si-, Al-, Fe-, and Mg-rich fluids into the host rock. The earliest changes observed in the protolith involved a recrystallisation of Cretaceous limestones to form coarse-grained marble (Figure 5.5A). This stage was followed by metasomatism of carbonate host rock, which produced anhydrous mineral assemblage characterised by andradite, grossular-andradite and clinopyroxene exoskarn (Figure 5.5B and C) with subordinate vesuvianite. The retrograde stage is characterised by epidote, chlorite, amphibole, calcite and quartz (Figure 5.5 D-F). During the retrograde stage, Fe-enriched minerals, such as magnetite, tremolite and Fe-chlorite (brunsvigite) were formed (full data given in Appendix 4). Garnet is optically isotropic to weakly anisotropic (Figure 5.5B). Its texture varies from very fine grained anhedral aggregates to coarse-grained sub to euhedral. Larger grains generally exhibit slight optical zoning (grossularite-andradite) which is parallel to crystal faces or sometimes show a sector zoning. Pyroxenes are generally anhedral to subhedral and occur either intergrown with garnet, or as thin, almost monomineralic layers (Figure 5.5C) rhythmically banded with garnet layers.

Subsequent hydrothermal mineralisation is characterised by a deposition of ore minerals (Figure 5.6), starting with an early pyrite-pyrrhotite assemblage (5.6A), followed by massive chalcopyrite (Figure 5.6B), arsenopyrite and iron-rich sphalerite. Pyrite and pyrrhotite are the most abundant sulphides, locally forming aggregates up to several centimetres. Pyrite also occurs disseminated throughout the host skarn. Pyrrhotite is locally replaced by chalcopyrite. In course of replacement of older silicates by pyrite-pyrrhotite aggregates, abundant grossular-rich garnets were enclosed in sulphides (Figure 5.6A). Arsenopyrite (Figure 5.6C and D) was the next sulphide phase. It is observed as irregular aggregates or single grains with typical rhombic shape of the crystals. In addition to chalcopyrite, arsenopyrite contains microscopic inclusions of löllingite, complex arsenian sulphosalt enriched in gold and irregular aggregates of Bi-minerals, distributed along microfractures and arsenopyrite growth zones. The Ni-Co association (Figure 5.6E), including minerals like krutovite, gersdorffite, gersdorffite-krutovite, nickeline is confined to a strongly silicified breccia, which is found in the eastern part of the skarn system. This Ni-Co association was not observed in the main skarn ore zone. The last sulphide phases deposited were sphalerite and galena (Figure 5.6E), which also occur as cross-cutting veins in the upper part of the skarn system (Figure 5.6F). Mineral chemistry data are presented in Appendix 4 on a CD-ROM enclosed at the back of this report.

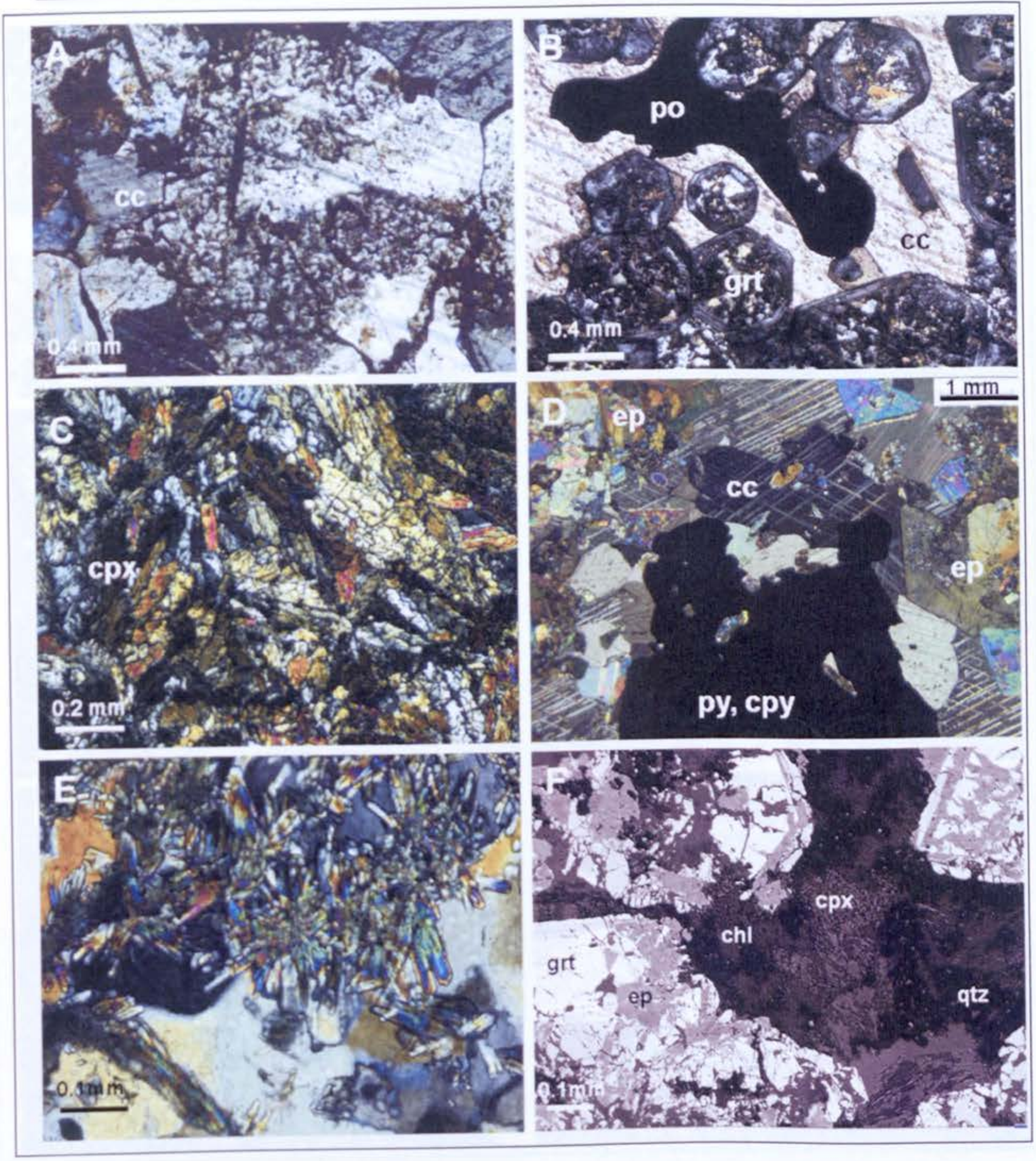

**Figure 5.5:** Photomicrograph taken under plain polarised (A) and cross polarised light (B-E) and BSE image (F) showing typical exoskarn textures from different stages of skarn formation. A) Marble showing the granoblastic texture produced by recrystallised twinned calcite; dark patches are dense fluid inclusions (doubly polished wafer 100 microns thick; sample NZ-7 from the outcrop at road cutting). B) The isotropic and anisotropic zoned grossular-andradite crystals at the garnet zone of the exoskarn, with calcite crystals and anhedral pyrrhotite filling intercrystal vugs (sample KU08-31-1). C) Monomineralic thin layer of clinopyroxene (sample KU08-31-4). D) Coarse-grained epidote and calcite completely replacing early prograde skarn minerals; single grains of mineral from the amphibole group are observed as sporadic long prismatic grains or aggregates with light greenish colour typical for tremolite; note pyrite and chalcopyrite mineralisation replacing late calcite cement (sample KU32). E) Spherullitic aggregate from epidote group mineral; epidote in the core and prismatic aggregates of zoisite at the periphery in the quartz groundmass; apart from granoblastic aggregates, quartz in this sample also occurs as prismatic crystals with feather-like extinction and it was used for fluid inclusion studies (sample KU69). F) Typical retrograde mineral assemblage with epidote replacing zoned grossular-andradite and chlorite replacing clinopyroxene during K-spar-quartz-chlorite alteration of the prograde calc-silicate skarn assemblage. Abbreviations: cc-calcite, chl-chlorite, cpx-clinopyroxene, cpy- chalcopyrite, ep-epidote, grt-garnet, py-pyrite.

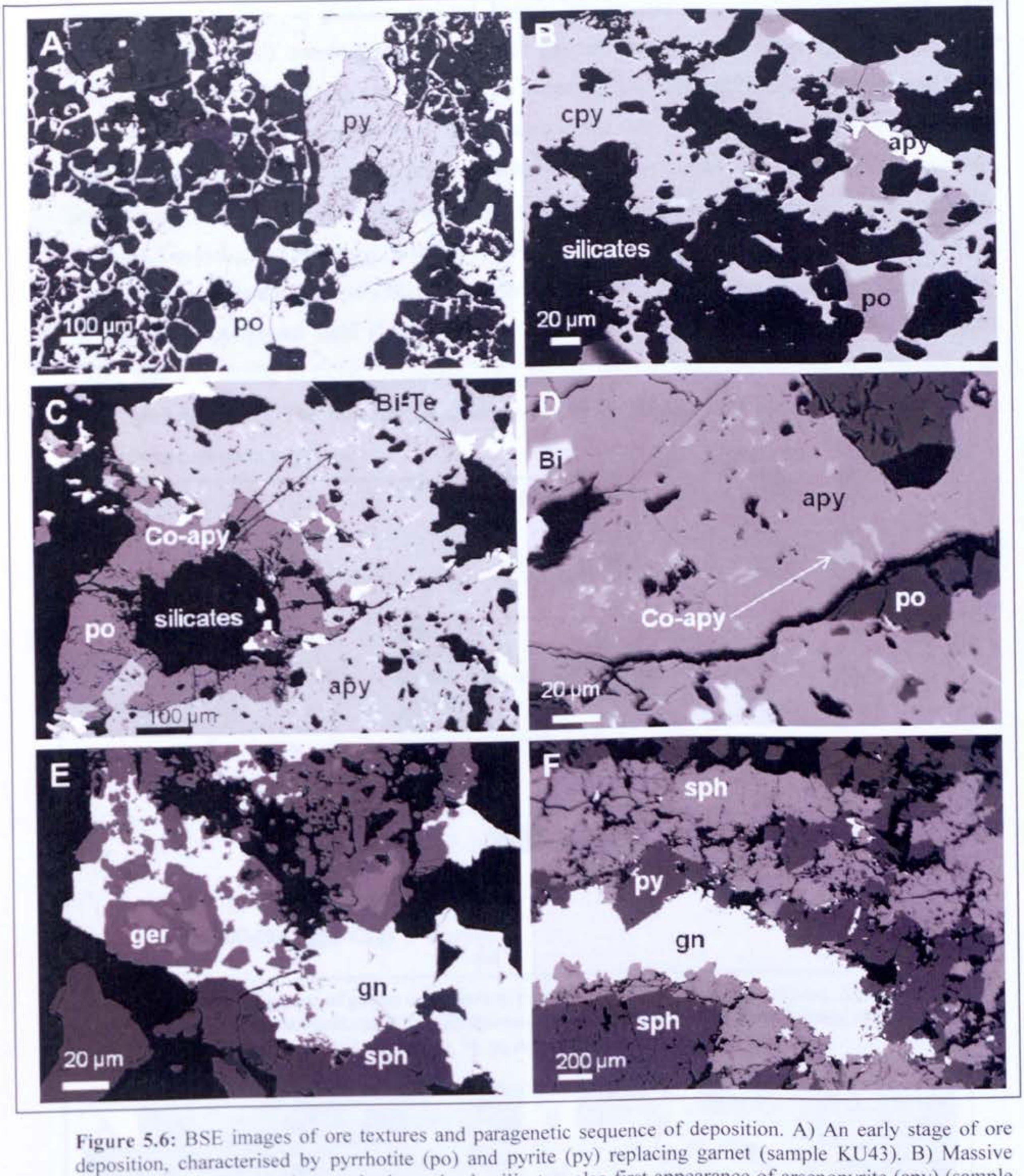

**Figure 5.6:** BSE images of ore textures and paragenetic sequence of deposition. A) An early stage of ore deposition, characterised by pyrrhotite (po) and pyrite (py) replacing garnet (sample KU43). B) Massive chalcopyrite (cpy) replacing pyrrhotite and calc-silicates; also first appearance of arsenopyrite (apy) (sample KU43). C and D) Anhedral arsenopyrite replacing pyrrhotite and hosting numerous inclusions of cobaltifferous-auriferous arsenopyrite and Bi-Te minerals (sample KU29). E) Sphalerite (sph) and galena (gn) replacing early gersdorffite (ger) in silica breccia (sample KU69). F) Pyrite-sphalerite-galena vein cross-cutting skarn mineralisation (sample KU07-24-3).

## 5.5 Garnet and pyroxene mineral chemistry

All ***garnets*** analysed belong to the grossular-andradite series (Figure 5.7A) and their compositions (Appendix 4) are close to those of garnets from Au-Cu and Fe-Cu skarns worldwide (Einaudi et al., 1981; Meinert, 1992). Broadly, two compositional types of garnets are observed in the exoskarn (i) fine- to medium-grained largely anisotropic grossular-andradite garnets with oscillatory zoning (ii) coarse-grained andraditic garnets, isotropic with thin "more grossularic" rims. Compositional zoning is also revealed by SEM analyses, but the trend of the change is not systematic. Most garnet grains show Fe enrichment in the rims and Al enrichment in the core. The composition changes from core to margin include: $Gr_{63}Ad_{36}$ to $Gr_{32}Ad_{67}$ (Figure 5.7B and 5.8). Some grains, however, have the opposite trend: from core to margin the compositions are $Gr_{0}Ad_{100}$, $Gr_{47}Ad_{53}$, $Gr_{57}Ad_{42}$, and $Gr_{66}Ad_{33}$ (grnt2 in Figure 5.8)

The ***pyroxenes*** are generally diopsidic to hedenbergitic, except for four samples which plot in the augite compositional field (Figure 5.9A). Their main composition is $Di_{32-72}$ $Hd_{26-67}$ (Figure 5.9B), which is similar to those pyroxenes from Au-Cu and Fe-Cu skarns worldwide (Einaudi et al. 1981; Meinert 1992). The average composition is $Di_{32-84}$ $Hd_{15-67}$ with minor contribution of the johansenite component ($Jo_{0.7-8}$).

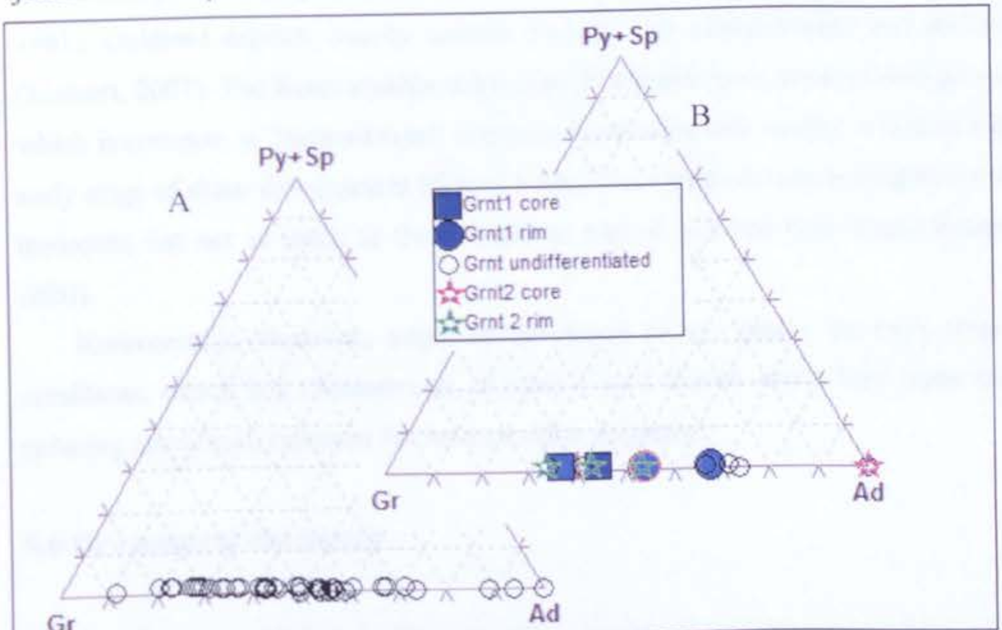

**Figure 5.7:** Ternary diagram of garnet composition based on recalculated SEM analyses. A) General composition of all analysed garnets. B) Detail showing two compositional types of garnets, within the same sample (KU29). Gr-grossular, Ad- andradite, Py-pyrope, Sp-spessartine.

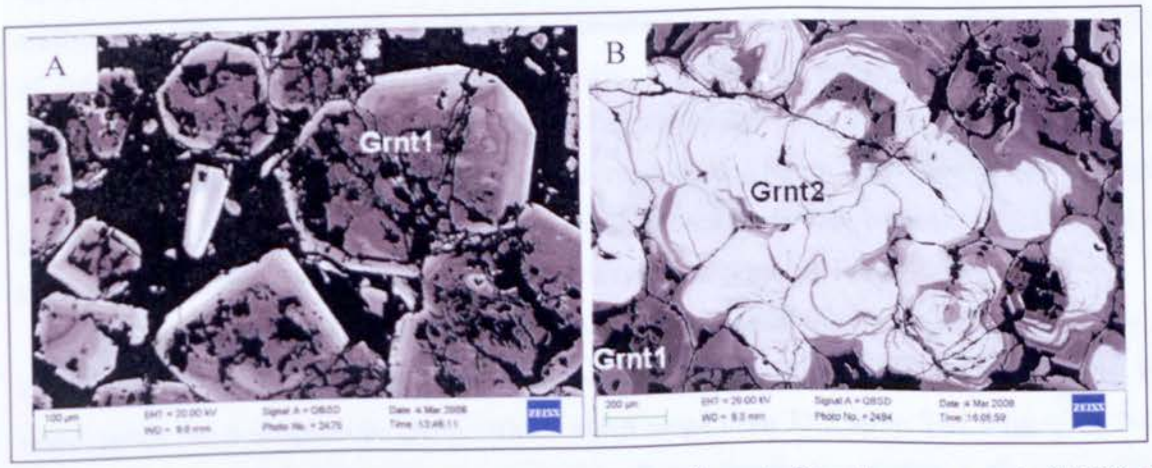

**Figure 5.8:** Textural evidence for two compositional types of garnets from the same sample (KU29). Both garnets show retrograde textures: garnet 1 (A) is fractured and brecciated and garnet 2 (B) exhibits shock-induced inhomogeneous edges (Ciobanu and Cook, 2004).

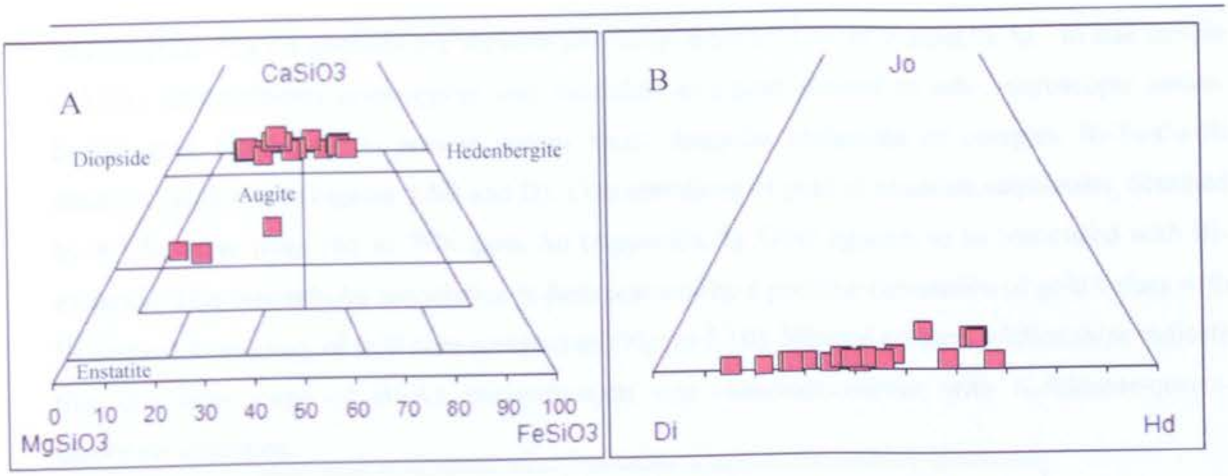

**Figure 5.9:** Ternary diagram of pyroxene composition based on recalculated SEM analyses.

Garnet and pyroxene compositions can indicate redox conditions of a skarn system (Einaudi et al., 1981). Oxidised deposits mainly contain diopside-rich clinopyroxene and andradite- rich garnet (Meinert, 2007). The Karavansalija skarn deposit contains both, predominant grossular-rich garnet, which is common in "reduced type" skarns and andradite-rich variety, which is mainly found in an early stage of skarn development (Figure 5.8B). The clinopyroxene is slightly enriched in diopside molecule, but not as much as those found in typical oxidised type skarns (Gaspar and Inverno, 2000).

Karavansalija, therefore, might be developed in two stages, an early stage with oxidising conditions, which is a characteristic of many Cu-Fe skarns, and a later stage indicative of more reducing conditions, common for Au-type skarn deposits.

### 5.6 Ore mineral chemistry

The ore assemblages in Karavansalija consist of variable proportions of a few common sulphide minerals. The sulphide mineralisation developed in three main stages. An early stage is represented by pyrrhotite ($Fe_{0.95}S$), chalcopyrite ($CuFeS_2$), iron-rich sphalerite ($Zn_{0.81}Fe_{0.22}S_{0.97}$), arsenopyrite [$(Fe_{0.99}Co_{0.01})AsS$], pyrite and subordinate magnetite. The intermediate stage consists of cobaltian arsenopyrite [$(Fe_{0.87}\ Ni_{0.01}Co_{0.13})\ As_{0.94}S_{1.05}$], pyrite, native Bi, bismuthinite, minor pyrrhotite ($Fe_{0.93}S$), chalcopyrite and As-Co-Bi-Te sulphosalts. The latest stage of ore deposition is characterised by sphalerite-galena-pyrite veins cross-cutting skarn formation at the uppermost portion of the mineralised system. Late stage sphalerite has lower iron content (6 – 13 mol.% FeS) compared to sphalerite from the early paragenesis (up to 20.5 mol.% FeS).

*Arsenopyrite* from Karavansalija deposit display high variability in As (25.5-34.9 at. %) and Co (up to 10 at. %) contents. Two compositional groups have been recognised. An early arsenopyrite has homogeneous compositions which range from 32.2 up to 34.1 atom.% As with a mean of 32.9 atom.% As. The second generation of arsenopyrite is enriched in Co (up to 16.6%) and Ni (up to 1.6%) and contains inclusions of native bismuth, bismuthinite and cobaltifferous arsenopyrite. The As contents are variable and range from 25.5 to 34.9 atom.% As. In one sample (KU29), cobaltifferous arsenopyrite was identified as a host mineral to sub- microscopic lattice-bound gold. Here, gold is present within small, irregular inclusions of complex Bi-Te-Co-Ni arsenian sulphosalts (Figures 5.6B and D). Concentrations of gold in arsenian sulphosalts, obtained by WDS, range from 161 to 790□ppm Au (Appendix 4). Gold appears to be associated with Bi-minerals. This bismuth-Au association is demonstrated by a positive correlation of gold values with Bi content from assay of drill core composites (Figure 5.10). Mineral textural relationships indicate that this later stage of Bi-Au mineralisation was contemporaneous with K-feldspar-quartz-carbonate alteration.

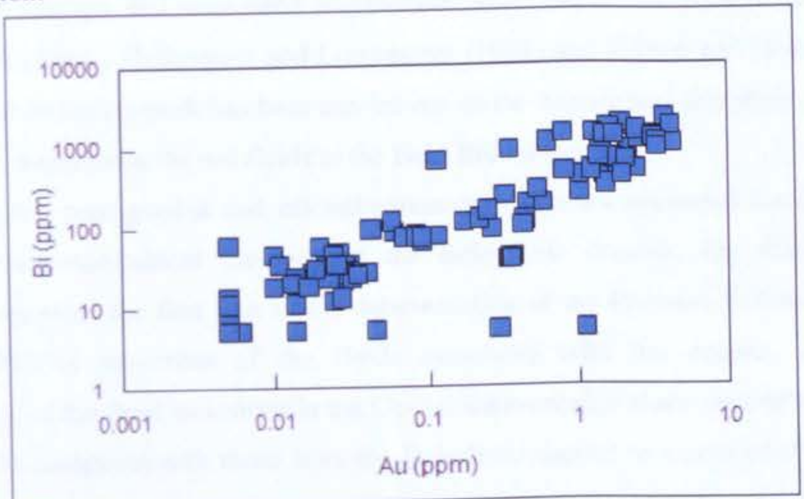

**Figure 5.10:** Bi-Au association; assays from the borehole PDMC 06-20 (data provided in Appendix 1; Boreholes)

## 5.7 Summary

- The Karavansalija Cu-Au skarn deposit is associated with an Oligocene quartz-latite dyke swarm. The quartz-latite dykes were emplaced along ENE-WSW faults perpendicular to the regional NNW-SSE structural trend of the Vardar Zone.
- Major and trace-element chemistry of the volcanic rocks indicate calc-alkaline metaluminous character, typical of intrusions associated with Fe, Cu, Au and Zn skarn deposits.
- Petrographic and mineral chemistry data show that the formation of skarn occurred in several stages. An early stage is characterised by a recrystallisation of Cretaceous limestones to form coarse-grained marble followed by metasomatism of carbonate host rock, which produced anhydrous mineral assemblage composed of andradite, grossular-andradite, diopside-hedenbergite and vesuvianite. The retrograde stage is characterised by epidote, chlorite, amphibole, calcite and quartz.
- The main-ore stage is represented by pyrite, pyrrhotite, chalcopyrite, arsenopyrite and iron-rich sphalerite. Accessory sulphides include Ni-Co-As mineral association.
- Gold is associated with Bi minerals, which occur as inclusions in cobaltifferous arsenopyrite.

# CHAPTER 6:

# FLUID INCLUSION STUDIES OF THE BELO BRDO DEPOSIT

## 6.1 Introduction

A fluid inclusion study of the Belo Brdo deposit was carried out in order to provide constraints on the temperature and composition of the ore-forming fluids. The study focuses on the question of whether the ore-forming fluids in Belo Brdo are of magmatic-hydrothermal type, similar to those in porphyry copper systems and associated polymetallic vein, skarn, and replacement deposits, as described by Cox (1986), Hedenquist and Lowenstern (1994) and Sillitoe and Hedenquist (2003). No previous fluid inclusion work has been carried out on the deposit and this study thus represents a first attempt to characterise the ore fluids in the Belo Brdo deposit.

In this chapter, petrographic and microthermometric data are presented for fluid inclusions from the carbonate-replacement ore-body of the Belo Brdo deposit. The microthermometric measurements represent the first step in the determination of the Pressure-Volume-Temperature-Composition (PVTX) properties of the fluids associated with the deposit. Additionally, a preliminary study of the fluid inclusions in the Cu-Au Karavansalija skarn deposit has been carried out and its results compared with those from the Belo Brdo deposit to assess whether they exhibit genetically similar properties.

## 6.2 Sampling

All available polished thin sections which were studied to document mineral paragenetic relationships (see Chapter 4), were also examined for the suitability of a particular mineral for fluid inclusion analysis. Although numerous samples were collected for fluid inclusion study, a total of seventeen doubly polished wafers, approximately 150 µm thick, were prepared. These sections define a depth range of 195 m of the main GII replacement type ore body of the Belo Brdo deposit. Most of the wafers were derived from specimens in which the paragenetic setting of the studied gangue and ore minerals could clearly be identified as belonging to the main mineralisation stage. No suitable host mineral (quartz or carbonates) was identified in the samples from the pre-ore mineralisation stage. Fluid inclusion analyses from the late ore-stage were conducted on two of the samples which contained quartz crystals of 4-5 mm in size (Figure 6.1A and B). For the main mineralisation stage, four doubly polished wafers from different underground levels (1055, 1080, 1099 and 1105m) contained quartz cogenetic with the sulphides that were selected for fluid inclusion study (Figure 6.1C), even though they contained inclusions of very small size (<10 µm) (Figure 6.1D). Quartz in the Belo Brdo deposit is the most suitable fluid inclusion host mineral because it is often highly transparent, has no cleavage and has high mechanical strength, so it can

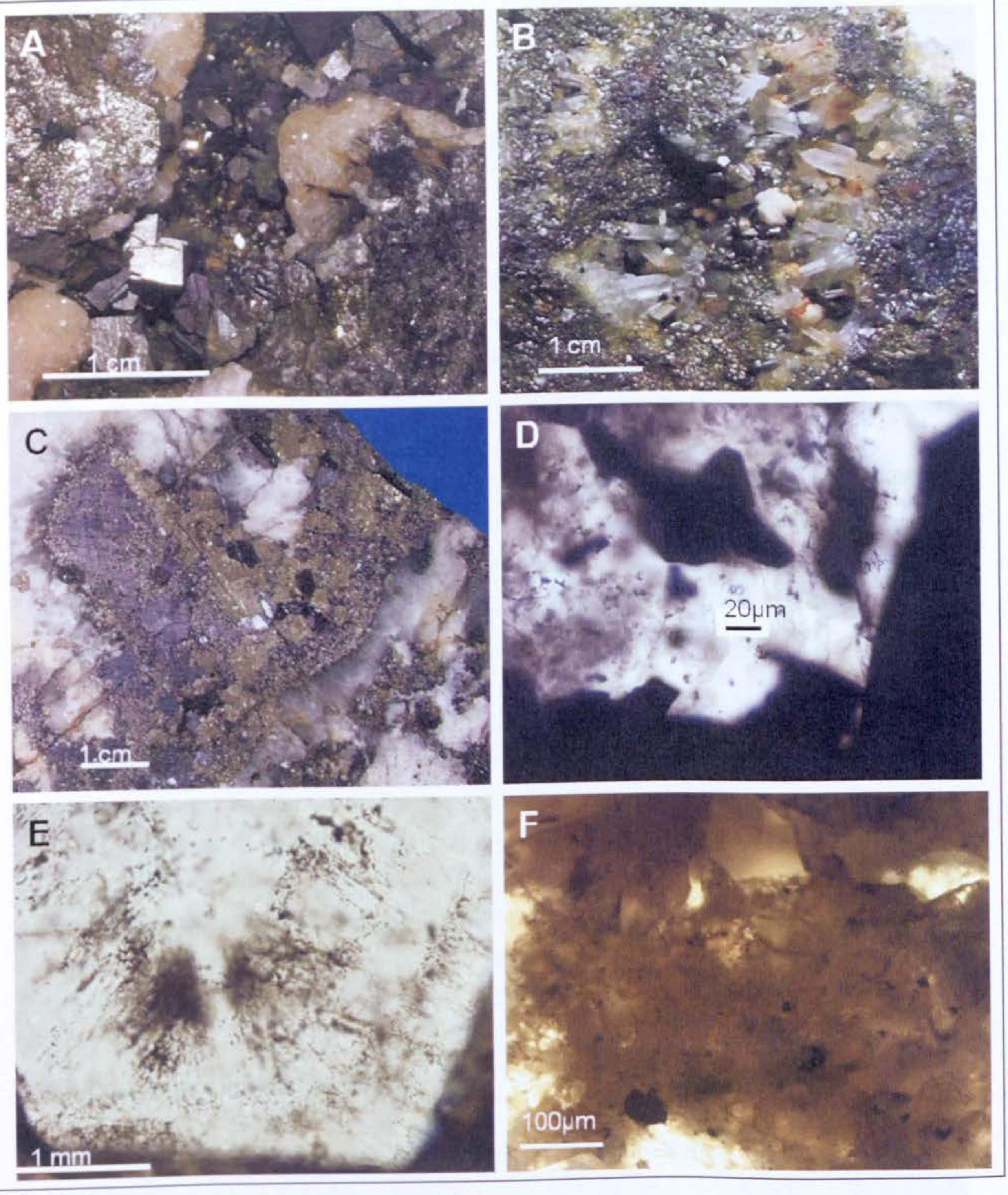

**Figure 6.1:** Examples of quartz crystals as the main fluid inclusion host mineral in the replacement-type ore body of the Belo Brdo deposit (A-E) and carbonate-quartz gangue minerals in vein-type ore body with no suitable fluid inclusions for microthermometric studies (F). A and B ) Quartz crystals (4-5 mm size), representing late stage mineralising fluids (Samples 1080/1D and 1099 respectively). C) Cut and lapped specimen showing breccia ore and quartz gangue mineral cementing pyrite, galena and sphalerite (Sample 1055/4D). D) Photomicrograph showing typical co-genetic quartz hosting isolated presumed primary inclusions (Sample 1105/4). E) Growth zones in euhedral quartz exhibiting a large number of very small (black patches) primary inclusions (*Type I*), which were not suited for microthermometry. F) Carbonates (brown) and quartz (light cream) with no suitable fluid inclusions for thermometric study (Sample 1235 from the vein-type ore body).

withstand large internal fluid pressures during heating experiments (Goldstein and Reynolds, 1994; Van den Kerkhof and Hein, 2001). As far as size and abundance of fluid inclusions are concerned, the majority of quartz crystals, however, did not contain inclusions of sufficient size (> 2-3 μm) and could not be studied in detail (Figure 6.1E). The number of inclusions analysed was small, between three and ten inclusions per sample for a total of 70 inclusions. Similarly, fluid inclusions in carbonates turned out to be very small (< 5 μm), and therefore were not suitable for microthermometric studies. Sphalerite could not be analysed because of its dark colour and lack of transparency due to the high iron content. A heating/cooling stage equipped with an infra-red light microscope was not available during this study. Despite the presence of common gangue minerals such as quartz, dolomite and barite, no systematic study of fluid inclusions was possible from the vein –ore body because of the fine-grained or cryptocrystalline character of their aggregates (Fig 6.1F).

Fluid inclusion types were documented, free-hand sketched and photographed. Suitable fluid inclusions from six samples were selected for microthermometry. Most fluid inclusions were also analysed using laser Raman spectroscopy at Kingston University for the presence of gaseous phases and the absence of major volatiles other than $H_2O$ was confirmed.

Many practical problems associated with the collection of valid microthermometric data were encountered during the fluid inclusion study. These include the following: lack of good host minerals, small inclusion size and poor abundance, poor optical clarity and sometimes leakage of inclusions during heating. Additionally, post-entrapment processes, which may significantly modify inclusions, include recrystallisation and replacement of host minerals. Nevertheless, great efforts were made to identify suitable inclusions for microthermometric measurements. Mainly those inclusions with consistent liquid: vapour phase ratios and only those samples that display the clearest textural evidence of primary growth were selected for analysis. Fluid inclusion assemblages (FIAs) as defined by Goldstein and Reynolds, (1994) were not recognised in samples from Belo Brdo.

## 6.3 Petrography of fluid inclusions

Fluid inclusions observed in quartz can be classified as primary, secondary or pseudo-secondary using criteria described in Roedder (1984). Classification of each inclusion in Belo Brdo was not always straight forward. Their primary nature was determined in cases where they occur parallel to growth zones in the quartz or in clearly isolated positions and small clusters without a clear textural relation to growth zones (Figure 6.2A-C). Inclusions, which mainly occurred in trails filling fractures in quartz or close to cleavage planes in carbonates and barite (barite only present in the vein ore-body), were excluded from thermometric study. Additionally, inclusions which were obviously secondary such as those that had variable liquid: vapour ratios or had necked down were

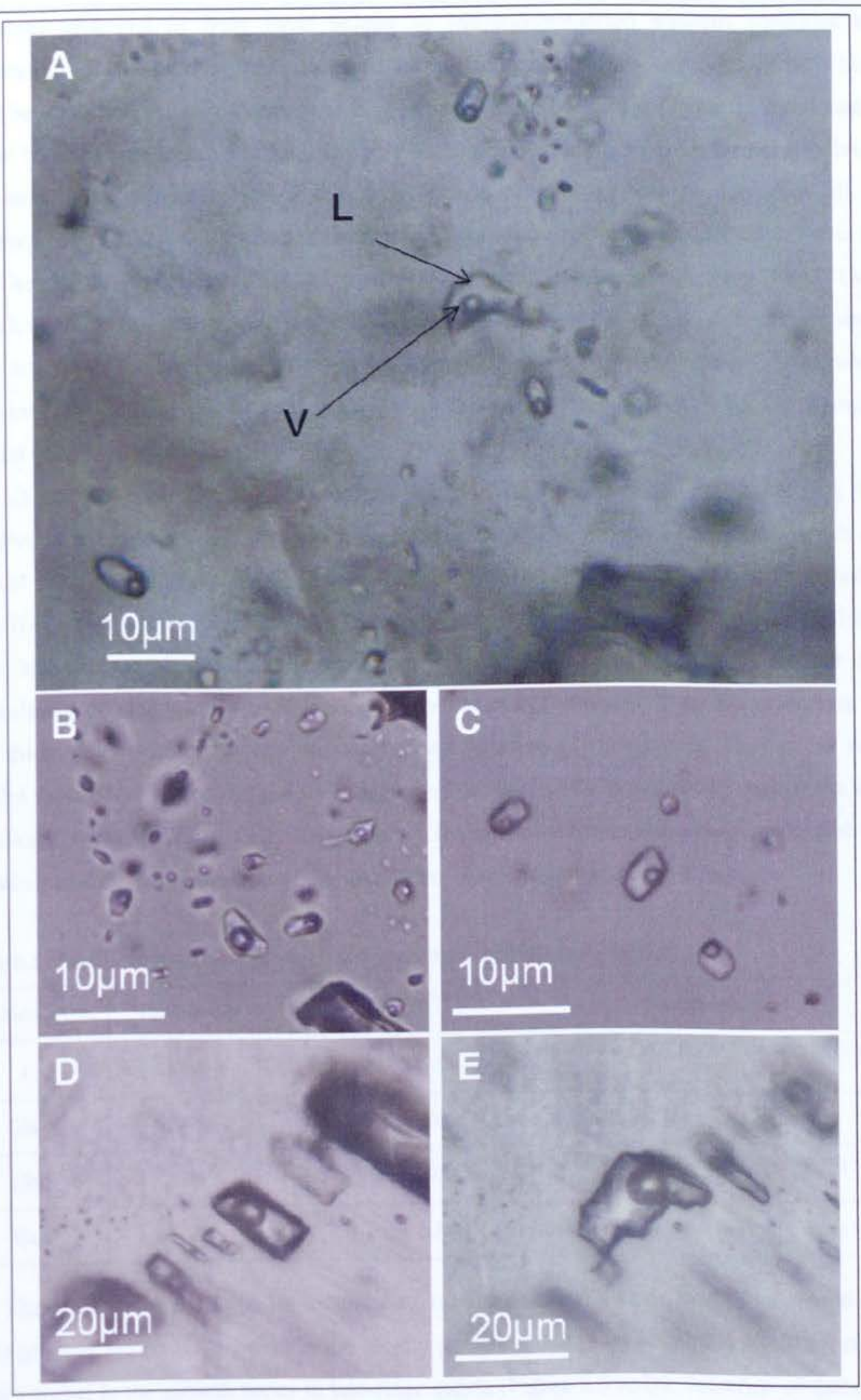

**Figure 6.2:** Photomicrographs of typical Type IIa (A-C) and Type IIb (D and E) aqueous fluid inclusions A) sample 180/1F; B) sample 1105/4-2-Fia-6; C) sample 1105/4-2 Q2; D) and E) sample 1080n Q3.

avoided. Inclusions with anomalously small or large gas bubbles relative to the surrounding ones were considered candidates for leakage and were also excluded from the study. Fluid inclusions were viewed through an Olympus optical microscope with up to 100x magnification. All the fluid inclusions observed in Belo Brdo belong to salt-undersaturated aqueous solutions at room temperature. Based on the phases observed at room temperature only two types of fluid inclusions could be identified, namely monophase liquid (Type I) and two-phase (Type II) liquid and a small vapour bubble (Figures 6.2 and 6.3). The two-phase aqueous solutions were further subdivided into three descriptive sub-categories on the basis of their morphology and the degree of fill. A brief summary of fluid inclusion types and their morphological properties are presented in Table 6.1.

The *Type I* inclusions include monophase liquid inclusions and very small two-phase inclusions (< 2 µm), which were not suited for microthermometric studies due to their small size. They are often concentrated along growth zones of euhedral quartz crystals. The monophase inclusions showed no phase transitions during microthermometric runs and the Raman study showed no presence of volatiles.

All of the observed fluid inclusions of *Type II* have a high degree of fill, (volume liquid/volume liquid + volume vapour), typically 0.7-0.9. The group of inclusions, which occur as isolated primary inclusions and have fairly regular oval and rounded outlines, are described here as Type IIa inclusions (Figure 6.2A-C). They vary in size from 2 µm to up to 10 µm and resemble those inclusions typical of epithermal environments (Bodnar et al., 1985). Neither daughter minerals nor other liquids (e.g.$CO_2$) were microscopically observed. Type IIb inclusions are dark with thick black outlines exhibiting angular and negative crystal shapes. They occur in groups parallel to the crystal growth and their degree of fill is slightly less than the rest of the observed inclusions (Figure 6.2D and E). Their slightly higher homogenisation temperatures and negative crystal shapes indicate primary entrapment during the main mineralisation stage.

**Table 6.1** Classification of aqueous fluid inclusions from the Belo Brdo deposit.

| Inclusion Type | Abundance | Size | Degree of fill | Morphology |
|---|---|---|---|---|
| I | Common | <2µm | 0.95-1 | Too small to be analysed; also monophase inclusions. |
| IIa | 51.4% | 2-10 µm | 0.85-0.9 | Oval or spherical; sometimes flat. |
| IIb | 20% | 5-15 µm | > 0.7-0.8 | Dark, "3D" appearance; some negative crystal shapes; rarely irregular. |
| IIc | 28.6% | 10-50 µm | 0.8-0.85 | Irregular, large, parallel to crystal growth. |

The majority of the Type IIc inclusions have flat irregular shapes, with a maximum diameter of 50 µm and are much larger than the locally present small primary inclusions. They commonly occur parallel to the growth zones in late-stage quartz (Figure 6.3 A-D). Selection of these types of inclusions ensures that the fluids were trapped during a final stage of quartz crystal growth. No evidence of $CO_2$-bearing fluid inclusions was found in any sample.

Vapour rich inclusions were present in two samples (180/new and 180/1D) within the late stage quartz crystals. These form a minor part of the total fluid inclusion population. It was difficult to distinguish weather those inclusions represent heterogeneous trapping or necking (Figure 6.4C and D). A few inclusions containing a solid phase were observed in two samples (1099, 1080/1D). Because of its random distribution and lack of dissolution on heating it is assumed that this solid phase represents a mineral trapped from the fluid during inclusion growth (Rankin and Alderton, 1983).

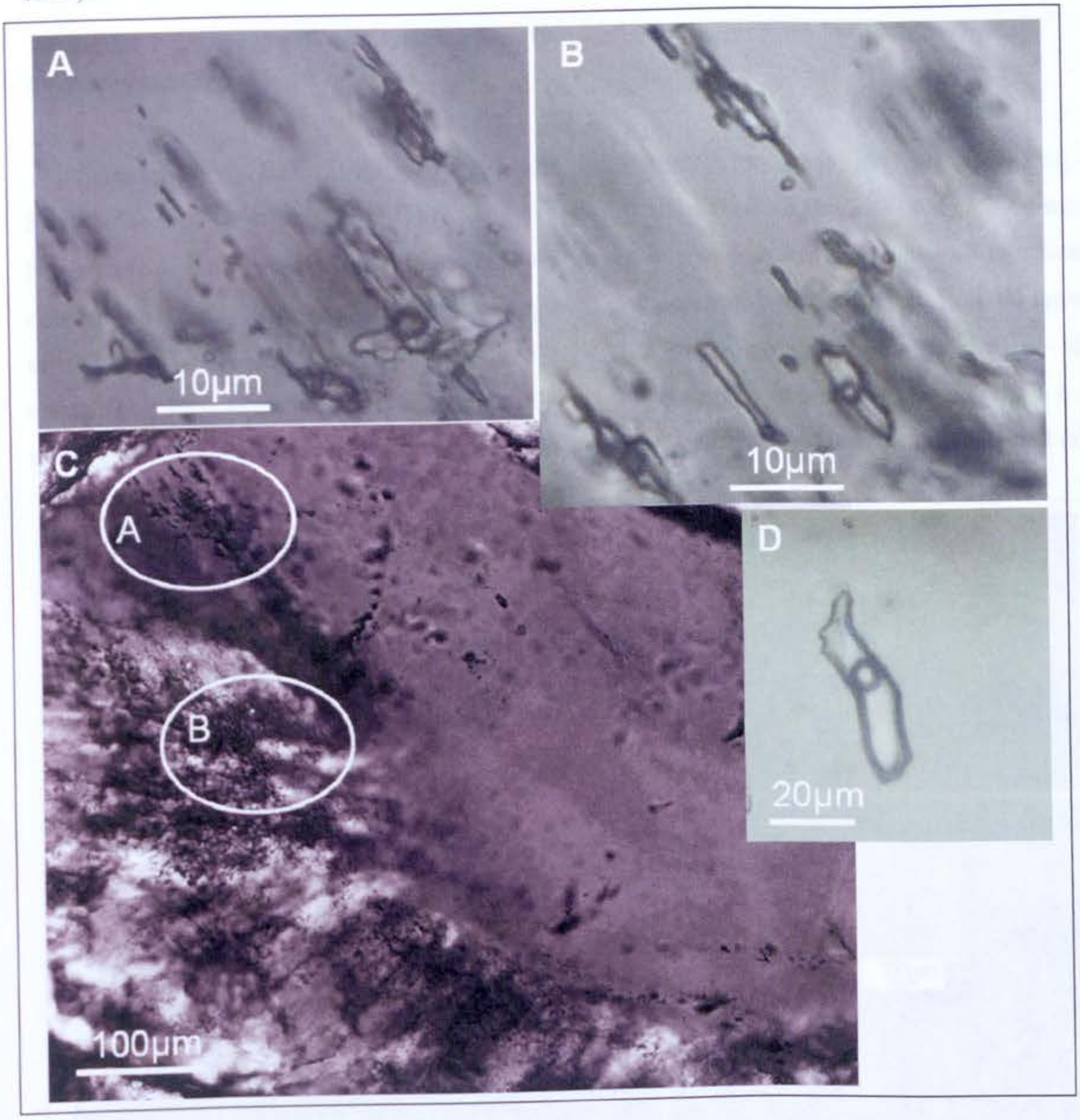

**Figure 6.3:** Photomicrographs of typical Type IIc fluid inclusions of irregular shape (A and B, position of insets shown in C) occurring parallel to the crystal growth and isolated (D) with no textural relation to the growth. Sample 1055/4D (A-C) and 1099 (D).

## 6.4 Microthermometric analysis

### *6.4.1 Introduction*

Microthermometry involves a non-destructive (optical) monitoring of the phase changes in fluid inclusions, including liquid, vapour, and solid daughter minerals during controlled heating and cooling (Bodnar, 2003). Microthermometry enables determination of general fluid properties such as salinity and basic compositions, including identification and semi-quantification of some volatiles such as carbon dioxide (Roedder, 1984; Haynes, 1985; Hall et al., 1988; Vanko et al., 1988; Bodnar, 1993). This technique is also used to infer minimum trapping temperatures and pressure conditions at entrapment (Potter, 1977; Roedder and Bodnar, 1980; Zhang and Frantz, 1987; Brown and Lamb, 1989).

### *6.4.2 Methodology*

Samples from Belo Brdo were selected for microthermometric analysis according to Roedder's (1984) criteria, implying a selection of the fluid inclusions with a constant, homogeneous liquid/vapour ratio. Great care was taken in ensuring that the inclusions represent a constant volume system, so that no post-entrapment processes took place such as: mineral growth on the inclusion walls; or leakage (Figure 6.4A and B); or re-equilibration of inclusions after entrapment, such as inclusions with scalloped walls (Figure 6.4C) or necking down (Figure 6.4D and E), which is illustrated by the presence of an unusually larger vapour bubble and extended tails.

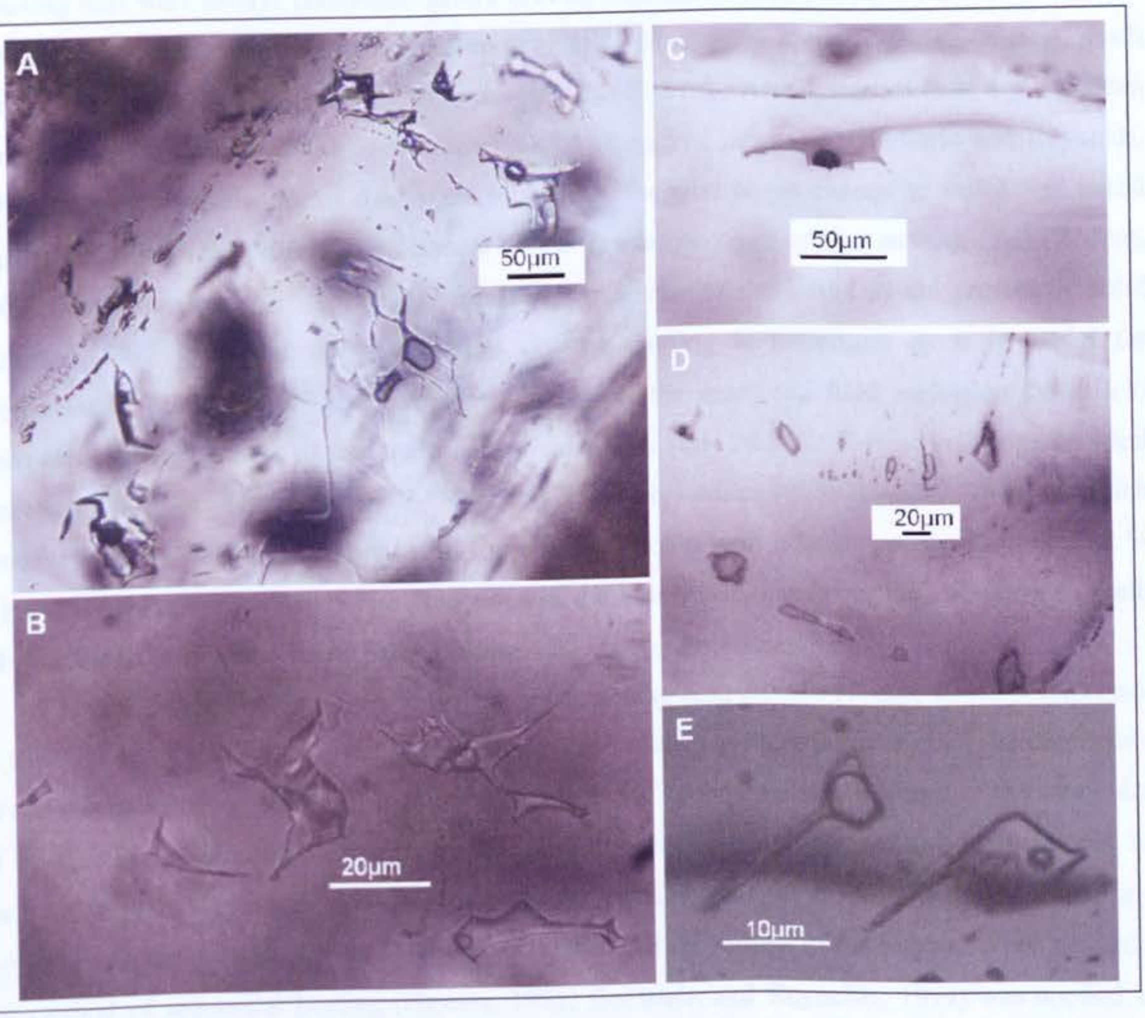

**Figure 6.4:** Photomicrographs of fluid inclusions exhibiting leaking and post-entrapment modification. A and B) Leaked and necked down inclusions; C) Re-equilibrated inclusions with "scalloped" walls; D and E) Heterogeneous trapping showing vapour-rich and liquid-rich inclusions, possibly a result of necking.

Microthermometric measurements were carried out using a Linkam MDS-600 heating-freezing stage mounted on a standard petrographic microscope with attached camera. The microscope field of view was displayed on an adjacent computer monitor and run by the computer programme Linkam Scientific Systems. The Linkam stage has a maximum temperature limit of 600°C and was calibrated using synthetic fluid inclusions containing pure water with melting temperature of 0°C. Results were reproducible to ±2.0°C for homogenisation temperatures (100-350 °C) and ±0.2°C for freezing experiments below +10 °C. A small fragment (~ 5 mm) of a fluid inclusion wafer was placed in the stage for cooling and freezing. The cooling of the wafer was done by controlled passage of liquid nitrogen through the stage, while heating was controlled by a heating element positioned in the stage.

### 6.4.3 General observations during heating and cooling

Phase changes were recorded by simple freezing and subsequent heating of the samples. Freezing runs were always performed before heating (Rankin and Shepherd, 1998). The inclusions were cooled rapidly from room temperature to -100°C. Most froze abruptly during cooling, much before reaching -100°C, generally between -40°C and -47°C, which was marked by a sudden contraction of the vapour bubble and sometimes a change of its shape (Goldstein and Reynolds, 1994). During slow heating of the frozen inclusions, the first phase change to occur was initial melting, known as the *eutectic* temperature ($T_e$) or the *temperature of first melting* ($T_{fm}$) (Bodnar, 2003). This temperature is marked by the first appearance of the liquid in the previously solid inclusion. Observation of the temperature of first melting is important, as it is useful for determination of the major fluid components. Most of the examined fluid inclusions from Belo Brdo exhibit temperatures of first melting between -22°C and -20.5°C. They are close to the ideal eutectic melting of -21.2°C in the $H_2O$-NaCl system (Borisenko, 1977; Roedder, 1984) at which hydrohalite ($NaCl.2H_2O$) decomposes to form ice and liquid with eutectic composition of 23.2 % (Figure 6.6). As the inclusion is heated beyond the eutectic temperature, ice continues to melt, diluting the salinity of the liquid phase (Bodnar, 2003)

The next phase change observed was *final ice melting temperature* ($Tm_{ice}$), which is important in fluid salinity calculations. Traditionally in the fluid inclusion literature, the observed depression of melting points is expressed in terms of equivalent NaCl concentration. Because of the small size of the inclusions, or poor optical clarity, the determination of final ice- melting temperatures, as well as the eutectic temperatures was not always possible (Figure 6.5). The final ice melting temperatures had to be determined sometimes by the final movement of the bubble. When possible, the method of sequential heating (Haynes, 1985; Goldstein and Reynolds, 1994) was applied to study subtle phase changes, especially to determine more accurately the final melting temperature of ice. The inclusions were first frozen and then carefully heated until only a single ice crystal remained attached to the vapour bubble. Inclusions were then cooled again to encourage the growth of a larger ice crystal and to test if hydrohalite was forming. Failure to recognise hydrohalite as the last melting solid phase (*temperature of hydrohalite melting*) can result in serious errors in salinity calculations (Bodnar, 2003). In this study however, upon repeated heating, the only phase that was melting above -21°C was ice. This was an important observation, as in the two-phase $H_2O$-NaCl system with salinity lower than 23.2wt. % NaCl, the ice is the last solid to melt. The melting of ice starts around the edges of the inclusion until the one single crystal remains (Figure 6.5).

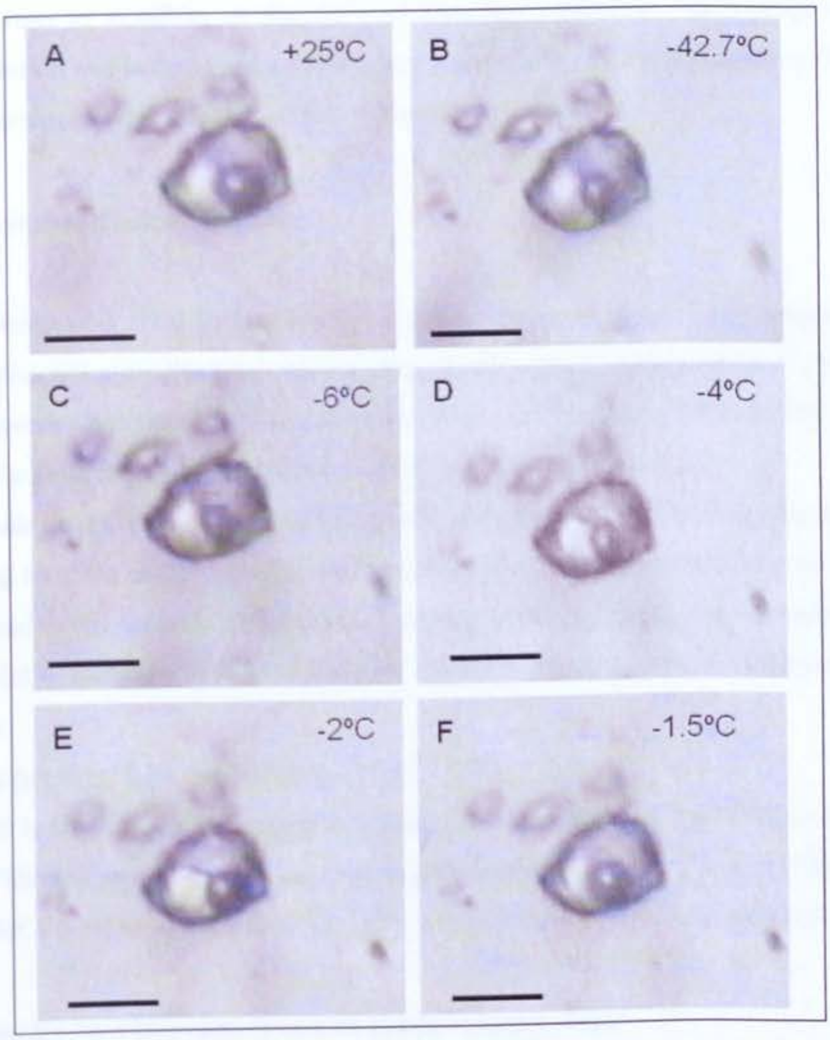

**Figure 6.5:** Phase changes observed in type IIa inclusion in quartz from Belo Brdo (sample 1055/4D). A) Two-phase liquid-vapour inclusion at room temperatures. B) Frozen inclusion content at -42.7°C; note a different position of the bubble, which also decreased in size. C) Ice crystal on the left side of the bubble; Eutectic melting was not possible to measure, as no difference in inclusion appearance was noticed between -42°C and -6°C. D) Melting of ice from the edge of the inclusion; ice forms a single, rounded crystal. E) Further melting of ice at -2°C; better visibility as the ice melts. F) Final ice melting just above -1.5°C; bubble moves to a new position as it's freed from ice. Scale bar 10 microns.

Only a few inclusions from the Type IIb inclusions froze between -51°C and -60°C. Their eutectic temperatures (~ -35°C) were slightly lower than those mentioned above, indicating that solutes other than NaCl were present in the system (Roedder, 1984; Shepherd et. al., 1985). However, this could not be confirmed as initial melting temperatures were not observed in most of the inclusions and salinity therefore remains unknown.

All inclusions analysed homogenised into the liquid phase on heating. The vapour bubble shrinks on heating above room temperature until eventual *vapour disappearance.* In two phase (liquid-vapour) inclusions this is known as ***homogenisation temperature*** (*Th*) and is important in the estimation of trapping temperatures and pressures, as well as for salinity calculations (Bodnar, 2003). In Belo Brdo, no halite-bearing inclusions were identified, so homogenisation by halite dissolution could not be observed. Collection of homogenisation data was carried out in as few heating runs as possible, so the risks of inclusion stretching and leakage could be minimised. Decrepitation and leakage were particularly common in some large carbonate hosted inclusions. No microthermometric data were collected from these inclusions.

### 6.4.4 Determinations of salinity

Salinity of a fluid inclusion can be calculated in different ways depending on the apparent fluid composition or chemical system, the phases present and transition of phases observed during thermometric experiments. Each method relies on the choice of chemical system on which to model the fluid ($NaCl-H_2O$; $NaCl-CaCl_2-H_2O$; $NaCl-KCl-H_2O$ etc.).

Bulk fluid salinity (expressed as equiv. wt % NaCl) for Belo Brdo deposit was determined by referring final ice melting temperatures to the $H_2O$–NaCl model fluid system. For example, the last ice crystal in the inclusion shown in Figure 6.5 melts at -5.0°C, corresponding to a salinity of 7.0 wt.% NaCl. Bodnar (1993) derived the equation which relates to freezing point to salinity as follows:

$$\text{Salinity (wt.\%)} = 0.00 + 1.78\Theta - 0.0442\,\Theta^2 + 0.000557\Theta^3 \qquad \text{(Equation 1)}$$

where $\Theta$ is freezing point depression (in degrees Celsius). Equation (1) is similar to that of Potter et al., (1978) and reproduces the original experimental data of Hall et al. (1988) to better than ±0.05 wt.% NaCl at all temperatures from 0.0°C to -21.2°C, the eutectic temperature for $H_2O$-NaCl.

## 6.5 Results and interpretation of thermometry data

In spite of difficulties encountered during collection of suitable specimens, paired Th-$T_m$ice data were obtained from 70 inclusions. However, at least twice as many have been investigated with no reliable results obtained. All inclusions analysed in quartz from the Belo Brdo deposit were aqueous and belong to the $H_2O$-NaCl system as evident from $T_{fm}$ values of -22°C to -20.5°C. The summary of phase transitions for the system $H_2O$-NaCl (Figure 6.6) is as follows:

1. Initial melting of hydrohalite ($T_i$ HH): HH + ice + vapour → liquid + ice + vapour
2. Final melting of ice ($T_m$ ice): ice + liquid + vapour→ liquid + vapour
3. Homogenisation (Th): liquid + vapour → liquid

Density and isochores of fluid inclusions were calculated using the computer program Flincor2 (Brown, 1989) and the equation of state defined by Zhang and Frantz (1987). Clathrates or liquid $CO_2$ were not observed in any of the fluid inclusions studied. Microthermometric results are tabulated in Table 6.2 and presented graphically in Figure 6.7.

**Figure 6.6:** Phase diagram for $NaCl-H_2O$ showing an example of a path (blue line), which an aqueous inclusion with salinity ~8 wt.% NaCl would follow when heated from freezing temperatures (below -30°C). Upon heating, hydrohalite melts first and at eutectic (E) hydrohalite is consumed and ice starts melting. The inclusion then follows the liquidus till the last ice melts (~ -5°C). P = peritectic (0.1°C, 26.3 wt.% NaCl); E = eutectic (-21.2°C, 23.2 wt.% NaCl)(Modified after Bodnar, 2003).

### *6.5.1 Homogenisation temperatures*

All analysed aqueous inclusions in quartz homogenised to the liquid phase. Homogenisation temperatures for a total of 70 analysed inclusions range between 165°C and 341°C, with 95% of all inclusions falling in the range of 165°C and 320°C. The mean value of all inclusions measured is 233°C ±10. This dataset can be broadly divided into two groups based on two different generations of quartz, namely quartz cogenetic to the main mineralising stage (CGQ) and late-stage quartz (LQ) that fills small open cavities (Table 6.2, Figure 6.7).

Homogenisation temperatures of all analysed inclusions, including Type IIa and IIb, within the quartz of the main mineralising stage (n=34) occupy a wide temperature range between 189°C and 341°C. They exhibit an average homogenisation temperature of 251°C ±17. The large spread of homogenisation temperatures is reflected by a high standard deviation of ±50°C. Distinction between homogenisation temperatures of Type IIa and Type IIb inclusions makes results more meaningful, although the datasets for each type are quite small. Microthermometric data for Type IIa inclusions (n=20) were derived mainly from the quartz which occurs as cement to the breccia, found in main-ore stage to post-ore stage. Microthermometric data for Type IIb inclusions (n=14) were collected from massive sulphide ore.

Homogenisation temperatures of fluid inclusions in the breccia range from 189°C to 277°C (standard deviation ±21°C) with a mean at 218°C ±10. A prominent *Th* mode is evident at 220°C (Figure 6.7 A). As compared to fluid inclusions from the breccia, the homogenisation temperatures of the main mineralisation stage are distinctly higher and show a somewhat wider spread, reflected in higher standard deviation (±39°C). They range from 220°C to 341°C with a mean at 299°C ±10. Frequency distribution histogram of *Th* indicates two possible weaker maxima occurring at 300°C and 340°C. These temperatures compare well to those obtained by arsenopyrite geothermometry carried out on samples taken from massive sulphide ore of the main mineralisation stage.

**Table 6.2**: Thermometric data for fluid inclusions in the Belo Brdo deposit. Abbreviations: CGQ = cogenetic quartz; LQ = late stage quartz.

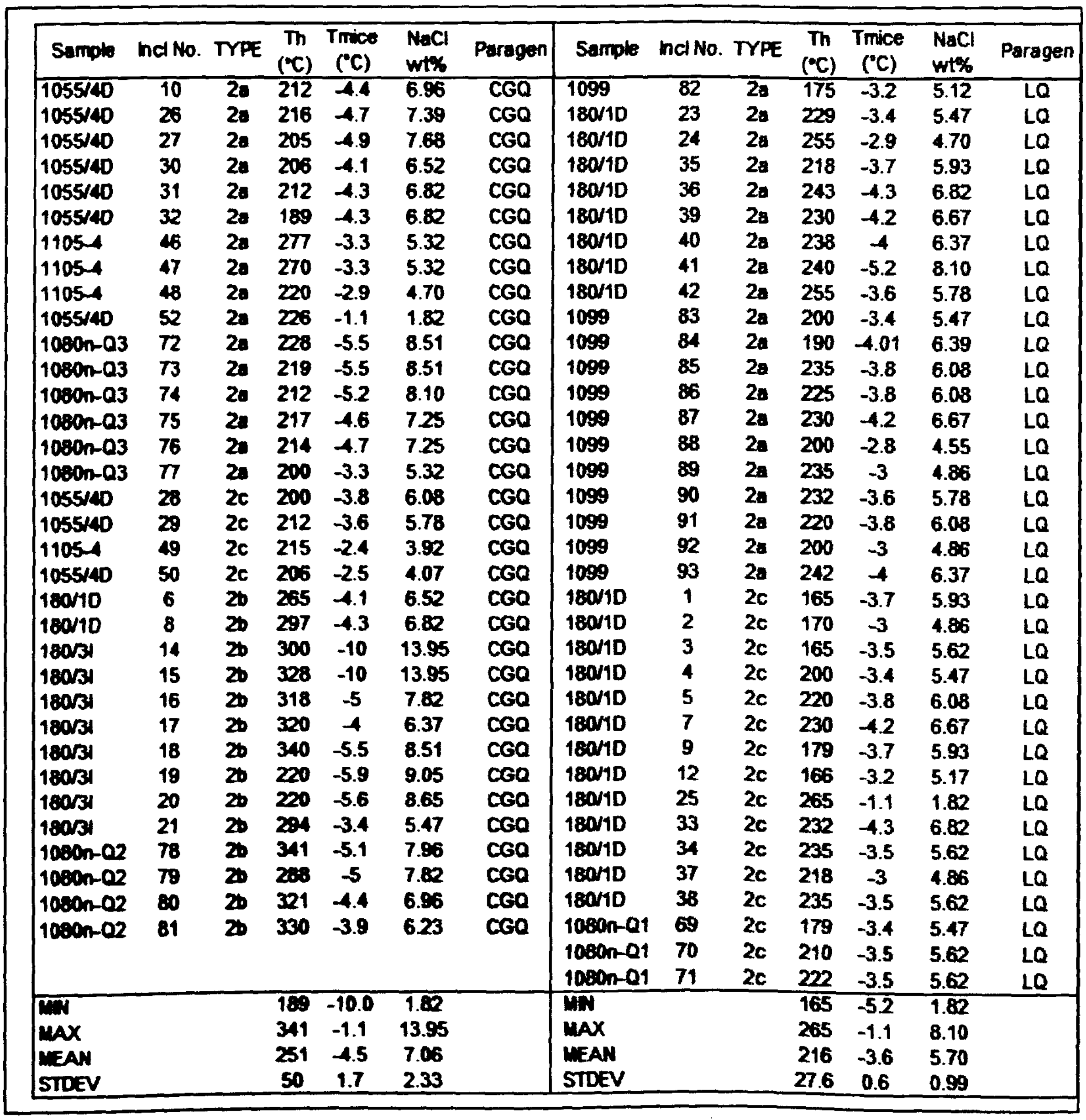

| Sample | Incl No. | TYPE | Th (°C) | Tmice (°C) | NaCl wt% | Paragen | Sample | Incl No. | TYPE | Th (°C) | Tmice (°C) | NaCl wt% | Paragen |
|---|---|---|---|---|---|---|---|---|---|---|---|---|---|
| 1055/4D | 10 | 2a | 212 | -4.4 | 6.96 | CGQ | 1099 | 82 | 2a | 175 | -3.2 | 5.12 | LQ |
| 1055/4D | 26 | 2a | 216 | -4.7 | 7.39 | CGQ | 180/1D | 23 | 2a | 229 | -3.4 | 5.47 | LQ |
| 1055/4D | 27 | 2a | 205 | -4.9 | 7.68 | CGQ | 180/1D | 24 | 2a | 255 | -2.9 | 4.70 | LQ |
| 1055/4D | 30 | 2a | 206 | -4.1 | 6.52 | CGQ | 180/1D | 35 | 2a | 218 | -3.7 | 5.93 | LQ |
| 1055/4D | 31 | 2a | 212 | -4.3 | 6.82 | CGQ | 180/1D | 36 | 2a | 243 | -4.3 | 6.82 | LQ |
| 1055/4D | 32 | 2a | 189 | -4.3 | 6.82 | CGQ | 180/1D | 39 | 2a | 230 | -4.2 | 6.67 | LQ |
| 1105-4 | 46 | 2a | 277 | -3.3 | 5.32 | CGQ | 180/1D | 40 | 2a | 238 | -4 | 6.37 | LQ |
| 1105-4 | 47 | 2a | 270 | -3.3 | 5.32 | CGQ | 180/1D | 41 | 2a | 240 | -5.2 | 8.10 | LQ |
| 1105-4 | 48 | 2a | 220 | -2.9 | 4.70 | CGQ | 180/1D | 42 | 2a | 255 | -3.6 | 5.78 | LQ |
| 1055/4D | 52 | 2a | 226 | -1.1 | 1.82 | CGQ | 1099 | 83 | 2a | 200 | -3.4 | 5.47 | LQ |
| 1080n-Q3 | 72 | 2a | 228 | -5.5 | 8.51 | CGQ | 1099 | 84 | 2a | 190 | -4.01 | 6.39 | LQ |
| 1080n-Q3 | 73 | 2a | 219 | -5.5 | 8.51 | CGQ | 1099 | 85 | 2a | 235 | -3.8 | 6.08 | LQ |
| 1080n-Q3 | 74 | 2a | 212 | -5.2 | 8.10 | CGQ | 1099 | 86 | 2a | 225 | -3.8 | 6.08 | LQ |
| 1080n-Q3 | 75 | 2a | 217 | -4.6 | 7.25 | CGQ | 1099 | 87 | 2a | 230 | -4.2 | 6.67 | LQ |
| 1080n-Q3 | 76 | 2a | 214 | -4.7 | 7.25 | CGQ | 1099 | 88 | 2a | 200 | -2.8 | 4.55 | LQ |
| 1080n-Q3 | 77 | 2a | 200 | -3.3 | 5.32 | CGQ | 1099 | 89 | 2a | 235 | -3 | 4.86 | LQ |
| 1055/4D | 28 | 2c | 200 | -3.8 | 6.08 | CGQ | 1099 | 90 | 2a | 232 | -3.6 | 5.78 | LQ |
| 1055/4D | 29 | 2c | 212 | -3.6 | 5.78 | CGQ | 1099 | 91 | 2a | 220 | -3.8 | 6.08 | LQ |
| 1105-4 | 49 | 2c | 215 | -2.4 | 3.92 | CGQ | 1099 | 92 | 2a | 200 | -3 | 4.86 | LQ |
| 1055/4D | 50 | 2c | 206 | -2.5 | 4.07 | CGQ | 1099 | 93 | 2a | 242 | -4 | 6.37 | LQ |
| 180/1D | 6 | 2b | 265 | -4.1 | 6.52 | CGQ | 180/1D | 1 | 2c | 165 | -3.7 | 5.93 | LQ |
| 180/1D | 8 | 2b | 297 | -4.3 | 6.82 | CGQ | 180/1D | 2 | 2c | 170 | -3 | 4.86 | LQ |
| 180/3I | 14 | 2b | 300 | -10 | 13.95 | CGQ | 180/1D | 3 | 2c | 165 | -3.5 | 5.62 | LQ |
| 180/3I | 15 | 2b | 328 | -10 | 13.95 | CGQ | 180/1D | 4 | 2c | 200 | -3.4 | 5.47 | LQ |
| 180/3I | 16 | 2b | 318 | -5 | 7.82 | CGQ | 180/1D | 5 | 2c | 220 | -3.8 | 6.08 | LQ |
| 180/3I | 17 | 2b | 320 | -4 | 6.37 | CGQ | 180/1D | 7 | 2c | 230 | -4.2 | 6.67 | LQ |
| 180/3I | 18 | 2b | 340 | -5.5 | 8.51 | CGQ | 180/1D | 9 | 2c | 179 | -3.7 | 5.93 | LQ |
| 180/3I | 19 | 2b | 220 | -5.9 | 9.05 | CGQ | 180/1D | 12 | 2c | 166 | -3.2 | 5.17 | LQ |
| 180/3I | 20 | 2b | 220 | -5.6 | 8.65 | CGQ | 180/1D | 25 | 2c | 265 | -1.1 | 1.82 | LQ |
| 180/3I | 21 | 2b | 294 | -3.4 | 5.47 | CGQ | 180/1D | 33 | 2c | 232 | -4.3 | 6.82 | LQ |
| 1080n-Q2 | 78 | 2b | 341 | -5.1 | 7.96 | CGQ | 180/1D | 34 | 2c | 235 | -3.5 | 5.62 | LQ |
| 1080n-Q2 | 79 | 2b | 288 | -5 | 7.82 | CGQ | 180/1D | 37 | 2c | 218 | -3 | 4.86 | LQ |
| 1080n-Q2 | 80 | 2b | 321 | -4.4 | 6.96 | CGQ | 180/1D | 38 | 2c | 235 | -3.5 | 5.62 | LQ |
| 1080n-Q2 | 81 | 2b | 330 | -3.9 | 6.23 | CGQ | 1080n-Q1 | 69 | 2c | 179 | -3.4 | 5.47 | LQ |
|  |  |  |  |  |  |  | 1080n-Q1 | 70 | 2c | 210 | -3.5 | 5.62 | LQ |
|  |  |  |  |  |  |  | 1080n-Q1 | 71 | 2c | 222 | -3.5 | 5.62 | LQ |
| MIN |  |  | 189 | -10.0 | 1.82 |  | MIN |  |  | 165 | -5.2 | 1.82 |  |
| MAX |  |  | 341 | -1.1 | 13.95 |  | MAX |  |  | 265 | -1.1 | 8.10 |  |
| MEAN |  |  | 251 | -4.5 | 7.06 |  | MEAN |  |  | 216 | -3.6 | 5.70 |  |
| STDEV |  |  | 50 | 1.7 | 2.33 |  | STDEV |  |  | 27.6 | 0.6 | 0.99 |  |

The late-stage quartz crystals from open cavities contain two types of inclusions namely Type IIa and IIc. The values for homogenisation temperatures obtained from both types of inclusions (a total of 36) are very similar, which is reflected in a good overlap of the data (Figure 6.7 B). They range from 165 °C to 265 °C with a mean at 216 °C ±10. The range of values, including minimum, maximum and mean between the two groups lies within the 95 % confidence for standard error. Therefore no significant difference in homogenisation temperatures between the two types of fluid inclusions (Figure 6.7 B) can be established. It is

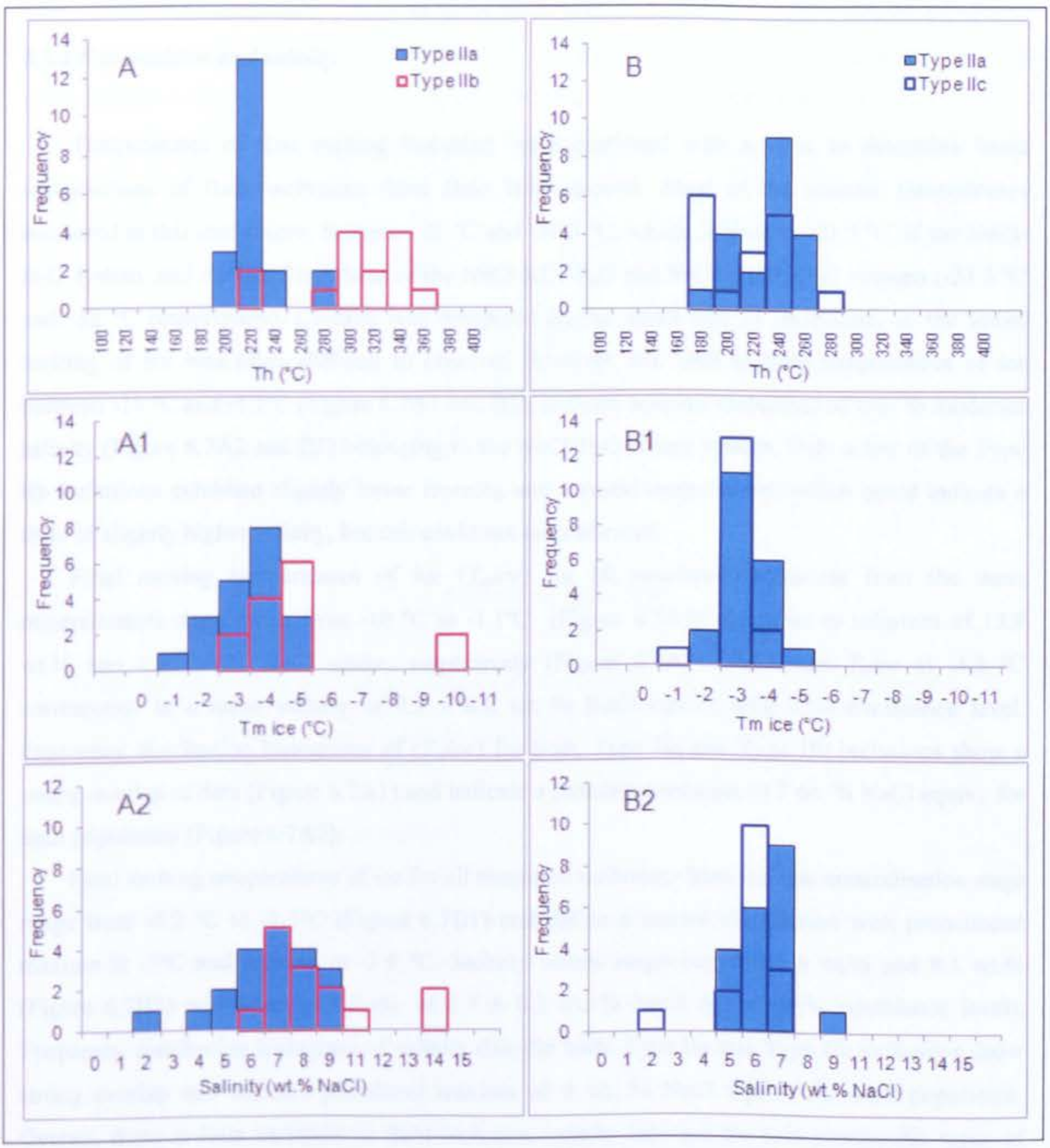

**Figure 6:7** Frequency histograms depicting thermometry results for primary fluid inclusions hosted by cogenetic quartz of the main mineralising stage (A, A1, A2) and quartz crystals filling cavities during later mineralising stage (B, B1, B2). Legend in the top right corner of A and B applies to all diagrams. **Main mineralising stage**: A) Frequency histogram of homogenisation temperatures (Th); A1) Frequency histogram of final ice melting temperatures ($T_m$ice); A2) Frequency histogram of salinity. **Late-ore stage**: B) Frequency histogram of homogenisation temperatures (Th); B1) Frequency histogram of final ice melting temperatures ($T_m$ice); B2) Frequency histogram of salinity expressed as wt.% NaCl equivalent.

also interesting that they compare well with the homogenisation temperatures obtained from the fluid inclusions in quartz from the breccias of the later main mineralising stage, suggesting that the temperatures of formation remained fairly constant during the precipitation of breccia and late stage quartz. As compared to fluid inclusions from the massive sulphide ore of the main mineralisation stage (Figure 6.7 A), the homogenisation temperatures of fluid inclusions in late stage quartz are lower and show a smaller spread (standard deviation ±27).

### *6.5.2 Composition and salinity*

Temperatures of first melting (eutectic) were examined with a view to determine basic compositions of fluid inclusions from Belo Brdo deposit. Most of the eutectic temperatures measured in this study were, between -22 °C and -20.5 °C, which is close to -21.2 °C of the NaCl-$H_2O$ system and distinct from those of the NaCl-KCl-$H_2O$ and NaCl-$CaCl_2$-$H_2O$ systems (-23.5 °C and -52 °C respectively). Cooling was hampered by the small size of inclusions, so the initial melting of ice was often difficult to observe. However, the final melting temperatures of ice between -10 °C and -1.1°C (Figure 6.7A1 and B1), indicate aqueous inclusions of low- to moderate salinity (Figure 6.7A2 and B2) belonging to the NaCl-$H_2O$ binary system. Only a few of the Type IIb inclusions exhibited slightly lower freezing and eutectic temperatures, which could indicate a fluid of slightly higher salinity, but this could not be confirmed.

Final melting temperatures of ice ($T_m ice$) for all measured inclusions from the main mineralisation stage range from -10 °C to -1.1°C (Figure 6.7A1) and point to salinities of 13.9 wt.% and 1.82 wt.% NaCl equiv., respectively (Figure 6.7A2). The mean $T_m ice$ at -4.5 °C corresponds to a mean salinity of 7.1 ± 0.8 wt. % NaCl equiv., with 95% confidence level. Frequency distribution histograms of ($T_m ice$) for both, Type IIa and Type IIb inclusions show a strong overlap of data (Figure 6.7A1) and indicate a prominent maxima of 7 wt. % NaCl equiv., for each population (Figure 6.7A2).

Final melting temperatures of ice for all measured inclusions from the late mineralisation stage range from -5.2 °C to -1.1°C (Figure 6.7B1) and define a narrow distribution with pronounced maxima at -3°C and a mean at -3.6 °C. Salinity values range between 1.8 wt.% and 8.1 wt.% (Figure 6.7B2) with a mean salinity of 5.7 ± 0.3 wt. % NaCl equiv. (95% confidence level). Frequency distribution histogram of salinity data for both, Type IIa and Type IIc inclusions show strong overlap and indicate prominent maxima of 6 wt. % NaCl equiv., for each population. Overall, there is little variation in fluid inclusion salinity between the two paragenetic types of quartz.

A salinity versus homogenisation temperature trend is presented in Figure 6.8 for the fluid inclusions of the two paragenetic groups. Overall, the diagram illustrates a linear, mostly continuous trend with moderate change from intermediate to low salinity and associated decrease in temperature reflecting ore formation conditions from the hotter, more saline fluid of the main mineralising stage to lower salinity fluid of the late mineralising stage. This trend could be interpreted as an effect of diluting fluids due to mixing of magmatic with meteoric water (Rankin, 1995). Such trends compare well with some of the known intermediate sulphidation Pb-Zn-precious metals deposits in Madjarovo district, Bulgaria (Rice et al., 2007); Pb-Zn-Ag Chihuahua district, Mexico (Grant and Ruiz, 1988 and references therein); the Eastern Cordilleran polymetalic deposits of the Peruvian Central Andes (Wagner et. al, 2009); Tertiary precious and base metal deposits of western Romania (Alderton and Fallick 2000; Grancea et al., 2002) etc. Although no magmatic characteristics of the fluid inclusions were directly observed, there is isotopic evidence for the presence of magmatic fluids in the system. These data will be presented in chapter 7.

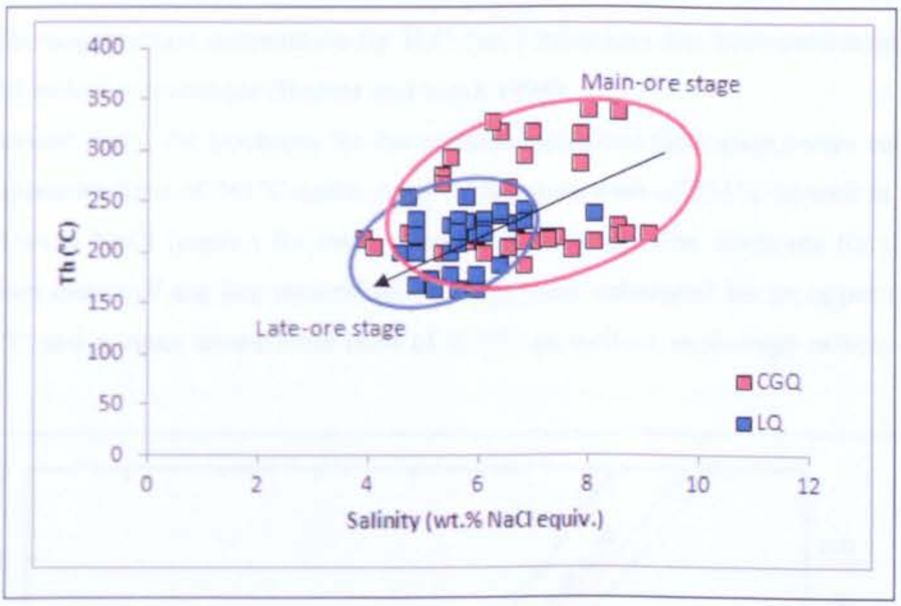

**Figure 6.8:** Bivariate plot of homogenisation temperature versus salinity for primary inclusions from the Belo Brdo deposit. Excluded from the diagram are two inclusions with highest salinity (~13.95 wt.% NaCl equiv) and two with lowest salinity (~1.82 wt.% NaCl equiv.). Abbreviations: CGQ= co-genetic quartz samples (red squares); LQ= Late quartz (blue squares).

### *6.5.3 Pressure and temperature estimates*

Determination of the temperature and pressure of formation of the inclusions is one of the most important goals in fluid inclusion studies. Fluid inclusions are usually homogeneous when trapped at the temperature and pressure of formation and additional phase states of the inclusion as observed at laboratory conditions (vapour bubble; solid daughter mineral), form during cooling as a result of differential contraction between the fluid and the host mineral (Shepherd et al., 1985; Bodnar, 2003). In the laboratory this process can be reversed by heating the inclusion and if the inclusions trapped in a boiling or immiscible fluid system, then the homogenisation temperature is equal to the trapping temperature and the trapping pressure is equal to the vapour pressure in the inclusion at the temperature of homogenisation (Bodnar, 2003). In the present study, however, immiscibility was suspected in only one sample, but could not be confirmed. Therefore, independent information about temperature or pressure was needed to locate a point of true trapping temperature along the constant density (isochore) of the fluid inclusion. The independent temperature information can be used to estimate pressures, or conversely, the independent pressure can be used to estimate the true trapping temperature. The latter technique is known as *pressure correction* and is routinely applied to homogenisation temperatures. The first step in estimating the trapping temperature is to determine the starting point for the isochore, on the bubble curve (liquid-vapour curve). This point corresponds to the measured temperature of homogenisation and the bubble curve pressure at the homogenisation temperature. Once the composition, homogenization temperature and vapour pressure in the inclusion at homogenisation have been determined, it is necessary to determine the slope of the isochore along which the inclusion was trapped in order to estimate a pressure correction. The relationship between trapping temperature and pressure, salinity, and homogenisation temperature for $H_2O$-NaCl inclusions has been determined using the synthetic fluid inclusion technique (Bodnar and Vityk 1994).

In the present study, the isochores for the aqueous inclusions from quartz were calculated for an upper temperature limit of 341°C and a mean temperature limit of 251°C as well as an average salinity of 7 wt.% NaCl (equiv.) for main mineralisation stage. The isochores for the aqueous inclusions from quartz of the late mineralisation stage were calculated for an upper temperature limit of 265°C and a mean temperature limit of 216°C as well as an average salinity of 7 wt.% NaCl equiv.

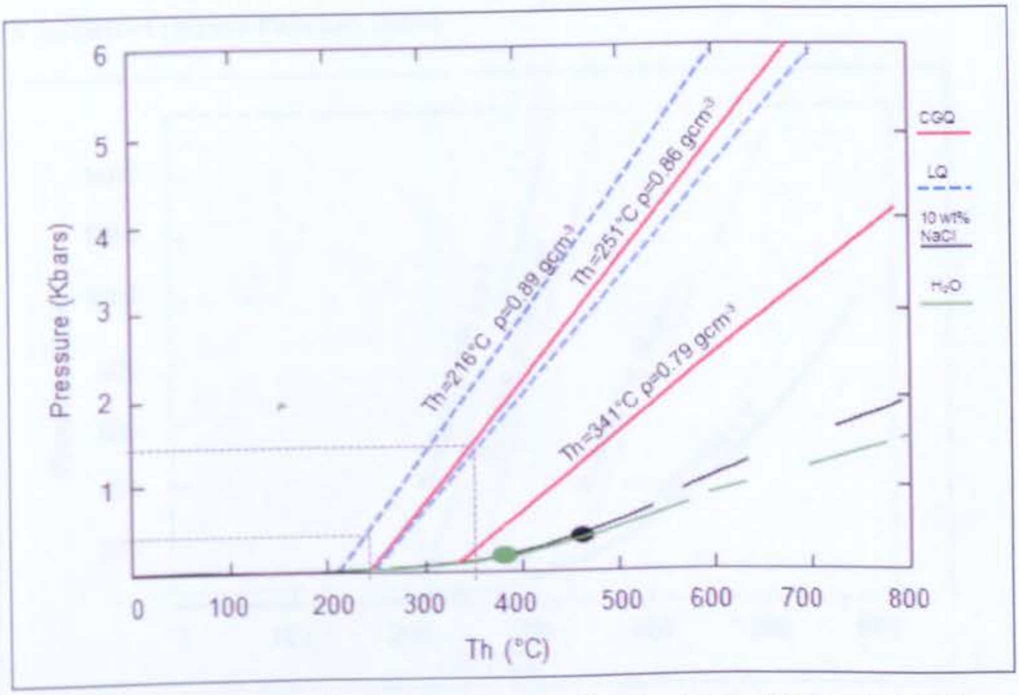

**Figure 6.9:** Pressure vs. Homogenisation temperature plot showing isochores calculated for average and maximum temperature limits for main mineralisation stage (red solid line) and late ore stage (blue dashed lines) for $H_2O$-NaCl aqueous inclusions, calculated using Bodnar and Vityk's (1994) equation. Independent temperature estimation was obtained from stable isotopes (256°C and 301°C for co-existing sulphides from breccia ore and 388°C for massive sulphide of the main mineralising stage; co-existing quartz-dolomite pairs from breccia ore yielded 320°C, 264°C, 217°C Ind 214°C), as well as arsenopyrite geothermometry (average at 350°C); the average temperature values of 250°C for late mineralising stage and 350°C for main ore stage have been projected onto the diagram for the pressure estimations (grey dotted lines).

Independent temperature estimates were obtained for Belo Brdo deposit using stable isotope data from co-existing mineral pairs (see Chapter 7). A co-existing pyrite-galena from one sample collected from breccia ore indicated temperature of 301°C, whist a co-existing sphalerite-galena pair from the late mineralising stage yielded a temperature of 256°C (samples 1055/4D and 180/1D). Co-existing sphalerite and galena from the main mineralisation stage indicate much higher temperatures of formation of between 388°C and 460°C. Those temperatures are higher than most of the fluid inclusion homogenisation temperatures obtained from the quartz (maximum obtained was 341°C, an average of 251°C). Co-existing quartz-dolomite pairs from breccia ore yielded temperatures of 214°C to 320°C with an average values of 250°C.

The mol.% CuS in sphalerite yielded temperatures between 290°C to 350°C for the main ore-stage, whilst arsenopyrite geothermometry indicated temperatures between 311°C to 348°C. Taking into account a slope of 13.9 bars/°C for the average isochore of the main mineralising stage and independent temperature of 350°C, as well as the slope of 15.6 bars/°C for the late ore-stage and average temperature of 250°C, the trapping pressures for the Belo Brdo deposit were between 1419 and 521 bars (Figure 6.9) under the lithostatic conditions, which would correspond to a minimum depths between 5 and 1.7 km. These are preliminary estimates for pressures and a depth of formation. They are consistent with formation in a shallow crustal environment. The fluids associated with the formation of the Trepca Pb-Zn carbonate-hosted deposit in Kosovo have similar PTVX properties (Strmić-Palinkaš, 2009).

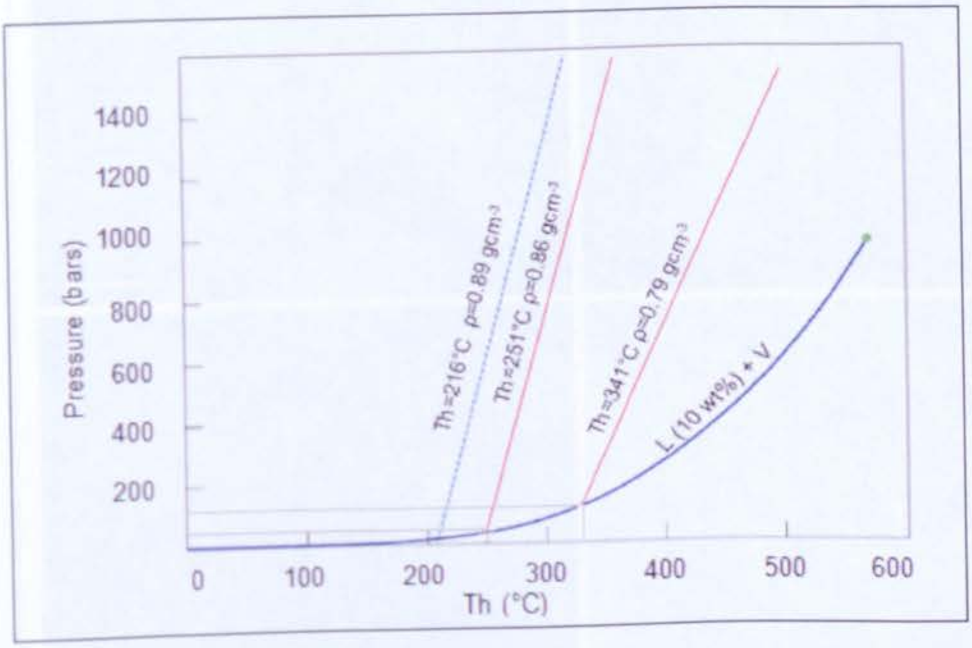

**Figure 6.10:** Pressure vs. temperature plot showing isochores calculated for an average (251°C) and maximum temperature limits (341°C) for the main mineralisation stage (red solid line) and late ore stage (blue dashed lines) for $H_2O$-NaCl aqueous inclusions, calculated using Bodnar and Vityk's (1994) equation. Hydrostatic pressure conditions assumed. Pressures estimated between 50 and 120 bars (after Haas, 1971).

No depth data from the reconstruction of stratigraphy is available, so whether the fluid pressure is close to lithostatic or hydrostatic conditions remains inconclusive. However, the presence of hydrothermal breccias in the deposit and the presence of vapour-rich inclusions in one sample, which unfortunately was not analysed here by microthermometry, indicate a possibility that pressure-temperature conditions were close to the liquid-vapour two phase curve. This in turn would indicate a hydrostatic pressure regime and trapping temperatures between 50 bars, corresponding to the mean homogenisation temperatures of 251°C and 120 bars corresponding to the maximum homogenisation temperature of 341°C (Figure 6.10).

## 6.6 Preliminary study of fluid inclusions in Karavansalija skarn prospect

### *6.6.1 Introduction*

Several samples were collected from drill-cores at the Karavansalija Cu-Au skarn deposit for a preliminary study of fluid inclusions. Since these samples were not obtained through systematic sampling, the petrographic and microthermometric data are only used for comparison with the fluid inclusion data from the Belo Brdo deposit. Quartz and calcite have been identified as the most suitable fluid inclusion host minerals. Numerous fluid inclusions were observed in "jigsaw"-textured quartz, which is a common quartz type found in the Karavansalija deposit (Figure 6.11A). It occurs as microcrystalline to crystalline aggregates with interpenetrating grain

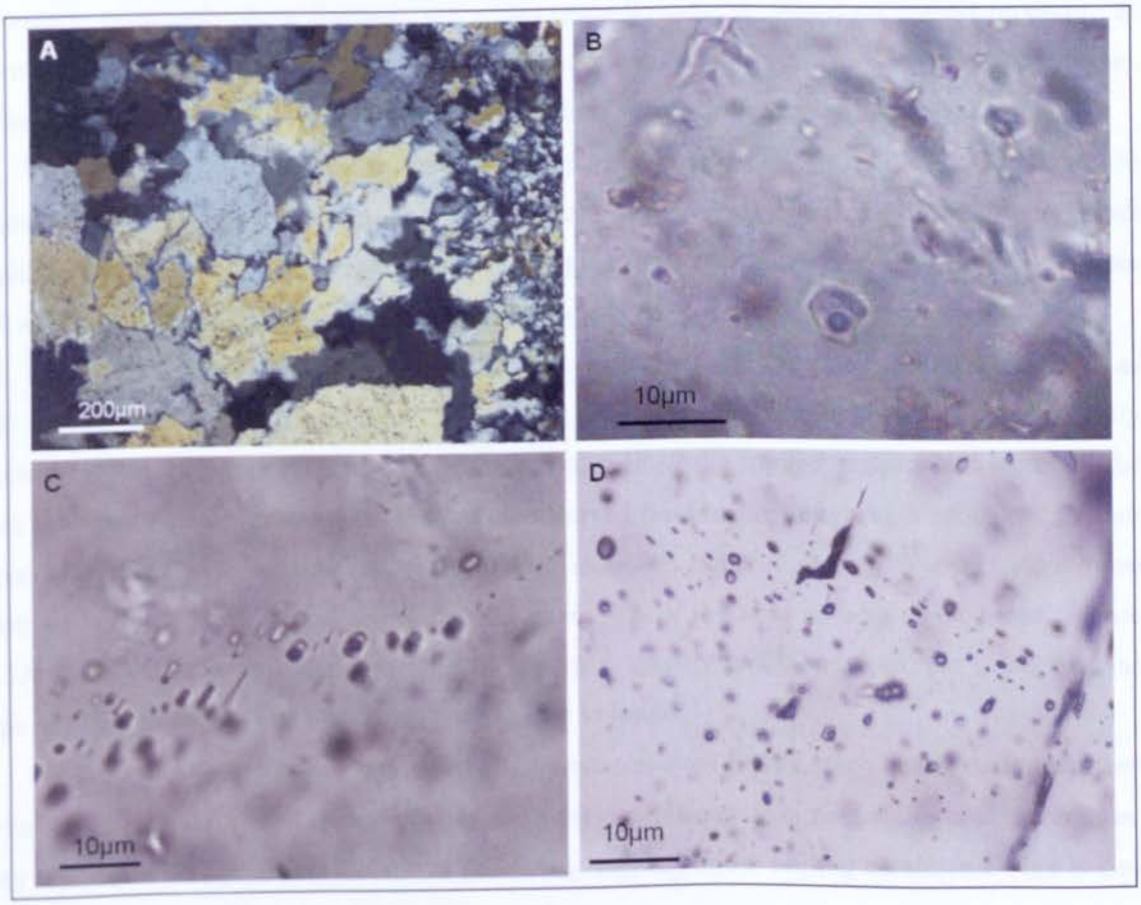

**Figure 6.11:** Photomicrographs showing jigsaw texture quartz, observed under cross polarised light (A) and examples of fluid inclusions (B-D) found in this type of recrystallised quartz (plane polarised light); B) primary two-phase liquid-rich aqueous inclusions and monophase liquid inclusions; C) secondary two-phase aqueous inclusions along healed fracture; D) two-phase aqueous inclusions with both, vapour-rich and liquid-rich inclusions along healed fractures (sample KU70).

boundaries and probably represents a recrystallised texture. Primary inclusions in this type of quartz (Figure 6.11B) were not analysed by microthermometry as they most likely do not record the original depositional conditions (Dong et al., 1995). Additionally, secondary inclusions, which occur along healed fractures (Figure 6.11C and D), were not considered for thermometric analysis.

Only two samples of clear euhedral quartz crystals growing into open spaces during late stage mineralisation were found to be suitable for preliminary microthermometric analysis (sample KU 72 of silicified breccia from PDMC-06-07, 282-286m and sample KU37 of skarn from PDMC-06-10 114m-116m).

### 6.6.2 Petrography of fluid inclusions

The classification of fluid inclusions in Karavansalija has been based on the same principles as for Belo Brdo, according to the nomenclature of Roedder (1984). The inclusions were considered primary or pseudosecondary, as they were formed isolated within the crystals (Figure 6.12A) or in planar arrays outlining growth zones. Inclusions in quartz and coarse-grained late-stage calcite that occur in planes of healed fractures that do not terminate against growth zones were considered secondary; commonly these fractures cut across grain boundaries. Based on optical properties at room temperature and the behaviour of phases during heating runs, three main end member types of fluid inclusions were recognized namely monophase, two-phase and polyphase inclusions.

Type I inclusions (L) are represented by monophase liquid inclusions, as seen in the Belo Brdo deposit and show no phase change during microthermometry. This group also includes very small liquid-vapour inclusions with vapour bubble occupying less than 10% of total inclusions volume and which, due to a small size could not be analysed.

Type II fluid inclusions are two-phase aqueous inclusions and they include liquid-rich (LV) as well as vapour-rich (VL) inclusions. In the LV inclusions the liquid phase is volumetrically dominant (>70%) (Figure 6.12B-F). They are common in all the studied samples and represent the most abundant type of inclusions (>80% of all observed fluid inclusion types). Vapour bubbles are variable in size, but constitute less than 30% of inclusion volume. Only a few inclusions were observed with the liquid phase occupying less than 70% of the total volume of inclusion (Figure 6.13A and B). The size of analysed fluid inclusions is usually less than 20μm, but a few were as large as 50μm in length. The inclusions homogenise to liquid.

The two-phase vapour rich inclusions (VL) were observed in late stage quartz that overgrows earlier euhedral quartz crystals and also as secondary inclusions occurring along healed fractures. They co-exist with liquid-rich inclusions indicating trapping under boiling conditions. This is also observed in the healed fractures in late stage calcite.

Type III fluid inclusions (LV+S) consist of liquid, vapour, halite, and sometimes other solids. They were only observed in one sample (KU73) where halite was identified by its cubic shape (Figure 6.13C) and represents the major crystal in this type of inclusion. Some polyphase inclusions were of irregular shapes often with long tails, and their origin and paragenetic characteristics were not clear as the distribution and volume of solid phases are not always regular. This suggests that they might represent trapped solids rather than daughter minerals. They commonly occur along microfractures, which suggest a secondary origin for them.

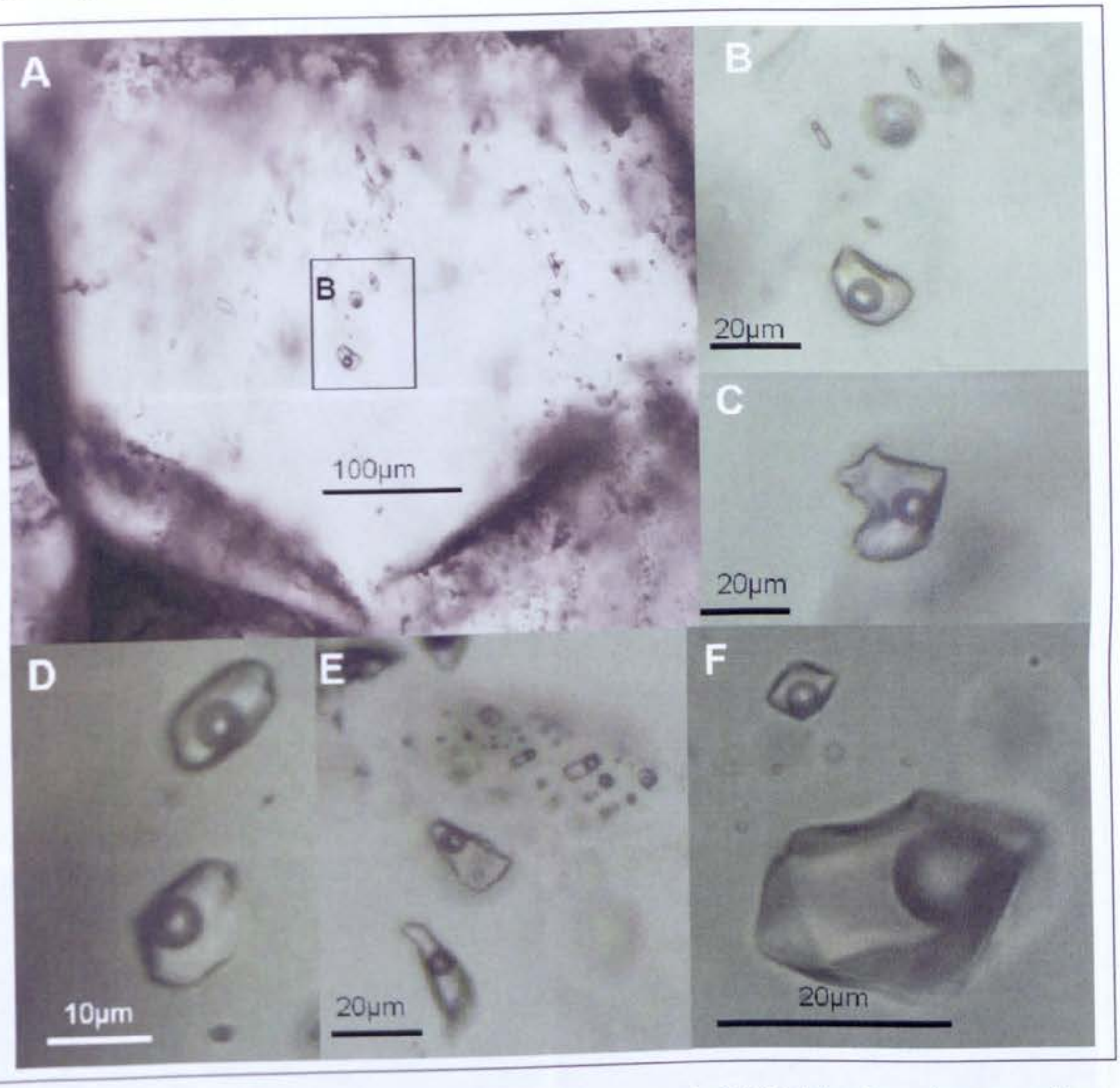

**Figure 6.12:** Photomicrographs of euhedral quartz crystal (A, sample KU37-1) hosting primary two-phase liquid-rich (LV) aqueous fluid inclusions (B-F) showing consistent liquid-vapour ratios and different shapes, such as rounded (B, sample Ku37-1), irregular (C, sample KU37-1), oval (D, sample KU37-4), elongated (E, sample Ku37-4) and negative crystal shape (F, sample KU26).

### *6.6.3 Results of microthermometric analysis*

Preliminary microthermometric data were obtained from 30 aqueous inclusions belonging to Type II. All inclusions froze between -70°C and -40°C into a dark granular mass. The temperatures of first ice melting were determined for fifteen inclusions, and on that basis they have been assigned to either the $H_2O$-NaCl binary system as evident from $T_{fm}$ values of -21°C to -20°C or to the NaCl-$CaCl_2$-$H_2O$ ternary system (Oakes et al., 1990) if the eutectic temperature is between -55°C to -45°C, which is indicative of the first melting of antarcticite ($CaCl_2 \cdot 6H_2O$). The phase transitions for the system NaCl-$CaCl_2$-$H_2O$ is as follows:

1. Initial melting of antarcticite ($T_iAA$): AA + HH + ice + vapour → liquid + HH + ice + vapour
2. Final melting of hydrohalite ($T_mHH$): HH + liquid + vapour + ice → liquid + ice + vapour
3. Final melting of ice ($T_m^{ice}$): ice + liquid + vapour → liquid + vapour
4. Homogenisation (Th): liquid + vapour → liquid

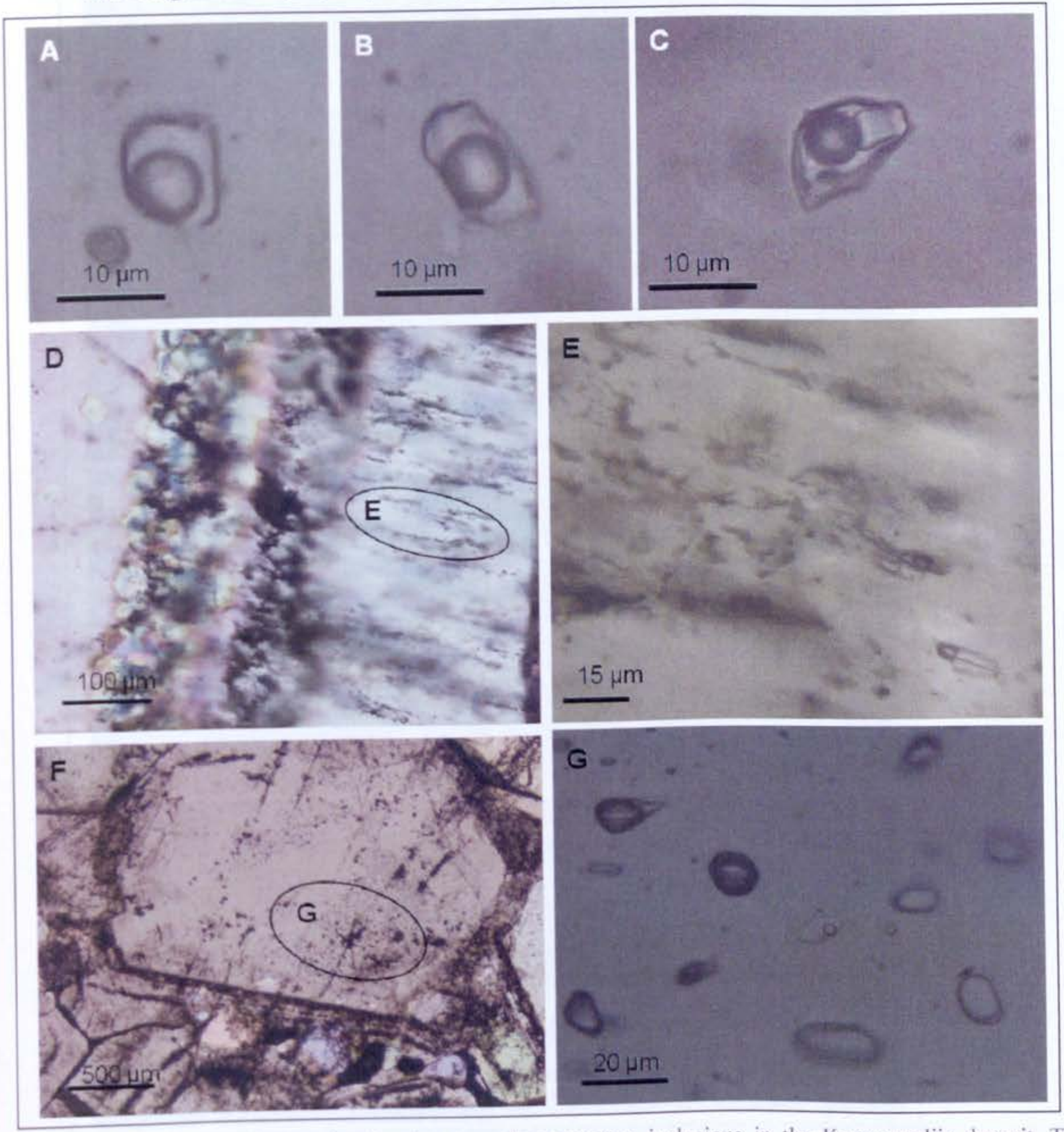

**Figure 6.13:** Photomicrographs showing two-phase aqueous inclusions in the Karavansalija deposit. The liquid phase occupys less than 70% of the total volume of inclusion (A and B, sample KU72-Q1); polyphase inclusion with halite daughter (C, sample KU72-Q2); pseudosecondary two-phase aqueous inclusions in feathery quartz (D and E, KU73) and inclusions with variable degree of fill, indicating boiling of fluids; they appear to be positioned along microfractures (F and G, KU73).

In three inclusions, eutectic temperatures were observed at higher temperatures (-37°C to – 26°C) which may suggest the presence of $FeCl_2$ in addition to $CaCl_2$ and NaCl, whilst in one inclusion it occurred between -20°C and -17°C, suggesting that KCl was an additional salt in

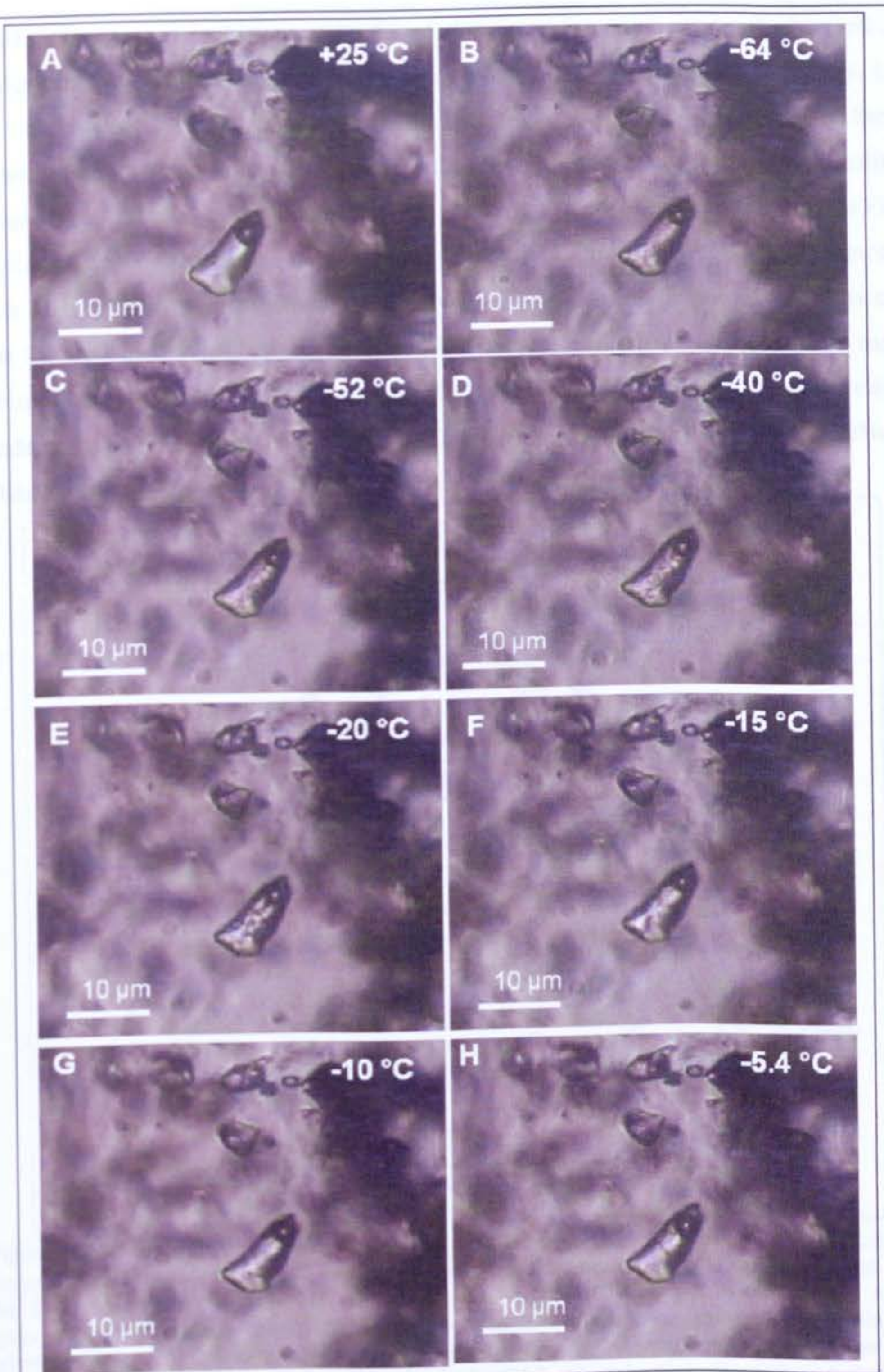

**Figure 6.14:** Photomicrographs of a cool/thaw run for an aqueous NaCl-$CaCl_2$-$H_2O$ inclusion in quartz (sample KU37-4). **A)** Room temperature conditions. **B)** Inclusion is frozen to mosaic of crystals at about -64°C and turned brownish colour; note the slight decrease in the bubble size. **C)** With slow warming to about -52°C the inclusion shows slightly crisper appearance indicating Te. **D)** By about -40°C crystals have better defined shapes indicating that melting has definitely occurred at this point, if it was not clear between -64°C and -40°C. **E)** More melting has occurred and crystals are more visible; the bright crystals are probably those of hydrohalite. **F)** Up to this point some clearing has occurred; rounded crystals are probably ice, but some hydrohalite might still be present. **G)** Only ice left, but it is not clear as at which exact temperature hydrohalite melted. **H)** Final ice melting at -5.4°C.

solution (Goldstein and Reynolds, 1994). It is not clear whether these temperature events represent true eutectic temperatures or perhaps metastable crystallisation of the inclusion contents (Bodnar, 2003). No gaseous inclusions were found. Clathrate formation was not observed in any of the inclusions, which rules out the presence of significant $CO_2$ (Hedenquist and Henley, 1985).

Because of the dark appearance of the inclusions, their small size as well as the small size of crystals within inclusions, it was not possible to record accurately hydrohalite dissolution temperatures and eutectic temperatures. An example of a cool/thaw run is shown in Figure 6.14. Therefore, more quantitative data on fluid salinity and the Ca/Na molar ratio cannot be expressed with any certainty using the ternary $H_2O$-NaCl-$CaCl_2$ diagram (Figure 6.15). It is clear however, that the ice was the last melting phase in all observed inclusions and the high- to moderately high ice melting temperatures (-17°C to -0.4°C, Table 6.3) can be used to predict relatively low- to moderately low salinities (< 20wt.% NaCl equiv.) regardless of the actual Ca/Na molar ratios (Oakes et al., 1990).

**Figure 6.15:** Illustration of phase transitions and melting paths for the presumed intermediate salinity inclusions (blue arrow lines) and low salinity aqueous fluid inclusions (red arrow line and red polygon) for the Karavansalija deposit in the ternary diagram $H_2O$-NaCl-$CaCl_2$. Cotectic curves separating halite, hydrohalite (HH) and ice stability fields are shown as thick black lines; isotherms are displayed as thin lines. Initial melting of inclusions commences with melting of antarcticite observed at temperatures between –55°C to –45°C, near the ideal eutectic temperature of –52°C. Upon heating, ice and hydrohalite melt and the composition of the remaining fluid moves along the cotectic curve separating the ice and hydrohalite fields (blue and red arrow lines). Assuming that hydrohalite disappears at -24°C, the inclusion will follow the path towards the $H_2O$ apex (blue dashed line) until the final ice melts about -14°C (blue circle). The bulk composition is defined by the intersection of the melting path with the appropriate isotherm in the ice-stable field, which in this case amounts to 18wt% NaCl+$CaCl_2$ and approximately 0.7 NaCl/$CaCl_2$ ratios. Eutectic melting of low salinity inclusions commences at temperatures around –21°C, indicating eutectic melting in the $H_2O$-NaCl system (red area). Final melting of ice for most of the inclusions in this study occurred at temperatures >-5°C ( modified after Shepherd et al., 1985; Vanko et al. 1988; Oakes et al, 1990 and Bodnar, 2003).

Microthermometric results for the Karavansalija skarn deposit are shown in Table 6.3 and graphically presented in Figure 6.16. During heating runs, all fluid inclusions homogenised to the liquid phase between 244°C and 402°C, with 95% of all inclusions falling in the range of 244°C and 396°C.The mean value of all inclusions measured is 316°C ±15. A prominent *Th* mode is evident at 340°C (Figure 6.16A). As compared to fluid inclusions from the Belo Brdo deposit, the homogenisation temperatures are distinctly higher, which is expected for skarn mineralisation. Weak bimodal distribution of homogenisation temperatures is apparent. The reason for this is that six low salinity aqueous inclusions from the late stage feathery textured quartz are included in the fluid inclusion dataset which exhibit higher calcic components, higher homogenisation temperatures and belong to paragenetically older quartz crystals. Those six inclusions were not treated as separate group. They exhibit lower homogenisation temperatures (244°C – 267°C) compared to the rest of the fluid inclusions whose homogenisation temperatures range from 270°C – 402°C. The wider spread of the data and higher standard deviation (±40 °C) could also be result of paucity of fluid inclusion data collected during this preliminary study.

**Table 6.3**: Thermometric data for fluid inclusions in Karavansalija deposit.

| Sample | No. Inclusion | Th(°C) | Tmice (°C) | NaCl wt% *equiv* | Dens (g/cm3) | Freez (°C) | Te(°C) | Comment-some melting |
|---|---|---|---|---|---|---|---|---|
| KU37 | 5 | 250 | -0.7 | 1.16 | 0.80 | -43 | -21 | |
| KU37 | 6 | 248 | -0.5 | 0.83 | 0.80 | -41 | -20 | |
| KU37 | 7 | 245 | -0.4 | 0.66 | 0.81 | -41 | | |
| KU37 | 8 | 244 | -0.6 | 0.99 | 0.81 | -40 | | |
| KU37 | 9 | 267 | -0.4 | 0.66 | 0.77 | -41 | -21 | |
| Ku72-Q1 | 1 | 378 | -3.9 | 6.23 | 0.62 | -47 | | |
| Ku72-Q1 | 2 | 402 | -4.6 | 7.25 | 0.58 | -50 | | |
| Ku72-Q2 | 3 | 286 | -4.5 | 7.11 | 0.82 | | | |
| Ku72-Q2 | 4 | 345 | -4.2 | 6.67 | 0.70 | -65 | -44 | |
| KU37 | 10 | 359 | -14 | 18.20 | 0.85 | -55 | -52 | -23 |
| KU37 | 11 | 345 | -4.8 | 7.54 | 0.72 | | -32 | |
| KU37 | 12 | 356 | -4.2 | 6.67 | 0.68 | | 26--30 | |
| KU37 | 13 | 360 | -3.9 | 6.23 | 0.66 | | -50 | |
| KU37 | 14 | 329 | -1.1 | 1.82 | 0.65 | -42 | -20 | |
| KU37 | 15 | 325 | -2.6 | 4.23 | 0.70 | -42 | | |
| KU37 | 16 | 334 | -3.2 | 5.17 | 0.70 | | | |
| KU37 | 17 | 320 | -3.4 | 5.47 | 0.73 | -56 | -40 | -15 |
| KU37 | 18 | 270 | -5 | 7.82 | 0.85 | -50 | -37 | -16 |
| KU37 | 19 | 327 | -4.8 | 7.54 | 0.75 | -55 | | -11 |
| KU37 | 20 | 327 | -4.7 | 7.39 | 0.75 | | | -14 |
| KU37 | 21 | 326 | -3.5 | 5.62 | 0.72 | | -45 | |
| KU37 | 22 | 326 | -4.5 | 7.11 | 0.75 | | | |
| KU37 | 23 | 319 | -3.1 | 5.01 | 0.73 | | | |
| KU37 | 24 | 319 | -3 | 4.86 | 0.73 | | | |
| KU37 | 25 | 320 | -3.8 | 6.08 | 0.74 | | -52 | -10 |
| KU37 | 26 | 320 | -3 | 4.86 | 0.72 | | | |
| KU37 | 27 | 332 | -4 | 6.37 | 0.72 | -43 | | |
| KU37 | 28 | 317 | -17 | 19.90 | 0.92 | -70 | -55 | -25 |
| KU37 | 29 | 316 | -17 | 20.20 | 0.91 | | | -24 |
| KU37 | 30 | 275 | -3.6 | 5.78 | 0.87 | | | -10 |
| Min | | 244 | -17.0 | 0.66 | 0.58 | | | |
| Max | | 402 | -0.4 | 20.20 | 0.92 | | | |
| Mean | | 316 | -4.5 | 6.51 | 0.75 | | | |
| Stdev | | 40 | 4.2 | 4.94 | 0.08 | | | |

The final melting temperatures of ice (*T<sub>m</sub>ice*) for all measured inclusions range from -17 °C to -0.4°C (Table 6.3; Figure 6.16B) and correspond to salinities of 20.2 and 0.66 wt.% NaCl equiv., respectively (Figure 6.16D). The mean $T_m ice$ at -4.5 °C corresponds to mean salinity of 6.5 ± 1.8 wt. % NaCl equiv., with 95% confidence level. A frequency distribution histogram of salinity data shows a wide distribution with pronounced maxima at 8 wt. % NaCl equiv. for the whole dataset. However, the data indicate a tri-modal distribution with maxima at 0.5wt%, 8wt% and smaller groupings at about 19wt% NaCl equiv. (Figure 6.16D). This could indicate the existence of three categories of aqueous fluid inclusions, namely (i) very low- salinity fluid (< 2 wt% NaCl equiv.); low- to moderate- salinity (4-8 wt% NaCl equiv wt% NaCl equiv) and an intermediate salinity fluid (~ 19wt% NaCl equiv.). It is apparent that the low- to moderate salinity inclusions are the most abundant type.

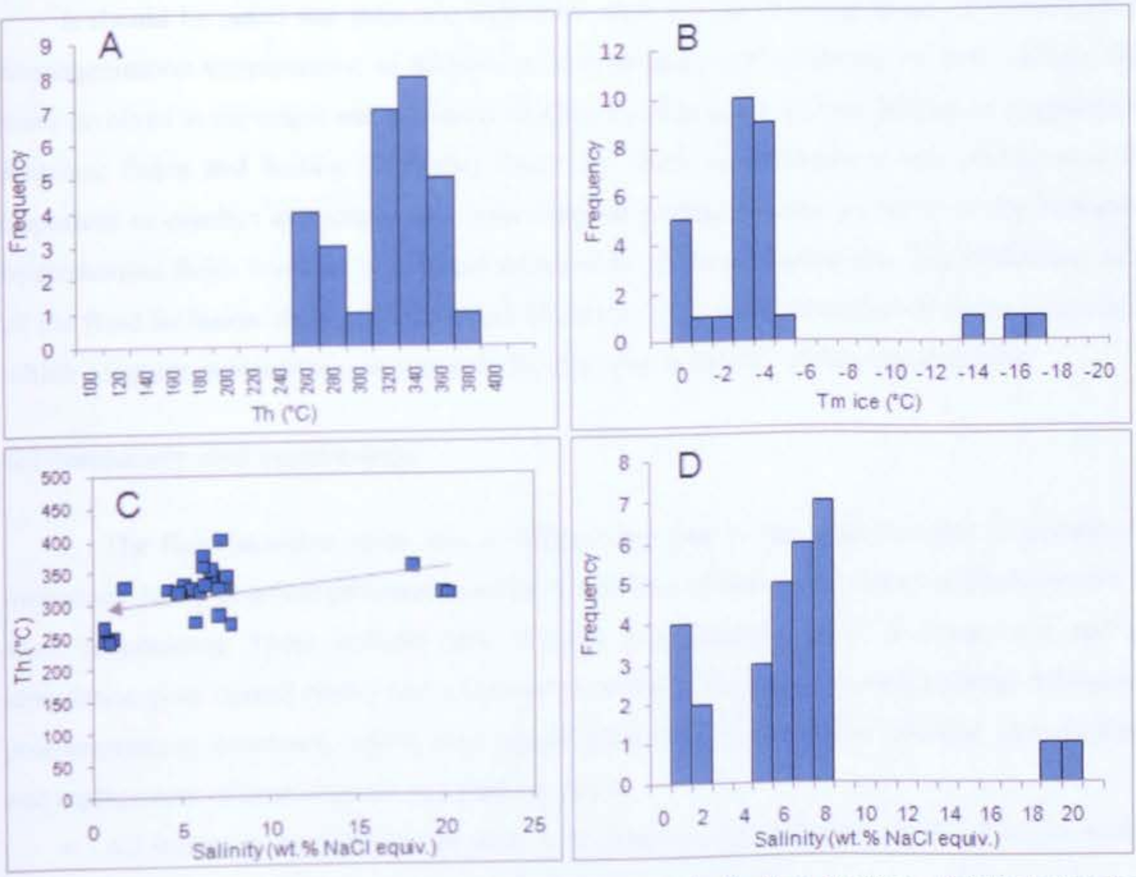

**Figure 6.16:** Frequency histograms depicting thermometry results for Type II primary fluid inclusions hosted by late stage quartz in Karavansalija skarn deposit. A) Distribution of homogenisation temperatures. B) Distribution of ice melting temperatures and corresponding salinity (D). C) Bivariate plot of salinity vs. liquid-vapour homogenisation temperatures; arrow represents regression line through the data and might indicate mixing of higher salinity fluids (presumed magmatic origin) with low salinity meteoric fluid. Besides mixing, the cooling trend is also indicated.

The lower salinity fluids might have been produced by dilution of the more saline fluid and boiling of the dilute fluids (Figure 6.13G). The dilution could have been caused by mixing with low salinity fluids, which are likely to be derived from meteoric water conductively heated by the Karavansalija dyke swarms. The meteoric origin of the fluids from the late stage quartz is evident from the results of the stable isotope studies and will be further discussed in Chapter 7. The apparent hiatus between the grouping of 5-10wt.% NaCl equiv. and that at 19wt.% NaCl equiv. might be a function of the quantity of data collected during this preliminary study.

Type III inclusions proved problematical in microthermometric studies as they failed to display observable changes on cooling. Also, some decrepitated on heating at temperatures up to 340°C without total homogenisation. Only three inclusions homogenised in the range of 350°C to 361°C by halite dissolution. Salinity estimates based on halite dissolution temperatures using the equation of Sterner *et al.* (1988) were about 42 wt % NaCl equiv. Due to low abundance and uncertainty of their classification, the hypersaline inclusions were not included in the graphical presentation of the data. At this stage of our investigation, it is not known, if the fluid in hypersaline inclusions was produced either by direct exsolution of the hypersaline fluid from magma (Roedder and Coombs, 1967) or boiling of an aqueous solution (Kodera et al., 2005).

It should be noted that there are indications that the high salinity fluids of moderately high homogenisation temperatures, in addition to intermediate- and moderate- to low- salinity fluids, were involved in the origin and evolution of Karavansalija skarn deposit. Mixing of magmatic with meteoric fluids and boiling of diluted fluids are likely mechanisms of ore precipitation. It is important to conduct systematic and more detailed studies in order to interpret the character of hydrothermal fluids involved in different stages of the skarn mineralisation. The preliminary results of the fluid inclusion study presented here illustrate the complex character of skarn evolution, for which adequate explanations are currently lacking, due to paucity of the data collected.

## 6.7 Summary and conclusions

- The fluid inclusion study was a difficult task due to the small number of suitable fluid inclusions. Many practical problems associated with the collection of valid microthermometric data were encountered. These include: lack of good host minerals, small inclusion size and poor abundance, poor optical clarity and sometimes leakage of inclusions during heating. Additionally, post-entrapment processes, which may significantly modify inclusions, include recrystallisation and replacement of host minerals and necking-down.
- All inclusions analysed in this study were aqueous and belong to the $H_2O$-NaCl system. No evidence of $CO_2$-bearing fluid inclusions was found in any sample.
- The fluid inclusion data suggests that the hydrothermal mineralisation at Belo Brdo was deposited from epithermal- to moderately high temperatures (160–350°C), and low- to moderate salinity (1.82-13.9wt.% equiv. NaCl) fluids.
- The trapping pressures were between 1419 and 521 bars and imply depths of between 5 and 1.7 km under lithostatic conditions. It is likely however, that pressures were fluctuating between lithostatic and hydrostatic conditions.
- The Cu-Au skarn mineralisation at Karavansalija is associated with moderately high temperatures (244-402°C) and low-to moderate salinity fluids (up to 20 eq. wt. % NaCl).

# CHAPTER 7:

# STABLE ISOTOPE GEOCHEMISTRY

## 7.1 Introduction

The elements sulphur, carbon, oxygen and hydrogen are important constituents of hydrothermal ore-forming systems. The stable isotope composition of hydrothermal minerals is a function of the initial isotopic composition of the hydrothermal fluid from which they precipitate and of the temperature-dependent isotopic fractionation processes during mineral precipitation and the effects of subsequent metasomatic alteration (Ohmoto, 1986; Ohmoto and Goldhaber, 1997; Zheng and Hoefs, 1993).The determination of light isotopes of S, C, O and H can provide powerful insights into the sources of the hydrothermal fluids, temperatures of mineralisation and physico-chemical conditions of mineral deposition (Ohmoto, 1986; Taylor, 1997; Hoefs, 2009).

In order to test the hypothesis that Belo Brdo represents a magmatic-hydrothermal type of deposit and to test whether mixing of magmatic and non-magmatic (i.e. meteoric) fluids played an important role in ore deposition, as indicated by the fluid inclusion study, a stable isotope analysis on the main ore and gangue minerals was carried out. No previous stable isotope data exist for the deposits considered here. Representative samples from all three stages of ore mineralisation from Belo Brdo deposit, as well as several samples from nearby porphyry and skarn deposits were selected for sulphur, carbon, oxygen and hydrogen isotope analysis with a view to gain a better understanding of the origin and evolution of mineralisation in the Kopaonik metallogenic district.

### *7.1.1 Basic terminology*

The absolute measurement of isotopic ratios is a difficult analytical task and, as a result, relative isotopic ratios of the two most abundant isotopes (i.e., $^{34}S/^{32}S$; $^{13}C/^{12}C$; $^{18}O/^{16}O$ and D/H) are measured. Variations in stable isotope ratios are expressed in per mil (‰), relative to an appropriate international standard by a relative difference value, $\delta$ ("delta"), which is defined as:

$\delta$ (in ‰) = ($R_{sample}$ - $R_{standard}$ -1) x1000 (Equation 7.1)

where "R" is the ratio of the heavy to the light isotope (i.e., $^{34}S/^{32}S$; $^{13}C/^{12}C$; $^{18}O/^{16}O$ and D/H) in the sample or standard (Faure, 1986; Hoefs, 2009).

## 7.2 Sulphur Isotope Geochemistry

### *7.2.1 Introduction*

The isotopic value ($\delta^{34}S$) of individual minerals is used to constrain sulphur sources and the physico-chemical dynamics of the mineralising systems. Ohmoto and Goldhaber (1997) indicate that the measured $\delta^{34}S$ value of a sulphide mineral is directly related to the reduced-sulphur ore-bearing fluid and therefore, is a powerful tool in determining the origin of the fluid. Furthermore, mineralising temperatures are constrained by the isotopic relationship between coexisting sulphides. Additionally, $\delta^{34}S$ is sensitive to changing redox conditions, so variations in the $\delta^{34}S$ values can trace changing oxidising or reducing conditions. Therefore, sulphur isotope geochemistry is recognised as an important tool in ore-deposit research (Ohmoto, 1986; Seward and Barnes, 1997; Ohmoto and Goldhaber, 1997).

### 7.2.2 *Objectives*

Sulphur isotopic studies in the Kopaonik mineral district were conducted with the following objectives:

1. To determine the sulphur isotope compositions from different types of Pb-Zn mineralisation in the study area in order to identify the most probable sulphur sources. The results of this study are expected to reveal if the sulphur is of magmatic, non-magmatic or mixed origin;
2. To compare the sulphur isotope signatures of different types of mineralisation, namely Pb-Zn (Ag) carbonate-replacement and vein-type mineralisation of the Belo Brdo deposit with those related to the Cu-Au skarn and Cu-Au porphyry systems and to delineate the conditions under which these deposits formed;
3. To compare the sulphur isotope geochemistry of different minerals and to test if sulphide precipitation took place under predominantly equilibrium or disequilibrium conditions by means of measuring sulphur isotope composition of cogenetic sphalerite-galena and pyrite-galena mineral pairs;
4. To help place constraints on the temperatures of mineralisation.

### *7.2.3 Sampling and Methods*

Sulphur isotope analysis was conducted on a total of 58 sulphide mineral separates including pyrite, sphalerite, galena and one stibnite. Apart from the Belo Brdo deposit, four other polymetalic occurrences in the Kopaonik metallogenic district were sampled for comparative stable isotope geochemical studies, namely the Karavansalija Cu-Au skarn, the Rudnitza Cu-Au porphyry, the Karadak Pb-Zn vein and the Kizevak Pb-Zn stockwork. A summary of all samples analysed.and their geological/mineralogical setting is provided in Table 7.1. All stable isotopic analyses in this study were performed at the stable isotope laboratory at the Scottish University Environment Research Centre (SUERC), East Kilbride, Scotland.

Sulphides from the Belo Brdo deposit count for most of the samples analysed. They include sphalerite, galena and pyrite from the main-ore stage, but also pyrite from the pre- and post- ore stage in order to track any changes in the ore-forming process. Barite of the vein ore-body in the Belo Brdo deposit could not be separated and hence could not be analysed. Most of the sulphide separates were identified and handpicked under a binocular microscope from 250µm sieved fractions derived from crushed ore-samples at Kingston University. Some monomineralic powders, which were also used for radiogenic isotope analysis, were obtained by hand-drilling coarse-grained sulphides using dental drill. Sulphur isotopic analyses of the sulphide minerals were performed by conventional methods following the procedure of Robinson and Kusakabe (1975), in which $SO_2$ gas is released by combustion with $Cu_2O$ and silica at 1070°C. The gas is further purified from water and $CO_2$ using standard separation acetone and pentane trap techniques. Isotopic compositions of the purified $SO_2$ gas were measured on a VG Isotech SIRA II mass spectrometer and standard corrections applied to raw $SO_2$ values to produce true $^{34}S$. Measurements were carried out using commercially available bottled $SO_2$ gas as a working standard, which was calibrated using certified reference materials supplied by the International Atomic Energy Agency (IAEA). The international reference standards NBS-123 (sphalerite) and IAEA-S-3 ($Ag_2S$), as well as the SUERC's internal laboratory standard CP-1(chalcopyrite) were repeatedly measured in-between samples to control the analytical reproducibility. They gave $^{34}S$ values of +17.1‰, –31.5‰ and –4.5‰ respectively, with overall reproducibility estimated to be around ±0.2 (1σ). All sulphur isotope compositions were calculated relative to Canon Diablo Troilite (V-CDT) and are reported in standard notation (per mil, ‰).

### *7.2.4 Results: Sulphur isotope composition of sulphides from the Kopaonik district*

Sulphur isotopic data for a total of 58 sulphide samples from four different deposit types, namely carbonate-replacement, vein, skarn and porphyry, are given in Table 7.1 and presented in Figures 7.1 and 7.2. The $\delta^{34}S$ values of the sulphides from the study area cover a relatively narrow range between 0.6 and 7.7 ‰ (Figure 7.1A), with 95% of the data falling into a range between 1.8 and 6.9‰. The frequency histogram of $\delta^{34}S$ compositions of sulphides exhibit a normal distribution with a mean $\delta^{34}S$ value of 4.4‰ ± 0.3 and a mode of 4.9‰ (Figure 7.1A). The $\delta^{34}S$ values of individual sulphides increasing in the order galena (0.6 to +4.6 ‰) $\leq$ pyrite (2.6 to 6.1 ‰) $\leq$ sphalerite (3.6 to 7.7‰) from four deposits show no significant variations (range $\leq$ 4‰) in the sulphur isotope compositions (Figure 7.1 B). Such a narrow range of $\delta^{34}S$ values suggests that there were no multiple components for the source of sulphur for these deposits.

In this study, a comparison has been made between sulphur isotope data from the Belo Brdo carbonate-replacement and vein-type deposit and several other polymetallic deposits in the Kopaonik Metallogenic district, namely the Karavansalija Cu-Au (Pb-Zn) skarn, the Rudnitza Cu-Au porphyry, the Karadak and Kizevak Pb-Zn vein and stockwork deposits (Figure 7.2). The sulphur isotope data for individual sulphides are arranged in the histograms according to the style of mineralisation (Figure 7.2A-D). The $\delta^{34}S$ values of pyrite from Belo Brdo are additionally arranged according to different generations of pyrite (pre-, main-, post-ore stage) to compare their isotopic signatures and track possible changes in ore forming processes between different stages of ore deposition (Fig 7.2A).

**Table 7.1** Sulphur isotope data obtained from sulphides from four deposits in the study area

| ID No | Sample | Mineral | $\delta^{34}S_{(V\text{-}CDT)}$ ‰ | Description | T in °C | $\delta^{34}S$ ($H_2S$) ‰ |
|---|---|---|---|---|---|---|
| *Belo Brdo (Pb-Zn ± Ag carbonate-replacement and vein-type)* | | | | | | |
| 33 | 1055_1B | Pyrite | 6.10 | Pre-ore carb-listwanite breccia | | |
| 26 | 1155/2B | Pyrite | 6.10 | Pre- ore; silicified carb. breccia | | |
| 34 | 1235/new | Pyrite | 3.60 | Pre-ore; dissemination in andesite | | |
| 63 | 1105/2A-2 | Pyrite | 3.10 | Pre-ore; dissemination in andesite | | |
| 68 | 1105/2A | Pyrite | 3.30 | Pre-ore; dissemination in Q-latite | | |
| 32 | 1105/3B | Pyrite | 2.60 | Pre-ore; pervasive listwanisation (Qtz, fuchsite) | | |
| 61 | 1055/2b | Pyrite | 3.20 | Pre-ore; dissemination in Qtz - tourm. breccia | | |
| 25 | 1055_T2 | Pyrite | 4.10 | Pre-ore; coarse-grained pyrite in listwanite | | |
| 56 | 1055_4A | Pyrite | 4.90 | Main-ore; massive sulphide | | $3.5^{c}$ |
| 57 | 1055_4A | Galena | 4.10 | Main-ore; massive sulphide | | $6.4^{c}$ |
| 20 | 1055_8 | Sphalerite | 5.20 | Main-ore; massive sulphide | $460^{a}$ | $4.9^{d}$ |
| 21 | 1055_8 | Galena | 3.90 | Main-ore; massive sulphide | | $5.7^{d}$ |
| 22 | 1055_8 | Pyrite | 4.50 | Main-ore; massive sulphide | | $3.4^{d}$ |
| 35 | 1105/halda | Sphalerite | 4.90 | Main-ore; massive sulphide | $434^{a}$ | $4.5^{c}$ |
| 36 | 1105/halda | Galena | 3.50 | Main-ore; massive sulphide | | $5.8^{c}$ |
| 37 | 1105/halda | Pyrite | 4.60 | Main-ore; massive sulphide | | $3.1^{c}$ |
| 13 | 1130_1B | Sphalerite | 5.40 | Main-ore; massive sulphide | $388^{a}$ | $5.1^{d}$ |
| 14 | 1130_1B | Galena | 3.80 | Main-ore; massive sulphide | | $5.6^{d}$ |
| 15 | 1130_1B | Pyrite | 4.70 | Main-ore; massive sulphide | | $3.5^{d}$ |
| 8 | 1155_1B | Sphalerite | 4.90 | Main-ore; massive sulphide | $525^{a}$ | $4.6^{d}$ |
| 9 | 1155_1B | Galena | 3.80 | Main-ore; massive sulphide | | $5.6^{d}$ |
| 62 | 180_3B | Pyrite | 3.80 | Main-ore; massive sulphide | | $2.4^{c}$ |
| 64 | 180_3B | Galena | 3.40 | Main-ore; massive sulphide | | $5.7^{c}$ |
| 65 | 180_3B | Sphalerite | 4.30 | Main-ore; massive sulphide | $609^{a}$ | $3.9^{c}$ |
| 4 | 180_1D | Sphalerite | 5.60 | Syn-to Late- stage ore breccia | $256^{a}$ | $5.2^{e}$ |
| 5 | 180_1D | Galena | 3.10 | Syn-to Late- stage ore breccia | | $5.7^{e}$ |
| 6 | 180_1D | Pyrite | 5.10 | Syn-to Late- stage ore breccia | | $3.4^{e}$ |
| 47 | 1055_4D | Galena | 4.10 | Syn-to Late- stage ore breccia | | $6.7^{e}$ |
| 48 | 1055_4D | Pyrite | 5.30 | Syn-to Late- stage ore breccia | | $3.6^{e}$ |
| 18 | BB-stock | Pyrite | 6.00 | Post-ore veins in contact with Cret. sediments | | |
| 41 | BB-m/dy | Pyrite | 5.30 | Post- ore; contact melange/dyke | | |
| 66 | 1055/6 | Sphalerite | 4.50 | Post-ore veins crosscutting listwanite | | |
| 67 | 1055/6 | Pyrite | 5.10 | Post-ore veins crosscutting listwanite | | |
| 59 | 1235_7B | Sphalerite | 4.90 | Vein ore body | $388^{a}$ | |
| 11 | 1235_7B | Galena | 3.30 | Vein ore body | | |
| 12 | 1235_7B | Pyrite | 4.90 | Vein ore body | | |
| 39 | 1235_5B | Galena | 3.50 | Vein ore body | | |
| 40 | 1235_5B | Pyrite | 5.50 | Vein ore body | | |
| 50 | 1235_5B1 | Stibnite | 3.60 | Vein ore body | | |
| *Karavansalija (Cu-Au ± Pb-Zn skarn)* | | | | | | |
| 52 | 07/24(3) | Pyrite | 5.30 | Skarn | $341^{b}$ | $4.1^{f}$ |
| 53 | 07/24(3) | Galena | 1.80 | Skarn | | $3.7^{f}$ |
| 69 | 07/24-2 | Pyrite | 4.80 | Skarn | $287^{b}$ | $3.6^{f}$ |
| 70 | 07/24-2 | Galena | 0.60 | Skarn | | $2.5^{f}$ |
| 29 | KU118 | Sphalerite | 7.70 | Skarn-Late vein | | $7.4^{f}$ |
| 28 | KU19 | Sphalerite | 3.60 | Skarn | | $3.3^{f}$ |
| 31 | KU43 | Pyrite | 3.00 | Skarn | | $1.8^{f}$ |
| 54 | KU47 | Pyrite | 5.40 | Skarn | | $3.8^{f}$ |
| 44 | KU69 | Pyrite | 5.00 | Skarn | $453^{b}$ | $4.0^{g}$ |
| 45 | KU69 | Galena | 2.50 | Skarn | | $4.2^{g}$ |
| *Rudnitza (Cu-Au porphyry)* | | | | | | |
| 42 | KU103 | Galena | 3.80 | Porphyry | | |
| 46 | KU103 | Pyrite | 2.60 | Porphyry | | |
| 19 | KU109 | Pyrite | 3.60 | Porphyry | | |
| 30 | KU90 | Galena | 3.10 | Porphyry | | |
| 51 | KU97 | Pyrite | 4.80 | Porphyry | | |
| *Kizevak-Karadak (Pb-Zn vein- and stockwork-type)* | | | | | | |
| 16 | R3/Q1 | Sphalerite | 6.20 | Karadak vein distal to porphyry | $388^{a}$ | |
| 17 | R3/Q1 | Galena | 4.60 | Karadak vein distal to porphyry | | |
| 60 | KZ5 | Sphalerite | 4.90 | Kizevak-vein and stockwork -dark sphalerite | | |
| 24 | KZ5 | Sphalerite | 7.60 | Kizevak-vein and stockwork (yellow sphalerite) | | |

**(a)** Sphalerite-galena and **(b)** pyrite-galena fractionation temperatures were calculated using the equations in Rye (1974), Czamanske and Rye (1974) and Ohmoto and Rye (1979). The **$\delta^{34}S_{(H2S)}$ ‰** is calculated utilising **(c)** average homogenisation temperature of 250°C of FIs from quartz of the main-ore stage; **(d)** average 325°C arsenopyrite and *(continued from previous page)* sphalerite geothermometry and (e) average homogenisation temperatures of 218°C from quartz of the late-ore stage; (f) average homogenisation temperature of 316°C from skarn and (g) average sulphur isotope temperature.

#### 7.2.4.1 Pyrite

The $\delta^{34}S$ values for 20 pyrite separates from Belo Brdo deposit range from 2.6 to 6.1‰, with an average of 4.6‰. Although there is considerable overlap, $\delta^{34}S$ values from the main-ore stage of the carbonate-replacement ore body (n=7) and late-stage veins, including the vein ore-body (n=4) (Figure 7.2A) are generally more homogeneous (3.8-5.3‰) compared to $\delta^{34}S$ values from pre-ore stage (n=8), which show a wider range of 2.6 and 6.1‰. The wider interval of $\delta^{34}S$ values from the pre-ore stage is clear when comparing $\delta^{34}S$ values from disseminated pyrites hosted in carbonate breccias (6.1‰) with respect to those disseminated in volcanic rocks (3.1-5.5‰) or associated with pervasive listwanisation (2.6-4.1‰). One pyrite sample from a late stage vein crosscutting Cretaceous sediments gave a $\delta^{34}S$ value of 6.0‰. Although slightly enriched in $^{34}S$, those pyrite samples that exhibit $\delta^{34}S$ values of ~6.0‰ are still within the 95% range of all analysed sulphides. In general, it can be concluded that $\delta^{34}S$ values of pyrite samples from Belo Brdo mineralisation overlap considerably with those derived from skarn and porphyry deposits, which show a narrow range between 2.6 and 5.4‰ (Fig 7.2B). Such $\delta^{34}S$ values have been reported in many Cu-Au and Cu-Mo porphyry and Pb-Zn skarn deposits worldwide (Rye and Ohmoto 1974; Gilmer et al.,1988; Megaw et al., 1988; Kalogeropoulos et al.,1989; Ohmoto and Goldhaber, 1997; Melfos, et al., 2002). They compare well to $\delta^{34}S$ values of pyrite from other Tertiary deposits within the Vardar Ophiolite zone, such as the Trepca skarn/replacement Pb-Zn deposit in Kosovo (Strmic-Palinkas, 2009) and Crnac Pb-Zn vein in southern Serbia (Borojevic-Sostaric, 2009). Slightly higher $\delta^{34}S$ values of pyrite from late-stage vein mineralisation crosscutting Cretaceous sediments and from those hosted in carbonate breccias might be a consequence of the ore fluid interacting with external, isotopically more positive sulphur sourced from country rocks (Ohmoto and Goldhaber, 1997).

#### 7.2.4.2 Sphalerite

Six sphalerite samples from the main-ore stage, one from the late veins crosscutting listwanite and one from the vein ore-body of the Belo Brdo deposit were analysed. Their $\delta^{34}S$ values occupy a very narrow interval between 4.3 and 5.6‰ and no difference in isotopic composition between early and late stages of Belo Brdo mineralisation can be established (Figure 7.2 C). Those values are close to the $\delta^{34}S$ value of one sphalerite sample from the skarn deposit (3.6) and one $\delta^{34}S$ value from the Karadak vein (4.9‰), which is located 1 km north from Rudnitza porphyry deposit (Radulović, 1992). However, small differences can be observed when comparing those values with $\delta^{34}S$ values of Fe-poor sphalerite samples derived from the Karadak and Kizevak vein and stockwork deposits. The Kizevak Pb-Zn deposit, situated 5 km north from Rudnitza porphyry deposit (Radulović and Savić, 1995), was not included in this study; however, one sample from mine dump found near the Rudnitza porphyry has been analysed for a comparative study. Both, the Kizevak and Karadak occurrences tend to display higher $\delta^{34}$S values then the sphalerites from the Belo Brdo and skarn deposits. They range from 4.9 to 7.6‰. No detailed investigation has been conducted on the Karadak and Kizevak Pb-Zn deposits in this study and their paragenetic textures are not known.

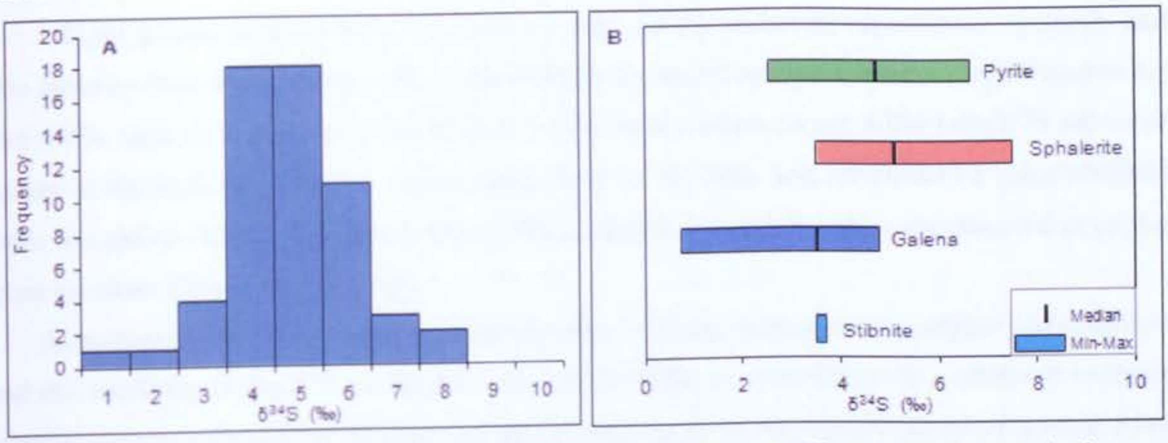

**Figure 7.1:** Sulphur isotope signatures for sulphide minerals from four different deposit types (carbonate-replacement, vein, skarn and porphyry) in the Kopaonik metallogenic district. A) Frequency histogram of $\delta^{34}$S compositions of all analysed sulphides showing normal distribution, with a mode at 4.9‰, indicative of magmatic source for sulphur. B) The range and median values of $\delta^{34}$S compositions for individual sulphides in the Kopaonik district.

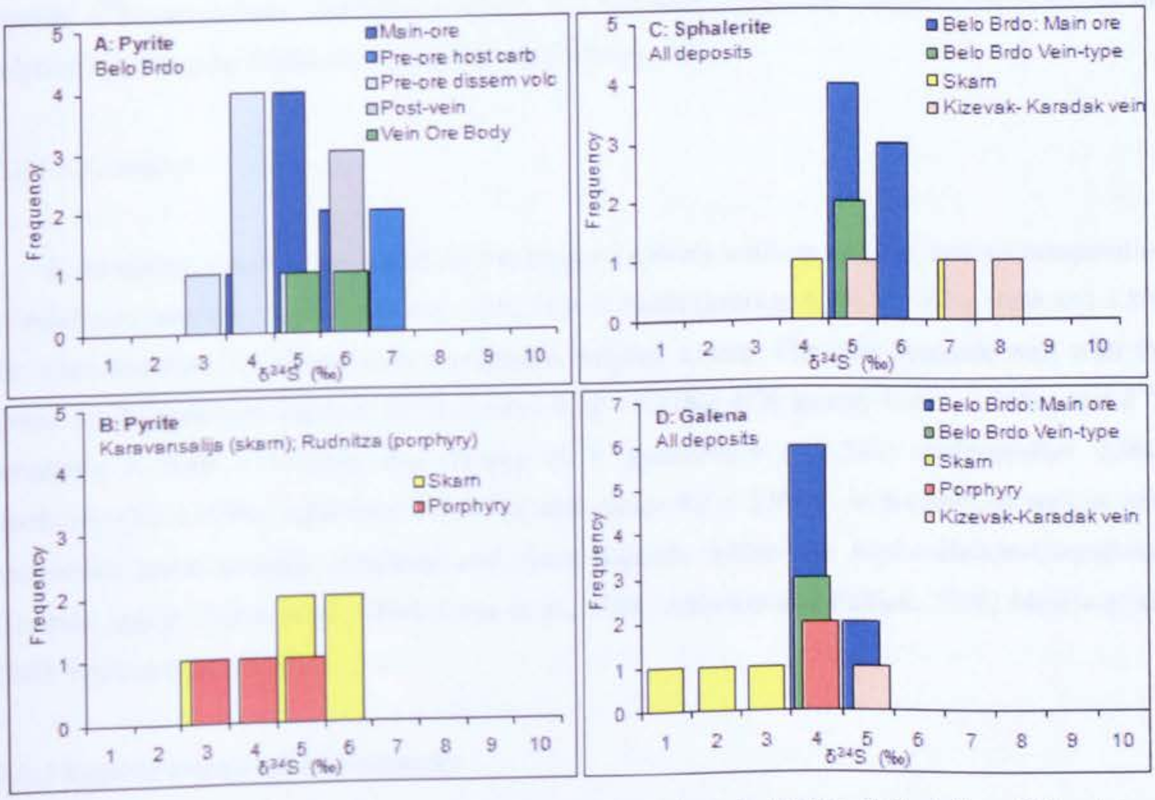

**Figure7.2:** Histograms of sulphide isotope data from 58 investigated sulphides derived from different types of deposits from the Kopaonik metallogenic district. A) Sulphur isotope values from different generations of pyrite from the Belo Brdo deposit) B) Sulphur isotope values from skarn and porphyry types; note a great overlap of sulphur values obtained from all three deposits. C) Sulphur isotope values for sphalerite. D) Sulphur isotope values for galena.

It has been observed, though, that the higher $\delta^{34}S$ values are obtained from honey-yellow Fe-poor sphalerite, which was not found in Belo Brdo. The higher $\delta^{34}S$ values of those samples may reflect a different hydrothermal event.

#### *7.2.4.3Galena*

Eight galena samples from the main-ore stage of the carbonate-replacement ore body and two samples from the vein ore body of the Belo Brdo deposit occupy a narrow range between 3.1 and 4.1‰, with an average of 3.5‰ (Figure 7.2D). Those values do not differ from $\delta^{34}S$ values of galena in the Rudnitza porphyry, which range from 3.1 to 3.8‰, and are close to a value obtained from one galena sample of Karadak vein (4.6‰). Slightly lower $\delta^{34}S$ values are observed in galena from the skarn deposit (0.6 – 2.5‰).

In summary, the data presented above indicate relatively homogeneous sulphur compositions and the similarity of the $\delta^{34}S$ values from all four localities is consistent with a relatively uniform igneous source, with sulphur derived directly by magmas or by the remobilisation of sulphur from igneous rocks (Ohmoto and Rye 1979; Ohmoto and Goldhaber, 1997). The absence of isotopically heavy $\delta^{34}S$, which is a characteristic of evaporitic sequences or seawater found in many MVT deposits, rules out evaporites as the potential source for sulphur in the studied deposits. The slightly heavier $\delta^{34}S$ values from carbonate breccias and late stage veins may suggest that some of the sulphur may have derived from Cretaceous sedimentary rocks.

#### *7.2.4.4 Summary*

In summary, the data presented above suggests a fairly uniform sulphur isotope composition of sulphides (average ~4.4‰) and coexisting $H_2S$ in fluids (average 4.7‰ for Belo Brdo and 3.8‰ for Karavansalija), consistent with a magmatic sulphur source. The data compare well with the Crnac Pb-Zn vein-type deposits ($\delta^{34}S$ pyrite= 0.32 - 3.11‰; $\delta^{34}S$ galena=0.42 - 3.05‰; and $\delta^{34}S$ sphalerite = 2.89 - 5.92‰), and Trepca ($\delta^{34}S$ galena=0..9 ± 2.3‰; chalcopyrite= 2.9‰; pyrrhotite=3.1 ± 0.8‰; sphalerite=3.7 ± 1.6; and pyrite 4.2 ± 2.8‰) in Kosovo, as well as with epithermal precious-metal, porphyry and skarn deposits within the Alpine-Balkan-Carpathian-Dinaride region (Vityk et al., 1994; Lexa et al., 1999; Alderton and Fallick, 2000; Melfos et al., 2002; Kodera et al., 2005).

### ***7.2.5 Sulphur isotope geothermometry***

Equilibrium sulphur isotope fractionation between coexisting sulphide minerals is strongly temperature-dependent and decreases with increasing temperature (Ohmoto and Goldhaber, 1997). It also depends on relative metal-sulphide bond strengths (Sakai, 1968; Bachiniski, 1969).

Thermodynamic considerations (Sakai, 1968) and experimental data (Kajiwara and Krouse, 1971; Grootenboer and Schwarcz, 1969) imply that under equilibrium conditions, and at a given temperature, the heavier isotope will be enriched in minerals with stronger sulphur bonds, so that the order of $^{34}$S enrichment in the sulphide minerals of the, for instance, Cu-Zn-Pb-Fe system would be pyrite>sphalerite>chalcopyrite>galena.

From a total of 38 sulphide separates (20 pyrites, 10 galenas and 8 sphalerites) from the Belo Brdo deposit, seven coexisting sphalerite-galena pairs indicated a possible precipitation under equilibrium conditions, based on the relation $\delta^{34}S_{galena} < \delta^{34}S_{sphalerite}$ (Ohmoto, 1986) (Table 7.1). The differences in $\delta^{34}S_{sphalerite} - \delta^{34}S_{galena}$ between the coexisting sulphide pairs are between 0.9 and 2.5‰, with an average of 1.47‰, yielding formational temperatures between 609°C and 251°C, with an average of 437°C. Additional geothermometry was carried out on the same samples using pyrite-galena pairs (Ohmoto and Rye, 1979), which revealed poor isotopic fractionation ($\delta^{34}S_{pyrite} - \delta^{34}S_{galena} \geq 0.6 \leq 2$) resulting in variable and unrealistically high temperatures (up to1200°C). It is well established that pyrite-galena pairs are often not the best suitable geothermometers (Hoefs, 2009). This is the case in Belo Brdo, where several generations of pyrite exist, indicating precipitation over much larger intervals than galena, suggesting that these two minerals were not contemporaneous.

Five sphalerite-galena pairs from the *main-ore stage* of the Belo Brdo deposit yielded much higher temperatures of between 388 and 609°C, indicating that sulphide pairs were not in equilibrium. They are higher than homogenisation temperatures obtained by fluid inclusion study of quartz (216 -251°C), which however, was not strictly contemporaneous with sulphide minerals. Furthermore, the sulphur isotope temperatures are higher than those obtained by arsenopyrite geothermometry (311 -348°C, average 330°C) and sphalerite geothermometry (290 -350°C, average 320°C) from the same paragenetic stage. The closest to those formation temperatures is the sulphur isotope temperature of 388°C, which is ~40°C higher than the maximum temperatures obtained by arsenopyrite and sphalerite geothermometers and the maximum homogenisation temperature obtained by fluid inclusion study of quartz from the main-ore stage.

One sphalerite-galena pair from the *syn- to late- ore stage* breccia separated from sample 180_1D yielded a temperature of 256°C, which is close to the average homogenisation temperature of 218°C obtained from the quartz in the same sample.

The sphalerite-galena pair from the vein ore body of the Belo Brdo deposit yielded 388°C. Unfortunately no microthermometric data could be collected from this ore body, so no homogenisation temperatures are available for comparison with stable isotope geothermometry results. However, several points of evidence suggest that the temperatures of ore formation in vein ore body were lower than 388°C and those from the replacement-type ore body, such as: numerous monophase fluid inclusions in late stage barite; presence of stibnite; lower concentrations of FeS in sphalerite and lower atomic% of As in arsenopyrite.

Most of the calculated temperatures presented above suggest an absence of isotopic equilibrium or noncontemporaneous precipitation of the co-existing sulphides. This is further supported by the fact that the sulphur isotope values for pyrite, sphalerite and galena do not always follow a normal order of $\delta^{34}S$ enrichment for these minerals. Where all three sulphides have been analysed from the same mineral assemblage, the order of relative $\delta^{34}S$ enrichment is sphalerite>pyrite>galena, indicating that the sulphides were not in isotopic equilibrium with each other (Kajiwara and Krouse, 1971; Czamanske and Rye, 1974).

As no sulphate minerals have been observed in the carbonate-replacement ore-body of the Belo Brdo deposit, a reduced, $H_2S$ dominated hydrothermal system can be inferred for the deposition of sulphides. The $\delta^{34}S$ values of sulphides deposited in an environment where $H_2S$ is presumed to be the main sulphur species in the fluid are generally close to the $\delta^{34}S$ values of the fluid (Ohmoto and Rye 1979). In this study, the $\delta^{34}S$ value of $H_2S$ in equilibrium with sulphides was calculated from the $\delta^{34}S$ value of sulphide minerals and the mineral-$H_2S$ fractionation factor of Ohmoto and Rye (1979) for pyrite and sphalerite, and of Li and Liu (2006) for galena. Assuming average formation temperatures of about 325°C for the main mineralising stage obtained from arsenopyrite and sphalerite geothermometry, and average homogenisation temperatures of 250°C and 218°C from quartz of syn- and late- ore stages respectively, the original $\delta^{34}S$ composition appears to be close to 4.7‰, which suggests a magmatic sulphur source (Table 7.1) (Ohmoto and Rye 1979; Field and Fifarek 1985).

Pyrite-galena pairs from three samples collected from the Karavansalija skarn deposit yielded more uniform temperatures compared to Belo Brdo. The results of sulphur isotope geothermometry indicate formation temperatures between 287 -453°C with an average of 360°C. Those temperatures compare well to preliminary homogenisation temperatures of fluid inclusions obtained from quartz. The calculated $\delta^{34}S$ value of $H_2S$ in equilibrium with sulphides is 3.8‰, utilising the average homogenisation temperature of fluid inclusions (316°C) for most samples and the average sulphur isotope temperature (360°C) for one sample, in which the homogenisation temperatures resulted in the highest values (286-402°C).

No sulphide pairs were collected from the Rudnitza porphyry deposit and only one sphalerite-galena pair was analysed from the nearby Karadak Pb-Zn vein. The formation temperature of 388°C far exceeds that obtained from a reconnaissance study of 16 fluid inclusions from quartz co-existing with sulphides in this sample. The homogenisation temperatures of aqueous fluid inclusions range from 220 -273°C with an average temperature of 230°C. Such temperatures are typical for epithermal vein deposits related to porphyry systems.

## 7.3 Oxygen and Carbon Isotope Geochemistry of carbonate phases

### *7.3.1 Introduction and objectives*

The study of the isotopic composition of carbonates including carbon ($\delta^{13}C$) and oxygen ($\delta^{18}O$) isotopic covariation in carbonate generations can be used to obtain information about the nature of the carbon species dissolved in mineralising fluid(s) and the oxygen isotopic composition of fluid(s) involved in mineralisation processes (Zheng and Hoefs, 1993). In this study, the carbon and oxygen isotopic compositions of several carbonate generations from the Belo Brdo deposit were determined in order to constrain the isotopic signature and nature of the fluid(s) involved, as well as to recognise possible trends in fluid evolution. Additionally, the isotopic compositions of carbonates from Karavansalija skarn and Rudnitza porphyry were determined for comparative study.

### *7.3.2 Sampling and Methods*

Carbon and oxygen isotope analyses of carbonates were performed on a total of 48 carbonate samples (36 dolomite and 12 calcite) from Belo Brdo (dolomite, n=34), Karavansalija (calcite, n=10) and Rudnitza (dolomite, n=2; calcite, n=2) localities. A summary of all samples analysed and the paragenetic setting of their generation is provided in Table 7.2.

Monomineralic carbonate separates were obtained from hand specimens (Belo Brdo) and drill core samples (Karavansalija and Rudnitza). Carbonate samples were carefully selected in order to accurately constrain the paragenetic setting of each carbonate generation from the Belo Brdo deposit. They include the following: unaltered Cretaceous limestone host rock ($d_1$); recrystallised carbonates ($d_1$-recryst); pre-ore listwanite and silicified carbonate breccia ($d_2$); dolomite from the main-stage mineralisation ($d_3$); the late-ore stage dolomites filling cavities ($d_4$); crosscutting veins ($d_4$-veins), as well as dolomites from the vein-type ore body (vein-BB) (Figure 7.3). Host rock was analysed proximal and distal to the Belo Brdo ore deposit in order to examine the isotopic effects of wall rock alteration. Note that the ore-stage dolomite ($d_3$) only occurs in microscopic amounts and could not be sampled. However, syn-to late dolomite which appears to coexist with massive sulphide ore was sampled and assigned to the $d_3$ generation.

Calcite samples from the Karavansalija skarn were derived from drill cores and include weakly mineralised carbonates, as well as calcite coexisting with arsenopyrite ± pyrite ± Bi-Te mineral assemblage and calcite coexisting with a later pyrite ± sphalerite ± galena assemblage. Calcite and dolomite from the Rudnitza porphyry deposit derived mainly from late stage calcite filling small cavities or coexisting with late-stage sphalerite-galena veinlets.

Prior to isotopic analysis samples were cleaned from surface impurities using 10% $HNO_3$ and deionised water. Carbonate powders were prepared in two ways. Cleaned fragments of non-mineralised host rocks were ground to powder with a mortar and pestle, whilst carbonates from ore

**Table 7.2:** C and O isotope data obtained from carbonates from three deposits in the study area

| Sample | Description | Carbonate Generation | $\delta^{13}C‰$ (VPDB) | $\delta^{18}O‰$ (VSMOW) |
|---|---|---|---|---|
| Belo Brdo (Pb-Zn ± Ag carbonate-replacement and vein-type) | | | | |
| LIM-1 | Cretaceous fossiliferous limestone | d1 | 2.66 | 27.65 |
| Z-3 | Zeljin bedded limestone | d1 | 2.86 | 25.43 |
| ZAP-1 | Massive limestone (adit) | d1 | 3.48 | 26.08 |
| NZ-7 | Non-min. recrystallised limestone - skarn | d1-recryst | 0.70 | 12.19 |
| 1055/1B(1) | Non-min. dark grey carbonate breccia fragment | d1-recryst | 0.49 | 11.78 |
| 1055_1C | Weakly mineralised listwanite breccia (Ni-Co; Py) | d2 | -1.66 | 13.10 |
| 1105_2B | Weakly mineralised silicified carbonate breccia | d2 | -1.52 | 13.00 |
| 1105_3B | Weakly mineralised listwanite (Ni-Co; Py) | d2 | -0.07 | 11.83 |
| 1155_2C | Weakly mineralised listwanite (Cr-mica) | d2 | -3.48 | 12.44 |
| 1055/1A | White dolomite cement in hydrothermal breccia | d2 | -0.17 | 12.85 |
| 1055/1B TC | White dolomite-hydrothermal breccia (Py, Cr-mica) | d2 | -1.92 | 13.54 |
| 1055/2B | Qtz-tourmaline breccia (Cr-mica) | d2 | -2.85 | 11.69 |
| 1055/T2 | Listwanite with coarse-grained pyrite (Cr-mica) | d2 | -1.76 | 13.82 |
| 1055_4A | Syn-to late-ore stage white-creamy dolomite | d3 | 0.69 | 11.47 |
| 1055_8 | Syn-to late-ore stage white-creamy dolomite | d3 | 1.70 | 10.03 |
| 1105/4 (1-2) | Syn-to late-ore stage white-creamy dolomite | d3 | -0.52 | 12.31 |
| 1105/4 (1) | Syn-to late-ore stage white-creamy dolomite | d3 | 0.04 | 13.09 |
| 1130/1B | Syn-to late-ore stage white-creamy dolomite | d3 | 0.74 | 11.43 |
| 1130/1B (1) | Syn-to late-ore stage white dolomite | d3 | -0.25 | 12.14 |
| 1155/1B | Syn-to late-ore stage yellow dolomite | d3 | 1.30 | 12.14 |
| 180/3B | Syn-to late-ore stage white-creamy dolomite | d3 | -0.18 | 12.94 |
| 1055_4D | Late-stage cavity filling yellow dolomite | d4 | 4.38 | 11.23 |
| 1105/H | Late-stage cavity filling creamy-yellow dolomite | d4 | 3.24 | 10.13 |
| 180/1D | Late stage yellow dolomite | d4 | 3.23 | 10.32 |
| 1105/H-2 | Late-stage breccia cement | d4 | 2.42 | 10.43 |
| 1105/4 (2 d2) | Creamy dolomite vein crosscutting main ore | d4- veins | -0.95 | 14.08 |
| 1105/4 (2 d1) | White dolomite vein crosscutting main ore | d4- veins | -1.56 | 13.89 |
| 1105/6(1) | White dolomite from quartz-dolomite vein | d4- veins | -4.41 | 13.62 |
| 1105_6 | Creamy dolomite from quartz-dolomite vein | d4- veins | -4.31 | 13.05 |
| 1235(2) | Early dolomite in contact with andesite | Vein ore body-early | -2.68 | 9.58 |
| 1235-5B-1-p | White-creamy dolomite associated with early pyrite | Vein ore body-early | 0.88 | 11.11 |
| 1235-5B-1s | Creamy dolomite coexisting with stibnite | Vein ore body | 0.69 | 10.66 |
| 1235-5B(3) | Late-stage white veinlets of dolomite | Vein ore body-late | 1.17 | 10.68 |
| 1235-5B(3-1) | Late-stage yellow dolomite | Vein ore body-late | 4.14 | 9.60 |
| 1235_7C | Late-stage dolomite in contact with pyrite | Vein ore body-late | 5.05 | 10.16 |
| Rudnitza (Cu-Au porphyry) | | | | |
| KU103 | Yellow dolomite associated with galena and sphalerite | porph-vein | -2.36 | 13.41 |
| KU103 | Late stage calcite vein | porph-vein | 2.06 | 14.4 |
| KU90 | Vein; yellow dolomite associated with galena | porph-vein | -2.43 | 18.24 |
| KU90-2 | Vein; late stage white calcite | porph-vein | -0.28 | 18.11 |
| Karavansalija (Cu-Au ± Pb-Zn skarn) | | | | |
| KU47 | Late-stage calcite, weakly mineralised (BH 06-19, 33m) | Late-skarn | -0.89 | 8.96 |
| KU41 | Late stage calcite filling cavity 9Bh 06-10, 208m) | Late-skarn | 1.51 | 14.86 |
| KU50 | Late calcite pods-non-mineralised skarn (BH 06-19, 75m) | Late-skarn | -0.22 | 11.43 |
| KU10 | Calcite pods with Py+Cpy (BH 06-18,40m) | skarn | -2.82 | 12.79 |
| KU31-1 | Calcite associated with Sph+Gn (BH 08 31, 432m) | skarn | -2.72 | 10.73 |
| KU6 | Calcite pods with dissemin. Py+Cpy (BH 18,13m) | skarn | -2.75 | 12.75 |
| KU19 | Calcite associated with Sph+Gn (BH 06- 11, 24m) | skarn-vein | -3.73 | 6.60 |
| KU25 | Calcite pods with dissemin Py, Apy; Bi-Te (BH 20, 224m) | Syn-skarn | -4.01 | 10.14 |
| KU07-24-3 | Calcite associated with Sph+Gn (BH 07-24,330m) | Syn-skarn | -2.78 | 9.89 |

samples were collected with a tungsten carbide drill-bit attached to the Dremel™ drilling tool to exclude contamination by sulphide minerals and mixing of different carbonate generations.

Oxygen and carbon isotope analyses were carried out at SUERC on an Analytical Precision automated AP 2003 continuous mass spectrometer, equipped with a fully automated sample preparation and sample processing unit. The sample powders (~2mg) were placed in 6 ml vacutainers, then sealed and loaded onto the autosampling unit. Sequentially, each sample tube was flushed by Helium, and then injected with 100% $H_3PO_4$ under at 70 °C (McCrea, 1950; Rosenbaum and Sheppard, 1986). The duration of the reaction was overnight for dolomites and 20 min for calcite samples. Removal of water vapour and purification of the $CO_2$ for subsequent analysis on the mass spectrometers, takes place in sample processor. Precision (1σ) based on replicate analysis of the SUERC laboratory standard (marble, MAB-2; $\delta^{13}C=2.4‰$ and $\delta^{18}O=-2.4‰$) was 0.02‰ for $\delta^{13}C$ and 0.03‰ for $\delta^{18}O$ during this study. Analytical raw data were corrected using standard procedures (Craig, 1957). The oxygen isotope data for dolomite was corrected using the fractionation factor given by Rosenbaum and Sheppard (1986). The carbon isotope data are reported relative to V-PDB (Vienna Pee Dee Belemnite) whereas the oxygen isotope data are relative to V-SMOW (Standard Mean Ocean Water).

### *7.3.3 Results: Carbon and oxygen isotope data of carbonates*

Carbon and oxygen isotopic results obtained on all analysed carbonates are listed in Table 7.2. The variation of the $\delta^{18}O$ and $\delta^{13}C$ values is shown in Figure 7.3. Carbon and oxygen isotopic signatures of carbonates are also presented in the form of stacked histograms in Figure 7.4. Based on textural and compositional characteristics, several generations of carbonates from Belo Brdo were analysed. Three non-mineralised samples of host rock Cretaceous limestones ($d_1$), two of which were collected ~5 km from the Belo Brdo deposit and one from the entrance to the mine, have very similar C and O isotope compositions. Their $\delta^{13}C$ values vary from 2.7 to 3.5‰ and $\delta^{18}O$ from 25.4 to 27.7‰, which correspond well to the world-wide Cretaceous marine carbonate values (Veizer and Hoefs, 1976; Vazquez et. al., 1998).

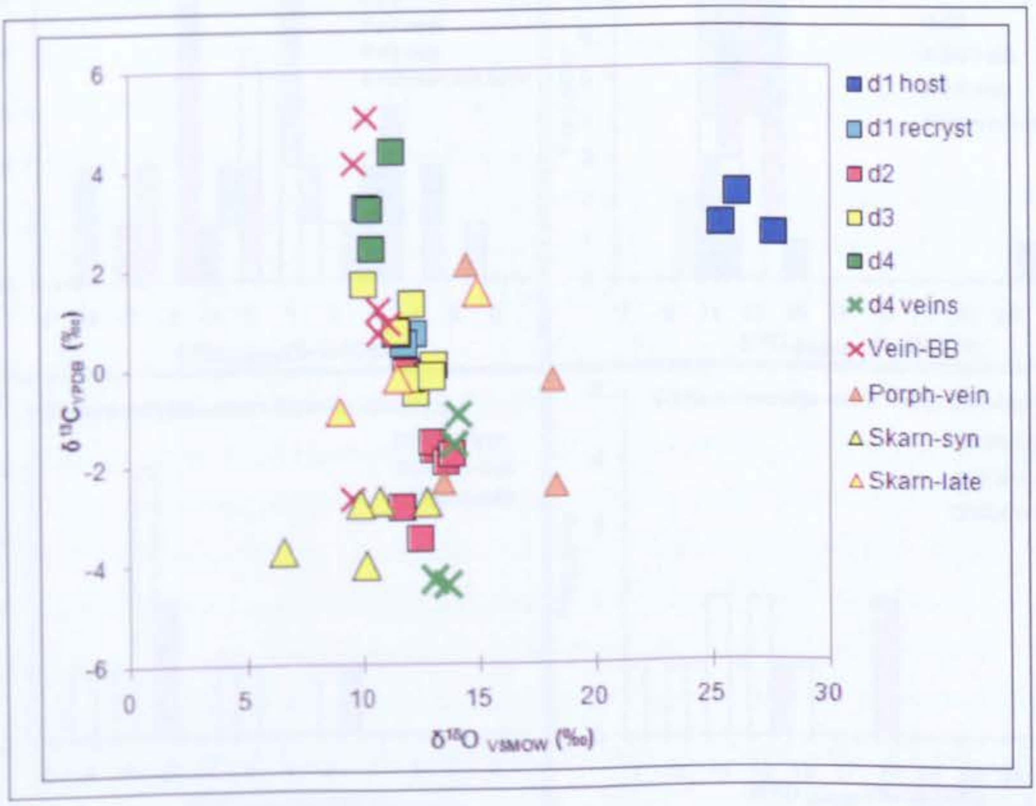

**Figure 7.3:** Carbon and Oxygen isotope signatures of carbonates from Belo Brdo (d2-d4 of the replacement-type and vein-BB of the vein-type ore body), Rudnitza (porphyry) and Karavansalija (skarn) deposits, compared to the isotopic composition of host rock carbonates from the Upper Cretaceous flysch unit ($d_1$).

In contrast, all other carbonate generations including recrystallised limestones (d$_1$-recryst), weakly mineralised carbonates (d$_2$), mineralised dolomites and ankerites (d$_3$), late stage dolomites and veins (d$_4$), as well as dolomites from Belo Brdo vein-type ore body show a considerable shift to lighter O isotopic values. Calcite samples from skarn and porphyry deposits also exhibit a similar shift to lighter O isotopic values (Figure 7.3).

The $\delta^{13}C$ values of the hydrothermal dolomites from the Belo Brdo deposit cover a relatively wide range between -4.4 and 5.1‰ with an average of 0.1 ±0.8‰ (Figure 7.4A). The large spread of data (n= 32; 1σ =2.4‰) reflects variable carbon signatures from different carbonate generations. The $\delta^{18}O$ values display a smaller range, between 9.6 and 14‰, with an average value of 12.1±0.5‰ (Figure 7.4C).

*The pre-ore carbonate generation* (d$_2$; n=8) is represented by dolomites of weakly mineralised listwanites, silicified carbonate breccias and hydrothermal dolomites from quartz-tourmaline breccias. This population exhibits depleted $\delta^{13}C$ values ranging from -3.5 to -0.1‰, with an average -1.7±0.8‰. They weakly overlap with $\delta^{13}C$ values of calcite coexisting with sphalerite ± galena ± chalcopyrite mineral assemblage of Karavansalija skarn deposit and chalcopyrite in porphyry deposits (Figure 7.4B). The lowest $\delta^{13}C$ values observed in this population might reflect

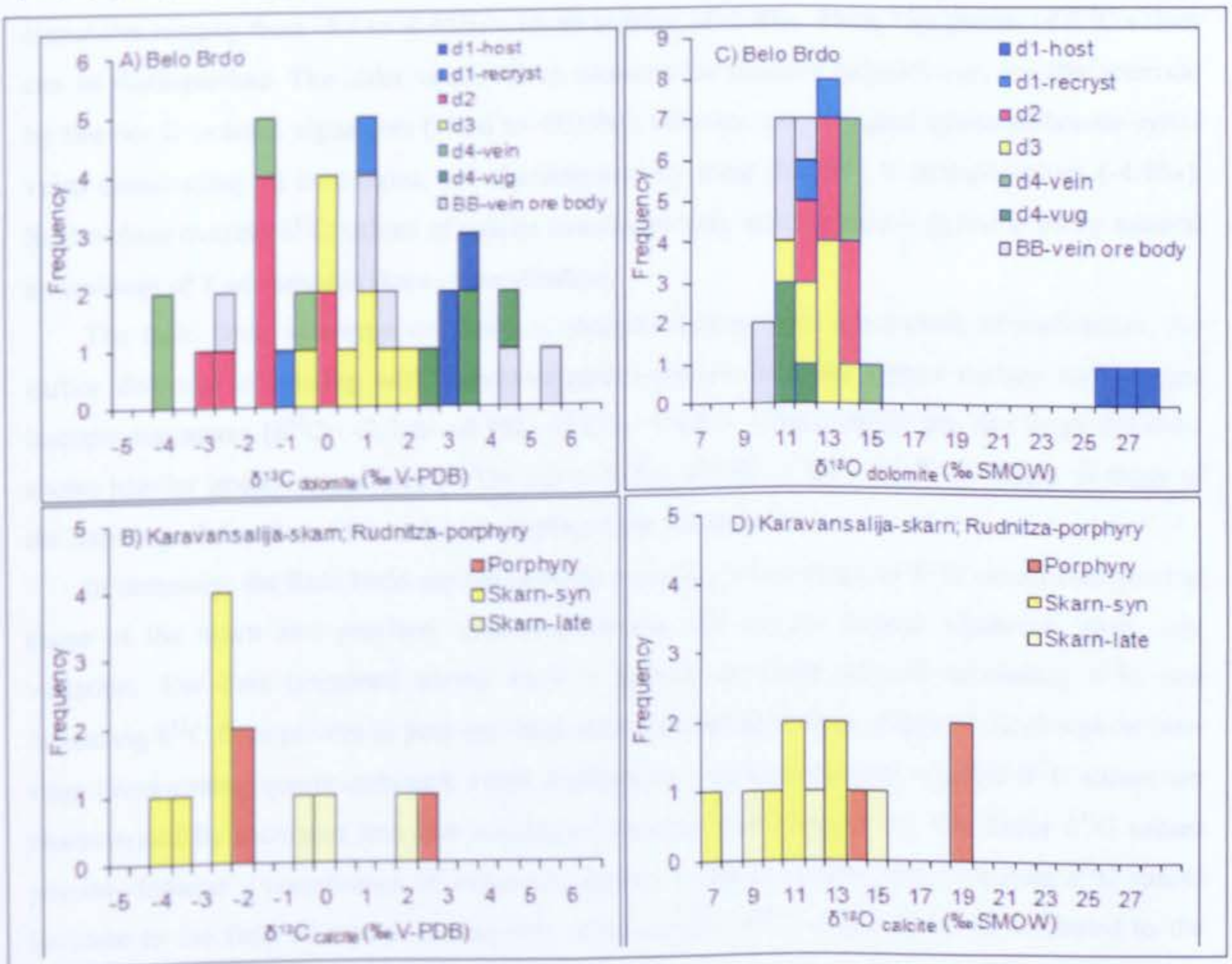

**Figure 7.4:** Stacked histograms showing distribution of $\delta^{13}C$ signatures (A and B) and $\delta^{18}O$‰ signatures (C and D) of carbonates in the studied area.

some input of magmatic carbon, whose value of $\delta^{13}C \sim 5‰$ has been identified as an isotope signature for the mantle (carbonatite and kimberlite carbonates, diamonds, and volcanic $CO_2$ exhalations) (Deines 2002, and references therein). The $\delta^{18}O‰$ values of $d_2$ carbonates show a narrow range from 11.7 to 13.8‰ with an average of 12.8±0.6‰ (Figure 7.4C).

*The syn- to late-ore carbonate generation* ($d_3$; n=8) include dolomites coexisting with sulphides of the main mineralisation stage. This group exhibits heavier C signatures then the pre-ore stage carbonates, with $\delta^{13}C$ values ranging from -0.5 to +1.7‰ and an average of +0.5± 0.4‰. The $\delta^{13}C$ signatures of this group overlap the $\delta^{13}C$ signatures of calcite coexisting with the late-stage pyrite ± sphalerite ± galena assemblage from the porphyry and skarn deposits (Figure 7.4B). The $\delta^{18}O‰$ values of the carbonates from this group show again a narrow range from 10 to 13‰ with an average 12±0.7‰ (Figure 7.4C).

*The post-ore carbonate generation* is represented by the late-stage dolomites infilling cavities and open voids ($d_4$; n=4) as well as late stage quartz-carbonate veins ($d_4$-veins; n=4). The $d_4$ carbonates are characterised by the heaviest $\delta^{13}C$ values, which range from 2.4 to 4.4‰ with an average of 3.3±0.4‰. Their $\delta^{18}O‰$ values show very narrow range from 10 to 11‰ with a mean value of 10.5±0.2‰. Late-stage quartz-dolomite veins are characterised by the most depleted $\delta^{13}C$ signatures ranging from -4.4 to -0.95‰ with an average of -2.8‰. Here, two groups of $\delta^{13}C$ values can be distinguished. The older veins, which crosscut the massive sulphide ore, are characterised by heavier C isotopic signatures (-1.56 to -0.95‰), whereas the youngest quartz-carbonate-pyrite veins crosscutting all lithologies, are characterised by most depleted C isotope values (-4.4‰). Such values overlap $\delta^{13}C$ values of calcite associated with arsenopyrite ± pyrite ± Bi-Te mineral assemblage of Karavansalija skarn mineralisation.

The Belo Brdo vein-type ore body is characterised by two generations of carbonates. An earlier dolomite coexisting with sphalerite-galena-stibnite exhibits lighter carbon and oxygen isotopic signatures ($\delta^{13}C$= -2.7 to +0.9‰; $\delta^{18}O‰$ = 9.6 – 11‰), whilst the late stage dolomite shows heavier isotopic signatures ($\delta^{13}C$= 1.2 to 5.0‰; $\delta^{18}O‰$ = 9.6 – 10.7‰), similar to those of the late-stage dolomites of the carbonate-replacement ore body.

In summary, the Belo Brdo deposit exhibits a slightly wider range of $\delta^{13}C$ values compared to those of the skarn and porphyry deposits, whereas the oxygen isotope signatures show less variation. The data presented above show a general tendency toward decreasing $\delta^{18}O$ and increasing $\delta^{13}C$ from pre-ore to post-ore stage carbonates of Belo Brdo (Figure 7.3), except for late-stage cross-cutting quartz-carbonate veins. Furthermore, carbonates with negative $\delta^{13}C$ values are characterised by increased iron and manganese contents (see Chapter 4). The lower $\delta^{13}C$ values possibly indicate a contribution of magmatic carbon, whereas the late-stage dolomite $\delta^{13}C$ values lie close to the field of marine limestones. Such variable $\delta^{13}C$ values could be attributed to the mixing of isotopically different waters or to the presence of various carbonate species derived from dissolution of host-rock carbonates (Velasco et. al., 2003). One possibility is the mixing of a deep fluid, having magmatic $\delta^{13}C$ signatures, with a fluid in equilibrium with marine limestones.

Alternatively, the observed variation could be the result of changes in pH, temperature and/or $fO_2$ conditions, which control the isotopic composition of the fluids (Ohmoto, 1972). The decrease of crystallisation temperature might be likely cause of increase in the $\delta^{13}C$ values of younger carbonates (Malý and Dolníček, 2005). This will be further tested in the following section.

## 7.4 Oxygen and Hydrogen Isotope Geochemistry

### *7.4.1 Introduction and objectives*

The hydrogen and oxygen isotope signature of hydrothermal fluids provides a powerful tool to trace the origin and evolution of the water involved in the formation of hydrothermal ore deposits (Taylor, 1979). This is because most natural fluid reservoirs exhibit characteristic $\delta D$ and $\delta^{18}O$ signatures that allow fluids of different origin to be distinguished (i.e. magmatic, metamorphic, meteoric, ocean, and connate). Hydrogen and oxygen isotope studies of fluid inclusions and hydrous minerals have proved to be of particular importance in deciphering the origins and evolution of magmatic-hydrothermal deposits, such as porphyry copper and associated polymetallic and epithermal deposits (Taylor 1973; 1974; 1979; Sheppard and Taylor, 1974; White 1981; O'Neil and Silberman 1974; Field and Fifarek 1985; Giggenbach, 1992; Rye 1993; Vennemann et al.,1993; Hedenquist et al., 1998). Modern interpretations suggest the involvement of multiple sources in the origin of mineralising fluids in the shallow crustal environment. They range from predominantly magmatic in the deeper porphyry setting to mixed magmatic-meteoric in the shallow epithermal environment Arribas 1995; Kouzmanov et al., 2003; Sillitoe and Hedenquist 2003; Heinrich 2005).

The $\delta D‰$ and $\delta^{18}O‰$ composition of hydrothermal fluids can be measured directly from fluids preserved in fluid inclusions, thus reflecting the true composition of the fluid at the time of entrapment in the mineral. Alternatively, it can be measured by analysis of the D/H and O isotopic composition of hydrous minerals (Ohmoto, 1986). The isotopic composition of hydrous minerals is affected by a temperature-dependent isotopic fractionation (Sheppard and Gilg, 1996). Hence the temperature of mineral formation is essential to obtain meaningful constraints on the isotopic signature of the fluid from which the mineral is precipitated.

Hydrogen and oxygen isotope analyses were used in this study in an attempt to (i) determine the nature and origin of the fluid(s) responsible for Pb-Zn (Ag) ore formation at the Belo Brdo Pb-Zn (Ag) deposit (ii) to quantify the potential mixing processes between fluids of magmatic and meteoric origin, and (iii) compare the O and H isotopic signatures of the Belo Brdo mineralising fluids with the other deposits in the area. Furthermore, oxygen isotope data derived from different generations of quartz from the Belo Brdo deposit would provide data to constrain the sources of oxygen responsible for the mineralisation.

### 7.4.2 Sampling and Methods

No previous stable isotope data exist for the Belo Brdo Pb-Zn (Ag), the Karavansalija Cu-Au skarn and the Rudnitza Cu-Au porphyry deposits considered here. A total of 46 oxygen isotopic analyses were conducted on mineral separates (quartz and hydrous minerals) and 7 on whole- rock powders during this study. Mineral separates analysed include quartz (n=31), sericite (n=3), tourmaline (n=1), garnet (n=3), epidote (n=1), biotite (n=4), hornblende (n=2) and magnetite (n=1). A total of 20 hydrogen isotope analyses were conducted on hydrous mineral separates (n=8), water contained in fluid inclusions in quartz (n=5) and whole-rock samples (n=7). Most of the minerals related to ore mineralisation were collected from the Belo Brdo deposit (n= 23), as the main focus of this study, whilst seven samples derived from skarn and four from porphyry deposits for comparison.

Prior to analysis, minerals were collected by handpicking under a binocular microscope, followed by cleaning in doubly distilled water. Whole-rock powders were prepared by standard crushing and milling techniques to -100 meshes (150 microns size). All mineral separates and whole-rock samples were dried at 90°C for several hours prior to isotopic analysis.

Water was extracted from 1-2g of quartz samples (n=4), containing mostly primary fluid inclusions. However, one sample from the skarn deposit contained almost as many secondary inclusions, so the δD value from the inclusions in this sample (KU 37) should be considered with care. Water was also extracted from 40 to 100 mg of hydrous minerals (sericite, biotite, hornblende, epidote and tourmaline), as well as from 100- 130 mg of whole rock powders. Hydrogen isotope compositions were determined using standard techniques (Donnelly et al., 2001) and a chromium reduction furnace to convert released $H_2O$ to $H_2$. Prior to extraction of water, samples were placed into Pt crucibles in previously degassed reaction tubes and heated overnight at 110°C to remove adsorbed surface water. Reaction tubes were placed on the hydrogen-line where water, released by heating at 220°C (or 500°C in case of fluid inclusion water) was trapped using liquid nitrogen and then acetone/dry-ice, purified by the removal of non-condensable gases. The condensable gases passed through a Cr furnace at 800°C and the water was reduced to hydrogen gas, which was pumped into a collector bottle. The yield was measured manometrically in a glass U-tube containing mercury prior to collected gas being passed to a mass spectrometer for D/H analysis. Hydrogen isotope ratios were determined by a V.G. Micromass 602D Isotope Ratio Mass Spectrometer. Replicate analyses of water standards with $\delta D_{SMOW}$ at 0.0‰ (international standard V-SMOW), -189.7‰ (international standard GISP) and -93.7‰ (internal standard Lt-STD), gave a reproducibility of ±3‰.

Oxygen isotopic composition of samples was determined by laser fluorination techniques following the Macaulay et al. (2000) modification of Sharp (1990). For $^{18}O/^{16}O$ measurement, 1 mg of oxygen bearing sample was reacted with purified chlorine trifluoride reagent at high temperature using $CO_2$ laser as a heat source to release oxygen. The reagent and other reaction products were then trapped using liquid nitrogen. The purified oxygen sample was then pumped through an in-line mercury diffusion pump to a hot graphite rod where it was converted to $CO_2$. The yield of $CO_2$ was measured by capacitance manometer before being passed to the V.G. PRISM III Mass Spectrometer, which uses a working standard bottle gas calibrated against MAB reference material. The precision and accuracy of the measurements was ±0.2‰ (1σ), based on replicate analysis of the SES quartz internal standard, which gave values of 10.3 ± 0·22‰ (1σ) during the course of the analyses. Oxygen and hydrogen isotope compositions are expressed relative to Vienna Standard Mean Ocean Water (V-SMOW) in per mil, as defined by Craig (1961).

Calculations of the oxygen and hydrogen fluid compositions from measured mineral $\delta^{18}O$ and $\delta D$ data were carried out using the equation:

$$1000 \ln \alpha_{(\text{min-wt})} = A\,(10^6/T^2) + B \qquad \text{(Equation 7.2)}$$

where 1000 ln α represents the per mil fractionation between a mineral and water (Taylor, 1997); T is temperature in Kelvin; A and B are experimentally determined constants appropriate to the minerals and to water at different temperatures. The sources for constants used in this study are listed in Table 7.3.

Calculations of the isotope equilibrium temperatures for a difference in measured isotopic composition ($\Delta_{A\text{-}B}$) were carried out using the equations of Chacko et al. (1996) for quartz-sericite; Bottinga and Javoy (1975) for quartz-biotite and Zheng (1999) for quartz-dolomite.

**Table 7.3**: Source of data for O and H mineral-water fractionation factors

| Fractionation | Reference for O fractionation | Reference for H fractionation |
|---|---|---|
| quartz-water | Matsuhisa et al. (1979) | - |
| sericite-water | O'Neil and Taylor (1969) | Suzuoki and Epstein (1976) |
| epidote-water | Zheng (1993) | Chacko et al. (1999) |
| tourmaline-water | Zheng (1993) | Kotzer et al. (1993) |
| hornblende-water | Zheng (1993) | Not determined |
| biotite-water | Bottinga and Javoy (1973, 1975) | Suzuoki and Epstein (1976) |
| garnet-water | Zheng (1993) | Not determined |

### *7.4.3 Results: Oxygen and hydrogen isotope data*

The measured values for oxygen and hydrogen isotopic compositions of mineral separates and whole- rock powder samples, together with the calculated values of fluid compositions (where possible) are listed in Table 7.4. Oxygen isotope compositions of mineral separates and whole-rock powder samples are also presented in Figure 7.5.

#### *7.4.3.1 Belo Brdo*

A total of 19 oxygen isotope analyses were conducted on quartz separates from various stages of the Belo Brdo mineralisation. Additionally, 3 sericite/Cr-mica samples (two from pre-ore stage and

**Table 7.4**: Oxygen and hydrogen isotope data from mineral separates and whole- rock samples from the Kopaonik district (n=53 oxygen analyses; n=20 hydrogen analyses)

| Sample No | Description | Mineral/ WR | $\delta^{18}O$ V-SMOW (‰) | $\delta D$ V-SMOW (‰) | T °C | Fluid $\delta^{18}O$‰ | Fluid $\delta D$ ‰ |
|---|---|---|---|---|---|---|---|
| Belo Brdo Pb-Zn (Ag) deposit | | | | | | | |
| 1105/2A | Pre-ore Qtz-Ser-Py alteration of andesite | Ser | 8.8 | -85 | 420 (a) | 7.7 | -58 |
| 1105/2A | Pre-ore Qtz-Py veins in andesite | Qtz | 11.6 | | 420 (a) | 7.9 | |
| 1055/T2 | Pre-ore listwanite | Qtz | 13.1 | | 300(b) | 6.5 | |
| 1055/1A | Pre-ore; Qtz-carbonate breccia | Cr-mica | 11.1 | -89 | 420 (a) | 10.0 | -62 |
| 1055/1A | Pre-ore; Qtz-carbonate breccia | Qtz | 12.1 | | 420 (a) | 8.5 | |
| 1055/2B | Pre-ore; Qtz -tourmaline breccia | Tm | 10.5 | -62 | 450(b) | 10.0 | -38 |
| 1055/2B | Pre-ore; Qtz -tourmaline breccia | Qtz | 12.1 | | 420 (a) | 8.5 | |
| BB-stwork | Pre-ore quartz-pyrite stockwork; surface sample | Qtz | 11.9 | | | | |
| 1130/1B | Main-ore stage | Qtz | 13.7 | | 325 (c) | 7.7 | |
| 1155/1B | Main-ore stage | Qtz | 13.7 | | 325 (c) | 7.7 | |
| 180/2A | Main-ore stage | Qtz | 12.6 | | 325 (c) | 6.6 | |
| 180/3B | Main-ore stage | Cr-mica | 9.3 | -87 | 325 (c) | 6.5 | -44 |
| 180/3B | Main-ore stage | Qtz | 11.9 | | 325 (c) | 5.9 | |
| 1105/4 | Syn-to late-ore stage | Qtz | 13.6 | | 252 d) | 4.8 | |
| 1105/H | Syn-to late-ore breccia | Qtz | 13.3 | | 250 (e) | 4.4 | |
| 1099- | Late- ore stage breccia | FI -Qtz | 14.2 | -93 | 220 (e) | 3.7 | -93 |
| 180/1D | Late- ore stage breccia | FI -Qtz | 12.8 | -96 | 220 (e) | 2.3 | -96 |
| BB/mel/dyke | Late- ore; contact melange/dyke; surface sample | Qtz | 11.7 | | | | |
| 1105/4 | Post-ore veins crosscutting main ore | Qtz | 13.3 | | | | |
| 1105/6-post | Post-ore veins crosscutting listwanite | Qtz | 16.8 | | | | |
| BB/mel/vein | Post-ore veins in melange; surface sample | Qtz | 16.4 | | | | |
| 1235/5B-1 | Vein ore body | Qtz | 17.3 | | | | |
| 1235/7B | Vein ore body | Qtz | 16.4 | | | | |
| Karavansalija Cu-Au skarn | | | | | | | |
| KU07/24-3 | Late stage Qtz ; Sph+Gn (PDMC 07-24,330m | Qtz | 2.4 | | 341 (g) | -3.1 | |
| KU29 | Skarn; Apy, Py, Bi (PDMC 06-20, 286m) | Grn (Gr) | 6.5 | | 350-500 | 9-9.3 | |
| KU29 | Skarn; Apy, Py, Bi (PDMC 06-20, 286m) | Grn(And) | 6.5 | | 350-500 | 9-9.3 | |
| KU31-1 | Skarn; Apy, Py, Bi (PDMC 08-31, 433m) | Grn (Gr) | 7.3 | | 350-500 | 9.8-10.1 | |
| KU37 | Late qtz ; Po ore (PDMC 06-10, 114m) | FI -Qtz | 5.7 | -93 | 320 (e) | -0.5 | -93 |
| KU71/72 | Late qtz; Apy,Py;Ni-Co (PDMC 06-07, 284m) | Ep | 8.1 | -89 | 320 (e) | 7.9 | -51 |
| KU71/72 | Late qtz ; Apy, Py; Ni-Co (PDMC 06-07, 284m) | FI -Qtz | 12.6 | -93 | 320 (e) | 6.4 | -93 |
| Rudnitza Cu-Au porphyry | | | | | | | |
| KU81 | Qtz-Py stockwork ; Cpy (PDRC 06-07, 308m) | Qtz | 8.6 | | | | |
| KU97 | Late Qtz-Py/ sulphate (PDRC 06-04, 289m) | Qtz | 11.1 | | | | |
| R3-Q | Karadak Qtz from Pb-Zn vein; surface sample | FI-Qtz | 11.7 | -88 | 235 (e) | 2.0 | -88 |
| RU-Q-(mgnt) | Qtz-mgnt stockwork; surface sample | Qtz | 8.8 | | | | |
| Whole-rock samples and mineral separates from fresh and mildly altered igneous rocks | | | | | | | |
| KU95 | Andesite (PDRC 05-04, 277m); | Ho | 5.6 | | 510 (f) | 7.8 | |
| KU95 | Andesite (PDRC 05-04, 277m) | Qtz | 9.7 | | | 8.0 | |
| KU95 | Andesite (PDRC 05-04, 277m) | Bi | 4.5 | | | 7.0 | |
| KOP-1 | Dacite dyke; Ser, argillic | Bi | 6.0 | -149 | | | |
| KOP-1 | Dacite dyke Ser, argillic | Mt | 2.9 | | | | |
| KOP-1 | Dacite dyke Ser, argillic | Qtz | 6.5 | | | | |
| KU45 | Dacite dyke; Qtz-Ser; (PDMC 06-19, 22 m) | Ho | -2.7 | -104 | | | |
| KU45 | Dacite dyke; Qtz-Ser (PDMC 06-19, 22 m) | Bi | 8.5 | | | | |
| KU45 | Dacite dyke Qtz-Ser (PDMC 06-19, 22 m) | Qtz | 9.6 | | | | |
| R3-A | Fresh granodiorite | Bi | 4.4 | -79 | 620(f) | 6.9 | -49 |
| R3-A | Fresh granodiorite | Qtz | 8.4 | | | 7.0 | |
| NZ4-1 | Andesitic pyroclastic rock | Qtz | 11.0 | | | | |
| 1105/2A | Q-Ser alteration in andesite | WR | 11.2 | -82 | | | |
| 180/3C | Qtz-Tm vein crosscutting andesite | WR | 10.1 | -72 | | | |
| 1105/3B | Listwanite (Carbonate; Qtz, Cr-mica) | WR | 12.7 | -92 | | | |
| BB2 | Andesite -mildly chloritised | WR | 6.3 | -97 | | | |
| 1235/1 | Andesite-mildly silicified | WR | 8.9 | -88 | | | |
| K8 | Q-latite dyke chloritised | WR | 5.3 | -90 | | | |
| KU/08/32-1 | Q-latite mildly silicified | WR | 8.0 | -84 | | | |

*Temperatures*: (a) $\Delta_{Qtz-Musc}$; (b) Gersdorffite geothermometry; (c) average temperature from sphalerite and arsenopyrite geothermometry; (d) $\Delta_{Qtz-Dolomite}$; (e) average homogenisation temperatures;
(f) $\Delta_{Qtz-Biotite}$; note: garnet temperatures adopted from literature (Einaudi et al.,1981); (g) $\Delta_{Py-Galena}$
*Abbreviations*: Qtz=quartz; Ser=sericite; Tm=tourmaline; Py=pyrite; Apy=arsenopyrite; Bi=biotite; Ho=hornblende; Ep=epidote; Mt=magnetite; Grn=garnet (Gr=grossular; And=andradite); FI-Qtz= water from fluid inclusions in quartz; WR= whole- rock

one from main-ore stage) and 1 tourmaline sample (pre-ore stage) were analysed. A total of 6 hydrogen isotope compositions were determined from sericite/Cr-mica and tourmaline (n=4) and from two samples of water contained in fluid inclusions in quartz from late- ore stage of the Belo Brdo mineralisation.

Quartz samples from carbonate replacement type of mineralisation of Belo Brdo show a narrow range of $\delta^{18}O$ values from 11.6 to 14.2‰ (Figure 7.5A). A slight increase in $\delta^{18}O$ values are observed from the *pre-ore stage* (11.6 to 13.1‰) through the *main-ore stage* (11.9-13.7‰) to the *syn- to late-ore stage* (11.7 to 14.2‰). Quartz samples from quartz-carbonate veins crosscutting the replacement type mineralisation, as well as from the *vein-type ore body* exhibit the highest $\delta^{18}O$ values (16.4 to 17.3‰) (Figure 7.5A). The $\delta^{18}O$ values of the pre-ore stage and an

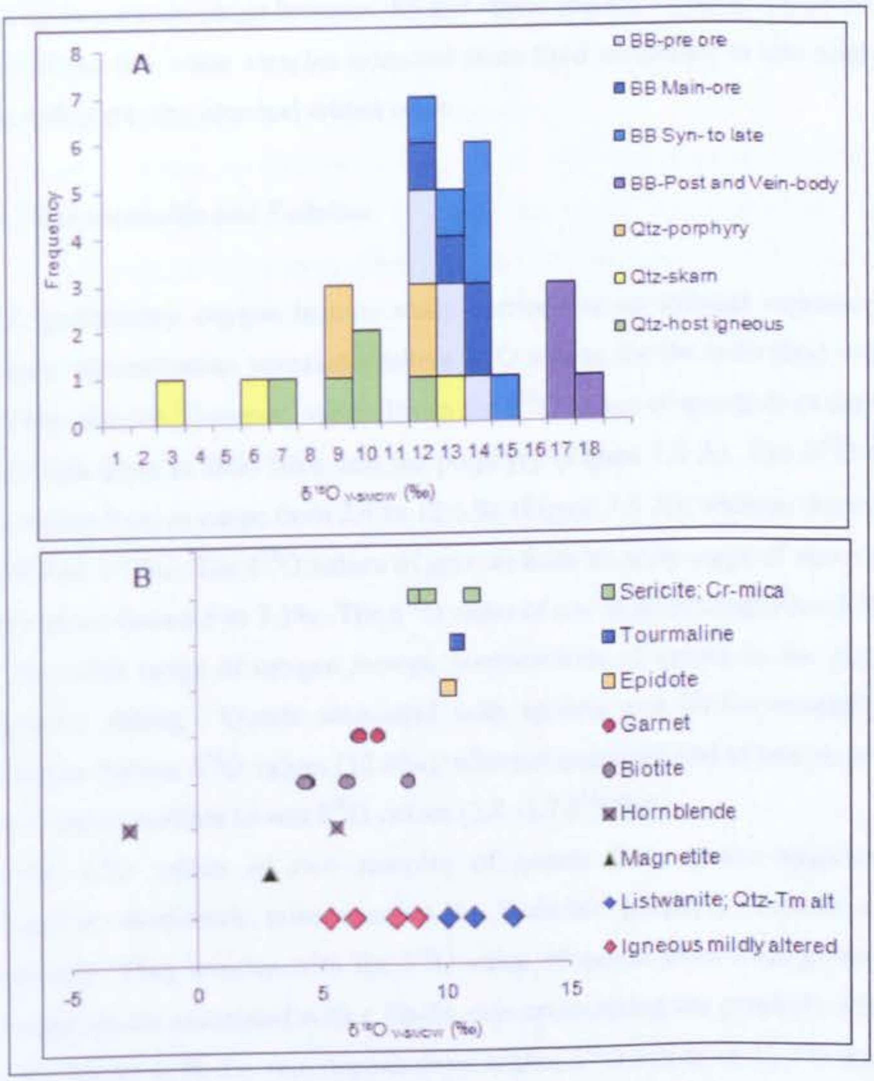

**Figure 7.5:** Stacked histogram showing distribution of $\delta^{18}O$ values of quartz from different settings (A) and $\delta^{18}O$ values of other mineral separates and whole- rocks (B) within the study area.

early main-ore stage overlap with hydrothermal quartz values obtained from a quartz-sulphide Karadak vein nearby the Rudnitza porphyry deposit (11.7‰) and with quartz associated with Ni-Co mineralisation in silicified breccias from the Karavansalija skarn deposit (12.6‰). They also overlap with $\delta^{18}O$ values obtained from quartz in andesitic pyroclastic rocks and with $\delta^{18}O$ values obtained from the whole- rock samples of hydrothermally altered andesites (quartz-sericite and quartz-tourmaline alteration).

One sample of tourmaline from quartz-tourmaline breccia yields 10.1‰, whereas sericite from an early sericitic alteration of host andesite has a $\delta^{18}O$ value of 8.8‰ and Cr-mica in quartz-carbonate breccia 11.1‰ (Figure 7.5B). The difference in $\delta^{18}O$ between the sericite in andesite and the Cr- mica from hydrothermal quartz-carbonate breccias could be caused by impurity of isotopically heavier quartz and carbonates as they form a fine intergrowth with the Cr-mica. One Cr-mica sample from the main-ore stage yields 9.3‰, which is close to the value of fine grained sericite from an early quartz-sericite alteration of andesites.

The hydrogen isotope composition of tourmaline is -62‰. The $\delta D$ values of sericite and Cr-micas lie in a narrow range between -85 and -89‰ and are identical within analytical error. The $\delta D$ values of the two water samples extracted from fluid inclusions in late stage quartz are -93 and -96‰, which are also identical within error.

### *7.4.3.2 Karavansalija and Rudnitza*

A preliminary oxygen isotope study carried out on mineral separates from the skarn and porphyry mineralisation revealed positive $\delta^{18}O$ values for the individual minerals, as seen in the Belo Brdo deposit. However, variability in the $\delta^{18}O$ values of quartz from the skarn deposit is much higher than those in Belo Brdo and the porphyry (Figure 7.5 A). The $\delta^{18}O$ values of quartz from skarn mineralisation range from 2.4 to 12.6 ‰ (Figure 7.5 A), whereas those in the porphyry range from 8.6 to 11.7‰. The $\delta^{18}O$ values of garnets from an early stage of skarn mineralisation show a narrow range from 6.5 to 7.3‰. The $\delta^{18}O$ value of one epidote sample has 8.1‰ (Figure 7.5B).

The wide range of oxygen isotope compositions of quartz in the skarn reflects a different paragenetic setting. Quartz associated with epidote and Ni-Co mineralisation from silicified breccia has highest $\delta^{18}O$ values (12.6‰), whereas quartz related to late stage sphalerite and galena mineralisation exhibits lowest $\delta^{18}O$ values (2.4 -5.7 $\delta^{18}O$‰).

The $\delta^{18}O$ values of two samples of quartz from quartz-magnetite and quartz-pyrite-chalcopyrite stockwork mineralisation in Rudnitza porphyry deposit are 8.8‰ and 8.6‰ respectively. They overlap with the $\delta^{18}O$ value of quartz from fresh granodiorite (Figure 7.5A). Late stage quartz associated with a Pb-Zn vein crosscutting the porphyry mineralisation as well as from the Karadak Pb-Zn vein deposit show higher $\delta^{18}O$ values of 11.1‰ and 11.7‰ respectively. The latter are close to those values of quartz from the early to main stage of Belo Brdo mineralisation.

Hydrogen isotopic compositions of water extracted from fluid inclusions in two samples of late stage quartz from skarn mineralisation gave the same values of -93‰, which are identical to those of the Belo Brdo deposit (Table 7.4). The $\delta D$ value of water from fluid inclusions in quartz from the Karadak Pb-Zn vein deposit is -88‰. The δD value of epidote also lies within the same range (-89‰).

### 7.4.3.3 The whole-rock data

Oxygen and hydrogen isotope ratios have been determined for seven whole- rock samples of variably altered wall rocks, ranging from mildly altered andesite and quartz-latite to pervasively sericitised andesite and listwanite, as well as for three mineral separates (biotite and hornblende). Additional oxygen isotope compositions were determined for nine mineral separates, including quartz, biotite, hornblende and magnetite from unaltered granodiorite and mildly altered volcanic rocks (Figure 7.5 B). Whole-rock samples were analysed with a view to determine their oxygen and hydrogen isotope compositions and the possible origins and thermal conditions of hydrothermal fluids associated with their formation.

The $\delta^{18}O$ values of whole-rock samples of unaltered to mildly altered volcanic rocks range from 6.3 to 8.9‰, with an average of 7.1±1.6‰, which is typical of calc-alkaline igneous rocks elsewhere (Taylor and Sheppard, 1986). The whole-rock samples from hydrothermally altered host rocks have different $\delta^{18}O$ values, depending on the type of alteration. Higher $\delta^{18}O$ values relative to unaltered igneous rocks are found in wall rocks affected by quartz-tourmaline (10.1‰), quartz-sericite (11.2 ‰) and listwanite alteration (12.7‰.), whereas chloritised quartz-latite is characterised by a lower $\delta^{18}O$ value (5.3‰) relative to unaltered volcanic rocks.

The oxygen isotope composition of individual minerals have a relatively wide range $\delta^{18}O$ values 4.4 to 8.5‰ for biotite and -2.7 to 5.6‰ for hornblende and relatively narrow range from 6.5 to 11.6‰ for quartz. Biotite from two relatively fresh rocks (granodiorite and andesite) yields oxygen isotope compositions of 4.4 and 4.5‰, which are in agreement with oxygen isotope values of biotite in granitic systems elsewhere (Taylor, 1974). Two biotite samples from dacite dykes affected by sericitic and argillic alteration yield much higher $\delta^{18}O$ values of 6‰ and 8.5‰. The latter need to be assessed with care, as it is unusually high. Such an increase in the $\delta^{18}O$ value of biotite compared to unaltered igneous biotite probably reflects its replacement by sericite or its hydrothermal origin. One sample of hornblende from altered dacite show depletion in $\delta^{18}O$ (-2.7‰) compared to hornblende from fresh granodiorite (5.6‰).

The δD values of whole-rock samples show a relatively narrow range of -72 to -97‰. The exceptions are biotite and hornblende from two samples of argillically altered dacites, exhibiting δD-depleted values (-145‰ and -109‰ respectively) compared to biotite from fresh granodiorite sample (-79‰) and to those reported elsewhere from porphyry copper deposits. This isotopic depletion suggests involvement of meteoric water (Sheppard and Taylor 1974; Taylor, 1992). However the data presented here are too few to draw any certain conclusions.

### *7.4.4 Isotopic compositions and source of the hydrothermal fluids related to mineralisation*

The oxygen and hydrogen isotope composition of the fluid in equilibrium with the fresh granodiorite, as well as fluids responsible for the mineralisation during early and late stages of the carbonate-replacement-type of the Belo Brdo deposit have been calculated to constrain the most likely fluid sources (Figure 7.6). Additionally, O and H isotope composition of fluids from four samples collected from skarn and porphyry-vein deposits have been calculated for comparison.

Calculated oxygen isotopic compositions of water in equilibrium with quartz and biotite from granodiorite at 610°C is consistent with magmatic water ($\delta^{18}O$=6.9-7.0‰; $\delta D$=-49‰ for biotite). The oxygen isotope composition of water in equilibrium with quartz, biotite and hornblende from andesite at 510°C is also in agreement with a magmatic origin ($\delta^{18}O$=7-8‰).

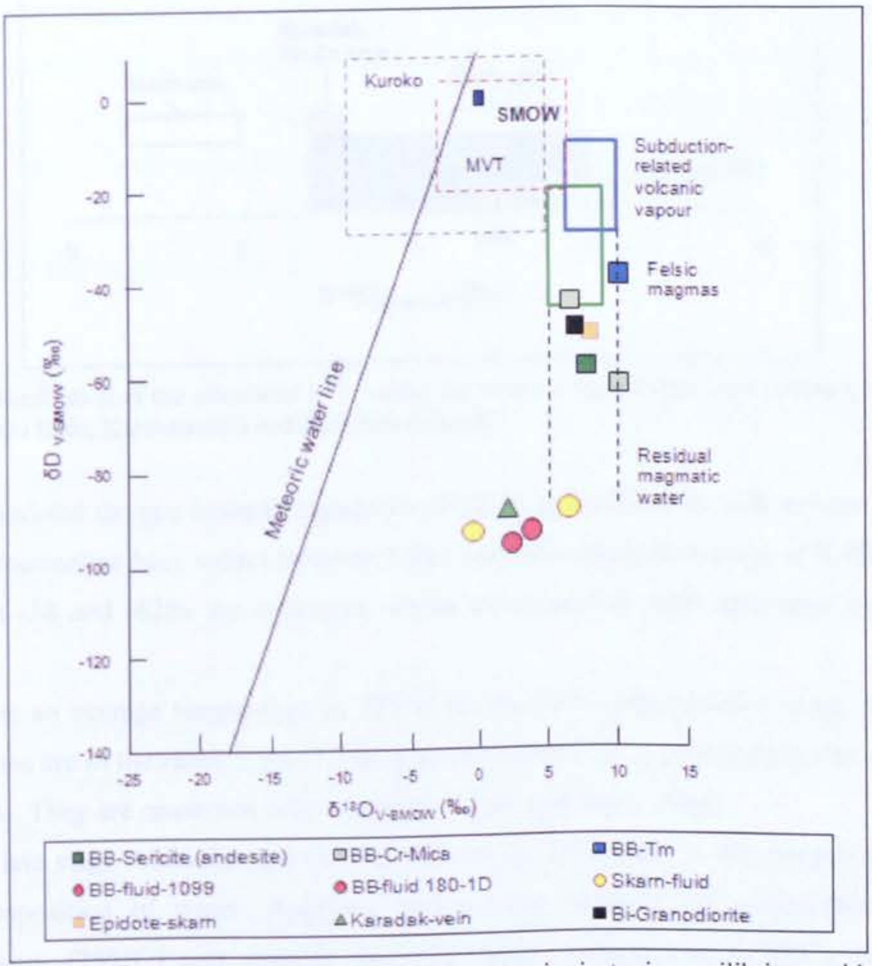

**Figure 7.6**: Plot of $\delta^{18}O$ versus $\delta D$ for calculated water in isotopic equilibrium with biotite (from granodiorite) and alteration minerals (tourmaline, sericite and epidote), as well as in fluid inclusions. The composition of water dissolved in felsic melts is based on Taylor (1992) volcanic vapour from Giggenbach (1992) and Hedenquist and Lowenstern (1994). Fields for Kuroko-type and MVT deposits (Ohmoto, 1986) are also plotted for comparison.

In Belo Brdo, the fractionation between co-existing quartz and sericite during an early stage of quartz-sericite alteration of andesite is 2.8‰, and corresponds to an equilibrium temperature of 420°C using the fractionation factors of Chacko et al. (1996) for quartz and muscovite. A fluid inclusion study was not carried out on minerals from the pre-ore stage of the Belo Brdo mineralisation, as no suitable quartz sample could be identified, whilst the high density of carbonate fracturing in listwanite lead to a lack of preservation of inclusions. Additionally, oxygen isotope fractionations among minerals in an early quartz-tourmaline-carbonate breccias were very low (or even negative between quartz-dolomite pairs), indicating that no isotope equilibrium was achieved between the minerals. Therefore the use of quartz-dolomite and quartz-tourmaline pairs for geothermometry of early stages of the Belo Brdo mineralisation was not appropriate, resulting in unreasonably high temperatures. Instead, independent temperature estimates were obtained using gersdorffite geothermometry (between 300°C and 450°C), as well as the quartz-sericite ($\Delta_{Qtz\text{-}musc}$) geothermometry.

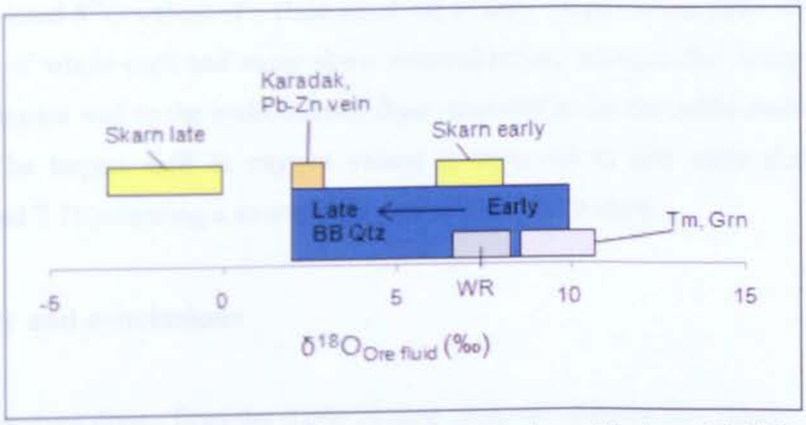

**Figure 7.7:** Distribution of the calculated $\delta^{18}O$ values for water in equilibrium with different ore and gangue minerals in Belo Brdo, Karavansalija and Rudnitza deposits.

The calculated oxygen isotopic signatures of fluids in equilibrium with pre-ore stage quartz, sericite and tourmaline have values between 5.9‰ and 10‰ (with an average of 8.4‰) for oxygen and between -38 and -62‰ for hydrogen, which are consistent with magmatic waters (Taylor, 1992).

Applying an average temperature of 325°C for the main-mineralisation stage, the calculated $\delta^{18}O_{water}$ values are in the range 5.9 to 7.7‰, and calculated $\delta^{18}D_{water}$ value from one sample of Cr-mica is -44‰. They are consistent with magmatic waters (Ohmoto, 1986).

Syn-to late stage mineralisation is characterised by a decrease in the oxygen and hydrogen isotopic composition of water. Applying temperatures obtained by quartz-dolomite isotope geothermometry (252°C) and average homogenisation temperatures (250°C), the calculated $\delta^{18}O_{water}$ values range from 4.8 to 2.3‰. The δD values of -93‰ and -96‰ measured in fluid-inclusion waters from two samples are depleted when compared to fluids involved in the early and main ore stages of carbonate-replacement mineralisation of Belo Brdo (Figure 7.6). The calculated $\delta^{18}O_{water}$ values from the same samples are also depleted (2.3 and 3.7‰), when compared to earlier mineral stages, indicating involvement of meteoric waters. Generally, the calculated oxygen isotope temperatures from Belo Brdo show a general decrease from an early, quartz-sericite-pyrite stage assemblage (420°C) to the late, quartz-carbonate assemblage (250°C), which is also marked by decrease of $\delta^{18}O$ values of hydrothermal fluid (Figure 7.7).

Oxygen isotope temperatures could not be calculated from an early skarn mineral assemblage, as no suitable mineral pairs could be collected. Instead, garnet crystallisation temperatures between 350 and 550°C were adopted from literature (Einaudi et al., 1981). For this temperature range, calculated $\delta^{18}O$ values of $H_2O$ in equilibrium with garnet are in range from 9.0 to 10.1‰.The oxygen isotope data are consistent with a predominantly magmatic source of the early skarn-forming fluids. In contrast, calculated $\delta^{18}O$ values of fluid in equilibrium with the late-stage quartz cogenetic with sphalerite and galena, have depleted values (-0.5 to -3.8‰) (Figure 7.7), suggesting the involvement of low $\delta^{18}O$ meteoric water in the system at this stage.

The calculated $\delta^{18}O$ values of a fluid involved in early stages of the Belo Brdo mineralisation overlap those of whole-rock and early skarn mineralisation, whereas the isotope composition of later fluids compare well to the hydrothermal fluid responsible for the epithermal-type Karadak Pb-Zn deposit. The largest shift in oxygen values is observed in late stage skarn mineralisation (Figures 7.6 and 7.7) indicating a strong influence of meteoric waters.

## 7.5 Summary and conclusions

The conclusions drawn from the stable isotope study are summarised below:

- The $\delta^{34}S$ values of sulphides (pyrite, sphalerite and galena) from four different deposit types in the Kopaonik region cover a narrow range between 1.8 and 6.9‰ V-CDT. The data suggests an uniform sulphur isotope composition of sulphides (average ~4.4‰) and coexisting $H_2S$ in fluids (average 4.7‰ for Belo Brdo and 3.8‰ for the Karavansalija skarn). The data compares well with the Pb-Zn skarn/replacement type of Trepca and polymetallic vein deposit of Crnac in the Western Vardar Ophiolite Zone and is consistent with a magmatic sulphur source for all deposits.
- The absence of isotopically heavy $\delta^{34}S$, which is a characteristic of evaporitic sequences or seawater found in many MVT deposits, rules out evaporites as the potential source for sulphur in the studied deposits.
- The carbon and oxygen isotopic compositions of several carbonate generations from the Belo Brdo deposit show general tendency toward decreasing $\delta^{18}O$ and increasing $\delta^{13}C$ from pre-ore to post-ore stage carbonates of Belo Brdo. Gangue carbonates are depleted in both $\delta^{18}O$ (6.6 to 18 ‰) and $\delta^{13}C$ (2 to -4.4 ‰) compared with Cretaceous limestones, suggesting the influx of an external magmatic fluid.
- Calculated isotope compositions of $\delta^{18}O$ (5.9 to 10 ‰ SMOW) and $\delta D$ (- 38 to - 62 ‰ SMOW) for waters in equilibrium with sericite and tourmaline of pre-mineralisation stage are consistent with the ore fluids being derived from the magmatic source, as are the calculated $\delta^{18}O_{water}$ values of the main-ore stage (5.9 to 7.7‰).

- Isotopic compositions of the fluid associated with the syn- to late- stage of the Belo Brdo mineralisation have isotopic characteristics that define a trend with an apparent decrease of $\delta\ ^{18}O$ and $\delta$ D calculated values ($\delta\ ^{18}O$ = 4.8 to 2.3 ‰ and $\delta$ D = -93 to -96 ‰), indicating an involvement of more dilute, low-temperature meteoric hydrothermal fluids.
- When different stages of the evolution of the Belo Brdo deposit are compared, the calculated oxygen isotope temperatures show a general decrease from the early stage assemblage (420°C) to the late quartz-carbonate assemblage (250°C), which is also marked by a decrease of $\delta^{18}O$ values of hydrothermal fluid. This means that cooling by mixing of hotter, magmatic fluid with cold meteoric water is a predominant process responsible for sulphide precipitation.

# CHAPTER 8:

# STRONTIUM AND LEAD RADIOGENIC ISOTOPE GEOCHEMISTRY

## 8.1 Strontium Isotope Geochemistry

### *8.1.1 Introduction and objectives*

Strontium isotopes are an important tool in the study of mineral deposits and are used in a wide range of applications, including characterisation of the original isotopic composition of the fluid, tracing the chemical and isotopic evolution of the mineralising fluids, defining possible sources of Sr and in the geochronological dating using the Rb-Sr system. Natural strontium varies in its isotope composition due to the radioactive decay of $^{87}$Rb to $^{87}$Sr with a half-life of 48.8 x $10^6$ years (Faure, 1986; Faure and Mensing, 2005). The natural variation in the ratio between radiogenic $^{87}$Sr and stable $^{86}$Sr (used as a reference isotope whose abundance remains unchanged with time) is derived from the radioactive decay of $^{87}$Rb to $^{87}$Sr. As a result of differing Rb/Sr ratios over time, the $^{87}$Sr/$^{86}$Sr ratio in rocks will depend on their age and composition, while in carbonate minerals the $^{87}$Sr/$^{86}$Sr ratio will reflect the isotopic composition of water from which they precipitated (Faure and Mensing, 2005). Sr closely mimics the behaviour of Ca, for example substituting for $Ca^{2+}$ in the lattices of minerals. Because of this, Sr isotope ratios are useful to trace Ca sources. Carbonates have very low Rb/Sr ratios and their $^{87}$Sr/$^{86}$Sr ratios do not change significantly with time as a result of radioactive decay (Faure, 1998). Therefore the $^{87}$Sr/$^{86}$Sr ratio will remain approximately constant over geological time, as long as they are not altered by subsequent metasomatic processes. For this reason, $^{87}$Sr/$^{86}$Sr ratios of carbonate minerals in this study have been used to infer the Sr-isotope signatures of the hydrothermal fluids from which the carbonates precipitated. Furthermore, the $^{87}$Sr/$^{86}$Sr ratios of different country rocks have been determined in order to identify the nature of the sources contributing Sr to the ore deposits.

Sr isotopes in the Belo Brdo and nearby base metal deposits have never previously been investigated. This study presents the first strontium isotope compositions of hydrothermal carbonates from three deposits in the Kopaonik metallogenic district including Belo Brdo, Rudnitza and Karavansalija.

### *8.1.2 Sampling and analytical techniques*

Sr isotopic ratios have been determined on ten whole-rock samples selected from various lithologies and on nine carbonate minerals (six from Belo Brdo, two from Rudnitza and one from Karavansalija). The $^{87}$Sr/$^{86}$Sr ratios were measured at the NERC Isotope Geosciences Laboratory

(NIGL), Keyworth, using a Thermo-Finnigan Triton thermal ionisation mass spectrometer (TIMS) following methods outlined in Royse et al. (1998) which are summarised below.

Whole-rock samples were prepared by standard crushing and milling to a fine powder in a tungsten carbide mill. The agate mill, which was used in preparation of samples for trace element and stable isotope analysis, was not used because of possible contamination of Sr and Pb. Splits of carbonate powders previously prepared for stable isotope analysis were used for Sr isotopes. For whole-rock samples, approximately 0.15-0.2 g of powder was leached with acetic acid to minimise the effects of secondary alteration. The dissolution was carried out in a fume cupboard on a hot plate in Teflon beakers using HF acid in combination with 16M $HNO_3$. Carbonates were dissolved in acetic acid. Strontium was separated from other components of the sample by the standard ion-exchange techniques using conventional Dowex AG 50W-X8 ion-exchange resin. Procedural blank and modern seawater samples were also prepared and measured along with each batch of chemical separations. The purified Sr was loaded onto a single Re filament using TaF activator after the method of Birck (1986) and analysed using TIMS. SRM987 was the primary standard used, and the $^{87}Sr/^{86}Sr$ ratios were normalised during run time to $^{86}Sr/^{88}Sr = 0.1194$. Sample data are reported relative to accepted values of SRM987 of 0.710235. Modern seawater ($^{87}Sr/^{86}Sr= 0.709168$) averaged 0.709172± 0.000008 (2SEM) at the time of analysis.

### *8.1.3 Results of strontium isotope analysis*

Strontium isotope analyses of various lithologies from the study area and carbonate minerals are given in Table 8.1 and presented in Figure 8.1. The measured $^{87}Sr/^{86}Sr$ ratios for whole-rock samples range from 0.70611 to 0.70943. Jurassic serpentinite exhibits the highest $^{87}Sr/^{86}Sr$ ratio of 0.70943 and the other values generally decrease with decreasing age. Listwanites have $^{87}Sr/^{86}Sr$ ratios between 0.708633 and 0.708695. Late Cretaceous limestone and a fragment of unmineralised carbonate from pre-ore breccia have less radiogenic ratios between 0.70748 and 0.70776, which fall within the range of Late Cretaceous seawater (Koepnick et al. 1985). Data for Tertiary igneous rocks plot within an interval of 0.70611 and 0.70784. The Belo Brdo andesite, which represents the first volcanic phase, has a less radiogenic composition and differs from dacite and quartz-latite of the second volcanic phase (Figure 8.1). The latter have $^{87}Sr/^{86}Sr$ ratios between 0.70769 and 0.70784. The Kopaonik and Zeljin granodiorites have compositions intermediate between the two volcanic phases. The $^{87}Sr/^{86}Sr$ ratios of quartz-latite overlap the Sr isotope ratios of the Upper Cretaceous carbonates, which might indicate a crustal component in their source. The $^{87}Sr/^{86}Sr$ ratios of rocks of the first volcanic phase match isotope ratios of calk-alkaline rocks (0.70632 - 0.70693) from the Lece-Chalkidiki metallogenic zone located east of the study area in the Eastern Vardar Ophiolite Zone (Serafimovski, 2000). The Sr isotope ratios of the rocks from the second volcanic phase compare well to the $^{87}Sr/^{86}Sr$ ratios of volcanic rocks from the Rogozna Mountain (in Serafimovski et al., 2006; precise location not known), which range from 0.7074 to 0.7085. Their Sr isotope ratios are also similar to the Tertiary high-K calc–alkaline basalts and shoshonites

**Table 8.1**: Sr isotopic compositions of whole-rock and carbonate samples from the study area.

| Sample | Rock type | $^{87}Sr/^{86}Sr$ | Error (±SEM) |
|---|---|---|---|
| Whole-rock | | | |
| LIM-1 | Light grey Cretaceous limestone | 0.707483 | 0.000006 |
| 1055/1B(1) | Dark grey carbonate breccia fragment | 0.707756 | 0.000010 |
| 1055_1C | Listwanite Ni-Co; Cr mica | 0.708695 | 0.000012 |
| 1155_2C | Silicified carbonate breccia | 0.708633 | 0.000008 |
| SRP-1 | Dark green serpentinite | 0.709430 | 0.000008 |
| KOP-1 | Dacite | 0.707839 | 0.000006 |
| BB-2 | Andesite | 0.706106 | 0.000006 |
| KG-1 | Qtz-latite | 0.707687 | 0.000006 |
| GND-Z | Granodiorite | 0.706754 | 0.000008 |
| R3-A | Granodiorite | 0.707131 | 0.000006 |
| Carbonates | | | |
| 1055/1B | Pre- ore stockwork (Ni-Co; Py; Cr-mica) | 0.708422 | 0.000008 |
| 1130/1B | Syn-to late dolomite (sulphide ore; Cr-mica) | 0.707966 | 0.000010 |
| 1105/h | Syn-to late ore breccia cement | 0.708085 | 0.000008 |
| 1055_4D | Post-ore cavity filling dolomite | 0.707763 | 0.000008 |
| 1105/6(1) | Post-ore vein in crosscutting serpentinites | 0.708208 | 0.000008 |
| 1235(3) | Dolomite in andesite-hosted vein ore body | 0.707851 | 0.000008 |
| KU19 | Late stage calcite; skarn Cu-Au | 0.708457 | 0.000008 |
| KU90 | Syn-ore calcite; Pb-Zn in porphyry | 0.707022 | 0.000006 |
| KU103 | Syn-ore calcite; Pb-Zn in porphyry | 0.707163 | 0.000008 |

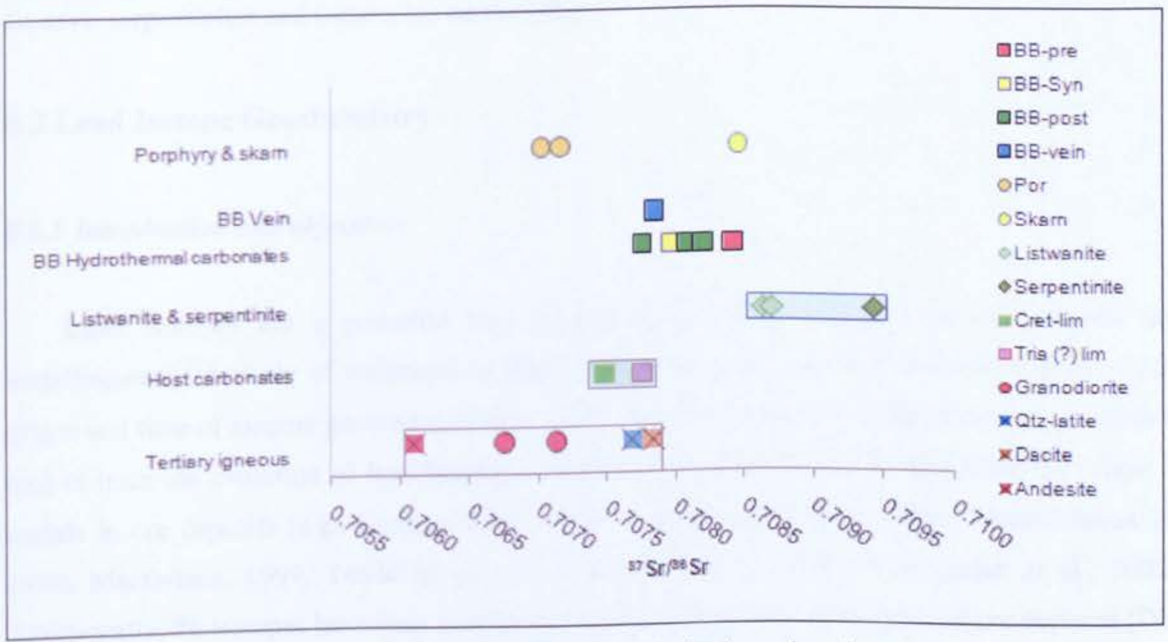

**Figure 8.1**: Strontium isotope data for host rocks and hydrothermal carbonates from the study area. Abbreviations: BB=Belo Brdo; pre=pre-ore stage; syn=syngenetic/main-ore stage; post=post-ore stage; Por=porphyry; Cret=Cretaceous; Tria=Triassic.

of Serbia, defined by Cvetković et al. (2004). The Sr isotope signatures of the granodiorite are similar to those of Serbian I-type granites (Karamata et al., 1990). The $^{87}Sr/^{86}Sr$ ratios of hydrothermal carbonates from the Belo Brdo deposit have a narrow range of values between 0.70776 and 0.70842 and plot between the isotopic compositions of the Tertiary magmatic rocks and the Upper Cretaceous limestones on one side and the more radiogenic serpentinite and listwanite on the other. Although the Sr isotope ratios span a narrow range, an important feature can be distinguished within the hydrothermal carbonates. Dolomite from the pre-ore stage quartz-carbonate stockwork, which developed within the brecciated zone in hydrothermally altered ultramafic rocks, is the most radiogenic (0.70842). A similar ratio is observed in dolomites of the post-ore vein that crosscut ultramafic rocks (0.70821), as well as in calcite from the skarn deposit. Such Sr isotopic ratios of carbonates indicate significant Sr input from the ultramafic rocks.

The post-ore carbonates that fill small cavities are characterised by lower $^{87}Sr/^{86}Sr$ ratios. The Sr isotope compositions of these carbonates overlap those of the Upper Cretaceous limestones, suggesting a predominant contribution of Sr from sedimentary rocks (Figure 8.1).

Two calcite samples from the Rudnitza porphyry deposit are less radiogenic compared to the rest and have $^{87}Sr/^{86}Sr$ ratios between 0.70702 and 0.70716. They overlap with the Sr isotopic composition of the granodiorite, suggesting a magmatic origin for the strontium in the hydrothermal fluid.

The data presented above show that the measured strontium isotopic compositions of hydrothermal carbonates of the Belo Brdo deposit lie within a narrow range and indicate Sr contribution from the Tertiary magmatic rocks and Cretaceous sediments on one end and the Jurassic serpentinites and listwanites on the other.

## 8.2 Lead Isotope Geochemistry

### 8.2.1 *Introduction and objectives*

Lead isotopes are a powerful tool in helping to solve problems of petrogenesis and metallogenesis. A study of variations in lead isotope ratios may provide answers to questions of origin and time of magma generation (Faure, 2001). Furthermore, lead isotope ratios are a sensitive tool to trace the evolution of lead-bearing minerals in ore deposits and to determine the origin of metals in ore deposits (e.g., Cannon et al., 1961; Vaasjoki and Gulson, 1986; Macfarlane et al., 1990; Macfarlane, 1999; Tosdal et al., 1999; Marcoux et al., 2002; Von Quadt et al., 2002). Additionally, Pb isotopes have been used as an exploration tool for some types of ore deposits (Doe and Stacey 1974; Gulson, 1986).

Variations in Pb isotopic compositions result from the radioactive decay of isotopes of uranium ($^{238}U \rightarrow {}^{206}Pb$ and $^{235}U \rightarrow {}^{207}Pb$) and thorium ($^{232}Th \rightarrow {}^{208}Pb$). Lead isotopic data are typically shown as plots of $^{207}Pb/^{204}Pb$ vs. $^{206}Pb/^{204}Pb$ (uranogenic) and $^{208}Pb/^{204}Pb$ vs. $^{206}Pb/^{204}Pb$

(thorogenic). Of the four significant naturally occurring Pb isotopes, only $^{204}$Pb is stable. The abundance of this isotope has remained constant throughout geological time and is therefore used as the reference isotope. Lead is the only ore metal other than osmium which shows large natural isotopic variability and has similar geochemical behaviour to other ore metals, such as zinc, copper, and silver. Therefore, comparison of ore lead isotope ratios with those of host rocks will suggest possible ore metal sources. The common lead isotope signatures of ore lead are directly related to the isotopic composition of lead in the source rock and commonly remain undisturbed after deposition (Dickin, 1995). Isotopic composition of Pb in source rocks evolves over time due to the radioactive decay of U and Th. However, the extraction of Pb from the source rock and its incorporation into an ore mineral, such as galena, terminates Pb evolution due to the absence of uranium and thorium in the galena crystal structure. The isotope composition preserved by Pb in an ore mineral can therefore constrain the isotopic composition of the source rocks at the time of Pb extraction or ore deposition. The isotope data can then be interpreted using, for example, the plumbotectonics model of Zartman and Doe (1981), which describes the composition and evolution of the mantle, and the lower and upper crust isotope reservoirs.

Pb isotope studies have been carried out in order to investigate the origin of ore metals in the Belo Brdo deposit and a possible genetic relationship with the nearby porphyry and skarn deposits. New data is compared with previously published Pb isotopic compositions for the Belo Brdo mineralisation (Jankovic, 1978), with an aim of providing a clearer view of mineralisation and magmatism in the study area.

### *8.2.2 Previous work*

Lead isotope compositions of Pb-Zn deposits in the Kopaonik metallogenic district were studied for the first time by Jankovic (1978) as part of a regional investigation of several deposits within the Serbo-Macedonian metallogenic province, including the Trepca skarn/hydrothermal deposit, the Crnac vein-type deposit (1.5 km south-east from Karavansalija skarn), the Belo Brdo carbonate-replacement and several other Pb-Zn deposits in Serbia and Macedonia. The data showed significant variations in lead isotope ratios, particularly at Trepca and Belo Brdo, where variations in $^{208}$Pb/$^{204}$Pb ratios were much greater than $^{206}$Pb/$^{204}$Pb ratios (Figure 8.2). This led Jankovic (1978) to suggest that the source of ore lead was nonhomogeneous. Nonetheless, the same author concludes that at Trepca, magmatic complexes and ore lead originated from the same source, based on similar lead isotope characteristics of magmatic rocks and galena. Furthermore Jankovic (1978) suggested that the timing of Pb-Zn ore deposition is close to that of granodioritic magma crystallisation.

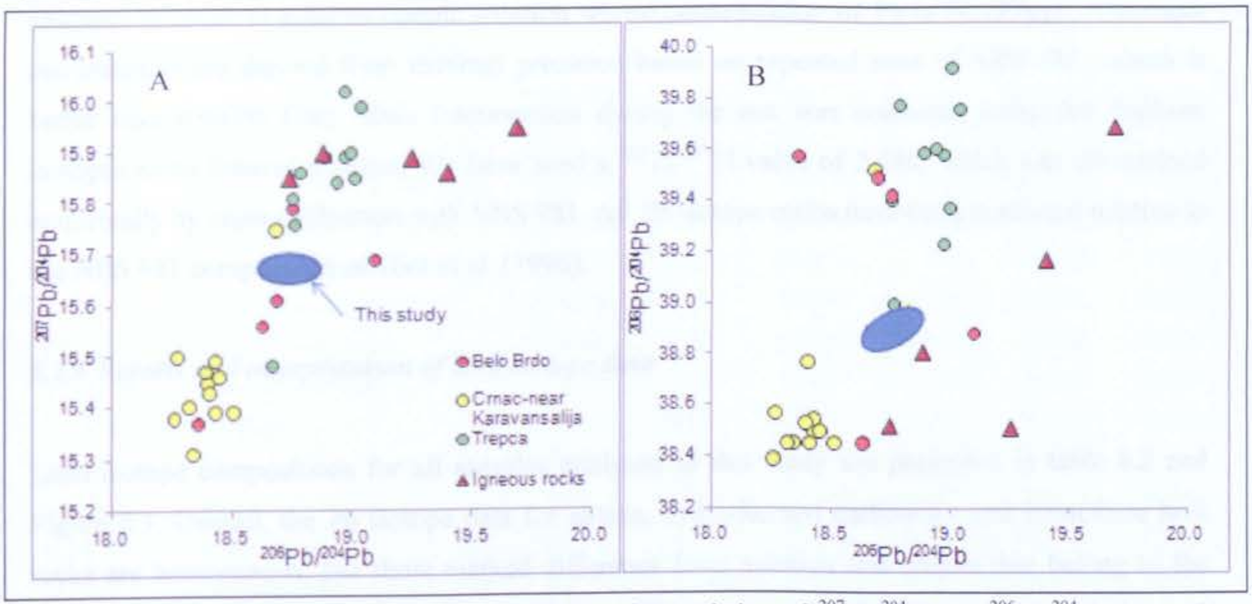

**Figure 8.2:** Data published by Jankovic (1978) showing variation of $^{207}Pb/^{204}Pb$ vs. $^{206}Pb/^{204}Pb$ (A) and $^{208}Pb/^{204}Pb$ vs. $^{206}Pb/^{204}Pb$ (B) for galena from the Belo Brdo, Crnac and Trepca deposits and igneous rocks from Trepca. Also included are data from this study (blue) for comparison.

### *8.2.3 Sampling and analytical techniques*

Pb isotope studies were carried out on 11 galena samples from various deposits in the study area, including the carbonate-replacement and vein-type ore bodies of the Belo Brdo deposit, the Rudnitza porphyry, the Karavansalija skarn, the Kizevak stockwork and Karadak vein-type deposits. Additionally, 12 whole-rock samples of various lithologies and 8 samples of hydrothermal carbonates were analysed. Names and brief descriptions of the samples are presented in Table 8.2.

The lead isotope ratios were determined by high precision plasma ionisation multi-collector mass spectrometry using a VG P54 at the NERC Isotope Geosciences Laboratory (NIGL), Keyworth, following procedures outlined in Kempton and McGill (2002), which are summarised below.

Monomineralic galena samples were separated by hand picking, as well as drilling using a dental drill and stored in polyethylene vials before analysis. Whole-rock samples were prepared at Kingston University by standard methods of trimming with a saw, crushing and milling in a tungsten carbide mill. For the Pb isotope analyses, 0.5-2mg of galena was dissolved first in 16M $HNO_3$ and then in HCl, without need for prior leaching, whereas whole-rock samples underwent acetic acid leaching prior to dissolution to remove possible contamination by secondary alteration processes. Whole-rock samples were digested using HF acid in combination with 16M $HNO_3$. Lead was separated from other components by cation exchange methods involving HCl and HBr and using Dowex 1 x 8, 200-400 mesh resin. A blank, spiked with $^{208}Pb$, and seawater were also prepared and measured along with each batch. Pb separates collected during ion exchange chemistry were dissolved in a dilute solution of nitric acid and doped with thallium prior to analyses in order to achieve sample solution whose concentration of Pb is 50-100ppb. Minimum uncertainties are derived from external precision based on repeated runs of NBS 981, which is better than 0.007% (1σ). Mass fractionation during the run was corrected using the thallium isotopes as an internal monitor. We have used a $^{205}Tl/^{203}Tl$ value of 2.388, which was determined empirically by cross calibration with NBS 981. All Pb isotope ratios have been corrected relative to the NBS 981 composition of Todt et al. (1996).

### 8.2.4 Results and interpretation of lead isotope data

Lead isotope compositions for all samples analysed in this study are presented in table 8.2 and Figure 8.3. Overall, the Pb isotope data for galena, hydrothermal carbonates and immediate host rocks are homogenous, but show marked difference from gabbros and basalts that belong to the Jurassic ophiolite suite (Table 8.2; Figure 8.3A and B).

The Pb isotopic ratios of galena and Tertiary igneous rocks show narrow range of values compared to the previously published data of Jankovic (1978). Lead isotopic composition of all analysed galena samples cluster with, $^{206}Pb/^{204}Pb$ ratios of 18.678 to 18.760 (mean=18.712 ±0.02), $^{207}Pb/^{204}Pb$ ratios of 15.669 to 15.680 (mean=15.675 ±0.002) and $^{208}Pb/^{204}Pb$ ratios of 38.867 to 38.915 (mean=38.888 ±0.008) (Table 8.3, Figure 8.3 C and D). Although very homogeneous in general, they exhibit distinguishable variations in their Pb isotopic compositions, with the Belo Brdo carbonate-replacement ore body having the most uniform Pb isotopic ratios. Lead isotopic compositions of five samples of galena from different mineralisation stages are nearly identical ($^{206}Pb/^{204}Pb$= 18.678 to 18.686, $^{207Pb}/^{204}Pb$= 15.674 to 15.677, and $^{208}Pb/^{204}Pb$ = 38.873 to 38.888), suggesting that fluids were well homogenised throughout the deposition of the carbonate-replacement mineralisation. Their Pb isotopic ratios are close to those of host limestones and serpentinites (Figure 8.3 C and D).

Six galena samples collected from various vein-; stockwork- and skarn-type deposits show slightly higher variations in their Pb isotopic compositions compared to Belo Brdo. Their $^{206}Pb/^{204}Pb$ ratios range between 18.710 and 18.760, $^{207Pb}/^{204}Pb$ between 15.669 and 15.680 and $^{208}Pb/^{204}Pb$ between 38.867 and 38.915. They are close to, and partially overlap those of Tertiary igneous rocks, whose $^{206}Pb/^{204}Pb$ ratios range between 18.759 and 18.821, $^{207Pb}/^{204}Pb$ between 15.664 and 15.678 and $^{208}Pb/^{204}Pb$ between 38.871 and 38.972.

**Table 8.2:** The Pb isotope composition of galena, host-rocks and hydrothermal carbonates from various deposits in the Kopaonik district.

| Sample | Description | $^{206}$Pb/$^{204}$Pb | % 1σ | $^{207}$Pb/$^{204}$Pb | % 1σ | $^{208}$Pb/$^{204}$Pb | % 1σ |
|---|---|---|---|---|---|---|---|
| Galena | | | | | | | |
| 1055/8 | Pre-syn; BB-carb. ore body | 18.679 | 0.005 | 15.674 | 0.006 | 38.873 | 0.008 |
| 1055/4D | Late; BB-carb. ore body | 18.680 | 0.005 | 15.676 | 0.006 | 38.882 | 0.008 |
| 1130/1B | Syn; BB-carb. ore body | 18.678 | 0.005 | 15.674 | 0.007 | 38.873 | 0.009 |
| 1155/1B | Syn; BB-carb. ore body | 18.686 | 0.005 | 15.677 | 0.006 | 38.888 | 0.008 |
| 1235/5A | BB-vein ore body | 18.682 | 0.005 | 15.676 | 0.006 | 38.882 | 0.008 |
| 1235/7B | BB-vein ore body | 18.726 | 0.005 | 15.671 | 0.006 | 38.867 | 0.009 |
| KU103 | Porphyry | 18.758 | 0.005 | 15.673 | 0.006 | 38.895 | 0.008 |
| 07/24-3 | Skarn | 18.710 | 0.005 | 15.680 | 0.006 | 38.905 | 0.008 |
| KU118 | Skarn | 18.729 | 0.006 | 15.678 | 0.008 | 38.915 | 0.009 |
| KZ4 | Kizevak-vein | 18.741 | 0.006 | 15.674 | 0.007 | 38.893 | 0.009 |
| R3/A1 | Karadak-vein | 18.760 | 0.006 | 15.669 | 0.007 | 38.891 | 0.009 |
| Host- rocks | | | | | | | |
| NZ1 | Gabbro | 18.176 | 0.005 | 15.606 | 0.006 | 38.190 | 0.007 |
| NZ2 | Basalt | 18.550 | 0.005 | 15.635 | 0.006 | 38.648 | 0.007 |
| SRP-1 | Serpentinite | 18.700 | 0.006 | 15.675 | 0.005 | 38.885 | 0.005 |
| 1055_1C | Listwanite | 18.712 | 0.006 | 15.672 | 0.005 | 38.865 | 0.006 |
| 1155_2C | Listwanite | 18.705 | 0.005 | 15.669 | 0.005 | 38.861 | 0.005 |
| LIM1 | Cret. Limestone | 18.700 | 0.006 | 15.673 | 0.005 | 38.867 | 0.005 |
| BB-2 | Andesite | 18.759 | 0.005 | 15.665 | 0.007 | 38.871 | 0.009 |
| KOP-1 | Dacite | 18.821 | 0.006 | 15.673 | 0.005 | 38.949 | 0.005 |
| KG-1 | Qtz-latite | 18.762 | 0.005 | 15.676 | 0.006 | 38.927 | 0.008 |
| 08/32-1 | Qtz-latite | 18.820 | 0.005 | 15.678 | 0.005 | 38.973 | 0.007 |
| R3-A | Granodiorite-Kopaonik | 18.772 | 0.005 | 15.668 | 0.006 | 38.916 | 0.008 |
| GND-2 | Granodiorite-Zeljin | 18.794 | 0.005 | 15.674 | 0.006 | 38.938 | 0.008 |
| Carbonates | | | | | | | |
| 1055/1B | BB: pre-ore | 18.676 | 0.007 | 15.675 | 0.007 | 38.869 | 0.010 |
| 1130/1B | BB: syn-to late | 18.682 | 0.004 | 15.676 | 0.005 | 38.883 | 0.008 |
| 1105/h | BB: syn-to late | 18.676 | 0.007 | 15.673 | 0.006 | 38.868 | 0.010 |
| 1055_4D | BB: post-ore | 18.679 | 0.007 | 15.675 | 0.006 | 38.878 | 0.010 |
| 1105/6(1) | BB: post-ore | 18.705 | 0.004 | 15.674 | 0.005 | 38.870 | 0.007 |
| 1235(3) | BB: vein ore body | 18.695 | 0.006 | 15.673 | 0.006 | 38.865 | 0.007 |
| KU90 | Porphyry vein | 18.768 | 0.007 | 15.669 | 0.006 | 38.894 | 0.010 |
| KU103 | Porphyry vein | 18.757 | 0.007 | 15.669 | 0.006 | 38.883 | 0.010 |

Lead isotopic compositions of hydrothermal carbonates are identical to those of galena from the respective deposits and their $^{206}$Pb/$^{204}$Pb ratios range from 18.675 to 18.705, $^{207Pb}/^{204}$Pb from 15.672 to 15.676 and $^{208}$Pb/$^{204}$Pb from 38.865 to 38.883.

It is also notable that the limestone, listwanites and serpentinite all show similar lead isotopic ratios to the unaltered igneous rocks. They are enriched in radiogenic components and their $^{206}$Pb/$^{204}$Pb ratios range from 18.700 to 18.712, $^{207Pb}/^{204}$Pb from 15.669 to 15.673 and $^{208}$Pb/$^{204}$Pb from 38.861 to 38.866. High radiogenic Pb-isotope values of serpentinites are a common feature of those rocks, reflecting strong influence of secondary alteration processes (Kempton and Stephens, 1997).

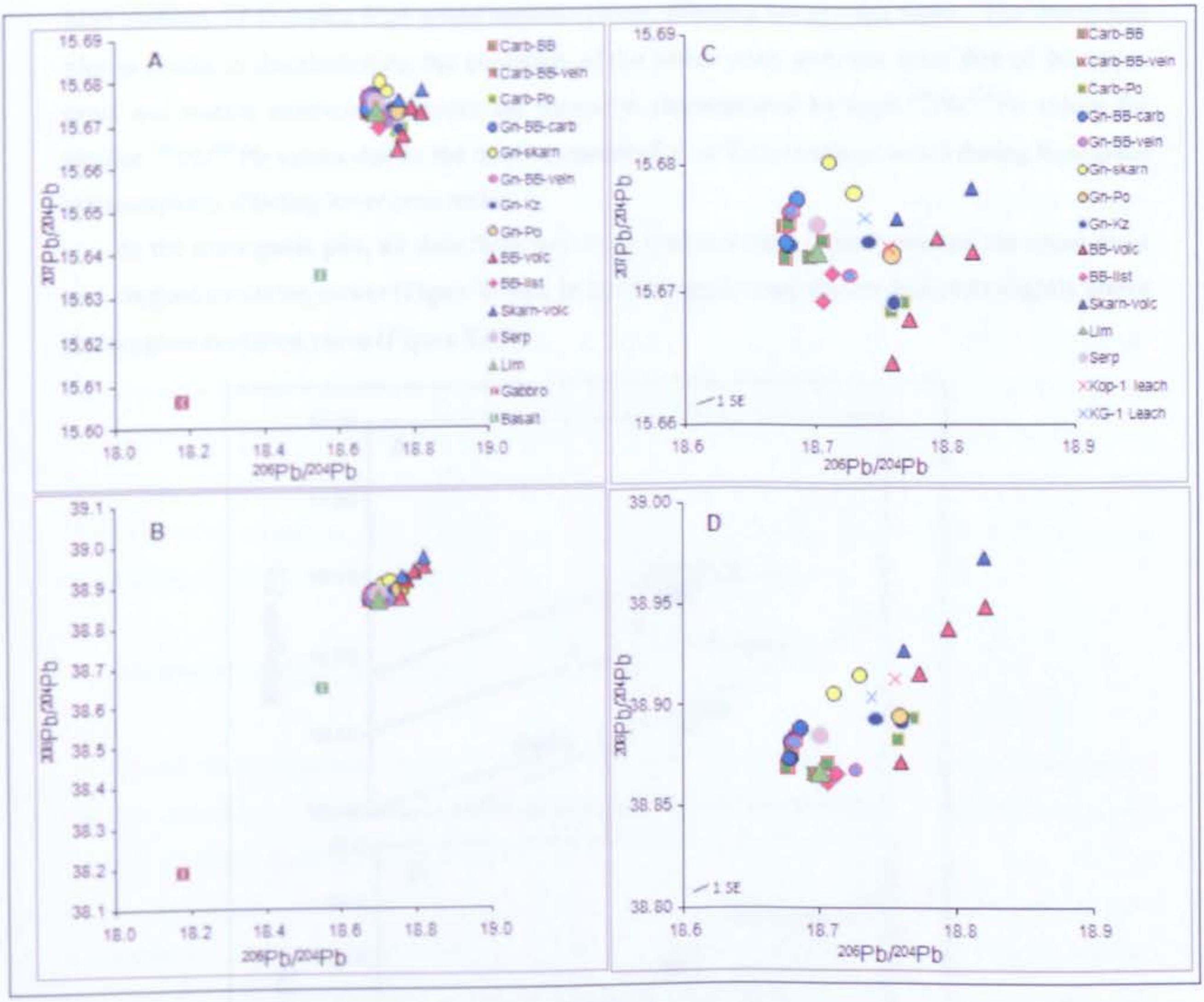

**Figure 8.3:** Variation of $^{207}$Pb/$^{204}$Pb vs. $^{206}$Pb/$^{204}$Pb and $^{208}$Pb/$^{204}$Pb vs. $^{206}$Pb/$^{204}$Pb (measured values) for galena, host rocks and hydrothermal carbonates from various deposits in the study area (A and B). Enlarged view of the same data, excluding gabbro and basalt, are shown in C and D. Legends in A and C apply to B and D respectively.

### *8.2.4.1 Source of lead*

The Pb-isotopic compositions of all samples are plotted against the evolution curves from one of the most used models (Zartman and Doe, 1981) that highlights the evolution through time of the upper crust, lower crust, and mantle reservoirs on uranogenic and thorogenic plots (Figure 8.4). Our database is too small to draw any certain conclusions; however an attempt is made to interpret the data in terms of derivation from one or more large-scale terrestrial reservoirs (e.g., upper and lower crust, mantle).

The Zartman and Doe model (1981) is based on geochemical partitioning of U, Th, and Pb during geological processes. In the uranogenic plot, the upper crust evolution curve has the highest $^{207}$Pb/$^{204}$Pb values, because upper crustal rocks are enriched in U due to the transfer of magma from mantle to crust. Because of the loss of U to the upper crust, the residual mantle curve has lower $^{207}$Pb/$^{204}$Pb values. The lower crust evolution curve has an even lower $^{207}$Pb/$^{204}$Pb value due to the high mobility of U during high-grade metamorphism affecting lower crust rocks. The thorogenic plot is useful in discriminating the evolution of the lower crust reservoir from that of the upper crust and mantle reservoirs, because the former is characterized by high $^{208}$Pb/$^{204}$Pb values for similar $^{206}$Pb/$^{204}$Pb values due to the relative immobility of Th (compared to U) during high-grade metamorphism affecting lower crust rocks.

In the uranogenic plot, all data from this study define a tight cluster between the upper crust and orogene evolution curves (Figure 8.4A). In the thorogenic diagram the data plots slightly above the orogene evolution curve (Figure 8.4B).

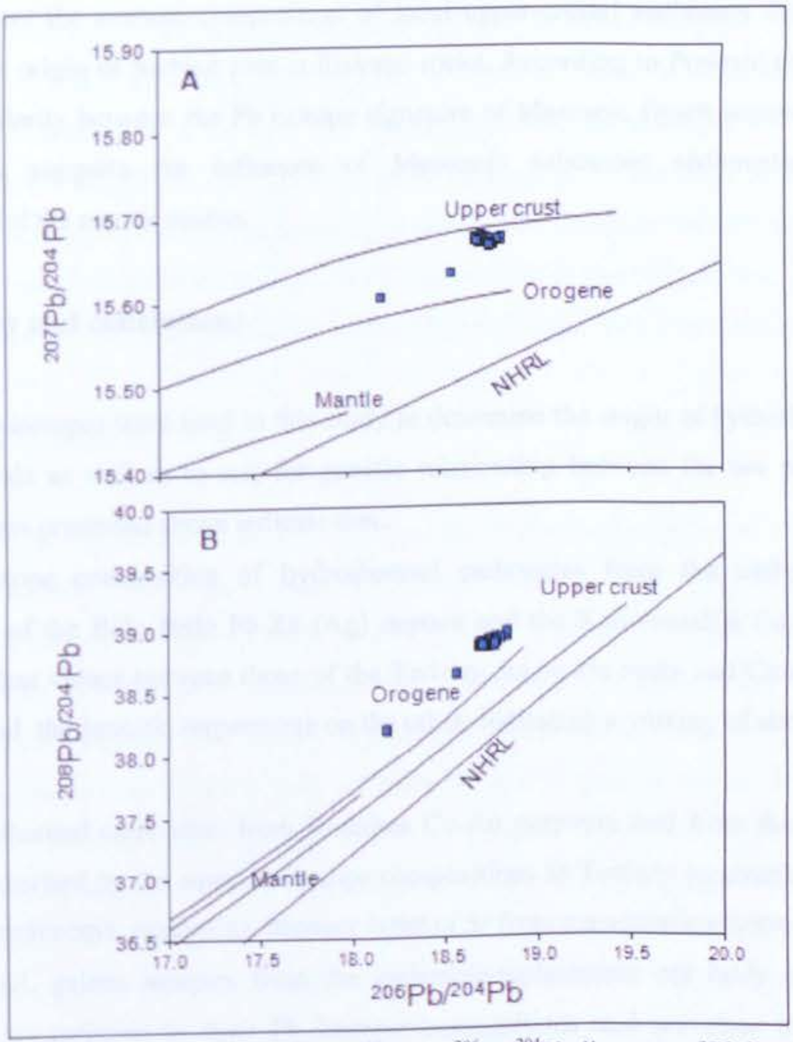

**Figure 8.4:** $^{207}$Pb/$^{204}$Pb vs. $^{206}$Pb/$^{204}$Pb and $^{208}$Pb/$^{204}$Pb vs. $^{206}$Pb/$^{204}$Pb diagrams of Pb isotopic compositions of all analysed samples. The upper crust, orogene, and mantle evolution curves are from Zartman and Doe (1981). NHRL-Northern Hemisphere reference line.

The signatures of galena and country rocks forming a tight cluster that plots slightly above the orogene curve indicate a homogeneous reservoir. Similar signatures are found in the continental arc environment where mantle-derived magmas become contaminated by continental crust rocks (Chiaradia et al., 2006). This interpretation is consistent with $^{87}$Sr/$^{86}$Sri data (0.7067 to 0.7078, described above) from magmatic rocks of the Kopaonik district that indicate mixed mantle and crustal sources.

Tertiary igneous rocks analysed in this study display very similar radiogenic Pb-isotope signatures with Oligocene-Miocene post-collisional igneous rocks located in the Vardar Ophiolite Suture Zone of Serbia, some 80 km north and south from the study area. This recently delineated igneous province is dominated by high-K calc-alkaline, shoshonitic and ultrapotassic rock types (Prelević et al., 2001; 2005; 2007; Cvetković at al., 2007) and show small variations of Pb isotope ratios ($^{206}$Pb/$^{204}$Pb = 18.58-18.83, $^{207}$Pb/$^{204}$Pb 15.62-15.70 and $^{208}$Pb/$^{204}$Pb 38.74-38.99) (Prelević et al., 2005). The Pb-isotope ratios of Tertiary rocks and Cretaceous limestone from this study also resemble those of Mesozoic flysch sediments studied by Prelević et al., (2005). The flysch sediments reflect the average composition of local upper-crustal sediments that may have been involved in the origin of Serbian post-collisional rocks. According to Prelević et al., (2005; 2007) the strong similarity between the Pb isotope signature of Mesozoic flysch sediments and the local igneous rocks suggests the influence of Mesozoic subducted sedimentary material and contamination of the mantle source.

## Summary and conclusions

Sr and Pb isotopes were used in this study to determine the origin of hydrothermal carbonates and ore minerals as well as to test for genetic relationship between the ore mineralisation and magma. The data presented above indicate that:

- Sr isotope composition of hydrothermal carbonates from the carbonate-replacement mineralisation of the Belo Brdo Pb-Zn (Ag) deposit and the Karavansalija Cu-Au skarn deposit have intermediate values between those of the Tertiary magmatic rocks and Cretaceous sediments on one hand and the Jurassic serpentinite on the other, indicating a mixing of strontium from those rocks.
- Hydrothermal carbonates from Rudnitza Cu-Au porphyry and from the Belo Brdo vein-type are characterised by the same Sr-isotope compositions as Tertiary magmatic rocks and partly as Cretaceous sediments, suggesting stronger input of Sr from a magmatic source.
- In detail, galena samples from the carbonate-replacement ore body of the Belo Brdo deposit show no variation in their Pb isotopic compositions and are close to those of Upper Cretaceous Flysch limestones. The vein-; stockwork- and skarn-type deposits exhibit slightly higher variations in their Pb isotopic compositions and are close to those of Tertiary magmatic rocks suggesting a similar source for felsic rocks and ore-related sulphide minerals.
- Generally, the Pb isotope data for 11 galena samples derived from four different deposits within the Kopaonik metallogenic district show uniform isotopic compositions ($^{206}$Pb/$^{204}$Pb=18.678-18.760; $^{207}$Pb/$^{204}$Pb=15.669-15.680; $^{208}$Pb/$^{204}$Pb= 38.867-38.915), suggesting that the deposits belong to the same metallogenic event and have possibly a common source of Pb.

# CHAPTER 9:
# DISCUSSION AND SYNTHESIS

## 9.1 Introduction

The variety and diversity of mineral deposits in the geographically restricted area of the Kopaonik metallogenic district indicates a complexity in both the geotectonic evolution and the ore-forming process. In this study, the Pb-Zn (Ag) carbonate-replacement deposit at Belo Brdo has been the target of detailed investigation. This has included petrography (textural and mineral chemistry studies), fluid inclusion analysis and stable and radiogenic isotope analysis. In addition, comparative stable (S, C-O, H-O) and radiogenic (Sr, Pb) isotope studies have been undertaken on nearby porphyry, skarn and vein- type deposits in order to enable a better understanding of the polymetallic mineralisation in the area. The wealth of data obtained during this research project is consistent with the hypothesis that the Belo Brdo Pb-Zn high temperature carbonate replacement mineralisation formed as a part of an evolving magmatic-hydrothermal system.

Data presented earlier in the thesis will be summarised in this chapter and a genetic model for the origin and evolution of the Belo Brdo Pb-Zn (Ag) deposit will be presented.

## 9.2 Regional geological setting

The Kopaonik metallogenic district is part of the Vardar ophiolite zone, which represents the easternmost tectonic unit of the Dinaride-Hellenide orogenic belt. Several models have been proposed to reconstruct the geodynamic evolution of the region, and there is an on-going debate about the number of basins and microcontinents involved in the origin of the Dinaride-Hellenide belt. In brief, the "multi-ocean" model (e.g. Robertson and Karamata, 1994; Karamata, 2006) suggests the existence of at least two different oceanic basins separated from each other by "terranes" of continental crust, namely the Drina-Ivanjica, Jadar and Kopaonik "terranes". In contrast, the "single-ocean" model (e.g. Schmid et al., 2008) suggests that the Jurassic-age ophiolites of the Dinarides originated from one and the same ocean and that the Kopaonik "terrane" represents thrust sheets derived from the distal Adriatic passive margin exposed in a tectonic window. Ophiolites, derived from the Vardar branch of the Neotethys Ocean ('Western Vardar Ophiolitic Unit' of Schmidt et al., 2008), were obducted during the latest Jurassic onto the Adriatic margin. Out-of-sequence thrusting, which produced a series of Dinaric composite nappes, occurred during Late Cretaceous to early Paleogene (Schmidt et al., 2008; Schefer et al., 2010a), followed by collisional (Eocene) and post-collisional (Oligocene-Miocene) stages (Cvetković et al., 2004). Composite tectonic nappes, consisting of continent-derived material in their lower part and ophiolitic material in the upper part make up the geological framework of the study area. It includes, from bottom to top (1) a Triassic Metamorphic Complex, structurally overlain by (2) an

Ophiolite Mélange Unit, which in turn is structurally overlain by (3) a Jurassic Ophiolite Unit and (4) an Upper Cretaceous Flysch Unit, which unconformably overlies all the other lithological units. The tectonic nappe pile was intruded by an I-type volcano-intrusive complex of Oligocene age (31.7 to 30.6 Ma, Schefer et al., 2010).

The Belo Brdo Pb-Zn (Ag) deposit and nearby polymetallic deposits are associated with Oligocene intrusive activity and are structurally controlled. The deposits within the Kopaonik metallogenic district are aligned along the regional NNW-SSE- trending structural zones, which coincide with the distribution of Paleogene magmatic rocks within the Alpine- Balkan-Carpathian-Dinaridic orogenic province.

## 9.3 Local geological setting: petrographic and geochemical constraints on the geo-tectonic setting of the Belo Brdo deposit

Petrographic data presented here show that listwanites, in addition to Cretaceous limestones, represent an important host rock to the carbonate-replacement type of mineralisation. Listwanites are metasomatic rocks derived from either an ultramafic or a mafic protolith and are characterised by the specific assemblage: chromian muscovite + quartz + Fe-Mg carbonates + pyrite (Halls and Zhao, 1995). An additional vein-type mineralisation in Belo Brdo is hosted by Tertiary andesites. Petrographic and geochemical data obtained from the peridotites and the Tertiary igneous rocks indicate a supra-subduction signature for the magmatic rocks.

### 9.3.1 *Peridotites*

In this study, harzburgite proved to be the most common peridotite and is the most likely protolith to listwanite. Although highly serpentinised, the harzburgites still preserve relics of primary phases (olivine > orthopyroxene >> clinopyroxene and Cr-spinel). The listwanites are an example of intensive mineral carbonation during serpentinisation. Relict chrome spinels are the sole remaining proof of a mantle peridotite protolith.

According to Dick and Bullen (1984), Cr-spinel chemistry [(Cr/Cr+Al) vs. Mg/Mg+Fe$^{2+}$ or Cr# vs. Mg#] can be used to classify mantle-derived peridotites in terms of geotectonic setting. Spinels from abyssal (MORB-type) peridotites are characterised by high Al and Mg and low Cr and Fe$^{2+}$ contents, resulting in low Cr# (Cr#=20-54) and high Mg#. In contrast, peridotites from supra-subduction environments exhibit high Cr# (38-84) and low Al content. High Cr# observed in many forearc peridotite spinels is also characteristic of spinels in high-Mg andesites and other boninitic lavas (Metcalf and Shervais, 2008). Spinels from peridotites associated with back-arc basins have compositions similar to those from abyssal peridotites (e.g., Ohara et al., 2002). In this study, Cr-spinels from non-mineralised peridotites are characterised by high Cr# (47-86), moderate Mg# (55-78) and low $Al_2O_3$ contents (up to 17%), similar to those of a supra-subduction setting.

The Mg# of some harzburgites in Belo Brdo is low (<20) owing to alteration of the harzburgites during serpentinisation. The effects of such alteration are well known (Prichard et al., 2001); they will cause an increase in $Fe^{3+}$ at the expense of Al (Evans and Frost 1975), and $Fe^{2+}$ will increase at the expense of Mg (Jan et al., 1985).

Other useful indicators of different tectonic settings are $TiO_2$ vs. $Al_2O_3$ contents of Cr-spinel (Beccaluva et al., 1989; Princiavalle et al., 1989; Kamenetsky at al., 2001). $TiO_2$ values higher than 0.2% and high Al contents (>25% $Al_2O_3$) are typical of mid-ocean-ridge magmatism. Peridotites containing spinel with $TiO_2$ values between 0.2 and 1% and $Al_2O_3$ between 15 and 25 are classified as subduction-related back-arc type, whereas those with $TiO_2$ values higher than 1% and 10-15% $Al_2O_3$ belong to intraplate environment. According to Beccaluva et al., (1989) high-Ti ophiolites compare favourably with the magmatic association occurring at mid-ocean ridges and well developed marginal basins, whereas low-Ti and very low-Ti ophiolites are best associated with the magmatic series of island arc and boninitic types respectively, generated in a supra-subduction zone settings.

Low-Ti (<1% $TiO_2$) and low- Al (< 17% $Al_2O_3$) values characterise Cr-spinel of Belo Brdo peridotites. Although limited, the mineral chemistry data indicate that Cr-spinel composition of the peridotites is different from MORB suites. Moderate- to high Cr#, low-$Al_2O_3$ and low-$TiO_2$ values suggest that the Cr-spinel grew in a supra-subduction setting.

### *9.3.2 Tertiary igneous rocks*

#### *9.3.2.1 Petrography*

Some important constraints on the geotectonic setting of the study area can be gained from the petrological and geochemical features of the volcanic rocks. Key petrological features are summarised below:

- All volcanic rocks are characterised by porphyritic and glomeroporphyritic textures, typical of those found in orogenic belts, with plagioclase being the predominant phenocryst phase in andesites and dacites. Alkali feldspar is common phase in quartz-latites.
- The water-rich nature of the magma is clearly indicated by the presence of hydrous mafic phenocrysts. The major ferromagnesian phase in the studied rocks from both volcanic phases is calcic amphibole, whilst biotite represents the second most common mafic mineral.
- Some andesitic lavas of the first volcanic phase display textural evidence for magma mixing. This is supported by disequilibrium textures such as: the existence of resorbed plagioclase phenocrysts; occurrence of both, normally and reversely zoned plagioclase phenocrysts in the same sample; and sieved-textured plagioclase.
- Disequilibrium textures are also noted in some quartz-latites of the second volcanic phase, where they are evident by rounding of euhedral crystal corners of plagioclase; deep embayment of quartz; and occurrence of quartz and plagioclase xenocrysts.

The observed disequilibrium textures are consistent with models involving magma mixing, where mixing is probably caused by the influx of a hotter basaltic magma into crustal magma chambers (Tsuchiyama, 1985; Altunkayna and Yilmaz, 1998; Kamaci and Altunkaynak, 2010).

Deep embayments of quartz phenocrysts and resorption of K-feldspar and plagioclase, can both occur due to resorption during the magmatic–hydrothermal transition, or due to under-saturation in the magma caused by rapid decompression as the magma ascended to a shallow magma reservoir (Nelson and Montana, 1992). Thus, shallow crustal processes probably had an important role in the petrogenesis of the felsic igneous rocks.

### *9.3.2.2 Geochemistry*

The geochemical data (Section 3.8) indicate that the volcanic rocks from the first and second volcanic phase exhibit several features that are typical of rocks associated with subduction zones. These are as follows:

- The rocks from both, the first and second volcanic phases classify as subalkaline and exhibit calc-alkaline to mildly alkaline metaluminous character.
- On "tectonomagmatic discrimination diagrams" (Rb vs. Y + Nb and Nb vs. Y) and the ternary Hf-Th-Ta and Zr-Th-Nb diagrams, they all plot in the field of magmas erupted in volcanic arc settings.
- Their trace-element chemistry (bivariate plots of Ni vs. V; and Zr vs. Rb/Sr) reflects compositions typical of intrusions associated with magmatic-hydrothermal, in particular Fe, Cu, Au and Zn skarn deposits which are often associated with the porphyry systems.
- On primitive mantle-normalised multi-element diagrams all the rocks display spiked patterns, which are typical of subduction-related magmatic rocks (Sun and Stern, 2001; Murphy, 2007). They show enrichment in large-ion lithophile elements (LILE [Cs, Rb, Th, U, K]) and Pb over light rare-earth elements (LREE) and MREE, and depletion in high-field-strength elements (HFSE [Zr, Nb, Ti, and P]).
- They display enrichment in LREE, flat HREE, and moderate to negligible negative Eu anomalies (Eu/Eu*: 0.7-0.9) on chondrite-normalised rare-earth diagrams. Negative Eu anomalies can be produced by plagioclase fractionation, residual plagioclase in the source, or source contamination by slab-derived fluids and sediments (Ellam and Hawkesworth, 1988). In general, the negative and mutually parallel REE slopes and multi-element variation diagrams of the rocks from both volcanic phases indicate the same magma source. However, bivariate plots (Zr-La and Zr-Th) indicate that the rocks first and second volcanic phases might not be co-genetic. Additionally, the rocks of the first volcanic phase show slightly lower Si contents than those of the second volcanic phase. As far as their trace element abundances are concerned, the rocks of the second volcanic phase are more enriched in incompatible elements with respect to primitive mantle, than the rocks of the first volcanic phase. Furthermore, the Sr isotopic ratios of the rocks of

the second volcanic phase are higher compared to the rocks of the second phase. Different degrees of partial melting of mantle sources heterogeneously enriched by fluids and melts derived from previous subduction can produce magmas variously enriched in K, incompatible elements, and isotopic composition (Foley, 1988; Pe-Piper et al., 1998). Geochemical variability observed in the rocks of the first and second volcanic phase may be explained by differing enrichments of subduction-related components (Prelević et al., 2005) or they are from different source regions.

Pb isotope ratios (Table 8.2, Section 8.2.4) for Tertiary igneous rocks ($^{206}Pb/^{204}Pb$ = 18.76-18.82, $^{207}Pb/^{204}Pb$ 15.66-15.68 and $^{208}Pb/^{204}Pb$ 38.87-38.97) are close to those of Upper Cretaceous limestones ($^{206}Pb/^{204}Pb$ = 18.70, $^{207}Pb/^{204}Pb$ 15.67 and $^{208}Pb/^{204}Pb$ 38.87) and similar to those of medium- to high-K calc-alkaline Oligocene lavas located elsewhere in the Alpine-Balkan-Carpathian-Dinaride province (Cvetković et al., 2004; Marchev et al., 2004). According to Prelević et al. (2005), elevated Sr and Pb isotope signatures reflect crustal contamination of their source through subduction of Mesozoic sedimentary material. Pb isotopes are useful indicators of contamination of the mantle by sediments (Ben Othman et al., 1989), because of the large contrast in Pb abundance between sediments and the mantle. Thus, a small addition of sediment will significantly affect the mantle Pb isotope ratios and the source will assume the isotopic characteristics of the sediments. Additionally, contribution by intracrustal materials can result in strongly radiogenic $^{87}Sr/^{86}Sr$ and $^{207}Pb/^{204}Pb$ values suggesting a contamination of mantle-derived magmas during ascent through the continental crust (Economou-Eliopoulos, 2005). Such isotope signatures are characteristics of many intrusions related to porphyry deposits.

The Kopaonik I-type granitoids of Oligocene age postdate the final stages of subduction of the Vardar branch of Neotethys and initial collision with Eurasia by ~30 Ma (Karamata et al., 1997; 1999), eliminating the possibility that the volcanism is directly related to subduction and early stages of collision. Therefore, it is clear that the Oligocene magmatism within the study area is post-collisional with respect to closure of the Vardar ocean. This magmatism is contemporaneous with the onset of extension in the Balkan area (Schefer et al., 2010). Various models have been proposed to explain the cause of post-collisional igneous activity in the region, namely: (1) Post-collisional orogenic collapse of an overthickened continental crust (e.g. Cvetković et al., 2004); (2) Back-arc magmatism (Pamić et al., 2002a; Kovacs et al. 2007); and (3) Slab delamination caused by roll-back (Funiciello et al., 2006) of the former lower plate after collision. Schefer et al., (2010) propose that after final closure of the Neotethys in the Eocene (Figure 9.1 A), the lithospheric mantle of the NE-ward subducted Adriatic plate started to delaminate (Figure 9.1 B) from the overlying crust and retreat. The resultant mantle flow gave rise to mantle-dominated magmas with various amounts of crustal contamination. This model allows for the generation of chemically variable magmas.

It is clear that the geochemical and isotopic variations in the Kopaonik magmatic complex suggest involvement of various crustal components in the evolution of the magmatic complex.

**Figure 9.1**: East-West profile sketches illustrating delamination model. A) Closure of the Neotethys; B) delamination of the Adria plate possibly associated with slab break-off; C) Present-day geometry (modified after Schefer et al. 2010).

### *9.3.3 Metallogenic significance of the Kopaonik Tertiary magmatism*

Petrological and geochemical data presented here reveal that the Kopaonik magmatism exhibits many characteristics similar to that of oxidised and hydrous I-type metaluminous subduction-related calc-alkaline magmatism associated with Cu-Au porphyry and related base-metal deposits (Einaudi, 2007). The majority of known porphyry deposits are genetically related to intermediate to felsic calc-alkaline arc-type magmatism that generates most of the hydrous and oxidised magmas above active subduction zones (Richards, 2003). In recent years, however, it has been reported that some porphyry copper deposits form in post-subduction and collisional settings (Richards, 2009). These deposits are associated with magmas produced by remelting of previously subduction-modified arc lithosphere triggered by post-subduction lithospheric thickening, lithospheric extension, or mantle lithosphere delamination caused by roll-back and break-off of the descending plate (Richards, 2009). The magmas with subduction-related geochemical signatures generated by melting of the previously metasomatised portion of the mantle wedge (i.e., "hybridised mantle"), as found in collisional zones, usually show larger variation in geochemistry than arc magmas (Foley and Wheeler, 1990; Hawkesworth et al., 1993).

Magmatism at Belo Brdo resembles that which occurs in post-subduction environments and arc contraction caused by collision, which leads to crustal thickening and delamination of the sub continental lithospheric mantle. Partial melting of lower crustal rocks caused by upwelling of hot asthenospheric melts in such settings produces felsic, calc-alkaline to mildly alkaline magmas with crustal radiogenic isotopic signatures (Kovacs, 1999; Richards, 2009 and references therein).

An example of a post-subduction setting is the Carpathian region in Romania, which is well known for its Miocene to Quaternary orogenic magmatism related to slab break-off (Grancea et al., 2002 and references therein). This magmatism was accompanied by widespread hydrothermal activity producing economic porphyry/skarn copper deposits and both high- and low-sulphidation epithermal mineralisation (e.g., Vityk et al. 1994; Lexa et al. 1999).

### *9.3.4 Summary*

- Petrographic and geochemical data obtained from the peridotites and the Tertiary igneous rocks indicate subduction-related signatures for the magmatic rocks.
- Moderate- to high Cr#, low-$Al_2O_3$ and low-$TiO_2$ values suggest that the Cr-spinel of the Belo Brdo peridotites grew in a supra-subduction setting.
- Tertiary volcanic rocks show typical “subduction-related” compositions as reflected by the enrichment of LIL elements and depletion of HFS elements.
- Pb isotope ratios for Tertiary igneous rocks are close to those of Upper Cretaceous limestones reflecting crustal contamination of their source through subduction of Mesozoic sedimentary material, or contamination during ascent of magma through the continental crust.
- Magmatism at Belo Brdo resembles that which occurs in post-subduction environments and arc contraction caused by collision, which leads to crustal thickening and delamination of the sub-continental lithospheric mantle. Such a setting is characterised by felsic, calc-alkaline to mildly alkaline magmas with crustal radiogenic isotopic signatures.

## 9.4 Evolution of the Belo Brdo Pb-Zn (Ag) deposit and genetic model for mineralisation

The mineralisation of the Belo Brdo Pb-Zn (Ag) deposit has the characteristics of an intermediate sulphidation base-metal deposit as described by Einaudi et al., (2003) displaying hydrothermal alteration styles similar to those of copper porphyry systems, and with significant input of trace elements from related ophiolites. Weak propylitic and argillic alteration of volcanic rocks occurs in the marginal parts of the mineralised area, whereas intense hydrothermal alteration (listwanisation, sericitisation, silicification, and tourmalinisation) is associated with the formation of the main ore bodies. Hydrothermal alteration and formation of irregular and tabular carbonate-replacement ore bodies is controlled by steeply dipping fault zones developed at contacts between different lithologies (serpentinites/Tertiary volcanics; Cretaceous limestones/ volcanics). The vein-ore body is hosted by hydrothermally altered andesite.

The genetic model for the origin and evolution of the Belo Brdo deposit proposed in this study involves three stages of mineral deposition, namely (1) pre-ore stage, characterised by strong hydrothermal alteration of host rocks and evolution of Ni-Co-As mineral assemblage; (2) main-ore stage, during which massive sulphides (sphalerite, galena, pyrite, chalcopyrite, tetrahedrite-tennantite) precipitated and (3) post-ore stage, characterised mainly by quartz and carbonates with minor pyrite.

### *9.4.1 Pre-ore stage*

This stage is characterised by formation of listwanites and intense quartz-sericite and quartz-tourmaline alteration of wall-rocks, as well as the presence of non-economic concentrations of predominantly Ni-Co-As sulphides, Ni-Co-As bearing pyrite, rare chalcopyrite and minor Bi-Te-bearing sulphosalts. No direct evidence, such as fluid inclusion data, is available to characterise the mineralising fluids. However, mineral chemistry and stable isotope data provide evidence for moderate- to high- formation temperatures (300-450°C) and a magmatic signature for the hydrothermal fluids involved in the early stages of Belo Brdo evolution.

#### *9.4.1.1 Formation of listwanites*

Petrographic and mineral chemistry data show that metasomatic transformation of ultramafic rocks to listwanites in Belo Brdo was a multi-stage process (Section 4.4.3) including (1) initial formation of serpentinites by hydration of harzburgites (hydration of olivine to form serpentine and magnetite; hydration of orthopyroxene to serpentine; O'Hanley, 1996) and formation of tremolite-chlorite schists at low-grade metamorphic conditions (with few carbonates); (2) intermediate stage characterised by brecciation and hydrothermal alteration of previously formed lithologies resulting in carbonate-veining of serpentinites and schists, grading into various listwanite-like rocks (i.e. serpentine-carbonate, talc-carbonate, talc-chlorite rocks), which are broadly grouped into *carbonate-serpentine listwanite breccias*; and (3) final stage of formation of *massive listwanites* through pervasive carbonatisation and sericitisation of carbonate-serpentine rocks along steeply dipping fault zones. The first two stages likely reflect sea floor hydration processes, whereas stage 3 represents a hydrothermal potassic alteration that stabilises the growth of Cr-mica. This is documented by textural and mineral chemistry data.

The two types of listwanites (carbonate-serpentine listwanite breccias and massive listwanites) are characterised by a distinct mineralogy. The carbonate-serpentine listwanite breccias contain Mg-Ca (±Fe) carbonates, serpentine minerals, magnetite, chromite, Cr-spinel, ± talc, ± chlorite ± quartz, Ni-Co-As sulphides and minor pyrite, whereas massive listwanites are characterised by Mg-

Fe (± Mn) carbonates, Cr-mica, Cr-chlorite, quartz and abundant sulphides (pyrite, arsenopyrite, gersdorffite and Bi-Te sulphosalts). Furthermore, carbonate-serpentine listwanite breccias are cross-cut by quartz-carbonate-fuchsite veins, clearly indicating that silicification and sericitisation postdate formation of early listwanite breccias. Massive listwanites show a direct spatial association with fault zones which served as conduits for K-rich hydrothermal fluids responsible for the alteration of Cr-spinel and formation of Cr-mica and Cr-chlorite.

The field relationships, textural features and distinct mineralogy of the two categories of listwanite rocks suggest differences in alteration intensity and characteristics of the hydrothermal fluids responsible for their formation. Several authors have proposed models for formation of various types of listwanites in ophiolite belts (e.g. Auclair et al., 1993; Ucurum, 2000; Akbulut et al., 2006), all of which include structural control (thrusts, faults or a micro-fractured and porous host-rock) as pathways for the hydrothermal fluid input and episodic carbonatisation of serpentinites. According to Akbulut et al. (2006) and Nasir et al., (2007) carbonatisation of non-silicified serpentinites is caused by fault controlled infiltration of alkaline, moderate- to high-temperature (300-400°C), Ca-, Mg- and $CO_2$- bearing fluid. Carbonatisation of the rock takes place through water–rock interaction. Similarly, the origin of the carbonate-serpentine listwanite breccias in Belo Brdo is likely associated with regional fault zones related to emplacement of ophiolites. Carbonate minerals, which replace the ultramafic rocks, formed by hydrolysis of iron, magnesium, calcium and manganese silicates, with the wall-rocks providing the necessary bivalent metal cations (Kerrich, 1983). In Belo Brdo, dolomite is the dominant product of carbonatisation of the serpentinite.

### *9.4.1.2 Evidence for externally derived moderate-to high temperature mineralising fluids with magmatic signatures responsible for the formation of massive listwanites and pre-ore stage sulphides*

Field evidence, microtextures, mineral chemistry and stable isotope data indicate that sulphide formation in massive listwanites was associated with quartz veining, carbonatisation and fuchsite (Cr-mica) metasomatism. As discussed above, the major petrographic difference between the massive listwanites and other listwanite-like rocks is in their mineralogy, which is characterised by presence of quartz, Cr-mica, Cr-chlorite, sulphides and absence of magnetite. A reasonable interpretation is that $Fe^{3+}$, present in the magnetite, was reduced to $Fe^{2+}$ in pyrite. This indicates that the fluids were reducing and sulphur bearing (Ash, 2001).

The origin of the chromium in listwanite depends on 1) the primary mineral acting as a source and its ability to release chromium and 2) the behaviour of Cr during metasomatism (Plissart et al., 2009). In an ultramafic rock, chromite is the primary source of chromium, which occurs as $Cr^{3+}$. However, $Cr^{3+}$ is known to be a chemically immobile cation and is not easily released from chromite. The destabilisation of Cr-spinel during hydrothermal alteration usually leads to the formation of a rim of Cr-$Fe^{3+}$ enriched spinel or Cr-rich magnetite and formation of chlorite aureoles (Shen et al. 1988, Kimball 1990, Mellini et al. 2005; Plissard et al., 2009). Such a feature is observed in the listwanite breccias of the Belo Brdo deposit. According to Kimball (1990) and Mellini et al. (2005), spinel destabilisation could be related to reaction with a fluid enriched in Mg and Si during high-T metasomatism (T > 400°C). Additionally, $Cr^{3+}$ mobilisation is seen in shear zones (Winchester and Max 1984), with strongly acidic conditions (pH < 4). In Belo Brdo, Mg-rich Cr-bearing chlorite in listwanite breccias was probably formed during a high-T metasomatism and prior to formation of massive listwanite. During subsequent stages of alteration, acidic, $SiO_2$- and K-rich hydrothermal fluids were responsible for leaching of chromium from Cr-chlorite and formation of Cr-mica-quartz assemblage.

Two distinct temperature events for the formation of sulphide mineralisation in different listwanite rocks are evident from the mineral compositions of gersdorffite. The As: S ratio and cation contents have been used to distinguish different types of gersdorffite. According to Hem et al. (2001), and Fanlo et al. (2004), both As and Ni contents in the gersdorffite-cobaltite solid solution are controlled by the fugacity of As in the mineralising fluid at high temperature. The temperature curves in the system NiAsS-CoAsS-FeAsS (Klemm, 1965) are not applicable to systems that show extensive substitutions and disequilibrium textures (Fanlo et al., 2006). Therefore, only gersdorffite compositions with As:S ratios of 0.96-1.01and those that show no substantial substitutions (Sb and Zn for As) were used to obtain the crystallisation temperatures. Two distinct groups were identified, a high temperature gersdorffite (>400°C) found in listwanite breccias, and a lower temperature gersdorffite (≤ 300 °C) which formed in massive listwanites (Section 4.6.1).

Quartz-sericite (phyllic), quartz-tourmaline, argillic and propylitic alteration of andesites in Belo Brdo are important indicators of involvement of hydrothermal fluids similar to those related to porphyry systems. There is robust stable isotope evidence that the fluids responsible for early alteration and sulphide precipitation have hydrothermal characteristics, albeit derived from a magmatic source. The main evidence for the magmatic component is: (1) moderately high temperature (~420°C) of the quartz-sericite alteration and magmatic $\delta^{18}O$ values for fluid in equilibrium with sericite and quartz (6.5 – 8.5‰); (2) magmatic δD value (-58‰) for fluid in equilibrium with sericite; (3) magmatic $\delta^{18}O$ and δD values of fluid in equilibrium with tourmaline (10‰ and -38‰ respectively) (Section 7.4.4); (4) magmatic $\delta^{13}C$ value of carbon in silicified listwanite (Section 7.3.3); and (5) magmatic $\delta^{34}S$ values of pyrite hosted by andesites and massive listwanite (2.6-4.1‰) (Section 7.2.4).

*Sericitic* alteration of volcanic rocks is characterised by the growth of sericite as a replacement of feldspars and mafic phases accompanied by quartz (± tourmaline), abundant disseminated pyrite and a small percentage of chalcopyrite. Temperature calculations based on stable isotope oxygen geothermometry between co-existing quartz and sericite is 420°C, which is consistent with the temperature range for sericitic alteration (350-450°C) from copper porphyry deposits (Rusk et al., 2008). Sericitic alteration implies low pH conditions. Whole-rock geochemical analyses of altered samples show enrichment in Si and K and depletion in Ca and Na. The source of the silica is most likely magmatic, based on $\delta^{18}O$ and $\delta D$ values of early hydrothermal fluids in equilibrium with quartz and sericite ($\delta^{18}O$ from 5 to 9 ‰, and $\delta D$ from about –20 to –80‰) (Table 7.4, Sections 7.4.3 and 7.4.4). Additional silica may be liberated from alteration products by way of feldspar hydrolysis reactions such as:

$$\underset{\text{K-feldspar}}{KAlSi_3O_8} + 2H^+ = \underset{\text{muscovite}}{KAl_2Si_3O_{10}(OH)_2} + \underset{\text{quartz}}{6SiO_2} + 2K^+ \qquad \text{(Equation 9.2)}$$

At Belo Brdo, the intensity of alteration decreases from intense sericitic and less advanced argillic to weaker and wider propylitic (Section 4.4). *Intermediate argillic* alteration of andesites is characterised by clay-bearing assemblages formed by hydrolytic alteration that typically forms at a lower temperature than sericitic alteration and at relatively low pH. In this alteration, clay minerals replace plagioclase and ferromagnesian minerals are replaced by chlorite and pyrite. *Propylitic alteration* refers to alteration of igneous rocks by hydration, carbonation, oxidation, and locally sulphidation reactions to form assemblages rich in hydrous minerals and containing minor carbonate (Robb, 2005). Typical assemblages at Belo Brdo contain epidote, chlorite, and minor pyrite. Preliminary chlorite mineral analyses were conducted on chlorite associated with propylitic alteration. On the basis of the chlorite geothermometer proposed by Cathelineau (1988), it was calculated that propylitic alteration assemblages formed at temperatures around 260°C. Such spatial zonation of hydrothermal alteration is typical of intermediate to shallow environments where cooling, acidic hydrothermal fluids, exsolved from metaluminous magma (or from magma with high K/Na), produce at depth higher- temperature sericitic alteration, overlain by lower temperature argillic and propylitic alterations (Hemley et al., 1980).

Tourmaline compositions in Belo Brdo are also good indicators of externally derived hydrothermal fluids (Section 4.4.2). Mineral chemistry data distinguish tourmalines from quartz-tourmaline listwanitic breccias and quartz-tourmaline veins associated with phyllic alteration of andesites. Tourmalines from the quartz-tourmaline veins are essentially dravite-schorl in their composition, whereas quartz-tourmaline listwanitic breccias contain both dravite-schorl and uvite-dravite, although dravite-schorl is more abundant. Vein-hosted tourmalines are notably higher in $Al_2O_3$, and $Na_2O$, and lower in CaO, relative to tourmalines from the breccia. Furthermore, tourmalines from quartz-tourmaline listwanitic breccias are characterised by high $Cr_2O_3$ contents (up to 3.2%) and are also associated with Cr-mica and pyrite. The chemical characteristics of tourmalines relate most likely to differences in host rock chemistry. The composition of Cr-bearing tourmaline is affected by the composition of the listwanitic breccias, which are the most likely source for Mg, Ca and Cr, whereas Si, Fe, Al, Na and B have been introduced by hydrothermal fluids. The hydrothermal origin of tourmalines is also evident by their association with quartz, mica, ± Cr-mica and pyrite in both, quartz-tourmaline veins and quartz-tourmaline listwanitic breccias. This is further supported by sulphur isotopic characteristics of pyrite associated with tourmaline in quartz-tourmaline listwanitic breccias, where sulphur isotopic values of pyrite show strong magmatic signatures (3.2‰) (Table 7.1 Section 7.2.4.1).

#### *9.4.1.3 Summary*

- Massive listwanites were formed through K-metasomatism of serpentinised harzburgites by acidic, $SiO_2$- and K-rich hydrothermal fluids.
- There is robust stable isotope evidence that the fluids responsible for early alteration and Ni-Co-As, Cu, ± Bi-Te sulphide precipitation have hydrothermal characteristics, albeit derived from a magmatic source.
- The main evidence for the magmatic component is: (1) moderately high temperature (~420°C) of the quartz-sericite alteration and magmatic $\delta^{18}O$ values for fluid in equilibrium with sericite and quartz; (2) magmatic $\delta D$ value for fluid in equilibrium with sericite; (3) magmatic $\delta^{18}O$ and $\delta D$ values of fluid in equilibrium with tourmaline; (4) magmatic $\delta^{13}C$ value of carbon in silicified listwanite; and (5) magmatic $\delta^{34}S$ values of pyrite hosted by andesites and massive listwanite.

### *9.4.2 Main-ore stage*

#### *9.4.2.1 Introduction*

The pre-ore stage hydrothermal alteration patterns, together with the main-stage sulphide paragenetic and mineral chemistry data, provide insights into general features of the hydrothermal fluids that formed the Belo Brdo deposit. Based on the criteria in Sillitoe and Hedenquist (2003), Belo Brdo can be described as an intermediate-sulphidation base-metal deposit, similar to those formed in transitional porphyry to epithermal environments (Figure 9.2). Sulphidation state refers to the oxidation state of sulphur (i.e. -2, 0, +2, +4 or +6) in hypogene sulphide assemblages (Hedenquist, 1987; Hedenquist et al., 2000; Sillitoe and Hedenquist, 2003). Based on the sulphidation state, three main types of epithermal deposits have been recognised: high-sulphidation (HS; $S^{4+}$ or $S^{6+}$); intermediate-sulphidation (IS; $S^{2+}$); and low-sulphidation (LS; S or $S^{2-}$) (Hedenquist et al., 2000; Sillitoe and Hedenquist, 2003).

End-member HS deposits are represented by pyrite-enargite-luzonite-famatinite-covellite sulphide assemblages, whereas end-member LS deposits are characterised by pyrite-pyrrhotite-arsenopyrite and Fe-rich sphalerite sulphide assemblages (Figure 9.2; Hedenquist et al. 2000; Einaudi et al., 2003).

**Figure 9.2:** $fS_2$-T diagram showing the variety of sulphide assemblages in epithermal deposits that reflect sulphidation state, from very low and low through intermediate to high and very high. Compositional fields of arc volcanic rocks, high-temperature volcanic fumaroles, magmatic-hydrothermal fluids, and geothermal fluids are shown (From Sillitoe and Hedenquist, 2003 after Einaudi et al., 2003). The red line indicates the compositional field of the main-ore stage in carbonate-replacement ore-body in Belo Brdo; formation temperatures and sulphur fugacity calculated by arsenopyrite and sphalerite geothermometry.

Intermediate-sulphidation deposits display intermediate sulphidation-state assemblages comprised of pyrite-tetrahedrite/ tennantite-chalcopyrite and sphalerite with variable FeS contents (1-20 mol %.). IS epithermal deposits mostly occur in andesitic-dacitic arc environments, but do not often show a close relationship with porphyry Cu deposits as do many of the HS deposits (Sillitoe & Hedenquist, 2003).

### *9.4.2.2 Mineralisation*

Ore textures in Belo Brdo indicate that replacement is the dominant process in the formation of sulphide mineralisation. Paragenetic studies have identified two sub-stages of the main stage mineralisation. An early stage is represented by sphalerite, galena, As-rich pyrite and arsenopyrite. A later, polymetallic mineralisation is characterised by the introduction of Cu-bearing phases, such as chalcopyrite, bornonite and Ag-bearing tetrahedrite-tennantite, in addition to sphalerite, galena, pyrite and arsenopyrite. Three main compositional populations of sphalerite have been identified. The most commonly occurring type is the Fe-rich variety with an average 17.5 mol.% FeS. Fe-rich sphalerite occurs throughout the main stage of mineralisation, including an earlier paragenesis with pyrite, arsenopyrite and galena in the carbonate-hosted ore body, as well as a later paragenesis in the vein ore body. The other two varieties have distinctly lower FeS contents with average values of 8.5 and 1 mol.%, respectively. The Fe-poor sphalerite is associated with late Cu-bearing sulphides. Sphalerite compositions in Belo Brdo are typical of intermediate-sulphidation states. Fluctuations in the FeS content of sphalerite may be caused by intermittent events such as boiling, local wall rock interaction, or by pulses of reduced fluids of magmatic and non-magmatic origin (Barton et al., 1977; Bethke and Rye, 1979). In Belo Brdo boiling was not observed in quartz samples syngenetic with main-ore sulphides. It is more likely that water-rock interaction and influx of new hydrothermal fluids may have caused such variability in sulphidation states.

Pyrite in the main-ore stage contains high As concentrations (up to 8 wt. %) and often exhibits usually oscillatory zoning defined by variations in As content. It contains variable concentrations of Ni and Co, although consistently lower than those of the pre-ore stage pyrite. Generally, the most common elements that can be incorporated into the pyrite lattice are As, Co and Ni. Mechanisms that can cause compositional changes in naturally zoned crystals include large-scale physical and chemical changes within the hydrothermal system (temperature, $fO_2$, fluid chemistry) that are independent of local crystallisation, or crystal growth can also be controlled by local, intrinsic phenomena, such as growth rate, solute diffusion through the crystal-fluid boundary layer, etc. (Shore and Fowler 1996). Pyrite in main-ore stage is locally auriferous.

The main-ore stage arsenopyrite is homogeneous and contains no significant amounts of Ni compared to the pre-ore stage, compositionally zoned arsenopyrite with respect to Ni content (up to 6 wt.%). The later stage of ore deposition is characterised by galena-pyrite-chalcopyrite- mineral assemblage followed by tennantite-tetrahedrite series minerals and bournonite. Tetrahedrite-tennantite is main carrier of Ag.

### *9.4.2.3 Ore-forming conditions*

Sulphidation state, referenced to stability fields of sulphide mineral assemblages as a function of log $fS_2$ and temperature, has been used to depict the ore-forming environment of the main sulphide-stage of the carbonate-replacement ore-body in the Belo Brdo deposit (Figure 9.2). In this study, sulphide mineral assemblages were used as a tool to provide information about the formation temperature, as it was not possible to find fluid inclusions for microthermometery in sphalerite, due to its opaque nature. Temperature estimates were obtained using arsenopyrite and sphalerite geothermometry.

Arsenopyrite is the most refractory of the common sulphides and has received considerable attention as a geothermometer for estimating the physicochemical conditions of ore deposits (Kretschmar and Scott, 1976). Arsenopyrite composition depends largely on temperature, sulphur fugacity and, to a lesser extent, pressure. However, the successful application of the arsenopyrite geothermometer is only possible where arsenopyrite, sphalerite, löllingite and iron sulphides are deposited under equilibrium conditions, and where the arsenopyrite composition does not change during subsequent processes. Equilibrium compositions of arsenopyrite are usually preserved in hydrothermal deposits that have undergone relatively rapid cooling, and their compositions are not typically subject to change during subsequent processes. Arsenopyrite co-existing with pyrite has As contents between 29.4 and 31.5 with a mean value of 30.05 atom.%., corresponding to formation temperatures between 311 and 348°C (see Section 4.6.3.1.) and logarithm of $fS_2$ between -8.3 and -10.5 (Fig. 4.18, Section 4.6.3.1). Arsenopyrite with lower arsenic content (27.2-27.9 atom.%) is recorded in one sample, where arsenopyrite occurs at a later stage of main-ore deposition, associated with more homogeneous pyrite. Because arsenopyrite is a refractory mineral it is unlikely that changed conditions would modify composition of already deposited arsenopyrite. Therefore, it is likely that As-depleted arsenopyrite represents lower-temperature, younger generation of sulphides. Equally, the very high As contents (32.5 to 33.9 atom.%) of some of the pre-ore stage arsenopyrite may be interpreted as a sign of high-temperature deposition of sulphides (>400°C). Therefore, arsenopyrite geothermometry indicates cooling of the hydrothermal system from >400°C in the pre-ore stage, to less than 300°C at the end of main-ore stage (Section 4.6.3). This is consistent with gersdorffite geothermometry data discussed previously.

The FeS content in sphalerite has been identified as a sensitive indicator of sulphur fugacity during ore precipitation (Barton and Toulmin, 1966). A $\log fS_2$–temperature (1000/K) composition diagram has been constructed by Lusk and Calder (2004) for a sequence of buffer reactions in the Cu–Fe–S and Fe–S systems. The equation:

$$\log_{10} fS_2 = 11.01 - 9.49(1000/K) + [0.187 - 0.252(1000/K)](\text{mol.\%FeS}) + [0.35 - 0.2(1000/K)](\text{mol.\% CuS in sphalerite}) \qquad \text{(Equation 9.3)}$$

can be applied to sphalerite that has equilibrated with buffer assemblages containing pyrite, or pyrite and pyrrhotite, in both the Fe-Zn-S and Cu-Fe-Zn-S systems at temperatures between 250 and 550°C at 1 bar (Lusk and Calder, 2004). In this study, sphalerite with mean composition of 18 mol.% FeS and CuS compositions between 0.009 and 0.12 mol.% CuS, was used to estimate formation temperatures, taking into consideration the sulphur fugacity of $10^{-8.3}$ and $\sim 10^{-10.5}$ obtained from arsenopyrite geothermometry. The calculated formation temperatures range between 290 and 350°C (Fig. 4.20, Section 4.6.5). This calculated temperature corresponds well to that deduced from arsenopyrite geothermometer (T = 311 - 348°C).

### *9.4.2.4 Characteristics of ore-forming fluids and sulphide precipitation*

Assuming that chloride complexes are responsible for metal transport, deposition of sulphides (Barnes, 1979) can be expressed as:

$$MeCl_2 + H_2S \rightarrow MeS + 2H^+ + 2Cl^-, \qquad \text{(Equation 9.3)},$$

where pH decreases in response to sulphide mineral precipitation, which yields $H^+$. Consequently, deposition of sulphides could result from (1) an increase in pH, (2) an increase in the concentration of $H_2S$ and (3) a decrease in the concentration of $Cl^-$. The pH increase, liberating sulphide from $H_2S$ or $HS^-$ to precipitate in sulphide minerals is one of the most common causes of sulphide precipitation. For example, under acidic conditions, galena is highly soluble as $PbCl_2$ and $PbCl_4^{2}$. The large galena solubility reflects the displacement of the following equilibrium equation to the right by a large $H^+$ activity at low pH:

$$PbS_{(galena)} + H^+_{(aq)} + 4Cl^-_{(aq)} = PbCl_4^{2-}{}_{(aq)} + HS^-_{(aq)} \qquad \text{(Equation 9.4)}$$

As pH increases equation 9.4 is driven to the left and essentially all aqueous Pb precipitates in galena as pH rises. The same basic characteristics of sulphide solubility apply to sphalerite and chalcopyrite. Deposits that form in this way clearly include all types of skarns, manto-type lead-zinc deposits and disseminated chalcopyrite in sericitised feldspar sites in alteration envelopes of veins related to porphyry copper deposits (Reed and Palandri, 2006). Sulphides such as sphalerite, galena and chalcopyrite precipitate in altered wall-rocks as feldspars or carbonates neutralise acid, metal-bearing fluid. The pH can also increase where a hydrothermal fluid boils out $CO_2$ to the gas phase, or where brine is diluted by fresh water.

In general, deposition of sulphides can also result from chemical reduction or cooling. Cooling can result either from dilution by cold water mixing or from heat conduction into cold wall rocks (Reed and Palandri, 2006). Cooling by mixing of hotter magmatic fluid with cold non-magmatic (meteoric) waters is seen in many porphyry-related epithermal precious and base metal deposits.

Fluid inclusion data from Belo Brdo suggest precipitation from low- to moderate salinity fluids (1.82-13.9wt.% equiv. NaCl) with predominantly Na-chloride composition (±Ca; ±Fe) (Section 6.5). Bulk fluid properties ($\rho = 0.86$ g/cm$^3$ for quartz) were calculated after the equation of state proposed by Zhang and Frantz (1987). Homogenisation temperatures of all analysed inclusions range between 189 and 341°C, with an average temperature of 251°C (Table 6.2, Section 6.5.1). However, the main-ore stage quartz exhibits higher homogenisation temperatures, which range from 220°C to 341°C with a mean at 299°C. These temperatures are consistent with those obtained by arsenopyrite geothermometry from the massive sulphide ore of the main mineralisation stage. Quartz from later stage main-ore breccia has lower homogenisation temperatures between 189 and 277°C with a mean at 218°C, whereas fluid inclusions from the late- to post-stage ore show even lower homogenisation temperatures (165-265°C) and salinities (1.82-8.19wt.% equiv. NaCl). Since homogenisation temperatures represent minimum trapping conditions and phase separation was not observed in quartz from main-ore stage, formation conditions were estimated from isochors intersected by temperatures calculated from arsenopyrite and sphalerite CuS geothermometers discussed above. The trapping pressures for the Belo Brdo deposit were between 1419 and 521 bars (Fig.6 9, Section 6.5.3) and imply depths of between 5 and 1.7 km under lithostatic conditions, taking into account a rock density of 2.5 g cm$^{-3}$. The presence of hydrothermal breccias in the deposit and the presence of vapour-rich inclusions in one sample, which unfortunately was not analysed here by microthermometry, indicate the possibility that pressure-temperature conditions were close to the liquid-vapour two phase curve. This would in turn indicate a hydrostatic pressure regime and trapping temperatures of between 50 and 120 bars. However, it is difficult to be more precise regarding the formation depth of the Belo Brdo mineralisation because of the lack of precise knowledge of the fluid pressure regime.

Decreases in both, homogenisation temperature and salinity from the main-ore stage to the late-ore stage indicates influence of cold, diluted meteoric waters. The correlation between homogenisation temperature and salinity (Fig. 6.8 Section 6.5.2) suggests that *cooling due to mixing with cold meteoric water* is an important process that may have contributed to sulphide precipitation. Fluid mixing is also indicated by $\delta^{18}O$ and $\delta D$ signatures of fluid inclusion water (Figure 7.5, Section 7.4.4) and $\delta^{13}C$- $\delta^{18}O$ signatures of different carbonate generations (Figure 7.3, Section 7.3.3). Calculated oxygen isotopic composition of water in equilibrium with quartz associated with massive sulphides is consistent with the ore fluids being derived from the magmatic source (5.9 to 7.7‰), whereas calculated isotopic composition of water in equilibrium with quartz from the ore breccia and late-ore stage show depletion in both oxygen and hydrogen values ($\delta^{18}O$ = 4.8 to 2.3 ‰ and $\delta D$ = -93 to -96 ‰), indicating influence of meteoric waters.

The carbon and oxygen isotopic compositions of several carbonate generations from the Belo Brdo deposit show a general tendency toward decreasing $\delta^{18}O$ and increasing $\delta^{13}C$ from pre-ore to post-ore stage carbonates of Belo Brdo. The lower $\delta^{13}C$ values (~-4‰) indicate a contribution of magmatic carbon, whereas the late-stage dolomite $\delta^{13}C$ values lie close to the field of marine limestones.

Sr isotope composition of hydrothermal carbonates from the carbonate-replacement mineralisation of the Belo Brdo deposit have intermediate values between those of the Tertiary magmatic rocks and Cretaceous sediments on one hand and the Jurassic serpentinite and listwanites on the other, indicating a contribution of Sr from those rocks.

REE geochemistry data clearly indicate that the REE distribution pattern for non-mineralised Cretaceous limestones reflects a marine environment, as they are characterised by negative $Eu_N$ and $Ce_N$ anomalies (Fig. 4.24, Section 4.8). Most of the other analysed carbonates show a positive $Eu_N$ anomaly and display no /or weak negative $Ce_N$ anomaly, which could be inherited from the primary carbonate sediments. The REE characteristics of hydrothermal carbonates are controlled by the composition of the fluid and physicochemical conditions during precipitation. The positive Eu anomalies directly reflect the $Eu^{2+}/Eu^{3+}$ ratio in the mineralising fluid (e.g. Zhong and Mucci, 1995). The $Eu^{2+}/Eu^{3+}$ ratio in a rock-buffered fluid is strongly dependent on temperature, and $Eu^{2+}/Eu^{3+}$ equilibrium is established at around 250°C (Bau & Möller, 1992). Therefore positive Eu anomalies are typical for carbonate precipitated at temperatures above 250°C and under at least mildly reducing conditions. Oxidising fluids will exhibit a negative Ce-anomaly, which is a typical feature of marine water (Hu et. al, 1988). Due to oxidising conditions in seawater, $Ce^{3+}$ is oxidised to $Ce^{4+}$ which is less mobile resulting in Ce depletion of the seawater itself. Therefore marine water commonly possesses a negative Ce anomaly (Elderfield and Greaves, 1982; de Baar et al., 1985), which is then inherited by carbonates formed in a marine environment.

Distinct positive $Eu_N$ anomalies in syn-ore dolomites and ankerites are typical of reducing, acidic, high temperature fluids (Bau and Möller, 1991), commonly of metamorphic or magmatic origin (McLennan, 1989).

*Neutralisation of acid fluids* with strong magmatic signatures may represent a second possible process for sulphide precipitation. This process could have taken place as acidic metalliferous fluids associated with calc-alkaline metaluminous magma entered the carbonate succession of the Upper Cretaceous Flysch Unit as well as listwanites. The rapid change of pH as a result of carbonate dissolution and buffering to mildly alkaline conditions could have triggered or at least contributed to sulphide precipitation (Seward and Barnes, 1997).

### *9.4.2.5 Source of sulphur*

The most important tool for tracing the source of S involved in ore formation at Belo Brdo are $\delta^{34}S$ studies of sulphide ore minerals (Section 7.2.4). The relatively low and uniform isotopic sulphur compositions of all main-ore sulphides (3.4-5.4‰; average 4.4‰) is consistent with an igneous source (0 ±5‰), with sulphur derived directly from magmas or by the remobilisation of sulphur from igneous rocks (Ohmoto and Rye 1979; Ohmoto and Goldhaber, 1997). As no sulphate minerals have been observed in the carbonate-replacement ore-body of the Belo Brdo deposit, a reduced, $H_2S$ dominated hydrothermal system can be inferred for the deposition of sulphides. Additionally, under the physical and chemical conditions illustrated for the main-ore stage of Belo Brdo ($T<350°C$, low pH and Eh), the major sulphur species would be $H_2S$. The $\delta^{34}S$ values of sulphides deposited in an environment where $H_2S$ is presumed to be the main sulphur species in the fluid are generally close to the $\delta^{34}S$ values of the fluid (Ohmoto and Rye 1979). In this study, the $\delta^{34}S$ value of $H_2S$ in equilibrium with sulphides was calculated from the $\delta^{34}S$ value of sulphide minerals and the mineral-$H_2S$ fractionation factor of Ohmoto and Rye (1979) for pyrite and sphalerite, and of Li and Liu (2006) for galena. Calculated $\delta^{34}S$ composition of $H_2S$ in equilibrium with main-ore sulphides is 4.7‰, which suggests a magmatic sulphur source (Section 7.2.4) (Ohmoto and Rye 1979).

A possible cause for $H_2S$ sulphur is the dissociation of $SO_2$. At high temperatures, magmatic-hydrothermal fluids have $SO_2$ greater than $H_2S$ (Einaudi et al., 2003; Field et al., 2005; Chambefort et al., 2008). As the magmatic-hydrothermal fluid cools, the sulphur dioxide disproportionate by reaction with water (Holland, 1965):

$$4SO_2 + 4H_2O = 3H_2SO_4 + 1H_2S = 3HSO_4^- + 3H^+ + H_2S \qquad \text{(Equation 9.5)}$$

The hydrogen sulphide produced by this reaction allows precipitation of galena, sphalerite and chalcopyrite. Ohmoto and Rye (1979) pointed out that this reaction favours $SO_2$ at 700°C, but on cooling to 400°C favours sulphuric acid and hydrogen sulphide. This reaction is also a function of pressure, such that hydrogen sulphide is produced at higher temperatures in deeper environments and lower temperatures in shallower environments (Field et al., 2005).

#### *9.4.2.6 Source of metals*

The lead isotopic compositions of galena from different mineralisation stages of the Belo Brdo carbonate-replacement ore body show little variation ($^{206}Pb/^{204}Pb$= 18.678 to 18.686, $^{207Pb}/^{204}Pb$= 15.674 to 15.677, and $^{208}Pb/^{204}Pb$ = 38.873 to 38.888), suggesting that fluids were well homogenised throughout the deposition of the carbonate-replacement mineralisation. The Pb isotope ratios are close to those of the Tertiary volcanic rocks, as well as the Cretaceous Flysch sediments. The strong similarity between the Pb isotope signature of Mesozoic flysch sediments and the local igneous rocks suggests a strong influence of the Mesozoic subducted sedimentary material and contamination of the mantle source. This implies a common source for both ore-galena and igneous rocks.

#### *9.4.2.7 Summary*

- Estimated formation temperatures using sphalerite with mean composition of 18 mol.% FeS and CuS compositions between 0.009 and 0.12 mol.% CuS, range between 290 and 350°C. Arsenopyrite geothermometry yielded formation temperatures between 311 and 348°C and sulphur fugacity ($fS_2$) of between $10^{-8.3}$ and ~$10^{-10.5}$ bar.
- Fluid inclusion data from the main-ore stage quartz suggest precipitation from low- to moderate salinity (1.82-13.9wt.% equiv. NaCl) and epithermal- to moderately high temperature (190- 341°C) fluids. The trapping pressures were between 1419 and 521 bars and imply depths of between 5 and 1.7 km under lithostatic conditions.
- Cooling by mixing of hotter, magmatic fluid with colder meteoric water is an important process that has contributed to sulphide precipitation. Calculated oxygen isotopic composition of the fluid responsible for the main-ore shows magmatic signatures (5.9 to 7.7‰), whereas calculated isotopic compositions of water responsible for sulphide precipitation in late ore breccia show depletion in both oxygen and hydrogen values ($\delta^{18}O$ = 4.8 to 2.3 ‰ and $\delta D$ = -93 to -96 ‰), indicating the influence of meteoric waters.
- The relatively low and uniform isotopic sulphur compositions for all main-ore stage sulphides (3.4-5.4‰; average 4.4‰) are consistent with an igneous source. The major sulphur species is $H_2S$. Calculated $\delta^{34}S$ composition of $H_2S$ in equilibrium with main-ore sulphides is 4.7‰, which suggests a magmatic sulphur source.
- The lead isotopic compositions of galena from different mineralisation stages of Belo Brdo deposit are homogeneous and similar to those of local calc-alkaline volcanic rocks, as well as the

Mesozoic flysch sediments, indicating contamination of the mantle source by subducted sediments and a genetic link between mineralisation and magma.

### *9.4.3 Post-ore stage*

The late mineral assemblages consist of quartz-dolomite cavity fillings as well as quartz-dolomite-pyrite veins crosscutting and replacing mineral assemblages from earlier stages. Homogenisation temperatures of two-phase aqueous fluid inclusions from the late-stage quartz crystals range from 165 to 265 °C with a mean of 216 °C. Salinities range from 1.8 to 8.1wt.% equiv. NaCl with a mean of 5.7 wt.% equiv. NaCl. The fluid salinity is much lower compared to the fluid inclusions from quartz in the main-ore stage, indicating that fluids were significantly diluted during the late stage of mineral deposition. The isotopic composition of water extracted directly from fluid inclusions hosted by late-stage quartz shows depletion in both oxygen and hydrogen values ($\delta\,^{18}O$ = 2.3 to 4.8‰ and δD = -93 to -96‰), reflecting the increased influence of meteoric waters during the waning stage of magmatic-hydrothermal activity.

Besides the listwanites, the Cretaceous shallow marine limestones are the host rocks of the replacement orebodies and have $\delta^{13}C$ values (2.7-3.5‰) and $\delta^{18}O$ values (25.4–27.7‰) typical of world-wide Cretaceous marine carbonate values (Veizer and Hoefs, 1976). Hydrothermal late-stage vein Ca-Mg-Fe carbonates that cross-cut altered serpentinites have $\delta^{13}C$ values (-4.4 to -0.95‰) and $\delta^{18}O$ values (13–14.5‰) that differ significantly from the $\delta^{13}C$ and $\delta^{18}O$ values of limestones. The lower $\delta^{13}C$ values indicate a stronger contribution of magmatic carbon. In contrast, late stage dolomites, which fill small cavities have the same carbon isotope signatures as unaltered host limestones ($\delta^{13}C$ = 2.4 to 4.4‰), suggesting that unaltered limestones are probably the source of carbon. Their oxygen isotope values however are much lower than those of unaltered limestones, and almost identical to those of syn-ore stage, reflecting interaction of hot hydrothermal fluids with the Upper Cretaceous Flysch Unit.

The slightly higher $\delta^{34}S$ values of 4.5 – 6‰ for late-stage pyrite and sulphides from late-stage vein mineralisation that crosscuts Cretaceous sediments and from those hosted in carbonate breccias might be a consequence of the ore fluid interacting with an external, isotopically more positive sulphur sourced from country rocks (Ohmoto and Goldhaber, 1997).

The data obtained by this study clearly suggest that Belo Brdo carbonate-replacement deposit formed from epithermal- to moderately-high temperatures (160-350 °C), low- to moderate- salinity aqueous fluids with strong magmatic signatures during the main-stage of ore deposition and with an increasingly significant involvement of meteoric waters during late-stage evolution.

## 9.5 Some comparisons with Mississippi-Valley-type (MVT) ores and high temperature carbonate-hosted Pb-Zn deposits

This study demonstrates that the Belo Brdo carbonate-replacement Pb-Zn (Ag) deposit contrasts sharply with those of MVT Pb-Zn deposits and exhibits similarities with the high temperature massive sulphide carbonate-hosted replacement ores of the North American Cordillera (Titley, 1996) and Northern Mexico (Megaw et al., 1988). The common features of both ore types are the epigenetic origin for the Pb-Zn ores that were deposited by hydrothermal solutions as replacements of the host rock, typically limestone or dolomite. They commonly form stratabound and stratiform massive sulphide orebodies containing Pb, Zn, Cu, ±Ag, ±Au and almost completely replace the carbonate host. The form and size of the ore-bodies are determined by structural and stratigraphic controls that localise the permeability of the ore-bearing fluids. The major differences between MVT and high temperature carbonate-replacement Pb-Zn (Ag) deposits, including Belo Brdo, are in their geotectonic setting and the characteristics of ore-forming fluids. MVT deposits are formed from low temperature (< 200°C) basinal brines. They are the product of regional to sub-continental-scale gravity driven fluid flow that led to ore precipitation typically in dolostone and limestone of stable, only weakly deformed carbonate platforms (Sverjensky, 1986). Large-scale fluid flow is commonly correlated with tectonic compression and uplift in the hinterland of the deposits (Leach et al., 2001). The majority of MVT deposits formed during periods of intense tectonic activity that occurred during the assimilation of Pangea in the Devonian to Permian time, as well as during a time of microplate assimilation along the western margin of North America and Africa-Eurasia during the Cretaceous to Tertiary (Leach et al., 2001). The MVT deposits are relatively poor in Ag and Fe.

In contrast, the high-temperature, carbonate-hosted Pb-Zn-Ag (±Cu; ±Au) deposits of western North America and Mexico are found in orogenic environments and are formed by high temperature (200-450°C) ore fluids. They often form mantos (tabular or cylindrical flatlying layers), pipes, and irregular and branching ore bodies. Ore systems are enriched in iron and silver and often exhibit zoned complex mineral assemblages. Metal sources are mixed, and range from magmatic to wall-rock or crustal sources. Some well known high temperature Pb-Zn deposits include Cerro de Pasco in Peru, Parana and Sao Paulo in Brazil, Tintic in Utah, Gilman and Leadville in Colorado, and Tsumeb in Namibia (Titley, 1996).

Similarities between Belo Brdo and the high-temperature, carbonate-hosted Pb-Zn-Ag (Cu) deposits of northern Mexico are seen in the structural control, the host-rock characteristics, and the sulphide mineralogy. The Mexican deposits occur in carbonate-dominant Jurassic-Cretaceous sedimentary sequences on the margins of a major fold-thrust zone. Silicic and intermediate volcanic and intrusive rocks of Tertiary age are associated with most of these deposits. Orebodies are represented by mantos, chimneys, and pods and are composed of massive sulphides and/or calc-silicate skarn (Megaw, 1988). The deposits commonly reveal strong structural controls and are stratigraphically discordant. Structural controls include intrusive contacts, faults, fold axes, fractures, fissures, and cavern zones. Intrusive contacts and intrusion-related faults are most important in the skarns, whereas regional fault, fold, and fracture systems are dominant controls on mantos and chimneys. Mineralisation commonly occurs below relatively impermeable shaly units, sills or volcanic rocks, although some extensive orebodies are restricted to specific horizons within apparently homogeneous carbonate successions. Zones of enhanced porosity and permeability induced by recrystallisation, heating, deformation, or hydrothermal dolomitisation are important controls of mineralisation. Fluid inclusion data indicate temperatures in the range 200-500 °C and salinities ranging from 1 to 60 wt.% equiv NaCl (Titley, 1996; Meinert, 2007). The hotter, more saline, solutions are typically from skarn zones. Evidence for boiling has not been reported. Stable isotope data for these deposits are sparse but show wide diversity and indicate mixing of magmatic and meteoric fluids (Megaw, 1988). The variety of mineralisation styles reflects variations in intrusive associations, depth of emplacement, host-rock characteristics, and geochemical evolution of the individual systems.

The major difference between Belo Brdo and the Mexican high temperature carbonate-hosted Pb-Zn (Ag) deposits is in its geotectonic setting within an ophiolite suture zone. The host lithologies, including ultramafic rocks, played an important role in the evolution of the varied ore mineralogy, and in the host rock alteration. The pre-ore evolution and the listwanite host rock, as well as Ni-Co and Cr enrichment is a result of the ophiolite influence. The alteration of andesitic-dacitic rocks is similar to those of porphyry copper deposits.

## 9.6 Comparison with other Pb-Zn deposits in the Kopaonik metallogenic district

Several Pb-Zn (Ag) veins, carbonate-replacement, skarn and stockwork deposits occur in the Kopaonik metallogenic district (Forgan, 1948; Schumacher, 1954; Jankovic, 1990). The deposits are related to Oligocene-Miocene post-collisional calc-alkaline volcanism as demonstrated by this study and two recently completed PhD research projects that focused on P-T-X formation conditions of the Crnac (Borojević-Šostarić, 2009) and Trepca Pb-Zn (Strmić-Palinkaš, 2009) deposits. Here, a brief summary of the Crnac and Trepca deposits are presented. The two deposits are than compared with the Belo Brdo deposit.

*The Crnac Pb-Zn (Ag)* deposit (Borojević-Šostarić, 2009) is located some 30 km southwest from Belo Brdo and 1.5 km northeast from the Karavansalija Cu-Au skarn mineralisation (Fig. 2.13, Section 2.6). Crnac is worked as an underground mine with total reserves of 4.4 Mt at 10% Pb, 4% Zn, and 100 - 150 g/t Ag and consists of a series of steeply dipping massive sulphide ore veins, 1 to 5 m thick. The veins are hosted by Jurassic amphibolites, which represent an amphibolite facies metamorphic sole of the Western Vardar zone, obducted 170.4± 1.2 - 164.9± 1.3 Ma ago and overlain by serpentinites of the same age (Borojevic-Sostaric, 2009). Additional irregular lenses and pods are hosted by listwanites, a common feature that Crnac shares with Belo

Brdo. Listwanite mineralisation occurs at the contact between amphibolites and overlying serpentinites. Intense volcanic activity produced shoshonitic and high-K calc-alkaline volcanic rocks and lasted from 32.4± 1.0 – 27.4± 0.3 Ma. The whole lithological sequence was intruded by the swarm of Tertiary, post-collisional quartz-latite dykes. Intrusion of the porphyry dykes generated NaCl– $H_2O$ rich magmatic fluids with temperatures of 280-400°C, salinities of 2–36wt.% equiv. NaCl. Fluids caused propylitic, potassic and sericitic-kaolinitic alteration of dykes and amphibolite hosts, dated at 28.6± 0.5 Ma. Similarly to Belo Brdo, pre- and syn- ore stage mineralisation (pyrite-arsenopyrite-quartz-kaolinite and galena-sphalerite-chalcopyrite respectively) are characterised by the introduction of low pH-high temperature-low salinity fluids of dominantly magmatic origin, and simple composition (Na-K-Cl). Late-stage mineralisation, represented by carbonates and subordinate galena and pyrite are precipitated from neutral fluids of more complex composition (Ca-Na-K-Cl-$CO_2$) with an increased influence of meteoric waters. Fluid inclusion data from quartz hosted by listwanite mineralisation reveal the presence of a high-temperature - low-salinity NaCl-$H_2O$ fluid (Th=249 - 324° C, 2.9 – 6.7 wt.% equiv. NaCl), similar to that seen in the Belo Brdo deposit.

The $\delta^{34}S$ values are also close to those of Belo Brdo and increase from the pre-mineralisation pyrite ($\delta^{34}S$ pyrite= 0.32 - 3.11‰), towards the major mineralisation stage sulphides ($\delta^{34}S$ galena=0.42 - 3.05‰; $\delta^{34}S$ sphalerite = 2.89 - 5.92‰). Generally the low $\delta^{34}S$ values indicate an influence of magmatic sulphur.

*The Pb-Zn-Ag Trepca* mineral deposit (Strmić-Palinkaš, 2009) is located around 40 km south from Belo Brdo. According to the ITT/UNMIK 2001 report, the potential ore reserve has been estimated at 29 million tons with grades varying from 3.40 to 3.45 % Pb, 2.23 to 2.36% Zn and 74 to 81 g/t Ag. Mineralisation is hosted by recrystallised Triassic limestone with a well developed palaeokarst, overlain by Triassic schists. The ore forming process is related to a phreatomagmatic eruption with a phreatomagmatic breccia developed at the contact between the host limestone and overlaying schist. The deposit is spatially and temporary related to post-collisional magmatism. The K/Ar and Ar/Ar dating of the breccia and associated igneous rocks suggest a Late Oligocene age (24.0 ± 0.7 to 25.1 ± 0.9 Ma). The mineralisation is represented by skarn and hydrothermal paragenesis as two end-member types. The skarns occur in the form of replacement of the recrystallised limestone, whereas hydrothermal mineralisation appears as replacements and as open-space fillings. Hedenbergite enriched in Mn represents the principal skarn mineral formed during the prograde stage under influence of Ca-Na-Cl fluids of magmatic origin. Formation temperature is between 380 and 500°C. The retrograde stage was initiated by phreatomagmatic explosions and formation of the breccia. The involvement of groundwater in the system increased oxygen fugacity and caused alteration of pyroxenes to ilvaite, magnetite, carbonates and quartz. The hydrothermal paragenesis comprises galena, sphalerite, pyrite, quartz and rhombohedral carbonates. Iron contents of sphalerite are higher than those of Belo Brdo and range from 17.6 and 22.5 mol% FeS, which represents a transition from low-sulphidation to an intermediate sulphidation state. The hydrothermal mineralisation is superimposed onto the skarn assemblages and was produced by mixing of magmatic fluids with the groundwaters under increased sulphur fugacity. Travertine deposition is related to very late stages of hydrothermal activity in the area.

Fluid inclusion studies were carried out on skarn (hedenbergite: Th=385-410°C, 14.8-16.5 wt.% NaCl equiv.), sulphide (sphalerite: Th=240-305°C, 8.0-14.6 wt.% NaCl equiv.) and gangue minerals (quartz: Th=295-355°C, 4.5-12.0 wt.% NaCl equiv.; carbonates: Th=295, 4.5-11.0 wt.% NaCl equiv.).

Stable isotope data for carbonate minerals point to the influence of magmatic fluids ($\delta^{13}C$ = -2.8 ‰; $\delta^{18}O$ = 12.5 ‰). The $\delta^{34}S$ values of the sulphides increase in the order galena (0.9 ± 2.3) $\leq$ chalcopyrite (2.9) $\leq$ pyrrhotite (3.1 ± 0.8) $\leq$ sphalerite (3.7 ± 1.6) $\leq$ pyrite (4.2 ± 2.8) and are consistent with a magmatic source of sulphur.

According to Strmić-Palinkaš (2009), the deposit can be classified as a high temperature carbonate-replacement/proximal calcic Pb-Zn-Ag skarn deposit as defined by Titley (1996) and Meinert (1992). However, it could also be considered as a polymetallic root of an eroded low-sulphidation epithermal-type system. An epithermal-style of mineralisation is also indicated by the presence of Mn-rich calcite (oligonite), together with rhodochrosite, silver and gold occurring in fractures and brecciated volcanic rocks (Féraud and Deschamps, 2009).

Despite the variations between ore types and host-rock characteristics, major similarities between the three deposits are seen in (1) fluid inclusion and stable isotope data; (2) structural controls and association with post-collisional calc-alkaline magmatism; and (3) the main sulphide mineral assemblages. It appears that the spectrum of mineralisation styles, shown by these three deposits represents different local responses to the same magmatic events. This could be largely a function of variation in host rock lithologies.

However, there are significant differences between the Pb-radiogenic values of ore-galena from the three deposits. The Pb isotopic ratios of galena from Trepca are the most radiogenic, whereas those from Crnac exhibit the least radiogenic signatures (Fig. 8.2, Section 8.2.2). Pb-radiogenic signatures of Crnac are similar to those of the Neogene Apuseni deposits in Romania, as well as Upper Cretaceous porphyry copper and massive sulphide deposits in the neighbouring region of Rhodopes, which are linked to subduction-related calc-alkaline magmatism (also known as 'banatitic') (Amov and Arnaudov 2000). Belo Brdo and nearby vein and stockwork polymetallic deposits exhibit Pb-isotope values that lie between those of Crnac and Trepca and show slightly higher crustal component signatures. Their Pb-radiogenic characteristics are close to those of the Baia Mare Neogene epithermal deposits in Romania (Marcoux, et al., 2002). It is not clear at this stage as to why there is such a difference in the Pb-radiogenic composition of the ore. One explanation is that ore-galena from Crnac deposit might be related to magma with minimal crustal contamination. Conversely, the compositional variation of the Trepca ore might be explained by significant contributions of Pb (and other metals) provided from the underlying metamorphic rocks. Therefore, variations in the isotopic signatures may also be due to a different basement lithology as well as to variations in crustal assimilation superimposed on variations in the igneous source composition.

Such variations in lead isotope compositions were also observed in the Cretaceous and Tertiary porphyry-type and epithermal-systems of Arizona, where magmatic, less radiogenic lead is exclusively present in major porphyry-type deposits located close to the parent pluton. Lead from more distal porphyry-type deposits and epithermal-systems is more radiogenic, reflecting an increased contribution of lead from regional rocks, acquired during widespread hydrothermal circulation (Bouse et al. 1999).

## 9.7 Brief comparison with other metallogenic zones within the Alpine-Balkan-Carpathian-Dinaride (ABCD) province and metallogenic implications

Generally, polymetallic mineralisation within the Kopaonik metallogenic district shares many common features with copper porphyry-epithermal systems and related Pb-Zn deposits located within the southern sectors of the Alpine-Balkan-Carpathian-Dinaride (ABCD) province (Fig.9.3).

The province includes well-known deposits such as: Buchim (Cu-Au porphyry), Kratovo, Zletovo (Pb-Zn-Ag volcanic hosted) in Macedonia, Skouries (Cu-Au-Ag porphyry) and Maronia (Cu-Au-Mo) in Greece, Madjarovo (Au-Ag-Pb-Zn hydrothermal veins) and Madan (Pb hydrothermal veins) in Bulgaria. The Kassandra mining district in Eastern Chalkidiki, Greece is one of many examples of a polymetallic area that hosts genetically linked porphyry copper, copper skarn and carbonate-hosted Pb-Zn (Ag, Au) ores within a large Tertiary magmatic- meteoric hydrothermal system related to the intrusion of quartz dioritic to granodioritic porphyries (Gilg, 1993). Some common features, which the Kopaonik deposits share with other polymetallic districts in the ABCD province, are as follows:

1) All the major deposits are intimately related to Oligocene-Miocene, mostly andesitic dacitic volcanic activity which lasted from 35-19 Ma. The magmatism is interpreted as collisional to post-collisional and is characterised by calc-alkaline, acidic, and in parts high-K volcano-intrusive complexes. The Pb-Zn deposits in the Kopaonik district are of same types as Pb-Zn-Ag deposits in the Madan and Laki ore districts of Bulgaria. In Bulgaria, the deposits comprise hydrothermal Pb–Zn veins, disseminated vein stockworks, and metasomatic replacements as the economically most important orebodies.

**Figure 9.3:** Simplified tectonic map displaying the distribution of major tectonic units and ore deposits in the Alpine-Balkan-Carpathian-Dinaride (ABCD) province (taken from Heinrich and Neubauer, 2002).

2) The mineralisation system of the Belo Brdo deposit exhibits some common characteristics of transitional intermediate-sulphidation copper porphyry-related deposits with respect to the main wall-rock alterations (sericitic, quartz-tourmaline, propylitic and intermediate argillic) and mineralisation style (pyrite, arsenopyrite, chalcopyrite, sphalerite, galena, Ag-rich tetrahedrite-tennantite, bornonite and minor Bi-Te mineralisation). Such a mineralisation style is common to many epithermal deposits across the ABCD province, including those in the Apuseni district of western Romania.

3) Listwanites occur in Bulgaria in the Central Srednogorie (Panagyurishte) Ore Region and in the Eastern Rhodopes (Laki Ore Field, Madan Ore Field) and are associated with Pb-Zn and gold mineralisation (Kunov, 2008).

4) Overall, the hydrothermal fluids at Belo Brdo, Crnac, Trepca and Karavansalija appear to be dominated by NaCl and are of low- to moderate salinity, epithermal- to moderately high temperatures, typical of those that form transitional porphyry-epithermal style mineralisation. They also have an isotopic composition similar to other, zoned polymetallic veins and epithermal precious-metal deposits in the ABCD province, including also deposits from the Carpathian chain such as at Baia Mare (Nedelcu et al. 1992; Cook and Damian 1997; Damian et al. 1998), Beregovo, Ukraine (Vityk et al. 1994) and Banska Stiavnica, Slovakia (Lexa et al. 1999). Most of these deposits show strong magmatic signatures in the early stages of ore precipitation with meteoric waters becoming dominant towards the later stages of ore deposits evolution.

At Belo Brdo, a moderate change from intermediate to low salinity and an associated decrease in temperature is interpreted as an effect of diluting fluids due to mixing of magmatic with meteoric water (Figure 6.8). Such a trend compares well with some of the known intermediate sulphidation Pb-*Zn*- *precious* metals deposits in the Madjarovo district, Bulgaria (Rice et al. 2007) and Tertiary precious and base metal deposits of western Romania (Alderton and Fallick 2009).

5) Sulphur isotope values of sulphides from all the studied deposits from the Kopaonik metallogenic district are similar to those of porphyry Cu-Mo deposits in Greece (Maronia; Melfos et al., 2002) and overlap with other porphyry copper, Pb-Zn and Sb-As vein deposits from the Lece-Chalkidiki metallogenic zone of Serbia, Macedonia and Greece (Serafimovski and Tasev, 2006), as well as with the Beregovo gold-silver-polymetallic deposit (Vityk et al., 1994).

The major difference between the Kopaonik deposits and those in Bulgaria, Romania and Greece is that in the Kopaonik district, typical epithermal end members of the magmatic-hydrothermal porphyry systems have not been discovered yet and presently the district lacks gold-rich deposits. The differences might result from a combination of several parameters such as (1) difference in magma composition, whereby gold-rich deposits tend to be associated with calc-alkaline magma with minimal crustal contamination, as in the Apuseni ore district or Upper Cretaceous part of ABCD belt; (2) a deeper present-day erosion level, as indicated by the presence of the large equigranular Kopaonik granodiorite pluton; (3) differences in host rocks and basement lithology are also apparent, with Belo Brdo and Crnac being dominated by ophiolites and Trepca by metamorphic and sedimentary sequences. It is clear that the polymetallic mineralisation of Belo Brdo, Crnac, Trepca, Rudnitza and Karavansalija formed at different stratigraphic levels (Triassic carbonates, Jurassic amphibolites, Cretaceous limestones and Tertiary volcanics) and were affected by different levels of erosion. As mentioned above, the Trepca deposit could be considered as an eroded epithermal low- sulphidation style system, whereas Crnac and Belo Brdo exhibit mineral characteristics similar to porphyry-related polymetallic deposits.

*Gold* in the Kopaonik metallogenic district was first reported by Titcomb et al., (1936) from the Trepca mine as traces in the Pb-Zn-Ag ore that could not be recovered. Schumacher (1950) reported grades <0.2g/t. Gold was reported by Djokic (in Janjusevic, 1974) as a by-product recovered from the lead smelter at Zvecani, together with indium and thallium. However, no other information exists regarding the mineralogy and type of occurrence. The GIS database compiled by Monthel et al., (2002) reports a total production of 8.7 t of gold between 1950 and 1985 from the Trepca deposit, which would indicate grades of 0.4 g/t Au in the ore. In recent years, gold has been reported from other deposits within the Kopaonik metallogenic district, such as: the Belo Brdo Pb-Zn (Ag) deposit, with 1-2.7 g/t Au (7t Au reserves with 1 g/t Au); Karavansalija Cu-Au skarn prospect (0.52 g/t Au over 113 m); Rudnitza Cu-Au porphyry prospect (0.37 g/t Au over 144m) as well as from deposits that have not been investigated by this study, such as: Novo Brdo Pb-Zn-Ag-Au deposit, with 3-4g/t Au (Figure 2.12; Section 2.6) and Lece Pb-Zn (Ag), with 2-6 g/t Au (Figure 2.12; Section 2.6); (Simić, 2000; Monthel, et al., 2002; Koželj, et a., 2007). These various occurrences of gold belong to several types of ore deposits including carbonate-replacement, skarn, porphyry, polymetallic veins and stockworks. However, they all probably belong to the same metallogenic events related to Oligocene magmatism and intersected by different levels of erosion.

It may therefore be that there remains scope for exploration for hitherto unrecognised epithermal precious metal deposits in the Kopaonik metallogenic district.

## 9.8 Summary of metallogenic characteristics indicating underlying porphyry system in the study area

Schematic representation of the spatial relationship between the alteration assemblages, mineralisation and igneous phases, indicating underlying porphyry system in the study area is shown in Figure 9.4.

Petrological and geochemical data presented here reveal that the Kopaonik magmatism exhibits many characteristics similar to that of oxidised and hydrous I-type metaluminous post-subduction- and collisional-related calc-alkaline magmatism associated with Cu-Au porphyry and related base-metal deposits worldwide (Richards, 2003; 2009; Einaudi et al., 2003).

The field work results, as well as petrological and mineral chemistry data, show that possibly three hydrothermal systems containing potassic, sericitic, propylitic and argillic alteration styles can be mapped in the study area. These systems display porphyry copper mineralisation in Rudnitza and Karavansalija and polymetallic mineralisation at Belo Brdo. Potassic alteration was responsible for the formation of listwanite (Figure 9.4). Intense iron oxide copper gold alteration and mineralisation occurs at Karavansalija and Rudnitza. Zones of intense hydrothermal alteration at the contacts of quartz-latite dykes and wall rocks, as well as pebble dyke brecciation and quartz-pyrite stockwork are present at Belo Brdo (Figure 9.4).

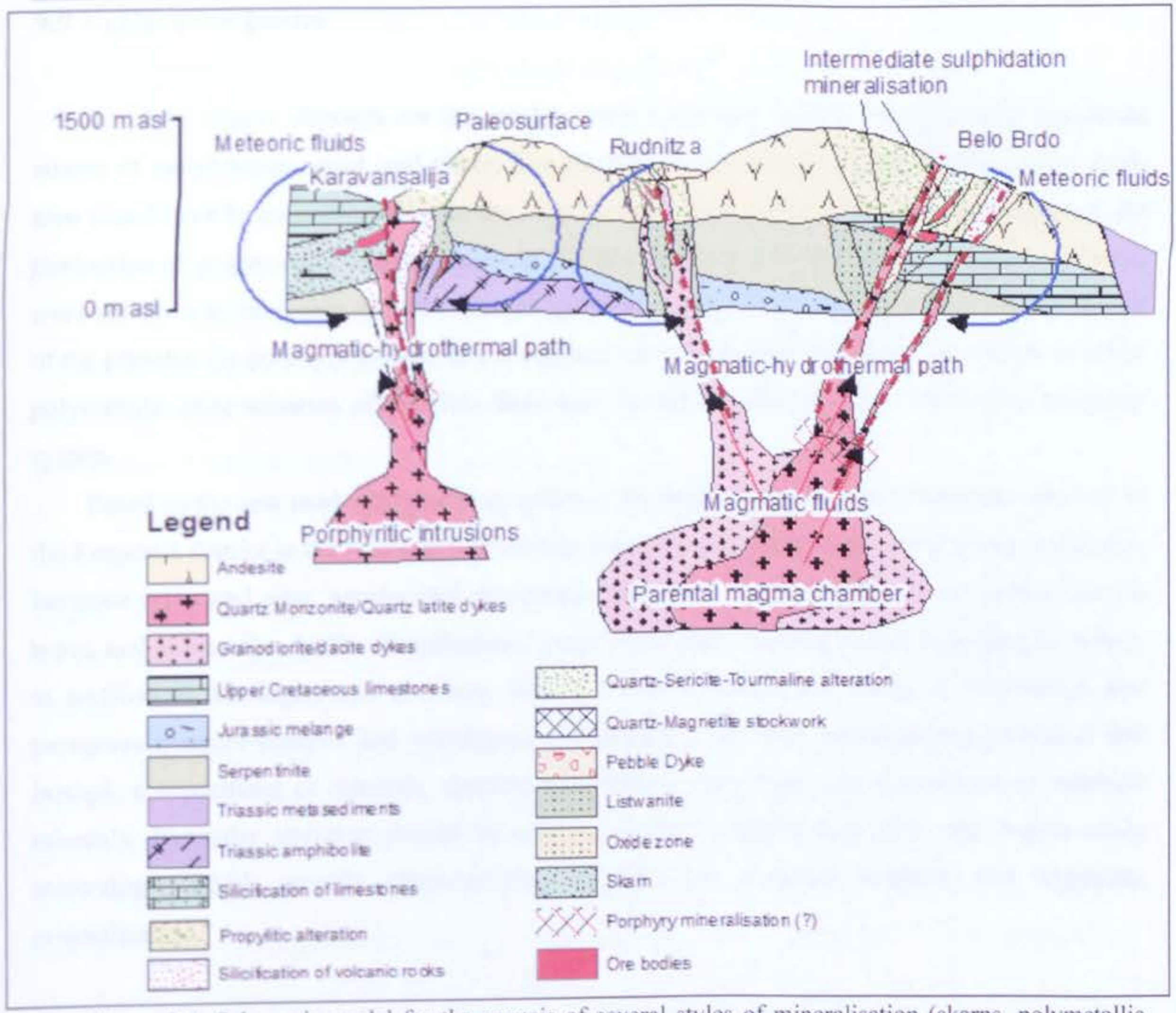

**Figure 9.4:** Schematic model for the genesis of several styles of mineralisation (skarns, polymetallic replacement, polymetallic intermediate sulphidation veins, and porphyry) in the study area.

The transitional magmatic-hydrothermal intermediate sulphidation type of polymetallic mineralisation, typical of those related to Cu porphyry deposits (Einaudi et al. 2003), is present at the Belo Brdo Pb-Zn, the Karavansalija Cu-Au skarn and the Rudnitza Cu-Au porphyry deposits (Figure 9.4).

The fluids responsible for the early hydrothermal alteration and the Ni-Co-As, Cu, ± Bi-Te sulphide precipitation at Belo Brdo have hydrothermal characteristics, derived from a magmatic source. As in many porphyry systems, cooling by mixing of hotter, magmatic fluid with cold meteoric water (Figure 9.4) is a predominant process responsible for main-stage sulphide precipitation. The trapping pressures were between 1419 and 521 bars and imply depths of between 5 and 1.7 km under lithostatic conditions.

## 9.9 Exploration guides

Porphyry copper deposits are the world's most important source of copper and significant source of molybdenum, gold, and silver. The discovery of porphyry copper systems in the study area would have broad implications for the local society. Despite a long history of investigation and production of polymetallic mineralisation in the Kopaonik district, the copper porphyry deposits were unknown in the region till 2004. One of the main reasons for this was a lack of understanding of the potential for porphyry systems at the regional level. This study represents an attempt to relate polymetallic mineralisation of the Belo Brdo and the nearby deposits to an underlying porphyry system.

Based on the new model for porphyry systems, the exploration for porphyry copper deposits in the Kopaonik district in the future should include regional-scale data, such as rock types, structures, intrusion types and ages, geophysical properties, spectral imagery, distribution of known deposit types, and prospective depths of unidentified porphyry copper deposits. Local-scale data including, in addition to lithologies and structure, distribution of hydrothermal minerals; mineralogy and paragenesis; minor-element and whole-rock geochemistry; fluid inclusion zoning; chemical and isotopic compositions of minerals; detailed geophysical properties; and distribution of sulphide minerals. Particular attention should be paid to leached capping and iron- and copper-oxide mineralogy, which *provide characteristics of subjacent enriched sulphide and hypogene* mineralisation.

# CHAPTER 10:
# CONCLUSIONS

- The Belo Brdo Pb-Zn (Ag) deposit of the Kopaonik metallogenic district is located within the NNW-SSE trending Vardar ophiolite zone, which represents the easternmost tectonic unit of the Dinaride-Hellenide orogenic belt and separates the Africa-Arabia plate from the Eurasian plate.
- The geology is characterised by a tectonic stack, which includes from bottom to top: a Triassic metamorphic complex; an Ophiolite mélange Unit; a Jurassic Ophiolite Unit; and an Upper Cretaceous Flysch Unit. During the Early Oligocene, the tectonic nappe pile was intruded by the I-type Kopaonik intrusive complex and erupted lavas.
- The Belo Brdo Pb-Zn (Ag) deposit and nearby polymetallic deposits are associated with post-collisional Oligocene intrusive activity and are structurally controlled. The deposits are aligned along the regional NNW-SSE- trending structural zones, which coincide with the distribution of Paleogene magmatic rocks within the Alpine- Balkan-Carpathian-Dinaridic orogenic province.
- Petrographic data presented here show that listwanites, in addition to Cretaceous limestones, represent an important host rock to the carbonate-replacement type of mineralisation at the Belo Brdo deposit. An additional hydrothermal vein deposit is located within Tertiary andesites. Listwanites formed by K-metasomatism of serpentinised harzburgites, and are characterised by the specific assemblage: chromian muscovite + quartz + Fe-Mg carbonates + pyrite.
- Petrographic and geochemical data obtained from the peridotites and the Tertiary igneous rocks indicate subduction-related signatures for the magmatic rocks. Moderate- to high Cr#, low-$Al_2O_3$ and low-$TiO_2$ values suggest that the Cr-spinel of the Belo Brdo peridotites grew in a supra-subduction setting. Tertiary volcanic rocks show typical "subduction-related" compositions as reflected by the enrichment of the LILE (Cs, Rb, Th, U, K) and Pb over LREE and MREE, and depletion of the HFSE (Zr, Nb, Ti, and P). The volcanic rocks classify as subalkaline and exhibit a calc-alkaline to mildly alkaline metaluminous character.
- The Belo Brdo Pb-Zn (Ag) deposit has the characteristics of an intermediate-sulphidation base-metal deposit, displaying hydrothermal alteration styles similar to those of copper porphyry systems, and with significant input of trace elements from related ophiolites.
- A genetic model for the origin and evolution of the Belo Brdo deposit involves three stages of mineral deposition, namely (1) pre-ore stage, characterised by hydrothermal alteration of host rocks (listwanisation, quartz-sericite-pyrite, quartz-tourmaline, propylitic and intermediate argillic) and evolution of Ni-Co-As mineral assemblage; (2) main-ore stage, represented by massive sulphides: sphalerite, galena, pyrite, arsenopyrite, chalcopyrite, Ag-tetrahedrite-tennantite, bournonite; and (3) post-ore stage (quartz, carbonates ±pyrite).

- The fluids responsible for the early hydrothermal alteration and the Ni-Co-As, Cu, ± Bi-Te sulphide precipitation have hydrothermal characteristics, derived from a magmatic source.
- There is robust stable isotope evidence for the magmatic component, such as: (1) moderately high temperatures (~420°C) for the quartz-sericite alteration and magmatic $\delta^{18}O$ values of fluid in equilibrium with sericite and quartz (6.5 – 8.5‰); (2) δD values of fluid in equilibrium with sericite (-58‰); (3) $\delta^{18}O$ and δD values of fluid in equilibrium with tourmaline (10‰ and -38‰ respectively); (4) $\delta^{13}C$ value of carbon in silicified listwanite (-3.5‰); and (5) $\delta^{34}S$ values of pyrite hosted by andesites and massive listwanite (2.6-4.1‰).
- Arsenopyrite co-existing with pyrite in the main-ore stage has As contents between 29.4 and 31.5 with a mean value of 30.05 atom.%., corresponding to formation temperatures between 311 and 348°C and sulphur fugacity ($fS_2$) between $10^{-8.3}$ and $\sim 10^{-10.5}$ bar.
- Estimated formation temperatures using sphalerite with a mean composition of 18 mol.% FeS and CuS compositions between 0.009 and 0.12 mol.% CuS, range between 290 and 350°C.
- Fluid inclusion data from main-ore stage quartz suggest precipitation from low- to moderate salinity (1.82-13.9wt.% equiv. NaCl) and epithermal- to moderately high temperature (190- 341°C) fluids. The trapping pressures were between 1419 and 521 bars and imply depths of between 5 and 1.7 km under lithostatic conditions.
- The presence of hydrothermal breccias in the deposit indicates the possibility that pressure-temperature conditions were close to the liquid-vapour two phase curve. This would indicate a hydrostatic pressure regime and trapping temperatures of between 50 and 120 bars.
- Gangue carbonates are depleted in both $\delta^{18}O$ (6.6 to 18 ‰) and $\delta^{13}C$ (2 to –4.4 ‰) compared with Cretaceous limestones, suggesting the influx of an external magmatic fluid. REE geochemistry of carbonates points to acidic, reduced, high-temperature hydrothermal fluids.
- Cooling by mixing of hotter, magmatic fluid with cold meteoric water is a predominant process responsible for sulphide precipitation. Calculated oxygen isotopic composition of main-ore fluid shows magmatic signatures (5.9 to 7.7‰), whereas calculated isotopic composition of water responsible for sulphide precipitation in late ore breccia show depletion in both oxygen and hydrogen values ($\delta\,^{18}O$ = 4.8 to 2.3 ‰ and δ D = -93 to -96 ‰), indicating an influence of meteoric waters.
- The relatively low and uniform isotopic sulphur compositions of all the main-ore stage sulphides (3.4-5.4‰; average 4.4‰) from Belo Brdo are consistent with an igneous source.
- The major sulphur species is $H_2S$. Calculated $\delta^{34}S$ composition of $H_2S$ in equilibrium with main-ore sulphides is 4.7‰, which suggests a magmatic sulphur source.
- Sr isotopic data of the hydrothermal carbonates from the carbonate-replacement mineralisation of the Belo Brdo deposit are consistent with a mixing line between a Sr contribution from the Tertiary magmatic rocks and Cretaceous sediments on one end and the Jurassic serpentinites and listwanites on the other.

- The lead isotopic compositions of galena from different mineralisation stages of Belo Brdo deposit are homogeneous and similar to those of local calc-alkaline volcanic rocks indicating genetic link between mineralisation and magma.
- This study demonstrates that the Belo Brdo carbonate-replacement Pb-Zn (Ag) deposit contrasts sharply with those of MVT Pb-Zn deposits which typically form from saline brines at temperatures between 100-180°C and in a different crustal setting within.
- The Belo Brdo deposit shares many common features with the nearby Cu-Au skarn (Karavansalija), Cu-Au porphyry (Rudnitza), Pb-Zn (Ag) vein (Crnac, Karadak, Kizevak) and Pb-Zn carbonate-replacement (Trepca) deposits, such as: (1) structural controls and association with post-collisional calc-alkaline magmatism; (2) epigenetic origin of mineralisation; (3) nature and origin of hydrothermal fluids (4) stable isotope characteristics of sulphides; and (3) composition of main sulphide mineral assemblages. It appears that the spectrum of mineralisation styles shown by these deposits represents different responses to the same magmatic events. .
- The data presented here are consistent with the hypothesis that the Pb-Zn mineralisation of the Kopaonik metallogenic district is genetically linked to the Cu-Au porphyry and skarn sequences in a magmatic-hydrothermal system.

## 10.1 Suggestions for future research

This study demonstrated that the polymetallic mineralisation in the Kopaonik metallogenic district shares many common features with deposits related to porphyry systems elsewhere in supra-subduction settings. The Karavansalija Cu-Au skarn and the Rudnitza Cu-Au porphyry deposits have only been recognised during the last decade. The obvious question is whether this porphyry is a small anomaly or whether there are porphyry-epithermal systems yet to be discovered in the Kopaonik district. To further clarify the genetic link between the deposits and their association with the Tertiary igneous rocks, the following recommendations for further research are proposed:

- Radiometric dating of Tertiary igneous minerals and hydrothermal minerals from the Belo Brdo deposit and the Karavansalija skarn deposit (sericite and fuchsite), as well as molybdenum from the Rudnitza Cu-Au porphyry deposit to constrain more precisely their absolute and relative age.
- Detailed petrological, mineral chemistry and fluid inclusion study in the Karavansalija Cu-Au skarn and Belo Brdo listwanites to locate Au-mineralisation and to clarify its association with As, Bi or Cu.
- More detailed fluid inclusion study should be undertaken on sphalerite (infrared microthermometry) from the Belo Brdo deposit, quartz and carbonates from the Karavansalija skarn and Rudnitza porphyry deposits, as well as on magmatic quartz from the quartz-latite. This

would enable further characterisation of fluids from the nearby deposits and from the various depths of igneous emplacement providing the information on the zonation of fluid temperatures and evolution of the mineralising fluids. Additionally, SEM and Laser Raman analyses should be carried out on daughter minerals in quartz from the Karavansalija and the Rudnitza deposits.

- A study of the hypersaline as well as low salinity fluid inclusions from Karavansalija and Rudnitza should be undertaken using LA-ICP-MS in order to gain quantitative concentrations on minor and trace elements in fluids (e.g. Bi, Cu, As, Au).
- Perform more D/H analyses in fluid inclusions and hydrothermal minerals to better quantify the relative abundances of magmatic and non-magmatic (e.g. meteoric) fluids in the study area.

# REFERENCES

Akbulut, M., Ozkan Pisikn, O., and Karayigit, A.I., 2006. The genesis of the carbonatized and silicified ultramafics known as listvenites: a case study from the Mihalıccık region (Eskisehir), NW Turkey. Geological Journal, 41, 557–580.

Alavi, M., 1994. Tectonics of the Zagros Orogenic belt of Iran: new data and interpretations. Tectonophysics 220, 211-238.

Alderton D.H.M., and Fallick, A.E., 2000. The Nature and Genesis of Gold-Silver-Tellurium Mineralization in the Metaliferi Mountains of Western Romania. Economic Geology, 95, 495-516.

Altunkaynak, S., and Yilmaz, Y., *The mount Kozak magmatic complex*, Western Anatolia, Journal of Volcanology and Geothermal Research, 85, 211-131, 1998.

Amov, B.G., and Arnaudov, V.S., 2000. Pb isotope data for Alpine magmatic rocks and related ore mineralization in the Srednogorie metallogenic zone and Madan region in the Central Rhodope. ABCD-Geode 2000 workshop, Bulgaria, abstracts.

*Andjelković, M., 1982. Geology of Yugoslavia-tectonics.* Monograph, Rudarsko Geoloski Fakultet, Beograd, 692p. (In Serbian).

Arribas, A.J., 1995. Characteristics of high-sulfidation epithermal deposits, and their relation to magmatic fluid. In: Thompson, J.F.H. (Ed.) Magmas, fluids, and ore deposits. Mineralogical Association of Canada, 419–454.

Ash, C.H., 2001. Relationship between ophiolites and gold-quartz veins in the North American Cordillera. B.C. Dep.of Energy, Mines and Petroleum Resources, Bulletin 108; 139pp.

Aubouin, J., 1973. Des tectoniques superposées et de leur signification par rapport aux modèles géophysiques: l'exemple des Dinarides; paléotectonique, tectonique, tarditectonique, neotectonique. Bulletin de la Société Géologique de France 15, 426-460.

Aubouin, J., Blanchet, R., Cadet, J.P., Culet, P., Charvet, J., Choroids, J., Cousin, M. and Rampnoux, J.P., 1970. Essai sur la géologie des Dinarides. Bulletin de la Société géologique de France 7 XII (6), 1060-1095.

Auclair, M., Gauthier, M., Trottier, J., Jébrak, M., and Chartrand, F., 1993. Mineralogy, geochemistry, and paragenesis of the Eastern Metals serpentinite-associated Ni-Cu-Zn deposit, Quebec Appalachians. Economic Geology, 88, 123–138.

Audétat, A., Günther, D., Heinrich, C.A., 1998. Formation of a magmatic-hydrothermal ore deposit: Insights with LA-ICP-MS analysis of fluid inclusions. Science, 279, 2091-2094.

Ault, W.V., and Jensen, M.L., 1963. Summary of sulphur isotope standards. In Jensen M.L. (ed.): Biochemistry of sulphur isotopes. National Science Foundation Symposium Proceedings, Yale University, 16-29.

Bachinski, D.J., 1969. Bond strength an d sulphur isotope fractionation in coexisting sulfides. Econ. Geol. 64, 56-65.

Barnes, H.L., 1979. Solubilities of ore minerals. In: Barnes. H.L. (Ed.) Geochemistry of hydrothermal ore deposits. 2nd edition, New York, John Wiley, 404-460.

Barton P.B., Jr., 1969. Thermochemical study of the system Fe–As–S. Geochimica et Cosmochimica Acta, 33, 841–857.

Barton, P.B.Jr., and Toulmin, P. III, 1966. Phase relations involving sphalerite in the Fe-Zn-S system, Econ. Geol., 61, 815-849.

Barton, P.B., Jr., Bethke, P.M. and Roedder, E., 1977. Environment of ore deposition in the Creede mining district, San Juan Mountains, Colorado. III. Progress toward interpretation of the chemistry of the ore-forming fluid for the OH vein. Econ. Geol. 72, 1-24.

Bau M. and Möller P., 1991. REE systematics as source of information on minerogenesis. In Pagel M. and Leroy J.L. (Eds.): Source, transport and deposition of metals. Balkema, Rotterdam, 17-20.

Bau, M. and Möller, P., 1992. Rare earth element fractionation in metamorphogenic hydrothermal calcite, magnesite and siderite. Mineralogy and Petrology, 45, 231–246.

Bazylev, B., Karamata, S. and Zakariadze, G.S., 2003. Petrology and evolution of the Brezovica ultrmafic massif, Serbia. In: Dilek, Y., Robinson, P.T. (Eds.): Ophiolites in Earth History. Geological Society, London Special Publications Vol. 218, 91-108.

Bazylev, B., Popević, A., Olujić, J., Vujnović, L., Karamata, S., Memović, E., Roshchina, I., and Rosmashova, T., 2006. Mantle peridotites from Dinaric Ophiolite belt and Vardar Zone: a preliminary petrological comparison based on petrographical and petrochemical data. Mesozoic Ophiolite Belts of northern part of the Balkan Peninsula, International Symposium, Belgrade-Banja Luka, May 21-June 6, 2006. Abstract, 8-11.

Bazylev, B., Popević, A., Karamata, S., Kononkova, N.N., Simakin, S.G., Olujić, J., Vujnović, L., and Memović, E., 2009. Mantle peridotites from the Dinaridic ophiolite belt and the Vardar zone western belt, central Balkan: a petrological comparison. Lithos, 108, 37-71.

Beccaluva, L., Maccciotta, G., Piccardo, G.B., and Zeda, O., 1989. Clinopyroxene composition of ophiolite basalts as petrogenetic indicator. Chem. Geol., 77, 165-182.

Ben Othman, D., White, W. M. and Patchett, J. 1989. The geochemistry of marine sediments, island arc magma genesis, and crust–mantle recycling. Earth and Planetary Science Letters 94, 1–21.

Bendezú, R., and Fontboté, L., 2009. Cordilleran Epithermal Cu-Zn-Pb-(Au-Ag) Mineralization in the Colquijirca District, Central Peru: Deposit-Scale Mineralogical Patterns. Economic Geology, 104, 905–944.

Bernoulli, D. and Laubscher, H. 1972. The palinspastic problem of the Hellenides. Eclogae Geologicae Helvetiae 65, 107-118.

Besić, Z., 1954. Some new opinions and ideas on the geotectonics of the Dinarides. Glasnik Prirodnjackog Muzeja, Beograd, 4, 1-22. (In Serbian)

Bethke, P.M. and Barton, P.B. Jr., 1971. Distribution of some minor elements between coexisting sulfide minerals Economic Geology, 66, 140-163.

Bethke, P. M., and Rye, R. O., 1979. Environment of ore deposition in the Creede mining district, San Juan Mountains, Colorado: Part IV, Source of fluids, from oxygen, hydrogen, and carbon isotope studies: Economic Geology, 74, 1832-1851.

Birck, J. L., 1986. Precision K-Rb-Sr Isotopic Analysis - Application to Rb-Sr Chronology. Chemical Geology, 56(1-2): 73-83.

Blundell, D.J., Neubauer, F. and Von Quadt, A. (Eds.), 2002. The Timing and Location of Major Ore Deposits in an Evolving Orogen. Geological Society, London, Special Publications, 204, 358p.

Blundell, D.J., Arndt, N., Cobbold, P. and Heinrich, C.A. (Eds.), 2005. Geodynamics and Ore Deposit Evolution in Europe. Thematic Issue with 9 papers, Ore Geology Reviews, 27, 349p.

Bodnar, R.J. 1993. Revised equation and table for determining the freezing point depression of H2O-NaCl solutions. Geochim. Cosmochim. Acta 57, 683-684.

Bodnar, R.J., 1995. Fluid inclusion evidence for a magmatic source of metals in porphyry copper deposits. In: Thompson, J.F.H. (Ed.). Magmas, Fluids and Ore deposits. Mineralogical Association of Canada Short Course Series, 23, 139-152.

Bodnar, R.J., 2003. Introduction to fluid inclusions. In I. Samson, A. Anderson, and D. Marshall, (Eds.): Fluid Inclusions: Analysis and Interpretation. Mineral. Assoc. Canada, Short Course 32, 1-8.

Bodnar R.J. and Vityk M.O., 1994. Interpretation of microthermometric data for H2O-NaCl fluid inclusions. In De Vivo B. and Frezzotti M.L. (Eds.): Fluid inclusions in minerals: methods and applications. Short course of the working group IMA (Inclusions in Minerals), (Pontignano-Siena, 1-4 September). Virginia Tech., 117-130.

Bodnar, R. J., Reynolds, T. J. and. Kuehn, C. A.,1985. Fluid Inclusion Systematics in Epithermal Systems. In: Berger, B. R. and Bethke, P. M. (Eds.): Geology and Geochemistry of Epithermal Systems. Reviews in Economic Geology, 2, 73-97.

Borisenko, A.,1977. Study of the salt composition of solutions of gas-liquid inclusions in minerals by the cryometric method. Geologiya i Geofizika, 18, (8), 16-27.

Borojević-Sostarić, S., 2004. Geneza Sideritno-Baritno-Polisulfidnih Rudnih Lezista Paleozoiku Unutarnjih Dinarida. Zagreb : Prirodoslovno-matematicki fakultet, M.Sc. theses, unpublished, 120pp..

Borojević-Sostarić, S., 2009. Genetic model of the Pb-Zn-Ag deposit Crnac, Mts. Rogozna, Kosovo. Zagreb University, Croatia, PhD thesis unpublished, 138pp.

Borojević-Sostarić, S Palinkaš, L. Cvetković, V., and Jorge Spangenberg, J. 2008. Ore-forming fluids in the Pb-Zn-Ag mineralization of the Crnac mine, Kosovo. Abstract, The 33rd IGC Oslo.

Bortolotti, V., Marroni, M., Nicolae, I., Pandolfi, L., Principi, G., and Saccani, E., 2002. Geodynamic implications of Jurassic ophiolites associated with island-arc volcanics, South Apuseni Mountains, western Romania. Int. Geol. Rev. 44, 938-955.

Bortolotti, V., Chiari, M., Marcucci, M., Marroni, M., Pandolfi, L., Principi, G. and Saccani, E., 2004. Comparison among the Albanian and Greek ophiolites, in search of constraints for the evolution of the Mesozoic Tethys ocean. Ofioliti, 29, 19-35.

Bortolotti V., Marroni M., Pandolfi L. and Principi G., 2005. Mesozoic to Tertiary tectonic history of the Mirdita ophiolites, northern Albania. In: Y. Dilek, Y. Ogawa, V. Bortolotti and P. Spadea (Eds.): Evolution of ophiolites in convergent and divergent plate boundaries. Isl. Arc, 14, 471-493.

Bottinga, Y. and Javoy, M. (1973). Comments on oxygen isotope geothermometry. Earth Planet. Sci. Lett. 20, pp. 250-265.

Bottinga, Y. and Javoy, M., 1975. Oxygen isotope partitioning among the minerals in igneous and metamorphic rocks. Rev. Geophys. Space Phys. 13, pp. 401-418.

Bouse, R.M., Ruiz, J., Titley, S.R., Tosdal, R.M., and Wooden, J.L., 1999. Lead isotope compositions of Late Cretaceous and Early Tertiary igneous rocks and sulfide minerals in Arizona: implications for the sources of plutons and metals in porphyry copper deposits. Econ Geol 94,211–244

Boyle, R.W., 1979. The geochemistry of gold and its deposits; Geological Survey of Canada, Bulletin 280, 584 pp.

Boynton, W.V., 1984. Cosmochemistry of the rare earth elements: meteorite studies. In: Henderson, P. (Ed.), Rare Earth Element Geochemistry. Elsevier, Amsterdam; 63-114.

Bralia, A., Sabatini, G., Troja, F., 1979. A revaluation of the Co/Ni ratio in pyrite as geochemical tool in ore genesis problems: evidences from southern Tuscany pyritic deposits. Mineralium Deposita 14, 353-374.

Brammall, A., 1930. Olovno-cinkovni rudnik Stantrg, Jugoslavia. Rudarski i topionicarski vesnik, br. 4 st. 154-159. Belgrade (In Serbian).

Brown P. E. and Lamb W. M.., 1989. P-V-T properties of fluids in the system H2O-CO2-NaCl: New graphical presentations and implications for fluid inclusion studies. Geochim. Cosmochim. Acta 53, 1209–1221.

Brown, P.R.,1989. FlinCor. A computer program for the reduction and investigation of fluid inclusion data. American Mineralogist 74, pp. 1390-1393.

Bryan, S.E., 2002. Facies Architecture of the Mount Janet Andesite, Pajingo Epithermal System, Stage 2 Report. Unpublished Report for Newmont Pajingo Pty Ltd, 91p.

Buckley, V.J.E., Sparks, R.S.J., Wood, B.J., 2002. Petrology of hornblende decompression reaction textures in the recent Soufrière Hills Volcano andesitic magma. IAVCEI Conference Abstracts, Saint Pierre, Martinique, May 12-16, p.56.

Burke, E.A.J. and Kieft, C., 1980. Roquesite and Cu-In-bearing sphalerite from Långban, Bergslagen, Sweden. Can. Mineral. 18, 361-363.

Burnham, C.W., 1967. Hydrothermal fluids at the magmatic stage. In: Barnes, H.L., (ed.), Geochemistry of hydrothermal ore deposits, 1st ed., New York, Holt, Rinehart and Winston, 34-76.

Burnham, C.W., 1979. Magmas and hydrothermal fluids. In: Barnes, H.L., (ed.), Geochemistry of hydrothermal ore deposits, 2nd ed., New York, Wiley, 71-136.

Burnham, C.W., 1997. Magmas and hydrothermal fluids. In: Barnes, H.L., (ed.), Geochemistry of hydrothermal ore deposits, 3rd ed., New York, John Wiley and Sons, 63-124.

Burnham, C.W. and Ohmoto, H.,1980. Late-stage processes of felsic magmatism. Mining Geology Special Issue 8, 1-11.

Campbell, F.A., Ethier, V.G., 1984. Nickel and cobalt in pyrrhotite and pyrite from the Faro and Sullivan orebodies. Canadian Mineralogist 22, 503- 506.

Camprubi, A. and Albinson, T. 2006. Depósitos epitermales en México: actualización de su conocimiento y reclasificación empírica. Boletín de la Sociedad Geológica Mexicana, 58, 27-81.

Canby, V.M., 2007. A brief review of Tethyan metal discoveries and developments since 1992. In: Andrew, C. et al., (Eds.): Digging deeper. Proceedings of the Ninth Biennial SGA Meeting, Dublin, Ireland, 97-100.

Cannon, R.S., Pierce, A.P., Antweiller, J.C., and Buck, K.L., 1961. The data of lead isotope geology related to problems of ore genesis. Economic Geology, v. 56, p. 1–38.

Carter, G.S., 2008. Technical report on the copper gold resources on the Karavansalija project, Serbia, on behalf of EuroMax Resources Limited. Unpublished Technical Report No: NI 43-101, 39pp.

Cathelineau, M., 1988. Cation site occupancy in chlorites and illites as a function of temperature. Clay Miner., 23, 471-485.

Chacko, T., Riciputi L.R., Cole D.R. and Horita J., 1999. A new technique for determining equilibrium hydrogen isotope fractionation factors using the ion microprobe: Application to the epidote-water system. Geochimica et Cosmochimica Acta, 63, p. 1-10.

Chacko, T., Hu, X.S., Mayeda, T.K., Clayton, R.N. and Goldsmith, J.R., 1996. Oxygen isotope fractionations in muscovite, phlogopite, and rutile, Geochimica et Cosmochimica Acta 60, 2595-2608.

Chambefort, I., Dilles, J.H., and Kent, A.J.R., 2008. Anhydrite-bearing andesite and dacite as a source for sulfur in magmatic-hydrothermal mineral deposits. Geology, 36, 719–722.

Chang, Z. and Meinert, L.D., 2004. The magmatic-hydrothermal transition-evidence from quartz phenocryst textures and endoskarn abundance in Cu-Zn skarns at the Empire Mine, Idaho, USA, Chem. Geol. 210, 149-171.

Christofides, G., Koroneos, A., Soldatos, T., Eleftheriadis, G. and Kilias, A. 2001. Eocene magmatism (Sithonia and Elatia plutons) in the Internal Hellenides and implications for Eocene-Miocene geological evolution of the Rhodope Massif (Northern Greece). In: Downes, H. and Vaselli, O. (Eds.): Tertiary magmatism in the Dinarides Balkan Peninsula. - Acta Vulcanologica 13, 73-89.

Christofides, G., Soldatos, T., Eleftheriadis, G. and Koroneos, A. 1998. Chemical and isotopic evidence for source contamination and crustal assimilation in the Hellenic Rhodope plutonic rocks. In: Christofides, G., Marchev, P. and Serri, G. (Eds.): Tertiary magmatism of the Rhodopian Region. Acta Vulcanologica 10, 305-318.

Ciobanu, C.L., and Cook, N.J., 2004. Skarn textures and a case study: the Ocna de Fier-Dognecea orefield, Banat, Romania, Ore Geology Reviews, 24, 315–370.

Ćirić, B. and von Gaertner, H.R., 1962. On the problem of Variscan Folding in Yugoslavia. Vesnik Zavoda geoloska i geofizicka istrazivanja XX, 303-312. Belgrade. (In Serbian).

Cook, N.J., 1996. Mineralogy of the sulphide deposits at Sulitjelma, Northern Norway. Ore Geology Reviews 11, 303-338.

Cook, N.J. and Damian, G., 1997. New data on plumosite and other sulphosalt minerals from the Herja hydrothermal vein deposit (Baia Mare district, Romania). Geol. Carpathica, Bratislava, 48, 6, 387-399.

Corbett, G.J., and Leach, T.M., 1998. Southwest Pacific gold-copper systems: Structure, alteration and mineralization. Special Publication 6, Society of Economic Geologists, 238pp.

Cox, D.P., 1986. Model 17-Descriptive model for porphyry Cu. In: Cox, D.P., and Singer, D.A., Mineral deposit models. U.S. Geological Survey Bulletin 1693, Washington; p. 76.

Craig J.R., and Vaughan, D.J., 1994. Ore Microscopy and Ore Mineralogy. John Wiley and Sons, New York, N.Y. 434p.

Craig, J.R., Vokes, F.M., *and Solberg, T.N., 1998. Pyrite: physical and chemical textures.* Mineralium Deposita 34, 82- 101.

Craig, J.R., Solberg, T.N., and Vaughan, D.J., 1983. Compositional variations in sphalerite ores of the East and Central Tennessee zinc district. In Tennessee Zinc deposits, field trip guide book, 1983. Virginia Tech. Dept. Geol. Sci., 152-164.

Craig, H., 1957. Isotopic standards and isotopic correction factors for mass spectrometric analysis of carbon dioxide. Geochim Cosmochim Acta 12, 133-149.

Craig, H., 1961. Isotopic variations in meteoric waters. Science, 133: 1702-1703.

Cvetković, V., 2002. Nature and origin of pyroclastic deposits of the Miocene Eruptive Complex of Borač (Central Serbia). Bull CXXV Acad. Serbe. Sci. Arts. Classe. Sci. Math. et Sci. Natur. 342; 209-215.

Cvetković, V., Karamata, S. and Knezević, V., 1995. Volcanic rocks of the Kopaonik district. Geology and Metallogeny of the Kopaonik Mt. Symposium, Belgrade, 185-194.

Cvetković, V., Prelević, D., and Pecskay, Z., 2000. Lamprophyric rocks of the Miocene Borac eruptive complex (central Serbia Yugoslavia). Acta Geologica Hungarica 43 (1), 25–41.

Cvetković, V., Poli, G., Resimić-Šarić, K., Prelević, D. and Lazarov, M., 2002. Tertiary post-collision granitoid of Mt. Kopaonik (Serbia)-Petrogenetic constraints based on new geochemical data. In: Michalık, J., Šimon, L., Vozar, J. (eds.) Proceedings of XVII. Congress of Carpathian-Balkan Geological Association Bratislava, September 1st–4th 2002. Geol. Carpathica, 53.

Cvetković, V., Prelević, D., Downes, H., Jovanović, M., Vaselli, O. and Pecskay, Z. 2004. Origin and geodynamic significance of Tertiary postcollisional basaltic magmatism in Serbia (central Balkan Peninsula). Lithos, 73, 161-186.

Cvetković, V., Downes, H., Prelević, D., Jovanović, M., Lazarov, M., 2004a. Characteristics of the lithospheric mantle beneath east Serbia inferred from ultramafic xenoliths in Palaeogene basanites. Contrib. Mineral. Petrol. 148 (3), 335–357..

Cvetković, V., Poli G., Christofides G., Koroneos A., Pécskay Z., Resimić-Sarić, K. and Eric V., 2007. The Miocene granitoid rocks of Mt. Bukulja (central Serbia): evidence for Pannonian extension-related granitoid magmatism in the northern Dinarides. Eur. J. Mineral., 19, 513-532.

Czamanske, G.K. and Rye, R.O., 1974. Experimentally determined sulfur isotope fractionations between sphalerite and galena in the temperature range 600°C to 275°C. Econ. Geol. 69, 17-25.

Damian, G., Marias, F., and Damian, F., 1998. Sulphur isotopes and lead from some hydrothermal mineralizations in the Baia Mare metallogenetic district. Rom. J. Miner. Deposits, 78, 1, 47-48.

De Baar H. J. W., Brewer P. G. and Bacon M.P., 1985. Anomalies in rare earth distributions in seawater: Cd and Tb. Geochim. Cosmochim. Acta 49, 1955- 1963.

De La Roche, H., Leterrier, J., Grande Claude, P. and Marchal, M., 1980. A classification of volcanic and plutonic rocks using R1-R2 diagrams and major element analysis, its relationship's and current nomenclature. Chemical Geology 29, 183- 210.

Deines, P., 2002. The carbon isotope geochemistry of mantle xenoliths. Earth. Sci. Rev. 58, 247-278.

Dercourt, J., Zonenshain, L.P., and Ricou, L.E., 1986. Geological Evolution of the Tethys from the Atlantic to the Pamirs since the Lias. Tectonophysics 123, 241-315.

Dercourt, J., Ricou, L.E., and Vrielynck, B., (Eds.), 1993. Atlas Pery-Tethys Palaeogeographical Maps. CCGM CGMW, Paris.

Dercourt, J., Gaetani, M., and Vrielynck, B., (Eds.), 2000. Pery-Tethys Palaeogeographical Atlas. Gauthier-Villars, Paris.

Deschamps, F., Guillot, S., Godard, M., Chauvel,C., Andreani, M., and Hattori, K., 2010. In situ characterization of serpentinites from forearc mantle wedges: Timing of serpentinization and behavior of fluid-mobile elements in subduction zones. Chemical Geology, 269, 262–277.

Dewey, J. F., Pitman, W. C. III, Ryan, W. B. F., Bonnin, J., 1973. Plate tectonics and the evolution of the Alpine system. Geological Society of America Bulletin, 84, 3137-3180.

Dick, H. J. B. and Bullen, T., 1984. Cr-spinel as a petrogenetic indicator in abyssal and alpine-type peridotites and spatially associated lavas. Contributions to Mineralogy and Petrology, 86, 54-76.

Dickin A.P., 1995. Radiogenic isotope geology. Cambridge University Press, 452pp.

Dilek, Y., 2006. Collision tectonics of the Mediterranean region: Causes and consequences. In: Dilek, Y. And Pavlides, S., (Eds.): Postcollisional tectonics and magmatism in the Mediterranean region and Asia. Geological Society of America Special Paper 409, 1-13.

Dilek, Y., Shallo, M. and Furnes, H., 2005. Rift-drift, seafloor spreding, and subduction zone tectonics of Albanian ophiolites: International Geology Review, 47, 147-176.

Dilek, Y., Shallo, M., Furnes, H., 2008. Geochemistry of the Jurassic Midiata Ophiolite (Albania) and the MORB to SSZ evolution of a marginal basin oceanic crust. Lithos 100, 174–209.

Dimitrijević, M. and Dragić, D., 1957. The structures and textures of the Kopaonik granodiorite massif. Vesnik, Geological and Geophysical Survey, vol 7 (in Serbian), Belgrade.

Dimitrijević, M. D., 1982. Dinarides: an outline of the tectonics, Earth Evolution Sciences, 1, 4-23.

Dimitrijević, M. D., 1995. The Kopaonik block-its position within the Vardar Zone. In Symposium-"Geology and Metallogeny of the Kopaonik Mt". Kopaonik- Belgrade, 33-40 (In Serbian, English Abstract).

Dimitrijević, M.D., 1997. Geology of Yugoslavia. Geological Institute GEMINI Special Publication, Belgrade, 187pp.

Dimitrijević, M.D., 2001. Dinarides and the Vardar Zone: a short review of the geology. Acta Vulcanologica 13, 1-8.

Dimitrijević, M.N., and Dimitrijević, M.D., 1973. Olistostrome melange in the Yugoslavian Dinarides and late Mesozoic plate tectonics. Journal of Geology 81, 328–340.

Dimitrijević, M. N. and Dimitrijević, M. D., 1985. The Paraflysch of the Central Vardar Subzone. In: Dimitrijević, M. N., Dimitrijević, M. D. (Eds.): Turbidite basins of Serbia. Monograph Serbian Academy of Science, 61, 79-100.

Dimitrijević, M.N. and Dimitrijević, M.D. 1987: The Titova Mitrovica Flysch. In: Dimitrijević, M.N. and Dimitrijević, M.D. (Eds.): The trubiditic basins of Serbia. Serbian Academy of Sciences and Arts Department of Natural andMathematical Sciences 61, 25-64.

Dini, A., Benvenuti, M., Lattanzi, P. and Tanelli, G., 1995. Mineral assemblages in the Hg-Zn-(Fe)-S system at Levigliani, Tuscany, Italy. Eur. J. Mineral. 7, 417-427.

Dixon, C. J. and Pereira, J., 1974. Plate tectonics and mineralization in the Tethyan region. Mineralium Deposita, 9, 185-198.

Dixon, J.E. and Robertson, A.H.F., (Eds.), 1984. The geological evolution of the Eastern Mediterranean. Geological Society, London, Special Publications, 17.

Djerić N., Gerzina N., 2008: Late Triassic radiolarians from the Ovcar-Kablar Gorge (SW Serbia). Geološki anali Balkanskog poluostrva, 69, 39-47, Beograd.

Doe, B.R., and Stacey, J.S., 1974. The application of lead isotopes to the problems of ore genesis and ore prospect evaluation-A review. Economic Geology, 69, 57–776.

Doe, B.R. and Zartman, R.E., 1979. Plumbotectonics. In: "Geochemistry of hydrothermal ore deposits". H.L.Barnes, ed. Wiley, 22-70.

Dong, G., Morrison, G., and Jaireth, S., 1995. Quartz textures in epithermal veins, Queensland; classification, origin and implication. Economic Geology, 90, (6), 1841- 1856.

Donnelly T., Waldron S., Tait A., Dougans J. and Bearhop S., 2001. Hydrogen isotope analysis of natural abundance and deuterium-enriched waters by reduction over chromium on-line to a dynamic dual inlet isotope-ratio mass spectrometer. Mass Spectrometry 15, 1297-1303.

Droop, G.T.R., 1987. A general equation for estimating $Fe^{3+}$ concentrations in ferromagnesian silicates and oxides from microprobe analyses, using stoichiometric criteria. Mineralogical Magazine, 51, (361) 431-435.

Dungan, M.A., and Rhodes, M.J., 1978. Residualg lassesa nd melt inclusions in basalts from DSDP legs 45 and 46. Evidence for magma mixing. Contributions to Mineralogy and Petrology, 67, 417-431.

Economou-Eliopoulos, M., 2005. PGE potential of porphyry deposits. In: Mungall J.E., (Ed): Exploration for Platinum-Group Elements Deposits. Mineralogical Association of Canada Short Course, 35 , 203-346.

Einaudi, M.T., Meinert, L.D. and Newberry, R.J. 1981. Skarn deposits. Economic Geology 75th Anniversary Volume, 317-391.

Einaudi, M.T., Hedenquist, J.W., Inan, E., 2003. Sulfidation state of hydrothermal fluids: The porphyry-epithermal transition and beyond: Society of Economic Geologists and Geochemical Society Special Publication 10, 285-313.

Elderfield, H. and Greaves, M.J.,1982. The rare earth elements in seawater. Nature, 296, 214-219.

Eliopoulos, D., et al. (Eds.), 2003. Mineral Exploration and Sustainable Development. Proceedings of the Seventh Biennial SGA Meeting on Mineral Exploration and Sustainable Development, Athens, Greece, August 24-28. Millpress, Rotterdam, 1328p.

Ellam, R.M., Hawkesworth, C.J., 1988. Elemental and isotopic variations in subduction-related basalts: evidence for a three component model. Contrib. Mineral. Petrol. 98, 72– 80.

Ellis, R., 2005. Kosovo - Land of opportunity for European mining and energy. Mining Journal special publication, London, October 2005.

Evans, B.W. and Frost, B.A., 1975. Chrome spinel in progressive metamorphism – a preliminary analysis. Geochim. Cosmochim. Acta 39, 959-972.

Fallick, A.E., Macaulay, C.I. and Haszeldine, R.S., 1993. Implications of linearly correlated oxygen and hydrogen isotopic compositions for kaolinite and illite in the Magnus Sandstones, North Sea. Clays & Clay Miner. 41, 184-190.

Fanlo, I., Subías, I., Gervilla, F., Paniagua, A. and García,B., 2004. The composition of Co–Ni–Fe sulfarsenides, diarsenides and triarsenides from the San Juan de Plan deposit, central Pyrenees, Spain. The Canadian Mineralogist, 42, 1221-1240.

Fanlo, I., Subías, I., Gervilla, F.,and Manuel, J., 2006. Textures and compositional variability in gersdorffite from the Crescencia Ni-(Co-U) Showing, Central Pyrenees, Spain: primary deposition or re-equilibration? The Canadian Mineralogist, 44, 1513-1528.

Faure, G., 2001. Origin of igneous rocks: the isotopic evidence. Springer Verlag Berlin, 496 pp.

Faure, G., 1998. Principles and applications of geochemistry. Prentice Hall, New Jersey, 600 pp.

Faure, G., 1986. Principals of Isotope Geology. 2nd Edition. Wiley and Sons. New York, 589 pp.

Faure, G., and Mensing, T.M., 2005. Isotopes: Principles and Applications. John Wiley and Sons, 897 pp.

Feeley, T.C., Sharp, Z.D., 1996. Chemical and hydrogen isotope evidence for in situ dehydrogenetion of biotite in silicic magma chambers. Geology 24, 1021-1024.

Féraud, J. and Deschamps, Y., 2009. French scientific cooperation 2007-2008 on the Trepca lead-zinc-silver mine and the gold potential of Novo Brdo-Artana tailings (Kosovo). BRGM report No 57204-FR, 92 p.

Field, C.W. and Fifarek, R.H., 1985. Light stable-isotope systematics in the epithermal environment. Rev Econ. Geol. 2, 99–128.

Field, C.W., Zhang, L., Dilles, J.H., Rye, R.O., and Reed, M.H., 2005. Sulfur and oxygen isotope record in sulfate and sulfide minerals of early, deep, pre-Main Stage porphyry Cu-Mo and late Main Stage base-metal mineral deposits, Butte district, Montana. Chemical Geology, 215, 61–93.

Foley, S.F., 1988. The genesis of continental basic alkaline magmas-an interpretation in terms of redox melting. J. Petrol. Spec. Lithosphere Issue, 139- 161.

Foley, S.F., and Wheeler, G.E., 1990. Parallels in the origin of the geochemical signatures of island arc volcanics and continental potassic rocks: the role of residual titanites. Chem. Geol. 85, 1-18.

Forgan, C.B., 1948. Ore deposits at the Stantrg lead-zinc mine, Yugoslavia. In: Dunham, K.C. (Ed): 18th International Geological Congress, London, 1948, Part VJJ, Section F symposium, 290-307.

Forward, P., 2008. Developing and expanding in the Tethyan belt. Conference presentation, Finex 08 - The role of the UK and Ireland in Global Mineral Exploration http: africaneagle.co.uk/finex/presentations2008.php

Frost, B. R., 1991. An introduction to oxygen fugacity and its petrologic importance. In: Lindsley, D. H. (Ed.). Oxide minerals: petrologic and magnetic significance. Mineralogical Society of America, Reviews in Mineralogy; 25, 1-10.

Frost B.R. and Lindsley D.H, 1991. Occurrence of iron-titanium oxides in igneous rocks. In: Lindsley, D. H. (Ed.). Oxide minerals: petrologic and magnetic significance. Mineralogical Society of America, Reviews in Mineralogy. 25, 433-468.

Frost, B.R., Calvin G. Barnes, Collins, W.J., R.J., Ellis, D.J. and Frost, C.D., 2001. A Geochemical Classification for Granitic Rocks. J. Petrology, 42(11), 2033-2048.

Funiciello, F., Moron,i M., Piromallo, C., Faccenna, C., Cenedese, A., and Bui, H.A., 2006. Mapping mantle flow during retreating subduction: laboratory models analyzed by feature tracking. J Geophys Res 111:B03402. doi:10.1029/2005JB003792

Garfunkel, Z., 2004. Origin of the Eastern Mediterranean basin: a re-evalaution. Tectonophysics 391, 11-34.

Gaspar, L.M., Inverno, C.M.C., 2000. Mineralogy and metasomatic evolution of distal strata-bound scheelite skarns in the Riba de Alva Mine, Northeastern Portugal. Econ. Geol. 95, 1259–1275

Gawlick H.-J., Frisch W., Hoxha L., Dumitrica P., Krystyn L., Lein R., Missoni S. and Schlagintweit F., 2008: Mirdita Zone ophiolites and associated sediments in Albania reveal Neotethys Ocean origin. Int. J. Earth Sci. (Geol. Rundsch.) 97, 865-881.

Geletii V.F., Chernishev L.V. and Pastushkova T.M., 1979. Distribution of cadmium and manganese between galena and sphalerite. Geologiia Rudnykh Mestoozhdenii 21, 66-75.

Gerzina, N., and Csontos, L. 2003: Deformation sequence in the Vardar Zone: surroundings of Jadar block, Serbia. Annales Universitatis Scientiarium Budapestinensis, Sectio Geologica 35, 139-140.

Giggenbach, W.F., 1992. SEG distinguished lecture-magma degassing and mineral deposition in hydrothermal systems along convergent plate boundaries. Econ. Geol. 87, 7, 1927-1944.

Gilg, H.A., 1993. Geochronology (K-Ar), fluid inclusion, and stable isotope (C,H,O) studies of skarn, porphyry copper, and carbonate-hosted Pb- Zn-(Ag,Au) replacement deposits in the Kassandra mining district (Eastern Chalkidiki, Greece). Unpub. PhD thesis, ETH Zurich, 152p.

Gill, J.B., 1981. Orogenic andesites and plate tectonics. Springer, Berlin, 390 p.

Gilmer, A.L., Clark, K.F., Conde, J.C., Hernandez, I.C., Figueroa, J.I.S., Porter, E.W., 1988. Sierra de Santa Maria, VelardenÃa mining district, Durango, Mexico. Econ. Geol. 83, 1802-1829.

Goldstein, R.H., and Reynolds, T.J., 1994. Systematics of fluid inclusions in diagenetic minerals: Society for Sedimentary Geology Short Course 31, 199pp.

Goncharenko, A.I., 1970. Auriferous listwanites as a new type of mineralization in the northern part of the Kuznetsk Alatau; Izvestiya Tomskogo Politekhnicheskogo Instituta (Reports of the Tomsk Polytechnical Institute), Volume 239, 110-114.

Grancea, L., Bailly, L., Leroy, J., Banks, D., Marcoux, E., Milési, J.P., Cuney, M., André, A.S., Istvan, D., Fabre, C., 2002. Fluid evolution in the Baia Mare epithermal gold/polymetallic district, Inner Carpathians, Romania. Mineralium Deposita, 37: 630-647.

Grant G.J., and Ruiz, J., 1988. The Pb-Zn-Cu-Ag Deposits of the Granadeha Mine, San Francisco del Oro-Santa Barbara District, Chihuahua, Mexico. Econom. Geology, 83, 1683-1702.

Grootenboer, J., and Schwarcz, H.P., 1969, Experimentally determined sulphur isotope fractionations between sulfide minerals: Earth and Planetary Science Letters, v. 7, p. 162-166.

Grubić, A. 1980. Yugoslavia - an outline of geology of Yugoslavia. Guide-book 15, 26th IGC, Paris, 49p.

Grubić, A. 1995. Schistes lustres in the Kopaonik area. In: Symposium- "Geology and Metallogeny of Kopaonik Mt.", Belgrade, 159-168 (In Serbian, English abstract).

Grubić, A., Đoković, I. and Marović, M. 1995. Tectonic outline of the Kopaonik area. In: Symposium- "Geology and Metallogeny of Kopaonik Mt.", Belgrade, 46-53. (In Serbian, English abstract).

Guilbert, J.M. and Parks, C.F., Jr., 1986. The geology of ore deposits. W.H. Freeman and Company, New York, 985p.

Gulson, B.L., 1986. Lead isotopes in mineral exploration. Developments in Economic Geology vol. 23, Elsevier, Amsterdam, 245 pp.

Haas, J.L., 1971. The effect of salinity on the maximum thermal gradient of a hydrothermal system at hydrostatic pressure: Economic Geology, 66 940–946.

Hajmolaali, A., Alavi, N.M., 1993. Geological map of Khezr-Abad area. Geological Survey of Iran, scale 1:100.000.

Hall, C. and Zhao, R., 1995. Listvenite and related rocks: perspectives on terminology and mineralogy with reference to an occurrence at Cregganbaun, Co. Mayo, Republic of Ireland; Mineralium Deposita, 30, 303-313.

Hall, D.L., Sterner, S.M. and Bodnar, R.J., 1988. Freezing point depression of NaCl-KCl-H2O solutions. Econ. Geol. 83, 197-202.

Halsor, S.P., Rose, W.I., 1991. Mineralogical relations and magma mixing in calc-alkaline andesites from Lake Atitlan, Guatemala. Mineral. Petrol. 45, 47-67.

Harangi, S., Downes, H., and Seghedi, I., 2006. Tertiary-Quaternary subduction processes and related magmatism in the Alpine-Mediterranean region: Geological Society, London, Memoirs 2006, 32:167-190.

Harkovska, A., Marchev, P. and Pecskay, Z., 1998. Paleogene magmatism in the central Rhodope area, Bulgaria - a review and new data. Acta Vulcanologica 10, 199-216.

Hawkesworth, C.J., Gallagher, K., Hergt, J.M. and McDermott, F. 1993. Mantle and slab contributions in arc magmas: Annu. Rev. Earth. Planet Sci., 21; 175-204.

Haynes, F.M. ,1985. Determination of fluid inclusion compositions by sequential freezing. Econ. Geol. 80, 1436-1439.

Hedenquist, J.W., 1987. Mineralization associated with volcanic related hydrothermal systems in the Circum Pacific Badin. In: Horn, M.K. (Ed.) Transactions of the 4th circum Pacific energy and mineral resources conference, 17-22 August 1987, Singapore: Tulsa, American Association of Petroleum Geologists, 513-523.

Hedenquist, J.W. and Henley, R.W., 1985.The importance of CO2 on freezing-point measurements of fluid inclusions - evidence from active geothermal systems and implications for epithermal ore deposition. Econ. Geol., 80, 1379–1406.

Hedenquist, J.W. and Lowenstern, J.B., 1994. The role of magmas in the formation of hydrothermal ore deposits: Nature, 370, 519-527.

Hedenquist, J.W., Arribas, A., Reynolds, T.J. 1998. Evolution of an intrusion-centered hydrothermal system: far Southeast-Lepanto porphyry and epithermal Cu-Au deposits, Philippines. Econ Geol 93,4, 373-404.

Hedenquist, J.W., Arribas, R.A., Gonzales, U.E., 2000. Exploration for epithermal gold deposits. In: S. Hagermann and P. E. Brown (Eds.): Gold in 2000. Society of Economics Geologists, Reviews in Economic Geology, 13, 245 - 277.

Heiken, G., Eichelberger, J.C., 1980. Eruptions at Chaos Crags, Lassen Volcanic National Park. J. Volcanol. Geotherm. Res. 7, 443-481.

Heinrich, C.A., 2005. The physical and chemical evolution of low-salinity magmatic fluids at the porphyry to epithermal transition: A thermodynamic study: Mineralium Deposita, 39, 864-889.

Heinrich, C.A. and Neubauer, F. (Eds.), 2002. Cu - Au - Pb - Zn - Ag metallogeny of the Alpine - Balkan - Carpathian - Dinaride geodynamic province. Thematic Issue, Mineralium Deposita 37, 533-678.

Hem, S.R., Makovicky, E. and Gervilla, F., 2001. Compositional trends in Fe, Co and Ni sulfarsenides and their crystal-chemical implications; results from the Arroyo de la Cueva deposits, Ronda Peridotite, southern Spain. Can. Mineral. 39, 831-853.

Hemley, J.J., Montoya, J.W., Marinenko, J.W., and Luce, R.W., 1980. Equilibria in the system Al2O3-SiO2-H2O and some general implications for alteration/mineralization processes: Economic Geology; 75, 210–228.

Herak, M., 1986. A new concept of the geotectonics of the Dinarides. Acta Geologica, 16, 1-42, Zagreb.

Hoefs J., 2009: Stable Isotope Geochemistry, 6th edition; Springer-Verlag, Berlin, 288pp.

Holland, H.D., 1965. Some applications of thermochemical data to problems of ore deposits, II. Mineral assemblages and the composition of ore-forming fluids. Economic Geology, 60, 1101–1166.

Hrvatović, H., 1999. Geological guidebook through Bosnia and Herzegovina Geological Bulletin. Book 25, 1-203. (in Bosnian).

Hrvatović, H., 2006. Geological guide book through Bosnia and Herzegovina. Geological Survey of Federation Bosnia and Herzegovina, Sarajevo, 163pp.

Hrvatović, H. and Pamić, J., 2005. Principal thrust-nappe structures of the Dinarides. Acta Geologica Hungarica 48/2, 133-151.

Hu, X., Wang, Y.L. and Schmitt, R.A., 1988. Geochemistry of sediments on the Rio Grande Rise and the redox evolution of the south Atlantic Ocean. Geochimica et Cosmochimica Acta, 52, 201–207.

Ilić, A. and Neubauer, F., 2005. Tertiary to recent oblique convergence and wrenching of the Central Dinarides: Constraints from a palaeostress study, Tectonophysics, 410, 465-484.

Irvine, T. N., Baragar, W. R. A., 1971. A guide to chemical classification of common volcanic rocks., Canadian Journal of Earth Sciences. 8, 523-547.

Ishihara, S. 1981. The granitoid series and minerallization. Economic Geology, 75th Anniversary Volume, 458-4584.

Ixer, R.A.,and P.R.Duller, P.R., 1998. Virtual Atlas of Opaque and Ore Minerals in their Associations - Website at http://www.smenet.org/opaque-ore.

Jan, M.Q., Windley, B.F., and Khan, A., 1985. The Waziristan ophiolite Pakistan: general geology and chemistry of chromite and associated phases. Econ. Geol. 80, 294-306.

Janjušević, M., (ed.) 1974. Trepca, Monografija Jubilare; Jubiläumsmonographie. Trepca Mining Kombinat Mitrovica.

Janković, S., 1977 The copper deposits and geotectonic setting of the Tethyan Eurasian metallogenic belt. Mineralium Deposita, 12, 37-47.

Janković, S., 1978. The isotopic composition of lead in some Tertiary lead-zinc deposits within the Serbo-Macedonian Metallogenic province. Geoloski Anali Balkanskog Poluostrva, 42, 507-525. (In Serbian).

Janković, S., 1990. The Ore Deposits of Serbia (Yugoslavia): Regional metallogenic settings, environments of deposition and types (In Serbian). Rep. Drust. Fond za geol. Istraz., Econ. Geol. Fakultet Beograd, 760p.

Janković, S., 1995. The principal metallogenic features of the Kopaonik District. In Symposium –"Geology and Metallogeny of the Kopaonik Mt", Kopaonik-Belgrade, 79-101(In Serbian, English Abstract).

Janković, S., 1997.The Carpatho-Balkanides and adjacent area: a sector of the Tethyan Eurasian metallogenic belt. Mineralium Deposita, 32 (5): 426-433.

Janković, S., Jelenković, R. And Vujić, S., 2003. Mineral resources and potential prognosis of metallic and non-metlic mineral raw materials in Serbia and Montenegro at the end of 20th Century; Engineering Academy of Serbia and Montenegro, Section of Mining and Geology sciences, Belgrade, 876p.

Jelenković, R., Kostić, A., Zivotić, D. and Ercegovac, M., 2008. Mineral resources of Serbia, Geologica Carpathica, 59, 4, 345-361.

Johan, Z., 1988. Indium and germanium in the structure of sphalerite: an example of coupled substitution with copper. Mineral. Petrol. 39, 211-229.

Jorge E. Spangenberg, Lluis Fontbote, and Stephen A. Macko An evaluation of the inorganic and organic geochemistry of the San Vicente mississippi valley-type zinc-lead district, central Peru; implications for ore fluid composition, mixing processes, and sulphate reduction (in A special issue on Organic matter and ore deposits; interactions, applications, and case studies, Gize,) Economic Geology and the Bulletin of the Society of Economic Geologists (November 1999), 94(7):1067-1092

Jovanović, M., Downes, H., Vaselli, O., Cvetković, V., Prelević, D. and Pécskay, Z. 2001. Paleogene mafic alkaline volcanic rocks of East Serbia. In: Downes, H. and Vaselli, O. (Eds.): Tertiary magmatism in the Dinarides Balkan Peninsula. - Acta Vulcanologica 13, 159-173.

Kajiwara, Y. and Krouse, H.R., 1971. Sulfur isotope partitioning in metallic sulfide systems. Can. J. Earth Sci. 8, pp. 1397-1408.

Kalogeropoulos, S.I., Kilias, S.P., Bitzios, D.C., Nicolaou, M., Both, R.A., 1989. Genesis of the Olympias carbonate-hosted Pb-Zn (Au, Ag) sulphide de ore deposit, eastern Chalkidiki Peninsula, northern Greece. Econ. Geol. 84, 1210-1234.

Kamaci, O., and Altunkaynak, S., 2010. Mineral Chemistry and Petrography of Lava Successions From Kepsut-Dursunbey Volcanic Field, NW Turkey: Implications For Magmatic Processes and Crystallization Conditions. World Academy of Science, Engineering and Technology, 71, 907-911.

Kamenetsky, V.S., Crawford, A.J., and Meffre, S., 2001, Factors controlling chemistry of magmatic spinel: An empirical study of associated olivine, Cr-spinel and melt inclusions from primitive rocks: Journal of Petrology, 42, 655–671.

Kandić, M., 1987. Basic geological investigations of Pb-Zn occurrences in the Kopaonik district during 1986- the Belo Brdo ore field. Fond Strucnih dokumenata "Geozavoda", Beograd unpublished report (In Serbian).

Karamata, S., 2006. The geodynamical framework of the Balkan Peninsula: its origin due to the approach, collision and compression of Gondwanian and Eurasian units. In: Robertson, A.H.F. and Mountrakis, D. (Eds.): Tectonic Development of the Eastern Mediterranean Region. Geological Society, London, Special Publication 260, 155-178.

Karamata, S., 1995. The Kopaonik block, its position and genesis. In Symposium-"Geology and Metallogeny of the Kopaonik Mt". Kopaonik- Belgrade, 41-45 (In Serbian, English Abstract).

Karamata, S. and Janković, S., 2000. Preface. In: Karamata, S. and Janković, S. (Eds.): Geology and Metallogeny of the Dinarides and the Vardar Zone. Academy of Science and Arts of the Republic of Srpska, Collections and Monographs, Banja Luka, Sarajevo Vol 1, 537p. (In Serbian).

Karamata, S. and Krstić, B. 1996. Terranes of Serbia and neighbouring areas. In: Knezević, V. and Krstić, B. (Eds.): Terranes of Serbia, Beograd, 25-40.

Karamata, S. and Vujnović, L., 2000. Correlation of Palaeozoic units of the Dinarides and the northern part of the Vardar zone. In: Karamata, S. and Janković, S. (Eds.): Geology and Metallogeny of the Dinarides and the Vardar Zone. Academy of Science and Arts of the Republic of Srpska, Collections and Monographs, Banja Luka, Sarajevo Vol 1, 71-78. (In Serbian).

Karamata, S., Majer, V., and Pamić, J., 1980. Ophiolites of Yugoslavia. Ofioliti, Tethian Ophiolites (special issue), 1, 105-125.

Karamata, S., Delaloye, M., Lovrić, A., Knežević, V., 1992. Two genetic groups of tertiary granitic rocks of Central and Western Serbia. Ann Géol Péninsule Balkan 56, 263–283.

Karamata, S., Pecskay, Z., Knezević, V., and Memović, E., 1994. Origin and age of Rogozna (central Serbia) volcanics in the light of new isotopic data. Bull Acad Serb Sci 35, 41-46.

Karamata, S., Knezević, V., Pecskay, Z. and Djordjević, M.,1997. Magmatism and metallogeny of the Ridanj–Krepoljin belt (eastern Serbia) and their correlation with northern and eastern analogues. Mineralium Deposita 32, 452–458.

Karamata, S., Dimitrijević, M. N. and Dimitrijević, M. D., 1999. Oceanic realms in the central part of the Balkan Peninsuladuring the Mesozoic. Slovak Geological Magazine, 5/3 173-177.

Karamata, S., Dimitrijević, M.D. and Dimitrijević, M.N., 2000. A correlation of ophiolitic belts and oceanic realms of the Vardar Zone and the Dinarides. In: Karamata, S. and Janković, S. (Eds.): Geology and Metallogeny of the Dinarides and the Vardar zone. Academy of Science and Arts of the Republic of Srpska, Collections and Monographs, Banja Luka, Sarajevo Vol 1, 191-194. (In Serbian).

Karamata, S., Olujić, J., Protić, L., Milovanović, D., Vujnović, L., Popević, A., Memović, E., Radovanović, Z., and Resimić-Sarić, K., 2000a. The western belt of the Vardar Zone - the remnant of a marginal sea. In: Karamata, S. and Janković, S. (Eds.): Geology and Metallogeny of the Dinarides and the Vardar Zone. Academy of Science and Arts of the Republic of Srpska, Collections and Monographs, Banja Luka, Sarajevo Vol 1, 131-135. (In Serbian).

Karamata, S., Stefanović, D., and Krstić, B., 2003. Permian to Neogene accretion of the assemblage of geologic units presently occuring to the south of the Pannonian basin- development of the Vardar Compoite Terrane and adjacent units. Acta Geologica Hungarica 46 (1), 63-76.

Karamata, S., Steiger, R., Đordjević, P., Knežević, V., 1990. New data on the origin of granitic rocks from western Serbia. Bulletin Académie des Serbe des Sciences et des Arts, Classe des Sciences Mathématiques et naturelles, Sciences naturelles, 32, 1 - 9.

Kempton, P.D. and McGill, R., 2002. Procedures for the analysis of common lead at the NERC Isotope Geosciences Laboratory and an assessment of data quality. NIGL Report Series No. 178, 60 pp.

Kempton, P.D. and Stephens, C.J., 1997. Petrology and geochemistry of nodular websterite inclusions in harzburgite, hole 920D1. In Karson, J.A., Cannat, M., Miller, D.J., and Elthon, D. (Eds.), 1997. Proceedings of the Ocean Drilling Program, Scientific Results, Vol. 153; Chapter 16.

Kerrich, R., 1983. Geochemistry of gold deposits in the Abitibi green Stone belt. Canadian Institute of Mining, Special Paper 27.

Kesler, S.E., 1994. Mineral resources, economics and the environment: New York, McMillan, 391 p.

Khalili, M., 1997. Petrography, mineral-chemistry and geochemistry of the Shir-Kuh granite, Southwest of Yadz, Central Iran. Unpublished Ph.D thesis, University of Hamburg, Germany, 143 pp.

Khosrotehrani, K., and Vazirimoghadam, H., 1993. Stratigraphy of Lower Cretaceous in south and southwest of Yazd: Journal of Earth Sciencs, Geological Survey of Iran7, 43-57 (in Persian).

Kimball, K.L., 1990. Effects of hydrothermal alteration on the compositions of chromian spinels. Contrib. Mineral. Petrol. 105, 337-346.

Klemm, D.D., 1965. Synthesen und Analysen in den Dreiecksdiagrammen FeAsS–CoAsS–NiAsS und FeS2–CoS2– NiS2. Neues Jahrb. Mineral., Abh. 103, 205-255.

Knežević, V. and Cvetković, V., 2000. Triassic rifting magmatism of the Dinarides. In: Karamata, S. and Janković, S. (Eds.): Geology and Metallogeny of the Dinarides and the Vardar zone. Academy of Science and Arts of the Republic of Srpska, Collections and Monographs, Banja Luka, Sarajevo Vol 1, 149-160.

Kober, F., 1924. Geologic der zentralen Balkanhalbinsel. - Die Krigschauplatze geol. gargestellt, Verl. Gebruder Borntraeger, Berlin, 198pp.

Kodera, P., Lexa, J. Rankin, A. H. And Fallick, A.E., 2005. Fluid inclusion and stable isotope evidence for the genesis of Epithermal Au-mineralization at Rozalia mine, Banska Hodrusa, Slovakia. Mineralium Deposita 39, 921-943.

Koepnick, R.B., Burke, W.H., Denison, R.E., Hetherington, E.A., Nelson, H.F., Otto, J.B., Waite, L.E., 1985. Construction of the Seawater $^{87}$Sr/$^{86}$Sr Curve for the Cenozoic and Cretaceous: Supporting Data. Chemical Geology 58, 55-8.

Kosmat, F. 1924. Geologie der zentralen Balkanhalbinsel, mit einer Übersicht des dinarischen Gebirgsbaus. In: Wilder J. (Ed.). Die Kriegsschauplätze 1914-1918 geologisch dargestellt. Verlag Gebrüder Bornträger, Berlin, 198p.

Kotzer, T.G., Kyser, T.K., King, R.W. and Kerrich, R., 1993. An empirical oxygen- and hydrogen-isotope geothermometer for quartz-tourmaline and tourmaline-water, Geochimica et Cosmochimica Acta 57, p. 3421-3426.

Kouzmanov, K., Bogdanov, K., and Ramboz, C., 2005. Te- and Bi-bearing assemblages in the Elshitsa and Radka epithermal deposits, Central Srednogorie, Bulgaria: Mineralogy and genetical features. In: Cook, N.J., Bonev, I.K. (Eds.): Au-Ag-Te-Se deposits, IGCP Project 486, Proceedings of the 2005 Field Workshop, Kiten, Bulgaria, 14-19 September, 108-112.

Kouzmanov, K., Ramboz, C., Lerouge, C., Deloule, E., Beaufort, D., Bogdanov, K., 2003. Stable isotopic constraints on the origin of epithermal Cu-Au and related porphyry copper mineralisations in the southern Pangyurishte district, Srednogorie zone, Bulgaria. In: Eliopoulos, D.G., (ed) Mineral exploration and sustainable development. Millpress, Rotterdam, pp 1181-1184

Kovacs, I., Csontos, L., Szabo, C., Bali, E., Falus, G., Benedek, K., and Zajacz, Z., 2007. Paleogene-early Miocene igneous rocks and geodynamics of the Alpine-Capathian-Pannonian-Dinaric region: an integrated approach. In: Beccaluva, L., Bianchini, G., Wilson, M., (Eds.): Cenozoic Volcanism in the Mediterranean Area. Geol. Soc. Am. Spec. Paper., 418, 93–112.

Kovacs, M., 1999. Tertiary calc-alkaline volcanism and geotectonic evolution in northwestern part of Romanian territory (Gutai Mts., Eastern Carpathians). Rom. J. Tec.t Reg. Geol., 77(1); 38

Kozelj, D., "Mac" Canby,V.M., Naftali, L. 2007. Rudnitza: New porphyry copper-gold occurrence in the Tertiary metallogenic belt, Serbia. In Andrew, C. et al., (Eds.): Digging deeper. Proceedings of the Ninth Biennial SGA Meeting, Dublin, Ireland, 20-23 August, 2007, 157-160.

Kretschmar, U., Scott, S.D., 1976. Phase relations involving arsenopyrite in the system Fe–As–S and their application. Canadian Mineralogist 14, 364–386.

Kuhlemann, J. and Zeeh, S., 1995. Sphalerite stratigraphy and trace element composition of east Alpine Pb-Zn deposits (Drau Range, Austria-Slovenia). Econ. Geol. 90, 2073- 2080.

Kuleshevich, L.V., 1984. Listwanites in the greenstone belts of eastern Karelia; Geologiya Rudnykh Mestorozhdenii (Geology of Ore Deposits), V3, 112-116 (Translated from the Russian, Geological Survey of Canada translation Number 2830).

Kunov, A., 2008. Metasomatic families in Bulgaria — a review. Geologica Balcanica, 37; 1-2, Sofia, 3-17.

Kuscu, G.G., and Floyd, P.A., 2001. Mineral compositional and textural evidence for magma mingling in the Saraykent volcanics. Lithos 56, 207-230.

Kwak, T.A.P. and White, A.J.R., 1982. Contrasting W-Mo-Cu and W-Sn-F skarn types and related granitoids: Mining Geology, v. 32, 339-351.

Le Bas M. J., Le Maitre, R. W., Streckeisen A., Zanettin, B., 1986. A chemical classification of volcanic rocks based on the total alkali-silica diagram. J. Petrol. 27, 745-750

Leach D.L., Bradley D., Lewchuk M., Symons D.T.A, Brannon J. and de Marsili G., 2001. Mississippi Valley- Type lead zinc deposits though geological time: Implications from recent age-dating research. Mineralium Deposita 36, 711-740.

Leake, B.E., 1978. Nomenclature of amphiboles. Mineral. Mag. 42, 533-563.

Leake, B.E., Woolley, A.R., Arps, C.E.S., Birch, W.D., Gilbert, M.C., Grice, J.D., Hawthorne, F.C., Kato, A., Kisch, H.J., Krivovichev, V.G., Linthout, K., Laird, J., Mandarino, J.A., Maresch, W.V., Nickel, E.H., Rock, N.M.S., Schumacher, J.C., Smith, D.C., Stephenson, N.C.N., Ungaretti, L., Whittaker, E.J.W., and Youshi, G., 1997. Nomenclature of amphiboles: Report of the subcommittee on amphiboles of the International Mineralogical Association, Commission on new minerals and mineral names: American Mineralogist, v. 82, 1019–1037.

Lentz, D.R. 2002. Sphalerite and arsenopyrite at ate Brunswick No. 12 massive-sulfide deposit, Bathurst Camp, New Brunswick: Constraints on P-T Evolution. The Canadian Mineralogist Vol. 40, pp. 19-31

Lescuyer, J.L., Hushmand Zadeh, A., and Deliran, F., 2003. Gold metallogeny in Iran: a preliminary review. In: Eliopoulis et al., (Eds.): Mineral Exploration and Sustainable Development , Millpress Rotterdam, 1185-1188.

Lexa, J., Stohl, J., Konecny, V., 1999. The Banska Stiavnica ore district: relationship between metallogenetic processes and the geological evolution of a *stratovolcano*. Miner. Deposita 34, (5-6), 639-655.

Li, Y.B., Liu, J.M., 2006. Calculation of sulfur isotope fractionation in sulfides. Geochimica et Cosmochimica Acta 70: 1789 - 1795.

Lips, A.L.W., 2007. Geodynamic causes of copper and gold concentrations in the Tethys Belt. In Andrew, C. et al., (Eds.): Digging deeper. Proceedings of the Ninth Biennial SGA Meeting, Dublin, Ireland, 20-23 August, 2007, 93-96.

Loftus-Hills, G., Solomon, M., 1967. Cobalt, nickel and selenium as indicators of ore genesis. Mineralium Deposita 2, 228- 242.

Lowell, J. and Guilbert, J., 1970. Lateral and Vertical Alteration-Mineralization Zoning in Porphyry Ore Deposits: Economic Geology, 64, 373-408.

Lugović, B., Altherr, R., Raczek, I., Hofmann, A.W., and Majer, V., 1991: Geochemistry of peridotites and mafic igneous rocks from the Central Dinaric Ophiolite Belt, Yugoslavia: Contributions to Mineralogy and Petrology 106, 201-216.

Luhr, J.F., Carmichael, I.S.E., 1980. The Colima volcanic complex, Mexico: I. Post-caldera andesites from volcano Colima. Contributions to Mineralogy and Petrology71, 343-372.

Lusk, J. and Calder, B.O.E, 2004. The composition of sphalerite and associated sulfides in reactions of the Cu Fe-Zn-S, Fe-Zn-S and Cu-Fe-S systems at 1 bar and temperatures between 250 and 535°C. Chemical Geology 203; 319-345.

Lusk, J. and Bray, D.M., 2002. Phase relations and sulfur fugacity for selected reactions in the Cu–Fe–S and Fe S systems at temperatures between 185 jC and 460 jC. Chem. Geol. 192, 227–248.

Lustrino, M., 2000. Volcanic activity from the Neogene to the Present evolution of the Western Mediterranean area. A review. Ofioliti, 25, 87-101.

Macaulay, C. I., Fallick A. E., Haszeldine R. S. and Graham C. M., 2000. Methods of laser-based stable isotope measurement applied to diagenetic cements and hydrocarbon reservoir quality. Clay Minerals 35, 313-322.

Macfarlane, A.W., 1999. Isotopic studies of northern Andean crustal evolution and ore metal sources, in Skinner, B.J., ed., Geology and ore deposits of the central Andes: Society of Economic Geologists, Special Publication, 7, 195–217.

Macfarlane, A.W., Marcet, P., LeHuray, A.P., and Petersen, U., 1990, Lead isotope provinces of Central Andes inferred from ores and crustal rocks: Economic Geology, 85, 1857–1880.

Malý K. and Dolníček Z. 2005. Pb-Zn-Ag vein mineralization of the central part of the Českomoravská vrchovina Upland (Czech Republic): S, C, and O stable isotope study . Bulletin of Geosciences, Czech Geological Survey, 80, 4, 307-319.

Marchev, P., Raicheva, R., Downes, H., Vaselli, O., Chiaradia, M., and Moritz, R., 2004. Compositional diversity of Eocene–Oligocene basaltic magmatism in the Eastern Rhodopes, SE Bulgaria: implications for genesis and tectonic setting. Tectonophysics, 393, 301–328.

Marchev, P., Downes H., Thirlwall, M. F., Moritz, R., 2002. Small-scale variations of 87Sr/86Sr isotope composition of barite in the Madjarovo low-sulfidation epithermal system, SE Bulgaria: implications for sources of Sr, fluid fluxes and pathways of the ore-forming fluids. – Mineral. Deposita, 37, 669-677.

Marchev, P., Rogers, G., Conrey, R., Quick, J., Vaselli, O. and Raicheva, R. 1998. Paleogene orogenic and alkaline basic magmas in the Rhodope zone: relationships, nature of magma sources, and role of crustal contamination. In: Christofides, G., Marchev, P. and Serri, G. (Eds.): Tertiary magmatism of the Rhodopian Region. - Acta Vulcanologica 10, 217-232.

Marcoux, E., Grancea, L., Lupulescu, M., and Milesi, J.P., 2002, Lead isotope signatures of epithermal and porphyry-type ore deposits from the Romanian Carpathian Mountains: Mineralium Deposits, 37, 173-184.

Marshall, D., Anglin, C.D., and Mumin, H., 2004. Ore mineral atlas: GAC, Mineral Deposits Division, p.112.

Matsuhisa, Y., Goldsmith, J.R. and Clayton, R.N., 1979. Oxygen isotopic fractionation in the system quartz-albite-anothite-water. Geoch. Cosmochim. Acta 43, 1131-1140.

McCallum, M.E., 1985. Experimental Evidence for Fluidization Processes in Breccia Pipe Formation. Economic Geology, 80, 1523-1543.

McCrea, J.M., 1950, On the isotopic geochemistry of carbonates and a paleotemperature scale: Journal of Chemical Physics, v. 18, p. 849-857.

McCulloch. M.T., and Gamble, J.A., 1991. Geochemical and geodynamical constraints on subduction zone magmatism. Earth Planet. Sci. Lett. 102, 358-374.

McDonough. W.F., 1990. Constraints on the composition of the continental lithospheric mantle. Earth Planet. Sci. Lett. 101, 1-18.

McKenzie D.P., 1972. Active Tectonics of the Mediterranean Region. Geophysical Journal of the Royal Astronomical Society, 30, 109-185.

McKenzie, D.P., 1978. Active tectonics of the Alpine-Himalayan belt: the Aegean Sea and surrounding regions. Geophysical Journal of the Royal Astronomical Society, 55, 217-354.

McLennan S.M., 1989. Rare earth elements in sedimentary rocks: influence of provenance and sedimentary processes. In Lipin B.R. and McKay G.A. (Eds.): Geochemistry and mineralogy of rare earth elements. Reviews in Mineralogy 21, pp. 1209-1264.

McLimans, R.K., Barnes, H.L., and Ohmoto, H., 1980. Sphalerite stratigraphy of the Upper Mississippi Valley zinc-lead district, southwest Wisconsin. Econ. Geol. 75, 351-361.

Megaw, P.K.M., Ruiz, J., and Titley, S.R., 1988. High-temperature, carbonate-hosted Ag-Pb-Zn(Cu) deposits of northern Mexico. Econ Geol 83, 1856-1885.

Meinert, L.D., 1993. Igneous petrogenesis and skarn deposits: Geological Association of Canada Special Paper 40, 569-583.

Meinert, L.D., 1995. Compositional variation of igneous rocks associated with skarn deposits - Chemical evidence for a genetic connection between petrogenesis and mineralization: in Thompson, J.F.H., ed., Magmas, fluids, and ore deposits, Min. Assoc. Can. Short Course Series, 23, 401-418.

Meinert, L.D.,1992. Skarns and skarn deposits. Geoscience Canada, 19, 145 -162.

Meinert, L.D., 2007. Exploration for skarn deposits; Short Course Notes; 9th Biennial SGA meeting, Dublin 182p.

Melfos, V., Vavelidis, M., Christofides, G., Seidel, E., 2002. Origin and evolution of the Tertiary Porphyry copper-molybdenum deposit in the Maronia area, Thrace, Greece. Miner Deposita, 37, 648-668.

Mellini, M., Rumori, C. and Viti, C., 2005. Hydrothermally reset magmatic spinels in retrograde serpentinites: formation of "ferritchromit" rims and chlorite aureoles. Contrib. Mineral. Petrol. 149, 266-275.

Mercier, J.C.C., 1985. Olivines and Pyroxenes. In Wenk, H.R. (Ed.), Preferred Orientation in Deformed Metals and Rocks: An Introduction to Modern Texture Analyses: New York (Academic Press), 407-430.

Metcalf R.V. and Shervais J.W., 2008. Suprasubduction-zone ophiolites: Is there really an ophiolite conundrum? In: Wright, J.E., and Shervais, J.W., (Eds.): Ophiolites, Arcs, and Batholiths: A Tribute to Cliff Hopson: Geological Society of America Special Paper 438, 191–222

Mićić, I., 1980. Contact, pneumatolytic and hydrothermal alterations in igneous rocks of Kopaonik region. Geological and Geophysical Survey Memoirs, Belgrade (in Serbian with Abstract in English),19, 138pp.

Mićić I., Urošević D., Kandić M., Klisić M. and Simić D. 1972. Findings of Triassic conodont fauna in the metamorphic complex of Kopaonik Mt. Zapisnici Srp. Geol. Druš. za 1968, 1969 i 1970 (Zbor 10. XII 1968), 103-104 (in Serbian, Cyrillic).

Miletić, G. and Mladenović, M., 1995. Promising areas lead and zinc deposit Belo Brdo. In Symposium – "Geology and Metallogeny of the Kopaonik Mt.", Kopaonik-Belgrade, 275-283.

Milovanović, D., 1984. Petrology of low metamorphics rocks of the middle part of the Drina-Ivanjica Paleozoic. Bulletin, Museum d'histoire naturelle de Belgrade A, Belgrade 39, 13-139. (In Serbian with a French abstract).

Milutinović, S., 2008. Elaborat o rezultatima geoloških istraživanja polimetaličnih mineralizacija (Cu, Au, Mo, Pb, Zn) na prostoru Medenovac - Karavansalija u rudnom polju Rogozna za 2007. Godinu. Internal report, unpublished.

Mitchell, A.H. and Garson, M.S., 1972. Relationship of porphyry copper and circum-Pacific tin deposits to palaeo-Benioff zones. Transaction of Institute of Mining and Metallurgy, 81, B10-25.

Mladenović, M, 2005. Methods of exploration for complex polymetallic ore bodies in the Belo Brdo ore field, Kopaonik district: Belgrade University; 60p: unpublished report (In Serbian)

Moh, G.H., 1980. Ore syntheses, phase equilibria studies and applications. Neues Jahrbuch fu¨ r Mineralogie, Abhandlungen 139, 114-154.

Möller, P., 1985. Development and application of the Ga/Ge-geothermometer for sphalerite from sediment-hosted deposits. Gebrüder Borntraeger Monograph Series on Mineral Deposits 25, 15-30.

Monthel J., Vadala P., Leistel J.M., Cottard F., with the collaboration of Ilić M., Strumberger A., Tosović R., Stepanović A., 2002. Mineral deposits and mining districts of Serbia. Compilation map and GIS databases. BRGM RC-51448-FR, 67p.

Morimoto, N., Fabries, J., Ferguson, A.K., Ginzburg, I.V., Ross, M., Seifert, F.A., Zussman, J., Aoki, K. and Gottardi, D., 1988, Nomenclature of pyroxenes. Am. Min., 62, 53-62.

Murphy, J.B., 2007. Igneous Rock Associations 8: Arc Magmatism II: geochemical and isotopic characteristics. Geoscience Canada 34, 7–36.

Nabavi, M. H., 1972, Geological map of Yazd quadrangle, scale 1:250,000: Tehran, Iran, Geological Survey of Iran.

Nakada, S., 1991. Magmatic processes in titanite-bearing dacites, central Andes of Chile and Bolivia. Am. Mineral. 76, 548-560.

Nakamura, K., and Kato, Y., 2004. Carbonatization of oceanic crust by the seafloor hydrothermal activity and its significance as a CO2 sink in the Early Archean. Geochimica et Cosmochimica Acta; 68; (22), 4595–4618.

Nasir, S., Al Sayigh, A. R., Al Harthy, A., Al-Khirbash, S., Al-Jaaidi, O., Musllam, A., Al-Mishwat, A., and Al-Busaidi, S., 2007. Mineralogical and geochemical characterization of listwaenite from the Semail ophiolite, Oman. Chemie Der Erde - Geochem. 67, 213-228.

Nedelcu, L., Voicu, G., Voicu, C., Rosu, E., Zamirca, A., and Gaftoi, F., 1992. Morphology of the pyrite crystals from the Main vein at Baia Sprie. Genetical significances. Rom. J. Mineral., 75,53–64.

Nelson, S.T., Montana, A., 1992. Sieved textured plagioclase in volcanic rocks produced by rapid decompression. Am. Mineral. 77, 1242-1249.

Neubauer, F. and Heinrich, C., with the GEODE ABCD Working Group including Tomek C., Lips A., Nakov R., A. von Quadt, Peytcheva I., Handler R., Bonev I., Ivascanu P., Rosu, Zivko Ivanov E., Kaiser-Rohrmeier M. and others, 2003. Late Cretaceous and Tertiary geodynamics and ore deposit evolution of the Alpine-Balkan-Carpathian-Dinaride orogen. In Eliopoulos et al. (Eds.): Mineral Exploration and Sustainable Development, Millpress, Rotterdam, 1133-1136.

Nicolas, A., and Poirier, J.P., 1976. Crystalline Plasticity and Solid State Flow in Metamorphic Rocks: New York (Wiley), 444pp.

Nixon, G.T., Pearce, T.H., 1987. Laser-interferometry study of oscillatory zoning in plagioclase: the record of magma mixing and phenocryst recycling in calc-alkaline magma chambers, Iztacc'chuatl volcano, Mexico. Am. Mineral. 72, 1144-1162.

Oakes, C.S., Bodnar, R.J. and Simonson, J.M.,1990. The system NaCl-CaCl2-H2O: the ice liquidus at 1 atm total pressure. Geochmica et Cosmochimica Acta 54, 603-610.

Oen, I.S., Kager, P. and Kieft, C.,1980. Oscillatory zoning of a discontinuous solid-solution series: sphalerite-stannite. Am. Mineral. 65, 1220-1232.

O'Hanley, D.S., 1996, Serpentinites: Records of Tectonic and Petrological History: New York, Oxford University Press, 277pp.

Ohara, Y., Stern, R.J., Ishii, T., Yurimoto, H., and Yamazaki, T., 2002. Peridotites from the Mariana Trough: First look at the mantle beneath an active backarc basin: Contributions to Mineralogy and Petrology, v. 143, p. 1-18.

Ohmoto, H., 1986. Stable isotope geochemistry of ore deposits. In Valley, J.W., et al., (Eds.): Stable isotopes in high temperature geological processes. Mineralogical Society of America.: Reviews in Mineralogy, v 16, 491-559.

Ohmoto, H., 1972. Sytematics of sulphur and carbon isotopes in hydrothermal ore deposits. Econ. Geol. 67, 551-578.

Ohmoto, H., and Goldhaber, M.B., 1997. Sulphur and Carbon isotopes. In Barnes, H.L (ed.) Geochemistry of hydrothermal ore deposits, 3rd ed. Wiley-Interscience, New York, 229-302.

Ohmoto, H., and Rye, R.O., 1979. Isotopes of sulfur and carbon. In: Barnes HL, (ed) Geochemistry of hydrothermal ore deposits, 2nd ed. Wiley-Interscience, New York, 509-567.

Olujić, J., 1978. Distribution and genesis of Mesozoic flysches in Bosnia and Herzegovina. Unpublished Manuscript, Geological Survey Sarajevo, Sarajevo. (In Serbian)

O'Neil, J.R., and Silberman, M.L., 1974. Stable isotope relations in epithermal Au-Ag deposits. Econ. Geol. 69, 902-909.

O'Neil, J. R., and Taylor, H. P., 1969. Oxygen isotope equilibrium between muscovite and water. Jour. Geophys Research, 74, 6012-6022.

Palinkaš, L. 1988. Geochemical Characteristics of Ljubija, Samoborska Gora, Gorski Kotar and Lika Metallogenic Ore Fields (in Croatian). Prirodoslovno-matematicki fakultet, 108 p. PhD thesis, unpublished.

Palinkaš, L. 2000. Mineral deposits related to geotectonic units of the Dinarides. Geoloske vijesti, Hrvatsko geolosko drustvo, 145-147.

Palinkaš, L.A., Borojević-Sostarić, S. and Strmić-Palinkaš, S., 2008. Metallogeny of the Northwestern and Central Dinarides and Southern Tisia. Ore Geology Reviews, 34, 501-520.

Pamić, J., 1984. Triassic magmatism of the Dinarides in Yugoslavia. Tectonophysics 109, 273-307.

Pamić, J., 1993. Eoalpine to Neoalpine magmatic and metamorphic processes in the northwestern Vardar Zone, the easternmost Periadriatic Zone and the southwestern Pannonian Basin. Tectonophysics 226, 503-518.

Pamić, J., 2000. The Sava–Vardar Zone (SVZ). In: Pamić, J., Tomljenović, B. (Eds.): Outline of Geology of the Dinarides and South Tisia with field guidebook. Vijesti 37/2, PANCARDI 2000, Dubrovnik, Croatia, 1-3/10/2000, 19–22.

Pamić, J. 2002. The Sava-Vardar Zone of the Dinarides and Hellenides versus the Vardar Ocean. Eclogae Geologicae Helvetiae 95, 99-113.

Pamić, J., Balen, D., Herak, M., 2002a. Origin and geodynamic evolution of Late Paleogene magmatic associations along the Periadriatic-Sava-Vardar magmatic belt. Geodin. Acta 15, 209–231.

Pamić J. and Balen D., 2001. Tertiary magmatism of the Dinarides and the adjoining South Pannonian Basin. Acta Vulcan., 13, 9- 24.

Pamić, J., Gusić, I. and Jelaska, V., 1998. Geodynamic evolution of the Central Dinarides. Tectonophysics, 297, 251-268.

Pamić, J., Gušić, I., and Jelaska, V., 2000. Basic geological features of the Dinarides and South Tisia. In: Pamić, J., Tomljenović, B. (Eds.), Outline of Geology of the Dinarides and South Tisia with field guidebook. Vijesti 37/2, PANCARDI 2000, Dubrovnik, Croatia, 1–3/10/2000, 9–18.

Pamić, J., McKee, E.H., Bullen, T.D. and Lanphere, M.A. 1995. Tertiary Volcanic Rocks from the Southern Pannonian Basin, Croatia. International Geology Review, 37, 259-283.

Pamić, J., Tomljenović, B. and Dražen, B., 2002. Geodynamic and petrogenetic evolution of Alpine ophiolites from the central and NW Dinarides: an overview. Lithos, 65: 113-142.

Pamić, J., Balen, D., Herak, M., 2002a. Origin and geodynamic evolution of Late Paleogene magmatic associations along the Periadriatic-Sava–Vardar magmatic belt. Geodin. Acta 15, 209-231.

Parkinson, I.J., and Pearce, J.A., 1998. Peridotites from the Izu-Bonin-Mariana forearc (ODP Leg 125): Evidence for mantle melting and melt-mantle interaction in a supra-subduction zone setting: Journal of Petrology, v. 39, p. 1577–1618.

Pattrick, R.A.D., Dorling, M. and Polya, D.A., 1993. TEM study of indium- and copper-bearing growth-banded sphalerite. Can. Mineral. 31, 105-117.

Pearce, J.A., 1982, Trace element characteristics of lavas from destructive plate boundaries. In Thorpe, R.S., (ed), Andesites Orogenic Andesites and Related Rocks, 525-548.

Pearce, J.A., and Cann, J.R., 1973. Tectonic setting of basic volcanic rocks determined using trace element analyses. Earth and Planetary Science Letters, 19, 290-300.

Pearce, J.A. and Parkinson, I.J., 1993. Trace element models for mantle melting: application to volcanic arc petrogenesis. In: Prichard, H.M., Alabaster, T., Harris, N.B.W. and Neary, C.R. (Eds.): Magmatic Processes and Plate Tectonics - Geological Society Special Publication 76, 373-403.

Pearce, J.A. and Peate, D.W. 1995. Tectonic implications of the composition of volcanic arc magmas. Annual Review of Earth and Planetary Sciences, 23, 251-285.

Pearce, J. A., Harris, N. W. and Tindle, A. G., 1984. Trace element discrimination diagrams for the tectonic interpretation of granitic rocks. Journal of Petrology 25, 956–983.

Pe-Piper, G., Christofides, G., and Elefftheriadis, G., 1998. Lead and neodymium isotopic composition of Tertiary igneous rocks of northern Greece and their regional significance. In: Christofides, G., Marchev, P., Serri, G. (Eds.): Tertiary Magmatism of the Rhodopian Region. Acta. Vulcanol., vol. 10(2), 255-263.

Petković, K., 1961. Tectonic map FNR Yugoslavia. - Glas SANU, 249p, Beograd (in Serbian).

Pirajno, F., 2009. Hydrothermal Proceses and Mineral Systems, Springer Netherlands, 1252p.

Plissart, G., Féménias, O., Măruntiu, M., Diot, H., and Demaiffe, D., 2009. Mineralogy and geothermometry of gabbro-derived listvenites in the Tisovita–Iuti ophiolite, southwestern Romania; The Canadian Mineralogist, 47; 81-105.

Porter, T.M., 1998. An overview of the world's porphyry and other hydrothermal copper and gold deposits and their distribution. In: Porter T.M., (ed). Porphyry and hydrothermal copper and gold deposits: a global perspective. Conference Proceedings. Australian Mineral Foundation, Glenside, South Australia, 3-17.

Potter, R.W., 1977. Pressure corrections for fluid-inclusion homogenization temperatures based on the volumetric properties of the system $NaCl-H_2O$. Journal of Research of the U.S. Geological Survey 5, 603-607.

Potter, R.W, Clynne, M.A. and Brown, D.L., 1978. Freezing point depression of aqueous sodium chloride solutions. Economic Geology, 73; 2; 284-285.

Prelević, D., Foley, S.F., and Cvetković, V., 2007. A review of petrogenesis of Mediterranean Tertiary lamproites: A perspective from the Serbian ultrapotassic province. In Beccaluva, L., Bianchini, G., and Wilson, M., (Eds.): Cenozoic Volcanism in the Mediterranean Area: Geological Society of America Special Paper 418, 113–129.

Prelević, D., Foley, S.F., Romer, R.L., Cvetković, V., and Downes, H., 2005. Tertiary ultrapotassic volcanism in Serbia: Constraints on petrogenesis and mantle source characteristics: Journal of Petrology, 46, p. 1443– 1487.

Prelević, D., Cvetković, V., Foley, S.F., Jovanović, M. and Melzer, S. 2001. Tertiary ultrapotassic-potassic rocks from Serbia, Yugoslavia. In: Downes, H., Vaselli, O. (Eds.): Tertiary magmatism in the Dinarides Balkan Peninsula. - Acta Vulcanologica 13, 101-115.

Prichard, H.M., Sá, J.H.S., and Fischer, P.C., 2001. Platinum-group mineral assemblages and chromite composition in the altered and deformed Bacuri Complex, Amapá, Northeastern Brazil: Canadian Mineralogist, v. 39, p. 377-396.

Princivalle, F., Della Giusta, A. and Carbonin, S. 1989. Comparative crystal chemistry of spinels from some suites of ultramafic rocks. Mineral. Petrol. 40, 117-126.

Protić, Lj., 2003. Iron Deposits Adamusa and Tomasica, Ljubija Metallogenic Field. In: Grubić, A. and Cvijić, R., (Eds.): Novi Prilozi za Geologiju i Metalogeniju Rudnika Gvozdja Ljubija. Mining Institute Prijedor, 134pp.

Radosavljević, M., 1989. Ore mineral study in the Belo Brdo and Crnac deposits; Institut za tehnologiju Nuklearnih i drugih mineralnih sirovina OOUR Institut za pripremu mineralnih sirovina, Beograd 38 pp; Unpublished report.

Radulović, B. 1992. Ležište cinka i olova Karadak.- Radovi Geoinstituta, Beograd, knjiga 27, 169-180.

Radulović, B., Savić, R. 1995. Deposits and potential for base and precious metals in the ore field Raska. Geology and Metallogeny of the Kopaonik Mountain, 284-298.

Ramdohr, P., 1980. The Ore Minerals and their Intergrowths, 2nd *edition* Pergamon *Press, Oxford 1202 pp.*

Rampnoux, J.-P., 1970. La géologie du Sandjak: mise en évidence de la nappe du Pešter: confines serbo-montenegrins (Yougoslavie). Bulletin de la Societé géologique de France, 7, XI, 881-893.

Rankin, A.H. 1995. Hydrothermal orefields and ore fluids. Geological Society, London, Memoirs, 16; 237-247.

Rankin, A.H. and Alderton, D.H.M., 1983. Fluid inclusion petrography of SW England granites and its potential in mineral exploration. Mineralium Deposita Supplement 2, 18, 335-347.

Rankin, A.H. and Shepherd, T.J. 1998. Fluid Inclusion techniques of analysis, In: Richards, J. P. and Hedenquist, J.W., (Eds.): Techniques in Hydrothermal Ore Geology . Revs. In Economic Geology, 7, 125-149.

Raymond, O.L., 1996. Pyrite composition and ore genesis in the Prince Lyell copper deposit, Mt Lyell mineral field, western Tasmania, Australia. Ore Geology Reviews 10, 231-250.

Reed, M.H., and Palandri, J., 2006. Sulfide Mineral Precipitation from Hydrothermal Fluids. Reviews in Mineralogy and Geochemistry 61, 609-631.

Rice, C.M., McCoyd, R.J., Boyce, A.J., and Marchev, P., 2007. Stable isotope study of the mineralization and alteration in the Madjarovo Pb–Zn district, south-east Bulgaria. Miner. Deposita, 42, 691–713

Richards, J.P., 2003. Tectono-magmatic precursors for porphyry Cu-(Mo-Au) deposit formation: Economic Geology and the Bulletin of the Society of Economic Geologists, 96, 1515–1533.

Richards, J.P., 2009. Postsubduction porphyry Cu-Au and epithermal Au deposits: Products of remelting of subduction-modified lithosphere. Geology; The Geological Society of America 37; 3; 247-250.

Robb, L. 2005. Introduction to Ore-forming Processes. Blackwell Publishing, Oxford, 373pp.

Roberts, F.I., 1982. Trace element geochemistry of pyrite: a useful guide to the occurrence of sulfide base metal mineralization. Journal of Geochemical Exploration 17, 49-62.

Robertson, A.H.F., 2002. Overview of the genesis and emplacement of Mesozoic ophiolites in the Eastern Mediterranean Tethyan region. Lithos 65, 1-67.

Robertson, A.H.F. and Dixon, J.E., 1984. Introduction: aspects of the geological evolution of the Eastern Mediterranean. In: Dixon, J.E., Robertson, A.H.F. (Eds.): The Geological Evolution of the Eastern Mediterranean. Geological Society, London Special Publication 17, 1–74.

Robertson, A.H.F. and Karamata, S., 1994. The role of subduction-accretion processes in the tectonic evolution of the Mesozoic Tethys in Serbia. Tectonophysics, 234: 73-94.

Robertson, A.H.F. and Mountrakis, D. (Eds.), 2006. Tectonic Development of the Eastern Mediterranean Region. Geological Society, London, Special Publication 260.

Robertson, A.H.F, Karamata, S. and Sarić, K. (Eds.), 2009. Ophiolites and related geology of the Balkan region, The Mesozoic ophiolite belts of the northern part of the Balkan Peninsula, 108, (1-4), 280pp.

Robertson, A.H.F, Karamata, S., Sarić, K., 2009a. Overview of ophiolites and related units in the Late Palaeozoic-Early Cenozoic magmatic and tectonic development of Tethys in the northern part of the Balkan region. Lithos, 108, 1-36.

Robertson, A.H.F., Clift, P.D., Degnan, P.J., and Jones, G., 1991. Palaeographic and palaeotectonic evolution of the eastern Mediterranean Neotethys. Palaeogeography, Palaeoclimatology, Palaeoecology 87, 289-343.

Robertson, A.H.F., Dixon, J.E., Brown, S., Collins, A., Morris, A., Pickett, E.A., Sharp, I., and Ustaömer, T., 1996. Alternative tectonic models for the Late Palaeozoic–Early Tertiary development of Tethys in the Eastern Mediterranean region. In: Morris, A., Tarling, D.H. (Eds.): Palaeomagnetism and Tectonics of the Mediterranean Region. Geological Society, London, Special Publications 105, 239–263.

Robertson, A.H.F., Ustaömer, T., Pickett, E., Collins, A., Andrew, T. and Dixon, J.E., 2004. Testing models of Late Palaeozoic–early Mesozoic orogeny in Western Turkey: support for an evolving open-Tethys model. Journal of the Geological Society, London 161, 501–511.

Robinson, B.W. and Kusakabe, M., 1975. Quantitative preparation of SO2 for 34S/32S analysis from sulfides by combustion with cuprous oxide: Analytical Chemistry, 47, 1179-1181.

Roedder, E., 1984. Fluid inclusions. Reviews in Mineralogy, 12, 644 pp.

Roedder, E. and Coombs, D. S., 1967.Immiscibility in granitic melts indicated by fluid inclusions in ejected granite blocks from Ascension Island. J. Petrol.8, 417–451.

Roedder, E., and Bodnar, R.J., 1980. Geologic pressure determinations from fluid inclusion studies. Ann. Rev. Earth Planet. Sci. 8, 263-301.

Roksandić, M., 1971. Geotectonic position and forms of large peridotite bodies in the Dinarides in the light of gephysical data. Vesnik, Zavod za geološka i geofizicka istraživanja, C, XII-XIII, 139-147. Belgrade. (In Serbian).

Rollinson, H.R., 1993. Using Geochemical Data: Evaluation, Presentation, Interpretation. Longman Harlow, 352pp.

Rosenbaum, J.M., and Sheppard, S.M.F. 1986. An isotopic study of siderites, dolomites and ankerites at high temperatures: Geochimica et Cosmochimica Acta, 50, 1147-1159.

Royse, K. R., P. D. Kempton, and D. P. F. Darbyshire, 1998. Procedure for the analysis for rubidium-strontium and samarium-neodymium isotopes at the NERC Isotope Geosciences Laboratory, NIGL Rep. Ser. 121, 28 pp., NERC Isotope Geosci. Lab., Keyworth, England.

Rusk, B.G., Reed, M.H., and Dilles, J.H., 2008. Fluid inclusion evidence for magmatic-hydrothermal fluid evolution in the porphyry copper-molybdenum deposit at Butte, Montana: Economic Geology; 103, 307-334.

Rutherford, M. J., P. M. Hill. 1993. Magma ascent rates from amphibole breakdown: An experimental study applied to the 1980-1986 Mount St. Helens eruption. J. Geophysical Research 98, 19667-19685.

Rye, R.O., 1993. The evolution of magmatic fluids in the epithermal environment-the stable isotope perspective. Econ. Geol., 88, 733-753.

Rye, R.O., 1974. A comparison of sphalerite-galena sulfur isotope temperatures with filling temperatures of fluid inclusions. Econ. Geol. 69, pp. 26-32.

Rye, R.O., and Ohmoto, H., 1974. Sulfur and carbon isotopes and ore genesis: a review. Econ. Geol. 69, 826-842.

Saccani, E., Beccaluva, L., Coltorti, M. and Siena, F., 2004. Petrogenesis and tectono-magmatic significance of the Albanide - Hellenide Subpelagonian ophiolites. Ofioliti, 29, 1, 75-93.

Sakai, H., 1968. Isotopic properties of sulphur compounds in hydrothermal processes: Geochem. Jour.( Japan), 2, 29-49.

Sakuyama, M., 1981. Petrological study of the Myoko and Kurohime Volcanoes, Japan: crystallization sequence and evidence for magma mixing. J. Petrol. 22, 553-583.

Šarić K., Cvetković V., Romer R.L., Christofides G. and Koroneos A., 2009. Granitoids associated with East Vardar ophiolites (Serbia, F.Y.R. of Macedonia and northern Greece): Origin, evolution and geodynamic significance inferred from major and trace element data and Sr-Nd-Pb isotopes. Lithos, 108: 131-150.

Saunders, A.D., Norry, M.J., Tarney, J., 1991. Fluid influence on the trace element compositions of subduction zone magmas. Philos. Trans. R. Soc. Lond. Ser. A: Math. Phys. Eng. Sci. 335, 377–392.

Schaefer, M.O., 2009. Paleoproterozoic Mississippi Valley-Type Pb-Zn deposits of the Ghaap Group, Transvaal Supergroup in Griqualand West, South Africa. PhD Thesis, 332pp: http://hdl.handle.net/10210/1969.

Schefer, S., Cvetković, V., Fügenschuh, B., Kounov, A.,Ovtcharova, M., Schaltegger, U., and Schmid, S.M., 2010. Cenozoic granitoids in the Dinarides of southern Serbia: age of intrusion, isotope geochemistry, exhumation history and significance for the geodynamic evolution of the Balkan Peninsula. Int J Earth Sci (Geol Rundsch).

Schefer, S., Egli, D., Missoni, S., Bernoulli, D., Fügenschuh, B., Gawlic, H.J., Jovanović, D., Krystyn, L., Lein, R., Schmid, S.M., and Sudar, M.N., 2010a. Triassic metasediments in the Internal Dinarides (Kopaonik area, southern Serbia): stratigraphy, paleogeographic and tectonic significance. Geol Carpathica 61,89–109

Schmid, S.M., Bernoulli, D., Fügenschuh, B., Matenco, L., Scheffer, S., Schuster, R., Tischler, M., Ustaszewski, K., 2008. The Alps-Carpathians-Dinarides-connection: a correlation of tectonic unit. Swiss Journal of Geosciences 101/1, 139-183.

Schumacher, F. 1950. Leziste Trepca i njegova okolina. Izdavacko Preduzece Saveta za Energetiku i Ekstrativnu Industriju vlade SFRJ, Beograd (Translation from German to Serbo-Croatian by Lj. Baric).

Schumacher, F. 1954. The ore deposits of Yugoslavia and the development of its mining industry. Economic Geology, 49, 451–492.

Scott, S.D.,1983. Chemical behaviour of sphalerite and arsenopyrite in hydrothermal and metamorphic environments. Mineral. Mag. 47, 427-435.

Scott, S.D., 1973. Experimental calibration of the sphalerite geobarometer. Econ. Geol. 68, 466–474.

Scott, S.D. and Barnes, H.L., 1971. Sphalerite geothermometry and geobarometry. Econ. Geol. 66, 653–669.

Şengör, A.M.C., 1984. The Cimmeride orogenic system and the tectonics of Eurasia. Geological Society of America Special Publication 195. 82pp.

Şengör, A.M.C., (Ed.) 1989. Tectonic evolution of the Tethyan Region. Proceedings of the NATO Advanced Study Institute on Tectonic Evolution of the Tethyan Region, the Faculty of Mines, Istanbul Technical University, Turkey, 740p.

Şengör, A.M.C., 1990. A new model for the Late Paleozoic- Mesozoic tectonic evolution of Iran and implication for Oman Region: Geological Society of London. Special Publication 49, 797-831.

Serafimovski, T., 2000. The Lece-Chalkidiki metallogenic zone: geotectonic setting and metallogenic features. Geologija, 42, 159-164. Ljubljana, 2000.

Serafimovski, T., and Tasev, G., 2006. Sulfur isotope study of sulfides from some mineral deposits from the Lece-Chalkidiki metallogenic zone. Geosciences, 251-254.

Seward, T.M., and Barnes, H.L., 1997. Metal transport by hydrothermal ore fluids. In Barnes, H.L (ed.) Geochemistry of hydrothermal ore deposits. 3rd ed. Wiley-Interscience, New York, 435-486.

Shand, S. J.,1943. Eruptive Rocks. Their Genesis, Composition, Classification, and Their Relation to Ore-Deposits with a Chapter on Meteorite. New York: John Wiley and Sons.

Sharp Z. D., 1990. A laser-based microanalytical method for the in situ determination of oxygen isotope ratios of silicates and oxides. Geochem. Cosmochim. Acta 54, 1353-1357.

Sharp, Z.D., Essene, E.J., and Kelly, W.C., 1985. A re-examination of the aresenopyrite geothermometer: pressure considerations and applications to natural assemblages. Can. Mineral. 23, 517-534.

Shelley, D., 1993. Igneous and metamorphic rocks under the microscope classification, features, microstructure, and mineral preferred orientations, Chapman and Hall, London, 405pp.

Shen, P., Hwang, S-L., Chu, H-T., and Jeng, R-C., 1988. STEM study of "ferritchromit" from the Heng-Chun chromitite. Am. Mineral. 73, 383-388.

Shepherd, T.J., Rankin, A.H. and Alderton, D.H.M.,1985. A practical guide to fluid inclusion studies. Blackie and Son Ltd., Glasgow and London, 240 pp.

Sheppard, S. M. F. and Gilg, H.A., 1996. Stable isotope geochemistry of clay minerals. Clay Minerals, 31, 1-24.

Sheppard, S. M. F., and Taylor, H. P., Jr., 1974, Hydrogen and oxygen isotope evidence for the origin of water in the Boulder Batholith and the Butte ore deposits, Montana. Econ. Geol., 69, 926-946.

Shore, M. and Fowler, D., 1996. Oscillatory zoning in minerals, a common phenomenon. Can. Mineral, 34. 1111-1126.

Sillitoe, R. H., 1972. A Plate Tectonic Model for the Origin of Porphyry Copper Deposits. Economic Geology, 67, 184-197.

Sillitoe, R.H., 1973. The tops and bottoms of porphyry copper deposits. Economic Geology, 68, 700-815.

Sillitoe, R.H., 1985. Ore-Related Breccias in Volcanoplutonic Arcs. Economic Geology, 80, 1467-1514.

Sillitoe, R.H., 1987. Copper, gold and subduction. A Trans-Pacific Perspective. In: Proceedings Pacific Rim Congress 1987, Australian Institute of Mining and Metallurgy, 399-403.

Sillitoe, R.H., 1989. Gold deposits in Western Pacific island arcs: The magmatic connection. Economic Geology Monograph 6, 274-291.

Sillitoe, R.H., 1991. Intrusion-related gold deposits. In Foster, R.P., (ed.), Gold Metallogeny and Exploration, Blackie, Glasgow, 165-209.

Sillitoe, R.H., 2000, Gold-rich porphyry deposits - Descriptive and genetic models and their role in exploration and discovery. Reviews in Economic Geology, 13, 315–345.

Sillitoe, R.H., 2010. Porphyry Copper Systems. Economic Geology, 105, 3-41.

Sillitoe, R.H. and Hedenquist, J.W., 2003. Linkages between volcanotectonic settings, ore-fluid compositions and epithermal precious metal deposits. In: Simmons SF, Graham I (Eds.): Volcanic, geothermal and ore-forming fluids: rulers and witnesses of processes within the earth. Econ. Geol. Spec. Publ. No 10, 315-345.

Simić, M., 2000. Metallogeny of Dražnja-Propaštica-Novo Brdo ore field in the Vardar Zone. In: Karamata, S. and Janković, S. (Eds.): Geology and Metallogeny of the Dinarides and the Vardar Zone. Academy of Science and Arts of the Republic of Srpska, Collections and Monographs, Banja Luka, Sarajevo Vol. I, 409–424. (In Serbian).

Simić, V. 1956. Zur Geologie des Studenicagebietes (Südwestserbien). Vesnik Bull. Serv. Geol. Geophys. 12, 5-66 (in Serbo-Croatian, with German summary).

Sinclair, W.D., 2007. Porphyry deposits. In: Goodfellow, W.D., (Ed.): Mineral Deposits of Canada: A Synthesis of Major Deposit-Types, District Metallogeny, the Evolution of Geological Provinces, and Exploration Methods: Geological Association of Canada, Mineral Deposits Division, Special Publication No. 5, 223-243.

Sladić-Trifunović, M., 1995. The Upper Cretaceous in the Kopaonik area. In: Symposium- "Geology and Metallogeny of Kopaonik Mt.", Belgrade, 122-146 (In Serbian, English abstract).

Smith, A.G., 1971. Alpine deformation and the alpine areas of Thetys, Mediterranean and Atlantic. Geological Society of America Bulletin, 82, 2039-2070.

Smith, A.G., 1993. Tectonic significance of the Hellenic–Dinaric ophiolites. In: Prichard, H.M., Alasbaster, T., Harris, N.B.W., Neary, C.R. (Eds.): Magmatic Processes and Plate Tectonics. Geological Society, London, Special Publication 76, 213–244.

Smith, A.G., 2006. Tethyan ophiolite emplacement, Africa to Europemotions, and Atlantic spreading. In: Robertson, A.H.F. and Mountrakis, D. (Eds.): Tectonic Development of the Eastern Mediterranean Region. Geological Society, London, Special Publication 260, 11-35.

Smith, A.G. and Spray, J.G., 1984. A half-ridge transform model for the Hellenic-Dinaric ophiolites. In: Dixon, J.E., Robertson, A.H.F. (Eds.): The Geological Evolution of the Eastern Mediterranean. Geological Society of London, Special Publication 17, 629-644.

Smith, A.G., Hynes, A.J., Menzies, A.J., Nisbet, E.G., Price, I., Welland, M.J.P., Ferrière, J., 1975. The stratigraphy of the Othris Mountains, eastern central Greece. Eclogae Geologicae Helvetiae 68, 463-481.

Spangenberg, J.E., Fontboté, L., and Macko, S. A., 1999. An Evaluation of the Inorganic and Organic Geochemistry of the San Vicente Mississippi Valley-Type Zinc-Lead District Central Peru: Implications of Ore Fluid Composition, Mixing Processes, and Sulfate Reduction. Economic Geology, 94 (7), 1067-1092.

Sparks, R.J.S., and Marshall, L.A., 1986. Thermal and mechanical constraints on mixing between mafic and silicic magmas: Journal of Volcanology and Geothermal Research 29, 99-124.

Spray, J.G., Bebien, J., Rex, D.C. and Roddick, J.C., 1984. Age constraints on the igneous and metamorphic evolution of the Hellenide-Dinaric ophiolites. In: Dixon, J.E., Robertson, A.H.F. (Eds.): The Geological Evolution of the Eastern Mediterranean. Geological Society, London, Special Publication 17, 619-627.

Stacey, J.S. and Kramers, J.D., 1975. Approximation of terrestrial lead isotope evolution by a two-stage model. Earth Plan.Sci. Lett. 26, 207-221.

Stamatelopoulou-Seymour, K., Vlassopoulos, D., Pearce, T.H., and Rice, C., 1990. The record of magma chamber processes in plagioclase phenocrysts at Thera Volcano, Aegean Volcanic Arc, Greece. Contributions to Mineralogy and Petrology104, 73-84.

Stampfli, G. M. and Borel, G. D. 2002. A plate tectonic model for the Palaeozoic and Mesozoic constrained by dynamic plate boundaries and restored synthetic oceanic isochrones. Earth and Planetary Science Letters, 169, 17-33.

Stampfli, G.M., Mosar, J., De Bono, A., Vavasis, I., 1998. Late Palaeozoic, early Mesozoic plate tectonics of the westernTethys. Bulletin of theGeological Society ofGreece 32,113–120. Stanton, R.L., 1972. Ore petrology. McGraw Hill Book Complex, N.Y., 713pp.

Stefanović, M. and Pavlović, Z., 1960. Petrographic characteristics of the Kopaonik granitoid massif. Vesnik, Geological and Geophysical Survey newsletters, vol 18, Belgrade (in Serbian).

Sterner, S. M., Hall, D. L., and Bodnar, R. J., 1988. Synthetic fluid inclusions. Solubility relations in the system NaCl-KCl-H2O under vapor-saturated conditions: Geochimica et Cosmochimica Acta, v. 52, p. 989-1006.

Stimac, J.A., Pearce, T.H., 1992. Textural evidence of mafic-felsic magma interaction in dacite lavas, Clear Lake, California. Am. Mineral. 77, 795-809.

Stocklin, J., 1968. Structural history and tectonics of Iran: A review. American Association of Petroleum Geologists Bulletin 52, 1229-1258.

Streckeisen, A., 1973. Plutonic Rocks. Classification and nomenclature recommended by the IUGS Subcommission on the Systematics of Igneous Rocks. Geotimes 18/10, 26–30.

Strmić, S., Spangenberg, J.E., Palinkas, L. and Borojević, S., 2003. The Ljubija siderite deposit, NW Bosnia: Fluid inclusions, stable isotopes, inorganic and organic geochemical constraints. Swiss Geoscience Meeting 2003, Abstract Volume / Bousquet, R., Dresmann, H., Groger, H.. (Eds.): University of Basel, 106p.

Strmić-Palinkaš, S., 2004. Organic and inorganic geochemistry of Ljubija mineral deposits, NW Bosnia). Prirodoslovno-matematicki fakultet, University of Zagreb, M.Sc. thesis, 102 p. unpublished (in Croatian).

Strmić-Palinkaš, S., 2009. Genesis of hydrothermal and skarn paragenesis in Pb-Zn-Ag mineral deposit Trepča (Stari Trg), Kosovo. Prirodoslovno-matematicki fakultet, University of Zagreb, PhD. thesis, unpublished, 148 p.

Sudar M., 1986. Triassic microfossils and biostratigraphy of the Inner Dinarides between Gučevo and Ljubišnja Mts., Yugoslavia. Ann. Géol. Péninsule Balkanique 50, 151-394 (in Serbo-Croatian, English summary).

Sudar, M. and Kovács S. *2006. Metamorphosed* and ductilely deformed conodonts from Triassic limestones situated between ophiolite complexes: Kopaonik Mountain (Serbia) and Bükk Mountains (NE Hungary) - a preliminary comparison. Geologica Carpathica 57, 157-176.

Sun, C.H., Stern, R.J., 2001. Genesis of Mariana shoshonites: contribution of the subduction component. Journal of Geophysical Research 106, 589-608.

Sun, S.S., and McDonough, W.F., 1989. Chemical and isotopic systematics of oceanic basalts: implications for mantle composition and processes. In: Saunders, A.D. and Norry, M.J. (Eds.): Magmatism in the Ocean Basins. - Geological Society Special Publication 42, 313-345.

Suzuoki, T. and Epstein, S., 1976. Hydrogen isotope fractionation between OH-bearing minerals and water. Geochim. Cosmochim. Acta 40, 1229-1240.

Sverjensky, D.A., 1984. Europium redox equilibria in aqueous solutions. Earth and Planetary Science Letters 67, 70-78.

Sverjensky, D.A. 1986. Genesis of Mississippi valley-type lead-zinc deposits. Annual Review of Earth and Planetary Sciences Letters 14, 177-199.

Symposium Committee, 1995: Symposium-"Geology and Metallogeny of the Kopaonik Mt"., 1995, June 19-22, Kopaonik-Belgrade; 518p. (In Serbian, English abstracts).

Takin, M., 1972. Iranian geology and continental drift in the Middle East. Nature 235, 147-150.

Tari, V. and Pamić, J., 1998. Geodynamic evolution of the northern Dinarides and the southern part of the Pannonian Basin. Tectonophysics, 297, 269 - 281.

Tatsumi, Y., Hamilton, D.L., and Nesbitt, R.W., 1986. Chemical characteristics of fluid phase released from a subducted lithosphere and origin of arc magma: evidence from high-pressure experiments and natural rocks. Journal of Volcanology and Geothermal Research 29, 293-309.

Taylor, B.E., 1992. Degassing of $H_2O$ from rhyolite magma during eruption and shallow intrusion, and the isotopic composition of magmatic water in hydrothermal systems. In: Hedenquist JW (Ed) Magmatic contributions to hydrothermal systems. Geol. Surv. Jpn. Rep. 279, 190-194.

Taylor, H.P. Jr.,1973. $^{18}O/^{16}O$ evidence for meteoric hydrothermal alteration and ore deposition in the Tonopah, Comstock Lode, and Goldfield mining districts, Nevada. Econ. Geol. 68, 747-764.

Taylor, H.P.Jr., 1974. The application of oxygen and hydrogen isotope studies to problems of hydrothermal alteration and ore deposition. Econ. Geol. 69, 843-883.

Taylor, H.P.Jr., 1979. Oxygen and hydrogen isotope relations in hydrothermal mineral deposits. In: Barnes, H.L. (Ed.) Geochemistry of hydrothermal ore deposits, 2nd edn. Wiley, New York, 236-277.

Taylor, H.P. Jr., 1997. Oxygen and hydrogen isotope relationships in hydrothermal mineral deposits. In: Barnes HL (Ed.) Geochemistry of hydrothermal ore deposits, 3rd ed. Wiley-Interscience, New York, 229-302.

Taylor, H.P Jr., and Sheppard, S. M. F., 1986. Igneous rocks: I. Processes of isotopic fractionation and isotope systematics. In: Valley, J. W., Taylor, H. P., Jr., and O'Neil, J. R. (Eds.): Stable Isotopes in High Temperature Geological Processes. Rev. Miner. 16, 227-71.

Taylor S. R. and McClennan S. M., 1985. The Continental Crust: Its Composition and Evolution Blackwell, Oxford, 312 pp.

Tindle, A.G. and Webb, P.C., 1994. PROBE-AMPH a spreadsheet program to classify microprobe-derived amphibole analyses. Computers and Geosciences, 20, 1201-1228.

Titcomb, H.A., Forgan Ch.B., Lorimer, J., Page, W.C., 1936. Trpca Mines Limited I-IV. Mining and Metallurgy, New York.17 (9): 424-426; 10:481-484; 11:514-518 and 527; 12: 584-585.

Titley, S. R., 1982. The style and progress of mineralization and alteration in porphyry copper systems, i n Titley, S. R., ed., Advances in geology of the porphyry copper deposits: Tucson, University of Arizona Press, 93-116.

Titley, S.R., 1993. Characteristics of porphyry Cu occurrences in the American Southwest: Geological Association of Canada Special Paper 40, 433-464.

Titley, S.R., 1996. Characteristics of high temperature, carbonate-hosted replacement ores and some comparisons with Mississippi Valley-type ores, in Sangster, D.F., ed., Carbonate-hosted lead-zinc deposits: Society of Economic Geologists, Special Publication Number 4, 244-254.

Titley, S.R. and Beane, R.E., 1981. Porphyry copper deposits. In: Skinner, B.J., (ed.). Economic Geology Seventy-fifth Anniversary Volume, 1905-1980, Economic Geology Publishing Co., 214-269.

Todt, W., Cliff, R.A., Hanser, A., Hofmann, A.W., 1996. Evaluation of a $^{202}Pb$– $^{205}Pb$ double spike for high-precision lead isotope analysis. In: Hart, S.R., Basu, A. (Eds.), Earth Processes: Reading the Isotope Code, vol. 95. American Geophysical Union, Washington, 429– 437.

Tosdal, R.M., Wooden, J.L., and Bouse, R.M., 1999. Pb isotopes, ore deposits, and metallogenic terranes: Society of Economic Geologists, Reviews in Economic Geology, 12, p. 1–12.

Trubelja, F., Marchig, V., Burgath, K. P. and Vujović, Z., 1995. Origin of the Jurassic Tethyan Ophiolites in Bosnia: A Geochemical approach to tectonic setting: Geologica Croatica, 48 (1); 49-66.

Tsuchiyama, A., 1985. Dissolution kinetics of plagioclase in melt of the system diopside-albite-anorthite and the origin of dusty plagioclase in andesites. Contributions to Mineralogy and Petrology, 89, 1-16.

Ucurum, A., 2000. Listwaenites in Turkey: perspectives on formation and precious metal concentration with reference to occurrences in East-Central Anatolia. Ofioliti 25, 15-29.

UNMIK, 2005. Summary description of the lead zinc silver resources and the Trepca mines in Kosovo: Handout , 30p, unpublished report.

Urošević M., Pavlović Z., Klisić M., Brković T., Malešević M. And Trifunović S. 1970: Basic Geological Map of the SFRY, 1: 100,000. Sheet Novi Pazar (K34-3). Sav. Geol. Zavod, Beograd (Zav. Geol. Geofiz. Istraž., Beograd, 1966).

Urošević M., Pavlović Z., Klisić M., Karamata S., Malešević M., Stefanović K., Marković O. and Trifunović S. 1973: Geology of Novi Pazar Sheet (K34-3). Explanatory notes. Sav. Geol. Zavod, Beograd (Zav. Geol. Geofiz. Istraž., Beograd, 1966) 1-77 (in Serbo-Croatian, English and Russian summaries).

Van den Kerkhof, A. M. and Hein, U. F., 2001. Fluid inclusion petrography. Lithos, 55, (1-4), 27-47.

Vanko, D.A., Bodnar, R.J. and Sterner, S.M. (1988): Synthetic fluid inclusions. VIII. Vaporsaturated halite solubility in part of the system NaCl-CaCl2-H2O, with application to fluid inclusions from oceanic hydrothermal systems. Geochim. Cosmochim. Acta 52, 2451-2456.

Vaasjoki M. And Gulson B.L., 1986. Carbonate-hosted base metal deposits; lead isotope data bearing on their genesis and exploration. Economic Geology 81, 156-172.

Vazquez, R., Vennemann, T.W., Kesler, S.E., and Russell, N., 1998. Carbon and oxygen isotope halos in the host limestone, El Mochito Zn-Pb-(Ag) skarn massive sulfide-oxide deposit, Honduras Economic Geology and the Bulletin of the Society of Economic Geologists, 93, 1, 15-31.

Veizer, J.D., Hoefs, J., 1976. The nature of $^{18}O/^{16}O$ and $^{13}C/^{12}C$ secular trends in sedimentary carbonate rocks. Geochim Cosmochim Acta 40, 1387-1395.

Velasco, F., Herrero, J.M., Yusta, I., Alonso, J.A., Seebold, I., and Leach D.L., 2003. Geology and geochemistry of the Reocin zinc-lead deposit, Basque-Cantabrian Basin, northern Spain. Economic Geology and the Bulletin of the Society of Economic Geologists, 98, 7, 1371-1396.

Vennemann TW, Muntean JL, Kesler SE, Oneil JR, Valley JW, Russell N (1993) Stable isotope evidence for magmatic fluids in the Pueblo-Viejo epithermal acid sulfate Au-Ag deposit, Dominican Republic. Econ. Geol. 88, 1, 55-71.

Viets, J.G., Hopkins, R.T. and Miller, B.M., 1992. Variations in minor and trace metals in sphalerite from Mississippi Valley-type deposits of the Ozark region: genetic implications. Econ. Geol. 87, 1897-1905.

Vishnevskaya V., Đerić N. and Karamata S., 2006. Ophiolite-related and non-ophiolite radiolarites of the Balkan Peninsula. Proceed. Ophiolites 2006, Mesozoic Ophiolite Belt of the northern part of the Balkan Peninsula. Belgrade-Banja Luka, May – June 2006, p. 139-143.

Vityk, M.O., Krouse, H.R., Szakun, L.Z., 1994. Fluid evolution and mineral formation in the Beregovo gold-base metal deposit, Transcarpathia, Ukraine. Econ Geol 89:547-565

Vojtěch J., Farrow, C.M., and Vojtěch, E., 2006. Technical Note; Interpretation of Whole-rock Geochemical Data in Igneous Geochemistry: Introducing Geochemical Data Toolkit (GCDkit). Journal of Petrology, 47(6): 1255–1259.

Von Quadt, A., Peytcheva, I., Kamenov, B., Fanger, L., Heinrich, C., and Frank, M., 2002. The Elatsite porphyry copper deposit in the Panagyurishte ore district, Srednogorie, Bulgaria-U-Pb zircon geochronology and isotope-geochemical investigations of magmatism and ore genesis. In Blundell, D.J., Neubauer, F., and von Quadt, Albrecht, (Eds.): The timing and location of major ore deposits in an evolving orogen: Geological Society of London, Special Publications, 204, 119–135.

Von Quadt, A., Driesner, T. and Heinrich, C.A., 2004. Geodynamics and Ore Deposit Evolution of the Alpine-Carpathian-Balkan-Dinaride Orogenic System. Schweizerische Mineralogische und Petrographische Mitteilungen 84, 1-2.

Von Quadt, A., Moritz, R., Peytcheva, I. and Heinrich, C.A., 2005. Geochronology and geodynamics of Late Cretaceous magmatism and Cu-Au mineralization in the Panagyurishte region of the Apuseni-Banat-Timok-Srednogorie belt (Bulgaria). In: Blundell, et al., (Eds.), 2005. Geodynamics and Ore Deposit Evolution in Europe. Thematic Issue with 9 papers, Ore Geology Review, 27, 95-126.

Von Quadt, A., Peytcheva, I., Heinrich, C.A., Cvetković, V. and Banjesević, M., 2007. Upper Cretaceous magmatic evolution and related Cu-Au mineralization in Bulgaria and Serbia. In: Andrew, C. et al.

(Eds.): Digging deeper. Proceedings of the Ninth Biennial SGA Meeting, Dublin, Ireland, 20-23 August, 861-864.

Wagner, T., Mlynarczyk, M.S.J., Williams-Jones, A.E., and Boyce, A.J., 2009. Stable Isotope Constraints on Ore Formation at the San Rafael Tin-Copper Deposit, Southeast Peru. Economic Geology, 104, 223-248.

Wallace, P.J., Carmichael, I.S.E., 1994. Petrology of Volcan Tequila, Jalisco, Mexico: disequilibrium phenocryst assemblages and evolution of the subvolcanic magma system. Contributions to Mineralogy and Petrology 117, 345-361.

Walshe, J.L., Solomon, M., 1981. An investigation into the environment of formation of the volcanic-hosted Mount Lyell copper deposits using geology, mineralogy, stable isotopes, and a sixcomponent chlorite solid solution model. Economic Geology 76, 246- 284.

White, D.E., 1981. Active geothermal systems and hydrothermal ore deposits. Econ. Geol. 75, 392-423.

Whitney, J., and Naldrett, A.J., 1989, Ore deposition associated with magmas: Reviews in Economic Geology, 4, 250pp.

Wilson, G., 1933. The geology, petrology and structure of the Brzece area, Kopaonik Mts, Yugoslavia; Geoloski Anali Balkanskog poluostrva, knj. XI, sveska 2, 1-53, Beograd.

Wilson, M., 1989. Igneous Petrogenesis. A Global Tectonic Approach, London, Boston, Sydney, Wellington: Unwin Hyman, 46pp.

Wilson, M. and Downes, H., 1991. Tertiary-Quaternary extension-related alkaline magmatism in Western and Central Europe. Journal of Petrology, 32, 811-849.

Wilson, M. and Bianchini, G., 1999. Tertiary-Quaternary magmatism within the Mediterranean and surrounding regions. In: Durand, B., Jolivet, L., Horváth, F. and Séranne, M. (Eds.): The Mediterranean Basins: Tertiary extension within the Alpine orogen. - Geological Society London Special Publication 156, 141-168.

Winchester, J.A. and Floyd, P.A., 1977. Geochemical discrimination of different magma series and their differentiation products using immobile elements. Chemical Geology 20: 325-343.

Winchester, J.A. and Max, M.D., 1984. Element mobility associated with syn-metamorphic shear zones near Scotchport, N.W. Mayo, Ireland. J. Metam. Geol. 2, 1-11.

Wood, D.A., 1980. The application of a Th Hf Ta diagram to problems of tectonomagmatic classification and to establishing the nature of crustal contamination of basaltic lavas of the British Tertiary volcanic province. Earth and Planetary Science Letters, 50, 11-30.

Yilmaz, Y. and Polat, A. 1998. Geology and evolution of the Thrace volcanism, Turkey. In: Christofides, G., Marchev, P. and Serri, G. (Eds.): Tertiary magmatism of the Rhodopian Region. - Acta Vulcanologica 10, 293-303.

Zarasvandi, A., Liaghat, S., Zentilli, M., 2004. Evolution of the Darreh-Zerreshk and Ali-Abad porphyry copper deposits, central Iran, within an orogen-parallel strike-slip system (abstract). In 30th Annual Meeting of Atlantic Geoscience Society, Monckton, New Brunswick, Canada, p.36.

Zarasvandi, A., Liaghat, S., Zentilli, M., 2005. Geology of the Darreh-Zerreshk and Ali-Abad porphyry copper deposits, central Iran. International Geology Review 47, 620-646.

Zelić, M., D'Orazio, M., Malasoma, A., Marroni, M. and Pandolfi, L., 2005. The metabasites from the Kopaonik metamorphic complex, Vardar zone, Southern Serbia: Remnants of the rifting-related magmatism of the Mesotethyan domain or evidence for Paleotethys closure in the Dinaric-Hellenic beltc Ofioliti, 30, 2, 91-101.

Zelić, M., Levi, N., Malasoma, A., Marroni, M., Pandolfi, L., And Trivić, B., 2010. Alpine tectono-metamorphic history of the continental units from Vardar zone: the Kopaonik Metamorphic Complex (Dinaric-Hellenic belt, Serbia). Geological Journal, 45, 59-77.

Zelić M., Samuele A., Marroni M., Pandolfi L. and Tonarini S., 2010a. Geological and geochemical features of the Kopaonik Intrusive Complex (Vardar Zone, Serbia). Ofioliti, 35, 1, 33-47.

Zhang, Yi-G. and Frantz, J.D., 1987.Determination of the homogenization temperatures and densities of supercritical fluids in the system NaCl-KCl-CaCl2-H2O using synthetic fluid inclusions. Chem. Geol. 64, 335- 350.

Zheng, Y.F., 1993. Calculation of oxygen isotope fractionation in hydroxyl-bearing silicates. Earth Planet. Sci. Lett. 120, 247-263.

Zheng Y.F., 1999. Oxygen isotope fractionation in carbonate and sulfate minerals. Geochemical Journal, 33, 109-126.

Zheng Y.F. and Hoefs J., 1993. Carbon and oxygen isotopic covariations in hydrothermal calcites; theoretical modeling on mixing processes and application to Pb-Zn deposits in the Harz Mountains, Germany. Mineralium Deposita, 28, 79-89.

Zhong, S. and Mucci, A., 1995. Partitioning of rare earth elements (REEs) between calcite and seawater solutions at 25 degrees C and 1 atm, and high dissolved REE concentrations. Geochim Cosmochim Acta 59:443–453